Methods in Molecular Biology 3089

Springer Protocols



Kristian M. Hargadon *Editor*

Melanoma

Methods and Protocols

Second Edition

Humana Press

METHODS IN MOLECULAR BIOLOGY

Series Editor
John M. Walker
School of Life and Medical Sciences
University of Hertfordshire
Hatfield, Hertfordshire, UK

For further volumes:
http://www.springer.com/series/7651

For over 35 years, biological scientists have come to rely on the research protocols and methodologies in the critically acclaimed Methods in Molecular Biology series. The series was the first to introduce the step-by-step protocols approach that has become the standard in all biomedical protocol publishing. Each protocol is provided in readily-reproducible step-by step fashion, opening with an introductory overview, a list of the materials and reagents needed to complete the experiment, and followed by a detailed procedure that is supported with a helpful notes section offering tips and tricks of the trade as well as troubleshooting advice. These hallmark features were introduced by series editor Dr. John Walker and constitute the key ingredient in each and every volume of the Methods in Molecular Biology series. Tested and trusted, comprehensive and reliable, all protocols from the series are indexed in PubMed.

Manuscript Instructions https://drive.google.com/file/d/1K4Az5vpAFVzYadJ3jKx2-QSo7Dqa_SNA/view?usp=sharing

Melanoma

Methods and Protocols

Second Edition

Edited by

Kristian M. Hargadon

Department of Biology, Hampden-Sydney College, Hampden-Sydney, VA, USA

Humana Press

Editor
Kristian M. Hargadon
Department of Biology
Hampden-Sydney College
Hampden-Sydney, VA, USA

ISSN 1064-3745 ISSN 1940-6029 (electronic)
Methods in Molecular Biology
ISBN 978-1-0716-5618-1 ISBN 978-1-0716-5619-8 (eBook)
https://doi.org/10.1007/978-1-0716-5619-8

1st edition: © Springer Science+Business Media, LLC, part of Springer Nature 2021
2nd edition: © The Editor(s) (if applicable) and The Author(s), under exclusive license to Springer Science+Business Media, LLC, part of Springer Nature 2027

This work is subject to copyright. All rights are solely and exclusively licensed by the Publisher, whether the whole or part of the material is concerned, specifically the rights of translation, reprinting, reuse of illustrations, recitation, broadcasting, reproduction on microfilms or in any other physical way, and transmission or information storage and retrieval, electronic adaptation, computer software, or by similar or dissimilar methodology now known or hereafter developed. Unless otherwise expressly agreed by the Publisher in writing, the Publisher does not authorize use or reproduction of all or any part of this work in any manner for the purpose of training, fine-tuning, evaluating, or developing artificial intelligence models, technologies, or systems. In accordance with Article 4(3) of the EU Directive 2019/790 on copyright and related rights in the Digital Single Market, the Publisher expressly reserves all rights with respect to this work under the text and data mining exception of the directive.
The use of general descriptive names, registered names, trademarks, service marks, etc. in this publication does not imply, even in the absence of a specific statement, that such names are exempt from the relevant protective laws and regulations and therefore free for general use.
The publisher, the authors and the editors are safe to assume that the advice and information in this book are believed to be true and accurate at the date of publication. Neither the publisher nor the authors or the editors give a warranty, expressed or implied, with respect to the material contained herein or for any errors or omissions that may have been made. The publisher remains neutral with regard to jurisdictional claims in published maps and institutional affiliations.

This Humana imprint is published by the registered company Springer Science+Business Media, LLC, part of Springer Nature.
The registered company address is: 1 New York Plaza, New York, NY 10004, U.S.A.

If disposing of this product, please recycle the paper.

Preface

In the summer of 2019, just months before the COVID-19 pandemic completely upended the world as we then knew it, I was on vacation with my family when I received an unexpected email from *Methods in Molecular Biology* Series Editor John Walker, inviting me to serve as editor of a new volume for the series focused on melanoma. Having entered graduate school to study tumor immunology in 2001, I had spent the formative part of my professional training studying immune suppression by melanoma, and I was fortunate to witness during this time the explosion of cancer immunotherapy as a result of early preclinical and clinical work focused largely on this particular disease. Almost 18 years to the day from when I first entered the field, and having by then established my own research program focused on anti-melanoma immunity and cancer genetics, I read John's email with keen interest and jumped at the opportunity to assemble a team of leading experts to contribute to the important volume. That decision culminated nearly 2 years later, in March 2021, with the publication of the first edition of *Melanoma: Methods and Protocols*, a collection of 45 chapters highlighting cutting-edge approaches for studying and treating the disease, developed and optimized by investigators who have dedicated their careers to this specific cancer.

Melanoma, much as it was in 2021 and just as it had been long before, remains today a disease of global public health significance. Although therapeutic advances over the last two and a half decades have dramatically improved the prognosis for patients with the disease, worldwide melanoma incidence has also steadily increased during this time, and at a faster rate than for most other cancers. As a result, annual mortality from the disease has continued to rise despite improved treatment options for patients. With such trends expected to continue until at least 2050, global melanoma incidence and mortality are both expected to nearly double—with nearly 600,000 new cases and 120,000 deaths anticipated per year—by the middle of the century. As I often impress upon my students when discussing the impact of the COVID-19 pandemic, a low mortality *rate* can still be quite tragic when disease *incidence* is high.

Recognizing the challenges that lie ahead, I nevertheless remain optimistic about the rapid progress that is being made in our understanding and treatment of melanoma. Even in the relatively short time since the first edition of this volume was published, several new therapeutics have garnered FDA approval based on their efficacy against the disease. Among these new therapies are novel immune checkpoint blockade regimens such as Opdualag®, which targets in tandem the PD-1 and LAG3 inhibitory receptors that often restrain anti-tumor T lymphocyte responses and which has proven superior to PD-1-blocking monotherapy; a first-in-class (for uveal melanoma) bispecific T-cell engager that directs CD3+ T cells to gp100-HLA-A*02:01 complexes on melanoma cells (KIMMTRACK®); and the first ever tumor-infiltrating lymphocyte (TIL)-based adoptive cell transfer therapy (AMTAGVI®) for any cancer. At the same time that these clinical breakthroughs have been made, technological advances have also revolutionized the ways in which we study and understand melanoma, with single-cell analysis and spatial biology emerging as particularly powerful tools that are yielding critical insights into overall tumor heterogeneity and the array of interactions between cancerous and non-cancerous cells that drive tumor evolution. In this regard, much of the

progress that we envision going forward will depend not only on achieving a more nuanced understanding of melanoma itself but also on gaining a greater appreciation of the ways in which melanoma progression is ultimately influenced by the ecological framework of the host.

With these ambitious goals in mind, we now present this second edition of *Melanoma: Methods and Protocols*, a comprehensive volume that features 14 chapters updated from the first edition together with 26 new chapters, all from leading investigators at the forefront of basic and clinical melanoma research. Divided into seven parts, the volume opens with an extensive review of the diverse model systems that have been developed to study melanoma, followed by chapters describing detailed methodology for genetically engineering melanoma cells for various research applications. Parts II and III include a series of chapters focused on 2D and 3D cell culture systems for investigating various aspects of melanoma biology, including tumor metabolism, cell migration/invasion, and adhesion. These chapters are followed, in Part IV, by several protocols that have been optimized for the isolation and study of circulating melanoma cells and melanoma-derived extracellular vesicles. Part V shifts focus toward melanoma imaging techniques and includes review and protocol chapters relevant to fluorescent and theranostic imaging as well as spatial imaging at both the intratumoral and intracellular levels. Part VI then transitions to computational omics-based approaches for studying melanoma and features chapters on microRNA profiling as well as several metabolomic and microbiomic profiling approaches that can be employed for biomarker identification in preclinical, clinical, and veterinary settings. Finally, the volume concludes in Part VII with methods related to the development and testing of melanoma diagnostics and therapeutics, including those relevant to monoclonal antibody generation and analysis, nucleic acid delivery to tumor tissue, assessment of microbiome-associated influences on immunotherapy, and the generation and characterization of tumor-targeting chimeric antigen receptor T (CAR-T) cells.

As with the first edition, I am indebted to many people who have sacrificed their time and energy to make this second edition possible. First, to my contributing authors, I am beyond grateful for your support of this project. I am inspired by your work and incredibly proud of the volume we have produced, and I know that it will be a tremendous resource for the many scientists and clinicians who share our passion for understanding and treating this cancer we have chosen. I thank you as well for your prompt responses to my inquiries throughout the editing process and for graciously putting up with what I suspect may have sometimes felt like "nagging" emails amidst your many other commitments! Though I am fortunate to have worked with some of you personally over the course of my career, I have come to view all of you as colleagues, and I hope to work with each of you again in the future.

I would also like to thank John Walker for once again inviting me to serve as editor of a second edition of this volume. You have built a true legacy with the *Methods in Molecular Biology* series, and it is an honor to be a small part of the MiMB team. Though I was fortunate to have a bit of experience on my side this second time around, your guidance throughout this project, not to mention your near-instantaneous responses to any questions I had along the way, was invaluable and greatly appreciated. I hope this new edition is as successful as the first!

My tremendous gratitude as well to the staff at Springer for their assistance throughout this process, from the early stages of the volume's inception to its ultimate publication. With particular thanks to Patrick Marton, David C. Casey, and Anna Rakovsky, I appreciate your support, not only of me but also of my authors, who occasionally posed questions that definitely left me out of my depth! Like John, you were always professional, helpful, and quick to respond to any queries I sent your way.

Finally, as I did in the first edition, I cannot end this preface without also thanking Patricia Hargadon and Michael Hargadon, otherwise known affectionately to me as Mom and Dad. You proudly have a copy of the first edition displayed at home, and I cannot wait to give you a copy of this new edition. Your support has always meant the world to me, and your enthusiasm for all I do has always fueled me. So many of my colleagues over the years have said to me, "My family has no idea what I do." I think it is so special that you actually do know what I do. You've read anything I've ever produced, even if it might sometimes seem like a foreign language. I am so blessed to have parents who want to know what I'm up to, and I can't tell you how much I love our coffee-time "journal club" conversations about my work! Your support, of course, extends far beyond my professional endeavors as well, and I am who I am because of you. As with the first edition of this volume, I dedicate this second edition to you, with love, ALWAYS.

Hampden-Sydney, VA, USA ***Kristian M. Hargadon***

Contents

Preface . . . . . *v*
Editors and Contributors . . . . . *xiii*

Part I Overview of Melanoma Models and Methods for Engineering Melanoma Cell Lines

1 Model Systems for the Study of Malignant Melanoma 3
Shannon Reed and Randal K. Gregg

2 Generation of Functional Gene Knockout Melanoma Cell Lines by CRISPR-Cas9 Gene Editing 25
Kristian M. Hargadon, David Z. Bushhouse, Coleman E. Johnson and Corey J. Willams

3 Establishment and Characterization of Model Antigen-Expressing Melanoma Cell Lines 47
Kristian M. Hargadon and Stephen L. Woodall II

Part II 2D Cell Culture-Based Approaches for Studying Melanoma Biology 71

4 A Fluorescence-Based Assay for Measuring Glucose Uptake in Living Melanoma Cells 73
Jelena Grahovac, Marijana Pavlović, Kristina Živić and Marija Ostojić

5 Indirect Coculture of Melanoma Cells with Stromal Cells Present in Their Microenvironment as a Method for Evaluation of Their Mutual Interactions 85
Aleksandra Simiczyjew, Katarzyna Pietraszek-Gremplewicz and Dorota Nowak

6 A Flow Cytometric Assay for Investigating Melanoma Cell Adhesion to Lymphatic Endothelial Cells 95
Kristian M. Hargadon and Coleman E. Johnson

7 Wound Healing Assay for Melanoma Cell Migration 107
Juliano T. Freitas

8 Evaluating Melanoma Cell Migration/Invasion in Transwell Assays by Flow Cytometry 115
Kristian M. Hargadon and James H. Lau

Part III 3D Cell Culture Systems for Studying Melanoma Biology

9 Skin Organ Constructs for In Vitro Modeling of Melanoma Invasion 133
Jelena Grahovac and Allan Wells

10 Modeling Proliferative Versus Migratory Melanoma Cell Phenotypes Using Biofabricated Matrices 143
Sonja K. Schmidt and Anja K. Bosserhoff

Part IV Techniques for Isolating and Studying Circulating Melanoma Cells and Melanoma-Derived Extracellular Vesicles

11 Capture and Isolation of Circulating Melanoma Cells Using Photoacoustic Flowmetry 159
Robert H. Edgar, Justin Cook, Madeline Douglas, Anie-Pier Samson and John A. Viator

12 A Rapid Exosome Isolation Using Ultrafiltration and Size Exclusion Chromatography (REIUS) Method for Exosome Isolation from Melanoma Cell Lines. 171
Shin La Shu, Cheryl L. Allen, Shawna Benjamin-Davalos, Marina Koroleva, Don MacFarland, Hans Minderman and Marc S. Ernstoff

13 Post-Lymphadenectomy Analysis of Small Extracellular Vesicles from Lymphatic Drainage/Exudative Seroma of Melanoma Patients. 189
Enrique Bastón de la Fuente, Pilar Ximénez-Embún, Javier Muñoz, Héctor Peinado and Susana García-Silva

14 Imaging and Analysis of Melanoma-Secreted Extracellular Vesicles in Tumor-Draining Lymph Nodes 209
Lucía Garrido-Miranda, Héctor Peinado and Susana García-Silva

15 Detection of Biomarkers for EMT-Associated Phenotype Switching in Melanoma-Derived Extracellular Vesicles 227
Quan Zhou, Jing Wang, Zhen Zhang, Matt Trau, Alain Wuethrich and Richard J. Lobb

Part V Melanoma Imaging Techniques and Methods for Spatial Analysis of Melanoma Tissue

16 Imaging and Isolation of Extravasation-Participating Endothelial and Melanoma Cells During Angiopellosis 241
Tyler A. Allen and Ke Cheng

17 Quantitative Mapping of Organelle Positioning in Cultured Cells Using Semi-Automated Image Analysis Pipeline 251
Katerina Jerabkova-Roda, Vincent Hyenne and Jacky G. Goetz

18 Design Strategies for Melanoma-Targeting Fluorescent Probes. 265
Emin Sahin, Safaa Altves and Sundus Erbas-Cakmak

19 Multi-Analyte Responsive Fluorescent Sensing of Pathological Cellular States in Melanoma 293
Safaa Altves, Emin Sahin and Sundus Erbas-Cakmak

20 Radiopharmaceuticals for Melanoma Theranostics 307
Chao Meng, Zhen Cheng and Xiaowei Ma

21 PET Imaging of Melanoma Using a Melanin-Targeted Probe. 317
Xiaowei Ma and Zhen Cheng

22 SPECT Imaging of Melanoma Using a ^{99m}Tc-Labeled Melanin-Targeted Probe 329
Ji Tao, Mei Tian and Zhen Cheng

23 PET Imaging of Melanoma Using a Melanocortin 1 Receptor-Targeted Probe 339
Tian Xiang, Mengshi Li, Nicholas J. Baumhover, Michael K. Schultz, Zhen Cheng and Xiaowei Ma

24 Preparation of Melanoma Tissue for Multiplex Immunofluorescence Histology Analysis of Immune Infiltration and Spatial Organization 349
Victoria Ann Remley, Marya Dunlap-Brown, Kelly T. Smith, Sheri Vanhoose, Sara J. Adair, Todd W. Bauer and Ileana S. Mauldin

25 A Method for Quantifying Immune Infiltrates and Tertiary Lymphoid Structures in Murine Melanoma Tumors by Multiplex Immunofluorescence . . . 363
Jackson R. Clark, Pallavi Rustogi and Ileana S. Mauldin

26 Methods for Analyzing Immune Infiltrates and Spatial Organization Within the Melanoma Microenvironment Using Multiplex Immunofluorescence 375
Jackson R. Clark, Kelly T. Smith, Marya Dunlap-Brown, Timothy N.J. Bullock, Craig L. Slingluff Jr. and Ileana S. Mauldin

Part VI Strategies for Diagnostic and Prognostic Metabolomic/Microbiomic Biomarker Identification for Melanoma and Computational/Bioinformatic Approaches to OMICS-Based Analysis of Melanoma

27 Integrated Functional and Metabolomic Profiling of Melanoma Cells Treated with Redox-Active Compounds 389
Marcella Bonanomi and Daniela Gaglio

28 Serum Peptidomic Profiling for Biomarker Discovery in Canine Oral Melanoma and Squamous Cell Carcinoma via MALDI-TOF and LC-MS/MS 403
Sekkarin Ploypetch, Sittiruk Roytrakul and Gunnaporn Suriyaphol

29 Discovery of Salivary Metabolomic Biomarkers for Canine Oral Melanoma and Squamous Cell Carcinoma via CIL LC-MS Analysis 417
Sekkarin Ploypetch, Xian Luo, Shuang Zhao, Gunnaporn Suriyaphol and Liang Li

30 Spatial Lipidomic Analysis Using Secondary Ion Mass Spectrometry (SIMS) 427
Simon Uzoni, John S. Fletcher and Noora Neittaanmäki

31 Unbiased Microbiome and Metabolomic Profiling of Fecal Samples from Patients with Melanoma 441
Animesh A. Mishra, Nicole Poulides, Aidan C. Morrill, Shuheng Gan, Gabriella Nguyen, Meagan A. Mollergren, Christina M. Zarek and Andrew Y. Koh

32 Assessment of Cell-Free MicroRNA by NGS Whole Transcriptome Analysis in Cutaneous Melanoma Patients' Blood 459
Kevin D. Tran, Rebecca Gross, Negin Rahimzadeh, Shanthy Chenathukattil, Dave S.B. Hoon and Matias A. Bustos

33 High-Throughput Identification of miRNA–Target Interactions in Melanoma Using miR-CATCHv2.0 471
Andrea Marranci, Romina D'Aurizio, Milena Rizzo, Catherine M. Greene and Laura Poliseno

Part VII Methods for Preclinical and Clinical Development/ Characterization of Melanoma Diagnostics and Therapeutics

34 Characterization of an Anti-Tryptophan 2,3-Dioxygenase Monoclonal Antibody and Use in a Melanoma Model 501
Summer Sedano, Kaylend Manley, George C. Prendergast, Marie R. Webster and Lisa D. Laury-Kleintop

35 Analytical Assessment of Fc-Receptor Binding of Therapeutic IgG1 Antibodies: A Surface Plasmon Resonance Approach 517
Silvia M. Bacot, Nozomi Sakakibara, Jessica Dement-Brown, Jordan D. Pritts, Devira Friedman, Kamai Patterson, Caroline Taylor, Jennifer Swisher, Gunther H. Boekhoudt, Venkateswara Simhadri, Carole Sourbier, V. Ashutosh Rao, Gerald M. Feldman and Tao Wang

36 In Vivo Reversible Electroporation for Melanoma Therapy 533
Namita Nanda and Joseph J. Skitzki

37 Lipoplex Nanoparticle-Based RNA Delivery to 3D Melanoma Spheroids 541
Rüdiger Rudolf, Tiziana Cesetti, Florian Keller and Mathias Hafner

38 Assessing the Antitumor Immune Effects of Gut Microbiota in a Preclinical Melanoma Model 551
Parastoo Sabaeifard, Wenling Li, Priscilla Del Valle, Rebecca Suet-Yan Chiu, Jana Dakour, Nicole Poulides, Shuheng Gan, Jake N. Lichterman, Christina M. Zarek, Xiaowei Zhan and Andrew Y. Koh

39 Generation of Murine Chimeric Antigen Receptor T Cells for Adoptive T Cell Therapy for Melanoma 591
Amorette Barber

40 Retroviral Transduction of Human T Cells with a Chimeric Antigen Receptor Targeting PD-1 Ligands for Melanoma Immunotherapy 603
Amorette Barber

Index. *613*

Editors and Contributors

About the Editors

Dr. Kristian M. Hargadon, *a Goldwater Scholar and graduate of Hampden-Sydney College (Valedictorian, Class of 2001), is the Trinkle and Spalding Professor of Biology at Hampden-Sydney College. Dr. Hargadon earned his Ph.D. in Microbiology in 2007 at the University of Virginia, where he studied immune suppression by melanoma in the laboratory of Dr. Victor Engelhard. After completing his Ph.D., Dr. Hargadon pursued his postdoctoral training, also at the University of Virginia, in the laboratory of Dr. Thomas Braciale, investigating influenza virus-dendritic cells interactions and their influence on anti-viral immunity and immunopathology. In 2009, he returned to Hampden-Sydney College as a faculty member in the Department of Biology, where he chairs the Health Sciences Advisory Committee and teaches courses in Immunology, Microbiology, Virology, the Biology of Cancer, Genetics, and Cell Biology. Dr. Hargadon maintains an active research program and has received over $300,000 in funding to support his cancer research, which has resulted in 44 articles and book chapters published in leading academic journals and book series. He is the editor of the 1st and 2nd Editions of the Melanoma: Methods and Protocols volume for the Methods in Molecular Biology series and serves as an Editorial Board member for the journals BMC Cancer, Discover Oncology, and Discover Immunity. The recipient of numerous awards for his research and mentoring efforts, Dr. Hargadon was recently recognized in 2023 with the University of Virginia School of Medicine's Early Achievement Award in Biomedical Sciences and in 2024 with the Council on Undergraduate Research Biology Division's Mid-Career Mentor Award, a national award given annually to a single biology faculty member from among all U.S. colleges and universities in recognition of sustained efforts in mentoring undergraduate research students, fostering their development, and providing an equitable learning environment. In both 2024 and 2025, Dr. Hargadon was also recognized as being among the top 2% of scientists worldwide (Subfield: Immunology), as ranked according to citation metrics published by Stanford University and Elsevier.*

Contributors

Sara J. Adair • *Department of Surgery, University of Virginia, Charlottesville, VA, USA*

Cheryl L. Allen • *Department of Medicine, Roswell Park Comprehensive Cancer Center, Buffalo, NY, USA*

Tyler A. Allen • *Department of Medicine, Division of Medical Oncology, Duke University Medical Center, Durham, NC, USA; Duke Cancer Institute, Duke University Medical Center, Durham, NC, USA*

Safaa Altves • *Department of Molecular Biology and Genetics, Necmettin Erbakan University, Konya, Turkey; Science and Technology Research and Application Center (BİTAM), Necmettin Erbakan University, Konya, Turkey*
V. Ashutosh Rao • *Office of Pharmaceutical Quality Assessment III, CDER, U.S. FDA, Silver Spring, MD, USA*
Silvia M. Bacot • *Office of Pharmaceutical Quality Research, CDER, U.S. FDA, Silver Spring, MD, USA*
Amorette Barber • *Department of Biological and Environmental Sciences, Longwood University, Farmville, VA, USA*
Enrique Bastón de la Fuente • *Microenvironment and Metastasis Laboratory, Tumor Biology Programme, Spanish National Cancer Research Center (CNIO), Madrid, Spain*
Todd W. Bauer • *Department of Surgery, University of Virginia, Charlottesville, VA, USA; Department of Pathology, Molecular and Cellular Basis of Disease Program, University of Virginia, Charlottesville, VA, USA*
Nicholas J. Baumhover • *Perspective Therapeutics Inc, Seattle, WA, USA*
Shawna Benjamin-Davalos • *Department of Medicine, Roswell Park Comprehensive Cancer Center, Buffalo, NY, USA*
Gunther H. Boekhoudt • *Office of Pharmaceutical Quality Assessment III, CDER, U.S. FDA, Silver Spring, MD, USA*
Marcella Bonanomi • *Institute of Bioimaging and Complex Biological Systems, National Research Council (CNR), Segrate, MI, Italy*
Anja K. Bosserhoff • *Institute of Biochemistry, FAU Erlangen-Nürnberg, Erlangen, Germany*
Timothy N. J. Bullock • *Department of Pathology, University of Virginia, Charlottesville, VA, USA*
David Z. Bushhouse • *Hargadon Laboratory, Department of Biology, Hampden-Sydney College, Hampden-Sydney, VA, USA*
Matias A. Bustos • *Department of Translational and Precision Medicine, Santa Monica, CA, USA*
Tiziana Cesetti • *CeMOS Research and Transfer Center, Technische Hochschule Mannheim, Mannheim, Germany; Institute of Molecular and Cell Biology, Technische Hochschule Mannheim, Mannheim, Germany*
Shanthy Chenathukattil • *Department of Translational Molecular Medicine, Santa Monica, CA, USA*
Ke Cheng • *Department of Biomedical Engineering, Columbia University, New York, NY, USA; Herbert Irving Comprehensive Cancer Center, Columbia University, New York, NY, USA*
Zhen Cheng • *State Key Laboratory of Drug Research, Molecular Imaging Center, Shanghai Institute of Materia Medica, Chinese Academy of Sciences, Shanghai, China; School of Pharmacy, University of Chinese Academy of Sciences, Beijing, China; Shandong Laboratory of Yantai Drug Discovery, Bohai Rim Advanced Research Institute for Drug Discovery, Yantai, China*
Rebecca Suet-Yan Chiu • *Department of Pediatrics, University of Texas Southwestern, Dallas, TX, USA*
Jackson R. Clark • *Department of Surgery, University of Virginia, Charlottesville, VA, USA*
Justin Cook • *Department of Radiology, Allegheny General Hospital, Pittsburgh, PA, USA*

Romina D'Aurizio • *Institute of Informatics and Telematics (IIT), CNR, Pisa, Italy*
Jana Dakour • *Department of Pediatrics, University of Texas Southwestern, Dallas, TX, USA*
Jessica Dement-Brown • *Office of Pharmaceutical Quality Research, CDER, U.S. FDA, Silver Spring, MD, USA*
Madeline Douglas • *Department of Bioengineering, University of Pittsburgh, Pittsburgh, PA, USA*
Marya Dunlap-Brown • *Department of Surgery, University of Virginia, Charlottesville, VA, USA*
Robert H. Edgar • *Department of Medicine, Vascular Medicine Institute, University of Pittsburgh, Pittsburgh, PA, USA*
Sundus Erbas-Cakmak • *Department of Molecular Biology and Genetics, Necmettin Erbakan University, Konya, Turkey; Science and Technology Research and Application Center (BİTAM), Necmettin Erbakan University, Konya, Turkey*
Marc S. Ernstoff • *Department of Medicine, Roswell Park Comprehensive Cancer Center, Buffalo, NY, USA*
Gerald M. Feldman • *Office of Pharmaceutical Quality Research, CDER, U.S. FDA, Silver Spring, MD, USA*
John S. Fletcher • *Department of Chemistry and Molecular Biology, University of Gothenburg, Gothenburg, Sweden*
Juliano T. Freitas • *Department of Specialty Medicine, Orlando College of Osteopathic Medicine, Winter Garden, FL, USA*
Devira Friedman • *Office of Pharmaceutical Quality Research, CDER, U.S. FDA, Silver Spring, MD, USA*
Daniela Gaglio • *Institute of Bioimaging and Complex Biological Systems, National Research Council (CNR), Segrate, MI, Italy*
Shuheng Gan • *Department of Population and Data Sciences, University of Texas Southwestern, Dallas, TX, USA; O'Donnell School of Public Health, The University of Texas Southwestern Medical Center, Dallas, TX, USA*
Susana García-Silva • *Melanoma Laboratory, Tumor Biology Programme, Spanish National Cancer Research Center (CNIO), Madrid, Spain*
Lucía Garrido-Miranda • *Microenvironment and Metastasis Laboratory, Tumor Biology Programme, Spanish National Cancer Research Centre (CNIO), Madrid, Spain; Microenvironment and Metastasis Laboratory, Immunology and Oncology Department, Spanish National Centre for Biotechnology (CNB-CSIC), Madrid, Spain*
Jacky G. Goetz • *Tumor Biomechanics, Strasbourg, France; INSERM UMR_S1109, Strasbourg, France; Université de Strasbourg, Strasbourg, France; Fédération de Médecine Translationnelle de Strasbourg (FMTS), Strasbourg, France; Equipe Labellisée Ligue Contre le Cancer, Paris, France*
Jelena Grahovac • *Experimental Oncology Department, Institute for Oncology and Radiology of Serbia, Belgrade, Serbia*
Catherine M. Greene • *Department of Clinical Microbiology, Royal College of Surgeons in Ireland, Dublin, Ireland*
Randal K. Gregg • *Dr. Kiran C. Patel College of Osteopathic Medicine, Nova Southeastern University, Clearwater, FL, USA*
Rebecca Gross • *Department of Translational Molecular Medicine, Santa Monica, CA, USA*

Mathias Hafner • *Institute of Molecular and Cell Biology, Technische Hochschule Mannheim, Mannheim, Germany*
Kristian M. Hargadon • *Hargadon Laboratory, Department of Biology, Hampden-Sydney College, Hampden-Sydney, VA, USA*
Dave S. B. Hoon • *Department of Genomic Sequencing Center, Saint John's Cancer Institute (SJCI) at Providence Saint John's Health Center (SJHC), Santa Monica, CA, USA; Department of Translational Molecular Medicine, Santa Monica, CA, USA*
Vincent Hyenne • *Tumor Biomechanics, Strasbourg, France; INSERM UMR_S1109, Strasbourg, France; Université de Strasbourg, Strasbourg, France; Fédération de Médecine Translationnelle de Strasbourg (FMTS), Strasbourg, France; Equipe Labellisée Ligue Contre le Cancer, Paris, France; CNRS, Strasbourg, France*
Katerina Jerabkova-Roda • *Tumor Biomechanics, Strasbourg, France; INSERM UMR_S1109, Strasbourg, France; Université de Strasbourg, Strasbourg, France; Fédération de Médecine Translationnelle de Strasbourg (FMTS), Strasbourg, France; Equipe Labellisée Ligue Contre le Cancer, Paris, France*
Coleman E. Johnson • *Hargadon Laboratory, Department of Biology, Hampden-Sydney College, Hampden-Sydney, VA, USA*
Florian Keller • *CeMOS Research and Transfer Center, Technische Hochschule Mannheim, Mannheim, Germany; Institute of Molecular and Cell Biology, Technische Hochschule Mannheim, Mannheim, Germany*
Andrew Y. Koh • *Department of Pediatrics, University of Texas Southwestern, Dallas, TX, USA; Department of Microbiology, The University of Texas Southwestern Medical Center, Dallas, TX, USA; Harold C. Simmons Comprehensive Cancer Center, The University of Texas Southwestern Medical Center, Dallas, TX, USA*
Marina Koroleva • *Department of Medicine, Roswell Park Comprehensive Cancer Center, Buffalo, NY, USA*
James H. Lau • *Hargadon Laboratory, Department of Biology, Hampden-Sydney College, Hampden-Sydney, VA, USA*
Lisa D. Laury-Kleintop • *Lankenau Institute for Medical Research, Wynnewood, PA, USA*
Liang Li • *The Metabolomics Innovation Centre, University of Alberta, Edmonton, Alberta, Canada; Department of Chemistry, University of Alberta, Edmonton, Alberta, Canada*
Mengshi Li • *Perspective Therapeutics Inc, Seattle, WA, USA*
Wenling Li • *Department of Pediatrics, University of Texas Southwestern, Dallas, TX, USA*
Jake N. Lichterman • *Department of Internal Medicine, University of Texas Southwestern Medical Center, Dallas, TX, USA*
Richard J. Lobb • *Centre for Personalized Nanomedicine, Australian Institute for Bioengineering and Nanotechnology (AIBN), The University of Queensland, Brisbane, QLD, Australia*
Xian Luo • *The Metabolomics Innovation Centre, University of Alberta, Edmonton, Alberta, Canada*
Xiaowei Ma • *Department of Nuclear Medicine, The Second Xiangya Hospital of Central South University, Changsha, Hunan, China*
Don MacFarland • *Pathology and Anatomical Sciences, Jacobs School of Medicine and Biomedical Sciences, University at Buffalo, Buffalo, NY, USA*
Kaylend Manley • *Lankenau Institute for Medical Research, Wynnewood, PA, USA*
Andrea Marranci • *Institute of Clinical Physiology (IFC), CNR, Pisa, Italy*

Ileana S. Mauldin • *Department of Surgery, University of Virginia, Charlottesville, VA, USA*
Chao Meng • *Department of Nuclear Medicine, The Second Xiangya Hospital of Central South University, Changsha, Hunan, China*
Hans Minderman • *Flow and Image Cytometry Shared Resource, Roswell Park Comprehensive Cancer Center, Buffalo, NY, USA*
Animesh A. Mishra • *Department of Pediatrics, University of Texas Southwestern, Dallas, TX, USA*
Meagan A. Mollergren • *Department of Pediatrics, University of Texas Southwestern, Dallas, TX, USA*
Aidan C. Morrill • *Department of Pediatrics, University of Texas Southwestern, Dallas, TX, USA*
Javier Muñoz • *Ikerbasque, Basque Foundation for Science, Bilbao, Spain*
Namita Nanda • *Department of Pathology, Case Western Reserve University School of Medicine, Cleveland, OH, USA*
Noora Neittaanmäki • *Department of Clinical Pathology, Sahlgrenska University Hospital, Region Västra Götaland, Gothenburg, Sweden; Department of Laboratory Medicine, Sahlgrenska Academy, University of Gothenburg, Gothenburg, Sweden*
Gabriella Nguyen • *Department of Pediatrics, University of Texas Southwestern, Dallas, TX, USA*
Dorota Nowak • *Department of Cell Pathology, Faculty of Biotechnology, University of Wroclaw, Wrocław, Poland*
Marija Ostojić • *Experimental Oncology Department, Institute for Oncology and Radiology of Serbia, Belgrade, Serbia*
Kamai Patterson • *Office of Pharmaceutical Quality Research, CDER, U.S. FDA, Silver Spring, MD, USA*
Marijana Pavlović • *Experimental Oncology Department, Institute for Oncology and Radiology of Serbia, Belgrade, Serbia*
Héctor Peinado • *Microenvironment and Metastasis Laboratory, Tumor Biology Programme, Spanish National Cancer Research Center (CNIO), Madrid, Spain; Microenvironment and Metastasis, Department of Immunology and Oncology, Centro Nacional de Biotecnología. Consejo Superior de Investigaciones Científicas (CNB-CSIC), Madrid, Spain; Microenvironment and Metastasis Laboratory, Immunology and Oncology Department, Spanish National Centre for Biotechnology (CNB-CSIC), Madrid, Spain*
Katarzyna Pietraszek-Gremplewicz • *Department of Cell Pathology, Faculty of Biotechnology, University of Wroclaw, Wrocław, Poland*
Sekkarin Ploypetch • *Department of Clinical Sciences and Public Health, Faculty of Veterinary Science, Mahidol University, Nakorn Pathom, Thailand*
Laura Poliseno • *Institute of Clinical Physiology (IFC), CNR, Pisa, Italy; Oncogenomics Unit, CRL-ISPRO, Pisa, Italy*
Nicole Poulides • *Department of Pediatrics, University of Texas Southwestern, Dallas, TX, USA*
George C. Prendergast • *Lankenau Institute for Medical Research, Wynnewood, PA, USA*
Jordan D. Pritts • *Office of Pharmaceutical Quality Research, CDER, U.S. FDA, Silver Spring, MD, USA*
Negin Rahimzadeh • *Department of Translational Molecular Medicine, Santa Monica, CA, USA*

Shannon Reed • *Dr. Kiran C. Patel College of Osteopathic Medicine, Nova Southeastern University, Clearwater, FL, USA*
Victoria Ann Remley • *Department of Surgery, University of Virginia, Charlottesville, VA, USA; Department of Pathology, Molecular and Cellular Basis of Disease Program, University of Virginia, Charlottesville, VA, USA*
Milena Rizzo • *Institute of Clinical Physiology (IFC), CNR, Pisa, Italy*
Sittiruk Roytrakul • *National Center for Genetic Engineering and Biotechnology, National Science and Technology Development Agency, Pathum Thani, Thailand*
Rüdiger Rudolf • *CeMOS Research and Transfer Center, Technische Hochschule Mannheim, Mannheim, Germany; Institute of Molecular and Cell Biology, Technische Hochschule Mannheim, Mannheim, Germany*
Pallavi Rustogi • *Department of Surgery, University of Virginia, Charlottesville, VA, USA*
Parastoo Sabaeifard • *Department of Pediatrics, University of Texas Southwestern, Dallas, TX, USA*
Emin Sahin • *Department of Molecular Biology and Genetics, Necmettin Erbakan University, Konya, Turkey; Science and Technology Research and Application Center (BİTAM), Necmettin Erbakan University, Konya, Turkey*
Nozomi Sakakibara • *Office of Pharmaceutical Quality Assessment III, CDER, U.S. FDA, Silver Spring, MD, USA*
Anie-Pier Samson • *Department of Biomedical Engineering, Duquesne University, Pittsburgh, PA, USA*
Sonja K. Schmidt • *Institute of Biochemistry, FAU Erlangen-Nürnberg, Erlangen, Germany*
Michael K. Schultz • *Perspective Therapeutics Inc, Seattle, WA, USA*
Summer Sedano • *Lankenau Institute for Medical Research, Wynnewood, PA, USA*
Shin La Shu • *Department of Medicine, Roswell Park Comprehensive Cancer Center, Buffalo, NY, USA*
Venkateswara Simhadri • *Office of Pharmaceutical Quality Research, CDER, U.S. FDA, Silver Spring, MD, USA*
Aleksandra Simiczyjew • *Department of Cell Pathology, Faculty of Biotechnology, University of Wroclaw, Wrocław, Poland*
Joseph J. Skitzki • *Department of General Surgery, Cleveland Clinic, Cleveland, OH, USA*
Craig L. Slingluff Jr. • *Department of Surgery, University of Virginia, Charlottesville, VA, USA*
Kelly T. Smith • *Department of Surgery, University of Virginia, Charlottesville, VA, USA*
Carole Sourbier • *Office of Pharmaceutical Quality Research, CDER, U.S. FDA, Silver Spring, MD, USA*
Gunnaporn Suriyaphol • *Biochemistry Unit, Department of Physiology, Faculty of Veterinary Science, Chulalongkorn University, Bangkok, Thailand; Companion Animal Cancer Research Unit, Faculty of Veterinary Science, Chulalongkorn University, Bangkok, Thailand*
Jennifer Swisher • *Office of Pharmaceutical Quality Assessment III, CDER, U.S. FDA, Silver Spring, MD, USA*
Ji Tao • *Huashan Hospital and Human Phenome Institute, Fudan University, Shanghai, China*

Caroline Taylor • *Office of Pharmaceutical Quality Research, CDER, U.S. FDA, Silver Spring, MD, USA; Medical College of Georgia, Augusta, GA, USA*
Mei Tian • *Huashan Hospital and Human Phenome Institute, Fudan University, Shanghai, China; State Key Laboratory of Genetics and Development of Complex Phenotypes, Fudan University, Shanghai, China*
Kevin D. Tran • *Department of Genomic Sequencing Center, Saint John's Cancer Institute (SJCI) at Providence Saint John's Health Center (SJHC), Santa Monica, CA, USA*
Matt Trau • *Centre for Personalized Nanomedicine, Australian Institute for Bioengineering and Nanotechnology (AIBN), The University of Queensland, Brisbane, QLD, Australia; School of Chemistry and Molecular Biosciences, The University of Queensland, Brisbane, QLD, Australia*
Simon Uzoni • *Department of Chemistry and Molecular Biology, University of Gothenburg, Gothenburg, Sweden*
Priscilla DelValle • *Department of Pediatrics, University of Texas Southwestern, Dallas, TX, USA*
Sheri Vanhoose • *Research Histology Core Facility, University of Virginia, Charlottesville, VA, USA*
John A. Viator • *Department of Biomedical Engineering, Duquesne University, Pittsburgh, PA, USA*
Jing Wang • *Key Laboratory of OptoElectronic Science and Technology for Medicine of Ministry of Education, Fujian Provincial Key Laboratory of Photonics Technology, Fujian Normal University, Fuzhou, China*
Tao Wang • *Office of Pharmaceutical Quality Research, CDER, U.S. FDA, Silver Spring, MD, USA*
Marie R. Webster • *Lankenau Institute for Medical Research, Wynnewood, PA, USA*
Allan Wells • *Department of Pathology, University of Pittsburgh, Pittsburgh, PA, USA*
Corey J. Willams • *Hargadon Laboratory, Department of Biology, Hampden-Sydney College, Hampden-Sydney, VA, USA*
Stephen L. Woodall II • *Hargadon Laboratory, Department of Biology, Hampden-Sydney College, Hampden-Sydney, VA, USA*
Alain Wuethrich • *Centre for Personalized Nanomedicine, Australian Institute for Bioengineering and Nanotechnology (AIBN), The University of Queensland, Brisbane, QLD, Australia; School of Chemistry and Molecular Biosciences, The University of Queensland, Brisbane, QLD, Australia*
Tian Xiang • *Department of Nuclear Medicine, The Second Xiangya Hospital of Central South University, Changsha, Hunan, China*
Pilar Ximénez-Embún • *Proteomics Unit, Spanish National Cancer Research Centre (CNIO), Madrid, Spain*
Christina M. Zarek • *Department of Pediatrics, University of Texas Southwestern, Dallas, TX, USA*
Xiaowei Zhan • *O'Donnell School of Public Health, The University of Texas Southwestern Medical Center, Dallas, TX, USA*
Zhen Zhang • *Centre for Personalized Nanomedicine, Australian Institute for Bioengineering and Nanotechnology (AIBN), The University of Queensland, Brisbane, QLD, Australia*

Shuang Zhao • *The Metabolomics Innovation Centre, University of Alberta, Edmonton, Alberta, Canada*

Quan Zhou • *Centre for Personalized Nanomedicine, Australian Institute for Bioengineering and Nanotechnology (AIBN), The University of Queensland, Brisbane, QLD, Australia*

Kristina Živić • *Experimental Oncology Department, Institute for Oncology and Radiology of Serbia, Belgrade, Serbia*

Part I

Overview of Melanoma Models and Methods for Engineering Melanoma Cell Lines



Chapter 1

Model Systems for the Study of Malignant Melanoma

Shannon Reed and Randal K. Gregg

Abstract

Since the first resection of melanoma by Hunter in 1787, efforts to treat patients with this deadly malignancy have been ongoing. Initial work to understand melanoma biology for therapeutics development began with the employment of isolated cancer cells grown in culture. However, these models lack in vivo interactions with the tumor microenvironment. Melanoma cell line transplantation into suitable animals, such as mice, has been informative and useful for testing therapeutics as a pre-clinical model. Injection of freshly isolated patient melanomas into immunodeficient animals has shown the capacity to retain the genetic heterogeneity of the tumors, which is lost during long-term culture of melanoma cells. Upon the advancement of technology, genetically engineered animals have been generated to study the spontaneous development of melanomas in light of newly discovered genetic aberrations associated with melanoma formation. Culturing melanoma cells in a matrix generates tumor spheroids, providing an in vitro environment that promotes the heterogeneity commonplace with human melanoma and displaces the need for animal care facilities. Advanced 3D cultures have been created simulating the structure and cellularity of human skin to permit in vitro testing of therapeutics on melanomas expressing the same phenotype as demonstrated in vivo. This review discusses these models and their relevance to the study of melanomagenesis, growth, metastasis, and therapy.

Keywords Bioprinting, B16, BRAF, NRAS, Genetically engineered mice, Malignant melanoma, Tumor spheroids, Ultraviolet light, Xenograft transplantation, YUMM, YUMMER, Zebrafish

1 Introduction

Aberrant changes at the molecular and biochemical levels underlie the development of a malignant tumor of melanocytes termed melanoma. The pigment-producing melanocytes of humans are primarily found in the skin, eyes, inner ear, and meninges, so primary malignancies develop at these sites. While basal and squamous cell carcinomas account for most cases of skin cancer, melanoma is responsible for the vast majority of skin cancer-related deaths [1]. The greatest risk factor is excessive exposure to the sun or ultraviolet (UV) light, which initially promotes protective melanin production by melanocytes to prevent cellular damage. Overexposure to UV light can cause mutations of genes associated with cell cycle regulation in melanocytes,

Kristian M. Hargadon (ed.), *Melanoma*, Methods in Molecular Biology, vol. 3089,
https://doi.org/10.1007/978-1-0716-5619-8_1,
© The Author(s), under exclusive license to Springer Science+Business Media, LLC, part of Springer Nature 2027

leading to transformation and cancer development. However, sunlight is not the only risk factor for melanoma; although not as common, inherited gene mutations can also contribute to cases, especially for patients with related diseases such as xeroderma pigmentosum [2]. In this condition, DNA repair systems are inefficient, and sun exposure can trigger damage that is not repaired properly, thereby potentially triggering unregulated cell cycle progression.

Melanoma is the most serious type of skin cancer due to its fast rate of growth and tendency to metastasize throughout the body, resulting in a 5-year survival rate of 5%–19% [3]. The aggressiveness of these tumors is related to the genetic instability or heterogeneity within the tumor mass. Heterogeneity arises in the tumor, given a mutation rate that surpasses all other cancers, fast growth rate, and environmental stresses such as immune reactivity and the differing oxygenation and nutrition availability to cancer cells within the tumor. Such heterogeneity greatly contributes to the lower rate of tumor regression, higher resistance to multiple therapeutics, and decreased survival rate seen in patients [4]. The extensive variety of mutations found in melanoma makes it difficult to determine which particular genetic aberration serves as the driver rather than a passenger mutation. Some of the more common gene mutations associated with melanoma involve pathways of cell cycle progression and differentiation, such as *CDKN2A* (cyclin-dependent kinase N2A), *BRAF* (B-raf proto-oncogene serine/threonine protein kinase), *NRAS* (N-rat sarcoma protein), and *TP53* (tumor protein 53) [5–7]. The *CDKN2A* gene encodes two tumor suppressor proteins by alternate reading frames, $p16^{INK4A}$ and $p14^{ARF}$ ($p19^{ARF}$ in mice). G_1 to S phase cell cycle progression is blocked when retinoblastoma (RB) protein remains unphosphorylated due to the action of $p16^{INK4A}$ that functions to inhibit cyclin D-cyclin-dependent kinase 4/6 from phosphorylating RB [8]. The action of $p14^{ARF}$ is to degrade MDM2 (E3 ubiquitin-protein ligase), which normally operates to promote TP53-mediated cell cycle arrest [9]. In melanoma patients, mutations of the *CDKN2A* gene diminish expression of both $p16^{INK4A}$ and $p14^{ARF}$, thereby leading to cellular progression through G_1 to S because of inactivation of RB and TP53, respectively [10]. RAS-mediated signaling is regulated by GDP-GTP modulation, where bound GTP to RAS recruits and activates RAF. In turn, RAF phosphorylates MEK (mitogen-activated protein kinase kinase), leading to phosphorylation of ERK (extracellular receptor-stimulated kinase) and, in turn, promoting translocation of ERK to the nucleus to mediate transcription factor activation resulting in mitotic stimulation [11]. Activating mutations of *BRAF* and *NRAS* together account for up to 80% of human melanomas [5, 12]. Thus, constitutively active BRAF and NRAS proteins in melanomas drive ERK activation and nuclear localization for a strong proliferation stimulus. Interestingly, *HRAS* and *KRAS* mutations are rare in human melanomas comparatively, but when present, can stimulate

growth. The most common mutation identified in human melanomas is *BRAF*V600E (*BRAF*^{V600E}) [13]. Identification of the genetic association with human melanoma has been exploited in the development of various animal models of melanoma. PTEN (phosphatase and tensin homolog) is a tumor suppressor protein that operates to remove phosphates from phosphatidylinositol (PI)-3,4,5-triphosphate (PIP3) to PI-4,5-biphosphate, thereby preventing the action of PI3K. This action blocks the activation of the serine/threonine kinase AKT or protein kinase B. Active AKT promotes cell growth, cell cycle progression, migration, and survival [14]. Mutant *PTEN* gene permits the unregulated activities of AKT. There are certainly other genetic aberrations associated with melanoma development and progression, but these are the most commonly observed in human melanomas and the focus of model development for the disease.

In addition, the number of melanoma cases has increased annually in the last 20 years [15], with the American Cancer Society predicting 324,000 new cases expected to be diagnosed worldwide in 2026. Given the growing number of cases each year and the high case fatality rate, a number of animal and human model systems continue to be developed to offer insight into the molecular and cellular characteristics of melanomas for the generation and testing of new therapeutics and vaccines. Much progress has been made in understanding the biology and genetics of melanomas using model systems. However, despite decades of research, malignant melanoma remains a common cause of morbidity and mortality in the world with limited treatment success. This review offers a survey of the past and present model systems for the investigation of melanoma epidemiology, pathogenesis, genetics, and pharmaceutical discovery and testing. These models have provided extensive information about the disease and are being modified or used to develop new models of melanoma to create innovative therapeutic approaches for successful tumor regression and possibly prevention.

2 Mouse Models of Melanoma

Although many advances have been made in the treatment of melanoma, patient outcomes remain poor, and the 5-year survival rate for metastatic melanoma patients is at best 19% [3]. For the development of new therapeutics such as ipilimumab and pembrolizumab, which restore some function to anti-melanoma T cells, a clearer picture of melanoma biology and the microenvironment is needed. This can be accomplished through the employment of in vitro and in vivo model systems that simulate the host-tumor interactions and growth characteristics of tumors in human patients. Indeed, model systems must recreate at least aspects of the microenvironment of the tumor, including the cellular constituents, blood network, and extracellular matrix. This is often accomplished by the use of preclinical

models, and the most widely utilized is the murine model. Several murine-based models have been generated, including transplanted (or injected) tumors into syngeneic animals, xenografts, genetically engineered mice, and UV-induced melanomas.

2.1 Transplantation of Murine Melanoma Cell Lines in Syngeneic Mice

Dating back to the mid-20th century, transplantation of murine melanoma cell lines into syngeneic animals is one of the oldest models used to study tumor biology. The most commonly used murine cell line is B16 and its sublines [16, 17]. Melanin-producing B16 melanoma cells (B16-F0) were originally harvested growing spontaneously from the posterior ears of C57Bl/6 mice in the 1950s. Once appropriate inoculation protocols were established in the 1970s, the B16 melanoma model provided a better understanding of tumor growth in vivo and served as a system for testing therapeutics. B16-F1 was established from one cycle of in vivo growth in the subcutaneous space of mice. Subsequently, B16-F0 cells were inoculated into mice, and the B16-F10 line was derived by selection for the capacity to form lung colonies in vivo following intravenous delivery, followed by in vitro culture of harvested cells after ten cycles of lung colonization [16]. Typically, B16-F1 cells are inoculated by subcutaneous injection into the nape of the neck or flank for the establishment of a solid tumor [17]. This tumor subline is minimally metastatic. It is used as a solid tumor model for testing melanoma progression and therapeutic efficacy. B16-F10 melanoma cells are injected intravenously and lodge in the lung to establish colonies at that site, thereby serving as a simulated model of metastasis [17]. A drawback of using this approach for metastatic modeling is that the events pertaining to metastasis are largely bypassed. Another metastatic model of melanoma involves the cell line, B16-4A5, which was harvested from a skin melanoma of C57Bl/6 mice [18]. When these cells are injected intraperitoneally into syngeneic mice, local colonies of the tumor are established in both the spleen and lung within 30 days of inoculation. These approaches are useful for tumor biology studies and drug effectiveness against melanoma at primary and metastatic sites.

To better assess the T and B cell responses to B16 melanoma, B16-F0 cells were transfected with a plasmid encoding full-length ovalbumin (OVA), creating the B16-OVA cell line [19, 20]. B16-F0 is weakly immunogenic, so any significant responses would be due to lymphocyte reactivity towards the liberated OVA peptides expressed by the cancer cells. This model system allows for a clearer understanding of the host-tumor interaction, as OVA-specific T cells can be assessed ex vivo for surface markers and secreted products. To improve OVA-specific T cell recovery, $CD8^+$ and $CD4^+$ T cells specific for OVA, derived from OT-I and OT-II TCR transgenic mice, respectively, can be transferred into the mice before B16-OVA inoculation [21, 22]. Moreover, T cells from OT-I and/or OT-II mice can be transferred into mice

with growing B16-OVA tumors to assess the potential efficacy of adoptive cell therapy [23].

B16 cancer cells also express self-antigens such as tyrosinase and gp100 for targeting T cell responses. However, similar to human melanomas, B16 variants express low levels of major histocompatibility complex I to display the antigens and thus are poorly immunogenic in terms of being recognized by activated $CD8^+$ cytotoxic T lymphocytes [24]. Additionally, B16 melanomas express B7 molecules and programmed cell death (PD-1) ligands for induction of T cell exhaustion through ligation of T cell surface CTLA-4 (cytotoxic T lymphocyte antigen-4) and PD-1, respectively [25]. Efficacy of the clinically approved checkpoint inhibitors, anti-CTLA-4 and anti-PD-1 antagonistic antibodies, in the regression of melanoma was initially tested using transplanted B16 melanoma in mice [26]. A disadvantage of this model system is the rapid growth of the tumors in vivo, which limits the therapeutic window. This rapid proliferation can also impair any long-term investigations of melanoma behavior, given that mice most often die within 3–4 weeks after transplantation with cancer cells. More importantly, B16 cancer cells, like other cultured melanoma lines, are different from their human counterparts in that human melanomas have much greater genomic heterogeneity [4]. B16 cancer cells possess inactivating mutations of *CDKN2A* but exhibit few modifications of the commonly implicated protein in human melanomas, BRAF [27]. Human melanomas are also known to have a deficiency of PTEN protein, while B16 and other melanoma lines express this protein [27]. Despite these genetic discrepancies, B16 variants have been used as a preclinical model for melanoma and have provided valuable information that has aided the design and testing of therapeutics for humans.

2.2 Xenograft Transplantation

To develop more clinically relevant models for human melanoma, xenografts of human cancer cells into immunocompromised mice were first implemented in the late 1960s and early 1970s [28]. In the years after and even today, cultured human cancer cells are injected either subcutaneously or intradermally into nude athymic or severe combined immunodeficient (SCID) mice. Nude athymic mice lack mature T cells, while SCID animals are deficient in both T and B cells [29, 30]. This model is useful for studying melanoma cell interactions with subcutaneous tissues, lymphatics, and blood vessels, with an emphasis on microenvironments, angiogenesis, and metastasis. Many of the subcutaneously delivered human melanoma lines metastasize to other anatomical sites, most often the lungs. Often, these melanoma cells are derived from metastatic sites in the immunocompromised mice after several in vivo passages, indicating that these cells are most likely subpopulations of cancer cells within the tumor population with the propensity to metastasize. A number of human melanoma cell lines are available for use as xenografts, including: A2058 (lymph node), A375 (skin), IGR-1 (lymph node), MEL290 (uvea), SK-MEL

(skin), WM-115 (metastatic skin), and UACC (skin). The relative importance of melanoma xenograft transplantation is that it allows investigations of tumor growth and progression in the presence of test drugs in vivo. An advantage of this system, like that of the B16 transplants, is the control of tumor induction and drug administration. Given that there are no T cells in either mouse, adaptive responses cannot contribute to this process. Thus, the data reflects more of the direct effects of the therapy on the tumor cells rather than what occurs in the context of a patient, where additional contributions by a more complex microenvironment play a role in the treatment outcome. In particular, melanoma-specific helper and cytotoxic T cells, natural killer T cells, and T regulatory cells are absent. These cells all play vital roles in tumor growth and survival. Furthermore, often the experiments are of short duration due to the ulceration and necrosis that occur at the tumor site, especially in animals inoculated with tumors via the intradermal route. For this reason, most xenografts are injected through the subcutaneous route; however, like the B16 model, the tumor that develops is comparable to a skin metastasis rather than the true primary tumor.

More recently, this model has been modified from cultured human cancer cells to freshly isolated tumor cells from patients. This approach is advantageous as the patient-derived xenografts retain their characteristics in the mice, including their histology, transcriptome, DNA polymorphisms, gene expression, and chromosomal architecture [31]. Given that the freshly derived human melanomas preserve the heterogeneity missing in other models, patient-derived xenografts are more appropriate for studying the mechanisms of metastasis and the cytotoxic potential of new drugs, as well as any tumor resistance mechanisms. Some patient-derived melanomas have been transplanted into immunodeficient mice and the animals treated with anti-cancer drugs for 8 weeks or more. Portions of surviving tumor cells are harvested, reimplanted, and again exposed to the same drug. Molecular studies can follow to discern the mechanism of tumor resistance to currently used or experimental therapeutics. Together, these studies have led to the development of clinical trials whereby patient tumors in mice are evaluated for response to therapy just ahead of treatment of the same patient with the same chemotherapy.

While there is much promise in patient-derived xenografts, clinical studies in mice can take a long time, and melanoma colonization may not occur in all of the animals. Additionally, as noted earlier, these host animals are immunodeficient, meaning that only direct effects of the drugs can be ascertained, and assessments of immune modulatory treatments are not possible. The costs of purchasing, care, and breeding of the mice can be high since the facilities must be germ-free and technicians must be highly skilled. Furthermore, since the patient-derived xenograft model is usually established from tumor biopsy fragments, methods of transfection to label or mark the

cells for detection in vivo are inefficient [32]. Finally, the growth rate of the fresh tumor fragments determines the success of the model, in that slow-growing cancer cells tend to be difficult to establish a model for study, whereas fast-growing tumor cells are much easier to develop a usable model [33].

2.3 Genetically Engineered Mice (GEM)

Thus far, the model systems for melanoma have relied upon established tumor lines or freshly isolated patient tumor fragments injected into wild-type and immunocompromised mice. There is no point in these systems where the transformation of normal cells occurs and where host-tumor interactions influence the outcome of melanomagenesis. Instead, the cultured or freshly isolated cancer cells, carrying pre-existing mutations and epigenetic landscapes, are injected into a naïve and unfamiliar environment within the subcutaneous region, intradermal space, or blood circulation. These models are very useful for therapeutic efficacy studies, given that treatments are usually administered to cancer patients with growing tumors, but they do not reflect the natural history of tumor progression that occurs over time in patients. Transgenic and knockout mice (i.e., genetically-engineered mice or GEM) have thus been generated to allow for investigation of the series of genetic and epigenetic changes that occur at the outset of spontaneous tumor formation [34–36]. Also, GEM models overcome issues that arise in cell culture and passage through mice, which can generate subpopulations within the tumor that become resistant to apoptosis. Another advantage of GEM is that tumors develop in an immunocompetent environment, which enables exploration of the initial host-tumor interactions in the tissues in which they would occur in humans. Moreover, cell line- and xenograft-based models have a bit more variability between the animals transplanted, as the populations are often heterogeneous for mutations, whereas GEM tumors possess the same basal mutations in all of the animals in the study. This permits an examination of subsequent signaling pathway alterations associated with tumor formation and the contribution of the immune response to melanoma biology and the drug resistance of the cancer cells as they accumulate further mutations. However, similar to xenograft models, GEM are costly and require skilled technicians for handling and care, as well as germ-free environments to house the animals.

One of the first melanoma GEM models developed was generated with a deletion of the *CDKN2A* gene, thereby eliminating both $p16^{INK4A}$ and $p19^{ARF}$ proteins to alleviate cell cycle regulation. In addition, the *HRAS* gene is overexpressed under the control of the promoter for the melanocyte differentiation and pigmentation pathway gene encoding tyrosinase, leading to a strong induction of mitosis. Together, this model is designated as the *HRAS CDKN2A*$^{-/-}$ mouse model [37]. In order to minimize the development of nonmelanoma tumors, melanocyte-specific promoters such as paired box 3 (*PAX3*), dopachrome tautomerase (*DCT*),

microphthalmia-associated transcription factor (*MITF*), and tyrosinase (*TYR*) are used to promote expression of oncogenes like *HRAS* [38–41]. *HRAS* activation drives proliferation through the MAPK pathway, which in human melanomas is often due to *NRAS* or *BRAF* mutations. Despite the use of melanocyte-specific promoters, one disadvantage of this model is that melanomas are still accompanied by the generation of B cell lymphomas and soft tissue sarcomas, and the melanomas that do form remain primary tumors without metastasis. However, the melanomas develop before the other tumors form in most of the animals examined. The *BRAF* mutation V600E ($BRAF^{V600E}$) is notable in human melanomas, and the GEM developed with this mutation produced spontaneous tumors, though only after long periods, necessitating the crossing of additional mutations into these animals to promote earlier melanomagenesis [42]. GEM have been developed to harbor a heterozygous germline $BRAF^{V600E}$ mutation, which is only expressed upon induction of Cre recombinase (Cre) in melanocytes, a model termed the $BRAF^{CA}$ mouse model [43]. Cre is expressed upon topical treatment of $BRAF^{CA}$ mice with 4-hydroxytamoxifen (4-HT) to facilitate recombination of conditional alleles ($BRAF^{V600E}$), and the animals develop hyperpigmented lesions at the application site within 3–4 weeks. This model allows for temporal and spatial control of target gene expression. However, melanocyte-specific expression of the $BRAF^{V600E}$ mutation alone did not produce spontaneous melanoma formation. Homozygous expression of $BRAF^{CA}$ generated highly pigmented hyperplasias upon topical 4-HT (at the application site and others), suggesting a dosage effect of $BRAF^{V600E}$ expression upon melanocyte proliferation. Given the association of *PTEN* deficiency and human melanoma, alleles of the *PTEN* gene were flanked with loxP sequences such that Cre expression would delete contributions by this gene in melanocytes upon 4-HT application. Within ten days after 4-HT, highly pigmented neoplasias develop that progress to malignant melanomas that metastasize. The $BRAF^{CA}$ $PTEN^{lox/lox}$ mice permit studies of the mechanisms of melanoma metastasis and application of therapeutics aimed at suppressing this process [43].

Most melanoma lines discussed above did not have defined mutations correlating with human melanomas, so that consistency among in vitro cultures and animals recipient of tumor transplants remained stringent. To address these issues, cell lines were developed from C57Bl/6 backcrossed GEM expressing melanocyte-specific driver mutations involving *BRAF* activation ($BRAF^{CA}$) as well as *PTEN* and *CDKN2A*. About 1–6 months after application of the 4-HT to the GEM-C57Bl/6 congenic mice, melanomas formed and were excised upon reaching 100 mm^3 in diameter. These melanomas were subsequently cultured to liberate cell lines termed Yale University Mouse Melanoma (YUMM) lines [44]. Different genetic aberrations have been incorporated into the GEM from which the lines were derived, and two numbers are applied for a particular

genotype to differentiate among the >37 congenic lines generated to date. For instance, YUMM1 lines are categorized by the gene profile *BRAF*^{V600E} *PTEN*$^{-/-}$ *CDKN2A*$^{-/-}$, while YUMM4 lines are deficient in expression of both *PTEN* and *CDKN2A*. Given YUMM lines are derived from C57Bl/6 mice, transplant into these immunocompetent animals permits an examination of the processes of tumor growth in the presence of unaltered immunity. That is, the mutations driving tumor growth are restricted to the cancer cells themselves and not expressed by all murine cells, as is the case for many GEM animals. YUMM lines are also advantageous to other melanoma lines, such as B16, which do not have the same genotype as most human melanoma cells. However, the transplantation of the YUMM lines again localizes them within the subcutaneous space rather than the native site of melanomas.

Given the involvement of ultraviolet radiation in melanogenesis, irradiation of the YUMM1.7 cell line yielded the YUMMER1.7 line (YUMM Exposed to Radiation), which, when transplanted into C57Bl/6 mice, gives rise to tumors that regress within 1–2 weeks, indicating an increased immunogenicity [45]. Interestingly, when high numbers of the YUMMER1.7 cells are injected, the resulting tumor escapes immune-mediated cytotoxicity and grows out. This model provides a platform to study immunotherapeutic agent impacts on the antimelanoma response.

Together, these different GEM have permitted an examination of the molecular events critical to melanomagenesis, establishing those that are driver mutations and revealing others that serve as bystander mutations. Furthermore, these model systems are developed in immunocompetent mice, which permit investigations of the interactions of host immunity and proliferating cancer cells.

2.4 Carcinogen- and UV-Induced Melanoma

Spontaneous melanoma models involving the transformation of melanocytes through exposure to UV light are the most relevant for studying melanoma development in humans, given the link between sun exposure and melanoma incidence [46]. However, the distribution of melanocytes in rodents differs from humans in that melanocytes in mice are localized to the hair follicles rather than the epidermis and epidermal-dermal junction of the skin [31, 47]. Accordingly, the hair follicle residence of melanocytes diminishes the invasiveness of developing melanomas, characteristic in human cases, into the skin in mouse models. One approach to circumvent this is to develop systems where melanocyte localization can be redirected to the epidermis. Induction of stem cell factor in keratinocytes of mouse skin has been shown to promote melanocyte localization to the epidermis [48]. An important murine melanoma model where melanocytes are localized to the epidermis is the *HGF/SF* (hepatocyte growth factor/scatter factor) transgenic mouse expressing the HGF receptor (or *MET* gene) under the control of the metallothionein (*MT-1*) promoter [49]. First identified as a protein tyrosine kinase

receptor in immature hematopoietic progenitor cells (HPC), the HGF receptor is triggered by bone marrow stromal cell ligands and promotes the proliferation, adhesion, and survival of HPC [50]. Ligation of the HGF receptor leads to MAPK and PI3K pathway signaling, and in the *HGF/SF* transgenic mouse, these pathways are then constitutively active. Interestingly, low-dose single exposure of neonatal (day 3.5) *HGF/SF* transgenic animals to UV radiation induces the formation of melanoma within 25 weeks in up to 30% of the mice exposed [51]. An increase in the percentage of animals developing melanoma is possible through the use of UVB radiation, with 56% of treated mice expressing melanoma at an average of 18 weeks of age after exposure [52]. Crossing the *HGF/SF* transgenic mice with $P16^{INK4A}/P19^{ARF-/-}$ mice was done to create the *HGF/SF* $P16^{INK4A}/P19^{ARF-/-}$ model in which UV-induced melanoma develops in 75% of the mice treated by 7 weeks of age [53].

While UV radiation-mediated melanomagenesis is the most relevant clinical model of spontaneous human melanoma, carcinogens have also been used to drive mutations for melanocyte transformation, albeit these chemicals are often used together with UV radiation. Transgenic overexpression of *HGF* has been coupled with the CDK4 mutation R24C (*HGF* $CDK4^{R24C}$) to generate a model inducible by the carcinogen, 7,12-dimethylbenz(a)anthracene (DMBA) in addition to repeated exposures to UV radiation [54]. Primary cutaneous melanomas form and spread to the lungs and lymph nodes. The DMBA-induced tumors can be harvested and transplanted into C57Bl/6 mice and used as a metastatic lung model.

Another model utilizes gene overexpression of an *HRAS* gene with the mutation given as G12V [55]. $HRAS^{G12V}$ is under the control of the tyrosinase promoter, which produces hyperpigmentation and hyperproliferation of melanocytes. However, this overexpressed mutant *RAS* does not generate spontaneous melanomas. Only when DMBA is applied will mice develop metastatic melanoma at 45 weeks in 80%–100% of mice treated [56]. In this same model, 12-*O*-tetradecanoylphorbol-13-acetate (TPA) or UVB radiation can also be used to generate melanomas with a penetrance of up to 40% and 57%, respectively.

Additionally, repeated UV irradiation of *RFP-RET* transgenic mice resulted in the development of cutaneous melanoma, and some of the animals also demonstrated metastases in the lungs [57]. The *RET* gene codes for a receptor tyrosine kinase proto-oncogene, which is placed under the control of the *MT-1* promoter in this transgenic model, and this model results in a slow course of metastatic melanoma without UV radiation. Following exposure to UV light, the *RET* gene is activated and underlies the rapid growth and metastasis of tumors by 7 weeks compared to 12 months without irradiation.

Inclusion of carcinogen- and UV radiation-mediated extensions of GEM have created model systems better able to serve as a preclinical system for human melanoma, especially those like *HGF/SF*

transgenic mice, where the melanocytes are localized to the epidermis and epidermis-dermis junction.

2.5 Humanized Murine Xenografts

A recent adaptation of the xenograft transplantation that has been developed involves the injection of human melanomas into immunodeficient mice that possess a human host response. The selection of the model depends upon the target of the investigation. NOD/SCID/γc (NSG) mice possess severe combined immunodeficiency and interleukin-2 receptor γc mutations, producing animals lacking B, T, and natural killer (NK) cells [58]. Subsequently, NSG mice are irradiated and then engrafted with human hematopoietic stem cells (HSC) or peripheral blood mononuclear cells (PBMC) [59, 60]. These humanized NSG mice can be injected with human melanoma cell lines or patient-derived xenografts (PDX). This system permits studies of therapeutics such as immune checkpoint inhibitors as well as investigations of the composition and action of the tumor microenvironment. Another model is NSG-SGM3 mice, where NSG animals are transgenic for stem cell factor (S), granulocyte-macrophage colony-stimulating factor (GMCSF), and interleukin-3 (IL-3). Inclusion of the cytokines improves engraftment of HSC and PBMC and especially enhances myeloid cell development [61]. MISTRG mice include knock-in expression of macrophage-colony stimulating factor (M-CSF), GM-CSF, IL-3, and thrombopoietin on a Rag2$^{-/-}$ IL-2Rγ$^{-/-}$ murine background. Populations of human monocytes, macrophages, and dendritic cells develop in the HSC-engrafted MISTRG mice. This model suggested that metastasis of human melanoma cell lines requires the action of macrophages, as a modified version of MISTRG mice lacking M-CSF did not support metastasis [59]. A major limitation to using humanized mice for xenograft studies is the potential development of graft-versus-host-disease (GVHD), due to the action of the engrafted human T cells attacking murine tissues, which can shorten the lifespan of the mice [62]. This complication has been reduced by transplantation with a matched patient tumor. Tumor growth is slower, and GVHD is reduced when compared to mismatched mice [63, 64].

3 Other Animal Models of Melanoma

Because of the cellular and physiological similarity with humans, extensive information about genetics, cost-effectiveness of care, and availability of reagents, mice are commonly used in melanoma research. However, it was recently reported that preclinical murine model translation into successful human treatments is about 8%, strongly suggesting that better model systems are needed [65]. Given melanoma has also been known to spontaneously develop in animals such as dogs, horses, and swine, these animals offer potentially informative models for studying human melanoma.

3.1 Dog Model

Domesticated animals such as dogs, cats, horses, and swine are known to develop spontaneous cases of melanoma; however, it is more common in dogs. Most cases of melanoma in dogs have been shown to develop in the oral mucosa with frequent metastases to the lungs and lymph nodes (up to 50%), as often occurs in humans [66]. Dogs may serve as a better model than mice in that canine DNA and proteins are more similar to humans than mice. This dog-human homology has eased the cost of reagents since many of the antibodies targeting human proteins also cross-react to bind well to dog antigens. However, oral mucosal melanoma of dogs differs from human and some mouse model melanomas in that melanomas in dogs are not strongly associated with UV radiation [67]. In fact, the etiology of canine melanomas is not known, but UV light is not an important factor. Indeed, the skin of dogs is covered by fur, which provides natural protection from UV light. Interestingly, melanomas are more prone to develop in dogs with dark coats, such as Scottish terriers, golden retrievers, dachshunds, and cocker spaniels [66]. Additionally, those melanomas that do appear in the skin originate from the dermis rather than the epidermis, despite the presence of melanocytes in both layers. Thus, dog melanomas resemble non-UV-induced melanomas of humans, with oral melanomas being the most similar. When evaluating the genetics of dog melanoma cells, *BRAF*^{V600E}, *NRAS*, and *PTEN* mutations are similar to those in humans [68, 69].

The first line of treatment of solid melanomas is surgical excision in dogs, as it is in humans [70]. Radiation can reduce tumor recurrence after surgical removal. Immune checkpoint inhibitors have become an important target for the treatment of advanced human metastatic cancers, including melanoma [71]. The inhibitory receptors on anti-tumor T cells, PD-1 (programmed death-1 receptor) and CTLA-4 (cytotoxic T lymphocyte antigen-4), have been shown to be overexpressed on T cells derived from dogs bearing cancers [72]. Accordingly, the ligand for PD-1 (i.e., PD-L1) has been shown to be expressed in oral melanomas derived from dogs. A blocking antibody for PD-L1 demonstrated efficacy against the oral melanoma [73]. Thus, dog oral mucosal melanoma models are useful for preclinical or co-clinical trials of cancer therapeutics and can be particularly informative given the shorter lifespan of a dog and the more rapid progression of tumors in the animals. Indeed, dogs currently serve as a model system for melanoma phase I safety clinical trials [74] and likely may offer a model to study novel drug efficacy against human melanomas.

3.2 Horse Model

Like dogs, melanomas are common in horses, though they develop as histopathologically similar lesions of two types: dermal melanomas and dermal melanomatosis. Some 80% of gray horses (>15 years of age) will develop melanomas in the chambers of the ear, salivary glands, lymph nodes, and neck region. However, not all are malignant, as some remain benign. Transformations of benign melanomas

are more common in non-gray horses, where both organ and lymphatic metastases are capable of developing [75]. Similar to dogs, UV radiation does not seem to be associated with horse melanomas, but there is a strong demonstration of constitutive activation of the MAPK pathway [76]. Cell lines derived from primary and metastatic horse melanomas serve as model systems for human studies, as they too can be transplanted as xenografts in immunocompromised mice.

3.3 Swine Model

Spontaneous melanoma development is not as common in pigs as it is in dogs and horses. However, three pig models that develop melanoma lesions have arisen through breeding, and these animals include the Sinclair miniature swine, Munich miniature swine Troll, and the Libechov minipig [77]. Black offspring of the Sinclair miniature swine develop superficial and disseminated melanoma (lungs, liver, and lymph nodes) during the first month after birth in up to 60% of piglets [78]. However, all or nearly all of the affected pigs will regress the melanomas, as T cells infiltrate the tumors by the fourth month of life. Thus, this model is a good system for assessing events associated with spontaneous regression and how that might be accentuated. The Munich miniature swine Troll, developed in Munich, Germany, was generated by breeding from founder animals possessing spontaneous melanomas [79]. Tumors are present at birth or develop within the first 2 months of life. As with the Sinclair, spontaneous regression occurs on a large scale along with skin depigmentation. Originally bred for blood group antigen studies in the 1960s, the melanoma-bearing Libechov minipigs were developed from crossbreeding Minnesota miniature pigs with several commercial breeds to create the first black piglets of the line with cutaneous lesions. Selective breeding increased melanoma incidence to 50%. The newly established line of melanoma pigs was termed melanoma-bearing Libechov minipig (MeLiM) [80]. This breed is mostly black pigmented, but there are varieties of colors, with the most frequent alternative being rusty-red, brown, or white. The black piglets of the MeLiM animals demonstrate the highest frequency of melanoma. Similar to the two previous swine models, MeLiM animals are born with melanomas or develop the lesions within the first 2 months of life. These animals also develop metastases to areas like the stomach, lung, liver, intestines, pancreas, kidneys, heart, lymph nodes, and thymus. Up to 30% of the MeLiM animals maintain tumor progression, while others in the population undergo spontaneous regression. Animals with progressive tumors often die within the first 3 months of life due to lung metastases. All three models permit the monitoring of spontaneous regression and the assessment of the involvement of immune function in these processes, making them applicable for studying human therapy for highly resistant melanomas. However, only MeLiM animals have a portion of the population that has cancer progression and death due to metastasis. Studies in these animals could help in the understanding of mechanisms of cancer progression

and metastasis-mediated death of patients and ultimately support the development of therapeutics. Furthermore, given their long lifespan of up to 18 years, these animals permit long-term studies, and the size of the animals allows for repeated tissue and blood sampling during the process of regression and/or tumor progression. Most important is the resemblance and distribution of pig melanocytes to human melanocytes.

3.4 Zebrafish Model

A recent addition to cancer models is the zebrafish, a small tropical fish, due to its 70% genetic similarity with humans, suitability for tumor induction (chemical means, genetic deletion, gene overexpression, xenotransplantation), and adaptation for different cancers (skin, pancreatic, breast, leukemia, glioma, lung, and melanoma) [81]. Additional advantages of using zebrafish are low costs of use, the rapid development of embryos (major organs developed by 5 days post-fertilization), a large number of offspring, 3–5 month lifespan and generation time, ease of drug testing for efficacy and toxicity (delivery of therapeutics into water), and optical transparency for superior in vivo imaging studies. In particular, zebrafish share similarities with humans in terms of the immune response, allowing for translatable pharmacologic studies [82]. As indicated above, human cancer cells can also be transplanted into zebrafish to establish xenograft models to study cancer growth, angiogenesis, metastasis, and drug responses. This is possible because the immune system of the zebrafish is only functional at ≥28 days of development. Thus, upon xenograft transplantation, the development of a tumor at the early stages can be followed visually. In addition to xenograft models using zebrafish, genetically engineered zebrafish similar to GEM have been developed to study melanoma.

3.4.1 Genetically Engineered Zebrafish (GEZ)

Genetically engineered zebrafish have been developed in the last 15 years. One of the first involves $BRAF^{V600E}$ under control of the melanocyte-specific promoter *mitfa* [83]. These animals develop spontaneous melanomas, and when crossed on a *P53*-deficient background, melanomas form at an increased rate in these fish. Subsequently, mutant *NRAS* expression was driven by the *mitfa* promoter in $NRAS^{Q61K}$ transgenic zebrafish [84]. The $HRAS^{G12V}$ mutant under the melanocyte-specific promoter *kita* gives rise to hyperpigmentation within 3-day-old embryos and melanomas by 1 month of age [85]. Tumors derived from this transgenic zebrafish are transplantable. These models are very useful in the examination of early events during the development of melanoma.

3.4.2 Xenograft Transplantation in Zebrafish

Human melanoma cell lines have been transplanted into zebrafish embryos, most often the yolk sac, allowing for the study of tumor establishment, angiogenesis, and metastasis [86]. Given that the zebrafish embryos are transparent, the cell lines can be fluorescently labeled before transplant to visualize their interaction with endothelia

and the process of metastasis [87]. An advantage of this system is the large number of embryos that can easily be obtained to provide adequate statistical power, and the ability to inject cell lines within 48 h of fertilization allows for routine experimental setup in the laboratory. Since the embryos are transparent, black-pigmented melanomas can easily be seen in the zebrafish. Again, the immune system of zebrafish is not established until 1 month of age, so the processes are assessed in the absence of a host response [88]. Transplants of cell lines into adult zebrafish must be performed after irradiation or treatment with dexamethasone of the zebrafish to avoid immune rejection of the xenografts. One disadvantage of using zebrafish for xenotransplantation is that the optimal growth of the zebrafish occurs at 28°C rather than 37°C for human cells, meaning that the impact of temperature on tumor growth and development must be considered during data analysis. Typically, transplanted embryos are incubated at a higher temperature, given that the cells are more sensitive to the temperature differential. However, xenograft transplantation of human melanoma cells into zebrafish has been informative in terms of the early events of tumor formation. Indeed, a vascular endothelial growth factor 2 inhibitor was shown to inhibit the growth and vascularization of a xenograft [89]. One of the advantages of the zebrafish is that the whole animal is treated since the drugs are added directly to the water. For instance, uveal melanoma cell lines, primary and metastatic, were transplanted into embryos and treated with anti-cancer drugs [90]. In these animals, a drug that blocked the anti-apoptotic factor BCL mediated decreased growth of melanoma of the primary human cancer line. This same study also demonstrated that treatment with a cell cycle blocking agent and pro-apoptotic factor suppressed the growth of both primary and metastatic cell lines in the zebrafish.

Thus, the zebrafish models of melanoma hold great promise for more translatable studies given the genetic similarity with humans, ease and low cost of care, statistical power in greater numbers of embryos, a short period of development, and growing interests in the generation of reagents for research.

4 Tissue-Engineered 3D Models of Melanoma

Two-dimensional (2D) cell cultures involve the growth of cancer cells in a monolayer on the surface of a plastic culture plate or flask. This method ensures optimal nutrition and oxygen for the cells, and drugs can be easily applied for testing. Moreover, 2D culture is the preferred method for culturing human melanoma cell lines before injection into live animals. The cultured melanoma cells can be assessed for gene and protein expression, cytotoxicity, and migration/adhesion properties in response to reagents or drugs. However, 2D cultures do not account for the oxygen and nutrient gradients observed within in vivo tumor settings. A more accurate representation of the in vivo

environment is the use of 3D culture systems [91]. Tumor spheroids can be generated by implanting melanoma cells into a gel matrix such as collagen prior to growing the cells in culture [92]. Given that the matrix permits 3D growth, this culture approach simulates tumor heterogeneity so commonly observed in melanomas resected from patients [93]. The levels of nutrition and oxygenation impact gene expression as cancer cells in the center of a 3D spheroid are likely not actively replicating in comparison to the proliferating cells at the tumor periphery. Thus, drugs targeting certain proliferative pathways may be effective against 2D growing monolayer cancer cells but have low to moderate impact upon cancer cells of a 3D tumor spheroid [94]. This phenomenon has been demonstrated for MAPK inhibitors [95]. What is interesting is that 3D spheroid models maintain the growth characteristics of different tumor types, including such behaviors as invasion, and they are likely more representative of the true response of a tumor to drugs in vivo. Indeed, BRAF inhibitors have been shown to translate from inhibition of 3D melanoma spheroid growth to successful inhibition of melanoma progression in clinical trials [96]. The gel matrix of the spheroids can also be altered to drive adherence-dependent cell signaling in the melanoma cells that impacts migration for studies on environmental influences upon melanoma growth, invasiveness, and metastasis [97]. Additional cell types can be co-cultured with tumor spheroids to determine how microenvironment constituents influence the growth of a particular tumor. This system was used in much of the work identifying the presence of cancer-associated fibroblasts [98].

A more advanced model for in vitro preclinical melanoma studies has been the creation of skin reconstructs [99]. These are generated by seeding culture systems with keratinocytes, melanocytes, and fibroblasts, all embedded in collagen. These collaborations operate to produce a basement membrane, extracellular matrix, and cellular composition similar to that found in human skin [100]. The introduced melanoma cells in this culture system retain the characteristics of the tumor itself in terms of growth, spread, invasiveness, metastasis, and drug resistance/susceptibility. An example of this type of system is the melanoma spheroid-loaded 3D skin model involving the use of the human melanoma cell line WM 1617 to generate melanoma spheroids, which were integrated into dermal equivalents [101]. The dermal equivalents are generated by fibroblasts that are added to a collagen-containing media which undergoes contraction, producing a high-density collagen matrix or artificial skin. The melanoma metastatic cell line WM 1617 spheroids are generated by the hanging drop method, involving the placement of a small drop of cells on a culture dish lid, which is then inverted over a reservoir of media, producing an aggregate of cancer cells as gravity pulls them to the bottom of the droplet. This approach provides a skin model that mimics melanoma progression in vivo. Another interesting find using this model is the ability to employ photodynamic therapy to selectively kill the

melanoma spheroid cells. While current therapies involve the use of alkylating agents as well as kinase and immune checkpoint inhibitors, photodynamic therapy has also been an effective approach to the treatment of various cancers, including melanoma [102, 103]. Monico et al. demonstrated that photodynamic therapy using visible red light led to the selective killing of melanoma cells while preserving healthy tissues [97]. Therefore, this system is useful for studying the inhibitory effects and specificity of anti-melanoma drugs in targeting abnormal vs normal melanocytes. At the same time, while the skin reconstruction is informative, they are costly to maintain and require a high level of technical skill as well as continuous care.

Bioprinting represents a new extension of the 3D model used for melanoma [104–106]. This process involves using a digital design of a structure, such as the skin and the precise laying of cells, thereby replicating the tissue of interest. Printing techniques vary from cell-laden hydrogels to droplets of bio-ink containing cells to laser pulsing to place bio-ink onto a substrate. This new approach offers investigators a recreation of tissue-specific environments that more accurately represent the setting for a tumor. This allows for the complexity of the tumor microenvironment in an in vitro setting. Indeed, in vitro skin models have been generated by incorporating fibroblasts, keratinocytes, melanocytes, endothelial cells, and adipocytes [107]. Recently, a bio-ink-generated three-layered construct has been prepared using melanoma cancer stem cells (from both the patient-derived cell line Mel-1 and the established cell line A375), keratinocytes, human umbilical vein endothelial cells, fibroblasts, collagen type I, and mesenchymal stem cells [108]. Cell metabolism, formation of extracellular matrix, detection of communicating extracellular vesicles, and early onset vascularization are present, demonstrating viability with adequate nutrient diffusion. Hydrogel degradation indicated that the cancer cells are remodeling the matrix to establish a tumor microenvironment. A375 hydrogels demonstrated resistance to the chemotherapeutic vemurafenib, which is normally effective against the BRAF-mutant cancer cells. Mel-1 hydrogel is non-responsive to any dose of vemurafenib used in the study. Given that both cancer cell lines possess the same mutation $BRAF^{V600E}$, the differential response may be due to differences in the characteristics of each tumor generated by the lines. Indeed, Mel-1 overexpresses ABC transporters in the hydrogel when compared to the A375 cells. Additionally, the tumor hydrogels were subcutaneously transplanted in NSG mice and demonstrated slower growth compared to injected melanoma lines, angiogenesis, and a structure consistent with a tumor microenvironment. Therefore, bioprinting has provided a tool to simulate skin structure and the tumor microenvironment in a way that may offer a model system to study therapeutics that not only target cancer cells in a more in vivo-like setting, but that also may interrupt the tumor microenvironment.

5 Conclusion

In the end, the object of developing a model system for disease is to provide a platform for discerning information about the growth and characteristics of a set of cancer cells and their responses to therapeutics before inclusion in the treatment of patients. Most likely, the best model for melanoma in the testing of therapeutics or vaccines is a combination of the models discussed above and the new approaches to follow this review. Certainly, 2D and 3D culture systems provide insight and strong indicators of drug responses, but in vivo testing using syngeneic cell line transplants or xenografts is an important measure of drug efficacy where melanomas are growing in the natural surroundings of the tumor microenvironment. The invention of genetically engineered animal models has permitted the assessment of tumor growth and drug responses of spontaneously developing or environmentally/chemically induced melanomas. The additional models to follow this review should advance our knowledge and understanding of melanoma dynamics in vivo and aid in the design and generation of the next phase of therapeutics and vaccines for melanoma treatment.

Competing Interests

The authors have no conflicts of interest to declare.

References

1. Preventive Service Task Force US, Grossman DC, Curry SJ et al (2018) Behavioral counseling to prevent skin cancer: US preventive services task force recommendation statement. JAMA 319(11):1134–1142
2. Paszkowska-Szczur K, Scott RJ, Serrano-Fernandez P et al (2013) Xeroderma pigmentosum genes and melanoma risk. Int J Cancer 133(5):1094–1100
3. Sandru A, Voinea S, Panaitescu E, Blidaru A (2014) Survival rates of patients with metastatic malignant melanoma. J Med Life 7(4):572–576
4. Grzywa TM, Paskal W, Wlodarski PK (2017) Intratumor and intertumor heterogeneity in melanoma. Transl Oncol 10(6):956–975
5. Leonardi GC, Falzone L, Salemi R et al (2018) Cutaneous melanoma: from pathogenesis to therapy (review). Int J Oncol 52(4):1071–1080
6. Rossi A, Roberto M, Panebianco M et al (2019) Drug resistance of BRAF-mutant melanoma: review of up-to-date mechanisms of action and promising targeted agents. Eur J Pharmacol 862:172621
7. Amann VC, Ramelyte E, Thurneysen S et al (2017) Developments in targeted therapy in melanoma. Eur J Surg Oncol 43(3):581–593
8. Serra S, Chetty R (2018) p16. J Clin Pathol 71(10):853–858
9. Wu C-E, Koay TS, Esfandiari A et al (2018) ATM dependent DUSP6 modulation of p53 involved in synergistic targeting of MAPK and p53 pathways with trametinib and MDM2 inhibitors in cutaneous melanoma. Cancers 11(1):3
10. Nelson AA, Tsao H (2009) Melanoma and genetics. Clin Dermatol 27(1):46–52
11. Yajima I, Kumasaka MY, Thang ND et al (2012) RAS/RAF/MEK/ERK and PI3K/PTEN/AKT signaling in malignant melanoma progression and therapy. Dermatol Res Pract 2012:354191
12. Erlich TH, Fisher DE (2018) Pathways in melanoma development. G Ital Dermatol Venereol 153(1):68–76

13. Ascierto PA, Kirkwood JM, Grob J-J et al (2012) The role of BRAF V600 mutation in melanoma. J Transl Med 10:85
14. Schadendorf D, Fisher DE, Garbe C et al (2015) Melanoma. Nat Rev Dis Primers 1:15003
15. Rastrelli M, Tropea S, Rossi CR, Alaibac M (2014) Melanoma: epidemiology, risk factors, pathogenesis, diagnosis and classification. In Vivo 28(6):1005–1011
16. Giavazzi R, Decio A (2014) Syngeneic murine metastasis models: B16 melanoma. Methods Mol Biol 1070:131–140
17. Overwijk WW, Restifo NP (2001) B16 as a mouse model for human melanoma. Curr Protoc Immunol Chapter 20(Unit 20):1
18. Danciu C, Falamas A, Dehelean C et al (2013) A characterization of four B16 murine melanoma cell sublines molecular fingerprint and proliferation behavior. Cancer Cell Int 13:75
19. Brown DM, Fisher TL, Wei C et al (2001) Tumours can act as adjuvants for humoral immunity. Immunology 102(4):486–497
20. Dobrzanski MJ, Reome JB, Dutton RW (1999) Therapeutic effects of tumor-reactive type 1 and type 2 CD8+ T cell subpopulations in established pulmonary metastases. J Immunol 162(11):6671–6680
21. Clarke SR, Barnden M, Kurts C et al (2000) Characterization of the ovalbumin-specific TCR transgenic line OT-I: MHC elements for positive and negative selection. Immunol Cell Biol 78(2):110–117
22. Robertson JM, Jensen PE, Evavold BD (2000) DO11.10 and OT-II T cells recognize a C-terminal ovalbumin 323-339 epitope. J Immunol 164(9):4706–4712
23. Ménager J, Gorin J-B, Maurel C et al (2015) Combining alpha-radioimmunotherapy and adoptive T cell therapy to potentiate tumor destruction. PLoS One 10(6):e0130249
24. Ouyang GF, Saio M, Suwa T et al (2006) Interleukin-2 augmented activation of tumor associated macrophage plays the main role in MHC class I in vivo induction in tumor cells that are MHC negative in vitro. Int J Oncol 28(5):1201–1208
25. Newton JM, Hanoteau A, Liu H-C et al (2019) Immune microenvironment modulation unmasks therapeutic benefit of radiotherapy and checkpoint inhibition. J Immunother Cancer 7(1):216
26. Zhang Y, Fang C, Wang RE et al (2019) A tumor-targeted immune checkpoint blocker. Proc Natl Acad Sci U S A 116(32):15889–15894
27. Melnikova VO, Bolshakov SV, Walker C et al (2004) Genomic alterations in spontaneous and carcinogen-induced murine melanoma cell lines. Oncogene 23(13):2347–2356
28. Giovanella BC, Yim SO, Stehlin JS, Williams JrLJ (1972) Development of invasive tumors in the "nude" mouse after injection of cultured human melanoma cells. J Natl Cancer Inst 48(5):1531–1533
29. Flanagan SP (1966) "Nude", a new hairless gene with pleiotropic effects in the mouse. Genet Res 8(3):295–309
30. Manning J, Pellegrini M, Davidson N (1977) A method for gene enrichment based on the avidin-biotin interaction. Application to the Drosophila ribosomal RNA genes. Biochemistry 16(7):1364–1370
31. Becker JC, Houben R, Schrama D et al (2010) Mouse models for melanoma: a personal perspective. Exp Dermatol 19(2):157–164
32. Ilie M, Nunes M, Blot L et al (2015) Setting up a wide panel of patient-derived tumor xenografts of non-small cell lung cancer by improving the preanalytical steps. Cancer Med 4(2):201–211
33. Xiao M, Rebecca VW, Herlyn M (2019) A melanoma patient-derived xenograft model. J Vis Exp May 20(147): 1–13.
34. Adams JM, Cory S (1991) Transgenic models of tumor development. Science 254(5035): 1161–1167
35. Frese KK, Tuveson DA (2007) Maximizing mouse cancer models. Nat Rev Cancer 7(9):645–658
36. Pérez-Guijarro E, Day C-P, Merlino G, Zaidi MR (2017) Genetically engineered mouse models of melanoma. Cancer 123(S11):2089–2103
37. Chin L, Pomerantz J, Polsky D et al (1997) Cooperative effects of INK4a and ras in melanoma susceptibility in vivo. Genes Dev 11(21):2822–2834
38. Galibert MD, Yavuzer U, Dexter TJ, Goding CR (1999) Pax3 and regulation of the melanocyte-specific tyrosinase-related protein-1 promoter. J Biol Chem 274(38):26894–26900
39. Ludwig A, Rehberg S, Wegner M (2004) Melanocyte-specific expression of dopachrome tautomerase is dependent on synergistic gene activation by the Sox10 and Mitf transcription factors. FEBS Lett 556(1–3):236–244
40. Yasumoto K, Yokoyama K, Shibata K (1994) Microphthalmia-associated transcription factor as a regulator for melanocyte-specific transcription of the human tyrosinase gene. Mol Cell Biol 14(12):8058–8070
41. Bentley NJ, Eisen T, Goding CR (1994) Melanocyte-specific expression of the human tyrosinase promoter: activation by the microphthalmia gene product and role of the initiator. Mol Cell Biol 14(12):7996–8006
42. Dhomen N, Reis-Filho JS, da Rocha Dias S et al (2009) Oncogenic Braf induces

melanocyte senescence and melanoma in mice. Cancer Cell 15(4):294–303
43. Dankort D, Curley DP, Cartlidge RA et al (2009) Braf(V600E) cooperates with Pten loss to induce metastatic melanoma. Nat Genet 41(5):544–552
44. Meeth K, Wang JX, Micevic G et al (2016) The YUMM lines: a series of congenic mouse melanoma cell lines with defined genetic alterations. Pigment Cell Melanoma Res 29(5):590–597
45. Wang J, Perry CJ, Meeth K et al (2017) UV-induced somatic mutations elicit a functional T cell response in the YUMMER1.7 mouse melanoma model. Pigment Cell Melanoma Res 30(4):428–435
46. Zaidi MR, Day CP, Merlino G (2008) From UVs to metastases: modeling melanoma initiation and progression in the mouse. J Investig Dermatol 128(10):2381–2391
47. Ha L, Noonan FP, De Fabo EC, Merlino G (2005) Animal models of melanoma. J Investig Dermatol Symp Proc 10(2):86–88
48. Vanover JC, Spry ML, Hamilton L et al (2009) Stem cell factor rescues tyrosinase expression and pigmentation in discreet anatomic locations in albino mice. Pigment Cell Melanoma Res 22(6):827–838
49. Takayama H, LaRochelle WJ, Sharp R et al (1997) Diverse tumorigenesis associated with aberrant development in mice overexpressing hepatocyte growth factor/scatter factor. Proc Natl Acad Sci U S A 942):701–706
50. Weimar IS, Miranda N, Muller EJ et al (1998) Hepatocyte growth factor/scatter factor (HGF/SF) is produced by human bone marrow stromal cells and promotes proliferation, adhesion and survival of human hematopoietic progenitor cells (CD34+). Exp Hematol 26(9):885–894
51. Noonan FP, Recio JA, Takayama H et al (2001) Neonatal sunburn and melanoma in mice. Nature 413(6853):271–272
52. De Fabo EC, Noonan FP, Fears T, Merlino G (2004) Ultraviolet B but not ultraviolet A radiation initiates melanoma. Cancer Res 64(18):6372–6376
53. Recio JA, Noonan FP, Takayama H et al (2002) Ink4a/arf deficiency promotes ultraviolet radiation-induced melanomagenesis. Cancer Res 62(22):6724–6730
54. Tormo D, Ferrer A, Gaffal E et al (2006) Rapid growth of invasive metastatic melanoma in carcinogen-treated hepatocyte growth factor/scatter factor-transgenic mice carrying an oncogenic CDK4 mutation. Am J Pathol 169(2):665–672
55. Powell MB, Hyman P, Bell OD et al (1995) Hyperpigmentation and melanocytic hyperplasia in transgenic mice expressing the human T24 Ha-ras gene regulated by a mouse tyrosinase promoter. Mol Carcinog 12(2):82–90
56. Broome Powell M, Gause PR, Hyman P et al (1999) Induction of melanoma in TPras transgenic mice. Carcinogenesis 20(9):1747–1753
57. Kato M, Takahashi M, Akhand AA et al (1998) Transgenic mouse model for skin malignant melanoma. Oncogene 17(14):1885–1888
58. Ito M, Hiramatsu H, Kobayashi K et al (2002) NOD/SCID/gamma(c)(null) mouse: an excellent recipient mouse model for engraftment of human cells. Blood 100(9):3175–3182
59. Voillet V, Berger TR, McKenna KM et al (2022) An in vivo model of human macrophages in metastatic melanoma. J Immunol 209(3):606–620
60. Yan C, Nebhan CA, Saleh N et al (2023) Generation of orthotopic patient-derived xenografts in humanized mice for evaluation of emerging targeted therapies and immunotherapy combinations for melanoma. Cancers 15(14):3695
61. Chuprin J, Buettner H, Seedhom MO et al (2023) Humanized mouse models for immuno-oncology research. Nat Rev Clin Oncol 20(3):192–206
62. Morton JJ, Ramos SA, Alzofon N et al (2025) Autologous thymic organoids support functional t-cell education and enhance antitumor immunity in humanized mice with melanoma xenografts. Cancer Res Commun 5(11):2053–2065
63. Morton JJ, Alzofon N, Keysar SB et al (2021) Studying immunotherapy resistance in a melanoma autologous humanized mouse xenograft. Mol Cancer Res 19(2):346–357
64. Chiorazzi M, Martinek J, Krasnick B et al (2023) Autologous humanized PDX modeling for immuno-oncology recapitulates features of the human tumor microenvironment. J Immunother Cancer 11(7):e006921
65. Mak IW, Evaniew N, Ghert M (2014) Lost in translation: animal models and clinical trials in cancer treatment. Am J Transl Res 6(2):114–118
66. Prouteau A, André C (2019) Canine melanomas as models for human melanomas: clinical, histological, and genetic comparison. Genes 2019 10(7):501
67. Nishiya AT, Massoco CO, Felizzola CR et al (2016) Comparative aspects of canine melanoma. Vet Sci 3(1):7
68. Gillard M, Cadieu E, De Brito C et al (2014) Naturally occurring melanomas in dogs as models for non-UV pathways of human melanomas. Pigment Cell Melanoma Res 27(1):90–102

69. Mochizuki H, Kennedy K, Shapiro SG, Breen M (2015) BRAF mutations in canine cancers. PLoS One 10(6):e0129534
70. Gardner HL, Fenger JM, London CA (2016) Dogs as a model for cancer. Annu Rev Anim Biosci 4:199–222
71. Hossain MA (2024) A comprehensive review of immune checkpoint inhibitors for cancer treatment. Int Immunopharmacol 143(Pt 2):113365
72. Tagawa M, Kurashima C, Takagi S et al (2018) Evaluation of costimulatory molecules in dogs with B cell high grade lymphoma. PLoS One 13(7):e0201222
73. Maekawa N, Konnai S, Takagi S et al (2017) A canine chimeric monoclonal antibody targeting PD-L1 and its clinical efficacy in canine oral malignant melanoma or undifferentiated sarcoma. Sci Rep 7(1):8951
74. Gardner HL, Fenger JM, London CA (2016) Dogs as a model for cancer. Annu Rev Anim Biosci 4:199–222
75. Valentine BA (1995) Equine melanocytic tumors: a retrospective study of 53 horses (1988 to 1991). J Vet Intern Med 9(5):291–297
76. Jiang L, Campagne C, Sundström E et al (2014) Constitutive activation of the ERK pathway in melanoma and skin melanocytes in Grey horses. BMC Cancer 14:857
77. Horak V, Palanova A, Cizkova J et al (2019) Melanoma-bearing Libechov minipig (MeLiM): the unique swine model of hereditary metastatic melanoma. Genes 10(11):915
78. Hook JrRR, Aultman MD, Adelstain EH et al (1979) Influence of selective breeding on the incidence of melanomas in Sinclair miniature swine. Int J Cancer 24(5):668–672
79. Müller S, Wanke R, Distl O (1995) Segregation of pigment cell anomalies in Munich miniature swine (MMS) Troll crossed with German Landrace. Dtsch Tierarztl Wochenschr 102(10):391–394
80. Bourneuf E (2017) The MeLiM minipig: an original spontaneous model to explore cutaneous melanoma genetic basis. Front Genet 8:146
81. Howe K, Clark MD, Torroja CF et al (2013) The zebrafish reference genome sequence and its relationship to the human genome. Nature 496(7446):498–503
82. Zhao S, Huang J, Ye J (2015) A fresh look at zebrafish from the perspective of cancer research. J Exp Clin Cancer Res 34(1):80
83. Patton EE, Widlund HR, Kutok JL et al (2005) BRAF mutations are sufficient to promote nevi formation and cooperate with p53 in the genesis of melanoma. Curr Biol 15(3):249–254
84. Dovey M, White RM, Zon LI (2009) Oncogenic NRAS cooperates with p53 loss to generate melanoma in zebrafish. Zebrafish 6(4):397–404
85. Santoriello C, Gennaro E, Anelli V et al (2010) Kita driven expression of oncogenic HRAS leads to early onset and highly penetrant melanoma in zebrafish. PLoS One 5(12):e15170
86. Hill D, Chen L, Snaar-Jagalska, Chaudhry B (2018) Embryonic zebrafish xenograft assay of human cancer metastasis. F1000Res 7:1682
87. Hoffman SJ, Psaltis P, Clark KJ et al (2012) An in vivo method to quantify lymphangiogenesis in zebrafish. PLoS One 7(9):e45240
88. Taylor AM, Zon LI (2009) Zebrafish tumor assays: the state of transplantation. Zebrafish 6(4):339–346
89. Zhao C, Wang X, Zhao Y et al (2011) A novel xenograft model in zebrafish for high-resolution investigating dynamics of neovascularization in tumors. PLoS One 6(7):e21768
90. van der Ent W, Burrello C, Teunisse AFAS et al (2014) Modeling of human uveal melanoma in zebrafish xenograft embryos. Investig Ophthalmol Vis Sci 55(10):6612–6622
91. Smalley KS, Lioni M, Noma K et al (2008) In vitro three-dimensional tumor microenvironment models for anticancer drug discovery. Expert Opin Drug Discov 3(1):1–10
92. Ishiguro T, Ohata H, Sato A et al (2017) Tumor-derived spheroids: relevance to cancer stem cells and clinical applications. Cancer Sci 108(3):283–289
93. Beaumont KA, Mohana-Kumaran N, Haass NK (2013) Modeling melanoma in vitro and in vivo. Healthcare 2(1):27–46
94. Zhuang L, Lee CS, Scolyer RA et al (2005) Activation of the extracellular signal regulated kinase (ERK) pathway in human melanoma. J Clin Pathol 58(11):1163–1169
95. Haass NK, Sproesser K, Nguyen TK et al (2008) The mitogen-activated protein/extracellular signal-regulated kinase kinase inhibitor AZD6244 (ARRY-142886) induces growth arrest in melanoma cells and tumor regression when combined with docetaxel. Clin Cancer Res 14(1):230–239
96. Bollag G, Hirth P, Tsai J et al (2010) Clinical efficacy of a RAF inhibitor needs broad target blockade in BRAF-mutant melanoma. Nature 467(7315):596–599
97. Tevis KM, Colson YL, Grinstaff MW (2017) Embedded spheroids as models of the cancer microenvironment. Adv Biosyst 1(10):1700083
98. Jeong SY, Lee J-H, Shin Y et al (2016) Co-culture of tumor spheroids and fibroblasts in a collagen matrix-incorporated microfluidic chip mimics reciprocal activation in solid tumor microenvironment. PLoS One 11(7):e0159013

99. Meier F, Nesbit M, Hsu MY et al (2000) Human melanoma progression in skin reconstructs: biological significance of bFGF. Am J Pathol 156(1):193–200
100. Berking C, Herlyn M (2001) Human skin reconstruct models: a new application for studies of melanocyte and melanoma biology. Histol Histopathol 16(2):669–674
101. Monico DA, Calori IR, Souza C et al (2022) Melanoma spheroid-containing artificial dermis as an alternative approach to in vivo models. Exp Cell Res 417(1):113207
102. Ulfo L, Costantini PE, Di Giosia M et al (2022) EGFR-targeted photodynamic therapy. Pharmaceutics 14(2):241
103. Turrini E, Ulfo L, Costantini PE et al (2024) Molecular engineering of a spheroid-penetrating phage nanovector for photodynamic treatment of colon cancer cells. Cell Mol Life Sci 81(1):144
104. Teixeira MC, Lameirinhas NS, Carvalho JPF et al (2024) Biobased hydrogel bioinks of pectin, nanocellulose and lysozyme nanofibrils for the bioprinting of A375 melanoma cell-laden 3D in vitro platforms. Int J Biol Macromol 282 5(Pt):136958
105. Jeong YM, Bang C, Park M et al (2021) 3D-printed collagen scaffolds promote maintenance of cryopreserved patients-derived melanoma explants. Cells 10(3):589
106. Vázquez-Aristizabal P, Henriksen-Lacey M, García-Astrain C et al (2024) Biofabrication and monitoring of a 3D printed skin model for melanoma. Adv Healthc Mater 13(27):e2401136
107. Fernandes S, Vyas C, Lim P et al (2022) 3D bioprinting: an enabling technology to understand melanoma. Cancers 14(14):3535
108. de Andres JL, Ruiz-Toranzo M, Antich C et al (2023) Biofabrication of a tri-layered 3D-bioprinted CSC-based malignant melanoma model for personalized cancer treatment. Biofabrication 15(3): 035016



Chapter 2

Generation of Functional Gene Knockout Melanoma Cell Lines by CRISPR-Cas9 Gene Editing

Kristian M. Hargadon, David Z. Bushhouse, Coleman E. Johnson and Corey J. Willams

Abstract

Recent advances in the treatment of metastatic melanoma have emerged only from advances in our understanding of melanoma development and progression at the cellular and molecular level. Despite the impact that such advances have made on the clinical management of this cancer over the last decade, additional insights into factors that promote melanoma progression and therapeutic resistance are needed to combat this disease. CRISPR-Cas9 gene editing technology is a powerful tool for studying gene function in a timely and cost-effective manner, enabling the manipulation of specific DNA sequences via a targeted approach. Herein, we describe a protocol for generating functional gene knockouts in melanoma cell lines by CRISPR-Cas9 gene editing, and we present an example application of this protocol for the successful knockout of the *Foxc2* transcription factor-encoding gene in the B16-F1 murine melanoma cell line.

Keywords CRISPR-Cas9, Gene editing, Melanoma, Gene knockout, B16, FOXC2, Transcription factor, Limiting dilution cloning

1 Introduction

Melanoma is the leading cause of skin cancer-related mortality, accounting for nearly 60,000 annual deaths worldwide [1]. The significance of this cancer as a global public health concern is underscored by the fact that its incidence has increased steadily over the last 40 years [2], a trend that is expected to continue until at least 2040 [1]. Although recent advances in our understanding of melanoma cell biology have led to the development of targeted and immunotherapeutic strategies that have improved the prognosis and clinical outcome for melanoma patients, there are still many patients who do not benefit from these regimens, and of those who do respond, a substantial number ultimately experience disease relapse as a result of tumor-acquired resistance [3–6]. Therefore, it is critical that we

Kristian M. Hargadon (ed.), *Melanoma*, Methods in Molecular Biology, vol. 3089,
https://doi.org/10.1007/978-1-0716-5619-8_2,
© The Author(s), under exclusive license to Springer Science+Business Media, LLC, part of Springer Nature 2027

gain additional insights into factors that promote melanoma progression and therapeutic resistance so that we may improve current and develop new strategies for the treatment of this cancer.

A number of technological advances have contributed to our understanding of cancer progression over the last two decades, and they continue to be useful tools for investigating important aspects of tumor biology. High throughput DNA and RNA sequencing efforts, such as those that have led to the large datasets publicly available through The Cancer Genome Atlas and AACR's Project GENIE consortium, have revealed specific driver mutations in various cancers, as well as distinct gene expression profiles in normal versus tumor tissue that demonstrate epigenetic dysregulation as a key contributor to tumor progression [7, 8]. Gene overexpression and silencing studies in various animal and preclinical models have in turn enabled direct assessment of the role of specific gene products in the development, progression, and therapeutic resistance of cancer. More recently, gene editing technologies have in many ways improved on these methods to understand gene function in cancer cells, allowing the introduction of specific nucleotide sequences at targeted sites within a cancer cell's genome or complete knockout of a specific gene's function (as compared to only the partial and less stable knockdown of gene function often achieved with gene silencing approaches).

A number of genome editing technologies have now been developed to study the function of specific genes and gene sequences within various cell types. One of the most widely used genome editing tools is the CRISPR-Cas9 system, which utilizes a specific guide RNA (gRNA) to direct the Cas9 endonuclease to a complementary DNA target sequence for cleavage. Specifically, Cas9 cleaves DNA at a defined site upstream of a protospacer adjacent motif (PAM) sequence found immediately 3′ to the gRNA (on the strand opposite to that complemented by the gRNA). Following cleavage, DNA is repaired by double-strand break repair machinery, enabling genome editing to be achieved in one of two ways: (1) homology directed repair (HDR) that introduces desirable nucleotide sequences (knock-ins) from a homologous repair template ("donor" DNA sequence) or (2) nonhomologous end joining (NHEJ) that rejoins the cleaved DNA sequences while often introducing mutations as a result of random nucleotide insertions/deletions (indels) during the repair process. In cases where indels are introduced in a way that disrupts the reading frame in all alleles of the target gene, a functional gene knockout is effectively introduced [9].

In this chapter, we describe a protocol for the generation of functional gene knockout melanoma cell lines using CRISPR-Cas9 gene editing technology, and we demonstrate in the B16-F1 melanoma model the successful application of this protocol to knock out *Foxc2*, a forkhead box transcription factor-encoding gene that has been linked to multiple oncogenic pathways in melanoma and

other cancers [10, 11] and whose expression is a poor prognostic factor for survival of melanoma patients treated with dacarbazine or ipilimumab [12, 13].

2 Materials

Store all media at 4°C in the dark. Store fetal bovine serum (FBS) at −20°C in the dark. Store all other supplies at room temperature. Use only sterile reagents for all procedures.

2.1 Cell Culture Media and Supplies

1. B16-F1 murine melanoma cell line.
2. Complete growth medium: Dulbecco's Modified Eagle's Medium (DMEM) containing 4 mM L-glutamine, 4500 mg/l glucose, 1 mM sodium pyruvate, and 1500 mg/l sodium bicarbonate, supplemented with 10% FBS.
3. Selection medium: Complete growth medium supplemented with 2 μg/ml of puromycin.
4. Freezing medium: Complete growth medium supplemented with 5% dimethyl sulfoxide (DMSO).
5. Trypsin-EDTA Solution (1×): 0.25% Trypsin/0.53 mM EDTA in Hanks Balanced Salt Solution without calcium or magnesium.
6. Tissue culture-treated 96-well plates.
7. Tissue culture-treated 24-well plates.
8. Tissue culture-treated 6-well plates.
9. Tissue culture-treated T25 flasks.
10. Nuclease-free, non-pyrogenic serological pipets and pipet tips.
11. Nuclease-free, non-pyrogenic 15 ml conical centrifuge tubes.
12. Nuclease-free, non-pyrogenic microcentrifuge tubes.
13. Tabletop centrifuge.
14. Hemocytometer.
15. Cryovials.
16. Light microscope.
17. Inverted light microscope.

2.2 Transfection Reagents

1. Attractene Transfection Reagent.
2. pSpCas9 BB-2A-Puro (PX459) V2.0 All-In-One plasmid vector (GenScript) encoding Cas9 and appropriately designed gRNA (*see* **Notes 1 and 2**) for target gene of interest (Fig. 1).
3. Opti-MEM I Reduced Serum Medium.

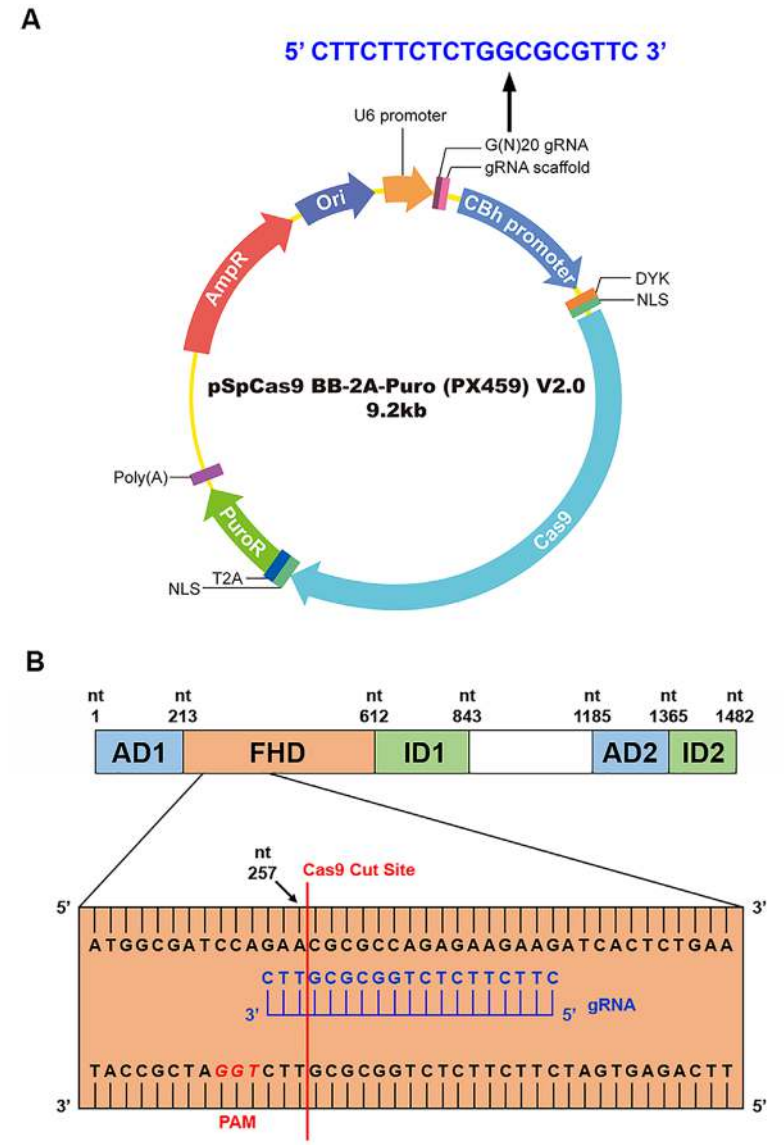


Fig. 1 Strategy for editing the *Foxc2* gene in the B16-F1 melanoma cell line using a CRISPR All-In-One plasmid-based genome editing approach. (**A**), Map of the pSpCas9 BB-2A-Puro (PX459) V2.0 All-In-One plasmid vector encoding Cas9 and a gRNA designed to target the murine *Foxc2* gene. In addition to these features, the plasmid carries an ampicillin resistance gene for selection of transformed bacterial cells and a puromycin resistance gene for selection of eukaryotic transfectants. (**B**), Schematic of the functional domains of the murine *Foxc2* gene and how the gRNA designed for the example gene editing approach described in this protocol targets a 5′ region of the gene encoding the N-terminal forkhead DNA-binding domain (FHD). AD activation domain, ID inhibitory domain. Portions of this figure are reproduced from Fig. 1 in our previously published article in *Cancer Genomics and Proteomics* [12] with permission from the International Institute of Anticancer Research

2.3 DNA Analysis

1. DNeasy Blood & Tissue Kit (Qiagen): This kit contains all proprietary buffers and the proteinase K reagent necessary for DNA extraction.
2. Endotoxin-free 1× phosphate-buffered saline (PBS), pH 7.4.
3. 100 mg/ml RNase A solution.
4. 100% ethanol.
5. Isopropanol.
6. Heat block.
7. Microcentrifuge.
8. Spectrophotometer.
9. Q5 Hot Start High Fidelity 2× Master Mix.
10. PCR primers (*see* **Note 3**).
11. 0.2 ml PCR reaction tubes.
12. Thermal cycler.
13. Nuclease-free water.
14. Agarose.
15. Ethidium bromide (EtBr).
16. Gel Loading Dye, Purple (6×).
17. Quick-Load® 100 bp DNA Ladder.
18. TAE Buffer (50×): Prepare 1 l of 50× TAE Buffer by dissolving 242 g of Tris-base in ~700 ml of deionized water and then adding 57.1 ml of 100% glacial acetic acid and 100 ml of 0.5 M EDTA (pH 8.0). Adjust the solution to a final volume of 1 l with deionized water. Store at room temperature. Make 1× TAE running buffer by diluting 50× stock 1:50 in deionized water.
19. UV light box.
20. Razor blades.
21. Laboratory analytical balance.
22. QIAquick Gel Extraction Kit (Qiagen): This kit contains all proprietary buffers necessary for DNA purification from agarose gel.
23. Parafilm.
24. DNA sequencer for Sanger sequencing.
25. CRISP-ID online tool [14].

3 Methods

Carry out all cell culture procedures in a biosafety cabinet to maintain sterility throughout the experiment. All steps following cell lysis may be performed under non-sterile conditions, though it is

important to maintain a nuclease-free environment throughout the entire protocol. A summary of the experimental workflow described below is shown in Fig. 2.

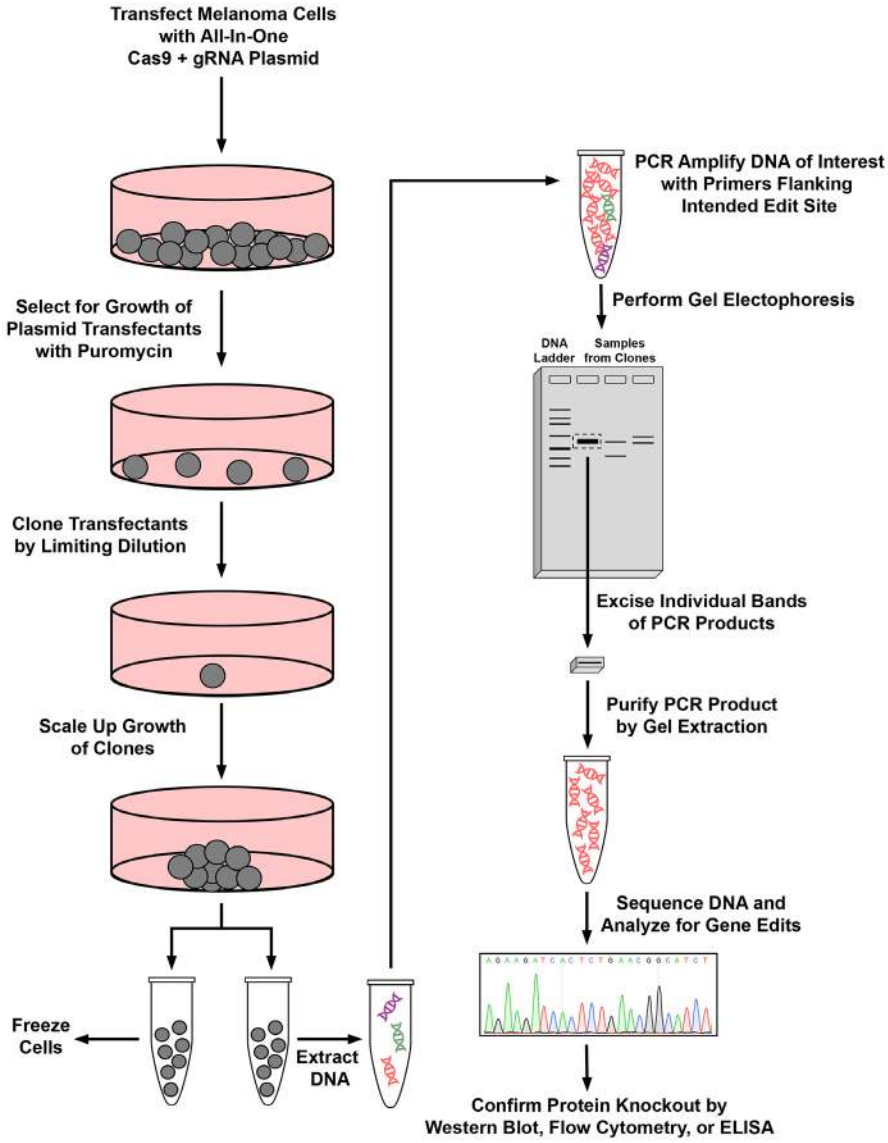


Fig. 2 Summary of the experimental workflow for CRISPR All-In-One plasmid-based genome editing of melanoma cell lines. Melanoma cells are transfected with a CRISPR All-In-One plasmid encoding Cas9 and a gRNA of interest. Polyclonal transfectants undergo puromycin selection, and clonal populations are generated by limiting dilution cloning. DNA is isolated from individual clones and the gene of interest is PCR amplified. PCR amplicons are gel purified and sequenced to screen clones for genome editing at the target site. Protein-based analysis is then performed to validate functional knockout in clones presenting with out-of-frame gene edits in all alleles

3.1 Designing a gRNA for CRISPR-Cas9 Gene Editing

For the protocol described herein, we utilize the pSpCas9 BB-2A-Puro (PX459) V2.0 All-In-One plasmid vector (GenScript) for delivery of both the Cas9 enzyme and the gRNA targeting the gene of interest. The GenScript sgRNA Design Tool (developed by the Broad Institute of Harvard and MIT and freely available at https://www.genscript.com/gRNA-design-tool.html) can be used to design an appropriate gRNA, whose coding sequence can then be engineered by GenScript into the Broad Institute-validated pSpCas9 BB-2A-Puro (PX459) V2.0 All-In-One plasmid.

1. Open the GenScript sgRNA Design Tool.
2. Input a sequence name, and select the desired Target Genome [in this case, Mouse (mm9)].
3. Search the National Center for Biotechnology Information (NCBI) for the gene sequence of interest.
4. Copy and paste into the Sequence box of the sgRNA Design Tool a region of up to 250 nucleotides from a portion of the gene's protein-coding sequence in which you wish to introduce an edit (*see* **Note 4**).
5. Click "Submit."
6. Retrieve the link that is emailed to the address used to register with GenScript, and click on the link to be taken to a list of potential gRNA sequences targeting the gene region of interest.
7. Choose an appropriate gRNA based on information in the gRNA sequence analysis, which is provided for all gRNAs generated when clicking on any one sequence from the list (*see* **Note 5**).
8. Input the desired gRNA sequence into GenScript's Custom CRISPR Plasmid Ordering form, along with the appropriate vector and species information, to order the All-In-One vector necessary for gene editing experiments (*see* **Note 6**).

3.2 Transfection of Melanoma Cells with CRISPR All-In-One Plasmid Vector

1. Harvest B16-F1 cells from culture and resuspend at a concentration of $1.6e^5$ cells/ml in complete growth medium.
2. Add 500 µl ($8.0e^4$ cells) to separate wells of a 24-well tissue culture plate. Set up three wells: one that will serve as an untransfected control, one that will serve as a mock transfection control, and one that will be transfected with the CRISPR All-In-One plasmid.
3. Incubate cells overnight at 37°C in a humidified incubator with 5% CO_2 (*see* **Note 7**).
4. The following morning, add 0.4 µg (4 µl of plasmid at a concentration of 0.1 µg/µl) of pSpCas9 BB-2A-Puro (PX459) V2.0 All-In-One plasmid encoding the gRNA of interest into 56 µl of Opti-MEM I Reduced Serum Medium in a microcentrifuge

tube. Mix gently by flicking the tube several times. Set up a separate microcentrifuge tube for the mock transfection group, but simply add 60 µl of Opti-MEM I Reduced Serum Medium to this tube (do not add plasmid).

5. To the above tubes, add 1.5 µl of Attractene Transfection Reagent, mix gently by flicking the tubes several times, and incubate at room temperature for 15 min to allow formation of transfection complexes.
6. During the 15-min incubation period, remove the medium from B16-F1 cultures in the 24-well plate, and wash once with fresh complete growth medium.
7. Discard the wash medium and replace with a fresh 500 µl of complete growth medium.
8. Add the transfection reagent mix with or without plasmid drop-wise onto the cells in the appropriate wells, gently swirling the culture plate after each drop to ensure uniform distribution of the transfection complexes.
9. Incubate cells overnight at 37°C in a humidified incubator with 5% CO_2.

3.3 Antibiotic Selection of Transfected Cells

1. The following morning, aspirate medium from cultures and add 250 µl of 1× Trypsin-EDTA Solution.
2. Return culture plate to the 37°C incubator long enough for cells to detach (*see* **Note 8**).
3. Following cell detachment (this can be evaluated by observation under an inverted light microscope), neutralize trypsin by adding 1 ml of complete growth medium (*see* **Note 9**).
4. Transfer cells to a nuclease-free, non-pyrogenic 15 ml conical tube and centrifuge at 450 × *g* for 5 min.
5. Remove supernatant, resuspend cells in complete growth medium, and count cells using a hemocytometer.
6. Centrifuge cells at 450 × *g* for 5 min, discard supernatant, and resuspend at a concentration of $5.0e^4$ cells/ml in Selection Medium containing 2 µg/ml of puromycin (*see* **Note 10**).
7. Plate 1 ml of cell suspension ($5.0e^4$ cells) into separate wells of a 6-well tissue culture plate in order to seed cells at a low density (≤10% confluence) and culture at 37°C in a humidified incubator with 5% CO_2.
8. Replace Selection Medium in cultures daily to remove dead cells and monitor cells for growth.
9. Once all untransfected and mock-transfected control cells have been killed (*see* **Note 11**), remove Selection Medium from plasmid transfectants, replace it with complete growth medium without puromycin (*see* **Note 12**), and continue to culture cells at 37°C in a humidified incubator with 5% CO_2.

3.4 Limiting Dilution Cloning of Transfected Melanoma Cells

1. One day after removing transfectants from puromycin selection, remove the medium and collect polyclonal cells by trypsinization for limiting dilution cloning (*see* **Note 13**).
2. Count cells on a hemocytometer and resuspend in complete growth medium to a concentration of $1.0e^6$ cells/ml.
3. Perform serial dilutions to achieve a concentration of 1 cell/400 µl of complete growth medium (Fig. 3).
4. Plate 200 µl of diluted cells into each well of a 96-well tissue culture plate such that a single cell is deposited into approximately every other well (*see* **Note 14**). Incubate cultures at 37°C in a humidified incubator with 5% CO_2.
5. Monitor cultures daily under an inverted microscope, taking care to note which wells contain single cells (*see* **Note 15**).
6. As clones from single cells expand over time, collect clonal populations and scale up growth by transferring cells to 24-well tissue culture plates.
7. Once clones approach confluence in 24-well plates, collect cells and continue to scale up growth by transferring to T25 flasks.
8. When T25 flasks reach confluence, collect cells and divide into two equal aliquots. Centrifuge cells at 450 × *g* for 5 min and discard supernatant. Resuspend one aliquot in freezing medium and store at −80°C for future use. Use the second aliquot for isolation of DNA.

3.5 Isolation of DNA from Melanoma Clones

In addition to isolating DNA from the potentially gene-edited clones, it is important to also isolate DNA from the unedited parental cell line for comparison during DNA sequence analysis. For DNA extraction, the DNeasy Blood & Tissue Kit should be used according to the manufacturer's protocol, with modifications as described below:

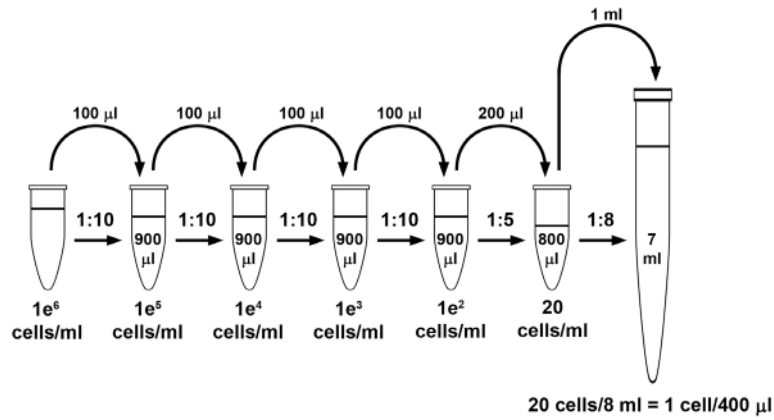


Fig. 3 Serial dilution scheme for limiting dilution cloning

1. Resuspend pelleted cells in 200 µl of 1× PBS.
2. Add 20 µl of proteinase K and 4 µl of RNase A, mix by vortexing, and incubate at room temperature for 2 min.
3. Add 200 µl of Buffer AL, mix thoroughly by vortexing, and incubate at 56°C on a heat block for 10 min (*see* **Note 16**).
4. Add 200 µl of 100% ethanol and mix thoroughly by vortexing.
5. Pipet the mixture into a DNeasy Mini spin column in a 2 ml collection tube, and centrifuge at ≥ 6000 × *g* for 1 min. Discard the flow-through and collection tube (*see* **Note 17**).
6. Place the DNeasy Mini spin column in a new 2 ml collection tube, add 500 µl of Buffer AW1, and centrifuge at ≥6000 × *g* for 1 min. Discard the flow-through and collection tube.
7. Place the DNeasy Mini spin column in a new 2 ml collection tube, add 500 µl of Buffer AW2, and centrifuge at 20,000 × *g* for 3 min. Discard the flow-through and collection tube.
8. Place the DNeasy Mini spin column in a new 1.5 ml microcentrifuge tube with a cap. Pipet 100–200 µl of nuclease-free water (volume will depend on the expected DNA yield) into the spin column, incubate at room temperature for 1 min, and centrifuge at ≥6000 × *g* for 1 min to elute the DNA (*see* **Note 18**).
9. Measure DNA concentration on a spectrophotometer (*see* **Note 19**).

3.6 PCR Amplification of DNA of Interest and Purification by Gel Extraction

1. Amplify DNA from the gene of interest by PCR using primers that flank the intended Cas9 cut site where gene editing is expected to occur (*see* **Note 3**).
   a. For DNA from each clone and parental sample to be analyzed, set up a PCR reaction tube as indicated in Table 1.
   b. Load thermal cycler and program the following conditions for the PCR reaction:
      i. Initial denaturation: 98°C for 30 s.
      ii. Denature at 98°C for 30 s.
      Anneal at 68°C for 30 s (*see* **Note 20**).
      Extend at 72°C for 30 s (*see* **Note 21**). Repeat for 35 cycles.
      iii. Final extension: 72°C for 2 min.
      iv. Hold at 4°C for ∞.
2. During the PCR reaction, prepare a 1.5% agarose gel containing 0.5 µg/ml of EtBr.
3. Submerge solidified gel in an electrophoresis chamber containing 1× TAE Buffer with 0.5 µg/ml of EtBr.

Table 1
PCR reaction setup for amplification of DNA from clonal melanoma cell populations

Reagent	Volume	Final concentration
Q5 Hot start high fidelity 2× Master mix	25 µl	1×
10 µM forward primer	2.5 µl	0.5 µM
10 µM reverse primer	2.5 µl	0.5 µM
Template DNA	*x*µl	500 ng
Nuclease-free water	*x*µl	
	Total volume = 50 µl	

4. After the PCR reaction, remove 40 µl of PCR product and mix with 8 µl of Gel Loading Dye, Purple (6×).
5. Load samples into separate gel wells. Also load one well with 10 µl of 100 bp DNA ladder (or other appropriate ladder based on the expected size of the PCR products).
6. Run the gel at an appropriate voltage for as long as necessary to separate PCR products (*see* **Note 22**).
7. Excise PCR products of interest from the gel using a clean razor blade (*see* **Note 23**).
8. Zero out an analytical balance with a microcentrifuge tube, and place the slice of agarose containing the DNA band of interest into the tube in order to weigh the agarose slice. The weight of the agarose is necessary to proceed with gel extraction using the QIAquick Gel Extraction Kit, which should be used according to the manufacturer's protocol with modifications as described here.
9. Add three volumes of Buffer QG to one volume of agarose gel (i.e., 300 µl of Buffer QG for every 100 mg of agarose gel).
10. Completely dissolve the agarose by incubating on a heat block at 50°C for 10 min (*see* **Note 16**).
11. Add one gel volume of isopropanol to the sample and mix by vortexing.
12. Apply the sample mixture to a QIAquick column that has been placed into a 2 ml collection tube, and centrifuge at 17,900 × *g* for 1 min. Discard the flow-through (*see* **Note 24**).
13. Place the QIAquick column back into the same 2 ml collection tube, add 500 µl of Buffer QG, and centrifuge at 17,900 × *g* for 1 min to remove all traces of agarose. Discard the flow-through and return column to the same 2 ml collection tube.

14. Add 750 µl of Buffer PE to the QIAquick column, incubate at room temperature for 5 min, and centrifuge at 17,900 × *g* for 1 min to wash the sample. Discard the flow-through and return the column to the same 2 ml collection tube.
15. Centrifuge again at 17,900 × *g* for 1 min to remove residual ethanol that is present in Buffer PE.
16. Transfer the QIAquick column to a new nuclease-free 1.5 ml microcentrifuge tube with a cap.
17. Add 25 µl of nuclease-free water directly to the QIAquick membrane and incubate at room temperature for 5 min.
18. Centrifuge tubes at 17,900 × *g* for 1 min to elute DNA.
19. Quantify DNA concentration on a spectrophotometer.

3.7 DNA Sequencing and Analysis

Sanger sequencing can be performed in-house, or samples can be submitted to a number of companies that provide DNA sequencing services. We use GenScript's DNA Sequencing Service and provide guidelines below for sample submission, along with sample data from *Foxc2* gene sequencing from wild-type B16-F1 and a series of B16-F1-derived gene-edited clones (Fig. 4).

1. Submit purified PCR product at a concentration ranging from 30–50 ng/µl in a nuclease-free microcentrifuge tube sealed with Parafilm. Include 10 µl of template DNA per sequencing reaction (*see* **Note 25**).
2. Submit the forward primer used for PCR amplification at a concentration of 5 µM in a separate microcentrifuge tube sealed with Parafilm, and include 10 µl of primer per sequencing reaction (*see* **Note 25**).
3. After Sanger sequencing is performed, review the sequencing chromatogram for the unedited wild-type sample and confirm that it matches the NCBI reference sequence for the gene of interest (Fig. 4A).
4. Review the sequencing chromatograms of the potentially gene-edited clones, and determine how any indels introduced impact the reading frame of the gene (*see* **Note 26**).
5. If sequence chromatograms for any samples reveal overlapping spectra (Fig. 4B–D), deconvolute the overlapping spectra using CRISP-ID [14], a freely available web application that distinguishes from a single sample the sequence of up to three alleles that are too similar in size to be separated by gel electrophoresis (*see* **Note 27**).
    a. Access the CRISP-ID application at http://crispid.gbiomed.kuleuven.be/
    b. Upload the sequence trace file in either ABI or SCF format.

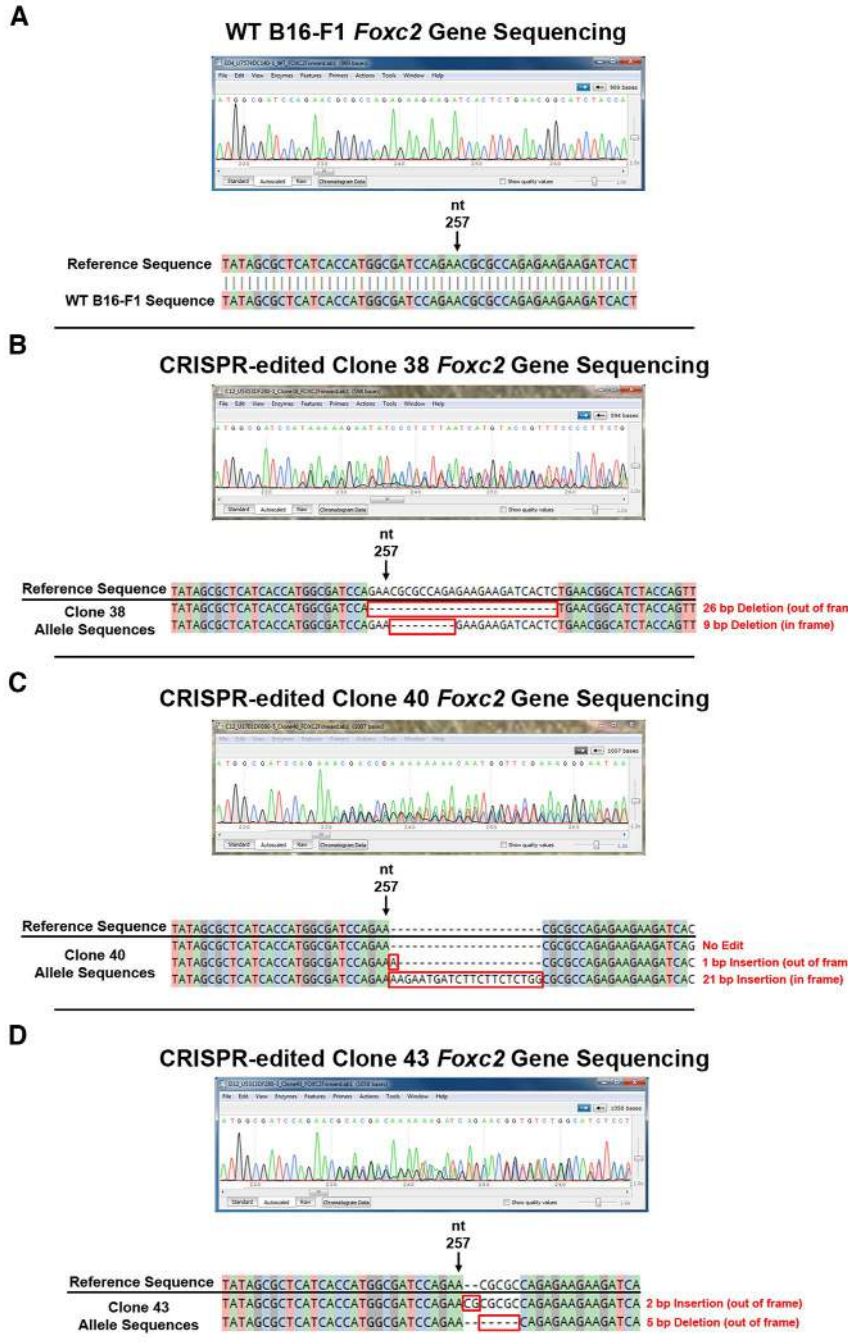


Fig. 4 Example DNA sequencing chromatograms and CRISP-ID deconvolution/alignment of *Foxc2* alleles from wild-type B16-F1 melanoma and gene-edited clones of B16-F1 carrying heterozygous alleles. (**A**), Sanger sequencing chromatogram of wild-type, parental B16-F1 melanoma cells, showing the region of the *Foxc2* gene that was targeted for gene editing in our study. CRISP-ID analysis shows perfect alignment of this sequenced DNA with the NCBI's reference sequence for the murine *Foxc2* gene. (**B**), An example of a clone in which both *Foxc2* alleles were edited at the target site, though with only one allele being edited out-of-frame. (**C**), An example of a clone in which CRISP-ID deconvolution yields three distinct alleles of the *Foxc2* gene (*see* **Note 27**).

c. Input the NCBI reference sequence for the gene of interest, using only the sequence of the PCR-amplified region of the gene.

d. Set the "Start position" and "End position" as necessary to exclude terminal ends of the sequence read where there may be less confidence in base calling.

e. Adjust the "Background cutoff (%)" to improve the accuracy of base calling as necessary (i.e., if there is a high background signal in the sequencing chromatogram).

f. Input the "Max insert size," which can be estimated for PCR products from gene-edited clones by comparing their electrophoretic mobility with that of a DNA ladder and the PCR product obtained from the wild-type sample.

g. Click "Analyze" and retrieve the data, which are reported as an alignment of resolved sequences with the reference sequence and which reveal the nature of individual indels from heterozygous alleles that had produced the originally overlapped sequencing chromatogram. Examples of several possible gene editing outcomes as identified by CRISP-ID are shown in Fig. 4.

6. Upon identifying a clone with out-of-frame edits in all alleles for the gene of interest, recover frozen cells of that clone and perform protein analysis by Western blot (Fig. 5), flow cytometry, or ELISA to verify functional knockout of the gene (*see* **Note 28**).

7. Use validated knockout as intended in functional studies (Fig. 6).

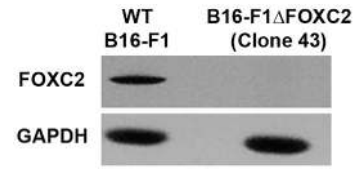


Fig. 5 Western blot validation of functional *Foxc2* gene knockout in a clone of B16-F1 melanoma cells edited as per the protocol described herein. This figure is reproduced from a portion of Fig. 1 in our previously published article in *Cancer Genomics and Proteomics* [12] with permission from the International Institute of Anticancer Research

Fig. 4 (continued) (**D**), An example of a clone (Clone 43) in which edits in both *Foxc2* alleles resulted in the desirable outcome of indels that produce out-of-frame mutations. Portions of this figure are reproduced from Fig. 1 in our previously published article in *Cancer Genomics and Proteomics* [12] with permission from the International Institute of Anticancer Research

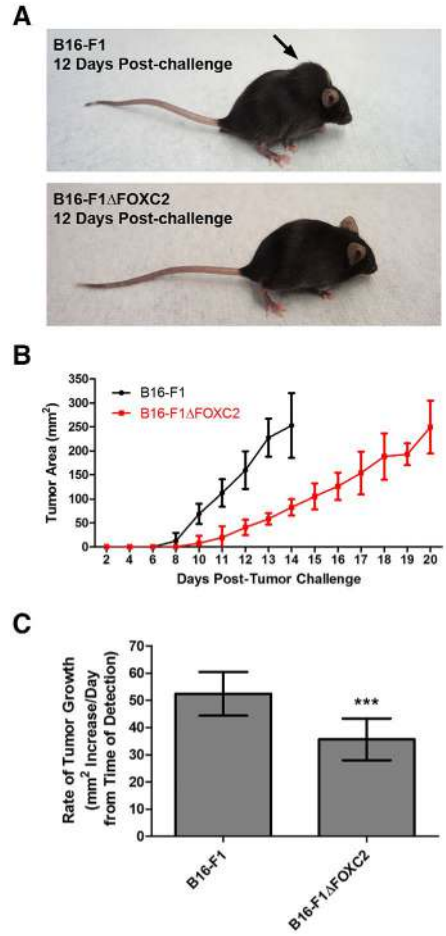


Fig. 6 Tumor challenge studies with wild-type versus CRISPR-Cas9 gene-edited, FOXC2-deficient B16-F1 melanoma. C57Bl/6 mice were challenged subcutaneously with 4×10^5 B16-F1 melanoma cells or B16-F1ΔFOXC2 melanoma cells (generated as described herein) and monitored for tumor growth and progression. Images of representative mice at day 12 post-challenge are shown in (**A**), and pooled data from three separate experiments, each with two to four mice per group, are shown in (**B**) and (**C**). The rate of tumor outgrowth was calculated as the size of tumor at the time of death divided by the number of days from the appearance of a measurable tumor to death. Data are graphed as the average of all replicates with error bars that represent the standard deviation of the mean. ***$p < 0.001$. This figure is reproduced from Fig. 2 in our previously published article in *Cancer Genomics and Proteomics* [12] with permission from the International Institute of Anticancer Research

4 Notes

1. When designing a gRNA to target a gene of interest for knockout, it is best to identify a targetable region near the

5′ end of the gene's coding sequence so that any translatable sequence yields only minimal C-terminal portions of the protein. This strategy will reduce the likelihood of translating protein with partial functionality or the ability to still participate in protein–protein or protein–DNA/RNA interactions. In the example highlighted herein, we targeted a region near the 5′ end of the murine *Foxc2* gene encoding the N-terminal forkhead DNA-binding domain of the FOXC2 transcription factor—the targeted Cas9 cut site was located after the 257th nucleotide of the gene's 1485-nucleotide-long coding sequence (Fig. 1B).

2. When designing a gRNA to target a gene of interest for knockout, care should also be taken as described in Sect. 3.1 to avoid/minimize off-target effects of the gRNA so that unintended gene edits are not introduced.
3. PCR primers should be designed to amplify a region of the target gene's DNA sequence that includes the intended site for gene editing, allowing for the possibility of the introduction of potentially large indels. In the example highlighted herein, we used forward primer 5′-CATGCAGGCGCGTTACTC-3′ and reverse primer 5′-ATAGCCCGCATACTGCACTGGTAG-3′ to amplify a 1005 bp region spanning nucleotide −1 to nucleotide +1004 of the *Foxc2* gene's coding sequence, in which gene editing was expected to occur near nucleotide +257 of the coding sequence.
4. In the example we describe here, nucleotides 187–396 of the murine *Foxc2* gene's coding sequence (beginning prior to and spanning the 5′ region that encodes the N-terminus of FOXC2's forkhead DNA-binding domain) were used to identify potential Cas9 target sites that would disrupt this key functional domain of the *Foxc2* gene.
5. Potential gRNA sequences are color-coded for quality, with high-quality gRNAs indicated by green, mid-quality gRNAs indicated by yellow, and low-quality gRNAs indicated by red. Additionally, for all gRNA sequences generated, a quality score that represents the inverse likelihood of off-target binding is provided. Upon selecting a particular gRNA, the number of potential off-target sites is also reported, and this list can be filtered down to include only those sites that are found within exonic regions of genes. It is best to choose a gRNA with a high-quality score and as few off-target sites as possible, particularly those within other exons. Should a desirable gRNA contain off-target sites within exonic regions, the NCBI reference sequences for such genes are provided, along with their chromosomal locations, so that investigators may perform quality control checks following gene editing to assess whether or not off-target mutations were introduced at these sites.

6. GenScript All-In-One vectors may be ordered as Research Grade, which require bacterial transformation to generate sufficient plasmid for multiple transfections, or as HT Transfection Grade or Industrial Grade, both of which are supplied in larger quantities and may not require scaling up of the plasmid before use.
7. Cells should be ~75% confluent at the time of transfection. Seeding at this density will achieve this level of confluence when working with B16-F1 melanoma cells.
8. The duration of trypsinization will vary by cell type and is dependent on the strength of cell adhesion to the culture plate. It is important not to trypsinize cells longer than necessary, as this enzymatic digestion will eventually damage the integrity of the cell membrane. B16-F1 melanoma cells typically detach within 2–3 min, and those that have not lifted from the plate after this time can be detached easily by gentle pipetting at this time.
9. FBS proteins in the complete growth medium serve as targets for trypsin and prevent overreactivity against cell membrane proteins.
10. The pSpCas9 BB-2A-Puro (PX459) V2.0 All-In-One plasmid carries a puromycin resistance gene (Fig. 1) to allow for selection of transfected cells. The 2 μg/ml dose of puromycin described here is specific for selection against untransfected B16-F1 melanoma cells. The dose of puromycin to use for selection must be empirically determined for different cell types by generating a dose–response curve following cell exposure to various dilutions of the antibiotic. The lowest dose that effectively kills 100% of untransfected cells should be used for selection of transfectants.
11. For B16-F1 melanoma cells, all control cells are typically killed within 3 days of puromycin selection.
12. Once all control cells have been killed by puromycin, antibiotic selection is no longer needed in the plasmid transfectants, which should be growing at this stage as tiny patches of cells. Maintenance of puromycin selection at this stage runs the risk of promoting plasmid integration into the host cell genome. Not only would such integration have unintended consequences on the host cell genome, it might also result in long-term expression of the puromycin resistance gene as well as the *S. pyogenes* Cas9 enzyme, which could in turn inadvertently result in presentation of foreign antigen on the melanoma cell surface and lead to altered immune reactivity against the melanoma in in vivo settings.
13. It is best to collect the patches of plasmid transfectants before they become too overgrown. Each patch of cells typically

represents a successful transfectant that grew into a small colony of cells, meaning that gene editing is likely identical in all cells in a given patch. Because the introduction of indels is random, many edits will not result in a functional knockout (i.e., small in-frame edits may yield a slightly truncated or elongated, but possibly still functional, protein), and if the patches of cells become too overgrown, there may be many cells arising from the same transfectant that all carry the same undesirable edit. Therefore, collecting cells after colonies have grown too large will most likely increase the number of clones that must be screened after limiting dilution cloning in order to identify one with the desirable knockout-inducing edit, making this process unnecessarily laborious. On the other hand, collecting the transfectants early means that more diverse clones are likely to be plated, thereby increasing the likelihood of identifying one with an edit that will yield a functional knockout.

14. Plating cells in this way will necessarily result in some wells receiving no cells but will also reduce the likelihood of depositing more than one cell into a given well. The number of plates loaded will likely depend on the melanoma cell line being used, as some cell lines are more easily cloned by limiting dilution than others. B16-F1 grows relatively well from single cells, and we typically generate 15–20 clones per 96-well plate. The growth and survival of other melanoma cell lines may depend more heavily on cell–cell contact, meaning that clones are less easily generated from single cells. For these cell lines, several plates must be used to generate a sufficient number of clones for analysis.
15. In many cases, it will be possible to visualize single cells that have adhered to the tissue culture plate. In some instances, though, cells may not be detected until a small colony forms, but it is important to identify these wells as soon as possible after plating. Effort should be made to avoid collecting cells from wells where two or more cells were originally deposited, as these wells will not yield clonal populations. Therefore, identifying wells with individual cells or single, small colonies early will reduce the unwanted outcome later of finding a well with a large patch of cells that could represent two or more colonies that have grown together.
16. It is recommended to add some water to the wells of the heat block in order to provide a more uniform temperature when heating the samples.
17. The DNA is trapped in the DNeasy Mini spin column at this stage and is subsequently washed to remove impurities prior to elution.

18. Though the kit comes with an elution buffer (Buffer AE), we prefer to elute DNA with nuclease-free water in order to avoid any potential impacts that Buffer AE components may have on downstream reactions in the workflow.
19. A260:280 values should ideally be ≥1.8, as this value indicates high DNA purity (minimal protein contamination) in the prep. We typically observe A260:280 values in the 1.9–2.0 range using this protocol on B16-F1 melanoma cells.
20. This annealing temperature is optimal for the primers used in our example for *Foxc2* DNA amplification described herein but will likely vary for other primer sets. We recommend utilizing the New England BioLabs Tm Calculator v1.12.0, a freely accessible web-based tool (https://tmcalculator.neb.com/#!/main) that calculates an optimal annealing temperature for the PCR reaction based on user-generated information on the PCR Master Mix, primer concentration, and primer sequences being used.
21. The duration of the extension stage may need to be altered depending on the length of the PCR amplicon. A 20–30-s extension period is recommended per kb of amplicon.
22. The gel should be removed from the electrophoresis chamber and monitored periodically to evaluate the size of bands. Though there is an expected product size in wild-type parental cells, the product sizes of the potentially edited clones may vary significantly based on the size of the indels introduced, which we have observed ranging from a single nucleotide to several hundred nucleotides.
23. While only a single PCR product should be generated in the wild-type parental cell line, clones generated from CRISPR All-In-One plasmid transfectants may yield one or multiple PCR amplicons. In some cases, even though cells are transfected and survive puromycin selection, no gene editing will occur, resulting in a PCR amplicon identical to that in wild-type cells. If only small indels are introduced in a gene-edited clone, the PCR product may run at the same speed as that from unedited parental cells. In these cases, one visible indication that an edit(s) has been introduced is the appearance of multiple faint bands that exhibit shifts in electrophoretic mobility as a result of heteroduplex formation between PCR products that are complementary in portions of their sequence but mismatched at a region where differential gene editing has occurred in different alleles. If editing results in two alleles of significantly different size, these heteroduplexes are readily apparent (Fig. 7).
24. The DNA is trapped in the QIAquick column at this stage and is subsequently washed to remove impurities prior to elution.



Fig. 7 Example of heteroduplex formation and the resulting shift in electrophoretic mobility that occurs when heterozygous alleles with partial complementarity anneal with one another after gene editing and PCR amplification. Note for Clone 12: the presence of multiple bands, three of which were purified for Sanger sequencing following PCR amplification of the region of interest from the *Foxc2* gene. The top band represents an unedited allele and aligns perfectly with the sequence obtained from wild-type, parental B16-F1 melanoma cells. The bottom band represents a PCR-amplified fragment of the *Foxc2* gene with a 628 bp deletion. The middle band that was sequenced produced an overlapping chromatogram. Deconvolution of this chromatogram by CRISP-ID revealed this band to be two distinct alleles, one equivalent to the wild-type allele and one equivalent to the allele carrying the 628 bp deletion

25. It is best to submit enough DNA and forward primer for two sequencing reactions per sample in case any technical issues arise and a repeat of the sequencing is required.
26. Indels that do not occur in multiples of three are desirable, as these will completely alter translation of any transcribed RNA from the point of editing. Indels that occur in multiples of three, on the other hand, will ultimately lead to restoration of the reading frame, meaning that proper translation will be restored following addition/deletion of some number of amino acids. In such a case, the resulting protein may retain some level of functionality.
27. Though counterintuitive, there are two ways by which one might obtain three different alleles from a population of cells that is diploid. The first way involves a technical issue with limiting dilution cloning, such that two cells are plated unknowingly into a single well, with one having two uniquely edited alleles and the other being unedited, or with each cell having single alleles edited in different ways (either outcome

yields two uniquely edited alleles and one unedited allele in the resulting population, which is not clonal). Alternatively, this outcome might also arise if gene editing is not complete at the time of limiting dilution cloning but instead continuing after division of a single plated cell, a phenomenon that would yield genetic mosaicism in the resulting population, which would no longer be clonal. In this scenario, a single allele is edited in one cell at the time of cloning, and upon cell division, one daughter cell is edited at the second allele while the other daughter cell remains unedited, or the second daughter cell is edited in a different way at a single allele and the cell originally edited at one allele does not undergo further editing (Fig. 4C). It should also be noted that many tumor cell lines amplify specific genes or are polyploid and may therefore carry more than two alleles of a given gene. Should sequencing chromatograms need to be deconvoluted for cell lines harboring more than three alleles of a gene, DECODR v3.0 (https://decodr.org/) [15] can be used as an alternative to CRISP-ID.

28. Be sure to use an antibody specific for a C-terminal region of the protein that should no longer be encoded by the edited gene. Antibodies that recognize linear or conformational epitopes of N-terminal regions of a protein encoded by DNA sequences prior to the site of gene editing will still bind to any partially translated amino acid sequences.

Acknowledgments

This work was supported by funding from Virginia's Commonwealth Health Research Board, a Jeffress Trust Awards Program in Interdisciplinary Research Grant from the Thomas F. and Kate Miller Jeffress Memorial Trust (Bank of America, N.A., Trustee), a Virginia Foundation for Independent Colleges (VFIC) Maurice L. Mednick Memorial Fellowship, and a Hampden-Sydney College Research Grant from the Arthur Vining Davis endowment (to KMH). This work was also supported by a VFIC Undergraduate Science Research Fellowship to CJW and a Virginia Academy of Science Undergraduate Research Grant to DZB. We also thank Mr Michael Hargadon and Mrs Patricia Hargadon for generous donations to support the involvement of Hampden-Sydney College undergraduate students in this research.

Competing Interests The authors have no conflicts of interest to declare that are relevant to the content of this chapter.

References

1. Arnold M, Singh D, Laversanne M et al (2022) Global burden of cutaneous melanoma in 2020 and projections to 2040. JAMA Dermatol 158:495–503. https://doi.org/10.1001/JAMADERMATOL.2022.0160
2. Howlader N, Noone AM, Krapcho M, Miller D, Brest A, Yu M, Ruhl J, Tatalovich Z, Mariotta A, Lewis DR, Chen HS, Feuer EJ, Cronin KA (eds) (2020) SEER cancer statistics review, 1975–2017. National Cancer Institute. Bethesda, MD. https://seer.cancer.gove/csr/1975_2017/. Based on November 2019 Seer data submission, posted to the SEER web site
3. Amann VC, Ramelyte E, Thurneysen S et al (2017) Developments in targeted therapy in melanoma. Eur J Surg Oncol 43:581–593. https://doi.org/10.1016/j.ejso.2016.10.014
4. Robert C, Grob JJ, Stroyakovskiy D et al (2019) Five-year outcomes with dabrafenib plus trametinib in metastatic melanoma. N Engl J Med 381:626–636. https://doi.org/10.1056/NEJMoa1904059
5. Hargadon KM, Johnson CE, Williams CJ (2018) Immune checkpoint blockade therapy for cancer: an overview of FDA-approved immune checkpoint inhibitors. Int Immunopharmacol 62:29–39. https://doi.org/10.1016/j.intimp.2018.06.001
6. Wolchok JD, Chiarion-Sileni V, Rutkowski P et al (2025) Final, 10-year outcomes with nivolumab plus ipilimumab in advanced melanoma. N Engl J Med 392:11–22. https://doi.org/10.1056/NEJMOA2407417
7. Lee JS (2016) Exploring cancer genomic data from the cancer genome atlas project. BMB Rep 49:607–611. https://doi.org/10.5483/bmbrep.2016.49.11.145
8. Pugh TJ, Bell JL, Bruce JP et al (2022) AACR project GENIE: 100,000 cases and beyond. Cancer Discov 12:2044–2057. https://doi.org/10.1158/2159-8290.CD-21-1547
9. Cong L, Ran FA, Cox D et al (2013) Multiplex genome engineering using CRISPR/Cas systems. Science 339:819–823. https://doi.org/10.1126/science.1231143
10. Hargadon KM, Williams CJ (2020) RNA-seq analysis of wild-type vs. FOXC2-deficient melanoma cells reveals a role for the FOXC2 transcription factor in the regulation of multiple oncogenic pathways. Front Oncol 10:267. https://doi.org/10.3389/fonc.2020.00267
11. Hargadon KM, Goodloe TB, Lloyd ND (2022) Oncogenic functions of the FOXC2 transcription factor: a hallmarks of cancer perspective. Cancer Metastasis Rev 41:833–852. https://doi.org/10.1007/S10555-022-10045-3
12. Hargadon KM, Györffy B, Strong EW et al (2019) The FOXC2 transcription factor promotes melanoma outgrowth and regulates expression of genes associated with drug resistance and interferon responsiveness. Cancer Genom Proteom 16:491–503. https://doi.org/10.21873/cgp.20152
13. Hargadon KM, Strong EW (2023) The FOXC2 transcription factor: a master regulator of chemoresistance in cancer. Technol Cancer Res Treat 22:15330338231155284. https://doi.org/10.1177/15330338231155284
14. Dehairs J, Talebi A, Cherifi Y, Swinnen JV (2016) CRISP-ID: decoding CRISPR mediated indels by Sanger sequencing. Sci Rep 6:28973. https://doi.org/10.1038/srep28973
15. Bloh K, Kanchana R, Bialk P et al (2021) Deconvolution of complex DNA repair (DECODR): establishing a novel deconvolution algorithm for comprehensive analysis of CRISPR-edited Sanger sequencing data. CRISPR J 4:120–131. https://doi.org/10.1089/crispr.2020.0022



Chapter 3

Establishment and Characterization of Model Antigen-Expressing Melanoma Cell Lines

Kristian M. Hargadon and Stephen L. Woodall II

Abstract

Significant advances in our understanding of antitumor immunity over the last two decades have ushered in an exciting era of cancer immunotherapy. During this time, several strategies have been developed to elicit robust antitumor immune responses by $CD8^+$ cytotoxic T lymphocytes. Despite the documented benefits of various approaches aimed at targeting these cells, however, there remains a substantial number of patients who either fail to respond to these regimens or who relapse after an initial response. Therefore, to gain insight into mechanisms of innate and acquired resistance to immune-based therapies for cancer, we must improve our understanding of factors that regulate the induction and maintenance of T cell responses against cancer antigens. In this regard, experimental systems that enable the study of cancer antigen-specific T cells are useful tools for investigating the activation and suppression of antitumor T lymphocytes. To this end, we describe herein a method for generating and characterizing model antigen-expressing melanoma cell lines, and we specifically validate this method using two variants of B16 murine melanoma that we engineered to express the OVA_{257} epitope of chicken ovalbumin, a model neoantigen against which both natural and T cell receptor (TCR) transgenic OT-I $CD8^+$ T cell responses can be monitored.

Keywords Melanoma, Tumor antigen, Neoantigen, $CD8^+$ T cell, Tumor immunity

1 Introduction

Over the last two decades, immunotherapy has emerged as a promising and viable treatment option for a diverse range of cancers. Among these, melanoma has proven to be particularly responsive to several types of immunotherapy, with cancer vaccines, checkpoint blockade, and adoptive cell therapy regimens each demonstrating success in clinical settings [1–3]. Though unique in their design, these interventions all ultimately harness the antitumor potential of $CD8^+$ cytotoxic T lymphocytes capable of recognizing and responding to cancer antigens. Understanding the nature of immune responses directed against such antigens is therefore critical to optimizing T cell-based immunotherapy and improving clinical outcomes for patients with melanoma and other cancers.

Kristian M. Hargadon (ed.), *Melanoma*, Methods in Molecular Biology, vol. 3089,
https://doi.org/10.1007/978-1-0716-5619-8_3,
© The Author(s), under exclusive license to Springer Science+Business Media, LLC, part of Springer Nature 2027

Since its discovery as a potential immunologic target, melanoma has been a focal point of research efforts aimed at identifying putative cancer antigens. One of the first classes of melanoma-associated antigens to be described is the family of melanocyte differentiation antigens (MDA) [4]. These tissue-specific antigens include epitopes derived from tyrosinase, tyrosinase-related protein 1/2, MART-1/Melan-A, and other proteins involved in the melanin biosynthesis pathway. Because expression of MDA is primarily restricted to cells of melanocytic origin, these antigens represent attractive targets of anti-melanoma immune responses since any reactivity against them carries minimal risk of inadvertent cross-reactivity against other tissue types. However, because MDA are shared between melanoma cells and normal melanocytes, issues of self-tolerance must be overcome in order to elicit robust antitumor immune responses against them.

Another class of shared tumor antigen frequently expressed by melanoma cells is the family of cancer/testis antigens, including NY-ESO-1, PRAME, and various MAGE family members [5]. These antigens, though expressed broadly during embryonic development, exhibit limited expression in adult tissues, where they are typically found only in immune privileged adult germ-line tissue. Because these embryonic genes are often reactivated in melanoma and other cancers, they too are amenable targets for antitumor immune responses, though mechanisms of self-tolerance may also limit their immunogenicity.

Finally, in an effort to overcome limitations imposed by various mechanisms of self-tolerance to shared tumor antigens, significant efforts have been made in recent years to target a third class of melanoma-specific neoantigens, which have emerged in the form of both novel, mutant protein-derived antigens as well as phosphopeptides that arise from proteins involved in aberrantly activated oncogenic pathways within melanoma cells [6]. Neoantigens have indeed proven to be highly immunogenic in melanoma patients [7], and tumor mutational burden/neoantigen load is a positive prognostic factor for melanoma patient response to various forms of immunotherapy [8–14]. Based on these observations, there is a growing desire in the field to better understand factors that regulate T cell reactivity against melanoma neoantigens.

Herein we describe a protocol for the generation and characterization of model antigen-expressing melanoma cell lines. Using an expression vector encoding the well-characterized chicken ovalbumin protein, we specifically validate this protocol as a means for engineering murine melanoma cell lines that express the H-2K^{b}-restricted OVA_{257} epitope as a model neoantigen. Included in this protocol are step-by-step procedures for characterizing expression of the OVA_{257} epitope by melanoma cells and for evaluating CD8^{+} T cell recognition of this antigen in both in vitro and in vivo experimental settings. Though our protocol is specific to engineering and evaluating this one model neoantigen in two variants of the B16 murine melanoma

cell line, it may easily be adapted for work with any cancer cell line and antigen of interest, and it therefore has broad applicability to any investigators wishing to pursue studies relevant to antitumor T cell immunobiology.

2 Materials

Store all media at 4°C in the dark. Store fetal bovine serum (FBS) and blasticidin selection antibiotic at −20°C in the dark. Store all other supplies at room temperature. Use only sterile reagents for cell culture work, and use nuclease-free, non-pyrogenic pipets and pipet tips for all work (*see* **Note 1**).

2.1 Cell Culture Media and Supplies

1. B16-F1 and D5.1G4 melanoma cell lines (*see* **Note 2**).
2. Complete growth medium for melanoma cell lines: Dulbecco's Modified Eagle's Medium (DMEM) containing 4 mM L-glutamine, 4500 mg/L glucose, 1 mM sodium pyruvate, and 1500 mg/L sodium bicarbonate, supplemented with 10% FBS.
3. Selection medium for transfected melanoma cell lines: Complete growth medium supplemented with 10 μg/ml blasticidin selection antibiotic (*see* **Note 3**).
4. Freezing medium: Complete growth medium supplemented with 5% dimethyl sulfoxide (DMSO).
5. Trypsin-EDTA Solution, 1×: 0.25% Trypsin/0.53 mM EDTA in Hanks Balanced Salt Solution without calcium or magnesium.
6. Endotoxin-free 1× phosphate buffered saline (PBS), pH 7.4.
7. Tissue culture-treated 96-well plates.
8. Tissue culture-treated 12-well plates.
9. Tissue culture-treated flasks (T25 and T75).
10. Nuclease-free, non-pyrogenic serological pipets and pipet tips.
11. Nuclease-free, non-pyrogenic 15 ml conical centrifuge tubes.
12. Nuclease-free, non-pyrogenic microcentrifuge tubes.
13. Tabletop centrifuge.
14. 0.4% trypan blue.
15. Hemocytometer.
16. Cryovials.
17. Light microscope.
18. Inverted light microscope.

2.2 Supplies and Reagents for Transfection of Melanoma Cells

1. Attractene Transfection Reagent.
2. pEF6-cOVA plasmid expression vector engineered to express cytoplasmic ovalbumin.
3. Opti-MEM I Reduced Serum Medium.

2.3 Supplies and Reagents for Characterization of OVA_{257} Expression and Presentation by Transfected Melanoma Cells

1. Recombinant murine interferon-γ (IFNγ).
2. APC-conjugated mouse H-$2K^b$ monoclonal antibody.
3. APC-conjugated mouse IgG2a, κ isotype control antibody.
4. APC-conjugated mouse H-$2K^b$-OVA_{257} (SIINFEKL epitope) monoclonal antibody (clone 25-D1.16).
5. APC-conjugated mouse IgG1, κ isotype control antibody.
6. BioLegend TruStain FcX™ PLUS (anti-mouse CD16/32) antibody.
7. FACS Buffer: 1× PBS supplemented with 2% FBS, 0.05% sodium azide, and 2 mM EDTA.
8. 96-well V-bottom plates.
9. Flow cytometry tubes.
10. Flow cytometer.

2.4 Supplies and Reagents for Characterization of Antigen-specific $CD8^+$ T Cell Recognition of OVA_{257} as a Model Neoantigen Presented by the H-$2K^b$ MHC Class I Molecule on Melanoma Cells

1. $RAG2^{-/-}$ OT-I TCR transgenic mice (8–10-week-old female mice).
2. CTL medium: RPMI-1640 Medium (1×) containing 2.05 mM L-glutamine, 10% FBS, 50 U/ml penicillin, 50 μg/ml streptomycin, 0.1 mM β-mercaptoethanol, 1 mM sodium pyruvate, 0.015 M HEPES, 1× MEM nonessential amino acids, 1× MEM essential amino acids. Adjust pH to 7.2–7.3 using 1 N NaOH.
3. Tissue homogenizer.
4. 70 μm cell strainer.
5. Nuclease-free, non-pyrogenic 15 ml conical centrifuge tubes.
6. Nuclease-free, non-pyrogenic 50 ml conical centrifuge tubes.
7. 10× Red Blood Cell Lysing Solution.
8. Sterile molecular biology grade H_2O.
9. Miltenyi Biotec $CD8a^+$ T Cell Isolation Kit.
10. Miltenyi Biotec MACS LS columns.
11. Miltenyi Biotec MidiMACS™ Separator and magnetic stand.
12. MACS Buffer: 1× PBS supplemented with 2% FBS and 2 mM EDTA.
13. 5-(and 6)-Carboxyfluorescein diacetate succinimidyl ester (CFSE): Reconstitute lyophilized CFSE with anhydrous dimethyl sulfoxide (DMSO) to a concentration of 10 mM

CFSE, and prepare single-use aliquots for storage (*see* **Note 4**).

14. 96-well U-bottom plates.
15. APC-conjugated mouse Thy1.2 (CD90.2) monoclonal antibody.

2.5 Additional Supplies and Reagents for Assessing H-2K^b-OVA$_{257}$ Recognition by CD8$^+$ T Cells in Melanoma Tumor-Bearing Mice

1. RAG2$^{-/-}$ OT-I TCR transgenic mice (8–10-week-old female mice).
2. Thy1.1 (CD90.1) congenic C57Bl/6 mice (8–10-week-old female mice).
3. 25G × 5/8 in. BD PrecisionGlide™ Needles.
4. 1 ml BD® Tuberculin Slip Tip syringes, sterile.
5. Infrared heat lamp.
6. Vortex.
7. Tailveiner® Restrainer for mice.
8. Kimwipes™.
9. Clotisol® Veterinary Blood Clotting Suspension.
10. Sterile dissecting instruments.
11. PE-conjugated mouse CD8α monoclonal antibody.
12. PerCP-Cy5.5-conjugated mouse Thy1.2 (CD90.2) monoclonal antibody.
13. APC-conjugated mouse CD69 monoclonal antibody.

3 Methods

Carry out all cell culture procedures in a biosafety cabinet to maintain sterility.

3.1 Routine Maintenance and Passaging of Cell Cultures

Maintain all cell lines at 37°C in a humidified incubator with 5% CO_2, and pass cell lines at 80%–90% confluency (*see* **Note 5**).

1. As cells require passaging, remove and discard cell culture medium from T75 flasks.
2. Add 4 ml 1× Trypsin-EDTA solution to flasks and return to cell culture incubator to promote cellular detachment (*see* **Note 6**).
3. Following cell detachment (this can be evaluated by observation under an inverted light microscope), neutralize Trypsin-EDTA solution with 10 ml of complete growth medium and transfer cells to a 15 ml conical centrifuge tube (*see* **Note 7**).
4. Centrifuge cells at 450× *g* for 5 min.

5. Decant supernatant and resuspend cells in an appropriate volume of complete growth medium.
6. Reseed new T75 flasks with necessary fraction of cells in a total volume of 15 ml of medium.
7. Use remaining cells as necessary for experimental work.

3.2 Determination of Appropriate Antibiotic Concentration for Selection of Plasmid Transfectants

Prior to transfecting cells with the antigen-encoding plasmid of interest, it is important to determine the optimal antibiotic concentration that should be used for selection of the cell lines that will be transfected. The protocol below describes this procedure when using blasticidin as a selection antibiotic for B16-derived melanoma cell lines.

1. Harvest melanoma cell line(s) as described in Sect. 3.1.
2. Following centrifugation of cells at 450 × *g* for 5 min, decant supernatant and resuspend cell pellet in an appropriate volume of complete growth medium.
3. Transfer 20 µl of cell suspension to one well of a 96-well plate, and mix with 20 µl 0.4% trypan blue.
4. Perform a live cell count on a light microscope using a hemocytometer and trypan blue exclusion (*see* **Note 8**).
5. After determining cell concentration, transfer a volume equivalent to $5.0e^4$ cells to a microcentrifuge tube. Repeat the setup such that there is one tube of cells for each antibiotic concentration that will be tested, and include as well a No Antibiotic control tube of cells.
6. Centrifuge cells at 450 × *g* for 5 min.
7. During the centrifugation in Step 6, prepare serial dilutions of selection antibiotic in complete growth medium. For blasticidin, prepare an 80 µg/ml solution in complete growth medium, and perform serial twofold dilutions to generate antibiotic concentrations of 40 µg/ml, 20 µg/ml, 10 µg/ml, and 5 µg/ml.
8. Following the centrifugation in Step 6, remove culture supernatant and resuspend cell pellets from individual tubes in 1 ml of the respective antibiotic dilutions prepared in Step 7. Resuspend the No Antibiotic control cells in 1 ml complete growth medium without selection antibiotic.
9. Plate the cells, now at a concentration of $5.0e^4$ cells/ml, in separate wells of a 6-well tissue culture-treated plate, and incubate at 37°C in a humidified incubator with 5% CO_2.
10. Observe cell growth daily, and replace media every 2 days with fresh media containing the appropriate concentration of selection antibiotic.

11. When the No Antibiotic control cells reach ~95% confluence, remove media from all wells, wash cells with 1 ml endotoxin-free 1× PBS, and trypsinize cells with 250 µl 1× Trypsin-EDTA solution.
12. Return culture plate to the 37°C incubator long enough for cells to detach (*see* **Note 6**).
13. Following cell detachment, neutralize trypsin with 1 ml complete growth medium, and centrifuge cells 450 × *g* for 5 min.
14. Perform a live cell count by trypan blue exclusion, and determine the lowest antibiotic concentration that kills 100% of cells to determine the concentration to use for selection during plasmid transfection in Sect. 3.3. For B16 melanoma cells and blasticidin, this appropriate antibiotic concentration for selection is 10 µg/ml (Fig. 1).

3.3 Transfection of Melanoma Cells with pEF6 Plasmid Vector Encoding Cytoplasmic Ovalbumin (pEF6-cOVA)

The protocol below is applicable to both the B16-F1 and D5.1G4 melanoma cell lines.

1. Harvest melanoma cells from culture as described in Sect. 3.1, and resuspend at a concentration of $1.6e^5$ cells/ml in complete growth medium.
2. Add 500 µl ($8.0e^4$ cells) to separate wells of a 24-well tissue culture plate. Set up three wells: one that will serve as an untransfected control, one that will serve as a mock transfection control, and one that will be transfected with the pEF6-cOVA plasmid (*see* **Note 9**).
3. Incubate cells overnight at 37°C in a humidified incubator with 5% CO_2.
4. The following morning, for each cell line to be transfected add 0.4 µg (0.4 µl of plasmid at a concentration of 1 µg/µl) of pEF6-cOVA plasmid encoding cytoplasmic ovalbumin into 59.6 µl of

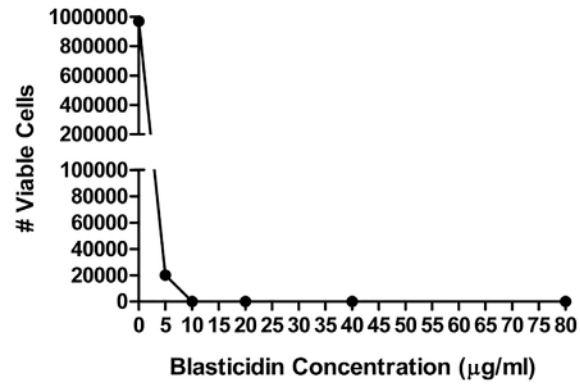


Fig. 1 Blasticidin dose–response curve for B16-F1 melanoma

Opti-MEM I Reduced Serum Medium in a microcentrifuge tube. Mix gently by flicking the tube several times. Set up a separate microcentrifuge tube for the mock transfection group, but simply add 60 µl of Opti-MEM I Reduced Serum Medium to this tube (do not add plasmid).

5. To the above tubes, add 1.5 µl of Attractene Transfection Reagent, mix gently by flicking the tubes several times, and incubate at room temperature for 15 min to allow formation of transfection complexes.
6. During the 15-min incubation period, remove medium from melanoma cultures in the 24-well plate, and wash once with fresh complete growth medium.
7. Discard the wash medium and replace with a fresh 500 µl of complete growth medium.
8. Add the transfection reagent mix with or without plasmid drop-wise onto the cells in the appropriate wells, gently swirling the culture plate after each drop to ensure uniform distribution of the transfection complexes.
9. Incubate cells overnight at 37°C in a humidified incubator with 5% CO_2.

3.4 Antibiotic Selection of Plasmid Transfectants

1. The following morning, aspirate medium from cultures and add 250 µl of 1× Trypsin-EDTA Solution.
2. Return culture plate to the 37°C incubator long enough for cells to detach.
3. Following cell detachment, neutralize trypsin by adding 1 ml of complete growth medium.
4. Transfer cells to a nuclease-free, non-pyrogenic 15 ml conical tube and centrifuge at 450 × *g* for 5 min.
5. Remove supernatant, resuspend cells in complete growth medium, and count cells using a hemocytometer.
6. Centrifuge cells at 450 × *g* for 5 min, discard supernatant, and resuspend at a concentration of $5.0e^4$ cells/ml in Selection Medium containing 10 µg/ml of blastocidin, as determined in Sect. 3.2.
7. Plate 1 ml of cell suspension ($5.0e^4$ cells) into separate wells of a 6-well tissue culture plate in order to seed cells at a low density (≤10% confluence) and culture at 37°C in a humidified incubator with 5% CO_2.
8. Replace Selection Medium in cultures daily to remove dead cells, and monitor cells for growth.
9. Once all untransfected and mock-transfected control cells have been killed (*see* **Note 10**), proceed to limited dilution cloning of polyclonal transfectants as described in Sect. 3.5 (*see* **Note 11**).

3.5 Limiting Dilution Cloning of Polyclonal Transfectants

1. Harvest polyclonal transfectants by trypsinization, and count viable cells under a light microscope using trypan blue exclusion.
2. Centrifuge cells at 450 × *g* for 5 min, discard supernatant, and resuspend at a concentration of 1.0e^5 cells/ml in Selection Medium containing blasticidin at a maintenance concentration of 5 μg/ml (*see* **Note 12**).
3. Perform serial dilutions to achieve a final concentration of 1 cell/400 μl in complete growth medium containing the maintenance concentration of blasticidin.
4. Plate 200 μl of diluted cells into each well of a 96-well tissue culture plate such that a single cell is deposited into approximately every other well (*see* **Note 13**). Incubate cultures at 37°C in a humidified incubator with 5% CO_2.
5. Monitor cultures daily under an inverted microscope, taking care to note which wells contain single cells (*see* **Note 14**).
6. As clones from single cells expand over time, collect clonal populations and scale up growth by transferring cells to 24-well tissue culture plates.
7. Once clones approach confluence in 24-well plates, collect cells and continue to scale up growth by transferring to T25 flasks.
8. When T25 flasks reach confluence, collect cells and divide into two equal aliquots. Centrifuge cells at 450 × *g* for 5 min and discard supernatant. Resuspend one aliquot in Freezing Medium and store at −80°C for future use. Use the second aliquot for characterization of OVA_{257} expression as described in Sect. 3.6.

3.6 Characterization of OVA_{257} Expression as a Model Neoantigen Presented by the H-2K^b MHC Class I Molecule on Melanoma Cells

1. Upon scaling up clonal populations of transfected cells for analysis, aliquot 1.0e^5 cells from each clone into two microcentrifuge tubes.
2. Centrifuge at 450 × *g* for 5 min, and discard supernatant.
3. For each clone to be analyzed, resuspend cell pellet from one tube in 500 μl complete growth media, and resuspend pellet from second tube in 500 μl complete growth media supplemented with 20 ng/ml recombinant murine IFNγ (*see* **Note 15**).
4. Plate cells in 12-well tissue culture plates, and incubate for 24 h at 37°C in a humidified incubator with 5% CO_2.
5. Collect cells by trypsinization using 250 μl of 1× Trypsin-EDTA Solution, and neutralize trypsin with 750 μl complete medium following detachment.
6. For each sample, transfer 250 μl to four separate wells of a 96-well V-bottom plate for flow cytometric staining.

7. Centrifuge plate at 450×*g* for 3 min at 4°C, and decant supernatant.
8. Fc block cells by resuspending pellets in 50 µl TruStain FcX™ PLUS (anti-mouse CD16/32) antibody diluted 1:50 in FACS Buffer (*see* **Note 16**).
9. Incubate cells at 4°C for 5 min.
10. Centrifuge plate at 450×*g* for 3 min at 4°C, and decant supernatant.
11. For each sample, resuspend pellets in 50 µl of the appropriate staining condition as outlined in Table 1.
12. Wrap plate in aluminum foil, and incubate at 4°C for 30 min (*see* **Note 17**).
13. Following this incubation, add 100 µl of FACS Buffer to all samples, and centrifuge plate at 450×*g* for 3 min at 4°C.
14. Decant supernatant, and wash cells 2× with 200 µl of FACS Buffer.
15. Resuspend cells in 250 µl of FACS Buffer, and collect each sample on a flow cytometer equipped with a 640 nm red laser and a 675/25 nm bandpass filter for fluorescence detection in the FL4 channel (*see* **Note 18**).
16. Use a consistent run speed for all samples.
17. Acquire desired number of cells for analysis.
18. Following sample collection, begin data analysis by creating a Forward Scatter/Side Scatter (FSC/SSC) dot plot, and draw a gate around all events that are not debris.
19. Create a histogram plot that displays FL4 fluorescence and that is gated on the FSC/SSC gate drawn in Step 18.
20. For each sample, generate an overlay that displays the appropriate isotype control histogram along with either the H-2K^b or H-2K^b-OVA$_{257}$ histogram, as shown in Fig. 2 for our analysis of wild-type B16-F1 and D5.1G4 melanoma cells as well as plasmid-transfected clones of these lines that we successfully

Table 1
Staining conditions for flow cytometric analysis of H-2K^b and H-2K^b-OVA$_{257}$ expression

	Antibody	Dilution
Group 1	Mouse IgG2a, κ APC	1:100
Group 2	H-2K^b APC	1:100
Group 3	Mouse IgG1, κ APC	1:100
Group 4	H-2K^b-OVA$_{257}$ APC	1:100

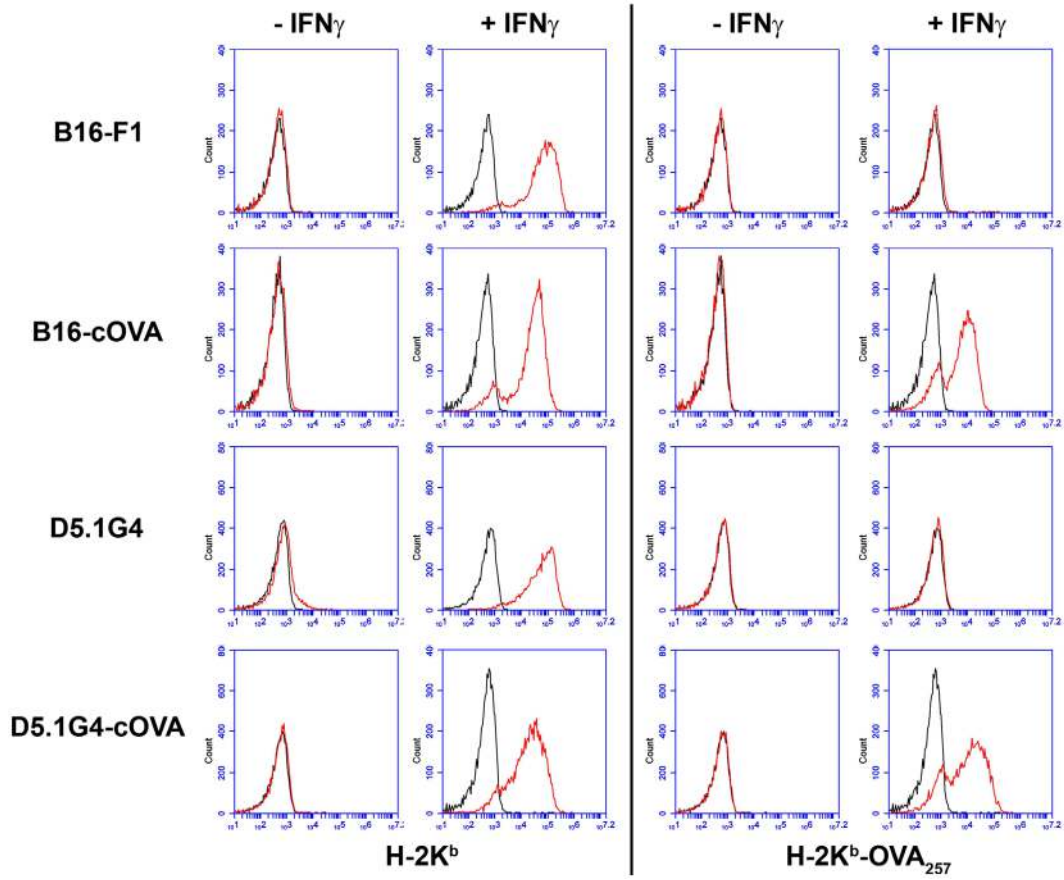


Fig. 2 Analysis of H-2K^b and H-2K^b-OVA$_{257}$ expression on melanoma cell lines. B16-F1, D5.1G4, and ovalbumin-encoding plasmid transfectants of these parental cell lines were left untreated or were pretreated for 24 h with IFNγ and then assayed for expression of H-2K^b and H-2K^b-OVA$_{257}$ complexes using flow cytometry. This figure is adapted from [15] with permission for reuse granted under the CC BY Creative Commons Attribution License (https://creativecommons.org/licenses/by/4.0/)

engineered with this protocol (and which we designate B16-cOVA and D5.1G4-cOVA, respectively).

3.7 Characterization of Antigen-Specific CD8$^+$ T Cell Recognition of OVA$_{257}$ as a Model Neoantigen Presented by the H-2K^b MHC Class I Molecule on Melanoma Cells

The protocol below takes advantage of the H-2K^b-OVA$_{257}$ specificity of CD8$^+$ T cells from OT-I TCR transgenic mice. For investigators interested in working with alternative model cancer antigens, other frequently employed TCR transgenic mouse systems include 2C TCR transgenic mice, which produce CD8$^+$ T cells specific for the H-2K^b-restricted model neoantigen SIYRYYGL, and P14 TCR transgenic mice, which produce CD8$^+$ T cells specific for an H-2D^b-restricted epitope of the lymphocytic choriomengitis virus GP33 protein, a commonly used system for evaluating immune responses to a model oncoviral antigen.

1. Harvest melanoma cells to be analyzed, and resuspend 1.0e^5 cells in 1 ml of complete growth medium with or without 20 ng/μl of recombinant murine IFNγ. Include blasticidin at a maintenance concentration of 5 μg/ml in cultures of transfected clones as well.
2. Incubate cells for 24 h at 37°C in a humidified incubator with 5% CO_2.
3. The next day, prior to collecting the cultured cells, isolate CD8$^+$ T cells by magnetic activated cells sorting and negative selection from the spleen of an 8–10-week-old female RAG2$^{-/-}$ OT-I TCR transgenic mouse.
    a. Place murine spleen into 5 ml CTL medium, and transfer to a tissue grinder for homogenization into a single-cell suspension.
    b. Moisten a 70 μm cell strainer placed over a 50 ml conical centrifuge tube, and pass splenic cell suspension through the filter to remove tissue debris.
    c. Rinse strainer with another 10 ml CTL medium.
    d. Centrifuge cells at 450 × *g* for 5 min, and decant supernatant.
    e. Resuspend cell pellet in 3 ml 1× RBC Lysing Solution (10× stock diluted 1:10 in molecular biology grade H_20), and incubate at room temperature for 4–5 min.
    f. Add 12 ml MACS Buffer, centrifuge cells at 450 × *g* for 5 min, and decant supernatant (*see* **Note 19**).
    g. Resuspend cells in 5 ml MACS Buffer, pass over another cell strainer, wash strainer with 20 ml MACS Buffer, and count cells.
    h. Centrifuge cells at 300 × *g* for 10 min, and aspirate supernatant completely.
    i. Resuspend cells in MACS Buffer at 4 μl buffer/1e^6 cells.
    j. From the Biotec CD8a$^+$ T Cell Isolation Kit, add 1 μl of Biotin-Antibody Cocktail/1e^6 cells, i.e., 1:4 ratio of antibody cocktail:buffer volume (*see* **Note 20**).
    k. Mix well, and incubate at 4°C for 5 min.
    l. Add 3 μl MACS Buffer/1e^6 cells.
    m. Add 2 μl Anti-Biotin MicroBeads/1e^6 cells.
    n. Mix well, and incubate at 4°C for 10 min.
    o. During the 10-min incubation, insert a MACS LS column in the magnetic field of a MidiMACS™ Separator on a magnetic stand, and prime the column with 3 ml of MACS Buffer, which should be collected in a waste tube.

p. Discard the waste tube and replace with a new 15 ml conical centrifuge collection tube.

q. Apply cell suspension to the column (bring to a volume of at least 500 µl/1.0e^8 cells with MACS Buffer if necessary), allowing unlabeled cells (representing the enriched T cells) to pass through (unwanted cells are bound by antibodies and are trapped in the column).

r. Wash the column with 3 ml MACS Buffer, and collect unlabeled cells (*see* **Note 21**).

s. Count purified CD8$^+$ T cells on a hemocytometer by trypan blue exclusion.

4. Label OT-I CD8$^+$ T cells with CFSE at a concentration of 1 µM (*see* **Note 22**).

   a. Centrifuge cells at 450 × *g* for 5 min, decant supernatant, and wash 2× in sterile, endotoxin-free 1× PBS to remove serum proteins that may interfere with dye labeling.

   b. Resuspend cells in 1× PBS at a concentration of no more than 1e^7 cells/ml.

   c. Add 1 µl/ml of 1 mM CFSE stock to stain cells at a concentration of 1 µM CFSE.

   d. Mix by vortexing, and incubate for 15 min at 37°C in a water bath in the dark.

   e. Quench unbound dye with four to five volumes of CTL medium.

   f. Wash cells 2× in CTL media, and then resuspend at a concentration of 1.0e^6 cells/ml in CTL medium.

5. 24 h post-plating/treatment of melanoma cells, collect cells by trypsinization using 250 µl of 1× Trypsin-EDTA Solution, and neutralize trypsin with 750 µl complete medium following detachment.

6. Wash cells twice with CTL medium, count cells on a hemocytometer by trypan blue exclusion, and resuspend at 5.0e^5 cells/ml in CTL medium.

7. Set up melanoma cell/OT-I cell cocultures by adding 100 µl of melanoma cells (5.0e^4 cells) and 100 µl of OT-I cells (1.0e^5 cells) to appropriate wells of a 96-well U-bottom cell culture plate.

8. Culture cells for 4 days at 37°C in a humidified incubator with 5% CO_2.

9. After 4 days of coculture, collect cells from culture wells and transfer to a 96-well V-bottom plate.

10. Centrifuge plate at 450×*g* for 3 min at 4°C, and decant supernatant.
11. Fc block cells as described in Steps 8–9 of Sect. 3.6.
12. Centrifuge plate at 450×*g* for 3 min at 4°C, and decant supernatant.
13. For each sample, resuspend pellets in 50 µl of FACS Buffer supplemented with APC-conjugated mouse Thy1.2 (CD90.2) monoclonal antibody at a 1:100 dilution (*see* **Note 23**).
14. Wrap plate in aluminum foil, and incubate at 4°C for 30 min.
15. Following this incubation, add 100 µl of FACS Buffer to all samples, and centrifuge the plate at 450×*g* for 3 min at 4°C.
16. Decant supernatant, and wash cells 2× with 200 µl of FACS Buffer.
17. Resuspend cells in 250 µl of FACS Buffer, and collect each sample on a flow cytometer equipped with a 488 nm blue laser and a 533/30 nm bandpass filter for fluorescence detection in the FL1 channel as well as a 640 nm red laser and a 675/25 bandpass filter for fluorescence detection in the FL4 channel.
18. Use a consistent run speed for all samples.
19. Acquire desired number of cells for analysis.
20. Following sample collection, begin data analysis by creating a Forward Scatter/Side Scatter (FSC/SSC) dot plot, and draw a lymphocyte gate.
21. Create a histogram plot gated that displays FL4 fluorescence and that is gated on the FSC/SSC gate drawn in Step 20.
22. Generate a second gate on Thy1.2+ cells.
23. Create another histogram plot that displays FL1 fluorescence and that is gated on the Thy1.2+ cells within the lymphocyte gate to assess CFSE dilution as a readout out of OT-I proliferation, as shown in Fig. 3 for our analysis of OT-I proliferation following coculture with B16-F1, D5.1G4, B16-cOVA, and D5.1G4-cOVA melanoma cells (*see* **Note 24**).

3.8 Assessing In Vivo H-2K^b-OVA$_{257}$ Recognition by OT-I Cells in Melanoma Tumor-Bearing Mice

This protocol can be used to establish whether the OVA_{257} model neoantigen is presented in the context of H-2K^b on engineered melanoma cells in vivo, and whether such antigen presentation persists over the course of tumor progression. It relies on an adoptive transfer system in which tumor-bearing mice are infused with H-2K^b-OVA_{257}-specific OT-I cells, which can subsequently be harvested and assessed for expression of CD69, a cell surface glycoprotein that is upregulated shortly after antigen recognition. We present here the application of this protocol within the context of a lung colonization

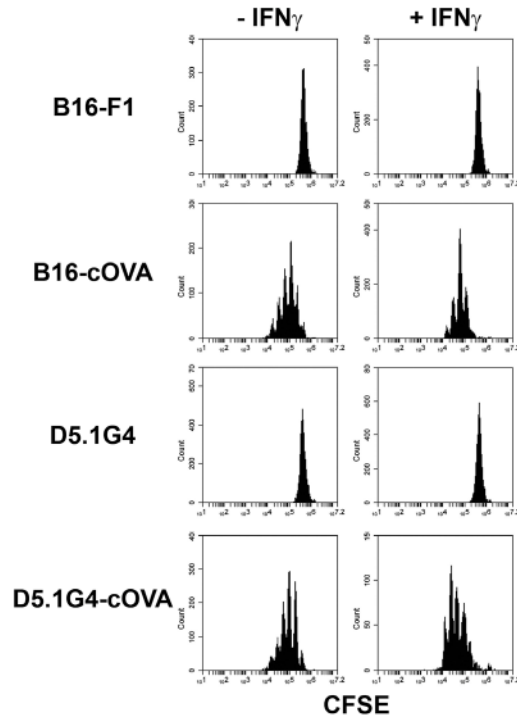


Fig. 3 Assessing OT-I recognition of H-2K^b-OVA$_{257}$ complexes on melanoma cell lines engineered to express the OVA$_{257}$ model neoantigen. B16-F1, D5.1G4, and ovalbumin-encoding plasmid transfectants of these parental cell lines were left untreated or were pretreated for 24 h with IFNγ and then cocultured for 4 days with CFSE-labeled H-2K^b-OVA$_{257}$-specific OT-I cells. Cultured cells were then collected, and Thy1.2+ T cells were assessed for CFSE dilution by flow cytometry. This figure is adapted from [15] with permission for reuse granted under the CC BY Creative Commons Attribution License (https://creativecommons.org/licenses/by/4.0/)

melanoma model, where OVA$_{257}$ antigen presentation is assessed in the lung-draining paratracheal lymph nodes of tumor-bearing mice. We have recently used this system to demonstrate that OVA$_{257}$ antigen derived from B16-cOVA and D5.1G4-cOVA is presented to OT-I cells in the context of both tumor-free and tumor-involved lymph nodes [15] (*see* **Note 25**).

1. Harvest melanoma cells from culture, and count cells on a hemocytometer by trypan blue exclusion.
2. Wash cells 2× in sterile, endotoxin-free 1× PBS.
3. Resuspend cells in sterile, endotoxin-free 1× PBS at a concentration of 2.0e^6 cells/ml.
4. Place Thy1.1 congenic C57Bl/6 mice to be injected under an infrared heat lamp for 5 min to promote vasodilation of the lateral tail vein (*see* **Note 26**).

5. Mix prepared melanoma cells by vortexing, draw an appropriate volume of cells into a 1 ml BD® Tuberculin Slip Tip syringe, and attach a 25G × 5/8 in. BD PrecisionGlide™ needle to the syringe (*see* **Notes 27 and 28**).
6. Place a mouse into a Tailveiner® Restrainer, and insert the plunger just far enough to restrict movement.
7. While holding the tail taut, insert the needle into the lateral tail vein, and inject the desired volume of cells (for the B16-cOVA and D5.1G4-cOVA melanoma lines we describe here, we challenge mice intravenously with $4.0e^5$ cells in a volume of 0.2 ml.
8. Upon removing the needle, if bleeding from the injection site continues after applying slight pressure with a Kimwipe™, apply a small amount of Clotisol® Veterinary Blood Clotting Suspension.
9. Following tumor challenge of individual mice, return the experimental animals to appropriate housing for the duration of the experiment.
10. At desired experimental time points post-tumor challenge, adoptively transfer $2.0e^6$ OT-I cells purified as described in Step 3 of Sect. 3.7 via the lateral tail vein into tumor-bearing mice (as well as nontumor-bearing control mice).
11. 24 h post-adoptive transfer, euthanize mice according to an IACUC-approved protocol, and dissect experimental animals to isolate the lung-draining paratracheal lymph node (*see* **Note 25**).
12. Transfer lymph nodes from individual mice to separate tissue homogenizers containing 1 ml of CTL medium.
13. Thoroughly homogenize lymph nodes to generate single-cell suspensions.
14. Pass single-cell suspensions of lymph node tissue through a 70 μm cell strainer attached to a 50 ml conical centrifuge tube in order to remove connective tissue debris.
15. Rinse the cell strainer with 4 ml of CTL medium, and transfer the single-cell suspension to a 15 ml conical centrifuge tube.
16. Centrifuge single-cell suspensions at 450 × *g* for 5 min, and decant supernatant.
17. Resuspend cell pellets in 250 μl of FACS Buffer, and transfer to a 96-well V-bottom plate.
18. Centrifuge plate at 450 × *g* for 3 min at 4°C, and decant supernatant.
19. Fc block cells as described in Steps 8 and 9 of Sect. 3.6.
20. Centrifuge plate at 450 × *g* for 3 min at 4°C, and decant supernatant.

21. For each sample, resuspend pellets in 50 µl of antibody cocktail (PE-conjugated mouse CD8α, PerCP-Cy5.5-conjugated mouse Thy1.2, and APC-conjugated mouse CD69 monoclonal antibodies, each diluted 1:100 in FACS Buffer).
22. Wrap plate in aluminum foil, and incubate at 4°C for 30 min (*see* **Note 17**).
23. Following this incubation, add 100 µl of FACS Buffer to all samples, and centrifuge plate at 450 × *g* for 3 min at 4°C.
24. Decant supernatant, and wash cells 2× with 200 µl of FACS Buffer.
25. Resuspend cells in 250 µl of FACS Buffer, and collect each sample on a flow cytometer equipped with a 488 nm blue laser and a 640 nm red laser, along with 585/40 nm, 670 LP, and 675/25 nm filters for fluorescence detection in the FL2, FL3, and FL4 channels, respectively (*see* **Note 18**).
26. Use a consistent run speed for all samples.
27. Acquire desired number of cells for analysis.
28. Following sample collection, begin data analysis by creating a Forward Scatter/Side Scatter (FSC/SSC) dot plot, and draw a lymphocyte gate.
29. Create a histogram plot gated that displays FL2 fluorescence and that is gated on the FSC/SSC gate drawn in Step 24.
30. Generate a second gate on the $CD8\alpha^+$ cells with positive FL2 fluorescence.
31. Create a 2D plot gated on the $CD8^+$ lymphocytes, and display FL3 fluorescence (for Thy1.2 detection) on the X-axis and FL4 fluorescence (for CD69 detection) on the Y-axis, as shown in Fig. 4 for our analysis of CD69 expression on Thy1.2+ OT-I cells from tumor-free controls as well as mice harboring B16-cOVA or D5.1G4-cOVA tumors for the indicated periods of time.

4 Notes

1. Pipet tips and serological pipets should be certified nuclease-free and non-pyrogenic. Nuclease-free tips are critical in order to avoid degradation of plasmid DNA during transfection of melanoma cells. Additionally, pyrogen exposure may alter gene expression/cellular behavior and could therefore influence downstream experimental outcomes when assessing T cell responses to engineered melanoma cells. It is also recommended that filter tips be used

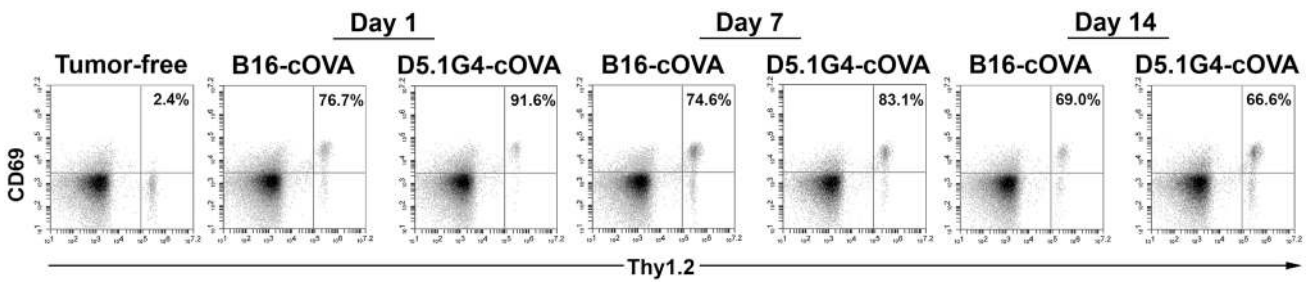


Fig. 4 Assessing OT-I recognition of melanoma-derived OVA_{257} neoantigen in tumor-bearing animals. Thy1.2+ OT-I cells were adoptively transferred into Thy1.1 congenic C57Bl/6 mice bearing B16-cOVA or D5.1G4 melanoma in the lungs for the indicated number of days. Lung-draining paratracheal LN were harvested 24 h post-adoptive transfer, and single-cell suspensions were stained for flow cytometric analysis of CD69 expression as a readout of OVA_{257} antigen recognition. Plots are gated on $CD8^+$ lymphocytes, and percentages in the upper right corner indicate the percentage of Thy1.2+ OT-I cells that are CD69+. This figure is adapted from [15] with permission for reuse granted under the CC BY Creative Commons Attribution License (https://creativecommons.org/licenses/by/4.0/)

for micropipettes in order to avoid cross contamination of samples.

2. The melanoma cell lines reported herein are of murine origin. B16-F1 is a commonly used melanoma model and is a highly aggressive, immunosuppressive, and lymph node-invasive cell line [15–19]. D5.1G4 is a chemically mutated variant of B16 melanoma that is poorly tumorigenic, less immunosuppressive, and lymph node-noninvasive [18–20].
3. The pEF6 vector encoding cytoplasmic ovalbumin carries a blasticidin resistance gene for selection of plasmid transfectants. The concentration of selection antibiotic should be determined empirically for specific cell lines as described in Sect. 3.2. The 10 μg/ml dose of blasticidin described here is specific for selection against untransfected B16-F1 melanoma cells (Fig. 1). In general, the lowest antibiotic dose that effectively kills 100% of untransfected cells should be used for selection of transfectants. Once the selection antibiotic has successfully killed 100% of untransfected control cells, its concentration in selection medium can be reduced by half (in our case to 5 μg/ml blasticidin) as a maintenance concentration.
4. Use CFSE within 6 months of reconstitution and avoid repeated freeze–thaw cycles to maintain consistency in CFSE labeling intensity. CFSE is light-sensitive and should be stored in the dark.
5. Do not allow cell lines to reach 100% confluency during routine maintenance, as this may result in contact inhibition, which can in turn interfere with downstream cell transfectability and behavior during experiments. As a guideline for passaging of cell lines, B16-F1 cells can be split 1:10 every 2 days or 1:30 every 3 days. D5.1G4 cells can be split 1:5 every 3 days or 1:10 every 4 days.
6. The duration of trypsinization is cell-line dependent and should be only long enough to promote cell detachment. As a recommendation for cell lines described in this procedure, trypsinize B16-F1 cells for 2–3 min and D5.1G4 cells for 5 min. If necessary, lightly tap the flasks to dislodge any cells that remain adherent. Avoid repeated or strong tapping of the flasks, however, so as not to promote clumping of trypsinized cells.
7. FBS proteins in the complete growth medium serve as targets for trypsin and prevent overreactivity against cell membrane proteins.
8. Cell viability should be >95% under standard culture conditions.

9. Cells should be ~75% confluent at the time of transfection. Seeding at this density will achieve this level of confluence when working with B16-F1 and D5.1G4 melanoma cells.
10. For B16-F1 and D5.1G4 melanoma cells, all control untransfected and mock-transfected cells are typically killed within 4–5 days of blasticidin selection.
11. We have sometimes found it necessary to extend the length of culture time for polyclonal transfectants an additional week before performing limited dilution cloning in order to ensure stable transfection. If no clones are recovered following a first round of limited dilution cloning, it is likely that the procedure was performed prior to plasmid integration, and cells that lost the plasmid were ultimately killed by the maintenance concentration of antibiotic. We recommend maintaining an ongoing culture of polyclonal transfectants while attempting to generate individual clones so that limited dilution cloning can be performed after an extended culture if necessary. Alternatively, polyclonal transfectants can be transferred to Freezing Medium and stored at −80°C for later recovery and extended culture should the limited dilution cloning procedure need to be repeated.
12. Due to blasticidin's toxicity, it is best to limit cell exposure to the full-strength selection concentration for as brief a time as is necessary to ensure successful transfection. Reducing the concentration of blasticidin to a maintenance level following successful transfection reduces unnecessary stress while ensuring that cells remain stably transfected (should the plasmid be retained as an independent episome rather than integrating into the host genome).
13. Plating cells in this way will necessarily result in some wells receiving no cells but will also reduce the likelihood of introducing more than one cell into a given well and thus yielding a non-clonal population. The number of plates loaded will likely depend on the melanoma cell line being used, as some cell lines are more easily cloned by limiting dilution than others. B16-F1 grows relatively well from single cells, and we typically generate 15–20 clones per 96-well plate when using this procedure. D5.1G4 melanoma cells, on the other hand, are more difficult to clone from single cells, and we typically generate only five to ten clones per 96-well plate. Because the growth and survival of some melanoma cell lines depend more heavily on cell–cell contact, clonal populations may not always be easily generated from single cells, and it may therefore be necessary to load several plates in order to generate a sufficient number of clones for analysis.

14. In many cases, it will be possible to visualize single cells that have adhered to the tissue culture plate. In some instances, though, cells may not be detected until a small colony forms, but it is important to identify these wells as soon as possible after plating. Effort should be made to avoid collecting cells from wells where two or more cells were originally deposited, as these wells will not yield true clonal populations. Therefore, identifying wells with individual cells or single, small colonies early will reduce the unwanted outcome later of finding a well with a large patch of cells that might actually represent two or more colonies that have grown together.
15. Some melanoma cell lines express no/low levels of class I MHC molecules under steady-state cell culture conditions. Pretreatment of cells with IFNγ prior to analysis may be necessary to induce MHC class I expression on such cells.
16. Fc blocking is necessary to prevent nonspecific antibody binding to cells that might express Fc receptors. Though this is most critical when analyzing certain immune cell populations, this blocking step is good practice, as other cell populations may also express low levels of Fc receptors, and nonspecific binding of experimental antibodies to such receptors will produce false-positive signals during analysis of flow cytometric data.
17. It is important to wrap plates in aluminum foil so that staining is performed in the dark. This practice prevents photobleaching of light-sensitive fluorochromes. Staining at 4°C rather than room temperature also reduces the likelihood of internalization of cell surface proteins.
18. Should it be necessary to delay sample acquisition, cells can be fixed by resuspending pellets in 100 µl of 2% paraformaldehyde and incubating at room temperature for 15 min. Following fixation, samples should be centrifuged at 450 × *g* for 3 min at 4°C so that the paraformaldehyde can be removed. Cells should then be resuspended in 200 µl of FACS Buffer and stored at 4°C in the dark until sample acquisition on a flow cytometer is possible. We recommend collecting samples as soon as possible and not storing them for more than 2 days.
19. MACS Buffer and cells should be kept on ice during the enrichment procedure to prevent cell surface receptor internalization and to promote more efficient binding of antibodies from the enrichment cocktail.
20. This kit utilizes a cocktail of biotin-conjugated antibodies against CD4, CD11b, CD11c, CD19, CD45R (B220), CD49b (DX5), CD105, Anti-MHC-class II, Ter-119, and TCRγ/δ, such that cell populations expressing these

biomarkers will be bound by magnetic anti-biotin microbeads and trapped within the MACS column during magnetic cell sorting. In this way, unlabeled CD8α$^+$ T cells can be enriched from the heterogeneous splenic population by negative selection.

21. We typically achieve >95% CD8$^+$ T cell purity by this protocol. If this level of purity is not achieved, or if greater purity is desired by the end user, the negatively selected sample collected from the first MACS LS column can be passed through a second primed MACS LS column.
22. To evaluate OT-I recognition of H-2K^b-OVA$_{257}$ complexes on engineered melanoma cell clones, we describe here a coculture system in which OT-I proliferation is assessed flow cytometrically by measuring dilution of CFSE, the fluorescent intensity of which is halved with each division of cells that have been pre-labeled with the dye.
23. Thy1.2 (CD90.2) is a cell surface glycoprotein expressed at high levels on murine T cells. It is being used here to stain OT-I cells so that during flow cytometric analysis they can be distinguished from the melanoma cells with which they were cocultured. Alternatively, users might also use an antibody directed against CD8 for this purpose.
24. Because some melanoma cells lines express very low cell surface H-2K^b expression under steady-state culture conditions, it is possible that the steady-state expression of H-2K^b-OVA$_{257}$ complexes will be below the level of detection by flow cytometric antibody staining without prior IFNγ treatment (as we demonstrate in Fig. 2). Nevertheless, such complexes may still be expressed at levels that are sufficient for recognition by highly sensitive OT-I cells even without prior IFNγ induction, as we demonstrate in Fig. 3 for the B16-cOVA and D5.1G4-cOVA melanoma cell lines.
25. For users who prefer to study CD8$^+$ T cell responses in the context of subcutaneous tumor challenge models, this protocol can easily be adapted to evaluate CD69 upregulation on adoptively transferred OT-I cells harvested from lymph nodes draining common subcutaneous tumor challenge sites, i.e., the axillary/brachial lymph nodes for tumors introduced in the nape of the neck and the ipsilateral inguinal lymph node for tumors introduced in the flank. We note that many investigators also study murine melanoma outgrowth following subcutaneous challenge in the flank or nape of the neck.
26. We recommend the use of Thy1.1 congenic mice in this setting so that adoptively transferred Thy1.2$^+$ OT-I cells can easily be distinguished from endogenous CD8$^+$ T cells during flow cytometric analysis.

27. Ensure that there are no air bubbles in the syringe.
28. Work quickly to perform tumor challenge before melanoma cells begin to settle so that the intended number of cells are injected.

Acknowledgments

D5.1G4 murine melanoma cells were a generous gift of Dr. Jerry Neiderkorn (University of Texas Southwestern Medical School). The pEF6 expression vector encoding cytoplasmic chicken ovalbumin was a generous gift of Dr. Timothy Bullock (University of Virginia School of Medicine). This work was supported by funding from Virginia's Commonwealth Health Research Board, a Jeffress Trust Awards Program in Interdisciplinary Research Grant from the Thomas F. and Kate Miller Jeffress Memorial Trust (Bank of America, N.A., Trustee), and a Hampden-Sydney College Research Grant from the Arthur Vining Davis endowment. We thank Mrs. Patricia Hargadon and Mr. Michael Hargadon for generous donations to support the involvement of a Hampden-Sydney College undergraduate student in this research.

Competing Interests The authors have no conflicts of interest to declare that are relevant to the content of this chapter.

References

1. Hargadon KM (2017) Strategies to improve the efficacy of dendritic cell-based immunotherapy for melanoma. Front Immunol 8:1594. https://doi.org/10.3389/fimmu.2017.01594
2. Hargadon KM, Johnson CE, Williams CJ (2018) Immune checkpoint blockade therapy for cancer: an overview of FDA-approved immune checkpoint inhibitors. Int Immunopharmacol 62:29–39. https://doi.org/10.1016/j.intimp.2018.06.001
3. Soleymanitabar A, Keshavarz-Fathi M, Hargadon KM, Rezaei N (2023) Immunotherapy for cutaneous melanoma. In: Rezaei N (ed) Handbook of cancer and immunology. Springer, Cham, pp 1–35. https://doi.org/10.1007/978-3-030-80962-1_237-1
4. Pitcovski J, Shahar E, Aizenshtein E, Gorodetsky R (2017) Melanoma antigens and related immunological markers. Crit Rev Oncol Hematol 115:36–49. https://doi.org/10.1016/J.CRITREVONC.2017.05.001
5. Tio D, Kasiem FR, Willemsen M et al (2019) Expression of cancer/testis antigens in cutaneous melanoma: a systematic review. Melanoma Res 29:349–357. https://doi.org/10.1097/CMR.0000000000000569
6. Xie N, Shen G, Gao W et al (2023) Neoantigens: promising targets for cancer therapy. Signal Transduct Target Ther 8:9. https://doi.org/10.1038/s41392-022-01270-x
7. Ott PA, Hu Z, Keskin DB et al (2017) An immunogenic personal neoantigen vaccine for patients with melanoma. Nature 547:217–221. https://doi.org/10.1038/nature22991
8. Snyder A, Makarov V, Merghoub T et al (2014) Genetic basis for clinical response to CTLA-4 blockade in melanoma. N Engl J Med 371:2189–2199. https://doi.org/10.1056/NEJMOA1406498
9. Van Allen EM, Miao D, Schilling B et al (2015) Genomic correlates of response to CTLA-4 blockade in metastatic melanoma. Science 350:207–211. https://doi.org/10.1126/science.aad0095
10. Hugo W, Zaretsky JM, Sun L et al (2016) Genomic and transcriptomic features of response to anti-PD-1 therapy in metastatic

melanoma. Cell 165:35–44. https://doi.org/10.1016/j.cell.2016.02.065
11. Hodi FS, Wolchok JD, Schadendorf D et al (2021) TMB and inflammatory gene expression associated with clinical outcomes following immunotherapy in advanced melanoma. Cancer Immunol Res 9:1202–1213. https://doi.org/10.1158/2326-6066.CIR-20-0983
12. Andrews MC, Li G, Graf RP et al (2024) Predictive impact of tumor mutational burden on real-world outcomes of first-line immune checkpoint inhibition in metastatic melanoma. JCO Precis Oncol 8:e2300640. https://doi.org/10.1200/PO.23.00640
13. Lauss M, Donia M, Harbst K et al (2017) Mutational and putative neoantigen load predict clinical benefit of adoptive T cell therapy in melanoma. Nat Commun 8:1–11. https://doi.org/10.1038/S41467-017-01460-0
14. Levi ST, Copeland AR, Nah S et al (2022) Neoantigen identification and response to adoptive cell transfer in anti–PD-1 naïve and experienced patients with metastatic melanoma. Clin Cancer Res 28:3042–3052. https://doi.org/10.1158/1078-0432.CCR-21-4499
15. Hargadon KM, Goodloe TB, Woodall SL (2025) Lymph node invasion by melanoma cells is not required for the induction of incomplete differentiation by tumor-specific CD8+ T cells. Cancer Rep 8:e70145. https://doi.org/10.1002/CNR2.70145
16. Fidler IJ, Gersten DM, Budmen MB (1976) Characterization in vivo and in vitro of tumor cells selected for resistance to syngeneic lymphocyte-mediated cytotoxicity. Cancer Res 36:3160–3165
17. Overwijk WW, Restifo NP (2001) B16 as a mouse model for human melanoma. Curr Protoc Immunol. https://doi.org/10.1002/0471142735.im2001s39
18. Hargadon KM, Forrest OA, Reddy PR (2012) Suppression of the maturation and activation of the dendritic cell line DC2.4 by melanoma-derived factors. Cell Immunol 272:275–282. https://doi.org/10.1016/j.cellimm.2011.10.003
19. Hargadon KM, Bishop JD, Brandt JP et al (2016) Melanoma-derived factors alter the maturation and activation of differentiated tissue-resident dendritic cells. Immunol Cell Biol 94:24–38. https://doi.org/10.1038/icb.2015.58
20. Knisely TL, Niederkorn JY (1990) Immunologic evaluation of spontaneous regression of an intraocular murine melanoma. Invest Ophthalmol Vis Sci 31:247–57

Part II

2D Cell Culture-Based Approaches for Studying Melanoma Biology



Chapter 4

A Fluorescence-Based Assay for Measuring Glucose Uptake in Living Melanoma Cells

Jelena Grahovac, Marijana Pavlović, Kristina Živić and Marija Ostojić

Abstract

Melanoma cells have high glycolytic capacity. Glucose uptake is a key rate-limiting step in glucose utilization. Here we describe a simple protocol for measuring direct glucose uptake in living melanoma cells by flow cytometry.

Keywords Melanoma, 2-NBDG, Glucose uptake, Flow cytometry

1 Introduction

Melanoma cells have high metabolic plasticity that sustains tumor growth and metastasis. About 50% of melanomas harbor BRAFV600E mutation that enhances glucose metabolism and represses oxidative phosphorylation [1, 2]. Increased expression of glucose transporter isoform 1 (GLUT1) enhances melanoma metastatic potential [3], and melanoma cells can metabolize glucose into lactose even in the presence of oxygen in the process of aerobic glycolysis [4]. Therefore, studying glucose metabolism and targeting metabolic flexibility in melanoma is of great interest and is an area of extensive research [5–8]. Here we describe a simple protocol for measuring glucose uptake in melanoma cells by flow cytometry. 2-NBDG (2-(*N*-(7-Nitrobenz-2-oxa-1,3-diazol-4-yl)Amino)-2-Deoxyglucose) is a fluorescent glucose analog [9] that is taken up by the glucose transporters but is not metabolized and accumulates in living cells [10]. It can be used for direct measurement of glucose uptake in single living melanoma cells. Given its emission peaking near 540 nm (green), it can also be combined with various dyes for multi-parametric imaging, provided they do not have significant spectral overlap or interfere with metabolic activity [11].

Kristian M. Hargadon (ed.), *Melanoma*, Methods in Molecular Biology, vol. 3089,
https://doi.org/10.1007/978-1-0716-5619-8_4,
© The Author(s), under exclusive license to Springer Science+Business Media, LLC, part of Springer Nature 2027

2 Materials

1. Melanoma cell lines: A375 (ATCC CRL-161), HTB-140 (ATCC HTB-140), and 518a2 (procured through inter-laboratory exchange).
2. 25 cm^2 cell culture flasks: polystyrene-treated, with filter caps, for adherent cells.
3. 15 ml conical centrifuge tubes.
4. 6-well cell culture plates.
5. Complete nutrient medium: Roswell Park Memorial Institute (RPMI) 1640 containing 2 g/L D-glucose, pH 7.2. Add fetal calf serum (FCS) to a final 10% and Penicillin–Streptomycin solution to a final concentration of 100 U/ml penicillin and 100 μg/ml streptomycin. Store at 4°C.
6. Phosphate-buffered saline (PBS), sterile-filtered. Store at 4°C.
7. Dissociation buffer: 0.25% Trypsin with 0.5 mM EDTA. Store at 4°C.
8. 10 mM 2-NBDG: Dissolve 1 mg of 2-NBDG (Mw 342.26) in 292.17 μL DMSO to get 10 mM stock solution and filter through 0.2 μm filter. The solution should be clear bright yellow-orange. We aliquot and store the stock solution at −20°C for up to 1 year (*see* **Note 1**).
9. Optional: MitoTracker Red CMXRos dye (M7512, Invitrogen) for concomitant measurement of glucose uptake and the status of active mitochondria.
10. Flow cytometer with FL-1/FITC (green fluorescence) channel (Ex/Em 485/535 nm) for detection of 2-NBDG. For concomitant detection of active mitochondria with MitoTracker Red, the flow cytometer will also need to be equipped with an additional red channel, preferably FL-3. For the procedures described herein, we used a BD Calibur flow cytometer with Cell Quest computer software (Becton Dickinson, Heidelberg, Germany) and a LongCyte flow cytometer with Model Flower computer software (Challen Biotechnology, Beijing, China).
11. Flow cytometry. 5 ml round-bottom tubes.

3 Methods

3.1 Cell Culture and Treatment

1. Culture melanoma cells in complete nutrient medium in 25 cm^2 cell culture flasks, at 37°C in an incubator with a humidified atmosphere of 5% CO_2. Pay attention to the level of glucose in

the medium (we use 2 g/L), and if comparing glucose uptake between the cell lines, culture cells under the same conditions.

2. After the cells have reached 80% confluence, subculture cells for experimentation.
3. Seed 200,000 cells per well into 6-well culture plates in 2 ml of RPMI per well. Make sure that cells are equally distributed across the well surface as single cells.
4. Allow cells to adhere overnight.
5. The next day, prepare working solution of 20 μM 2-NBDG in RPMI (*see* **Notes 2 and 3**).
6. Design experimental conditions according to the desired investigation:
   a. For comparing glucose uptake between cell lines, set up unstained samples (negative control; with only RPMI) and stained samples (treated with 2-NBDG) for every cell line.
   b. For examining the effect of drugs on direct glucose uptake in a given cell line, add an appropriate concentration of the drug into the 2-NBDG working solution. In the example given here, we treated A375 cells with 50 μM pioglitazone hydrochloride, which stimulates glucose uptake [12] and is a candidate for drug repurposing in oncology [13]. If the viability of cells in the presence of the drug tested is a concern (*see* **Note 4**).
   c. For co-staining of active mitochondria, set up an unstained sample, single-stained controls, and the combination-stained sample. In the example given here, we first stained cells for 30 min at 37°C with 1 μM MitoTracker Red CMXRos in medium alone or in the presence of 50 μM pioglitazone hydrochloride and then washed off the stain before commencing with the incubation with 2-NBDG.
7. Aspirate the medium from the 6-well plate, and add 1 ml of working 2-NBDG solution per well.
8. Incubate cells for 1 h in a 37°C incubator with a humidified atmosphere of 5% CO_2 (*see* **Note 3**).
9. After incubation, remove the 2-NBDG solution and wash the cells with 2 ml of PBS.
10. Add 0.5 ml of 0.25% Trypsin-0.5 mM EDTA per well, and incubate at 37°C until the cells round up and detach. Depending on the cell line, start with 5 min and observe under the microscope.
11. Neutralize Trypsin-EDTA by adding 2 ml of RPMI. Gently disperse by pipetting up and down to obtain a single-cell suspension.

12. Transfer cell suspension to a 15 ml centrifuge tube, and centrifuge at 400 × *g* for 5 min at room temperature.
13. Carefully discard supernatant without disturbing the cell pellet.
14. To wash the pellet, add 1 ml of PBS, and resuspend by gently pipetting up and down.
15. Centrifuge at 400 × *g* for 5 min at room temperature.
16. Resuspend the cells in 1 ml of PBS, transfer to a flow tube and keep on ice until measurement on the Flow cytometer. For the highest fluorescence signal, analyze cells immediately, as 2-NBDG decomposes into nonfluorescent derivative over time [14, 15] (*see* **Note 5**).

3.2 Flow Cytometric Analysis of Glucose Uptake

3.2.1 Flow Cytometry Set Up

1. Prepare the flow cytometer for analysis.
2. Fluorescence of 2-NBDG can be detected in the FL-1/FITC (green fluorescence) channel (Ex/Em 485/535 nm) (*see* **Note 6**).
3. Set the acquisition to 20,000 events for each sample.
4. By adjusting FSC and SSC parameters, position cell population at the center of the FSC/SSC plot, and gate out debris (Fig. 1).
5. Set the laser so that the unstained sample positions on the left side of the histogram plot. The stained sample should have the highest peak around the center of the X-axis (around 10^2) (Fig. 2).
6. After the parameters are set for the first recorded cell line, proceed to other samples (unstained and stained or untreated and treated with the drug of interest) and collect them without any further adjustments.

3.2.2 Comparison of Glucose Uptake Between the Cell Lines

1. Overlay histograms of the unstained and stained samples for each cell line, and set the gate (M1) to collect the signal from the stained sample (Fig. 2). Export statistics. For quantification, we use the mean fluorescence intensity of an event in the gate M1 (Table 1, *see* **Note 7**).
2. For creating the image for illustration, overlay all the stained samples for each cell line (Fig. 3A). Perform three biological replicates of the experiment, and plot the average of the mean (We use PRISM 7 from GraphPad for plotting and statistical analysis) (Fig. 3B). When comparing multiple cell lines, we use

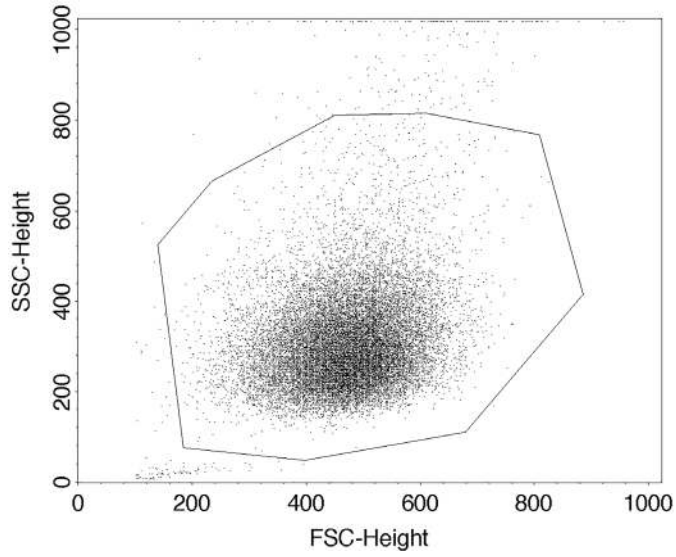


Fig. 1 Scatter plot and gating of A375 cells incubated with 2-NBDG

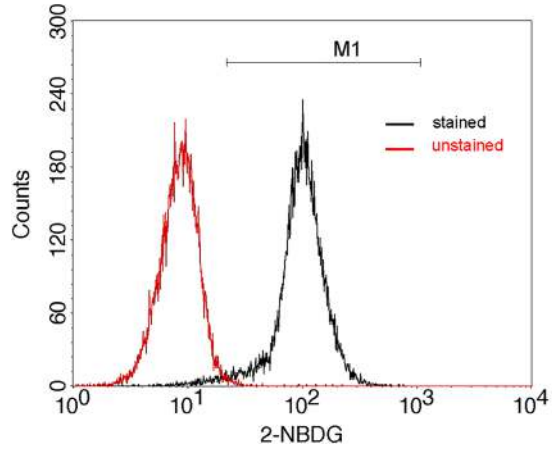


Fig. 2 Overlay of histograms for unstained and 2-NBDG stained A375 line and example of the M1 gate

Table 1
Example of the exported statistics for the graph in Fig. 3A

Cell line	Events	% Gated	Mean	CV	Median	Peak Ch
A375	19,669	99.51	105.83	46.58	98.22	98
518a2	19,362	98.97	109.08	55.57	101.82	110
HTB-140	19,718	99.68	63.61	57.78	56.23	59

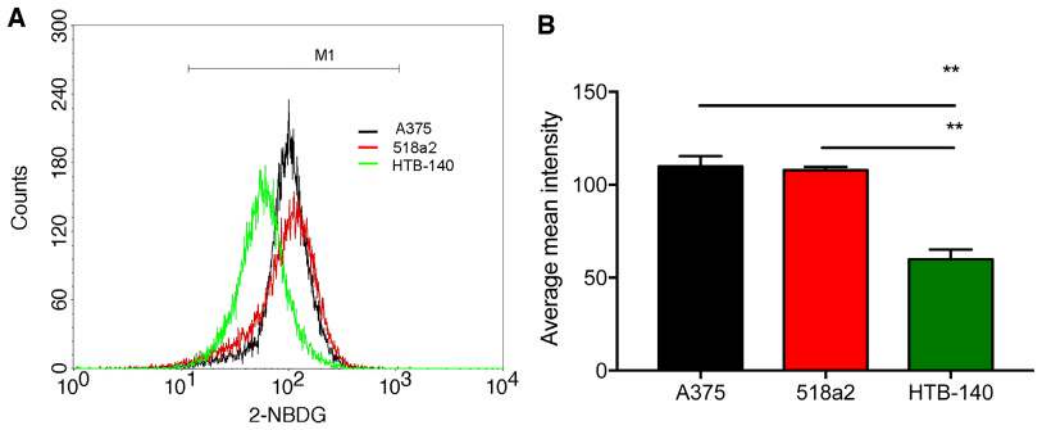


Fig. 3 (**A**), Overlay of 2-NBDG histograms for the three cell lines and example of the M1 gate. (**B**), Quantification of the average fluorescent intensity per cell from biological replicates of the experiment. $^{**}p < 0.005$ One-way ANOVA with Tukey's multiple comparisons test

one-way ANOVA and Tukey's multiple comparisons test (*see* **Note 8**).

3.2.3 Measurement of the Effects of Drugs on Glucose Uptake

1. Overlay histograms of the untreated (control) and treated (pioglitazone) samples to observe the shift, and set the gate (M1) to collect the signal from both (Fig. 4A).
2. Export statistics for each treatment separately. For quantification, we use the mean fluorescence intensity of an event in the gate M1 (Table 2, *see* **Notes 7, 9, and 10**).
3. Perform three biological replicates of the experiment, and plot the average of the mean. We use PRISM 7 from GraphPad for plotting and statistical analysis (Fig. 4B). When comparing control versus treated, we use Unpaired *t*-test. When comparing multiple treatments, we use one-way ANOVA and Tukey's multiple comparisons test.

3.2.4 Concomitant Detection of Glucose Uptake and Active Mitochondria

MitoTracker Red CMXRos dye accumulates in active mitochondria dependent on the mitochondrial membrane potential and can be detected in both FL-2 (PE) and FL-3 (PerCP) channels. Dual staining with MitoTracker Red and 2-NBDG allows live-cell analysis of the relationship between mitochondrial function and cellular glucose metabolism. However, bright 2-NBDG signal can also spillover into both FL-2 and FL-3 channels. We recommend collection of the MitoTracker Red CMXRos signal in the FL-3 channel (PerCP), as it is distinct enough to allow specific quantification in co-stained samples (Fig. 5).

1. Set up laser power based on the unstained control and single-stained controls in untreated cells. In the example given

Table 2
Example of the exported statistics for the graph in Fig. 4A

A375	Events	% Gated	Mean	CV	Median	Peak Ch
Control	19,092	97.49	12.58	38.15	11.76	11
Pioglitazone	17,213	88.38	28.62	34.26	28.13	33

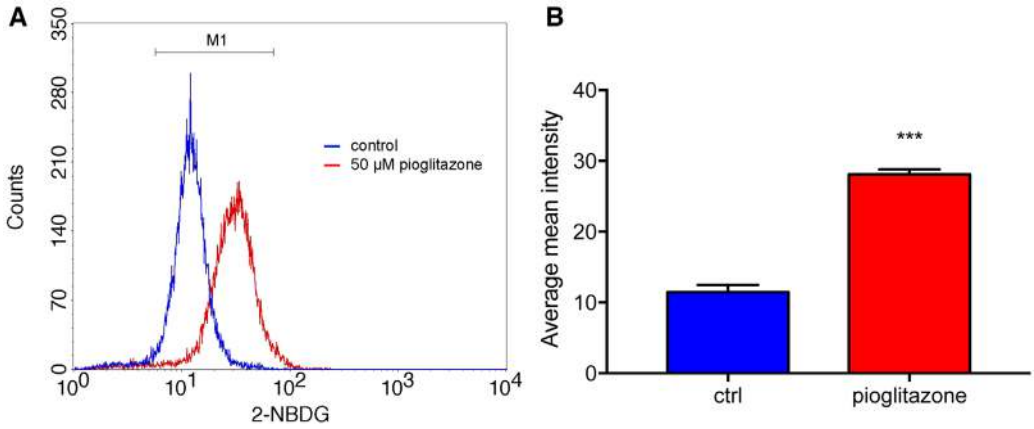


Fig. 4 (**A**), Overlay of 2-NBDG histograms of untreated (ctrl) and pioglitazone-treated A375 cells. (**B**), Quantification of the average fluorescent intensity per cell from biological replicates of the experiment. $^{**}p < 0.005$ Unpaired *t*-test

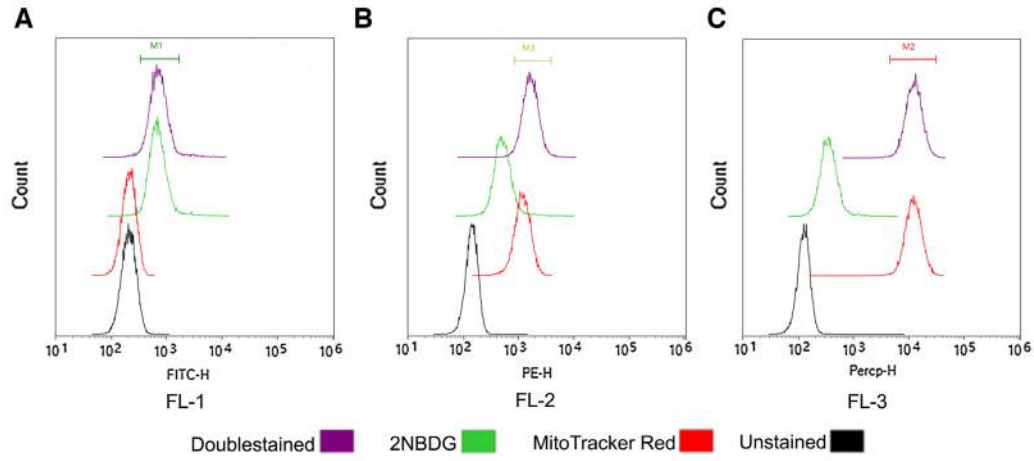


Fig. 5 Histogram overlays of the fluorescence of the unstained, 2-NBDG-stained, MitoTracker Red-stained, and double-stained A375 cells in FL-1 (**A**), FL-2 (**B**), and FL-3 (**C**) channels

in Fig. 6, we treated the cells with 50 μM pioglitazone. Pioglitazone increases glucose uptake (Fig. 6A) and induces transient mitochondrial membrane depolarization, observed as a decrease in MitoTracker Red fluorescence (Fig. 6B).

2. Overlay histograms for the untreated (control) and treated (pioglitazone) samples to observe the shift, and set the gate (M1, M2) to collect the signal from both (Fig. 6A, B).
3. Export statistics for each treatment and dye separately. For quantification, use mean fluorescence intensity as described in Sect. 3.2.3.

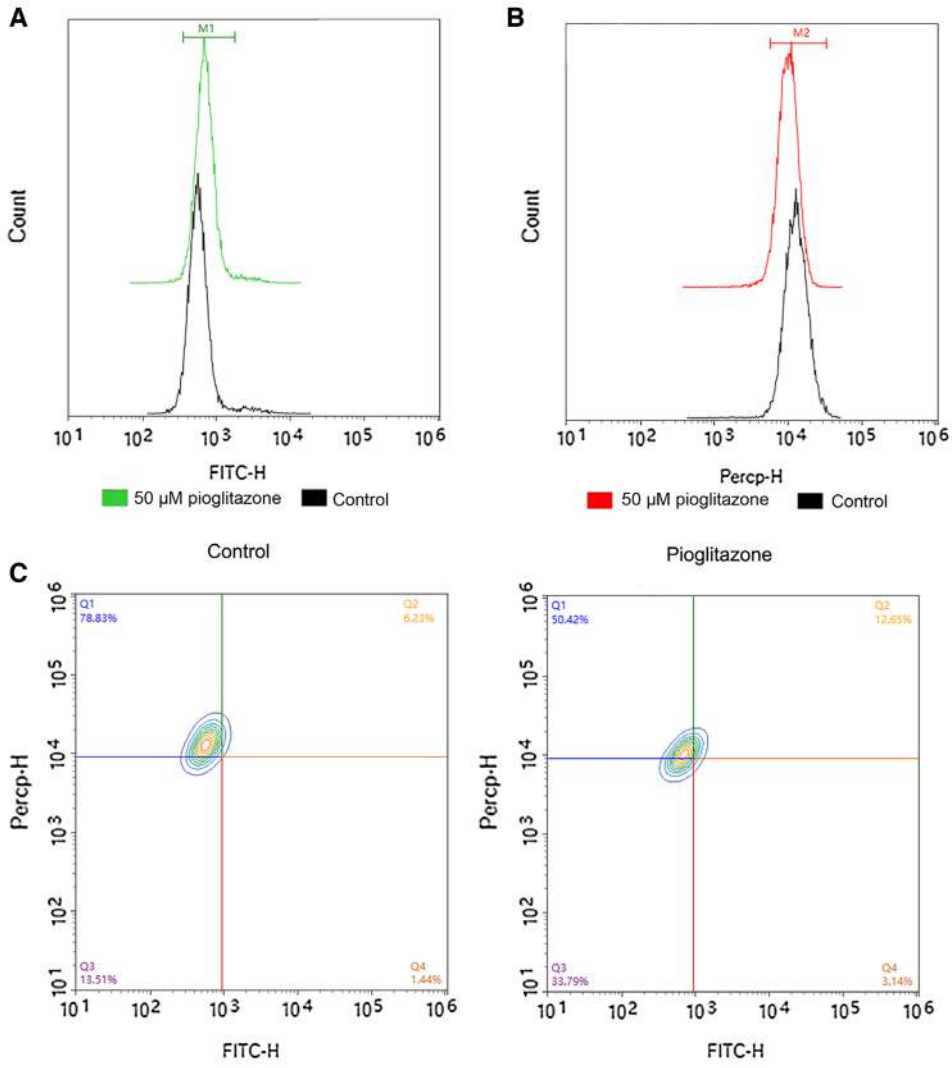


Fig. 6 Overlay of histograms of 2-NBDG (**A**) and Mitotracker Red CMXRos (**B**) fluorescence of untreated (control) and pioglitazone-treated, double-stained A375 cells. **C**, Contour plots of fluorescence of 2-NBDG and Mitotracker Red CMXRos in untreated and pioglitazone-treated, double-stained A375 cells

4. For observation of simultaneous change of 2NBDG and Mitotracker fluorescence, plot FL-1 and FL-3 channels in a contour plot (Fig. 6C).
5. Set the gate based on the fluorescence intensity in the untreated samples, and export statistics from the quadrants as percent population (Table 3).
6. Perform three biological replicates of the experiment.

4 Notes

1. Although breakdown of 2-NBDG upon freezing has been reported [10], in our hands, 10 mM 2-NBDG stock solution stored at −20°C could be thawed and refrozen several times without losing potency, maintaining stability for 1 year.
2. If the cells used in experimentation grow in high glucose medium (4.5 g/L), replace the medium with low or no glucose prior to cell labeling, as glucose in the medium and 2-NBDG compete for glucose transporters.
3. For increasing the fluorescence signal, cells can be incubated in glucose-free medium, or 2-NBDG concentrations can be increased up to 100 μM. Concentrations higher than 250 μM have been reported to cause self-quenching [16]. For further enhancement of the fluorescence signal, incubation time can be increased up to 3 h without affecting the cell viability.
4. When the viability of cells is a concern, after labeling with 2-NBDG and washing in Step 16 of Sect. 3.1, resuspend the cells in PBS with 1 μg/ml Propidium Iodide (PI), keep the cells on ice, and measure viability within 30 min.
5. Keep the cells on ice until flow cytometry is performed to slow down the 2-NBDG loss of signal.
6. If including PI stain for cell viability, collect the signal in the FL3 channel, and gate out PI-positive (dead) cells.
7. We export (see Tables 1 and 2) Mean (average fluorescence intensity of an event within the gate M1, which is a measure

Table 3
Example of the exported statistics from the graph in Fig. 6C

Treatment	Events	Q1 (%)	Q2 (%)	Q3 (%)	Q4 (%)
Control	15,000	78.83	6.23	13.51	1.44
Pioglitazone	15,000	50.42	12.65	33.79	3.14

of the average glucose uptake per cell), CV (coefficient of variation that is equal to standard deviation divided by the mean expressed as percentage; and is a measure of variation in glucose uptake in the cell population), Median (intensity value that divides a histogram into two equal parts with equal number of events), and Peak Channel Intensity (the peak within the gate M1, the highest fluorescence detected in the population). We usually graph and compare mean fluorescence intensity.

8. In the example in Fig. 3, one can observe higher glucose uptake in BRAFV600E mutated cell lines A375 and 518a2 compared to the BRAF WT cell line HTB-140.
9. If the population of the cells investigated is heterogeneous and has several subpopulations with different GLUT expression, one might observe two peaks and analyze the shift between populations upon treatment with the tested drug.
10. One also has to bear in mind to set up appropriate unlabeled controls for drugs that exhibit autofluorescence and compounds with emission wavelength close to 2-NBDG cannot be tested by this protocol.

Acknowledgments

This work was supported by the grant Agreement No. 451-03-136/2025-03/200043 with the Ministry of Education, Science, and Technological Development of the Republic of Serbia.

Competing Interests The authors have no conflicts of interest to declare that are relevant to the content of this chapter.

References

1. Abildgaard C, Guldberg P (2015) Molecular drivers of cellular metabolic reprogramming in melanoma. Trends Mol Med 21(3):164–171. https://doi.org/10.1016/j.molmed.2014.12.007
2. Haq R, Fisher DE, Widlund HR (2014) Molecular pathways: BRAF induces bioenergetic adaptation by attenuating oxidative phosphorylation. Clin Cancer Res 20(9):2257–2263. https://doi.org/10.1158/1078-0432.CCR-13-0898
3. Koch A, Lang SA, Wild PJ et al (2015) Glucose transporter isoform 1 expression enhances metastasis of malignant melanoma cells. Oncotarget 6(32):32748–32760. https://doi.org/10.18632/oncotarget.4977
4. Fischer GM, Vashisht Gopal YN, McQuade JL et al (2018) Metabolic strategies of melanoma cells: mechanisms, interactions with the tumor microenvironment, and therapeutic implications. Pigment Cell Melanoma Res 31(1):11–30. https://doi.org/10.1111/pcmr.12661
5. Brummer C, Faerber S, Bruss C et al (2019) Metabolic targeting synergizes with MAPK inhibition and delays drug resistance in melanoma. Cancer Lett 442:453–463. https://doi.org/10.1016/j.canlet.2018.11.018
6. Grahovac J, Srdic-Rajic T, Francisco Santibanez J et al (2019) Telmisartan induces melanoma cell apoptosis and synergizes with vemurafenib in vitro by altering cell bioenergetics.

Cancer Biol Med 16(2):247–263. https://doi.org/10.20892/j.issn.2095-3941.2018.0375
7. Chaube B, Malvi P, Singh SV et al (2015) Targeting metabolic flexibility by simultaneously inhibiting respiratory complex I and lactate generation retards melanoma progression. Oncotarget 6(35):37281–37299. https://doi.org/10.18632/oncotarget.6134
8. Vukadinovic D, Damjanovic A, Vukovic M et al (2025) Newly synthesized telmisartan-amino acid conjugates exhibit enhanced cytotoxic effects in malignant melanoma cells. Molecules 31(1):125. https://doi.org/10.3390/molecules31010125
9. Yoshioka K, Takahashi H, Homma T et al (1996) A novel fluorescent derivative of glucose applicable to the assessment of glucose uptake activity of *Escherichia coli*. Biochim Biophys Acta 1289(1):5–9. https://doi.org/10.1016/0304-4165(95)00153-0
10. Lloyd PG, Hardin CD, Sturek M (1999) Examining glucose transport in single vascular smooth muscle cells with a fluorescent glucose analog. Physiol Res 48(6):401–410
11. Hogan AM, Swaminathan V, Pallegar N, Christian SL (2016) Nile red and 2-NBDG are incompatible for the simultaneous detection of lipid and glucose accumulation. Int J Spectrosc 2016:215086. https://doi.org/10.1155/2016/5215086
12. el-Kebbi IM, Roser S, Pollet RJ (1994) Regulation of glucose transport by pioglitazone in cultured muscle cells. Metabolism 43(8):953–958. https://doi.org/10.1016/0026-0495(94)90173-2
13. Dinic J, Efferth T, Garcia-Sosa AT et al (2020) Repurposing old drugs to fight multidrug resistant cancers. Drug Resist Updat 52:100713. https://doi.org/10.1016/j.drup.2020.100713
14. Yoshioka K, Saito M, Oh KB et al (1996) Intracellular fate of 2-NBDG, a fluorescent probe for glucose uptake activity, in *Escherichia coli* cells. Biosci Biotechnol Biochem 60(11):1899–1901. https://doi.org/10.1271/bbb.60.1899
15. Zou C, Wang Y, Shen Z (2005) 2-NBDG as a fluorescent indicator for direct glucose uptake measurement. J Biochem Biophys Methods 64(3):207–215. https://doi.org/10.1016/j.jbbm.2005.08.001
16. Ball SW, Bailey JR, Stewart JM et al (2002) A fluorescent compound for glucose uptake measurements in isolated rat cardiomyocytes. Can J Physiol Pharmacol 80(3):205–209. https://doi.org/10.1139/y02-043s



Chapter 5

Indirect Coculture of Melanoma Cells with Stromal Cells Present in Their Microenvironment as a Method for Evaluation of Their Mutual Interactions

Aleksandra Simiczyjew, Katarzyna Pietraszek-Gremplewicz and Dorota Nowak

Abstract

A tumor tissue consists not only of cancer cells but also of stromal cells, which often support cancer cell progression. Therefore, oncology research utilizes models that enable the study of cancer cell characteristics in the presence of noncancereous cells that, in vivo, also form the tumor. The following protocol describes the culturing of cancer cells with stromal cells (such as keratinocytes, fibroblasts, and adipocytes) in an indirect coculture model, in which both cell types exchange secretory factors in the culture medium but do not interact directly. This system allows for the assessment of the influence of one cell type on the other without the need to separate them through sorting to conduct further experiments based on only one selected cell type.

Keywords Melanoma, Stromal cells, Fibroblasts, Keratinocytes, Adipocytes, Indirect coculture

1 Introduction

Melanoma originates from melanocytes, which are pigment-producing cells. In healthy skin, melanocytes interact with keratinocytes and other adjacent cells to protect DNA from UV-induced damage, primarily through melanin-dependent mechanisms [1]. However, when melanocytes undergo neoplastic transformation, the cells present in their microenvironment, including keratinocytes, fibroblasts, and adipocytes, may promote the progression of melanoma [2]. Indeed, solid tumors in general are composed not only of malignant cells but also of various nonmalignant cellular components within the tumor niche. Additional elements, such as the composition of the extracellular matrix (ECM) and factors such as hypoxia, must also be considered [3]. Initially, the tumor microenvironment (TME) may act as a physical barrier that limits drug delivery to tumor cells [4]. In the next stages of cancer progression, factors present in the TME

Kristian M. Hargadon (ed.), *Melanoma*, Methods in Molecular Biology, vol. 3089,
https://doi.org/10.1007/978-1-0716-5619-8_5,
© The Author(s), under exclusive license to Springer Science+Business Media, LLC, part of Springer Nature 2027

can support tumor growth, invasive abilities, and angiogenic potential by secreting growth factors, chemokines, and cytokines, affecting not only neighboring cells within the niche but also distant sites in the organism [5]. Moreover, fibroblasts and keratinocytes secrete matrix metalloproteinases (MMPs), which degrade ECM components, forming a pathway facilitating cancer cell invasion through surrounding tissues [6–8]. Additionally, adipocytes secrete high-energy metabolites, which may be utilized by melanoma cells [9].

The most commonly applied current melanoma treatment methods are immunotherapy and targeted therapy based on BRAF/MEK inhibitors. Unfortunately, resistance to these drugs often occurs in patients within a few months of starting treatment [10]. One of the factors influencing the effectiveness of cancer therapy is the TME, which exerts diverse effects on the development of treatment resistance. Due to the significant impact of stromal cells on melanoma progression and response to therapy, it seems crucial to study the biology of melanoma cells in the presence of selected elements of their niche. Therefore, this protocol describes an indirect melanoma cell culturing model with surrounding cells (keratinocytes, fibroblasts, and adipocytes) using Transwell filters. Application of this method enables the exchange of the secretome between two types of cocultured cells. However, owing to the spatial separation inherent to this system, the cocultured cells can be used immediately after culturing for further experiments without the need for sophisticated methods for their separation.

2 Materials

The entire procedure should be performed under a laminar flow hood, in sterile conditions, and all materials and reagents used should also be sterile.

2.1 Supplies for Coculture Experiments

1. 6- or 24-well plates of appropriate height, suitable for coculture.
2. Transwell insert with transparent polyethylene terephthalate (PET) membrane with a pore size of 0.4 μm, suitable for cell culture in 6- or 24-well plates.
3. Tweezers.

2.2 Cell Culture

1. Melanoma cell lines:
   a. A375.
   b. WM9.
   c. Hs294T.
   d. WM1341D.
2. Fibroblasts: human normal dermal fibroblasts (neonatal).
3. Keratinocytes: human immortalized keratinocytes HaCaT.

4. Adipocytes differentiated from mouse 3T3L1 preadipocytes.
5. 0.25% trypsin/0.05% EDTA solution.
6. Melanoma Cell Culture Medium: Dulbecco's Modified Eagle's Medium (DMEM) containing 4.5 g/l glucose and 1.5 g/l $NaHCO_3$ and supplemented with 10% fetal bovine serum (FBS), antibiotics (10,000 U/ml penicillin, 10 mg/ml streptomycin, 25 µg/ml amphotericin B), and 2 mM glutamine.
7. Fibroblast Culture Medium: Fibroblasts Growth Basal Medium (FBM), which is supplemented with FGM™-2 SingleQuots™, containing insulin, human basic fibroblast growth factor (hFGF-B), gentamicin sulfate-amphotericin (GA-1000), and 10% FBS.
8. Immortalized Keratinocyte (HaCaT) Culture Medium: DMEM containing 4.5 g/l glucose and 3.7 g/l $NaHCO_3$ supplemented with 10% FBS, 2 mM glutamine, and antibiotics (10,000 U/ml penicillin, 10 mg/ml streptomycin, 25 µg/ml amphotericin B).
9. 3T3L1-derived Pre-Adipocyte Culture Medium: DMEM containing 4.5 g/l glucose and 1.5 g/l $NaHCO_3$ and supplemented with 10% bovine calf serum (BCS), antibiotics (10,000 U/ml penicillin, 10 mg/ml streptomycin, 25 µg/ml amphotericin B), and 2 mM glutamine.
10. Adipocyte Culture Medium: 3T3L1-derived Pre-Adipocyte Culture Medium supplemented with 2 µM rosiglitazone, 0.5 mM 3-Isobutyl-1-methylxanthine (IBMX), 1 µg/µl insulin, and 0.25 µM dexamethasone.
11. Melanoma and Fibroblast Coculture Medium: Melanoma Cell Culture Medium and Fibroblast Culture Medium mixed in a 1:1 ratio to meet the needs of both cell types.
12. Melanoma and Immortalized Keratinocyte Coculture Medium: Melanoma Cell Culture Medium and Immortalized Keratinocyte Culture Medium mixed in a 1:1 ratio to meet the needs of both cell types.
13. Melanoma and Adipocyte Coculture Medium: Melanoma Cell Culture Medium and Adipocyte Culture Medium mixed in a 1:1 ratio to meet the needs of both cell types.
14. Automated cell counter, e.g., EVE Automated Cell Counter or Burker Chamber.
15. 0.4% trypan blue solution in 1× phosphate-buffered saline (PBS).
16. T25 or T75 cell culture flasks.
17. Water bath.
18. Inverted microscope.

19. Sterile tubes suitable for centrifugation, e.g., 15 ml Falcon tubes.
20. Centrifuge suitable for cell culture.
21. Incubator suitable for cell culture.

3 Methods

3.1 Cell Passage

1. Warm cell culture medium and trypsin/EDTA solution to 37°C in a water bath.
2. Aspirate and discard cell culture medium from cell culture flasks.
3. Remove the remaining cell culture medium by washing the flask with attached cells with 1 ml (for T25 flask) of 0.25% trypsin/0.05% EDTA solution.
4. Aspirate and discard the liquid.
5. To detach adherent cells, add 1 ml of 0.25% trypsin/0.05% EDTA solution to the flask and incubate the cells in the incubator (37°C) until they round up. Support cell detachment by tapping the flask. Monitor cell detachment under the inverted microscope (*see* **Note 1**).
6. After cell detachment, add 3 ml of cell-specific culture medium to stop trypsin activity, rinse the cell surface with the medium, and collect the cell suspension. Transfer it to the 15 ml centrifuge tube.
7. Centrifuge cells at $100 \times g$ for 5 min at room temperature.
8. Discard the supernatant, and resuspend the pellet in fresh cell-specific culture medium.
9. Count cells with a suitable method, e.g., using a Burker chamber or an automatic counter. Assess cell viability using the trypan blue staining.

3.2 Adipocyte Differentiation

Adipocytes may be obtained from mouse 3T3L1 fibroblasts by their differentiation according to the protocol described earlier by Zebisch et al. [11].

1. Seed 3T3L1 fibroblasts in 3T3L1-derived Pre-Adipocyte Culture Medium into appropriate 6- or 24-well plates suitable for co-culturing cells (2×10^5–4×10^5 cells/well are typically appropriate for seeding a 6-well plate).
2. Culture cells until they reach 100% confluence (*see* **Note 2**).
3. Two days after reaching confluence, replace 3T3L1-derived Pre-Adipocyte Culture Medium with Adipocyte Culture Medium (*see* **Notes 3 and 4**).

4. Incubate cells for 48 h.
5. Replace Adipocyte Culture Medium with fresh 3T3L1-derived Pre-Adipocyte Culture Medium supplemented only with 1 μg/μl insulin.
6. Incubate cells for another 48 h.
7. Replace cell culture medium with 3T3L1-derived Pre-Adipocyte Culture Medium (without any other additives) for another 7 days, at which point cells are fully differentiated (*see* **Note 5**, Fig. 1).

3.3 Seeding Cells

1. Fibroblasts should be seeded on the bottom of 6- or 24-well plates (*see* **Notes 6 and 7**).
2. Keratinocytes should be seeded on the bottom of the 6- or 24-well plates (*see* **Notes 6 and 7**).

3.4 Coculture

Normal cells can be cultured in the presence of melanoma cells using a Transwell insert with 0.4 μm pores, which allows for the exchange of secretory factors between cells. However, the pores in the insert's membrane are too small for whole cells to pass through to the other side of the filter. A photographic demonstration of the individual steps of the procedure for establishing indirect coculture is presented in Fig. 2.

1. Replace the culture medium from the previously seeded monocultures of nontumor cells with the appropriate 1:1 mixture of coculture medium suitable for the cell types under study [2 ml for 6-well plate or 1 ml for 24-well plate (*see* **Note 8**)].
2. Place into each well a Transwell insert, onto which the melanoma cells will subsequently be seeded (*see* **Notes 9 and 10**, Fig. 3).

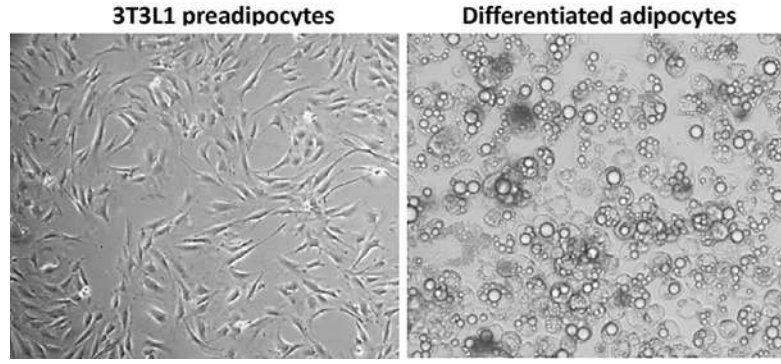


Fig. 1 Representative transmitted light images of 3T3L1 preadipocytes (before reaching 100% confluence) and differentiated adipocytes

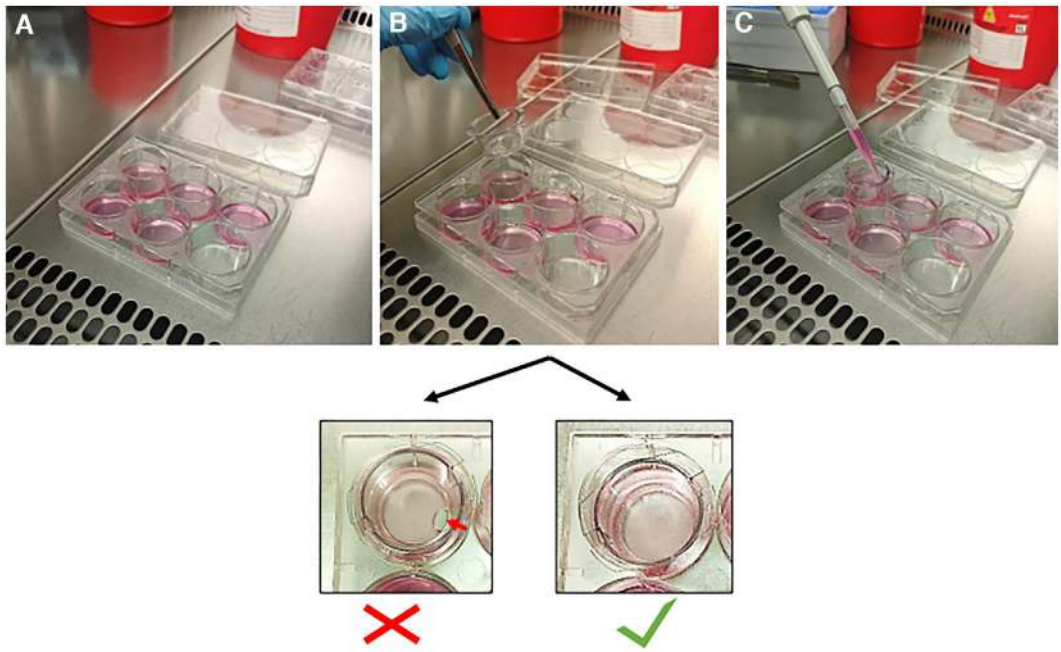


Fig. 2 Photographic demonstration of the individual steps of the procedure for establishing indirect coculture. (**A**), Seed stromal cells (keratinocytes, fibroblasts, and preadipocytes) at the bottom of the well. (**B**), After 24 h (in the case of fibroblasts or keratinocytes) or after the preadipocytes have differentiated into adipocytes, place the insert in the well. Be sure to do this slowly to avoid forming air bubbles between the fluid layer and the insert (marked with a red arrow in the photo). (**C**), Seed cancer cells at the top of the insert

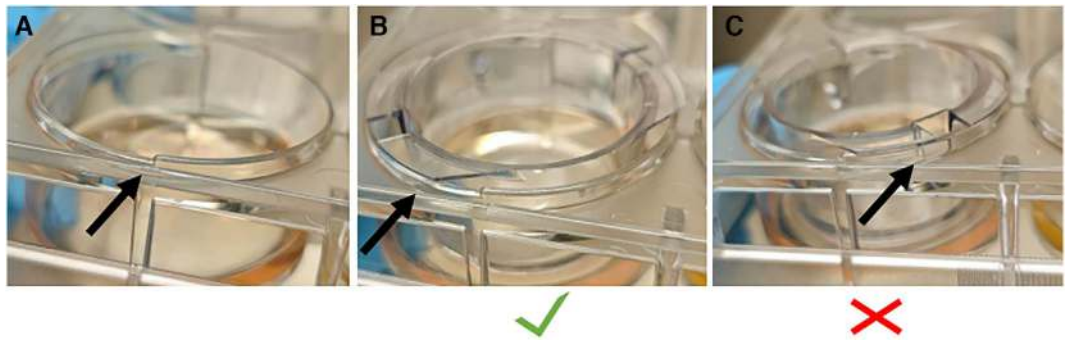


Fig. 3 Photographic presentation of the proper placement of the insert. (**A**), Illustration of the notches present in the top of the well of the plate suitable for cell coculture. (**B**), Correct positioning of the flanges of the insert in the notches of the well. This will minimize media wicking and ensure proper plate lit-fit. (**C**), Incorrect positioning of the insert in the well of the plate

3. Seed melanoma cells into the bottom of the insert in 1 ml (insert for 6-well plate) or 0.5 ml (insert for 24-well plate) of the appropriate coculture medium for the given type of melanoma–stromal cell interaction under study (*see* **Note 11**). This medium is a 1:1 mixture of media used for the individual cell types used to create the coculture (*see* **Note 12**).

4. The indirect coculture should be maintained for 7 days. During this period, the appropriate coculture medium should be replaced once (after 3–4 days of coculture) (*see* **Notes 8 and 12**). To change the medium, remove it from the insert, then lift the insert with tweezers and collect the medium from the bottom of the well. Then, gently add the medium to the bottom of the well and onto the insert (Fig. 4).

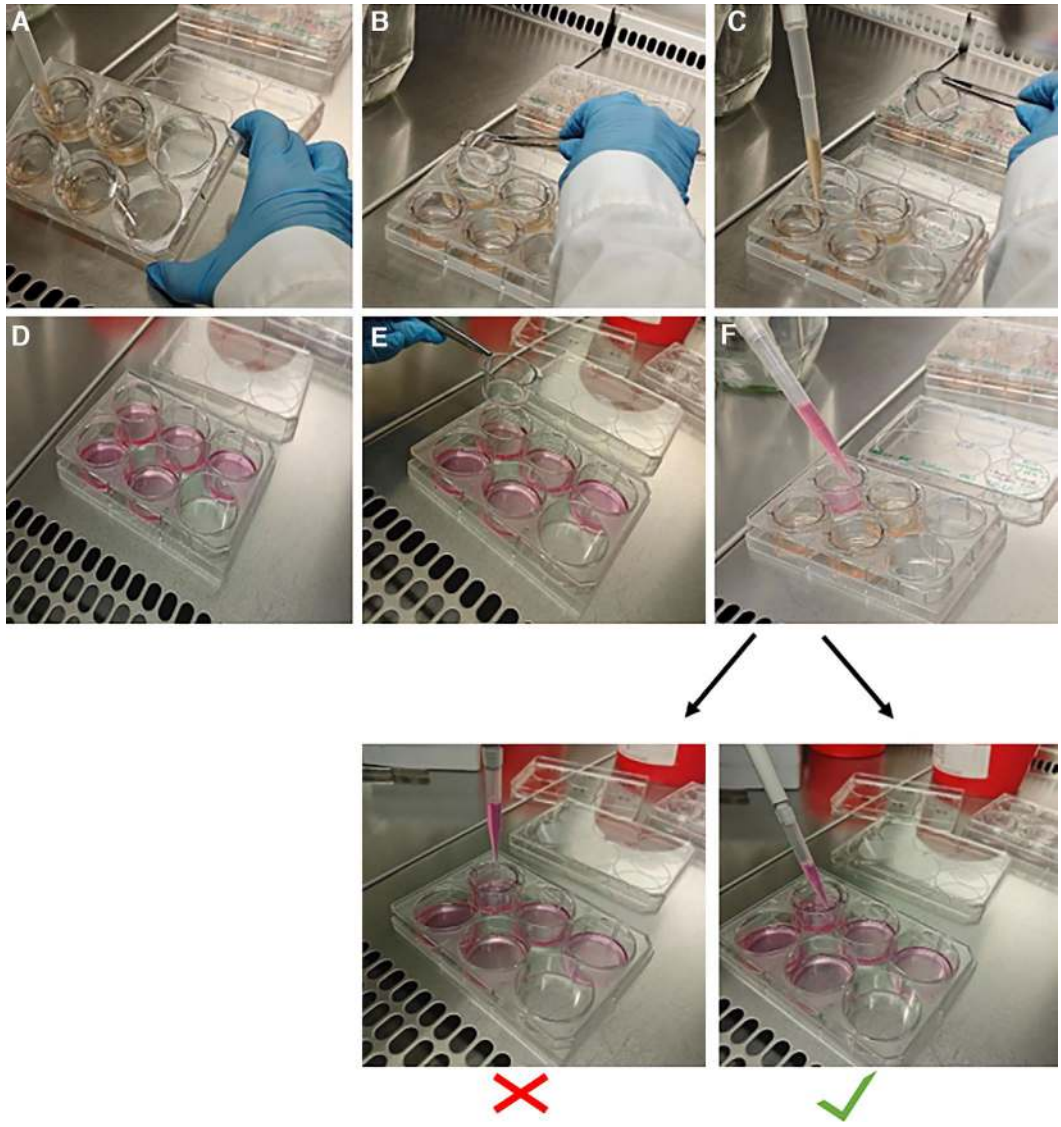


Fig. 4 Photographic demonstration of the exchange of cell culture medium in a coculture of stromal cells and melanoma. (**A**), Removing the medium from the insert where the melanoma cells are growing. (**B**), Removing the insert from the well. (**C**), Removing the medium from the bottom of the well where the stromal cells (fibroblasts, keratinocytes, or adipocytes) are growing. (**D**), Adding the fresh medium to the bottom of the well where the stromal cells are growing. (**E**), Placing the insert back into the plate well. **F**, Gently adding the medium to the insert. Remember to add the medium to the wall of the insert, not directly onto the cells, as the latter approach may cause cells to detach

5. For users wishing to compare the results for cells grown in the presence of stromal cells to melanoma cells grown as a monoculture, it is important to plan an appropriate number of controls (*see* **Note 13**).
6. After the coculture, cells may be easily separated and used for further experiments, e.g.:
    a. Cells may be used to prepare lysates for qPCR or Western blotting analyses.
    b. Cells may be passaged and seeded for subsequent experiments, such as proliferation or migration assays, and immunocytochemical staining.
    c. Cell culture medium may be replaced with one devoid of FBS, and after 72 h, cell-conditioned medium may be collected and used for further experiments.

4 Notes

1. The time of rounding and detachment of cells depends on the cell line used. In the case of HaCaT cells, which are difficult to detach, after the aspiration of medium, wash cells and then incubate with 0.05% EDTA for 10 min at 37°C, followed by incubation with a freshly prepared mixture of 0.05% trypsin (without EDTA) and 0.025% EDTA (Invitrogen) for 3 min at 37°C.
2. It is important to reach a high level of cell confluency before the induction of adipocyte differentiation. Otherwise, the efficiency of differentiation may be affected.
3. Prepare Adipocyte Culture Medium only in the volume necessary for direct use. Do not store it for a long time, and always use freshly prepared medium. Before use, warm Adipocyte Culture Medium in a 37°C water bath.
4. IBMX may precipitate if it is added to the medium at a temperature lower than 37°C. To solubilize it, warm up the liquid in a water bath set to 37°C.
5. You can see that the cells have been differentiated because, under an inverted microscope, you will notice large lipid droplets within the differentiated adipocytes. To confirm that the structures you see are lipid droplets, you can stain them with an appropriate fluorescent dye, such as Lipid Spot, and observe them under a fluorescent microscope.
6. Be sure first to prepare the cell suspension in the appropriate cell culture medium, and only add the suspension to the

wells after thorough mixing. Do not add the cells directly to the medium in the well, as this will make the cell suspension difficult to mix and may cause cells to attach unevenly to the bottom of the well.

7. The number of cells seeded for coculture should be appropriately selected. Considering the proliferative capacity of the cells, we selected them so that after 7 days of indirect coculture, the ratio of normal cells to cancer cells was approximately 1:1, and both cell types achieved about 90% confluence. To select the appropriate number of cells to seed for coculture experiments, the proliferation of individual cell lines should be assessed within 7 days after seeding. This rule does not apply to adipocytes, which must be confluent at the time of initiation of differentiation.
8. As normal cells, especially differentiated adipocytes tend to be poorly adherent to the bottom of the well; the medium should be replaced slowly and gently.
9. Make sure to place the insert in the well in the correct position. The wells of the plates intended for coculture have special grooves into which the insert should be placed (Fig. 3).
10. When placing the insert into the well, ensure no air bubbles form between the liquid in the well and the insert (Fig. 2).
11. Since the indirect coculture conditions must be suitable for both cell types, the coculture should be conducted using a 1:1 mixture of optimal medium for each of the normal and cancer cells. Appropriate controls should be performed to ensure that the cells representing a specific type, such as fibroblasts, keratinocytes, or melanoma cells do not change their characteristics in the media mixture used. Cell shape, proliferation, and typical biomarker expression should be checked.
12. If using 6-well plates, cells growing at the bottom of the well should be cultured in the presence of 2 ml of appropriate coculture medium, while those seeded on the insert should be grown in 1 ml of appropriate coculture medium. In the case of 24-well plate cocultures, cells growing at the bottom of the well should be cultured in the presence of 1 ml of medium, while those seeded on the insert should be grown in 0.5 ml of medium.
13. Cells cultured as a monoculture (normal ones or melanoma cells) should be grown in an analogous media mixture as used for the coculture experiment in order to ensure that medium composition does not influence experiment results.

Acknowledgments

This research was funded by the National Science Centre, Poland, with a grant received by Aleksandra Simiczyjew (SONATA, 2020/39/D/NZ5/02330).

Competing Interests The authors have no conflicts of interest to declare that are relevant to the content of this chapter.

References

1. Williams PF, Olsen CM, Hayward NK et al (2011) Melanocortin 1 receptor and risk of cutaneous melanoma: a meta-analysis and estimates of population burden. Int J Cancer 129:1730–1740. https://doi.org/10.1002/ijc.25804
2. Mazurkiewicz J, Simiczyjew A, Dratkiewicz E et al (2021) Stromal cells present in the melanoma niche affect tumor invasiveness and its resistance to therapy. Int J Mol Sci 22:529. https://doi.org/10.3390/ijms22020529
3. Dratkiewicz E, Simiczyjew A, Mazurkiewicz J et al (2021) Hypoxia and extracellular acidification as drivers of melanoma progression and drug resistance. Cells 10:862. https://doi.org/10.3390/cells10040862
4. Sriraman SK, Aryasomayajula B, Torchilin VP (2014) Barriers to drug delivery in solid tumors. Tissue Barriers 2:e29528. https://doi.org/10.4161/tisb.29528
5. Labrousse A-L, Ntayi C, Hornebeck W et al (2004) Stromal reaction in cutaneous melanoma. Crit Rev Oncol Hematol 49:269–275. https://doi.org/10.1016/j.critrevonc.2003.10.007
6. Shiga K, Hara M, Nagasaki T et al (2015) Cancer-associated fibroblasts: their characteristics and their roles in tumor growth. Cancers 7:2443–2458. https://doi.org/10.3390/cancers7040902
7. Mazurkiewicz J, Simiczyjew A, Dratkiewicz E et al (2022) Melanoma cells with diverse invasive potential differentially induce the activation of normal human fibroblasts. Cell Commun Signal 20:63. https://doi.org/10.1186/s12964-022-00871-x
8. Mazurkiewicz J, Simiczyjew A, Dratkiewicz E et al (2022) Melanoma stimulates the proteolytic activity of HaCaT keratinocytes. Cell Commun Signal 20:146. https://doi.org/10.1186/s12964-022-00961-w
9. Simiczyjew A, Wądzyńska J, Pietraszek-Gremplewicz K et al (2023) Melanoma cells induce dedifferentiation and metabolic changes in adipocytes present in the tumor niche. Cell Mol Biol Let 28:58. https://doi.org/10.1186/S11658-023-00476-3
10. Luebker SA, Koepsell SA (2019) Diverse mechanisms of BRAF inhibitor resistance in melanoma identified in clinical and preclinical studies. Front Oncol 9:268. https://doi.org/10.3389/fonc.2019.00268
11. Zebisch K, Voigt V, Wabitsch M et al (2012) Protocol for effective differentiation of 3T3-L1 cells to adipocytes. Anal Biochem 425:88–90. https://doi.org/10.1016/j.ab.2012.03.005



Chapter 6

A Flow Cytometric Assay for Investigating Melanoma Cell Adhesion to Lymphatic Endothelial Cells

Kristian M. Hargadon and Coleman E. Johnson

Abstract

Lymph node invasion by tumor cells is an important process in the progression of melanoma and is a poor prognostic factor for patients with this cancer. Before they are able to spread to regional lymph nodes, though, melanoma cells must first adhere to lymphatic endothelium and transmigrate into the lymphatic vasculature. In order to study melanoma cell adhesion to lymphatic endothelial cells and the factors that regulate this process, we have developed an in vitro flow cytometry-based assay to measure melanoma cell attachment to lymphatic endothelial cells. This assay will be a useful tool for investigating the interactions that take place between melanoma cells and lymphatic endothelial cells during the adhesion process.

Keywords Cell adhesion, Tumor, Melanoma, Lymphatic endothelium, Flow cytometry

1 Introduction

The prognosis for early-stage melanoma is excellent, with minimally invasive surgical removal of primary lesions being largely curative. However, many melanoma patients are not diagnosed until later stages of metastatic disease, and despite advances in targeted and immune-based therapies for melanoma patients in recent years [1–3], the 5-year survival rate for this cancer remains significantly lower in these more advanced cases. Importantly, during tumor progression, one of the first sites to which melanoma spreads is the regional lymph nodes. Lymph node involvement is indeed a poor prognostic factor for melanoma patients [4, 5], and tumor burden within regional lymph nodes also correlates negatively with survival [6–10]. Notably, recent studies in murine models have shown that lymph node invasion by melanoma and other cancer types provides tumor cell access to vasculature for subsequent metastatic dissemination to vital organs [11, 12]. Additionally, lymph node invasion by melanoma has also been linked with antitumor immune tolerance [13], thus highlighting the significance of this process to cancer progression.

Kristian M. Hargadon (ed.), *Melanoma*, Methods in Molecular Biology, vol. 3089,
https://doi.org/10.1007/978-1-0716-5619-8_6,
© The Author(s), under exclusive license to Springer Science+Business Media, LLC, part of Springer Nature 2027

Based on these findings, it is critical to gain insight into the processes that regulate lymph node invasion by melanoma.

The transition of a tumor from a benign, localized mass to a state in which invasive cells are capable of infiltrating regional lymph nodes is a multistep process that involves several hallmarks of cancer progression. Production of lymphangiogenic factors by various cell populations in the tumor microenvironment [14, 15], detachment of tumor cells from a primary mass and the surrounding tissue architecture [16, 17], remodeling of the extracellular matrix (ECM), and migration toward/invasion through various ECM components [18], expression of lymphatic-homing chemokine receptors on tumor cells [19], and tumor cell adhesion to lymphatic endothelium followed by transendothelial migration into the lymphatic vasculature [20, 21] are all crucial steps required for lymph node invasion by melanoma cells. Understanding each of these processes and the factors that regulate them is important to the discovery of key biomarkers for melanoma progression and could also lead to the development of novel therapeutics designed to interfere with lymph node invasion by melanoma cells. To this end, we describe here a flow cytometry-based technique for evaluating melanoma cell adhesion to lymphatic endothelial cells. This method will serve as a useful tool for in vitro studies aimed at understanding the ligand–receptor interactions that occur between melanoma cells and lymphatic endothelial cells as well as the signaling pathways/genetic factors that regulate this cell–cell adhesion process.

2 Materials

Store all media and bovine serum albumin (BSA) at 4°C in the dark. Store fetal bovine serum (FBS) and carboxyfluorescein succinimidyl ester (CFSE) at −20°C in the dark. Store all other supplies at room temperature. Use only sterile reagents for all procedures.

2.1 Cell Culture Media and Supplies

1. Growth medium for SV-LEC lymphatic endothelial cell line [22]: Dulbecco's Modified Eagle's Medium (DMEM) containing 4 mM L-glutamine, 4500 mg/L glucose, 1 mM sodium pyruvate, and 1500 mg/L sodium bicarbonate, supplemented with 10% FBS.
2. Growth medium for melanoma cell lines (*see* **Note 1**): Dulbecco's Modified Eagle's Medium (DMEM) containing 4 mM L-glutamine, 4500 mg/L glucose, 1 mM sodium pyruvate, and 1500 mg/L sodium bicarbonate, supplemented with 10% FBS.
3. Tissue culture-treated T75 flasks.
4. Trypsin-EDTA Solution, 1×: 0.25% Trypsin/0.53 mM EDTA in Hanks Balanced Salt Solution without calcium or magnesium.

5. Nuclease-free, non-pyrogenic serological pipets and pipet tips.
6. Nuclease-free, non-pyrogenic 15 ml conical centrifuge tubes.

2.2 Supplies and Reagents for Melanoma Cell/Lymphatic Endothelial Cell Adhesion Assay

1. Tissue culture-treated 6-well plates.
2. Tissue culture-treated 48-well plates.
3. Accutase Cell Detachment Solution.
4. Endotoxin-free 1× phosphate-buffered saline (PBS), pH 7.4.
5. Adhesion assay medium: DMEM supplemented with 0.5% BSA.
6. 5-(and-6)-Carboxyfluorescein diacetate succinimidyl ester (CFSE): Reconstitute lyophilized CFSE with anhydrous dimethyl sulfoxide (DMSO) to a concentration of 10 mM CFSE, and prepare single-use aliquots for storage (*see* **Note 2**).
7. Flow cytometry tubes (Titertube micro test tubes or 1.5 ml microcentrifuge tubes).
8. Flow cytometer (equipped with a 488 nm laser and a 533/30 nm bandpass filter for fluorescence detection in the FL1 channel).

3 Methods

Carry out all cell culture procedures in a biosafety cabinet to maintain sterility throughout the experiment. A summary of the experimental workflow described below is shown in Fig. 1.

3.1 Routine Maintenance and Passaging of Cell Cultures

Maintain all cell lines at 37°C in a humidified incubator with 5% CO_2, and passage cell lines at 80%–90% confluency (*see* **Note 3**).

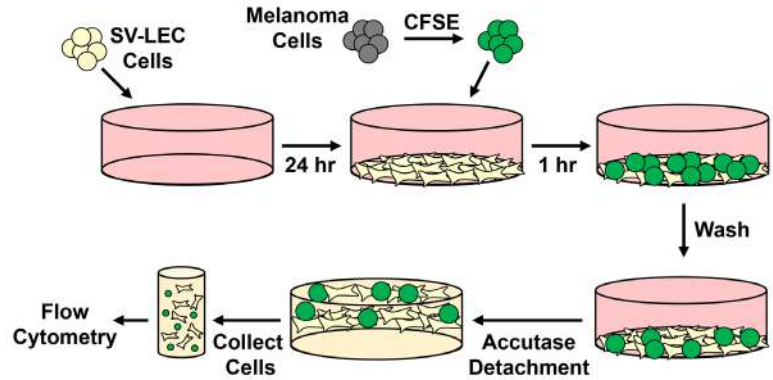


Fig. 1 Schematic of experimental workflow for the melanoma cell/lymphatic endothelial cell adhesion assay

1. As cells require passaging, remove and discard cell culture medium from T75 flasks.
2. Add 4 ml 1× Trypsin-EDTA solution to flasks and return to cell culture incubator to promote cellular detachment (*see* **Note 4**).
3. Neutralize Trypsin-EDTA solution with 10 ml of the relevant complete growth medium and transfer cells to a 15 ml conical centrifuge tube. Centrifuge cells at 450 × *g* for 5 min.
4. Decant supernatant and resuspend cells in an appropriate volume of complete growth medium.
5. Reseed new T75 flasks with necessary fraction of cells in a total volume of 15 ml of medium.
6. Use remaining cells to perform the cell adhesion assay.

3.2 Preparation of Lymphatic Endothelial Cell Monolayers

1. Harvest SV-LEC cells as described in Sect. 3.1 (*see* **Note 5**).
2. Resuspend SV-LEC cells at a concentration of 3.75e^5 cells/ml in complete growth medium (*see* **Note 6**).
3. Plate 200 µl of SV-LEC cells (7.5e^4 cells) per well into 48-well tissue culture-treated plates (*see* **Note 7**), and incubate for 24 h at 37°C in a humidified incubator with 5% CO_2 to generate 100% confluent monolayers (*see* **Note 8**).

3.3 Preparation and CFSE Labeling of Melanoma Cells

1. On the same day that SV-LEC cells are plated to generate monolayer cultures, harvest melanoma cells as described in Sect. 3.1.
2. Plate 1e^6 melanoma cells in 1 ml of tumor growth medium per well into 6-well tissue culture-treated plates, and incubate for 24 h at 37°C in a humidified incubator with 5% CO_2 (*see* **Note 9**).
3. 24 h post-plating melanoma cells, remove and discard the culture medium and any nonadherent cells from the 6-well culture plates and add 500 µl of Accutase Cell Detachment Solution to each well (*see* **Note 10**).
4. Incubate melanoma cells with Accutase Cell Detachment Solution at room temperature (*see* **Note 11**) on a rotating platform set to 100 rpm until all cells are dislodged (*see* **Note 12**).
5. Add 2 ml of tumor growth medium, and transfer cells to a 15 ml conical centrifuge tube. Centrifuge cells at 450 × *g* for 5 min, completely remove supernatant, and resuspend cells in 1 ml of tumor growth medium.
6. Count live cells using a hemocytometer and trypan blue exclusion of dead cells (*see* **Note 13**).
7. Transfer 7.5e^5 tumor cells to a 15 ml conical centrifuge tube, spin at 450 × *g* for 5 min, completely remove supernatant,

and wash cells twice with 5 ml of endotoxin-free 1× PBS (*see* **Note 14**).

8. During the preceding Step 7 PBS washes, prepare a 0.25 μM solution of CFSE in endotoxin-free 1× PBS by performing a 1:40,000 dilution of a single-use 10 mM CFSE stock.
9. Following the Step 7 PBS washes, remove supernatant and resuspend melanoma cell pellets in 1 ml of the 0.25 μM CFSE solution prepared in Step 8. Incubate for 15 min in a 37°C water bath in the dark.
10. Stop the labeling reaction by quenching with 5 ml of complete tumor growth medium (containing 10% FBS), centrifuge at 450 × *g* for 5 min, and wash tumor cell pellets twice with 1× PBS as described in Step 7.
11. Resuspend tumor cell pellets in 1 ml DMEM medium supplemented with 0.5% BSA (*see* **Note 15**).

3.4 Melanoma Cell/Lymphatic Endothelial Cell Adhesion Assay

1. During the CFSE labeling of tumor cells in Steps 9–11 from Sect. 3.3, remove medium from the SV-LEC monolayer cultures and wash the monolayers gently three times with 250 μl of endotoxin-free 1× PBS (*see* **Note 16**).
2. Gently add 100 μl of DMEM supplemented with 0.5% BSA to the SV-LEC cultures (*see* **Note 17**).
3. Using the tumor cells resuspended in DMEM supplemented with 0.5% BSA from Step 11 of Sect. 3.3, gently add 100 μl ($7.5e^4$ cells) to the SV-LEC monolayer (*see* **Note 18**).
4. Incubate cocultures for 1 h at 37°C in a humidified environment with 5% CO_2.
5. In order to remove nonadherent melanoma cells, remove the medium and wash the wells gently three times with 250 μl of endotoxin-free 1× PBS as described in Step 1.
6. Add 200 μl of Accutase Cell Detachment Solution and incubate at room temperature on a rotating platform set to 100 rpm until all cells are dislodged (*see* **Note 19**).
7. Vigorously pipet the mixed cell culture up and down several times to ensure a single-cell suspension is generated, and transfer 175 μl to a tube appropriate for use in flow cytometry (*see* **Note 20**).

3.5 Flow Cytometry Sample Acquisition and Analysis

1. Collect each sample on a flow cytometer equipped with a 488 nm laser and a 533/30 nm bandpass filter for fluorescence detection in the FL1 channel.
2. Use a consistent run speed for all samples.
3. Select a run limit of 150 μl for each sample (*see* **Note 21**).

4. Following sample collection, begin data analysis by creating a Forward Scatter/Side Scatter (FSC/SSC) dot plot, and draw a gate around all events that are not debris.
5. Create a histogram plot that displays FL1 fluorescence and that is gated on the FSC/SSC gate drawn in Step 4.
6. On the histogram plot, draw a vertical marker that divides the cell populations into $CFSE^-$ SV-LEC cells and $CFSE^+$ melanoma cells (Fig. 2A).
7. Graph data as either % of Tumor Cells in the mixed population (Fig. 2B) or # of Adherent Tumor Cells (Fig. 2C).

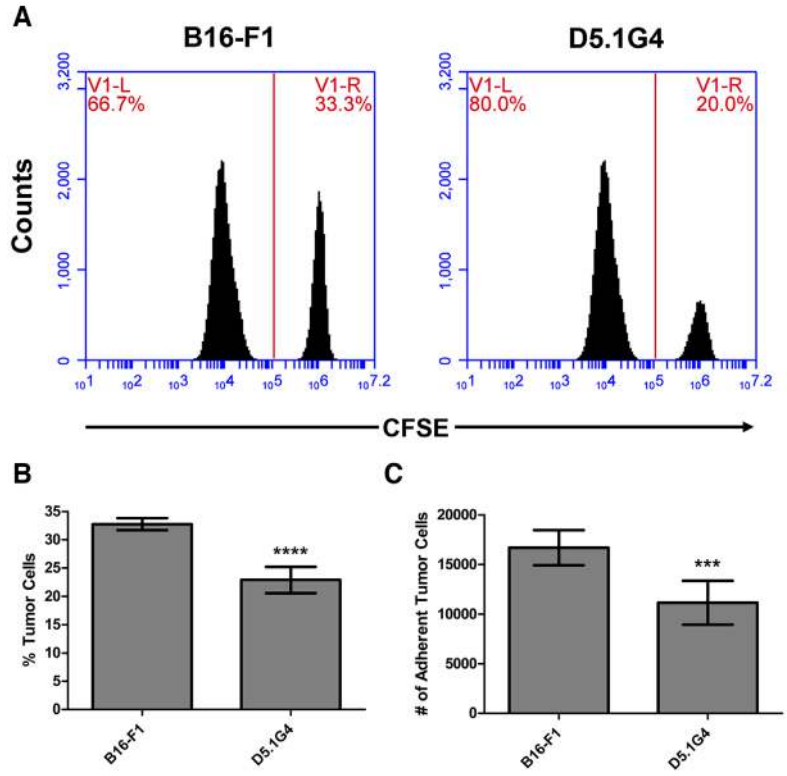


Fig. 2 Sample flow cytometric data acquired from the melanoma cell/lymphatic endothelial cell adhesion assay. (**A**), Representative histogram plots showing differential adhesion of the lymph node-invasive B16-F1 melanoma cell line and the lymph node-noninvasive D5.1G4 melanoma cell line to SV-LEC cells. Plots are gated on all FSC/SSC events that are not debris, and melanoma cells are represented by the $CFSE^+$ events shown to the right of the vertical marker in the plots. Data can be reported as % tumor cells in the mixed population (**B**) or as the number of adherent tumor cells (**C**). In the graphs shown here, data are pooled from two independent experiments, each with three replicates for B16-F1 and D5.1G4. Data are plotted as the average with error bars representing the standard deviation of the mean. *** = $p < 0.001$, **** = $p < 0.0001$

4 Notes

1. The melanoma cell lines reported herein are of murine origin. B16-F1 is a commonly used melanoma model and is a highly aggressive, lymph node-invasive cell line [23, 24]. D5.1G4 is a chemically mutated variant of B16 melanoma that is poorly tumorigenic and lymph node-noninvasive [25, 26].
2. Use CFSE within 6 months of reconstitution and avoid repeated freeze–thaw cycles to maintain consistency in CFSE labeling intensity. CFSE is light-sensitive and should be stored in the dark.
3. Do not allow cell lines to reach 100% confluency during routine maintenance, as this may result in contact inhibition and interference with cell adhesion properties during subsequent assays. As a guideline for passaging of cell lines, B16-F1 cells can be split 1:10 every 2 days or 1:30 every 3 days. D5.1G4 cells can be split 1:5 every 3 days or 1:10 every 4 days. SV-LEC cells can be split 1:3 every 3 days or 1:5 every 4 days.
4. The duration of trypsinization is cell-line dependent and should be only long enough to promote cell detachment. As a recommendation for cell lines described in this procedure, trypsinize B16-F1 cells for 2–3 min, D5.1G4 cells for 5 min, and SV-LEC cells for 10 min. If necessary, lightly tap the flasks to dislodge any cells that remain adherent. Avoid repeated or strong tapping of the flasks, however, as this will result in clumping of trypsinized cells.
5. $7.5e^4$ SV-LEC cells will be needed per replicate in the assay.
6. We typically achieve this concentration by resuspending $7.5e^5$ cells in 2 ml of complete growth medium. However, the cell number and volume can be scaled accordingly as needed.
7. It may be desirable to utilize other lymphatic endothelial cell lines or primary lymphatic endothelial cells for this assay. If using any cells other than the SV-LEC line, the number of cells needed to generate a 100% confluent monolayer within 24 h should be determined experimentally. For this purpose, it is recommended that a series of twofold dilutions that span our recommended SV-LEC cell concentration be plated in triplicate for microscopic observation after 24 h.
8. It is critical to obtain a 100% confluent monolayer of lymphatic endothelial cells in order to prevent nonspecific binding of melanoma cells to any exposed surface on the tissue culture-treated plate, which would lead to an overestimation of melanoma cell adhesion to lymphatic endothelial cells. Likewise, overgrowth of SV-LEC cells beyond a single monolayer may result in melanoma cells binding to lymphatic

endothelial cells growing on top of the monolayer. Such conjugates are more likely to be removed during subsequent wash steps, leading to an underestimation of melanoma cell adhesion to lymphatic endothelial cells.

9. This step is necessary to synchronize different melanoma cell lines that may be in different stages of growth in their routinely maintained cell culture flasks.
10. Accutase Cell Detachment Solution is a nonenzymatic alternative to trypsin-EDTA for cell detachment and is used here to prevent the potential enzymatic cleavage of melanoma cell surface adhesion molecules. Trypsin-mediated cleavage of such adhesion molecules could interfere with ligand–receptor interactions between melanoma cells and lymphatic endothelial cells in the assay.
11. Unlike trypsin-EDTA, Accutase Cell Detachment Solution is inactivated at 37°C.
12. If cells have not completely detached within 10 min, they may be dislodged by holding the 6-well plate at a 45° angle and washing the wells by pipetting the Accutase solution across the entire surface of the wells several times.
13. Cell viability should be >95%.
14. These PBS washes are necessary to remove serum proteins that are present in the FBS component of the tumor growth medium. CFSE binds to FBS proteins, and failure to remove these proteins will interfere with the subsequent CFSE staining of melanoma cells.
15. DMEM supplemented with 0.5% BSA is used here in place of complete growth medium containing 10% FBS in order to eliminate attachment factors found in FBS. Use of medium containing FBS at this stage might otherwise result in nonspecific adherence of melanoma cells to exposed tissue culture plastic should any small gaps in the lymphatic endothelial cell monolayer be exposed during wash steps in the subsequent adhesion assay.
16. Take care not to disturb the SV-LEC monolayer during medium removal and all wash steps. During washing, do not pipet the 1× PBS directly onto the monolayer. Rather, gently pipet 1× PBS onto the side of the wells in the 48-well plate, and allow it to slowly rinse across the bottom of the wells. When removing the 1× PBS, tilt the plate at a 45° angle and pipet out the solution from the bottom of the well.
17. As with the previous 1× PBS washes, do not pipet directly onto the monolayer but allow the DMEM with 0.5% BSA to slowly run from the side of the well down across the surface of the monolayer. Medium with BSA is again used in this step

so that attachment factors found in FBS are not introduced into the assay system.

18. Again, pipet tumor cells gently along the side of the well so as not to disturb the SV-LEC monolayer. Once tumor cells have been added, the plate can be gently swirled and moved left–right and up–down to distribute the cells evenly within the well. The assay should be performed in triplicate for each cell type or experimental condition.
19. If cells have not completely detached within 10 min, they may be dislodged by holding the 48-well plate at a 45° angle and washing the wells by pipetting the Accutase solution across the entire surface of the wells several times.
20. Because it will be difficult to recover the full 200 µl volume of cells in Accutase solution from the wells without introducing varying levels of air bubbles in each sample, it is better to collect a consistent volume of 175 µl across each sample. Collecting equal volumes at this stage will allow for a consistent volumetric acquisition of samples during the subsequent flow cytometry and is crucial to accurate quantitation when comparing the number of adherent tumor cells across samples.
21. For each sample, collect only 150 µl of the 175 µl volume so as not to run the flow cytometer dry. As alluded to in **Note 20**, collecting equal volumes for each sample makes it possible during data analysis to compare across samples the number of melanoma cells that had adhered to the SV-LEC monolayer.

Acknowledgments

D5.1G4 murine melanoma cells were a generous gift of Dr. Jerry Neiderkorn (University of Texas Southwestern Medical School). The SV-LEC murine melanoma cell line was kindly provided by Dr. Jonathan Alexander (Louisiana State University Health Sciences Center). This work was supported by funding from Virginia's Commonwealth Health Research Board, a Jeffress Trust Awards Program in Interdisciplinary Research Grant from the Thomas F. and Kate Miller Jeffress Memorial Trust (Bank of America, N.A., Trustee), and a Hampden-Sydney College Research Grant from the Arthur Vining Davis endowment to KMH. We also thank Mr. Michael Hargadon and Mrs. Patricia Hargadon for generous donations to support the involvement of Hampden-Sydney College undergraduate students in this research.

Competing Interests The authors have no conflicts of interest to declare that are relevant to the content of this chapter.

References

1. Luke JJ, Flaherty KT, Ribas A, Long GV (2017) Targeted agents and immunotherapies: optimizing outcomes in melanoma. Nat Rev Clin Oncol 14:463–482. https://doi.org/10.1038/nrclinonc.2017.43
2. Hargadon KM, Johnson CE, Williams CJ (2018) Immune checkpoint blockade therapy for cancer: an overview of FDA-approved immune checkpoint inhibitors. Int Immunopharmacol 62:29–39. https://doi.org/10.1016/j.intimp.2018.06.001
3. Soleymanitabar A, Keshavarz-Fathi M, Hargadon KM, Rezaei N (2023) Immunotherapy for cutaneous melanoma. In: Rezaei N (ed) Handbook of cancer and immunology. Springer, Cham, pp 1–35. https://doi.org/10.1007/978-3-030-80962-1_237-1
4. Chen J, Xu Y, Zhou Y et al (2016) Prognostic role of sentinel lymph node biopsy for patients with cutaneous melanoma: a retrospective study of surveillance, epidemiology, and end-result population-based data. Oncotarget 7:45671–45677. https://doi.org/10.18632/oncotarget.10140
5. Doepker MP, Thompson ZJ, Harb JN et al (2016) Dermal melanoma: a report on prognosis, outcomes, and the utility of sentinel lymph node biopsy. J Surg Oncol 113:98–102. https://doi.org/10.1002/jso.24088
6. Pilko G, Zgajnar J, Music M, Hocevar M (2012) Lower tumour burden and better overall survival in melanoma patients with regional lymph node metastases and negative preoperative ultrasound. Radiol Oncol 46:60–68. https://doi.org/10.2478/v10019-011-0028-1
7. Kim C, Economou S, Amatruda TT et al (2015) Prognostic significance of microscopic tumor burden in sentinel lymph node in patients with cutaneous melanoma. Anticancer Res 35:301–309
8. Ulmer A, Dietz K, Hodak I et al (2014) Quantitative measurement of melanoma spread in sentinel lymph nodes and survival. PLoS Med 11:e1001604. https://doi.org/10.1371/journal.pmed.1001604
9. Kretschmer L, Mitteldorf C, Hellriegel S et al (2021) The sentinel node invasion level (SNIL) as a prognostic parameter in melanoma. Mod Pathol 34:1839–1849. https://doi.org/10.1038/s41379-021-00835-5
10. Cochran AJ, Wen DR, Huang RR et al (2022) Sentinel lymph node melanoma metastases: assessment of tumor burden for clinical prediction of outcome in the first Multicenter Selective Lymphadenectomy Trial (MSLT-I). Eur J Surg Oncol 48:1280–1287. https://doi.org/10.1016/j.ejso.2022.01.021
11. Pereira ER, Kedrin D, Seano G et al (2018) Lymph node metastases can invade local blood vessels, exit the node, and colonize distant organs in mice. Science 359:1403–1407. https://doi.org/10.1126/science.aal3622
12. Brown M, Assen FP, Leithner A et al (2018) Lymph node blood vessels provide exit routes for metastatic tumor cell dissemination in mice. Science 359:1408–1411. https://doi.org/10.1126/science.aal3662
13. Reticker-Flynn NE, Zhang W, Belk JA et al (2022) Lymph node colonization induces tumor-immune tolerance to promote distant metastasis. Cell 185:1924–1942.e23. https://doi.org/10.1016/J.CELL.2022.04.019
14. Cianfarani F, Mastroeni S, Odorisio T et al (2012) Expression of vascular endothelial growth factor-C in primary cutaneous melanoma predicts sentinel lymph node positivity. J Cutan Pathol 39:826–834. https://doi.org/10.1111/j.1600-0560.2012.01955.x
15. Peppicelli S, Bianchini F, Calorini L (2014) Inflammatory cytokines induce vascular endothelial growth factor-C expression in melanoma-associated macrophages and stimulate melanoma lymph node metastasis. Oncol Lett 8:1133–1138. https://doi.org/10.3892/ol.2014.2297
16. Van Marck V, Stove C, Van Den Bossche K et al (2005) P-cadherin promotes cell-cell adhesion and counteracts invasion in human melanoma. Cancer Res 65:8774–8783. https://doi.org/10.1158/0008-5472.CAN-04-4414
17. Kreiseder B, Orel L, Bujnow C et al (2013) α-Catulin downregulates E-cadherin and promotes melanoma progression and invasion. Int J Cancer 132:521–530. https://doi.org/10.1002/ijc.27698
18. Botti G, Cerrone M, Scognamiglio G et al (2013) Microenvironment and tumor progression of melanoma: new therapeutic prospectives. J Immunotoxicol 10:235–252. https://doi.org/10.3109/1547691X.2012.723767
19. Jacquelot N, Duong CPM, Belz GT, Zitvogel L (2018) Targeting chemokines and chemokine receptors in melanoma and other cancers. Front Immunol 9:2480. https://doi.org/10.3389/fimmu.2018.02480
20. Rebhun RB, Cheng H, Gershenwald JE et al (2010) Constitutive expression of the alpha4 integrin correlates with tumorigenicity and lymph node metastasis of the B16 murine melanoma. Neoplasia 12:173–182. https://doi.org/10.1593/neo.91604
21. Jeong K, Murphy JM, Rodriguez YAR et al (2019) FAK inhibition reduces metastasis of

α4 integrin-expressing melanoma to lymph nodes by targeting lymphatic VCAM-1 expression. Biochem Biophys Res Commun 509:1034–1040. https://doi.org/10.1016/j.bbrc.2019.01.050

22. Ando T, Jordan P, Joh T et al (2005) Isolation and characterization of a novel mouse lymphatic endothelial cell line: SV-LEC. Lymphat Res Biol 3:105–115. https://doi.org/10.1089/lrb.2005.3.105
23. Fidler IJ, Gersten DM, Budmen MB (1976) Characterization in vivo and in vitro of tumor cells selected for resistance to syngeneic lymphocyte-mediated cytotoxicity. Cancer Res 36:3160–3165
24. Overwijk WW, Restifo NP (2001) B16 as a mouse model for human melanoma. Curr Protoc Immunol Chapter 20(Unit 20):1. https://doi.org/10.1002/0471142735.im2001s39
25. Knisely TL, Niederkorn JY (1990) Immunologic evaluation of spontaneous regression of an intraocular murine melanoma. Invest Ophthalmol Vis Sci 31:247–257
26. Hargadon KM, Forrest OA, Reddy PR (2012) Suppression of the maturation and activation of the dendritic cell line DC2.4 by melanoma-derived factors. Cell Immunol 272:275–282. https://doi.org/10.1016/j.cellimm.2011.10.003



Chapter 7

Wound Healing Assay for Melanoma Cell Migration

Juliano T. Freitas

Abstract

Cell migration is a critical process involved in morphogenesis, inflammation, and cancer metastasis. The wound healing assay is a simple, nonexpensive, and highly reproducible method to study cancer cell migration in vitro. It is based on the observation that cells growing in a monolayer migrate to re-establish cell contacts after the development of an artificial wound. The assay involves creation of a wound in a monolayer, image acquisition during wound closure, and comparison of migrated area at initial and final time points.

Keywords Melanoma, Metastasis, Cell migration, Wound healing, Wound scratch

1 Introduction

Cell migration is a pivotal process involved in physiologic and pathologic events, including morphogenesis, immune cell trafficking, inflammation, and cancer metastasis [1, 2]. In the context of cancer, metastasis is the ultimate cause of death in 90% of patients, and there are still many remaining gaps in our understanding of metastasis formation [3]. The establishment of metastases involves a series of intricate events. Cancer cells have to detach from the primary tumor and migrate through the extracellular matrix. Once invasive cells access the blood or lymphatic vessels, they can disseminate and establish new tumor colonies at distant sites [4].

Melanoma is a highly metastatic cancer that is responsible for 75% of all deaths related to cutaneous tumors. Once melanoma becomes metastatic, the patient has a very poor prognosis with the median survival of 6–12 months [5]. Therapeutic strategies aiming to disrupt the metastatic process are imperatively required for patients with melanoma. Along these lines, a better understanding of melanoma cell migration becomes essential as migration is an early event during melanoma metastasis formation [6].

The wound healing assay is a simple, nonexpensive, and highly reproducible method to study melanoma cell migration in vitro

Kristian M. Hargadon (ed.), *Melanoma*, Methods in Molecular Biology, vol. 3089,
https://doi.org/10.1007/978-1-0716-5619-8_7,
© The Author(s), under exclusive license to Springer Science+Business Media, LLC, part of Springer Nature 2027

[7, 8]. Wound healing assays can replicate key features of cell migration observed in vivo. The foundation of this assay is the fact that the creation of an artificial wound in cells growing in a monolayer initiates cell migration. Cells migrate perpendicularly to the wound edge until cellular contacts are re-established. The wound healing assay is appropriate to study cell–cell and cell–extracellular matrix interactions during cell migration [9]. The conventional wound healing assay requires the formation of a cell monolayer that is scratched in order to create a wound. Cell migration is monitored as images are captured immediately after wound creation and at given time points during wound closure. Images are then compared in order to calculate cell migration [10, 11].

2 Materials

1. Growth Medium: DMEM supplemented with 10% fetal bovine serum (FBS), 1× nonessential amino acids, 2.5 μg/ml of Plasmocin and 50 μg/ml of Gentamicin.
2. Serum-Free Medium: DMEM.
3. Migration Medium: Serum-free medium supplemented with 1% FBS.
4. Proliferation Inhibitor: Mitomycin C.
5. Migration Inhibitor (negative control): Dexamethasone.
6. Migration Stimulator (positive control): Epidermal growth factor (EGF).
7. Phosphate-buffered saline (PBS).
8. Incubator (5% CO_2, 37°C).
9. Six-well plate (or other size).
10. 200 μl micropipette tip (sterile).
11. Ultrafine tip marker.
12. Inverted microscope with camera.
13. ImageJ software (https://imagej.nih.gov/ij/download.html).

3 Methods

1. Seed 5×10^5 cells per well of a six-well dish and grow to 90%–95% confluence (1–2 days) (*see* **Note 1**).
2. When cells reach desirable confluency, serum-starve overnight using serum-free medium (*see* **Note 2**).

3. The following morning, treat all cells with mitomycin C (5 µg/ml–8 µg/ml) for 1 h to remove any effects of proliferation on wound closure [12] (*see* **Note 3**).
4. Use an ultrafine tip marker to draw a reference line on the exterior plastic surface of each well (*see* **Note 4**).
5. Make three separate wounds per well by scratching the monolayer culture using a sterile 200-µl micropipette tip. To create a wound, move the micropipette tip through the cells. Each wound should be perpendicular to the line drawn in Step 4. The layout of the wounds is illustrated in Fig. 1 (*see* **Note 5**).
6. Carefully rinse the cells 3× with PBS to remove cell debris and to eliminate any remaining mitomycin C.
7. Using the reference line drawn in Step 4 as a guide, acquire six images of each well (as shown in Fig. 1) on an inverted microscope at 40× (*see* **Note 4**).
8. Incubate cells with negative (10 µM dexamethasone) and positive (10 ng/ml EGF) controls for cell migration, as well as test compounds (dissolved in migration medium) at 37°C for 12–36 h (*see* **Notes 6 and 7**).
9. After the desirable incubation time, use the reference line drawn in Step 4 to monitor the same region (as described in

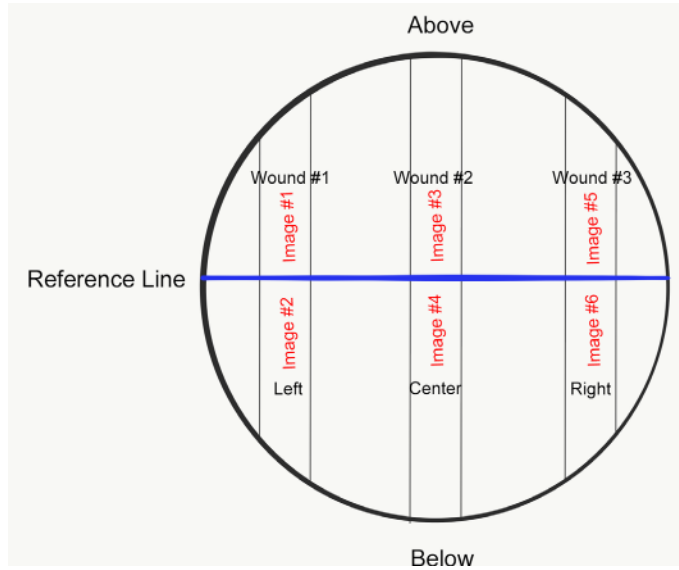


Fig. 1 Layout of wounds. Three wounds per well are created in the cell monolayer. The first wound is close to the left end of the well, the second is central to the well, and the third is close to the right end of the well. Two images are acquired for each wound: one below and the other above the reference line

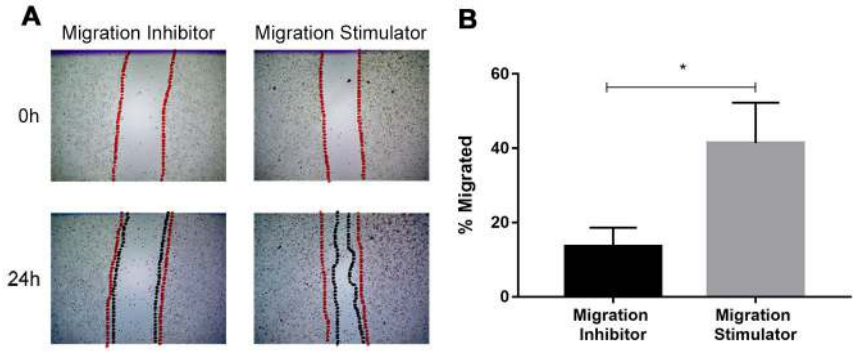


Fig. 2 Cell migration of melanoma cells. (**A**), Representative images acquired at 0 and 24 h post-wounding of A375 human melanoma cells treated with migration inhibitor (10 μM dexamethasone) or migration stimulator (10 ng/ml EGF). The initial wound area is represented in red while the migrated area is shown in black. (**B**), Percentage invaded area was determined by calculating the invaded area at 24 h to that at time 0 h. Six wound fields per treatment were examined. Data are presented as mean ± SEM. $*p < 0.05$

Step 7), and acquire a second image of the same wound field (*see* **Note 4**).

10. Quantify the migrated area in each image using ImageJ software:

    a. Select the edge of a cohesive group of cells using the *free-hand selection tool.*

    b. Under the *Analyze* tab, select the option *Measure* (or Press M key) and the software will automatically calculate the selected area (*see* **Note 8**).

    c. Calculate **migrated ratio** as the migrated area of each image normalized to its respective time 0 [13, 14] (*see* **Note 9**).

    d. Alternatively, the **migration effect** of each treatment can be calculated as: 1—migrated ratio (*see* **Note 9**) and is presented as percentage migrated. The migration effect of a migration inhibitor (dexamethasone) and a migration stimulator (EGF) on human A375 melanoma cells is shown in Fig. 2.

4 Notes

1. Experiments should be performed to empirically determine the cell density and time required for each cell line tested to reach 90%–95% confluence [8].

2. In order to form a monolayer, cells are cultivated in growth medium containing regular amount of serum (around 10% FBS). Before scratching the monolayer, cells should be serum-starved since serum contains growth factors that might stimulate cell proliferation. Additionally, to reduce the effect of proliferation, the migration medium should have a lower percentage of serum than growth medium. The amount of serum in the migration medium should be just enough to avoid cell death [9].
3. It is very important to prevent the confounding effect of cell proliferation during the wound healing assay. It has been suggested that mitogenic stimuli are released when the cell monolayer is scratched [15, 16]. Consequently, wound closure could be interpreted as a result of cell proliferation rather than cell migration. Treatment with proliferation inhibitors (i.e., mitomycin C) minimizes the impact of cell proliferation during the wound healing assay. Experiments should be performed to establish the ideal concentration at which the proliferation inhibitor prevents cell proliferation, and this can be easily achieved by counting the number of cells treated with the proliferation inhibitor. Previous experiments using cell counting are also helpful to validate that test conditions do not affect cell proliferation.
4. For quantitative analysis, it is crucial to acquire images of the same wound field during wound closure. As cells migrate, it might become difficult to match the initial and final wound field. Reference points on the bottom of the dish made using a razor blade can be used to monitor the same wound field. Alternatively, a reference line drawn using an ultrafine tip marker helps to match the same wound field for images acquired at time 0 and the next time point [9, 10, 17]. The reference line is also useful to increase the sample size of wound fields, as from the same scratch different images could be acquired above and below the reference line. An alternative approach that reduces the chances to acquire images of different wound fields is the employment of a time-lapse microscope. When using an automated time-lapse microscope, the plates are placed under the microscope in the same position at all times. Hence, the same wound field is consistently monitored during time-lapse acquisition [10].
5. To avoid contamination, scratching should be performed in sterile conditions [13]. Wounds should be as wide as possible since narrow wounds usually close faster [17]. Wounds must have similar width to reduce the variation that is not a consequence of different treatments [9]. To obtain wounds with similar sizes, move the micropipette tip slowly and continuously when scratching the cell monolayer [7]. It is possible

that some wounds have slightly different sizes. This may lead to misleading migratory rates. In order to minimize this bias, during the quantification process, the final area of each wound is normalized to its respective initial area.

6. In addition to the tested conditions, proper controls for cell migration should be included in the experimental design. For example, dexamethasone inhibits cell migration [18] and can be used as a negative control for cell migration. On the other hand, EGF [19] stimulates cell motility and can be considered a positive control for cell migration.
7. The amount of time cells migrate under different conditions should be determined based on previous trials by monitoring cell migration at different time points during wound closure. The ideal incubation time is determined by the time it takes cells moving under the fastest migration condition to reach imminent wound closure [9, 10].
8. During the quantification process, it is critical to standardize the cut-off point for what is included in the area of migration. When measuring collective cell migration, the migratory area is determined as the edge of a cohesive group of cells that can be visually identified, which excludes cells that migrated individually.
9. After incubation, experimental conditions that stimulate cell migratory behavior will result in a smaller migrated area, and therefore, a reduced migrated ratio when normalized to time 0. Conversely, experimental conditions that inhibit cell migration will generate a larger migrated area, resulting in an increased migration ratio. To facilitate intuitive data interpretation, the migration effect is calculated as 1—migration ratio and presented as % migrated, such that treatments that induce cell migration yield higher values, while treatments that inhibit migration yield lower values.

References

1. Stehbens SJ, Scarpa E, White MD (2024) Perspectives in collective cell migration—moving forward. J Cell Sci 137:jcs261549. https://doi.org/10.1242/jcs.261549
2. Yamamoto A, Doak AE, Cheung KJ (2023) Orchestration of collective migration and metastasis by tumor cell clusters. Annu Rev Pathol Mech Dis 18:231–256. https://doi.org/10.1146/annurev-pathmechdis
3. Chaffer CL, Weinberg RA (2011) A perspective on cancer cell metastasis. Science 331:1559–1564. https://doi.org/10.1126/science.1203543
4. Gerstberger S, Jiang Q, Ganesh K (2023) Metastasis. Cell 186:1564–1579. https://doi.org/10.1016/j.cell.2023.03.003
5. Schadendorf D, Fisher DE, Garbe C et al (2015) Melanoma. Nat Rev Dis Primers 1:15003. https://doi.org/10.1038/nrdp.2015.3

6. Nascentes Melo LM, Kumar S, Riess V et al (2023) Advancements in melanoma cancer metastasis models. Pigment Cell Melanoma Res 36:206–223. https://doi.org/10.1111/pcmr.13078
7. Pijuan J, Barceló C, Moreno DF et al (2019) In vitro cell migration, invasion, and adhesion assays: from cell imaging to data analysis. Front Cell Dev Biol 7:1–16. https://doi.org/10.3389/fcell.2019.00107
8. Justus CR, Leffler N, Ruiz-Echevarria M et al (2014) In vitro cell migration and invasion assays. J Vis Exp 88:51046. https://doi.org/10.3791/51046
9. Liang C-C, Park AY, Guan J-L (2007) In vitro scratch assay: a convenient and inexpensive method for analysis of cell migration in vitro. Nat Protoc 2:329–333. https://doi.org/10.1038/nprot.2007.30
10. Rodriguez LG, Wu X, Guan J-L (2005) Wound-healing assay. Methods Mol Biol 294:23–29. https://doi.org/10.1385/1-59259-860-9:023
11. Grada A, Otero-Vinas M, Prieto-Castrillo F et al (2017) Research techniques made simple: analysis of collective cell migration using the wound healing assay. J Invest Dermatol 137:e11–e16
12. Jozic I, Sawaya AP, Pastar I et al (2019) Pharmacological and genetic inhibition of caveolin-1 promotes epithelialization and wound closure. Mol Ther 27:1992–2004. https://doi.org/10.1016/j.ymthe.2019.07.016
13. Moreno-Bueno G, Peinado H, Molina P et al (2009) The morphological and molecular features of the epithelial-to-mesenchymal transition. Nat Protoc 4:1591–1613. https://doi.org/10.1038/nprot.2009.152
14. Zhang P, Huang C, Fu C et al (2015) Cordycepin (3'-deoxyadenosine) suppressed HMGA2, Twist1 and ZEB1-dependent melanoma invasion and metastasis by targeting miR-33b. Oncotarget 6:9834–9853. https://doi.org/10.18632/oncotarget.3383
15. Kramer N, Walzl A, Unger C et al (2013) In vitro cell migration and invasion assays. Mutat Res 752:10–24. https://doi.org/10.1016/j.mrrev.2012.08.001
16. Cory G (2011) Scratch-wound Assay. In: Wells CM, Parsons M (eds) Cell migration. Methods Mol Biol. Humana Press, New York, p 769
17. Valster A, Tran NL, Nakada M et al (2005) Cell migration and invasion assays. Methods 37:208–215. https://doi.org/10.1016/j.ymeth.2005.08.001
18. Han S, Bui NT, Ho MT et al (2016) Dexamethasone inhibits TGF-β1–induced cell migration by regulating the ERK and AKT pathways in human colon cancer cells via CYR61. Cancer Res Treat 48:1141–1153. https://doi.org/10.4143/crt.2015.209
19. Wickert LE, Pomerenke S, Mitchell I et al (2016) Hierarchy of cellular decisions in collective behavior: implications for wound healing. Sci Rep 6:20139. https://doi.org/10.1038/srep20139



Chapter 8

Evaluating Melanoma Cell Migration/Invasion in Transwell Assays by Flow Cytometry

Kristian M. Hargadon and James H. Lau

Abstract

Cell migration and invasion are vital aspects of melanoma biology that are critical to the progression of this aggressive cancer. Numerous in vitro assays are available to study these hallmark properties of cancer, including two-dimensional wound healing ("scratch") and transwell (Boyden chamber) assays, as well as three-dimensional microfluidic-based video microscopy assays and matrix/skin organ construct-based assays. Though each of these assays has unique advantages depending on the experimental question at hand, transwell assays are highly adaptable and thus particularly well-suited for investigating the role of specific stimulators/inhibitors of cancer cell migration and invasion. Traditionally, quantification of migrating/invading cells that are capable of transiting the Boyden chamber utilized in these assays is achieved by manual counting of cells that have reached the bottom chamber or by colorimetric/fluorometric detection of transited cells that were preloaded with specific dyes prior to assay initiation. These approaches, while commonly used, have inherent limitations in their design, including the introduction of quantification artifacts that arise from human error during direct cell counting or uneven/inconsistent cell labeling within/across experiments. To overcome these limitations, we have optimized a non-fluorescent flow cytometry-based assay for quantifying melanoma transwell migration and invasion, and we present herein an application of this assay to assess the role of the FOXC2 transcription factor in these processes.

Keywords Melanoma, Cell migration, Cell invasion, Transwell assay, Flow cytometry

1 Introduction

Tissue invasion and metastasis, one of the original core hallmarks of cancer as defined by Douglas Hannahan and Robert Weinberg in their seminal publication in *Cell* more than 25 years ago [1], are central processes that mark the transition of a primary tumor from a benign, localized state to a disseminated, malignant disease. Driven by a reversible genetic program in cancer cells that supports their phenotypic plasticity, the epithelial-mesenchymal transition (EMT) that accompanies cancer cell metastasis is marked by a shift in cells from a highly proliferative to a highly migratory and invasive phenotype [2]. Importantly, although EMT was originally described in the context

Kristian M. Hargadon (ed.), *Melanoma*, Methods in Molecular Biology, vol. 3089,
https://doi.org/10.1007/978-1-0716-5619-8_8,
© The Author(s), under exclusive license to Springer Science+Business Media, LLC, part of Springer Nature 2027

of cancer as a phenomenon shared by carcinomas of epithelial origin, evidence has since accumulated documenting an EMT-like program as a critical driver of melanoma progression as well [3, 4]. Indeed, the acquisition of migratory and invasive properties by melanoma cells contributes not only to the radial and vertical growth phases of primary melanomas but also to the seeding of metastatic growths characteristic of aggressive malignant melanomas.

Several in vitro assays and experimental systems have been developed to study cancer cell migration/invasion, and many of these have specifically been used to investigate these processes in the context of melanoma. Traditional wound healing ("scratch") assays rely on introduction of an artificial "wound" to a confluent monolayer of cells in culture, followed by real-time or endpoint monitoring of wound closure as a readout of cell migration. Such assays typically involve the use of a pharmacologic inhibitor of cell proliferation, such as mitomycin C, to prevent artifactual wound closure by proliferating cells, thus ensuring that any measured wound repair is achieved by actively migrating cells [5, 6] (see **Chap. 7 by Freitas JT in this volume**). Transwell (Boyden chambers) assays are useful for studying both migration and invasion, as these assays allow for the quantification of cells that have transited a porous membrane, which is either left uncoated (in the case of cell migration assays) or which is precoated with various matrices or cell monolayers of interest (in the case of cell invasion assays). In either case, migration/invasion of cells across the membrane from one chamber towards the other is typically directed by inclusion of some form of chemoattractant in the initially cell-free chamber [7, 8]. In addition to these two-dimensional cell migration/invasion assays, three-dimensional assays employing systems that more closely resemble the tumor microenvironment (TME) have also been developed. Among these systems are a range of microfluidics-based approaches [9, 10] and matrix/skin organ construct models [11–14] (see **Chap. 9 by Grahovac J, Wells A and Chap. 10 by Schmidt SK, Bosserhoff AK in this volume**).

Though transwell assays lack the complexity and microenvironmental nuances of tumor tissue that are advantages of more advanced experimental systems, they nevertheless remain useful tools for studying cancer cell migration and invasion, particularly as they are highly adaptable and thus well-suited for studies that aim to investigate the role of specific stimulators/inhibitors of these hallmark processes. Historically, however, transwell assays have been limited by their potential to be impacted by quantification artifacts that may arise from human error at various stages of experimental design, as their readout usually relies on direct counting of migrated/invaded cells or colorimetric/fluorescent-based detection that may be influenced by uneven/inconsistent cell labeling within/across experiments. To overcome these limitations, we describe herein an optimized non-fluorescent flow cytometry-based assay for quantifying melanoma cell transwell migration and invasion, and we present an application of this assay to assess the role of the EMT-associated transcription factor FOXC2 [15] in these processes.

2 Materials

Store all media and bovine serum albumin (BSA) at 4°C in the dark. Store fetal bovine serum (FBS) at −20°C in the dark. Store all other supplies at room temperature, unless otherwise indicated. Use sterile reagents and supplies for all procedures, and utilize non-pyrogenic pipets, pipet tips, and cell culture vessels for all work (*see* **Note 1**).

2.1 Cell Culture Media and Supplies

1. Melanoma cell lines: Herein, we describe the application of this protocol for use with the B16-F1 murine melanoma cell line and a CRISPR-Cas9 gene edited FOXC2-deficient variant of B16-F1 that we previously generated (B16-F1ΔFOXC2) [16, 17].
2. Complete Growth Medium (*see* **Note 2**): Dulbecco's Modified Eagle's Medium (DMEM) containing 4 mM L-glutamine, 4500 mg/L of glucose, 1 mM sodium pyruvate, and 1500 mg/L of sodium bicarbonate, supplemented with 10% FBS (*see* **Note 3**).
3. Starvation Medium: Serum-free DMEM containing 4 mM L-glutamine, 4500 mg/L of glucose, 1 mM sodium pyruvate, and 1500 mg/L of sodium bicarbonate, supplemented with 0.5% BSA. Filter-sterilize through a 0.22 μm filter following preparation.
4. Tissue culture-treated T75 flasks.
5. Trypsin-EDTA Solution, 1×: 0.25% Trypsin/0.53 mM EDTA in Hanks Balanced Salt Solution without calcium or magnesium.
6. Non-pyrogenic serological pipets and pipet tips.
7. Non-pyrogenic 15 ml conical centrifuge tubes.
8. Tabletop centrifuge.

2.2 Supplies and Reagents for Melanoma Cell Migration and Invasion Assays

1. Serum-free DMEM containing 4 mM L-glutamine, 4500 mg/L of glucose, 1 mM sodium pyruvate, and 1500 mg/L of sodium bicarbonate.
2. Endotoxin-free 1× phosphate-buffered saline (PBS), pH 7.4.
3. 0.4% trypan blue.
4. 96-well plate.
5. Hemocytometer.
6. Light microscope.
7. Tissue culture-treated six-well plates.
8. Corning® 6.5 mm Transwell® with 8.0 μm Pore Polycarbonate Membrane Insert (*see* **Note 4**), prepackaged as 12 inserts in a 24-well tissue culture-treated plate (for migration assays).
9. Corning® BioCoat® Growth Factor Reduced Matrigel Invasion Chamber with 8.0 μm PET Membrane (*see* **Note 4**),

prepackaged as 12 inserts in a 24-well tissue culture-treated plate (for invasion assays) (*see* **Note 5**). Store at −20°C.

10. 24-well plates (in addition to the prepackaged plates listed in **items 7** and **8** of this section).
11. Forceps.
12. Accutase Cell Detachment Solution.
13. Rotating platform.
14. Flow cytometry tubes (Titertube micro test tubes or 1.5 ml microcentrifuge tubes).
15. Flow cytometer.

3 Methods

Carry out all cell culture procedures in a biosafety cabinet to maintain sterility throughout the experiment.

3.1 Maintenance and Passaging of Cell Cultures

Maintain all cell lines at 37°C in a humidified incubator with 5% CO_2, and passage cell lines at 80%–90% confluency (*see* **Note 6**).

1. Propagate melanoma cells in Complete Growth Medium in tissue culture-treated T75 flasks.
2. As cells approach 80%–90% confluency and require passaging, remove and discard cell culture medium from T75 flasks.
3. Add 4 ml of 1× Trypsin-EDTA solution to flasks, and return to cell culture incubator to promote cellular detachment (*see* **Note 7**).
4. Neutralize Trypsin-EDTA solution with 10 ml of Complete Growth Medium, and transfer cells to a 15 ml conical centrifuge tube. Centrifuge cells at 450 × *g* for 5 min.
5. Decant supernatant and resuspend cells in appropriate volume of Complete Growth Medium.
6. Reseed new T75 flasks with necessary fraction of cells in a total volume of 15 ml of medium.
7. Use remaining cells to perform the cell migration (see Sect. 3.2) and/or cell invasion (see Sect. 3.3) assays.

3.2 Cell Migration Assay

A schematic of the transwell cell migration assay is depicted in Fig. 1, along with example data collected in replicate experiments in which serum-starved B16-F1 and B16-F1ΔFOXC2 cells were assessed for migration toward Complete Growth Medium. The assay can be easily adapted to monitor cell migration toward any chemoattractant in the bottom chamber, and cells may also be pretreated with putative

inhibitors/stimulators of migration to monitor their effects on cell motility.

1. Harvest melanoma cells as described in Sect. 3.1.

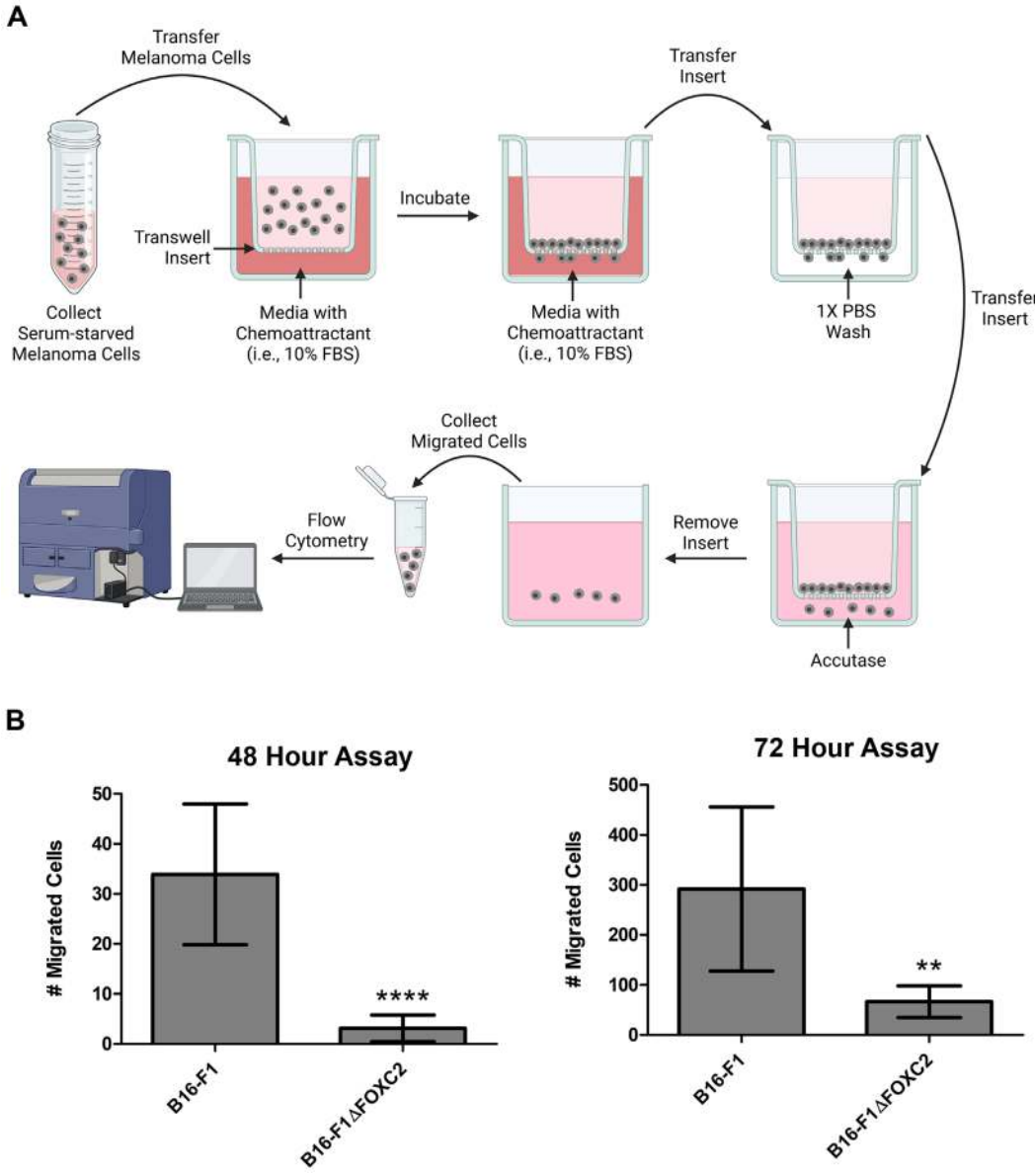


Fig. 1 (**A**), Schematic of the flow cytometry-based transwell migration assay. (**B**), Representative data from 48-h (left) and 72-h (right) migration assays performed with B16-F1 and B16-F1ΔFOXC2 melanoma cells. Data are pooled from three independent experiments, each with three replicates per group, and are graphed as the average of all replicates with error bars that represent standard deviation of the mean. * = $p < 0.05$, ** = $p < 0.01$, *** = $p < 0.001$, **** = $p < 0.0001$. Portions of this figure were created in BioRender [Hargadon, K. (2026) https://BioRender.com/l9yvzqo]

2. Following centrifugation of cells at 450 × *g* for 5 min, decant supernatant and resuspend cell pellet in an appropriate volume of Complete Growth Medium.
3. Transfer 20 µl of cell suspension to one well of a 96-well plate, and mix with 20 µl of 0.4% trypan blue.
4. Perform a live cell count on a light microscope using a hemocytometer and trypan blue exclusion (*see* **Note 8**).
5. To prepare cells for serum starvation, wash cells twice in endotoxin-free 1× PBS, and resuspend cells at 1.0e^6 cells/ml in serum-free Starvation Medium.
6. Plate 1.0e^6 cells for each cell type under study into separate wells of a six-well tissue culture-treated plate.
7. Culture cells for 24 h at 37°C in a humidified incubator with 5% CO_2 (*see* **Note 9**).
8. After the 24-h serum starvation period, transfer medium containing floating cells to a 15 ml conical centrifuge tube.
9. Collect remaining adherent cells by trypsinization with 500 µl of 1× Trypsin-EDTA solution, and transfer detached cells to the 15 ml conical centrifuge tube containing the previously collected nonadherent cells from Step 8 of this section.
10. Add 2 ml of Starvation Medium, and centrifuge at 450 × *g* for 5 min.
11. Discard supernatant, and resuspend cell pellet in an appropriate volume of Starvation Medium for cell counting as described in Steps 3 and 4 of this section (*see* **Note 10**).
12. Resuspend cells at a concentration of 2.5e^5 cells/ml in Starvation Medium (*see* **Note 11**).
13. Remove transwell inserts from a prepackaged 24-well tissue-cultured treated plate (Corning® 6.5 mm Transwell® with 8.0 µm Pore Polycarbonate Membrane Insert), and add 600 µl of Complete Growth Medium to the appropriate number wells needed for the experiment (*see* **Notes 12 and 13**).
14. Replace transwell inserts, ensuring that the entire bottom surface is in contact with the medium in the lower chamber of the plate.
15. To the upper chamber of the transwell insert, add 100 µl (2.5e^4 cells) of tumor cell suspension prepared in Step 12 of this section (*see* **Note 12**). Add another 200 µl of Starvation Medium to this upper chamber to ensure that the chamber does not dry out in experiments assessing migration at extended time points.
16. Culture cells for the appropriate period of time (as determined by experimental optimization for specific cell lines) at 37°C in a humidified incubator with 5% CO_2 (*see* **Note 14**).

17. At the appropriate experimental time point(s), remove the transwell insert from the migration assay plates using forceps, and transfer the insert to a new 24-well plate preloaded with 400 µl of endotoxin-free 1× PBS to wash the underside of the transwell membrane.
18. Immediately transfer the inserts again to another 24-well plate in which the wells have been preloaded with 400 µl of Accutase Cell Detachment Solution (*see* **Note 15**).
19. Incubate plates at room temperature for 10 min with gentle shaking on a rotating platform set to 100 rpm to dislodge cells that have migrated to the underside of the membrane.
20. Following incubation, collect 370 µl of the cell suspension in Accutase Cell Detachment Solution from each well, and transfer samples to tubes suitable for use with a flow cytometer (*see* **Note 16**).
21. Run samples on a flow cytometer, setting either a standard time of sample collection or a standard volume of sample collection to ensure consistency in collection across all samples within and across experiments (*see* **Note 17**).
22. To analyze the flow cytometric data, draw a live cell gate to exclude debris, and record the number of live cells collected as the number of migrated cells for each sample. Data from replicate samples should be averaged and used to calculate the standard deviation for graphing purposes.

3.3 Cell Invasion Assay

A schematic of the transwell cell invasion assay is depicted in Fig. 2, along with example data collected in replicate experiments in which serum-starved B16-F1 and B16-F1ΔFOXC2 cells were assessed for invasion of Corning® BioCoat® Growth Factor Reduced Matrigel toward Complete Growth Medium (*see* **Note 18**). Although Matrigel is a commonly used matrix for cell invasion studies, this assay can be easily adapted to monitor cell invasion through various other matrices should investigators wish to coat transwell membranes with their own matrix proteins of interest, rather than using pre-coated membranes as described herein. Additionally, as with the cell migration assay described in Sect. 3.2, this invasion assay can also be refined to include pre-treatment of cells with putative inhibitors/stimulators of invasion to monitor their effects on this hallmark cancer process.

1. Harvest melanoma cells as described in Sect. 3.1.
2. Following centrifugation of cells at 450 × *g* for 5 min, decant supernatant and resuspend cell pellet in an appropriate volume of Complete Growth Medium.
3. Transfer 20 µl of cell suspension to one well of a 96-well plate, and mix with 20 µl of 0.4% trypan blue.

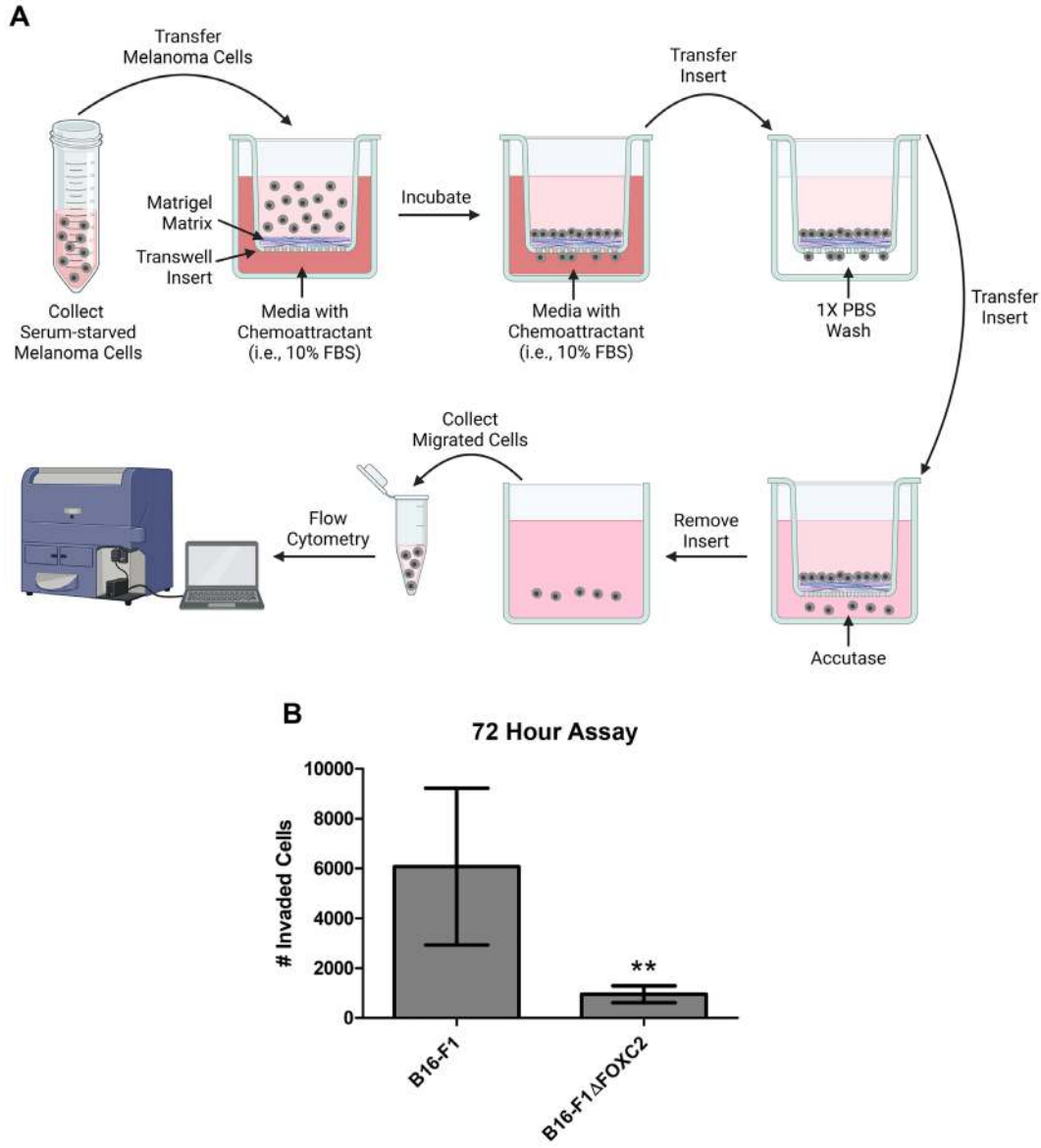


Fig. 2 (**A**) Schematic of the flow cytometry-based transwell invasion assay. (**B**), Representative data from a 72-h invasion assay performed with B16-F1 and B16-F1ΔFOXC2 melanoma cells. Data are pooled from two independent experiments, each with three replicates per group, and are graphed as the average of all replicates with error bars that represent standard deviation of the mean. * = $p < 0.05$, ** = $p < 0.01$, *** = $p < 0.001$, **** = $p < 0.0001$. Portions of this figure were created in BioRender [Hargadon, K. (2026) https://BioRender.com/boshy43]

4. Perform a live cell count on a light microscope using a hemocytometer and trypan blue exclusion (*see* **Note 8**).
5. To prepare cells for serum starvation, wash cells twice in endotoxin-free 1× PBS, and resuspend cells at 1.0e^6 cells/ml in serum-free Starvation Medium.
6. Plate 1.0e^6 cells in for each cell type under study into separate wells of a six-well tissue culture-treated plate.
7. Culture cells for 24 h at 37°C in a humidified incubator with 5% CO_2 (*see* **Note 9**).
8. ~1.5 hours before the end of the 24-h serum starvation period, remove a 24-well plate containing Corning® BioCoat® Growth Factor Reduced Matrigel Invasion Chambers with 8.0 μm PET Membranes from the −20°C freezer, and bring the plate to room temperature for 30 min (*see* **Note 19**).
9. Following the 30-min incubation at room temperature, rehydrate the Matrigel coating by adding 500 μl of serum-free DMEM to the interior of the insert (i.e., the upper chamber). Incubate plates for 2 h at 37°C in a humidified incubator with 5% CO_2.
10. After the 24-h serum starvation period (and during the last hour of Matrigel rehydration), collect serum-starved melanoma cells by first transferring medium containing floating cells to a 15 ml conical centrifuge tube.
11. Collect remaining adherent cells by trypsinization with 500 μl of 1× Trypsin-EDTA solution, and transfer detached cells to the 15 ml conical centrifuge tube containing the previously collected nonadherent cells from Step 10 of this section.
12. Add 2 ml of Starvation Medium, and centrifuge at 450 × *g* for 5 min.
13. Discard supernatant, and resuspend cell pellet in an appropriate volume of Starvation Medium for cell counting as described in Steps 3 and 4 of this section (*see* **Note 10**).
14. Resuspend cells at a concentration of 2.5e^5 cells/ml in Starvation Medium (*see* **Note 11**).
15. Remove the Corning® BioCoat® Growth Factor Reduced Matrigel Invasion Chamber plate from the incubator.
16. Add 600 μl of Complete Growth Medium to the bottom chamber of appropriate wells as needed for the experiment (*see* **Notes 12 and 13**).

17. Replace transwell inserts, ensuring that the entire bottom surface is in contact with the medium in the lower chamber of the plate.
18. Carefully remove the rehydration medium from the transwell insert, using precaution not to disturb the Matrigel matrix coating the membrane (*see* **Note 20**).
19. To the upper chamber of the transwell insert, add 100 µl ($2.5e^4$ cells) of tumor cell suspension prepared in Step 14 of this section (*see* **Note 12**). Add another 200 µl of Starvation Medium to this upper chamber to ensure that the chamber does not dry out in experiments assessing invasion at extended time points.
20. Culture cells for the appropriate period of time (as determined by experimental optimization for specific cell lines) at 37°C in a humidified incubator with 5% CO_2 (*see* **Note 14**).
21. At the appropriate experimental time point(s), remove the transwell insert from the invasion assay plates using forceps, and transfer the insert to a new 24-well plate preloaded with 400 µl of endotoxin-free 1× PBS to wash the underside of the transwell membrane (*see* **Note 21**).
22. Immediately transfer the inserts again to another 24-well plate in which the wells have been preloaded with 400 µl of Accutase Cell Detachment Solution (see Note 15).
23. Incubate plates at room temperature for 10 min with gentle shaking on a rotating platform set to 100 rpm to dislodge cells that have migrated to the underside of the membrane.
24. Following incubation, collect 370 µl of the cell suspension in Accutase Cell Detachment Solution from each well, and transfer samples to tubes suitable for use with a flow cytometer (see Note 16).
25. Run samples on a flow cytometer, setting either a standard time of sample collection or a standard volume of sample collection to ensure consistency in collection across all samples within and across experiments (see Note 17).
26. To analyze the flow cytometric data, draw a live cell gate to exclude debris, and record the number of live cells collected as the number of invaded cells for each sample. Data from replicate samples should be averaged and used to calculate the standard deviation for graphing purposes.

4 Notes

1. Pipet tips, serological pipets, and cell culture vessels should be certified non-pyrogenic, as pyrogen exposure may alter gene expression/cellular behavior and could therefore influence experimental outcomes.
2. The Complete Growth Medium described here is optimal for propagation and maintenance of the B16-F1 murine melanoma cell line and should be adjusted accordingly based on supplier recommendations for alternative melanoma cell lines.
3. We recommend using a high-grade FBS that has been tested and verified to have a low endotoxin level so as to minimize the risk of endotoxin signaling that could alter gene expression and cellular behavior. For the work described herein, we used Premium Select FBS from GeminiBio (SKU #S11550).
4. Corning® Transwell® membrane inserts are available in various pore sizes, ranging from 0.4 μm to 8.0 μm. For the study of migration/invasion by large tumor cells, the largest 8.0 μm pore size should be used.
5. We recommend the use of Growth Factor Reduced Matrigel Invasion Chambers for these assays so as to avoid artifacts that might be introduced by cellular stimulation with growth factor-enriched Matrigel, including the potential such stimulation might have to reduce cellular invasion through Matrigel toward the chemoattractant under investigation.
6. Do not allow cell lines to reach 100% confluency during routine maintenance as this may result in contact inhibition and interference with cell behavior during subsequent assays. As a guideline for passaging of the B16-F1 cell line used in the application of the protocol presented in this chapter, cells can be split 1:10 every 2 days or 1:30 every 3 days.
7. The duration of trypsinization is cell-line dependent and should be only long enough to promote cell detachment. As a recommendation for the B16-F1 cell line described in this procedure, trypsinize cells for 2–3 min. If necessary, lightly tap the flasks to dislodge any cells that remain adherent. Avoid repeated or strong tapping of the flasks, however, as this action will result in clumping of trypsinized cells.
8. Cell viability should be >95% under standard culture conditions.
9. Note that B16-F1 melanoma cells, a typically adherent cell line, become less adherent and begin to grow as clumps of floating cells following serum starvation. After a 24-h serum starvation period, the culture will have a mix of both lightly adherent and floating cells.

10. Because melanoma cells tend to become clumpy during serum starvation, it is important to mix the resuspended cells well by pipetting and vortexing to generate a single cell suspension for accurate cell counting at this stage.
11. The recommendations provided herein should yield a sufficient number of cells to allow for multiple replicates in the assay, as our protocol requires $2.5e^4$ cells per replicate.
12. We recommend running each cell line under investigation in triplicate wells.
13. As an optional negative control, additional wells can be filled with 600 μl of Starvation Medium (i.e., no chemoattractant), such that the bottom receiving chamber is filled with the same medium as the upper chamber into which cells will be loaded.
14. Because specific cell lines exhibit differences in migratory/invasive properties and thus are likely to migrate/invade at different rates in these assays, we recommend that initial experiments be designed as time course studies in which cells are collected at various time points to monitor migration/invasion across the transwell insert. It is important to identify cells shortly after they have transited the insert in order to identify true differences in migration/invasion between experimental samples, as delayed collection will allow time for transited cells to proliferate within the lower chamber and thus interfere with data interpretation. Specifically, proliferation of cells that migrate/invade at different rates but whose collection is delayed will artifactually inflate apparent differences in migratory/invasive capacity of the distinct samples under study. Likewise, different samples that migrate/invade similarly but which proliferate at different rates will also exhibit artifactual differences in the number of cells entering the lower chamber if cells are collected too long after their initial migration/invasion. We suggest setting up time course studies to assess migration/invasion at 12, 24, 48, and 72 h to determine the optimal time of collection.
15. At this stage, we recommend the use of Accutase Cell Detachment Solution, as opposed to a 1× Trypsin-EDTA Solution, because it can be run directly through a flow cytometer without the need for centrifugation and resuspension of cells in another buffer. Additionally, Accutase is a gentler cell dissociation agent than trypsin and thus better maintains cell surface marker expression and overall health of fragile cells. Though gentle dissociation is not particularly necessary for the application we describe herein, which aims only to quantify the number of migrated cells, it is particularly important for investigators who may wish to couple

this quantitative readout with other analyses (such as surface molecule phenotyping) of migratory cells.

16. To avoid introducing air bubbles into the collected sample that could negatively affect flow cytometric performance, we recommend that users of this protocol collect only 370 µl of the 400 µl sample volume.
17. Failure to set a consistent sample collection method will render the interpretation of any data obtained with this protocol invalid, as it will not be possible to make fair comparisons of the number of migrated cells if different sample volumes are collected from distinct samples.
18. It is expected that invasion assays will exhibit a smaller number of cells transiting the membrane filter than migration assays that are conducted over the same period of time, since cells must also degrade and penetrate the matrix coating the transwell filter during an invasion assay. However, even when using Growth Factor Reduced Matrigel Invasion Chambers as we describe herein, the presence of trace growth factors can still promote proliferation of melanoma cells prior to invasion, meaning that a larger number of cells may indeed end up being detected in the invasion assay as compared to the migration assay, as is the case in the example data we provide in Figs. 1 and 2.
19. The Corning® BioCoat® Growth Factor Reduced Matrigel Invasion Chambers come prepackaged as 12 inserts in a Falcon® 24-well cell culture insert companion plate. If the 12 inserts are not all needed for a single assay, remove only the necessary number of inserts, and transfer them to a separate Falcon® 24-well cell culture insert companion plate. It is critical to use only Falcon® 24-well cell culture insert companion plates, as these plates have predesigned notches to ensure proper positioning of inserts. Be sure to transfer any inserts using sterile forceps while working in a laminar flow biosafety cabinet to avoid contamination, as invasion assays may require up to a 72-h culture period. Additionally, return unused inserts to the −20°C freezer quickly so that they do not thaw, as repeated freeze-thaw cycles will damage the Matrigel matrix barrier coating the membrane.
20. We recommend gently pipetting rehydration medium out of the chamber by touching the pipet tip only to the side of the insert so that the Matrigel matrix is left undisturbed.
21. Optimal culture periods for invasion assays will necessarily be longer than for migration assays, as cells must first penetrate the Matrigel matrix before transiting the insert membrane pores.

Acknowledgments

This work was supported by funding from Virginia's Commonwealth Health Research Board, a Jeffress Trust Awards Program in Interdisciplinary Research Grant from the Thomas F. and Kate Miller Jeffress Memorial Trust (Bank of America, N.A., Trustee), and a Hampden-Sydney College Research Grant from the Arthur Vining Davis endowment to KMH. This work was also supported by a Sigma Xi Grant-in-Aid of Research to JHL. We also thank Mrs. Patricia Hargadon and Mr. Michael Hargadon for generous donations to support the involvement of a Hampden-Sydney College undergraduate student in this research.

Conflict of Interest The authors have no conflicts of interest to declare that are relevant to the content of this chapter.

References

1. Hanahan D, Weinberg RA (2000) The hallmarks of cancer. Cell 100:57–70. https://doi.org/10.1016/s0092-8674(00)81683-9
2. Lambert AW, Weinberg RA (2021) Linking EMT programmes to normal and neoplastic epithelial stem cells. Nat Rev Cancer 21:325–338. https://doi.org/10.1038/S41568-021-00332-6
3. Caramel J, Papadogeorgakis E, Hill L et al (2013) A switch in the expression of embryonic EMT-inducers drives the development of malignant melanoma. Cancer Cell 24:466–480. https://doi.org/10.1016/j.ccr.2013.08.018
4. Pedri D, Karras P, Landeloos E et al (2022) Epithelial-to-mesenchymal-like transition events in melanoma. FEBS J 289:1352–1368. https://doi.org/10.1111/febs.16021
5. Capparelli C, Purwin TJ, Glasheen MK et al (2022) Targeting SOX10-deficient cells to reduce the dormant-invasive phenotype state in melanoma. Nat Commun 13:1381. https://doi.org/10.1038/s41467-022-28801-y
6. Freitas JT, Jozic I, Bedogni B (2021) Wound healing assay for melanoma cell migration. Methods Mol Biol 2265:65–71. https://doi.org/10.1007/978-1-0716-1205-7_4
7. Xuan X, Cao J, Chen L et al (2024) DTL promotes the growth and migration of melanoma cells through the ERK/E2F1/BUB1 axis. Sci Rep 14:26288. https://doi.org/10.1038/s41598-024-76477-9
8. Justus CR, Marie MA, Sanderlin EJ, Yang LV (2023) Transwell in vitro cell migration and invasion assays. Methods Mol Biol 2644:349–359. https://doi.org/10.1007/978-1-0716-3052-5_22
9. Mehta P, Rahman Z, Dijke PT, Boukany PE (2022) Microfluidics meets 3D cancer cell migration. Trends Cancer 8:683–697. https://doi.org/10.1016/j.trecan.2022.03.006
10. Ayuso JM, Sadangi S, Lares M et al (2021) Microfluidic model with air-walls reveals fibroblasts and keratinocytes modulate melanoma cell phenotype, migration, and metabolism. Lab Chip 21:1139–1149. https://doi.org/10.1039/d0lc00988a
11. Grahovac J, Becker D, Wells A (2013) Melanoma cell invasiveness is promoted at least in part by the epidermal growth factor-like repeats of tenascin-C. J Invest Dermatol 133:210–220. https://doi.org/10.1038/jid.2012.263
12. Hill DS, Robinson NDP, Caley MP et al (2015) A novel fully humanized 3D skin equivalent to model early melanoma invasion. Mol Cancer Ther 14:2665–2673. https://doi.org/10.1158/1535-7163.MCT-15-0394
13. Aranha ESP, Mendonça L deS, Almeida B deL et al (2024) Three dimensional reconstruction of skin with melanoma: a model for study of invasion in vitro. Toxicol Vitr 99:105883. https://doi.org/10.1016/j.tiv.2024.105883
14. de Barros DPC, Ventura S, Duque M et al (2026) Development of a 3D skin model for studying melanoma progression. Cells 15:379. https://doi.org/10.3390/cells15040379
15. Hargadon KM, Goodloe TB, Lloyd ND (2022) Oncogenic functions of the FOXC2 transcription factor: a hallmarks of cancer perspective. Cancer Metastasis Rev 41:833–852. https://doi.org/10.1007/S10555-022-10045-3

16. Hargadon KM, Györffy B, Strong EW et al (2019) The FOXC2 transcription factor promotes melanoma outgrowth and regulates expression of genes associated with drug resistance and interferon responsiveness. Cancer Genom Proteom 16:491–503. https://doi.org/10.21873/cgp.20152

17. Hargadon KM, Williams CJ (2020) RNA-seq analysis of wild-type vs. FOXC2-deficient melanoma cells reveals a role for the FOXC2 transcription factor in the regulation of multiple oncogenic pathways. Front Oncol 10:267. https://doi.org/10.3389/fonc.2020.00267

Part III

3D Cell Culture Systems for Studying Melanoma Biology



Chapter 9

Skin Organ Constructs for In Vitro Modeling of Melanoma Invasion

Jelena Grahovac and Allan Wells

Abstract

Melanoma progression from an in situ lesion to an invasive dermal tumor is strongly associated with poor patient prognosis, with depth of invasion serving as a predictor of survival. Increasing evidence indicates that remodeling of the extracellular matrix (ECM) plays a central role in this transition by altering both mechanical and biochemical cues within the tumor microenvironment. To facilitate mechanistic studies of ECM-mediated melanoma invasion, we developed a reproducible in vitro skin organ construct (SOC) model that recapitulates key structural and cellular features of human skin. The SOC system is assembled using a two-layer collagen-based dermal equivalent containing primary human dermal fibroblasts, overlaid with normal human epidermal keratinocytes to generate a stratified epidermis. Melanoma cells are subsequently seeded onto the reconstructed epidermal surface and cultured under defined conditions, including staged modulation of epidermal growth factor and exposure to an air–liquid interface to promote keratinization. The model permits incorporation of defined ECM components or genetically modified melanoma cells to evaluate their impact on tumor invasion. Melanoma progression is assessed by measuring radial growth and quantifying invasion depth and patterns in paraffin-embedded sections using histological and immunohistochemical analyses. This SOC platform provides a physiologically relevant and customizable system to investigate ECM-driven mechanisms of melanoma invasion and to evaluate candidate therapeutic targets that modulate tumor–microenvironment interactions.

Keywords Melanoma invasion, In vitro modeling, Skin organ constructs, Extracellular matrix

1 Introduction

In order to develop better therapies for metastatic melanoma, it is important to identify the mechanisms by which tumor cells invade into surrounding tissues. While melanoma in situ has a high cure rate by surgical resection, invasive melanoma that has penetrated dermis has very poor prognosis with the depth of invasion in primary tumors highly correlating with patient survival [1]. Elucidating changes that precede and/or induce melanoma invasion from the epidermis into the dermis is of critical importance. Remodeling of the extracellular matrix (ECM) plays a significant role in melanoma invasion as ECM

Kristian M. Hargadon (ed.), *Melanoma*, Methods in Molecular Biology, vol. 3089,
https://doi.org/10.1007/978-1-0716-5619-8_9,
© The Author(s), under exclusive license to Springer Science+Business Media, LLC, part of Springer Nature 2027

proteins provide both mechanical and chemical cues to the tumor cells [2, 3]. Indeed, production of ECM proteins is significantly altered in melanoma compared to the normal skin: components characteristic of an immature and healing dermis, such as Tenascin C (TNC), Fibronectin, certain laminins, and SPARC, are upregulated [4–7], while components characteristic of a mature matrix, such as Decorin, Lumican, and certain collagens, are down-regulated [8].

Here, we present a protocol developed for assembling in vitro skin organ constructs (SOCs), in part based on the three-dimensional organotypic raft cultures [9], that can be fine-tuned to study the influence of ECM components on melanoma invasion.

2 Materials

1. Normal human epidermal keratinocytes (NHEKS) obtained from Invitrogen (Grand Island, NY, USA) and cultured on collagen-coated dishes in Epilife medium with growth supplements [e.g., Keratinocyte Medium Supplement, Product No. K 2007 from Sigma containing bovine pituitary extract, bovine insulin, hydrocortisone, bovine transferrin, and human epidermal growth factor (EGF) (*see* **Note 1**)].
2. Neonatal human dermal fibroblasts cultured in DMEM with 10% fetal bovine serum (FBS), used under the sixth passage (*see* **Note 2**).
3. Melanoma cell line: We used WM1158 (stably transfected with GFP) from the Wistar Institute (Philadelphia, PA, USA), cultured in DMEM:L15 medium at a 3:1 mixture supplemented with 10% FBS.
4. Collagen Resuspension Buffer: Dissolve 2.2 g of $NaHCO_3$ and 4.77 g of HEPES in 100 ml of 0.05 N NaOH. Filter-sterilize the solution, aliquot (2–5 ml), and store long-term at −20°C. Working buffer aliquots can be stored at 4°C for a couple of months.
5. SOC Maintenance Medium: For 1 L of medium, mix 750 ml of DMEM (4.5 g/l glucose) and 250 ml of F12 Ham's nutrient mixture. Remove 100 ml to achieve a 900 ml volume of medium, and supplement with the following additives to restore the final volume to 1 L: 10 ml of Penicillin–Streptomycin stock (final concentration of 100 U/mL of penicillin and 100 µg/mL of streptomycin), 50 ml of fetal calf serum (FCS), 25 ml of 1 M HEPES (25 mM final concentration), 1 ml of 1000× hydrocortisone (0.4 ng/ml final concentration), 1 ml of 1000× cholera toxin (0.1 nM final concentration), and 10 ml of 10X medium cocktail (10 µM adenine, 5 µg/ml of insulin, 5 µg/ml of transferrin, and 5 µg/

ml of T3 final concentrations). Just prior to use, also add 5 ng/ml of EGF (*see* **Note 4**).

6. 25 cm^2 cell culture flasks: polystyrene-treated, with filter caps, for adherent cells.
7. 15 mL conical centrifuge tubes.
8. Six-well cell culture plates.
9. 4.7 mm R cloning rings (e.g., Bel Art, 14-512-78, Thermo Fisher Scientific).
10. 0.45 μm pore size culture plate inserts (e.g., Millicell-HA, Cat. #PIHA 03050).
11. Metal mesh grids, optional (*see* **Note 3**).
12. Small sterile spatula.
13. ~4 mg/ml of bovine collagen.
14. Hank's balanced salt solution (HBSS).
15. Fetal calf serum.
16. F12 Ham's nutrient mixture.
17. Dulbecco Modified Eagle Medium (DMEM) with L-glutamine and 4.5 g/l glucose.
18. Penicillin–Streptomycin stock solution.
19. 10× Minimal Essential Medium with Earl salts (10× EMEM) without additives.
20. 0.25% Trypsin with 0.5 mM EDTA.
21. Phosphate-buffered saline (PBS), sterile-filtered.
22. 10% formalin fixing solution.
23. Image J or Imaris software.

3 Methods

3.1 Assembly of the SOC Dermal Part

On Day 1, dermal SOC layers are made in a six-well plate. Keep all the reagents on ice. Perform all the mixing gently to avoid forming bubbles. Perform all mixing on ice to prevent premature polymerization of collagen.

1. To prepare the *acellular layer*, mix the following:
   a. 0.6 ml of Collagen Resuspension Buffer.
   b. 0.6 ml of 10× EMEM.
   c. 4.2 ml of collagen solution.
   d. 0.6 ml of NaOH to neutralize.

2. Aliquot 1 ml of the above mixture per well of a six-well plate, and distribute evenly to cover the bottom of the well.
3. Place the plate into a humidified incubator with 5% CO_2 at 37°C to form a gel while you prepare the cellular part.
4. To prepare the *cellular layer*, harvest at least 1.8×10^6 fibroblasts (300,000 per SOC), spin cells at $450 \times g$ for 5 min, and decant the supernatant. Wash the pellet once with PBS and decant (*see* **Note 5**).
5. Add 1.8 ml of Collagen Resuspension Buffer and 1.8 ml of 10× EMEM directly to the cell pellet, and gently resuspend. Mix thoroughly. The mixture will be ruby red.
6. Add 8.4 ml of cold collagen and mix well, but very gently to avoid generation of bubbles. The mixture will turn straw yellow.
7. Add 1.8 ml of NaOH to neutralize, and mix well until the mixture becomes light pink.
8. At this stage, different ECM proteins can be added into the cellular layer, as desired based on investigator interest (*see* **Note 6**).
9. Aliquot 3 ml of the mixture per well on top of the acellular layer in the six-well plate.
10. Incubate the plate for 30 min at 37°C to allow the mixture to solidify.
11. After 30 min, add 4 ml of DMEM containing 10% FBS on top of the gel.
12. The next day (Day 2), release the gels from the edges of the six-well plate with a small aluminum spatula or scoop so that they can contract equally.
13. Change the medium to DMEM containing 10% FBS every other day. At this point, the gels might float off the surface so be careful not to aspirate them when changing the medium (*see* **Note 7**).

3.2 Assembly of the SOC Epidermal Part

1. Inspect the gels every day. On Days 4 or 5, depending on the cell passage of fibroblasts (younger cells will contract faster), gels should be contracted almost to half of their initial size, forming a concave surface.
2. Change the medium to HBSS for 1 h to wash the calcium off from the gels.
3. Harvest at least 3×10^6 keratinocytes for six SOCs. The more keratinocytes are seeded, the more layers will form the epidermis. 500,000 cells is the minimal number for the epidermis to properly form on this surface.

4. Spin keratinocytes down at 450 × *g* for 5 min, decant the supernatant, and resuspend in 1.2 ml of SOC Maintenance Medium containing 5 ng/ml of EGF.
5. Aspirate HBSS from the dermal parts, and add 200 µl of keratinocyte mixture on top of each gel drop-wise into the concave area.
6. Place the plate into the incubator for 30 min without adding extra medium to allow the keratinocytes to attach.
7. After 30 min, add enough of SOC Maintenance Medium containing 5 ng/ml of EGF on top and around the gel, so that it is fully immersed.

3.3 Seeding of Melanoma Cells into SOC

1. Prepare 600,000 melanoma cells (100,000 cells per SOC), and resuspend in 600 µl of SOC Maintenance Medium containing a reduced EGF concentration of 2.5 ng/ml. At this stage, melanoma cells stably transfected to produce ECM proteins or their fragments of interest can be seeded [7].
2. Aspirate medium from the SOCs, and gently put the small cloning ring on top.
3. Aliquot 100 µl of the melanoma cell suspension into the cloning ring (Fig. 1, **left panel**).
4. Return culture to the incubator for 1 h to allow melanoma cells to attach.
5. After 1 h, add SOC Maintenance Medium containing 2.5 ng/ml of EGF around the cloning ring and fully submerge

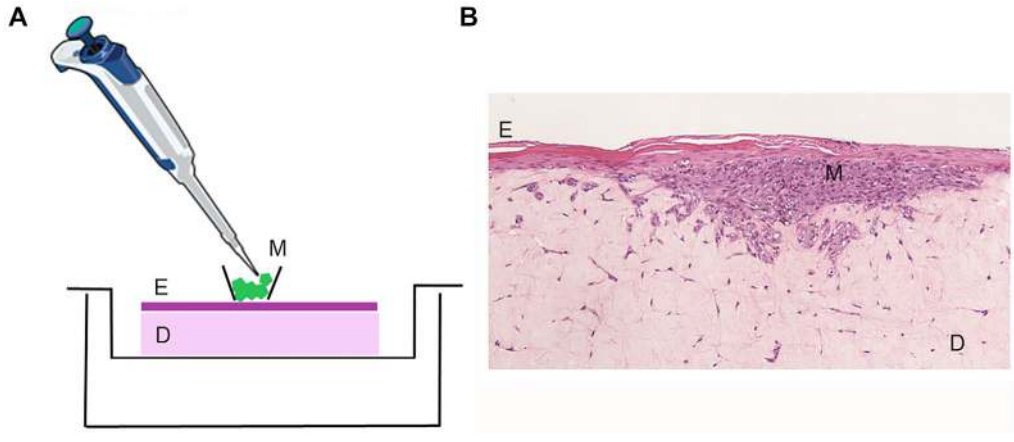


Fig. 1 (**A**), Schematic representation of the procedure for seeding melanoma cells into the SOC. (**B**), Photomicrograph of H&E-stained SOC. D-dermis, E-epidermis, M-melanoma cells

the entire SOC in medium, before carefully removing the cloning ring.

6. On the fourth day after seeding of keratinocytes and second day after seeding of melanoma cells, expose the SOC to air to allow keratinization of the epidermal layer:
   a. Transfer SOCs carefully with an aluminum spatula/spoon under the gel, either into the 0.45 μm pore size culture plate inserts in six-well plates or onto the metal grids in 60 mm dishes (place the gel in the center of the grid if using this latter option).
   b. Add SOC Maintenance Medium without EGF into the wells in the six-well plate or around the grid in the dishes so that the liquid reaches the bottom of the skin but does not overflow to the top.
7. Change medium every other day until collection. SOCs can be maintained without degradation for up to 20 days after seeding of melanoma cells, depending on the melanoma cell line seeded (Fig. 2).
8. Quantify radial spread of melanoma on the surface with a caliper.

3.4 SOC Collection and Immunohistochemistry

1. On the 14th to 20th days after seeding melanoma cells, carefully transfer the SOC into the 10% formalin fixing solution (*see* **Note 8**).
2. After overnight fixation, proceed with the standard paraffin embedding and processing (*see* **Note 9**).
3. Cut 5 μM sections of the paraffin-embedded SOC tissue, and proceed with the preferred immunohistochemistry protocol. As an example, Fig. 3 displays sections that were stained with hematoxylin and eosin (H&E) [panels on the left] or with anti-TNC antibody (panels on the right).
4. Quantify the depth and pattern of invasion with Image J or Imaris software.



Fig. 2 SOC on a metal grid. (**A**) SOC without melanoma. (**B**) SOC seeded with GFP-expressing WM1158 melanoma cells on Day 10 after seeding. (**C**) SOC seeded with GFP-expressing WM1158 melanoma cells on Day 20 after seeding

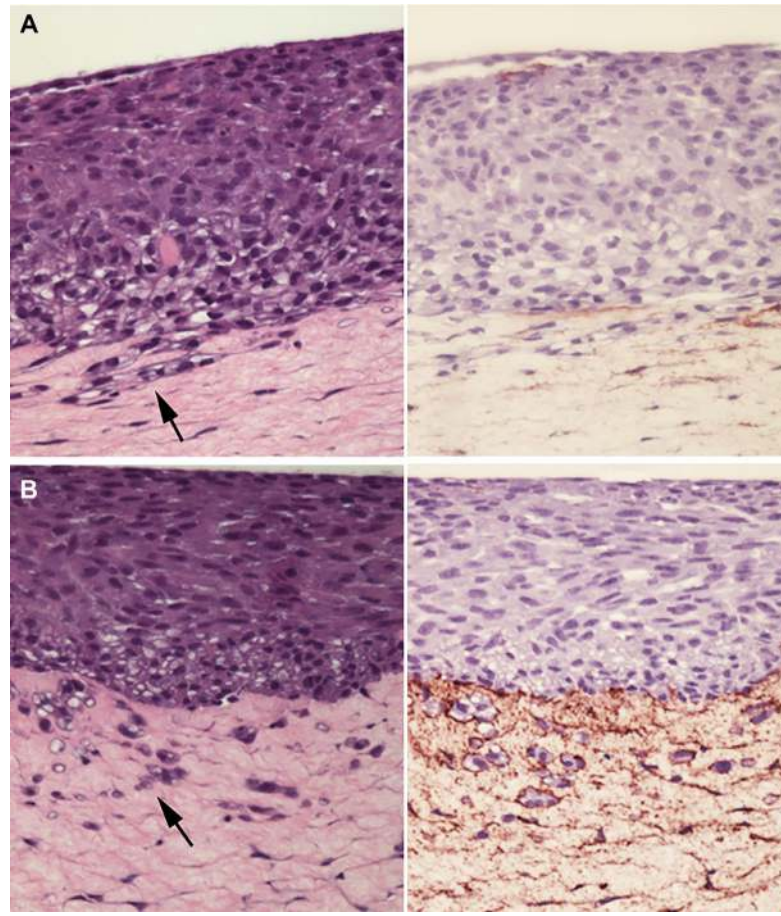


Fig. 3 Representative images of SOCs seeded with WM1158 melanoma cells after 20 days of culture in SOCs with the standard collagen dermis (**A**) or dermis with the addition of 4 μg/ml of the EMC protein TNC (**B**). H&E staining on the left and TNC staining on the right. Note the change in shape/mode of the invading cells between the two conditions (arrowheads)

4 Notes

1. An immortalized cell line such is HaCat can also be used, though it forms a very thin epidermal layer.
2. Try to use primary cells under the sixth passage for consistent results. The Hs68 (ATCC® CRL-1635™) cell line can also be used, but it does not contract the dermis as primary freshly isolated fibroblast cells do.
3. For culture at the air-liquid interface, SOCs can be placed in a transwell insert in a six-well plate, or they can be placed on

a sterile mesh grid (Fig. 2) in a 10 cm dish, allowing for maintenance of several SOCs in the same dish for high-throughput experiments.

4. A concentration of 5 ng/ml of EGF allows keratinocyte proliferation that will form several layers in the epidermis. At the time of melanoma seeding, this concentration is lowered to 2.5 ng/ml of EGF, and at exposure of SOCs to the air–liquid interface, EGF is excluded to allow keratinization of the top layer. Always add fresh EGF to the maintenance medium prior to use, as EGF degrades quickly in aqueous solutions at room temperature.
5. 300,000 early passage dermal fibroblasts contract the collagen gel within 4 days of culture. For later passages, optimization of the cell number per SOC may be needed. Optimization may also be required when including ECM components that impact cell contractility, such as fibronectin, tenascin C, or hyaluronan.
6. In the example shown in Fig. 3, we added 4 μg/ml of TNC.
7. Cultures can be left over the weekend without changing the medium; they will do just fine if enough medium is added to the rim of the well.
8. SOCs can be analyzed by any molecular biology technique used for fresh or paraffin-embedded tumor tissue. For RNA and protein isolation, do not fix, but instead proceed to isolation straight after a gentle wash with PBS.
9. To maximize representation of the "tumor" in the SOC specimen, fixed SOC can be cut with a sterile scalpel into strips and placed into the cassette so that the vertical edges are exposed for sectioning.

Acknowledgments

The authors would like to thank Dr. Arthur Huen for the help in establishment of SOCs and Diane George for paraffin embedding and SOC sectioning. JG was supported by the grant Agreement No. 451-03-136/2025-03/200043 with the Ministry of Education, Science, and Technological Development of the Republic of Serbia.

Conflict of Interest The authors have no conflicts of interest to declare that are relevant to the content of this chapter.

References

1. Wanebo HJ, Woodruff J, Fortner JG (1975) Malignant melanoma of the extremities: a clinicopathologic study using levels of invasion (microstage). Cancer 35(3):666–676. https://doi.org/10.1002/1097-0142(197503)35:3<666::aid-cncr2820350320>3.0.co;2-4
2. Wells A, Grahovac J, Wheeler S et al. (2013) Targeting tumor cell motility as a strategy against invasion and metastasis. Trends Pharmacol Sci 34(5):283–289. https://doi.org/10.1016/j.tips.2013.03.001
3. Grahovac J, Wells A (2014) Matrikine and matricellular regulators of EGF receptor signaling on cancer cell migration and invasion. Lab Invest 94(1):31–40. https://doi.org/10.1038/labinvest.2013.132
4. Ilmonen S, Jahkola T, Turunen JP et al. (2004) Tenascin-C in primary malignant melanoma of the skin. Histopathology 45(4):405–411. https://doi.org/10.1111/j.1365-2559.2004.01976.x
5. Ledda F, Bravo AI, Adris S et al. (1997) The expression of the secreted protein acidic and rich in cysteine (SPARC) is associated with the neoplastic progression of human melanoma. J Invest Dermatol 108(2):210–214
6. Pyke C, Romer J, Kallunki P et al. (1994) The gamma 2 chain of kalinin/laminin 5 is preferentially expressed in invading malignant cells in human cancers. Am J Pathol 145(4):782–791
7. Grahovac J, Becker D, Wells A (2013) Melanoma cell invasiveness is promoted at least in part by the epidermal growth factor-like repeats of tenascin-C. J Invest Dermatol 133(1):210–220. https://doi.org/10.1038/jid.2012.263
8. Hood BL, Grahovac J, Flint MS et al. (2010) Proteomic analysis of laser microdissected melanoma cells from skin organ cultures. J Proteome Res 9(7):3656–3663. https://doi.org/10.1021/pr100164x
9. Simpson CL, Kojima S, Getsios S (2010) RNA interference in keratinocytes and an organotypic model of human epidermis. Methods Mol Biol 585:127–146. https://doi.org/10.1007/978-1-60761-380-0_10



Chapter 10

Modeling Proliferative Versus Migratory Melanoma Cell Phenotypes Using Biofabricated Matrices

Sonja K. Schmidt and Anja K. Bosserhoff

Abstract

Biofabrication enables the controlled generation of three-dimensional cell cultures that can be highly useful to study different cellular phenotypes. As melanoma cells reveal high plasticity, and the "phenotype switching model" defining the cells as either proliferative or migratory active has been described, we recently developed a 3D bioprinted model mimicking these phenotypes. Here, we describe the generation of these bioprinted models based on either Matrigel or Cellink Bioink, which can be used with various cell lines and which allows for the analysis of cell response on microscopic and molecular levels. This model system offers novel opportunities for fundamental research and drug testing on heterogeneous tumors like melanoma.

Keywords Bioprinting, 3D cell culture, Hydrogel, Plasticity, Heterogeneity

1 Introduction

Melanomas are highly heterogeneous tumors in which the tumor cells can constantly change and adapt to microenvironmental cues due to their cellular plasticity. This involves reprogramming of gene expression patterns, whereby a previously proliferative cell can transition to a migratory state or vice versa. These processes are crucial for the development and progression of melanoma, and a deeper understanding may help to find molecular targets that control them.

In vivo, cells are confronted with various stimuli, including those of the extracellular matrix, which changes during migration and invasion into new tissues. In order to analyze if this can be modeled using 3D, we cultured cells on classic 2D culture dishes or in 3D in alginate hydrogel, observed cell behavior over 7 days and performed transcriptome analysis by RNA sequencing (RNA-Seq) [1]. The different morphologies, growth rates, and the plethora of differentially regulated genes exhibited by cells grown under these distinct

Kristian M. Hargadon (ed.), *Melanoma*, Methods in Molecular Biology, vol. 3089,
https://doi.org/10.1007/978-1-0716-5619-8_10,
© The Author(s), under exclusive license to Springer Science+Business Media, LLC, part of Springer Nature 2027

conditions impressively demonstrated the impact of the matrix and the ability of the cells to adapt to it (Fig. 1).

Moreover, we analyzed whether we can induce different phenotypes by different hydrogels, in a controlled manner [2]. To ensure the creation of reproducible 3D cultures in vitro, we used extrusion-based 3D printing, which allows us to deposit the bioinks with spatial control. Since all hydrogels, have different properties, different protocols must be used for printing the inks (Fig. 2A). In first screenings, we observed that different melanoma cell behavior can be triggered by the matrix, making hydrogel cultures, an extremely interesting platform to analyze molecular patterns of distinct cellular phenotypes (Fig. 2B).

For this reason, we have developed a 3D model that, in two separate approaches, allows us to map a proliferative and a nonproliferative but migratory phenotype of a cell line, enabling us to study and compare their regulation in greater detail. This 3D model is based on the two hydrogels, Matrigel and Cellink Bioink (CIB) (Fig. 2). Like most hydrogels suitable for cell culture, CIB and Matrigel have in common that they are mixed with the cells, printed, and cross-linked afterwards to maintain a stable structure. This cross-linking is induced chemically or by a temperature shift, respectively. Once cross-linked, the hydrogel-cell constructs can be submerged in the cell's culture medium and cultivated for the desired period of time.

We revealed that melanoma cells proliferate in Matrigel in vitro, while cells from the same cell line establish a G1 arrest when cultured in CIB [3]. Surprisingly, despite G1 arrest, we observed strong cell growth on the well bottom after a few days in culture. In addition, scattered directed structures are found in the constructs, indicating cell migration. In addition, the invasive capacity of the cells in CIB was proven in vivo in the arteriovenous (AV) loop model in rats [4].

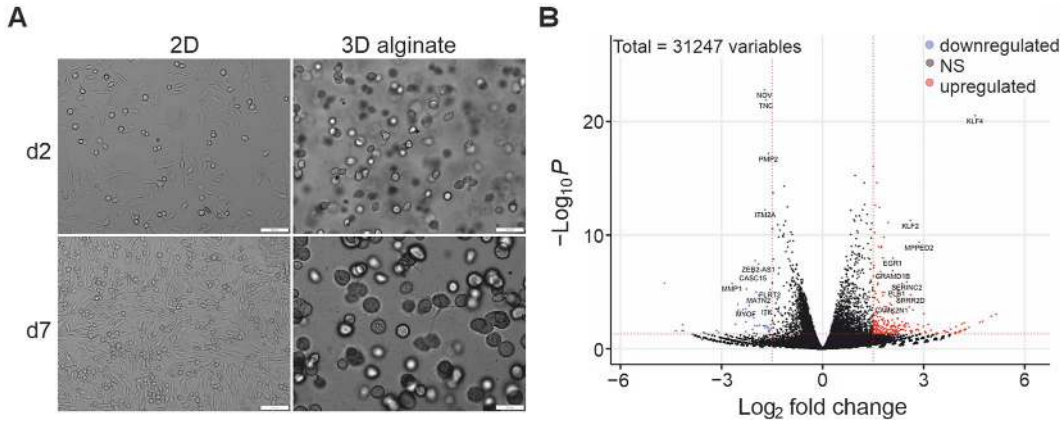


Fig. 1 Comparison of melanoma cell line Mel Im cultured on 2D culture dishes or in 3D alginate hydrogel. Reproduced from [1], under a CC BY license. (**A**), Microscope images from respective cultures on days 2 (d2) or 7 (d7). Scale bar = 100 μm. (**B**), Volcano plot of differentially expressed genes in 3D alginate versus 2D culture

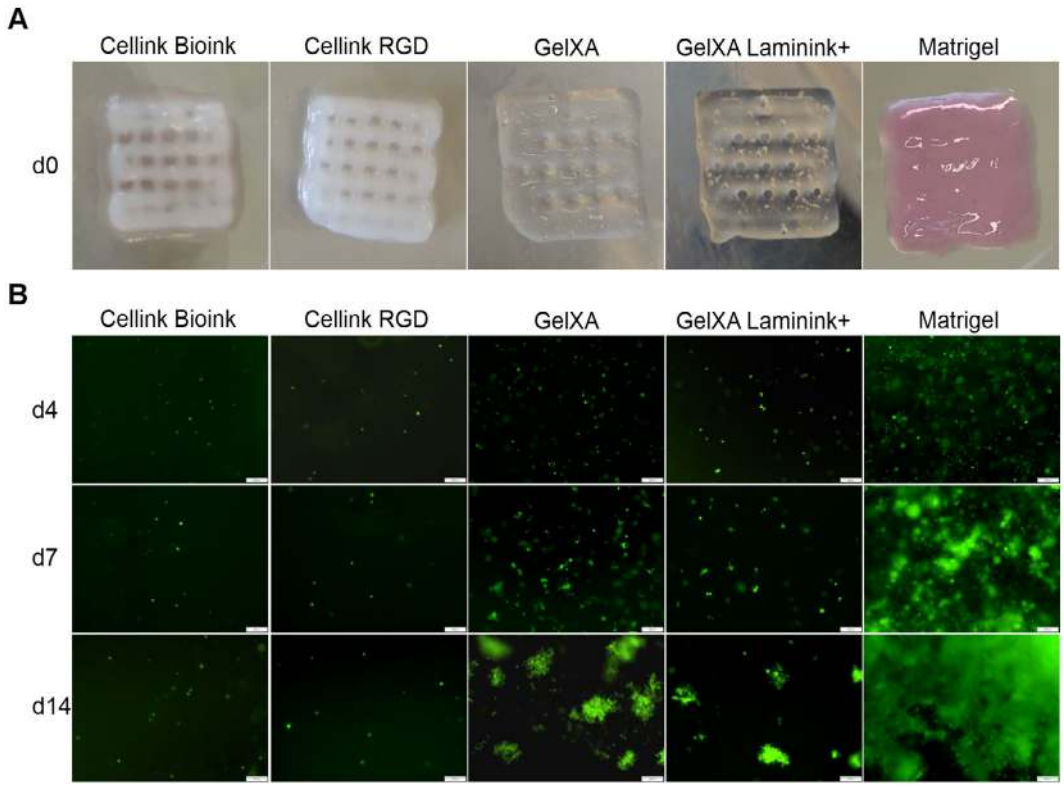


Fig. 2 Different hydrogels induce different cell behavior. Reproduced from [2], under a CC BY license. (**A**), Macroscopic images of exemplary hydrogels after cross-linking. (**B**), Behavior of the fluorescently labeled melanoma cell line Mel Im (GFP) on days 4, 7, and 14 (d4, d7, and d14) in these hydrogels. Scale bar = 200 μm

In summary, in this experiment, the bioink (=CIB + cells) is filled into a closed chamber that is connected to the rat only via a blood vessel loop, where it is stably cross-linked and left in the animal for 4 weeks. After completion of the experiment, metastases were detected in the animals' lymph nodes, demonstrating that cells invaded into the enclosed blood vessel and traveled from there to the lymph vessels and ultimately to the lymph nodes, where they could proliferate again.

RNA-Seq data from cells from in vitro CIB or Matrigel culture and their bioinformatic evaluation once again confirmed our hypothesis that the cells in CIB establish not only a migratory and mesenchymal but also a neural-crest- or stem-like character [5]. We, therefore, recommend our comparative model as a cell culture assay for analyzing the relevance of a gene of interest in the development or maintenance of a mesenchymal phenotype.

Our published analyses of the relevance of the transcription factors AP2ε and FHL2 in this process exemplify how the assay can be integrated into a research project answering questions like, How is a particular gene expressed at a defined time point in the mesenchymal

versus mitotic phenotype? Or, in the case of transcription factors, how active are they in the respective phenotype? This can, of course, be analyzed for different cell lines (also from different tumor types) and at different time points. Although we have not observed any cell lines being able to proliferate in CIB without prior genetic modification, we recommend verifying the G1 arrest and cell survival in CIB prior to further testing using the FUCCI cell cycle reporter system over at least 7 days.

2 Materials

1. Cellink® Bioink.
2. Corning® Matrigel® Basement Membrane Matrix, LDEV-free (~10 mg/ml protein).
3. Cross-linking solution: 50 mM $CaCl_2$.
4. Extrusion-based 3D bioprinter.
5. 3cc cartridges with piston and tip cap.
6. 22G conical nozzles.
7. 1 ml syringes.
8. Female–female luer lock adapter for syringes.
9. Thin spatula.
10. Cells + cell culture equipment (sterile hood, incubator, etc.).
11. Cell culture medium with supplements as appropriate for specific cell lines: Dulbecco's Modified Eagle Medium (DMEM) with 10% fetal calf serum (FCS) and penicillin (400 U/ml)/streptomycin (50 µg/ml) (P/S) for the lines described herein.
12. 6-well plates.

3 Methods

All steps are carried out at room temperature, unless otherwise specified.

3.1 Preparations for Bioprinting

1. Generate a G-code for one grid structure (10 mm × 10 mm × 1.2 mm; three layers; flow rate 600 mm/min) per well of a 6-well plate (*see* **Textbox 1** for G-code for Cellink + bioprinter).
2. Thaw Matrigel overnight in a refrigerator (4°C) (*see* **Note 1**).
3. Let CIB warm up to room temperature (*see* **Note 1**).
4. To prepare the cell suspension, harvest cells from the culture plate as usual, centrifuge, and resuspend pellet in fresh culture medium. Count the cells, and set the cell number to 11× of the

desired final concentration (3.3 million cells/ml for a final concentration of 300,000 cells/ml in the hydrogel) in cell culture medium including supplements (*see* **Note 2**).

3.2 Bioprinting Matrigel

1. Mix 500 µl Matrigel on ice with 50 µl of the prepared cell suspension (*see* **Note 3**).
2. Pipette the Matrigel-cell mix into a 3cc cartridge with tip cap, and add piston using a thin spatula. Make sure air can pass by the piston to avoid the Matrigel-cell mix getting compressed in the cartridge.
3. Incubate at room temperature for 45 min to pre-cross-link the mixture.
4. Remove the tip cap and apply a 22G conical nozzle.
5. Print three grid structures into a 6-well plate using a 3D bioprinter at ~5–15 kPa.
6. Incubate printed constructs for 30 min at 37°C.
7. Add 2 ml cell culture medium per well.
8. Incubate under the cells' usual culture conditions.
9. Perform subsequent analysis (see Sect. 3.4).

3.3 Bioprinting Cellink Bioink According to Manufacturer's Description

1. Mix 500 µl CIB carefully with 50 µl of the prepared cell suspension by pushing back and forth between two 1 ml syringes connected by a luer lock adapter four times until the mixture looks homogeneous (*see* **Notes 3 and 4**).
2. Transfer the bioink via a luer lock adapter into a 3cc cartridge with piston.
3. Add 22G conical nozzle and directly print six grid structures into a 6-well plate, using a 3D bioprinter at ~15–30 kPa.
4. Gently cover the constructs in cross-linking solution for 5 min.
5. Take off the cross-linking solution and wash the constructs once with cell culture medium.
6. Add 2 ml cell culture medium per well.
7. Incubate under the cells' usual culture conditions.
8. Perform subsequent analysis (see Sect. 3.4).

3.4 Subsequent Analyses

Based on the different composition and properties of the hydrogels, experimental procedures necessarily have to be adjusted. For subsequent analyses, in order to maintain best comparability between the two conditions, equal or at least highly similar protocols should be used for the materials whenever possible. Below is guidance for various downstream analyses that can be performed following experiments using this protocol (*see* **Note 5**):

1. Microscopy: Imaging of printed constructs should be carried out in an incubator microscope to maintain ideal culture conditions for the cells at all times. Be aware that CIB is a semitranslucent material (Fig. 3). Best microscopy images and documentation of the cells can be obtained using fluorescently labeled cells, e.g., cells with cytoplasmic expression of GFP or specific reporters (see below). However, for certain molecular analyses (e.g., RNA-Seq), unmodified cells need to be used to avoid artifacts.
2. Fluorescent reporter assays: Fluorescent reporter cells are a very helpful tool for the analysis of cell behavior in the 3D materials over time, as they enable real-time observation of cell behavior with spatial resolution without termination of the experiment. Briefly, reporter cells express a fluorescent signal upon a respective stimulus, which can be detected in the 3D constructs by fluorescence microscopy. In order to generate reporter cell lines, they need to be stably transduced with a reporter plasmid of interest. Many reporter plasmids already exist, including the FUCCI cell cycle reporter, as well as reporters for morphology, hypoxia, p21, p53, caspase, or transcription factor activity, and many more (Fig. 4).
3. RNA analysis: As the cellulose in CIB leads to clogging in filter columns, we highly recommend using TRIzol reagent to isolate RNA from the cells cultured in hydrogels, as this procedure is based on phase separation. Depending on the cell concentration, we suggest pooling multiple constructs (for 300,000 cells/ml pool three CIB grids) to increase RNA yields.
4. Gene knockdown or overexpression studies: Gene knockdown or overexpression should be carried out by transfecting cells in 2D, e.g., 24 h prior to seeding the cells into the 3D cultures (time point has to be established for each gene and cell line). It has to be confirmed prior to the experiment that the respective

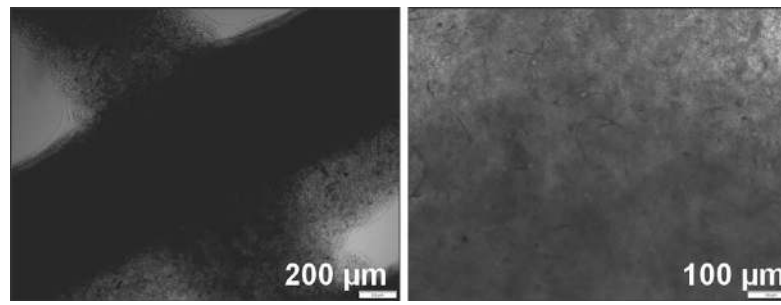


Fig. 3 Brightfield microscopy images of CIB with melanoma cells in two different magnifications reveal that it is semitranslucent. Images were taken with an Olympus IX83 epifluorescence microscope

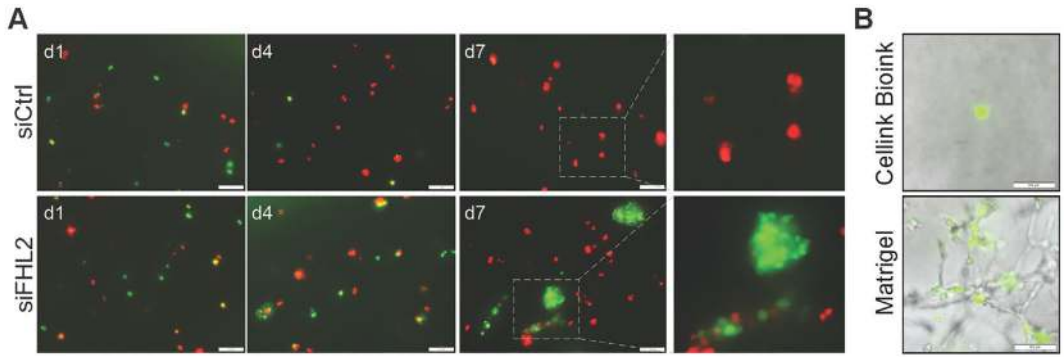


Fig. 4 Reporter cells are a helpful tool to visualize cells in 3D materials, including semitranslucent materials like Cellink Bioink and may deliver further information about the cells. (**A**), Exemplary fluorescence images of FUCCI-labelled melanoma cells in Cellink Bioink over 7 days. Upon treatment, here with a pool of short interfering RNAs (siRNAs) against FHL2, Mel Im cells overcome G1 arrest and proliferate again. Scale bar = 100 μm. Reproduced from [5] under a CC BY license. (**B**), Brightfield and fluorescence overlay images of MV3 cells in Cellink Bioink or Matrigel expressing GFP under transcription factor TEAD control. Only cells with active TEAD binding express GFP. Scale bar = 100 μm. Reproduced from [2], under a CC BY license

alteration is induced at the chosen time point and that it is maintained over the desired culture duration.

5. Histology: Fixation and dehydration of the hydrogels, has to be done very carefully, as constructs tend to dissolve or get brittle during the process. For Matrigel, a 2% paraformaldehyde (PFA) solution, and for CIB, a 4% PFA solution, each for 10 min at room temperature has proven suitable. We recommend carrying out the first steps of dehydration with 2% × 70% EtOH for 30 min in the well plate before constructs get transferred into embedding cassettes for the subsequent dehydration steps.
6. Immunostainings are suitable to determine relative protein expression and protein localization within a cell (Fig. 5). To obtain comparable results and guarantee exact same handling, sections from CIB and Matrigel cultures should be on the same slide.
7. Luciferase assays: For luciferase assays to analyze transcription factor activity in promoter assays, we use a dual LUC assay kit and lyse the whole constructs using a positive displacement pipette in the lysis buffer provided. We pool three constructs of CIB for lysis in 300 μl buffer and centrifuge all samples after lysis. Be very careful not to transfer cellulose fibers or air bubbles to the luminometer plate, as these may significantly impair luciferase activity measurements.

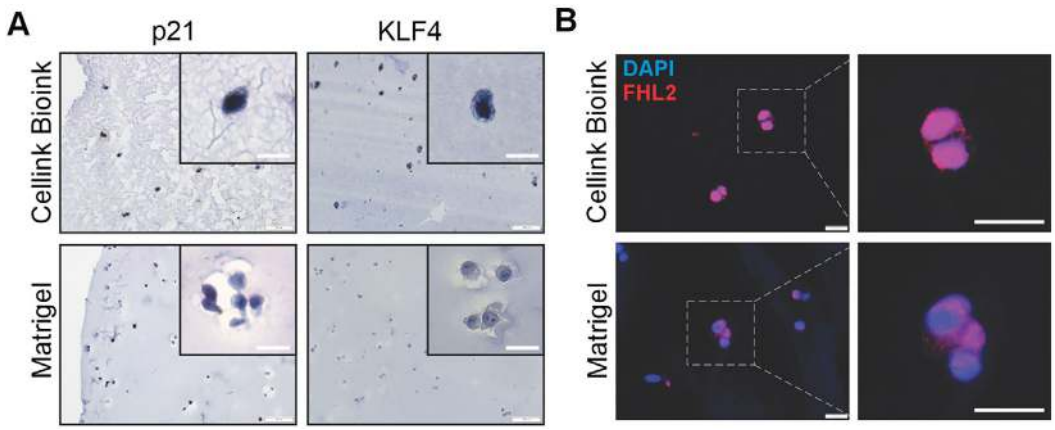


Fig. 5 Exemplary immunostainings of melanoma cells Mel Im in Cellink Bioink and Matrigel. Reproduced from [5], under a CC BY license. (**A**), Immunohistochemistry for p21 and KLF4 to compare staining intensities. Scale bar overview = 100 μm; Scale bar inserts = 20 μm. (**B**), Immunofluorescence staining for FHL2 is suitable to detect staining intensity and localization. Scale bar = 20 μm

4 Notes

1. Before/during printing: A comparison with 2D cultured cells instead of Matrigel would also be possible; however, a comparison between different two 3D culture models is far more meaningful. There are alternatives for Matrigel, including alginate or Alg/HyA/Gel, in which tumor cells also proliferate. Alternatives for CIB are hydrogels-like AlgCell [6] or, as shown for breast cancer cells, stiff nondegradable and nonadherent alginate [7]. However, it has to be considered that for different hydrogels, different protocols are required and, as illustrated in Fig. 2, cells grow in each of the bioinks slightly differently (e.g., spheroids in soft alginate, invasive cluster in Matrigel). Moreover, we have published RNA-Seq datasets for the CIB-MG comparison, which can be helpful in the selection of relevant genes [5]. The RNA-Sequencing data used in that study have been deposited in the NCBI BioProject database (https://www.ncbi.nlm.nih.gov/bioproject/) and can be accessed with the BioProject accession number PRJNA1197413.
2. In general, highly standardized cell culture procedures are needed to rely on results using cell lines, and even more for primary cell culture. This includes defined seeding densities, supplements, and being aware of lot-to-lot differences.
3. The volume of 500 μl hydrogel + 50 μl cell suspension is the absolute minimum for printing. Smaller amounts will significantly decrease printing quality. Using larger volumes is

possible but will hamper mixing of CIB with the cell suspension. Additionally, pre-cross-linking times for Matrigel in the cartridge may have to be increased.

4. Mix the cell suspension with CIB very carefully to avoid shearing or compressing the cells. Too harsh mixing may lead to significant loss of viable cells.
5. So far, we have not established an ideal way to isolate protein from the hydrogels, as residual FCS in the gels causes high levels of serum proteins in the protein lysate, hampering downstream applications. By using standard protein isolation (RIPA lysates), strongly expressed proteins like β-actin can be determined; however, detection of weakly expressed proteins like transcription factors is limited.

Textbox 1: G-Code for Cellink+ Printer; 6 grid structures, one per 6-well.

```
Tissue model; Size = 10x10x1.2mm; Single PH, 3
layers, Line space 2mm; Feed rate = 600mm/min
G90
G0 Z30
G0 X-47 Y25
G0 Z0.40
M760; Turn on PH1
G1 X-37 Y25 F600
G1 X-37 Y23
G1 X-47 Y23
G1 X-47 Y21
G1 X-37 Y21
G1 X-37 Y19
G1 X-47 Y19
G1 X-47 Y17
G1 X-37 Y17
G1 X-37 Y15
G1 X-47 Y15
G0 Z0.80
G1 X-47 Y25
G1 X-45 Y25
G1 X-45 Y15
G1 X-43 Y15
G1 X-43 Y25
G1 X-41 Y25
G1 X-41 Y15
G1 X-39 Y15
G1 X-39 Y25
G1 X-37 Y25
G1 X-37 Y15
M761; Turn off PH1
G0 Z1.20
M760; Turn on PH1
G1 X-47 Y15
```

```
G1 X-47 Y17
G1 X-37 Y17
G1 X-37 Y19
G1 X-47 Y19
G1 X-47 Y21
G1 X-37 Y21
G1 X-37 Y23
G1 X-47 Y23
G1 X-47 Y25
G1 X-37 Y25
M761; Turn off PH1
G0 Z30
G0 X-5 Y25
G0 Z0.40
M760; Turn on PH1
G1 X5 Y25 F600
G1 X5 Y23
G1 X-5 Y23
G1 X-5 Y21
G1 X5 Y21
G1 X5 Y19
G1 X-5 Y19
G1 X-5 Y17
G1 X5 Y17
G1 X5 Y15
G1 X-5 Y15
G0 Z0.80
G1 X-5 Y25
G1 X-3 Y25
G1 X-3 Y15
G1 X-1 Y15
G1 X-1 Y25
G1 X1 Y25
G1 X1 Y15
G1 X3 Y15
G1 X3 Y25
G1 X5 Y25
G1 X5 Y15
M761; Turn off PH1
G0 Z1.20
M760; Turn on PH1
G1 X-5 Y15
G1 X-5 Y17
G1 X5 Y17
G1 X5 Y19
G1 X-5 Y19
G1 X-5 Y21
G1 X5 Y21
G1 X5 Y23
G1 X-5 Y23
G1 X-5 Y25
G1 X5 Y25
M761; Turn off PH1
G0 Z30
```

```
G0 X37 Y25
G0 Z0.40
M760; Turn on PH1
G1 X47 Y25 F600
G1 X47 Y23
G1 X37 Y23
G1 X37 Y21
G1 X47 Y21
G1 X47 Y19
G1 X37 Y19
G1 X37 Y17
G1 X47 Y17
G1 X47 Y15
G1 X37 Y15
G0 Z0.80
G1 X37 Y25
G1 X39 Y25
G1 X39 Y15
G1 X41 Y15
G1 X41 Y25
G1 X43 Y25
G1 X43 Y15
G1 X45 Y15
G1 X45 Y25
G1 X47 Y25
G1 X47 Y15
M761; Turn off PH1
G0 Z1.20
M760; Turn on PH1
G1 X37 Y15
G1 X37 Y17
G1 X47 Y17
G1 X47 Y19
G1 X37 Y19
G1 X37 Y21
G1 X47 Y21
G1 X47 Y23
G1 X37 Y23
G1 X37 Y25
G1 X47 Y25
M761; Turn off PH1
G0 Z30
G0 X-47 Y-25
G0 Z0.40
M760; Turn on PH1
G1 X-37 Y-25 F600
G1 X-37 Y-23
G1 X-47 Y-23
G1 X-47 Y-21
G1 X-37 Y-21
G1 X-37 Y-19
G1 X-47 Y-19
G1 X-47 Y-17
G1 X-37 Y-17
```

```
G1 X-37 Y-15
G1 X-47 Y-15
G0 Z0.80
G1 X-47 Y-25
G1 X-45 Y-25
G1 X-45 Y-15
G1 X-43 Y-15
G1 X-43 Y-25
G1 X-41 Y-25
G1 X-41 Y-15
G1 X-39 Y-15
G1 X-39 Y-25
G1 X-37 Y-25
G1 X-37 Y-15
M761; Turn off PH1
G0 Z1.20
M760; Turn on PH1
G1 X-47 Y-15
G1 X-47 Y-17
G1 X-37 Y-17
G1 X-37 Y-19
G1 X-47 Y-19
G1 X-47 Y-21
G1 X-37 Y-21
G1 X-37 Y-23
G1 X-47 Y-23
G1 X-47 Y-25
G1 X-37 Y-25
M761; Turn off PH1
G0 Z30
G0 X-5 Y-25
G0 Z0.40
M760; Turn on PH1
G1 X5 Y-25 F600
G1 X5 Y-23
G1 X-5 Y-23
G1 X-5 Y-21
G1 X5 Y-21
G1 X5 Y-19
G1 X-5 Y-19
G1 X-5 Y-17
G1 X5 Y-17
G1 X5 Y-15
G1 X-5 Y-15
G0 Z0.80
G1 X-5 Y-25
G1 X-3 Y-25
G1 X-3 Y-15
G1 X-1 Y-15
G1 X-1 Y-25
G1 X1 Y-25
G1 X1 Y-15
G1 X3 Y-15
G1 X3 Y-25
```

```
G1 X5 Y-25
G1 X5 Y-15
M761; Turn off PH1
G0 Z1.20
M760; Turn on PH1
G1 X-5 Y-15
G1 X-5 Y-17
G1 X5 Y-17
G1 X5 Y-19
G1 X-5 Y-19
G1 X-5 Y-21
G1 X5 Y-21
G1 X5 Y-23
G1 X-5 Y-23
G1 X-5 Y-25
G1 X5 Y-25
M761; Turn off PH1
G0 Z30
G0 X37 Y-25
G0 Z0.40
M760; Turn on PH1
G1 X47 Y-25 F600
G1 X47 Y-23
G1 X37 Y-23
G1 X37 Y-21
G1 X47 Y-21
G1 X47 Y-19
G1 X37 Y-19
G1 X37 Y-17
G1 X47 Y-17
G1 X47 Y-15
G1 X37 Y-15
G0 Z0.80
G1 X37 Y-25
G1 X39 Y-25
G1 X39 Y-15
G1 X41 Y-15
G1 X41 Y-25
G1 X43 Y-25
G1 X43 Y-15
G1 X45 Y-15
G1 X45 Y-25
G1 X47 Y-25
G1 X47 Y-15
M761; Turn off PH1
G0 Z1.20
M760; Turn on PH1
G1 X37 Y-15
G1 X37 Y-17
G1 X47 Y-17
G1 X47 Y-19
G1 X37 Y-19
G1 X37 Y-21
G1 X47 Y-21
```

```
G1 X47 Y-23
G1 X37 Y-23
G1 X37 Y-25
G1 X47 Y-25
M761; Turn off PH1
G0 Z30
G0 X0 Y0
M84;END;END
◄
```

Competing Interests

The authors have no conflicts of interest to declare that are relevant to the content of this chapter.

References

1. Kappelmann-Fenzl M, Schmidt SK, Fischer S et al (2021) Molecular changes induced in melanoma by cell culturing in 3D alginate hydrogels. Cancers 13:4111. https://doi.org/10.3390/CANCERS13164111/S1
2. Schmidt SK, Schmid R, Arkudas A et al (2019) Tumor cells develop defined cellular phenotypes after 3D-bioprinting in different bioinks. Cells 8:1295. https://doi.org/10.3390/CELLS8101295
3. Staebler S, Rottensteiner-Brandl U, El Ahmad Z et al (2024) Transcription factor activating enhancer-binding protein 2ε (AP2ε) modulates phenotypic plasticity and progression of malignant melanoma. Cell Death Dis 15:351. https://doi.org/10.1038/S41419-024-06733-3
4. Schmid R, Schmidt SK, Schrüfer S et al (2024) A vascularized in vivo melanoma model suitable for metastasis research of different tumor stages using fundamentally different bioinks. Mater Today Bio 26:101071. https://doi.org/10.1016/J.MTBIO.2024.101071
5. Schmidt SK, Fischer S, El Ahmad Z et al (2025) Modeling a mesenchymal cell state by bioprinting for the molecular analysis of dormancy in melanoma. Mater Today Bio 32:101674. https://doi.org/10.1016/J.MTBIO.2025.101674
6. Eckert C, Schmidt S, Faber J et al (2025) An alginate-cellulose based bioink mimics the viscoelastic features of the melanoma microenvironment and its influence on cell cycle and invasion. Bioprinting 46:e00384. https://doi.org/10.1016/J.BPRINT.2024.E00384
7. Bakhshandeh S, Heras U, Taïeb HM et al (2024) Dormancy-inducing 3D engineered matrix uncovers mechanosensitive and drug-protective FHL2-p21 signaling axis. Sci Adv 10:eadr3997. https://doi.org/10.1126/sciadv.adr3997

Part IV

Techniques for Isolating and Studying Circulating Melanoma Cells and Melanoma-Derived Extracellular Vesicles



Chapter 11

Capture and Isolation of Circulating Melanoma Cells Using Photoacoustic Flowmetry

Robert H. Edgar, Justin Cook, Madeline Douglas, Anie-Pier Samson and John A. Viator

Abstract

Early detection of cancer has been a goal of cancer research in general and melanoma research in particular. Early detection of metastasis has been targeted as pivotal to increasing survival rates. Melanoma, though curable in its early stages, has a dramatic decrease in survival rates once metastasis has occurred. The transition to metastasis is not well understood and is an area of increasing interest. Metastasis is always premeditated by the shedding of circulating tumor cells (CTCs) from the primary tumor. The ability to isolate rare CTCs from the bloodstream has led to a host of new targets and therapies for cancer. Detection of CTCs also allows for disease progression to be tracked in real time while eliminating the need to wait for additional tumors to grow. Using a photoacoustic flow cytometer, in which we induce ultrasonic responses from circulating melanoma cells (CMCs), we identify and quantify these cells in order to track disease progression. Additionally, these CMCs are captured and isolated, allowing for future analysis such as RNA-Seq or microarray analysis. Finally, anticipating the need to streamline clinical workflow, a method for testing in whole blood is offered.

Keywords Diagnostic, Metastasis, Optical, Optoacoustic, Ultrasound

1 Introduction

Traditional cancer treatment, including that for melanoma, involves the removal of suspected tumors and close monitoring for additional tumor sites [1–5]. Aggressive melanoma treatment may involve interferon therapy or other chemotherapy and close monitoring for recurring tumors [6]. Each stage of treatment involves a substantial waiting period to assess disease progression or treatment success. CTCs are tumor cells that have separated from the main tumor and have entered the blood or lymphatic system. CTCs allow the cancer to spread and to develop secondary tumors, which is integral to metastatic progression [7]. Detection of CTCs allows for the real-time assessment of a therapy's efficiency and has a strong prognostic value for cancer advancement.

Kristian M. Hargadon (ed.), *Melanoma*, Methods in Molecular Biology, vol. 3089,
https://doi.org/10.1007/978-1-0716-5619-8_11,
© The Author(s), under exclusive license to Springer Science+Business Media, LLC, part of Springer Nature 2027

Many methods for detecting CTCs have been developed, including immunocytochemical, immunomagnetic, microfluidic, and molecular methods. Each of these methods has certain advantages and disadvantages. Some demonstrate excellent sensitivity while lacking the ability to recover identified CTCs. Similarly, a method might be able to capture cells but lack the ability to yield quantitative results, and each method may require a skilled technician or cytologist. Photoacoustic flow cytometry (PAFC), also known as photoacoustic flowmetry, offers both a high degree of specificity and the ability to recover detected cells with high reproducibility [8]. The PAFC method in this chapter provides immediate, sensitive, and unambiguous detection and recovery of CMCs.

Photoacoustics is a process using light to create sound. Photoacoustic flow cytometry generates ultrasonic waves resulting from absorption of light in particles under flow [9]. These ultrasonic waves are often created by thermoelastic expansion and contraction of an object that absorbed laser light [10, 11].

In our photoacoustic flow cytometry setup, a nanosecond laser operating at 532 nm is used to irradiate a sample under flow. The ultrasonic waves are detected by a piezoelectric transducer and recorded onto a computer. The advantage of using photoacoustic detection over conventional flow cytometry is that cells can be specifically targeted, and the ultrasonic wave generated by these cells is strong enough to allow for single-cell detection. Additionally, since the cells remain in suspension, recovery of the cells is straightforward with high CTC viability for later analysis. Though most testing is done after separation of leukocytes from whole blood to avoid optical excitation of erythrocytes, we offer a method for testing for CMCs in whole blood. Since erythrocytes generally have high absorption in the visible spectrum [13], we have relied on the separation method to avoid drowning out the photoacoustic signature from CMCs from the signature from erythrocytes. However, some research groups have successfully performed in vivo photoacoustic flow cytometry [14], and thus we have added a method for whole blood testing to improve clinical workflow.

2 Materials

2.1 Blood Separation

1. BD Vacutainer® Blood Collection Tube with Sodium Heparin.
2. Histopaque®-1077 or Ficoll-Paque™PLUS.
3. Red Blood Cell (RBC) Lysis Buffer, 10× (Tonbo Biosciences).
4. Phosphate-buffered saline (PBS).

5. Neutral Density Solution (NDS): Prepare in a 50 ml Falcon tube by adding 0.56 ml of PBS to 49.44 ml of Histopaque® 1077.
6. DNase1.
7. 100–1000 µl micropipette.
8. 10 ml serological pipette.
9. 15 ml Falcon tube.
10. Centrifuge (capable of 414 × *g* or greater).

2.2 Photoacoustic Flow Cytometry

1. Photoacoustic flow cytometry system consisting of a nanosecond laser, acoustic chamber, transducer, oscilloscope, and data recording device.
2. Mineral oil, light.
3. 5 ml syringe.
4. Sonotech LithoClear acoustic gel.
5. Tegam 4040B amplifier.
6. LabView software (National Instruments).

2.3 Capture and Isolation

1. Fraction collector, e.g., Gilson FC 203B fraction collector with three-way valve kit.
2. Microscope with micro injection system, e.g., Leica DMI4000B with Eppendorf Microinjection System.
3. 96-well flat-bottom plate.

2.4 Immunohistochemistry

1. PBS.
2. 1% bovine serum albumin (BSA) solution in PBS.
3. 10% normal mouse serum solution in PBS.
4. Formalin (4% formaldehyde).
5. Shaker.
6. Melan-A monoclonal primary antibody raised in mouse (Invitrogen, Thermo Fisher MA5-15237).
7. Melan-A secondary antibody (Goat anti-mouse IgG-Alexa Fluor 647; Invitrogen, Thermo Fisher A-21235).
8. CD-45 monoclonal primary antibody raised in mouse (Invitrogen, Thermo Fisher MA1-19111).
9. CD-45 secondary antibody (Goat anti-mouse IgG-Alexa Fluor 488; Invitrogen, Thermo Fisher A28175).
10. 96-well flat-bottom plate coated with 1% poly-L-lysine.
11. 0.1 µg/ml solution of DAPI in PBS.

2.5 RT-PCR and cDNA Library Preparation

1. SuperScript® VILO® cDNA Synthesis kit (Invitrogen).
2. 10% NP40 (CAS 9016-45-9)
3. SUPERase-in™.
4. T4 Gene 32 Protein.
5. Nuclease-free water.
6. Thermocycler.
7. 96-well Skirted PCR plate.

3 Methods

3.1 Blood Separation

1. Obtain blood samples in vacutainer tubes (*see* **Note 1**).
2. Place 10 ml of Histopaque 1077 in a 15 ml Falcon tube.
3. Carefully layer 3–4 ml of blood onto the ficoll layer without breaking the surface tension of ficoll.
4. Centrifuge the sample at 1600 × *g* at 20°C for 30 min (*see* **Note 2**).
5. Carefully pipette out the buffy coat, which is situated above ficoll and below the plasma layer (*see* **Note 3**).
6. Pipette the white blood cell layer into a separate 15 ml Falcon tube.
7. Dilute one volume of extracted buffy coat into ten volumes of 1× RBC Lysis Buffer.
8. Incubate buffy coat/RBC Lysis Buffer at 24°C for 15–30 min with periodic agitation or gentle vortexing (*see* **Note 4**).
9. Centrifuge the cells at 400 × *g* at 20°C for 15 min, pipet out supernatant, and resuspend cells in 1–4 ml of NDS.
10. Add 20 units of DNase 1/ml, and incubate at room temperature (RT) for 15 min.

3.2 Photoacoustic Flow Cytometry

Our PAFC system consists of an Nd:YAG laser coupled into a 1000 μm, 0.39 numerical aperture optical fiber. This system is used to produce 532 nm laser light with 5 ns pulses. Laser beam energy coupled through the optical fiber is maintained and measured from 1.9–2.1 mJ for melanoma CTC detection. Laser light is directed toward a quartz tube with 10 μm thick walls passing through a 3D-printed flow chamber (Fig. 1). The 10 μm thick walls allow for the propagation of ultrasonic waves, as well as provide an optically transparent pathway for the sample to flow through. The optical fiber is placed 5 mm from the quartz tube to create a detection volume of 0.04 μl. Laser beam shape is assumed to be Gaussian, and fluence is calculated to be 0.014 mJ/cm^2. A 2.25 MHz transducer (immersion transducer,

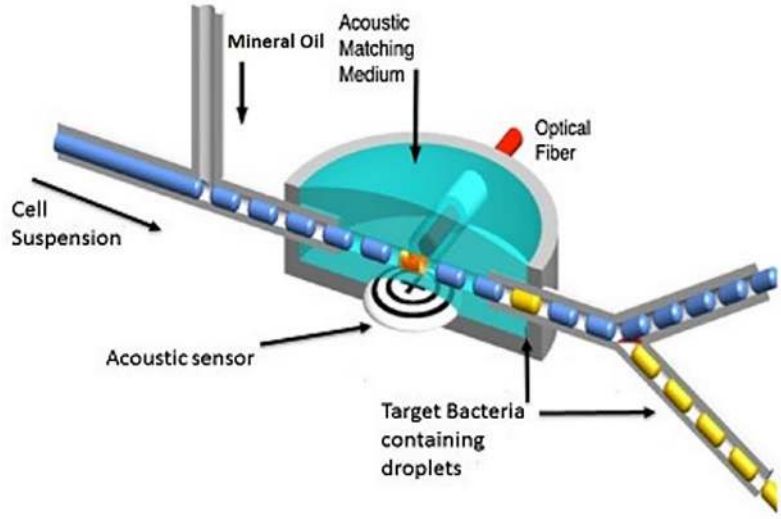


Fig. 1 Schematic of photoacoustic flow chamber with parts labeled for identification

0.50 in. element diameter $F = 0.80$ in.) focused on the quartz sample tube is fitted to the base of the 3D-printed flow chamber. The transducer focal point is aligned to incorporate the quartz tube illuminated by the laser beam. The internal volume of the chamber is filled with Sonotech LithoClear acoustic gel to provide a medium for the propagation of acoustic waves. Syringe pumps create an alternating flow of sample and mineral oil equal to a 60 µl/min flow rate. The introduction of sample and the immiscible mineral oil induces two-phase flow [12]. Two-phase flow is employed to allow for sample collection and further analysis while eliminating the possibility of samples becoming stuck or delayed inside the tubing. Signals are amplified with a gain of 50 using a Tegam 4040B amplifier and sent to a desktop computer running a customized LabView program (Fig. 2).

1. Allow a 1% BSA solution to sit in the sample syringe, tubing, and the flow chamber for 1 h prior to use to create a hydrophobic barrier inside the tubing/syringe.
2. Turn on the laser system, and allow it to establish thermal equilibrium.
3. Layer 1 ml of mineral oil on top of the sample in a 5 ml syringe.
4. Place the sample syringe in the first syringe pump, and place the second syringe with mineral oil in the second syringe pump.

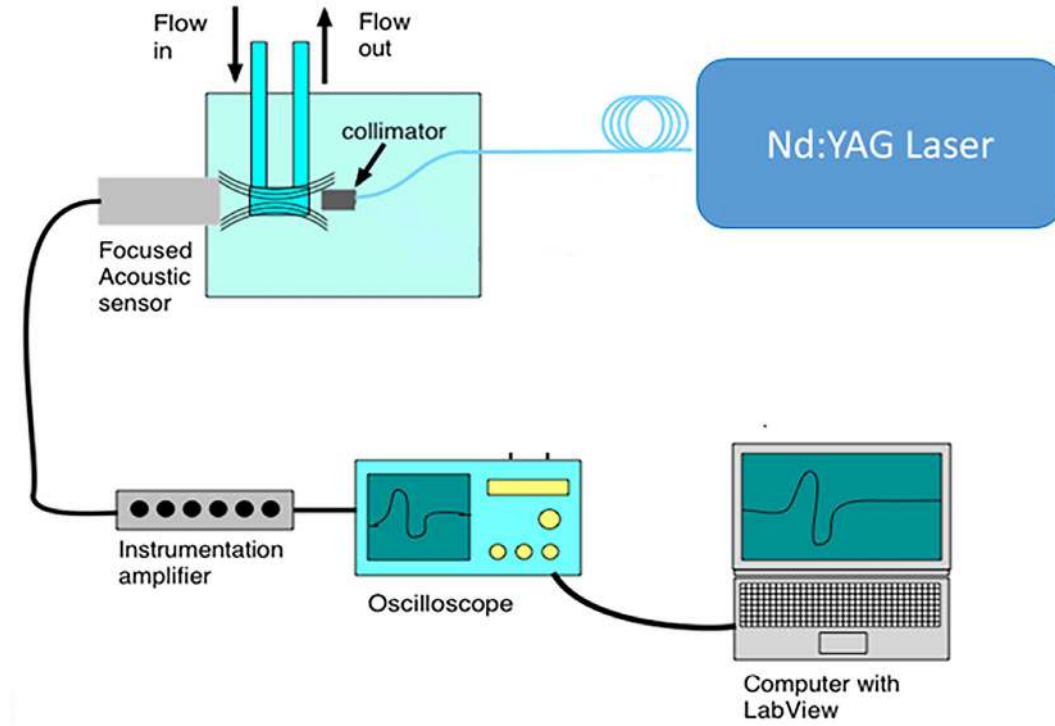


Fig. 2 Schematic of photoacoustic flow setup with parts labeled for identification

5. Turn on the syringe pumps, and watch for air bubbles to pass through the Quartz tube in the flow chamber before beginning the test.
6. Start the computer interface and the fraction collector.
7. Begin the test once any air bubbles have cleared the flow chamber.
8. Set the oscilloscope to take a minimum of four averages to reduce noise.
9. Set the RITEC system on 32 dB amplification, with a 1 MHz high-pass filter.
10. When capturing and isolating melanoma cells, collect detected volumes directly into a 96-well flat-bottom plate coated with 1% poly-L-lysine (*see* **Notes 5 and 6**). Collected cell volumes can be further analyzed by visual inspection, RT-PCR, or immunocytochemistry.

3.3 Analysis of CTC

Once a CTC has been detected, it can be captured for additional testing. Cells can either be stained/imaged, or RNA can be isolated for RT-PCR and the creation of a cDNA library for analysis.

3.3.1 Immunocytochemistry

1. Collect single droplets containing detected cells in 96-well plates coated with 1% poly-L-lysine.
2. Place the 96-well plate containing cells into a 5% CO_2 incubator set at 37°C for 15–60 min.
3. Centrifuge the plate at 100 × *g* at RT for 3–5 min.
4. Using a micropipetter, gently remove the supernatant.
5. Add 100 µl of Formalin (4% Formaldehyde).
6. Place the 96-well plate on a shaker for 1 min.
7. Incubate on the bench top at RT for 15 min.
8. Centrifuge plate at 100 × *g* for 2–3 min.
9. Using a micropipetter, gently remove the supernatant.
10. Wash cells by adding 100 µl of PBS.
11. Centrifuge plate at 100 × *g* at RT for 2–3 min.
12. Repeat cell washing (Steps 9–11 from this section) three times.
13. Remove PBS, and add 100 µl of 10% mouse serum for 1 h at RT.
14. Remove mouse serum solution, and add 100 µl of the primary antibody solution (1% CD-45 antibody and 1% Melan-A antibody in 10% goat serum solution). Incubate at RT for 1 h.
15. Remove antibody solution using a micropipetter.
16. Wash the cells three times with 100 µl of PBS for 10 min (repeat Steps 9–11 from this section).
17. Remove PBS, and add 100 µl of secondary antibody solution (1% CD-45 secondary antibody and 1% Melan-A secondary antibody in 10% mouse serum). Incubate at RT for 1 h.
18. Remove antibody solution with a micropipetter.
19. Wash the cells three times with 100 µl of PBS for 10 min (repeat Steps 9–11 from this section).
20. Add 0.1 µg/ml of DAPI. Incubate at RT for 1 min.
21. Remove DAPI solution, and wash three times (repeat Steps 9–11 from this section).
22. Image cells in PBS with a fluorescence imaging microscope. An example of an isolated CTC is shown following staining for Melan-A in Fig. 3 (*see* **Notes 7 and 8**).

3.3.2 Isolation of CTC RNA and Generation of cDNA Library

1. For each 96-well plate, prepare the appropriate amount of RT Mix Solution 1 according to Table 1. The following steps accomplish lysis of cells and stabilizing of isolated RNA.
2. Pipette 5 µl of RT Mix Solution 1 into each well to be used on the 96-well PCR plate.



Fig. 3 Captured melanoma cell stained with Melan-A antibody and Alexa Fluor 647 secondary antibody

Table 1
RT Mix Solution 1

Component	Volume (µl)	48 samples w/ overages (µl)	96 samples w/ overages (µl)
5× VILO™ Reaction Mix	1.2	72.0	144.0
20 U/µl SUPERase-in™	0.3	18.0	36.0
10% NP40	0.25	15.0	30.0
Nuclease-free Water	3.25	195.0	390.0
Total	5.0	300.0	600.0

3. Sort individual cells directly into the same plate containing RT Mix Solution 1.
4. Seal the plate and vortex thoroughly for 15 s.
5. Centrifuge plate for 30 s in a centrifuge prechilled at 4°C.
6. Immediately freeze (−20°C) the sealed plate, or immediately perform cDNA generation.
7. If previously frozen, thaw the sealed plate on ice.
8. Centrifuge plate for 30 s in a centrifuge prechilled at 4°C.

9. Preheat the thermocycler to 65°C.
10. Transfer samples to thethermocycler and incubate at 65°C for 90 s.
11. Immediately remove the plate, and snap-chill on ice for 5 min.
12. Centrifuge plate for 30 s in a centrifuge prechilled at 4°C.
13. Prepare RT Mix Solution 2 according to Table 2. The following steps are for the amplification of cDNA.
14. Aliquot 1 µl of RT Mix Solution 2 into each well, and centrifuge for 30 s in a centrifuge prechilled at 4°C.
15. Perform Reverse Transcriptase (RT) cycling in thermocycler according to conditions shown in Table 3.
16. Centrifuge plate for 30 s in a centrifuge prechilled at 4°C and store at −20°C.
17. Samples are now ready for cDNA sequencing.

3.4 Whole Blood Treatment and Testing (Optional)

1. Obtain a 1 ml blood sample in vacutainer tubes (*see* **Note 1**).
2. Dilute one volume of whole blood into ten volumes of 1× RBC Lysis Buffer.
3. Incubate whole blood/RBC Lysis Buffer at 24°C for 15 min with periodic agitation or gentle vortexing (*see* **Note 4**).
4. Introduce to photoacoustic flow cytometer with laser wavelength tuned to 700 nm. All other procedures are identical to processing in the flow cytometer with centrifuge-separated samples.

Table 2
RT Mix Solution 2

Component	Volume (µl)	48 samples w/ overages (µl)	96 samples w/ overages (µl)
10× SuperScript® Enzyme	0.15	9.0	18.0
T4 Gene 32 Protein	0.12	7.2	14.4
Nuclease-free water	0.73	43.8	87.6
Total	1.00	60.0	120.0

Table 3
RT thermocycler parameters

Temperature	25°C	50°C	55°C	60°C	70°C	4°C
Time	5 min	30 min	25 min	5 min	10 min	Infinity



Fig. 4 Cultured HS936 melanoma cells are shown fully adhered to the culture flask without staining

4 Notes

1. Blood must be processed within 24 h of specimen collection.
2. Blood must be 18°C–25°C for correct centrifugation to occur.
3. RBC will pellet through ficoll to the bottom of the tube. Plasma and buffy coat containing white blood cells and CTCs will be layered on top of ficoll.
4. If visible RBC contamination remains, ensure the cells are mixed up so that the lysis buffer can lyse the RBC, and repeat the lysis steps at RT before diluting cells into the desired amount of NDS buffer.
5. The fraction size containing a positively detected cell should be large enough to eliminate the possibility of dehydration before the test concludes. Droplet size from our PAFC system can range from 10 to 30 μl.
6. A consistent droplet size will increase the chances of appropriate staining of detected cells.
7. The typical staining of captured melanoma cells is shown in Fig. 3. Green fluorescence staining using Mart1 primary and green AlexaFluor secondary antibody delineates the captured melanoma cell. The image is created as an overlay using ImageJ software. The antibody concentration can be increased

or decreased to modulate fluorescence and background staining. In contrast to CTC, cultured HS936 melanoma cells fully adhere to culture flasks (Fig. 4). When cultured cells adhere, they elongate and display a different morphology than circulating cells.

8. When staining cells, if the image background looks washed out or overly green, try a 1:10, 1:100, and 1:1000 dilution series of both primary and secondary antibodies.

Acknowledgments

We would like to acknowledge support by the National Cancer Institute of the National Institutes of Health under award number 1R01CA161367-01. We also acknowledge Acousys Biodevices Inc. for their support.

Competing Interests The authors have no conflicts of interest to declare that are relevant to the content of this chapter.

References

1. Birnbaum JK, Duggan C, Anderson BO, Etzioni R (2018) Early detection and treatment strategies for breast cancer in low-income and upper middle-income countries: a modelling study. Lancet Glob Health 6(8): e885–e893
2. Alendar F, Drljević I, Drljević K, Alendar T (2009) Early detection of melanoma skin cancer. Bosnian J Basic Med Sci 9(1):77–80
3. Menezes M, Das S, Minn I et al (2016) Detecting tumor metastases: the road to therapy starts here. Adv Cancer Res 132:1–44
4. Sharma S, Zhuang R, Long M et al (2018) Circulating tumor cell isolation, culture, and downstream molecular analysis. Biotechnol Adv 36(4):1063–1078
5. Micalizzi DS, Maheswaran S, Haber DA (2017) A conduit to metastasis: circulating tumor cell biology. Genes Dev 31(18):1827–1840
6. Board PATE (2019) Intraocular (uveal) melanoma treatment (pdq®). PDQ cancer information summaries [Internet]. Bethesda (MD): National Cancer Institute (US) https://www.ncbi.nlm.nih.gov/books/NBK65836/
7. Zhou L, Dicker DT, Matthew E et al (2017) Circulating tumor cells: silent predictors of metastasis. F1000 Res 6:F1000 Faculty Rev-1445 https://doi.org/10.12688/f1000research.11313.1
8. Edgar RH, Cook J, Noel C et al (2019) Bacteriophage-mediated identification of bacteria using photoacoustic flow cytometry. J Biomed Opt 24(11):1–7
9. Manohar S, Razansky D (2016) Photoacoustics: a historical review. Adv Opt Photon 8(4):586–617
10. Paltauf G, Schmidt-Kloiber H, Guss H (1996) Light distribution measurements in absorbing materials by optical detection of laser-induced stress waves. Appl Phys Lett 69(11):1526–1528
11. Kruger RA, Liu P, Fang YR, Appledorn CR (1995) Photoacoustic ultrasound (PAUS) reconstruction tomography. Med Phys 22(10):1605–1609
12. O'Brien CM, Rood K, Bhattacharyya KD et al (2012) Capture of circulating tumor cells using photoacoustic flowmetry and two phase flow. J Biomed Opt 17(6):061221
13. Viator JA, Prahl SA (1999) Laser thrombolysis using long pulse frequency-doubled ND:YAG lasers. Laser Surg Med 25(5):379–388
14. Galanzha EI, Shashkov EV, Spring PM et al (2009) In vivo, noninvasive label-free detection and eradication of circulating metastatic melanoma cells using two-color photoacoustic flow cytometry with a diode laser. Cancer Res 69(20):7926–7934



Chapter 12

A Rapid Exosome Isolation Using Ultrafiltration and Size Exclusion Chromatography (REIUS) Method for Exosome Isolation from Melanoma Cell Lines

Shin La Shu, Cheryl L. Allen, Shawna Benjamin-Davalos, Marina Koroleva, Don MacFarland, Hans Minderman and Marc S. Ernstoff

Abstract

Cells release extracellular vesicles (EVs) that can be detected both in vivo and in cell culture medium. Among EVs, exosomes are 50–150 nm vesicles that are systematically packaged into multivesicular bodies for release into the external environment. In cancer, these intentionally packaged exosomes carry a payload of molecules such as protein, RNA, and surface receptors that facilitate the reprogramming of proximal cells to assemble a pro-tumor microenvironment. Exosomes have been implicated as an important intermediary extracellular communication pathway between cells, including in melanoma. Human melanoma-derived exosomes (HMEX) have been demonstrated to modulate the extracellular environment and inhibit immune cell activation. There are many methods to isolate and enrich for exosomes, and the method applied can impact yield and purity of the isolates. In this chapter, we describe the REIUS (Rapid Exosome Isolation Using Size exclusion chromatography) method to isolate HMEX from melanoma cell cultures and then demonstrate their enrichment using molecular and microscopic approaches.

Keywords Extracellular vesicles, EV, Isolation techniques, Melanoma, Exosomes, Size exclusion Chromatography, Ultrafiltration, REIUS

1 Introduction

1.1 Background

Inter-communication between cells in a tumor microenvironment (TME) is multifactorial. Release of soluble signaling factors such as cytokines and chemokines that attract or repulse cells (particularly immune cells) controls the tissue microenvironment, providing a dynamic environment down to the cellular level. Malignant cells manipulate extracellular signaling systems that disrupt the normal stromal environment by promoting cell plasticity and creating a tumor niche in the TME [1, 2]. Cancer cells do this in part by releasing extracellular vesicles (EVs) that are lipid bilayer vesicles

Kristian M. Hargadon (ed.), *Melanoma*, Methods in Molecular Biology, vol. 3089,
https://doi.org/10.1007/978-1-0716-5619-8_12,
© The Author(s), under exclusive license to Springer Science+Business Media, LLC, part of Springer Nature 2027

containing a payload of proteins, RNA, and surface receptors capable of modulating both the immediate microenvironment and the macroenvironment [3–6]. Among many subsets of EVs, exosomes are intentionally packaged vesicles ranging from 50 to 150 nm in size and are generated through the endocytic pathway via the endosomal sorting complexes required for transport (ESCRT) complex. The control of the microenvironment by tumor through exosome release is swift and sustained, and some cancer cells can release manyfold more exosomes than normal stromal cells [7]. In this context, the study of exosomes and how they contribute to tumor control of the microenvironment is an active area of research interest [8].

Melanoma-derived exosomes are rapidly taken up by stromal cells and control the metabolic programming in those cells to generate a pro-tumorigenic niche [9]. The exact mechanisms by which exosomes affect their target cells remain insufficiently understood [10, 11]. The field is further complicated by the various exosome isolation methods employed to date, which result in different levels of recovery and purity [12, 13]. Exosome isolation methods have advanced significantly over the past decade, and deeper investigations into exosomes and their control over the TME may reveal their use as targets for manipulation and therapeutic intervention [14, 15].

In this chapter, the REIUS method for isolating exosomes from cell cultures is introduced in detail [1, 9]. We have taken efforts to optimize the centrifugation speed to match most 50 ml tube benchtop centrifuges while retaining the same efficiency as that in enrichment and isolation of human melanoma-derived exosomes (HMEX). Isolation of exosomes using the REIUS method is simple, effective, and easily scalable to accommodate larger experiments (Fig. 1). We have also included the minimum molecular and microscopic methods necessary to validate a successful exosome isolation through the use of western blot, nanoparticle tracking analysis (NTA), and transmission electron microscopy (TEM) [14].

1.2 Continued Relevance and Applications

The International Society for Extracellular Vesicles (ISEV) promotes the use of "Extracellular Vesicles (EVs)" as a general descriptor for vesicles derived from cells regardless of the isolation method. However, REIUS isolates a tightly distributed ~70 nm population that demonstrates clear exosome-associated markers (e.g., TSG101), making the term "exosomes" appropriate and more specific for this preparation. To remain aligned with current ISEV terminology trends, the terms "EV" and "exosome" shall be used interchangeably in this section.

Recent comparative studies continue to support size exclusion chromatography (SEC) as one of the more reliable ways to separate extracellular vesicles from complex biofluids. SEC generally produces cleaner preparations with less soluble protein carryover, recovers vesicles in the expected size ranges, and maintains a high degree of

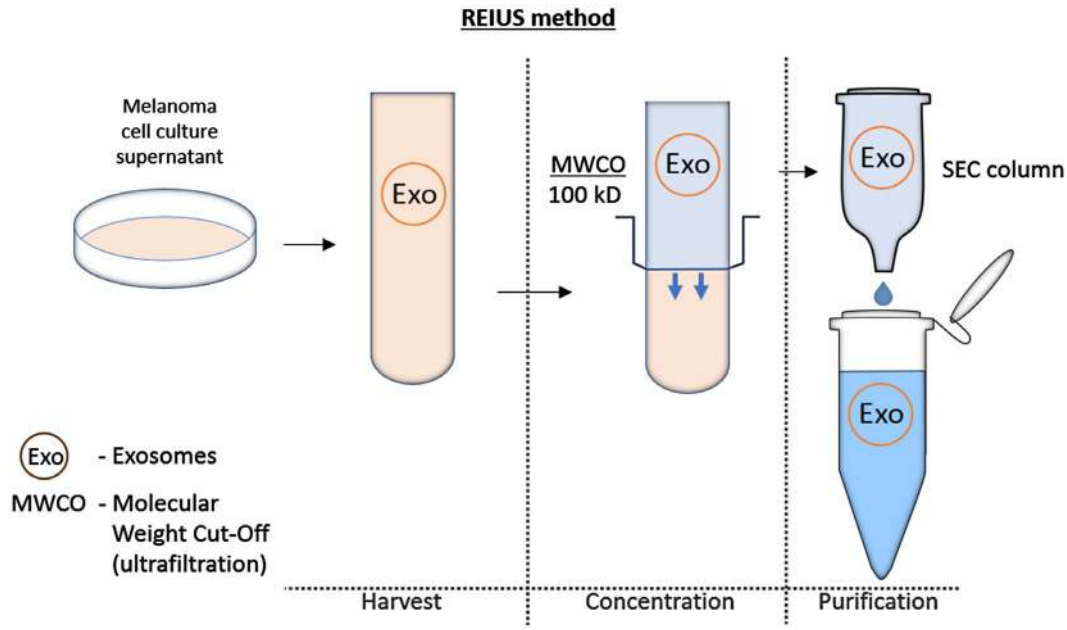


Fig. 1 The REIUS method has three general steps performed in the following order: 1, Harvest: supernatants are collected from cell cultures, spun using a benchtop centrifuge to remove cells and debris, and then particulates are removed for size stringency by passing through a 0.2 μm syringe-based filter. This restricts the EV to under 200 nm in size, consistent with the physiological exosome size limit. 2, Concentration: cleared supernatants are concentrated using an ultrafiltration column to reduce volumes to those appropriate for the SEC Step. 3, Purification (SEC): exosomes are isolated using SEC columns and are used immediately or frozen for future use. To scale up, combine exosome isolates after the SEC step

reproducibility across operators and sample types [16, 17]. Because REIUS is built around SEC, these observations reinforce the method's continued relevance. The REIUS workflow also incorporates a sterile 0.22 μm filtration step before SEC and restricts collection to the well-defined exosome-enriched fraction, yielding a preparation that is both consistent and suitable for downstream biological use.

Interest in in vivo applications of EVs has grown, and several reports now describe tissue-localized or compartment-specific administration of serum- or cell-derived vesicles. For example, one study evaluating a single intratesticular dose of serum-derived exosomes found no acute safety signals and suggested potential therapeutic activity in a localized injury model [18]. These observations align with internal findings in which REIUS-purified EVs delivered subcutaneously to multiple mice produced no noticeable local reaction. Although the formulation and injection route differ across studies, together these findings suggest that SEC-based preparations, including those produced by REIUS, are broadly compatible with animal work and may offer advantages over methods that introduce more debris or soluble protein contaminants.

As the field moves toward clinical applications, the contamination of cytokines during EV isolation has become increasingly important to understand. Cytokines occupy a size range that makes it difficult to determine if they are embedded as cargo or are instead co-eluting during SEC isolation, and current data do not clearly distinguish whether cytokines travel as luminal cargo within EV. The proportion of surface-associated versus internal cytokines may vary with inflammatory state or disease context, but this has not been resolved in a systematic way. Because cytokines have potent biological activity independent of EVs, unintentional co-isolation can complicate interpretation of functional studies. SEC-based workflows (including REIUS) typically show lower levels of soluble protein contamination relative to ultracentrifugation or precipitation approaches [1], yet further work will be needed to determine whether cytokine-EV associations carry diagnostic or therapeutic significance.

2 Materials

2.1 Cell Culture

1. Melanoma cell lines (e.g., 2183-Her4, 526-mel, or 888-mel: all high exosome-producing lines).
2. 150 mm tissue culture plates or T175 flasks.
3. Complete cell culture medium: RPMI-1640 supplemented with antibiotics, GlutaMAX or L-glutamine, and 5%–10% fetal bovine serum (FBS), as optimized for specific cell lines of investigator interest.
4. Dulbecco's phosphate-buffered saline (DPBS): 1× solution.
5. 0.4% trypan blue.
6. Cell dissociation reagent (e.g., TrypLE Express Enzyme).
7. RPMI-1640 cell culture medium without supplements.
8. Exosome-depleted cell culture medium: complete cell culture medium containing 5%–10% exosome-depleted FBS (*see* **Note 1**).

2.2 Harvesting of Supernatants and Exosome Isolation

1. Sterile 50 ml conical tubes.
2. Benchtop centrifuge capable of spinning 50 ml conical tubes at 3000 ×*g* (e.g., Eppendorf 5810/5810 R with A481 rotor or Sorvall Legend X1/X1R with TX-400 rotor).
3. Polyethersulfone (PES) syringe filters, 0.20 μm.
4. Sterile 30 ml syringes.
5. 100 kDa MWCO centrifugal ultrafilter devices (e.g., Amicon Ultra-15 Centrifugal Filter devices, 100 K MWCO).

6. Size exclusion chromatography (SEC) columns (e.g., Exo-spin columns—EX03).
7. 0.20 μm filter-sterilized 1× PBS (fresh).
8. 1.5–1.7 ml low protein and nucleic acid-binding microcentrifuge tubes.
9. Microcentrifuge or benchtop centrifuge capable of spinning at 50 $\times g$ (e.g., Eppendorf 5810 R with bucket adapters for microcentrifuge tubes).

2.3 Counting of Exosomes by NTA

1. Nanoparticle tracking analyzer (*see* **Note 2**).
2. 100 nm beads (for instrument calibration).
3. 0.20 μm filter-sterilized 1× PBS (fresh).
4. Sterile 1 cc syringes.

2.4 Western Blot

1. Ice-cold 1× DPBS.
2. Protease and phosphatase inhibitors.
3. RIPA buffer: 25 mM Tris-HCL pH 7.6, 150 mM NaCl, 1% NP-40, 1% sodium deoxycholate, 0.1% sodium dodecyl sulfate (SDS). Just prior to use, add Halt™ Protease Inhibitor Cocktail (100×) protease/phosphatase inhibitors (Aprotinin, Bestatin, E-64, Leupeptin, Sodium Fluoride, Sodium Orthovanadate, Sodium Pyrophosphate, and β-glycerophosphate) to achieve a 1× final concentration.
4. 5 ml microcentrifuge tubes or equivalent.
5. 21-G needles and syringes.
6. Refrigerated microcentrifuge.
7. Protein assay kit: Pierce BCA Protein Assay Kit.
8. Laemmli SDS sample loading buffer (6×): 375 mM Tris-HCl pH 6.8, 9% SDS, 50% glycerol, 0.03% bromophenol blue. Add 2-mercaptoethanol (2-ME) at 9% (V/V) before use.
9. Protein molecular weight standard: Precision Plus Protein Dual Color Standards.
10. Heating block.
11. PAGE Protein gels: precast 4%–20% Tris-Glycine gels.
12. Tris/Glycine/SDS running buffer, 10× (Bio-Rad): Dilute stock solution to 1× with water to achieve a working solution of running buffer that is 25 mM Tris, 192 mM glycine, 0.1% SDS, and pH 8.3.
13. Protein gel electrophoresis system.
14. 0.45 μm low-fluorescence polyvinylidene difluoride (PVDF) membrane.
15. Gel transfer system (e.g., Trans-Blot Turbo Transfer System).

16. Transfer buffer as recommended for the user's specific transfer system (proprietary for the Trans-Blot Turbo Transfer System).
17. 100% ethanol or methanol for activating PVDF membrane.
18. Blocking buffer (e.g., AdvanBlock).
19. Primary antibodies: rabbit anti-CD63, rabbit anti-TSG101, mouse anti-β-tubulin, and mouse anti-cytochrome C (Table 1).
20. Tube rotator or rocker (for 50 ml conical tubes).
21. 1× TBS.
22. 1× TBS/0.1% Tween 20.
23. 10% SDS.
24. Secondary antibodies (detection system dependent, e.g., IRDye secondary antibodies 680RD Goat anti-Mouse, 680RD Goat anti-Rabbit, 800CW Goat anti-Mouse, and 800CW Goat anti-Rabbit).
25. Blot imaging system (e.g., Odyssey Fc Imaging System).

2.5 Transmission Electron Microscopy (TEM)

1. 2% Methyl cellulose, viscosity: 25 cP (optional).
2. Parafilm.
3. Nickel EM grids (e.g., 10 nm Formvar/1 nm carbon-coated square 300 mesh nickel grids).
4. EM grid tweezers.
5. Filter paper (e.g., Whatman).
6. UranyLess™ EM Stain.
7. Transmission electron microscope (e.g., JEOL 100CX II TEM 100 kV).

Table 1
Table of antibodies used and their concentration

Name of antibody	Company	Mono/ polyclonal	Molecular weight (kDa)	Species	Dilution for WB	Secondary antibody dilution
CD63	Sigma (Cat #HPA010088)	Poly	50–60	Rabbit	1:1000	1:5000
TSG101	Abcam (Cat #ab125011)	Mono	50	Rabbit	1:1000	1:5000
Cytochrome C	ThermoFisher (Cat #66264-1-IG)	Mono	14	Mouse	1:1000	1:5000
β-tubulin	Cell Signaling (Cat #86298 S)	Mono	55	Mouse	1:1000	1:5000

3 Methods

3.1 Cell Culture for Exosome Production

The following is the general protocol for culturing adherent cells to obtain exosomes. In our hands, we found that melanoma cell lines can vary up to 2.5-fold in the number of exosomes they secrete. Thus, for each sample of exosomes, the appropriate number of plates to seed in Step 5 will need to be determined for each cell line. In order to isolate exosomes from the cells in culture and limit contamination from exosomes present in FBS, the cells must be grown in exosome-depleted medium (*see* **Note 3**). To maximize growth, expand the melanoma cell lines in a medium containing normal FBS, and replace with exosome-depleted medium the day before harvesting the supernatants.

1. Once cell lines are 70%–90% confluent in complete medium, wash the plates/flasks with 1× DPBS, and add dissociation reagent until the cells have rounded up and started detaching.
2. Add an equal volume of complete medium, and transfer to a conical tube.
3. Count the cells, and determine percent viability using trypan blue or another method. Ensure that viability is greater than 95%.
4. Pellet the cells at 300 × *g*, and discard supernatant.
5. Resuspend pellet in complete medium, and seed cells into each of three to five plates at a density that will reach a confluency of 70%–85% in 2–4 days. Monitor the plates of cells daily, replacing medium as necessary (*see* **Notes 4 and 5**).
6. When cells reach 70%–85% confluency, aspirate off all medium. Wash monolayer by adding 10 ml of plain medium without supplements, making sure to tilt the plate back and forth and side to side. Aspirate medium completely.
7. Add 12–16 ml of exosome-depleted medium, and culture for 18–24 h. The volume of medium added will depend on the metabolic activity of the cells (*see* **Note 6**).

3.2 REIUS Method for Isolating Exosomes

All centrifuge spins are performed at room temperature (RT). In order to maintain sterility, all steps should be performed in a biosafety cabinet (*see* **Notes 7 and 8**).

1. Tilt plates back and forth to wash and pool supernatant. While the plate is tilted, use a pipet to transfer all supernatant to a 50 ml conical tube. Supernatant from multiple plates can be added to the same tube (*see* **Note 9**).

2. Centrifuge tubes at 300×*g* for 5 min to pellet any cells. Pour supernatants into new 50 ml tubes, and discard emptied tubes.
3. Centrifuge tubes at 3000×*g* for 15 min to pellet any cell debris. Pour supernatants into new 50 ml tubes and discard emptied tubes.
4. Using 0.20 μm PES syringe filters, filter the supernatants into new 50 ml tubes. Keep these clarified supernatants at 4°C until the remaining steps can be performed, up to 3 days.
5. Add 15 ml of clarified supernatant to ultrafiltration devices, using one device for each predetermined exosome sample.
6. Centrifuge at 3000×*g* for 15 min. Carefully lift the sample reservoir, and aspirate away the filtrate that has passed through the reservoir into the tube. Reinsert the reservoir into the tube.
7. Apply another 15 ml of clarified supernatant to the ultrafiltration unit, and centrifuge and aspirate as in Step 6, repeating until all clarified supernatant has been filtered (*see* **Note 10**).
8. Measure the volume in the sample reservoir using a micropipette. If the volume is much greater than 100 μl, centrifuge the filter device for another 15 min at 3000×*g* (the Amicon devices will not "overspin" or release all liquid as flowthrough). We routinely measure 115–120 μl of concentrated supernatant even after this extra spin.
9. Bring the SEC spin columns to RT for 15 min, one for each ultrafiltration unit used, keeping the columns upright. Check the integrity of the columns to be sure there are no bubbles, air pockets, or "breaks" in the matrix. If so, do not use that column. Throughout the SEC spin column procedure, take care to avoid introducing bubbles while adding the 1× PBS washes and samples.
10. After removing the bottom plug, place the SEC spin columns into the provided collection tubes. Remove the cap of each column, and immediately screw it back on (*see* **Note 11**). Remove the cap again, and using a micropipette, discard the 20% ethanol above the frit of the column. To prevent the column matrix from drying, immediately add 250 μl of filtered PBS to the top of the column, replace the cap, and continue with the protocol (*see* **Note 12**).
11. Centrifuge the columns at 50×*g* for 10 s. Pour off the flowthrough. If PBS still sits above the frit in any of the columns, spin those columns for 5 s at 50×*g*, repeating if necessary. Check the integrity of the spin column matrix as in Step 9.

12. Add another 250 µl of filtered PBS, replace the caps, and centrifuge at 50 × *g* for 10 s. Aspirate or pour off the flow-through. Again, check the integrity of the spin column matrix.
13. Carefully add a maximum of 100 µl of the ultrafiltered supernatant to each column and replace the cap. This time, centrifuge at 50 × *g* for 1 min. If the cell culture medium contained phenol red, the spin columns will have a pink to orange tint at the top of the matrix, depending on how spent the culture medium was.
14. Transfer the columns to prelabeled and sterile low-binding microcentrifuge tubes.
15. Add 200 µl of filtered PBS onto the columns. Replace caps, and centrifuge at 50 × *g* for 1 min. The pink to orange color should now be seen throughout the column matrix.
16. The resultant flow-through in the low-binding microcentrifuge tubes contains concentrated stock exosomes in approximately 200 µl of PBS. Discard the spin columns. Measure and note the final exosome sample volumes. At this point, NTA can be used to determine exosome concentration and size. We routinely perform the dilutions for NTA on freshly isolated exosome samples. The stock exosomes are then frozen at −80°C.
17. If multiple ultrafiltration units were used for the same cell line undergoing the same treatment in Step 5 and there is extra concentrated supernatant still present in those ultrafiltration units after Step 13, the excess can be pooled. Adjust the total volume to 100 µl with filtered PBS, and isolate the exosomes using a freshly prepped new SEC column (*see* **Note 13**).

3.3 NTA by ZetaView

1. Prepare the following dilutions of the stock exosomes (dilutions can be kept overnight at 4°C):
   a. 1:100 = 990 µl of filtered PBS + 10 µl of concentrated stock exosomes.
   b. 1:1000 = 900 µl of filtered PBS + 100 µl of 1:100 dilution.
   c. 1:10,000 = 900 µl of filtered PBS + 100 µl of 1:1000 dilution (if necessary).
2. Count exosomes using NTA. We use the following ZetaView settings: 25°C, 488 nm laser, shutter speed of 400, frame rate of 60, and sensitivity of 89. Calibrate the instrument using 100 nm beads, and prime the instrument with filtered 1× PBS since the exosomes are isolated in PBS (*see* **Notes 14 and 15**).
3. Inject exosome samples into the instrument using a 1 cc syringe. Individual particles are visualized in real-time (Fig. 2A). The results are collected from ten positions and analyzed.

Wash with 2–5 ml of filtered PBS after each sample. A mean diameter of ~50–60 nm and concentration of approximately 1×10^{11}–1×10^{12} exosomes/ml can be expected (Fig. 2B, C).

3.4 Western Blot Analysis of Exosome Samples

When preparing western blots, include cell lysates to serve as controls for the exosome samples. Samples of enriched exosomes should show expression of CD63 and TSG101 but very little to no expression of β-tubulin (or other cytoplasmic housekeeping genes such as β-actin) and cytochrome C (to demonstrate absence of organelle contamination from mitochondria). Cell lysates should show expression of all four proteins (Fig. 3).

1. Cell lysates can be prepared directly from monolayers in 150 mm dishes (or T175 flasks) or from cell pellets.
2. Prepare lysates from monolayers as follows:
   a. Place dishes/flasks on ice and wash with ice-cold 1× DPBS.
   b. Aspirate away DPBS and add 3 ml of RIPA buffer with protease/phosphatase inhibitors for 5 min.

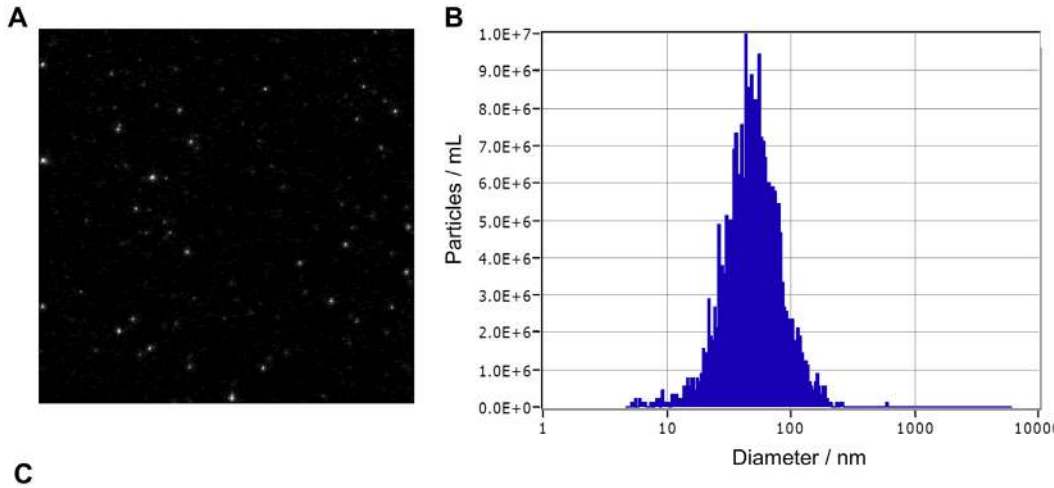


Fig. 2 Breakdown of Nano Tracking Analysis (NTA) report generated by ZetaView. (**A**), A snapshot of the particles visualized in the particle counting chamber. Particle count should be between 50 and 500 (maximum). (**B**), Size distribution graph with a single, normal-like curve (mean, median, and mode are of similar values) indicating a successful exosome isolation. (**C**), Concentration of particles in the chamber should range between 1×10^7 and 9.9×10^8. The dilution factor used is multiplied to give the original exosome concentration of the sample. Mean diameter is 50–70 nm, depending on the cell line from which the exosomes are derived. The exosome polydispersity index (NePdi) is a ratio of the standard deviation divided by the mean exosome size based on NTA (ZetaView). NePdi higher than 1.0 could indicate that the sample was not passed through a 0.22 μm syringe-filter before ultrafiltration or that a faulty SEC column was used

c. Using a cell scraper and pipet, transfer cell suspension to a 5 ml microcentrifuge tube, and incubate for 15 min on ice.

d. Pass cell suspension through a 21-G needle five times. Incubate for another 15 min on ice.

e. Split lysate into 1.5 ml microcentrifuge tubes, and continue to Step 4.

3. Prepare lysates from cell pellets as follows:

a. Add 1 ml of RIPA buffer with protease/phosphatase inhibitors to 5×10^6 cells.

b. Resuspend to disperse the pellet, transfer to a 1.5 ml microcentrifuge tube, and place on ice for 15 min.

c. Pass cell suspension through a 21-G needle five times. Incubate for another 15 min on ice.

4. Centrifuge cell lysates in a microcentrifuge at full speed for 10 min at 4°C. Transfer supernatants to a new microcentrifuge tube. Store at −80°C.

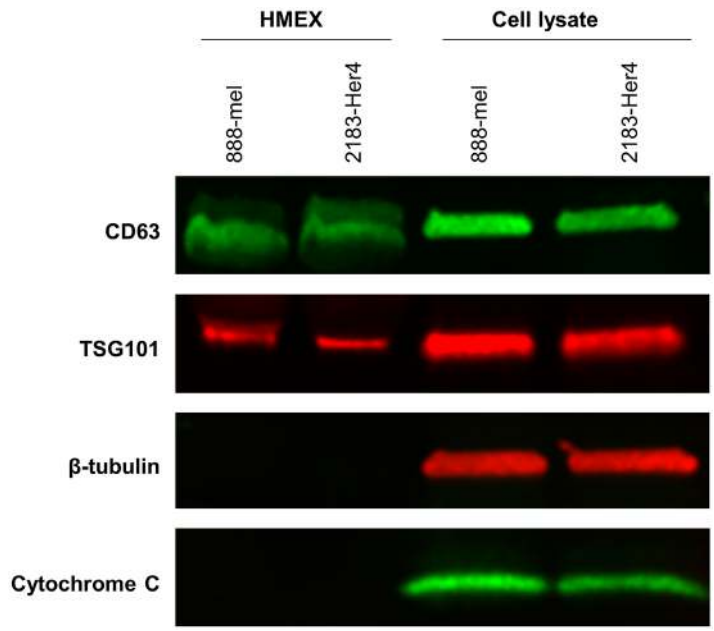


Fig. 3 Western blot analysis of exosomes. Cell lysates are included as positive controls for proteins absent in exosomes, such as β-tubulin (cytoplasmic) or cytochrome C (mitochondrial). Most reviewers expect at least two probes for the absence of non-exosomal protein, preferably one cytoplasmic and one organelle-specific protein. Both TSG101 and CD63 must be present for the sample to be defined as an exosome isolate. If only CD63 is present but not TSG101, it is still considered an EV isolate if β-tubulin and/or cytochrome C are not present

5. Measure the protein concentration of both the cell lysates and exosome samples using a protein assay kit. We typically dilute an aliquot of cell lysate 1:10 and 1:25 in RIPA buffer + protease/phosphatase inhibitors for protein analysis. An aliquot of exosome samples is diluted 1:5 in RIPA buffer + protease/phosphatase inhibitors. For the exosome samples, a protein concentration of 1–2 μg/μl can be expected after dilution.
6. Prepare 20 μg of cell lysate and 20 μg of exosome samples for electrophoresis by adding 6× Laemmli SDS sample loading buffer/2-ME up to a maximum volume of 50 μl (or the maximum volume that can be loaded in the gel wells). Heat samples for 5 min at 95°C. Centrifuge briefly.
7. Load samples and molecular weight standard on the gel, and run at 200 V for approximately 30 min, or as is appropriate for your electrophoresis system.
8. Presoak PVDF membrane in 100% ethanol (or methanol) to activate the membrane, and then rinse it in transfer buffer. Transfer proteins from the gels to the PVDF membrane as directed by your transfer system. For the Trans-Blot Turbo System, we use the preprogrammed protocol "1 Mini-TGX."
9. After transfer, rinse the membranes in H_2O for several minutes to remove any gel debris. Proceed with antibody incubations (using antibodies against CD63, TSG101, Cytochrome C, or β-tubulin) as described below in Step 11, or allow the membrane to air dry for ≥2 h (*see* **Note 16**).
10. If membranes were dried, activate the membrane by soaking in ethanol or methanol and rinse twice with H_2O.
11. Place membranes in blocking buffer for 1 h, rocking at room temperature. Dilute primary antibodies to the appropriate concentration in blocking buffer (Table 1). For us, all four antibodies (CD63, TSG101, β-tubulin, and cytochrome C) are diluted 1:1000. Incubate blots overnight at 4°C with rocking, or in 50 ml conical tubes on a rotator.
12. Rinse blots with 1× TBS/0.1% Tween 20 four times for 5 min per wash. Centrifuge antibodies for 5 min at 10,000 × *g* to remove any aggregates that may occlude bands during imaging. Dilute secondary antibodies to the appropriate dilution (Table 1) in blocking buffer with 0.01% SDS and incubate blots for 1 h, either on a rocker in dark boxes or in conical tubes on a rotator in the dark (*see* **Notes 17 and 18**).
13. Making sure to minimize light exposure, rinse blots in TBS/0.1% Tween 20 four times for 5 min per wash. Finally, rinse once in 1× TBS for 5 min to remove any residual Tween.
14. Blots can be imaged immediately or allowed to air-dry for at least 2 h in the dark. They then can be stored in the dark at RT for imaging in the future.

3.5 Preparation of Exosomes for TEM

The defining feature of exosomes is inherent in the phospholipid bilayer that keeps the internal region of exosomes discrete from their surroundings. Previously, TEM was used for the morphological characterization of an exosome, primarily based on the presence of the lipid bilayer. While not solely reliant upon TEM for exosome characterization, it is important that isolated exosomes maintain their integrity as demonstrated by an intact bilipid membrane, which can be visualized by combining TEM with negative staining (Fig. 4).

1. As the structure of the exosomes will not be preserved by the chemicals used in this protocol, the resultant EM grid exosome sample should be imaged by TEM as soon as possible. If the exosomes are not immediately imaged after Step 6, combine

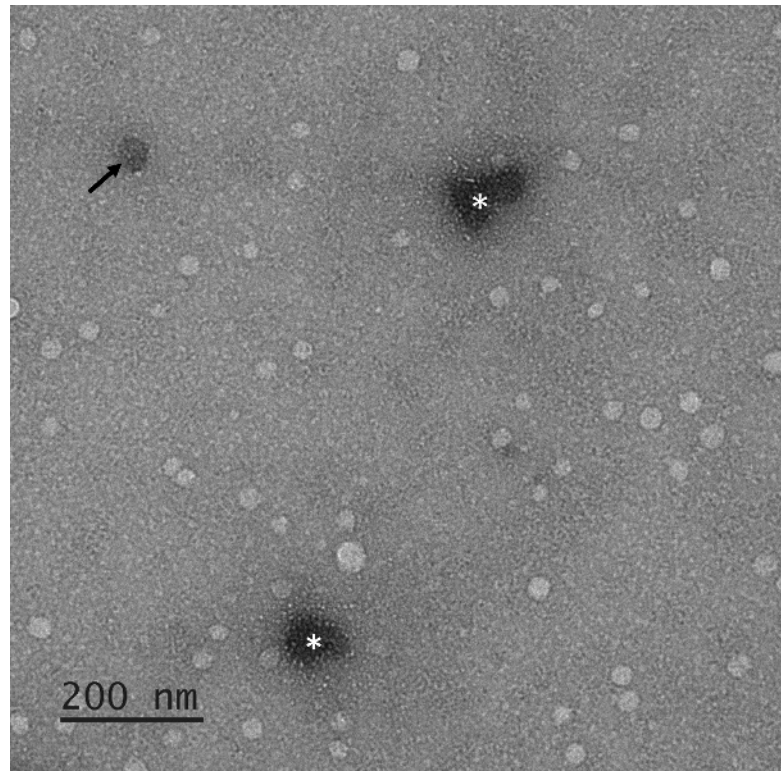


Fig. 4 TEM image of exosomes. Due to the compartmentalized nature of exosomes, negative staining by Uranyless™ highlights intact bilipid-layered vesicles as bright spherical spots relative to the darker, even background stained by Uranyless™. If an exosome is structurally compromised, it can appear as a darkened round spot as the stain is absorbed and retained within the vesicles (black arrow). Darker spots of undefined shapes are concentrations of stain (white asterisks). This phenomenon can be minimized by reducing the duration of time the sample is exposed to Uranyless™, but optimization requires a balance, as too short of an exposure would give a lighter background and may impair the contrast provided by the vesicles, which, if present, could appear unstained

6 μl of isolated exosomes (in 1× PBS) and 6 μl of 2% methyl cellulose before continuing to Step 2.

2. Place one drop (approximately 10 μl) of exosomes at a concentration of at least 1×10^{11} exosomes/ml onto parafilm.
3. Using tweezers, invert an EM grid onto the exosome drop for 1 min. Electrostatic forces and osmosis are sufficient for the exosomes to be uniformly distributed across the grid; this distribution occurs very quickly (1 min). Remove excess liquid by touching the edge of the grid with the edge of filter paper.
4. Place a drop (10 μl) of UranyLess™ solution onto the parafilm (*see* **Note 19**).
5. Invert the EM grid containing exosomes onto the UranyLess™ drop for 1 min only to limit aggregation of the stain. Remove excess UranyLess™ by touching the edge of the grid with the edge of the filter paper (*see* **Note 20**).
6. Leave to air-dry for at least 30 min, and then image by TEM.

4 Notes

1. The quality of exosome-depleted FBS is critical in regard to its exosome concentration. To verify its quality, prepare an aliquot of medium containing 5% normal FBS and another vial with medium containing 5% exosome-depleted FBS, and then analyze by NTA. The medium with exosome-depleted FBS should have approximately 1000-fold fewer particles. This step assures a more accurate quantification of exosomes after isolation.
2. ZetaView (Particle Metrix) is well-suited for use as a shared laboratory facility instrument, as it contains an automatic wash-pump system that allows quick turnaround of sample measurements and eliminates contamination from previous user samples without the need to dismantle the instrument to clean it in preparation for the next user.
3. Exosome-depleted FBS is not only higher in cost but is inferior at supporting the growth of melanoma cell lines when compared to normal FBS.
4. We have found that a confluency less than 70% will yield too few exosomes. We typically seed $0.7–1.2 \times 10^6$ cells per plate.
5. Cells produce more exosomes when confluency is between 85% and 95%. When confluency reaches 100%, the yield drops considerably. Therefore, cells should be seeded in a uniform layer by giving the plates a gentle lateral shake (in perpendicular motion, i.e., left to right then front to back) several times before placing in the incubator. Observe under the microscope for uniform confluency. Uneven seeding can

cause some areas to be 100% confluent, which may cause a reduction in exosome production, yielding an inadequate number for downstream experiments.

6. Caution is advised when using this small volume of medium in 150 mm plates (or T175 flasks). Check that the incubator shelves do not have a slant that may cause certain areas of the plates to be devoid of medium, which could otherwise lead to cell death and contamination of the supernatant with exosomes released by dead cells.
7. As NTA is extremely sensitive, any bacterial growth in an isolated exosome sample due to contamination would severely compromise both the NTA and the sample.
8. The isolated exosomes are not considered sterile, as the ultrafilters we use are not sterile and the SEC columns are not manufactured in a GMP facility. However, the SEC column matrix is preserved in 20% ethanol and therefore unlikely to carry contamination. When our exosomes were used for downstream cell culture experiments, no contamination was observed for in vitro experiments that lasted 24 h. We also performed in vivo studies where exosomes were injected into the tail-vein of severe combined immunodeficient (SCID) mice, and no blood-based complications were observed after 30 days. To limit the potential for contamination, use a biosafety cabinet for all steps.
9. After supernatants have been collected, the cells can be dissociated from the plates and counted in order to calculate the number of exosomes per cell once the exosome count is determined. Otherwise, discard the monolayers as we have observed that cell proliferation slows in the presence of medium containing exosome-depleted FBS.
10. Although repeated additions of supernatant from one sample can be added to the ultrafiltration units, it is not recommended to "wash and re-use" the units for a different sample because their membranes can clog with use.
11. We have found that this removal and replacement of the cap helps to maintain both the packing of the matrix and a consistent flowrate.
12. The SEC columns are stored in a preservative that contains enough alcohol to weaken or damage the integrity of the exosome lipid bilayers. Therefore, the PBS wash steps of the columns are critical.
13. In accordance with the manufacturer's instructions, the reuse of SEC columns is not recommended, as trace amounts of proteins will continue to be released.
14. The recommended settings may vary depending on the user's NTA instrument. Please consult the manufacturer for calibration of the instrument to detect spherical liposomes sized 50–100 nm. For consistency, calibrate the instrument using

100 nm microbeads. S.D. should fall between the bead manufacturer's QC certification fact sheet specifications, including concentration.

15. There is no need to filter PBS before use if the specific brand/lot of PBS is checked by NTA for particulates by running a PBS-only sample on the NTA instrument. It should register only background levels of particles (the same as reverse-osmosis filtered distilled water). The PBS should be kept at 4°C when not in use, and procedures should be followed to ensure that sterility is not compromised. If the PBS is kept for an extended period of time, check it by NTA before use. If exosome yield following isolation is unusually high, check by NTA to see if the PBS is contaminated. It is advisable to check for particles whenever a new lot of PBS is used.
16. Drying the PVDF membrane allows it to be used at a future time but can also improve the eventual signal by increasing the retention of the proteins on the membrane. Place the dry membranes in a zip-lock bag, and store at 4°C for up to 2 weeks, −20°C for up to 2 months, or at −70°C for longer storage [19]. When ready to use, bring membranes to RT and activate.
17. SDS is included in the secondary fluorescent antibody blocking buffer to reduce background fluorescence [20].
18. We typically use IRDye 800CW secondary antibodies to detect protein targets with low abundance and IRDye 680RD secondary antibodies to detect more abundant proteins.
19. In the past, negative staining could only be done using heavy metals such as uranyl acetate, which also had radioactive properties. In this TEM staining procedure, UranyLess™ can be used in place of uranyl acetate with similar results.
20. A wash step following incubation with UranyLess™ is not required. We found that without the wash, the exosome images were more accurate and that most exosomes are spherical and rarely cup-shaped.

Acknowledgments

We would like to thank Dr. Teresa Whiteside and her team for their technical advice. This work was supported by The Katherine Anne Gioia Endowed Chair in Cancer Medicine, Roswell Park Comprehensive Cancer Center; National Cancer Institute (NCI) grant P30CA016056 involving the use of Roswell Park Comprehensive Cancer Center's Flow and Image Cytometry Shared Resources.

Competing Interests The authors have no conflicts of interest to declare that are relevant to the content of this chapter.

References

1. Shu S, Yang Y, Allen C et al (2020) Purity and yield of melanoma exosomes are dependent on isolation method. J Extracell Vesicles 9(1):1692401. https://doi.org/10.1080/20013078.2019.1692401
2. Ludwig N, Lotze MT (2020) A treatise on endothelial biology and exosomes: homage to Theresa Maria Listowska Whiteside. HNO 68(2):71–79. https://doi.org/10.1007/s00106-019-00803-1
3. Whiteside TL (2016) Tumor-derived exosomes and their role in cancer progression. Adv Clin Chem 74:103–141. https://doi.org/10.1016/bs.acc.2015.12.005
4. Kalluri R (2016) The biology and function of exosomes in cancer. J Clin Invest 126(4):1208–1215. https://doi.org/10.1172/JCI81135
5. Valadi H, Ekström K, Bossios A et al (2007) Exosome-mediated transfer of mRNAs and microRNAs is a novel mechanism of genetic exchange between cells. Nat Cell Biol 9(6):654–659. https://doi.org/10.1038/ncb1596
6. Wang S, Li X, Zhu R et al (2016) Lung cancer exosomes initiate global long non-coding RNA changes in mesenchymal stem cells. Int J Oncol 48(2):681–689. https://doi.org/10.3892/ijo.2015.3272
7. Whiteside TL (2017) Exosomes in cancer: another mechanism of tumor-induced immune suppression. Adv Exp Med Biol 1036:81–89. https://doi.org/10.1007/978-3-319-67577-0_6
8. Whiteside TL (2015) The potential of tumor-derived exosomes for noninvasive cancer monitoring. Expert Rev Mol Diagn 15(10):1293–1310. https://doi.org/10.1586/14737159.2015.1071666
9. Shu S, Yang Y, Allen C et al (2018) Metabolic reprogramming of stromal fibroblasts by melanoma exosome microRNA favours a pre-metastatic microenvironment. Sci Rep 8(1):12905. https://doi.org/10.1038/s41598-018-31323-7
10. Kahlert C, Kalluri R (2013) Exosomes in tumor microenvironment influence cancer progression and metastasis. J Mol Med 91(4):431–437. https://doi.org/10.1007/s00109-013-1020-6
11. Kalluri R, LeBleu VS (2020) The biology, function, and biomedical applications of exosomes. Science 367(6478), eaau6977. https://doi.org/10.1126/science.aau6977
12. Wong CH, Chen YC (2019) Clinical significance of exosomes as potential biomarkers in cancer. World J Clin Cases 7(2):171–190. https://doi.org/10.12998/wjcc.v7.i2.171
13. Alegre E, Zubiri L, Perez-Gracia JL et al (2016) Circulating melanoma exosomes as diagnostic and prognosis biomarkers. Clin Chim Acta 454:28–32. https://doi.org/10.1016/j.cca.2015.12.031
14. Théry C, Whitwer K, Aikawa E et al (2018) Minimal information for studies of extracellular vesicles 2018 (MISEV2018): a position statement of the International Society for Extracellular Vesicles and update of the MISEV2014 guidelines. J Extracell Vesicles 7(1):1535750. https://doi.org/10.1080/20013078.2018.1535750
15. Altevogt P, Bretz N, Ridinger J et al (2014) Novel insights into exosome-induced, tumor-associated inflammation and immunomodulation. Semin Cancer Biol 28:51–57. https://doi.org/10.1016/j.semcancer.2014.04.008
16. Benjamin Davalos S, Koroleva M, Allen CL et al (2021) Co-isolation of cytokines and exosomes: implications for immunomodulation studies. Front Immunol 12:638111. https://doi.org/10.3389/fimmu.2021.638111
17. Robinson SD, Samuels M, Jones W et al (2024) Confirming size-exclusion chromatography as a clinically relevant extracellular vesicles separation method from 1 mL plasma through a comprehensive comparison of methods. BMC Methods 1(1):7. https://doi.org/10.1186/s44330-024-00007-2
18. Keivan M, Mansouri Torghabeh F, Davoodi S et al (2022) Single intratesticular injection of blood serum derived exosomes can potentially alleviate testopathy following testicular torsion. Animal Model Exp Med 5(4):362–368. https://doi.org/10.1002/ame2.12232
19. EMD-Millipore (2017) Protein blotting handbook: tips and tricks, 6th edn. MilliporeSigma. https://www.sigmaaldrich.com/content/dam/sigma-aldrich/docs/Sigma-Aldrich/General_Information/1/protein-blotting-handbook.pdf
20. Li-COR Biosciences (2008) Good westerns gone bad: tips to make your NIR western blot great. http://biosupport.licor.com



Chapter 13

Post-Lymphadenectomy Analysis of Small Extracellular Vesicles from Lymphatic Drainage/Exudative Seroma of Melanoma Patients

Enrique Bastón de la Fuente, Pilar Ximénez-Embún, Javier Muñoz, Héctor Peinado and Susana García-Silva

Abstract

Circulating extracellular vesicles (EVs) have emerged as a promising source of disease biomarkers in biofluids. Although multiple isolation methods are available, differential ultracentrifugation remains a gold standard for small EV purification. Small EVs purified using this approach retain functional activity both in vitro and in vivo and are suitable for downstream applications, including proteomics, electron microscopy, mass spectrometry, and nucleic acid analysis. An additional purification step, either by density gradient centrifugation or size-exclusion chromatography, allows for the isolation of highly pure EV fractions for subsequent biomarker analysis. Here, we describe a protocol based on differential ultracentrifugation followed by a density gradient centrifugation or size exclusion chromatography step for the recovery of highly pure small extracellular vesicles (EVs) from lymphatic exudate (seroma) collected following lymphadenectomy, with the aim of supporting biomarker discovery and liquid biopsy applications.

Keywords Lymphatic exudate, Lymphatic drainage, Lymphadenectomy, Extracellular vesicles, Exosomes, Ultracentrifugation, Iodixanol gradient, Size-exclusion chromatography, Biomarker discovery

1 Introduction

Extracellular vesicles (EVs) are cell-secreted particles characterized by a lipid bilayer that display a broad range of sizes and biogenesis pathways. Due to this heterogeneity, they are commonly classified based on size into small (sEVs) and large (lEVs) vesicles [1]. Exosomes, migrosomes, and other vesicles with sizes around 50–150 nm are considered sEVs. Microvesicles (200 nm–1 μm), apoptotic bodies (1–5 μm) exophers (4 μm), and oncosomes (1–10 μm), among others, are considered lEVs [1, 2]. EVs carry a complex molecular cargo that includes cytosolic and membrane-anchored proteins, glycoproteins, lipids, nucleic acids, and metabolites [3]. Large EVs such

Kristian M. Hargadon (ed.), *Melanoma*, Methods in Molecular Biology, vol. 3089,
https://doi.org/10.1007/978-1-0716-5619-8_13,
© The Author(s), under exclusive license to Springer Science+Business Media, LLC, part of Springer Nature 2027

as microvesicles or exopheres are generated by budding from the plasma membrane, whereas exosomes are generated through the endosomal pathway [4]. More specifically, exosomes arise during the formation of the multivesicular bodies (MVBs) that subsequently fuse with the plasma membrane releasing their content of exosomes into the extracellular milieu [4, 5].

Vesicle secretion is an evolutionarily conserved mechanism present from bacteria to vertebrates. Its primary function is the selective transport of cargo, enabling cells to communicate over short and long distances across tissues [6, 7]. This cargo influences the behavior of recipient cells. Remarkably, EVs have been detected in most biological fluids [8]. Most of the knowledge about EVs has been focused on exosomes, and subsequently the methods and applications developed for liquid biopsy are predominantly based on these EVs. Exosomes have been involved in numerous physiological and pathological processes such as the adaptive immune response [9], mother–fetus communication [10], neurodegenerative processes [11], and cancer progression [12], including the formation of the pre-metastatic niche [13, 14] and metastatic organotropism [15].

Several methods have been described for the purification of exosomes and other sEVs [16]. Differential ultracentrifugation is a widely used technique for the isolation of sEVs from cell cultures and biological fluids such as serum, plasma, cerebrospinal fluid, or urine [17, 18]. This method is based on the different densities of bodies under a rotary force. Several steps with increasing centrifugation forces allow for the removal of cellular debris, platelets, and large EVs such as microvesicles [17]. Ultracentrifugation at $100{,}000 \times g$ yields a pellet enriched in exosomes and other sEVs. Due to the presence of protein aggregates, apolipoproteins, and other contaminants in the pellet, an additional purification step is currently recommended. An additional centrifugation using an iodixanol density-gradient medium or a sucrose gradient could be performed for the recovery of highly purified exosomes [19, 20].

Although differential ultracentrifugation enables high vesicle yields, it is time-consuming, has limited compatibility with high-throughput applications, and may cause structural damage to EVs [17]. To address these limitations, alternative methods have been developed for EV isolation [18]. Size-exclusion chromatography (SEC) employs columns containing heterogeneous pores [21, 22]. Another size-based isolation method is ultrafiltration that segregates EV using membranes with specific cutoff molecular weights [23]. These methods have limitations in the in/out volumes and the presence of contaminants with a similar size. However, their coupling with differential ultracentrifugation substantially increases the purity of sEV preparations [24]. Precipitation with hydrophobic polymers such as Polyethylene glycol (PEG) allows for the capturing of sEVs in the polymer net that precipitates [25]. Based on this principle,

several commercial kits have been developed to enable rapid and straightforward exosome isolation; however, the coprecipitation of contaminants may compromise downstream analyses.

A high-purity isolation of sEVs can be performed using immunoaffinity techniques based on the use of exosome/sEV-specific antibodies attached to magnetic beads or other matrices [26]. Although this approach provides isolation of specific sEV subpopulations, scaling up for the purification of large amounts of sEVs is challenging and expensive. Recently, new techniques based on microfluidic devices are being developed. These platforms apply strategies based on hydrodynamic-based microfluidics, affinity-based capture chips, size-based sorting using nano/micro porous membrane on chips, or field-based microfluidics mostly applying electrical or acoustic forces to achieve particle separation [27–29]. Compared to more traditional methods, microdevices allow for shorter processing times (often under an hour), higher purity, and easier integration with downstream analytic pipelines [30]. However, they still face challenges regarding standardization, throughput for large clinical cohorts, and cross-platform comparability of yield and purity parameters.

Isolation of sEVs allows the analysis of EV content, which reflects the cell of origin. Besides that, the stability of EVs in body fluids facilitates their study in biobanked samples and enables multiplexed analytics [20]. Thus, sEVs are powerful tools to provide information in a noninvasive way about diseases such as cancer, neurological syndromes, or cardiovascular diseases [31]. Thanks to their complex cargo, sEVs/exosomes can be exploited for the detection of mutations, SNPs, and epigenetic changes [31–33], as well as RNA, miRNA [34], and other noncoding RNA profiles [35], apart from the analysis of protein, lipid, and metabolic biomarkers [36–38].

Due to the presence of nucleic acids in EVs, detection of mutations located in the coding region has been shown in exosome-derived RNA/DNA isolated from cell cultures [39]. In liquid biopsies, the use of EV-derived DNA has been first focused on the analysis of EGFR in lung cancer and glioblastoma [32, 33] and KRAS and TP53 in pancreatic cancer [40, 41]. In melanoma, combined analysis of BRAF mutation in tissue and in plasma-derived EVs is more informative than each biopsy type alone [42]. Concerning protein biomarkers, many studies propose the detection of EV-associated proteins as cancer diagnostic or prognostic tools. For example, the levels of PD-L1 in plasma-derived exosomes correlated with the response to immunotherapy in melanoma patients [37]. The analysis of prostate-specific antigen (PSA) in plasma-derived exosomes from prostate cancer patients has been shown to be a more reliable marker than serum PSA [38, 43]. Furthermore, proteomic analysis combined with machine learning applied to EVs and other secreted particles isolated from various sources, including plasma, can determine tumor type and even classify tumors with an unknown primary origin [44].

Tumor progression to the metastatic phase represents the deadliest stage of cancer, accounting for an estimated 70%–90% of cancer-related deaths. Although not life-threatening, lymph node (LN) metastases are associated with poor prognosis in cancer patients, and the number of LNs with metastases is a strong prognostic factor in multiple cancer types, including melanoma, pancreatic cancer, breast cancer, or prostate cancer [45, 46]. Exudative seroma (also denominated lymphatic exudate or lymphatic drainage) is a biofluid obtained post-lymphadenectomy, a technique frequently performed in cancer patients for the removal of regional sentinel LNs after tumor resection [47]. This seroma is a lymph-like fluid with some similarities to plasma and to wound exudates [48]. In the clinical setting, this fluid has been used to profile disease markers in melanoma, showing better discrimination of patients with high risk of relapse than an equivalent analysis in blood [49–51]. Remarkably, the trafficking of sEVs via the lymphatic system and their contribution to pre-metastatic niche (PMN) formation in sentinel LNs have been reported [52–56]. In agreement with these reports, seroma is a biofluid highly enriched in sEVs that contain proteins and microRNAs associated with melanoma progression [57, 58]. Interestingly, the proteomic profiling of EVs purified from afferent lymphatic vessels in early-stage melanoma patients revealed proteins differentially expressed in the sentinel LNs during pre-metastatic niche formation [59]. Furthermore, we have shown that a combined approach analyzing seroma-derived EVs and circulating nucleic acids estimated that the genetic material obtained from seroma was around 650 times more abundant compared to plasma and that determination of BRAFV600E mutation in EVs derived from lymphatic drainage provided a strong prognostic value in a small cohort of stage III melanoma patients [58]. Recently, immunocapture of seroma-derived aspartate β-hydroxylase$^+$ EVs on a microfluidic platform allowed for fast detection of postoperative minimal residual disease in oral squamous cell carcinoma patients [60].

In summary, the isolation of small extracellular vesicles (sEVs) from seroma fluid represents a highly sensitive and promising approach for liquid biopsy applications, particularly for cancer diagnosis and the detection of minimal residual disease. In this chapter, we provide a detailed methodology for the analysis of sEV derived from exudative seroma collected post-lymphadenectomy in melanoma patients. This strategy may facilitate biomarker discovery in seroma fluid across diverse cancer types and lymphatic disorders and could be adapted to other biofluids.

2 Materials

1. Surgical drain tubes for postoperative fluid collection.
2. Commercially available red blood cell lysis buffer (*see* **Note 1**).

3. Refrigerated ultracentrifuge and swinging-bucket or fixed-angle rotor (*see* **Note 2**).
4. Ultracentrifuge-suitable tubes (*see* **Note 3**).
5. 15 ml collection Falcon tubes.
6. Phosphate Buffered Saline (PBS) without Mg^{+} and $Ca2^{+}$ (1×): 137 mM NaCl, 10 mM Na_2HPO_4, 2.7 mM KCl, 1.8 mM, KH_2PO_4, pH 7.4.
7. OptiPrep™ (containing iodixanol) density gradient medium (60%, w/v) (*see* **Note 4**).
8. Diluent mix: 0.25 M sucrose, 1 mM EDTA, 10 mM Tris-HCl, pH 7.5.
9. Iodixanol gradient solutions: Prepare 40%, 20%, 10%, and 5% (w/v) iodixanol solutions by diluting a stock solution of OptiPrep™ in the diluent mix.
10. Fresh 0.5 M NaOH solution filtered with a 0.22 μm pore-size sterile filter (*see* **Note 5**).
11. Fresh PBS solution containing 0.05% azide filtered with a 0.22 μm pore-size sterile filter (*see* **Note 5**).
12. qEVoriginal columns, 70 nm, 500 μL (Izon).
13. Automatic Fraction Collector (AFC) V2 (Izon).
14. Amersham™ Protran® western blotting nitrocellulose membrane.
15. Tris-buffered saline-Tween (TBST): 20 mM Tris base, 150 mM NaCl (pH adjusted to 7.6), 0.1 % Tween-20.
16. 5% nonfat dry milk in TBST
17. Appropriate unconjugated primary antibodies for sEV detection (e.g., anti-TSG101, anti-ALIX, anti-Syntenin-1, anti-CD9, anti-CD63).
18. Appropriate IRDye-conjugated secondary antibodies.
19. Amicon® Ultra-2 Centrifugal Filter with an Ultracel®-10k membrane (NMWL = 10 kDa).
20. Odyssey Infrared Imaging System (LI-COR Biosciences).
21. QIAamp DNA Mini kit (Qiagen) (*see* **Note 6**).
22. Milli-Q water.
23. Bicinchoninic acid-based assay kit (*see* **Note 7**).
24. Standard spectrophotometer or plate reader.
25. Nanoparticle tracking analysis (NTA) system.
26. Glow-discharged carbon-coated 400-mesh copper electron microscopy (EM) grids.
27. Uranyl acetate (1%).

28. Transmission electron microscope.
29. Freshly prepared solubilization solution: 8 M urea in 100 mM Tris-HCl (pH 8.0).
30. Microcon-30 kDa centrifugal filter units.
31. 2 M urea in 100 mM Tris-HCl (pH 8.0).
32. 1 M Tris(2-carboxyethyl)phosphine (TCEP).
33. 0.5 M 2-chloroacetamide (CAA).
34. Lys-C and Trypsin proteases.
35. Mass Spectrometer.
36. ExoLution™ Plus cfDNA + exoRNA Isolation Kit (Biotechne) or AllPrep DNA/RNA Mini Kit (Qiagen).

3 Methods

Carry out all procedures at room temperature unless otherwise specified. We encourage users of this protocol to carefully read notes on each step. A summary of the experimental workflow described here is shown in Fig. 1.

3.1 Purification of sEVs from Human Exudative Seroma/ Lymphatic Exudate

1. Collect the seroma (3–10 mL) from postoperative surgical drains for 24–48 h after radical lymphadenectomy.
2. Centrifuge at 500 × *g* for 10 min.
3. Discard the pellet, and incubate the supernatant with red blood cell lysis buffer for 10 min on ice.
4. Spin samples at 1100 × *g* for 10 min.
5. Transfer the supernatant fraction into a new collection tube, and immediately freeze at −80°C for storage (*see* **Note 8**).
6. When ready for analysis (*see* **Note 9**), allow samples to thaw at 37°C for 3–5 min.
7. Spin samples at 3000 × *g* for 10 min.
8. Place the supernatants into 13.5 mL or 4 mL polycarbonate thick-walled tubes (*see* **Note 10**).
9. Place a mark on the top of the tube, and align it with the exterior of the rotor (*see* **Note 11**).
10. Centrifuge at 12,000 × *g* for 20 min at 10°C (*see* **Note 12**).
11. Transfer the supernatants into new polycarbonate thick-walled tubes.
12. Measure particles in the supernatant by NTA or another similar technique to determine the initial sEV content (see Sect. 3.7).

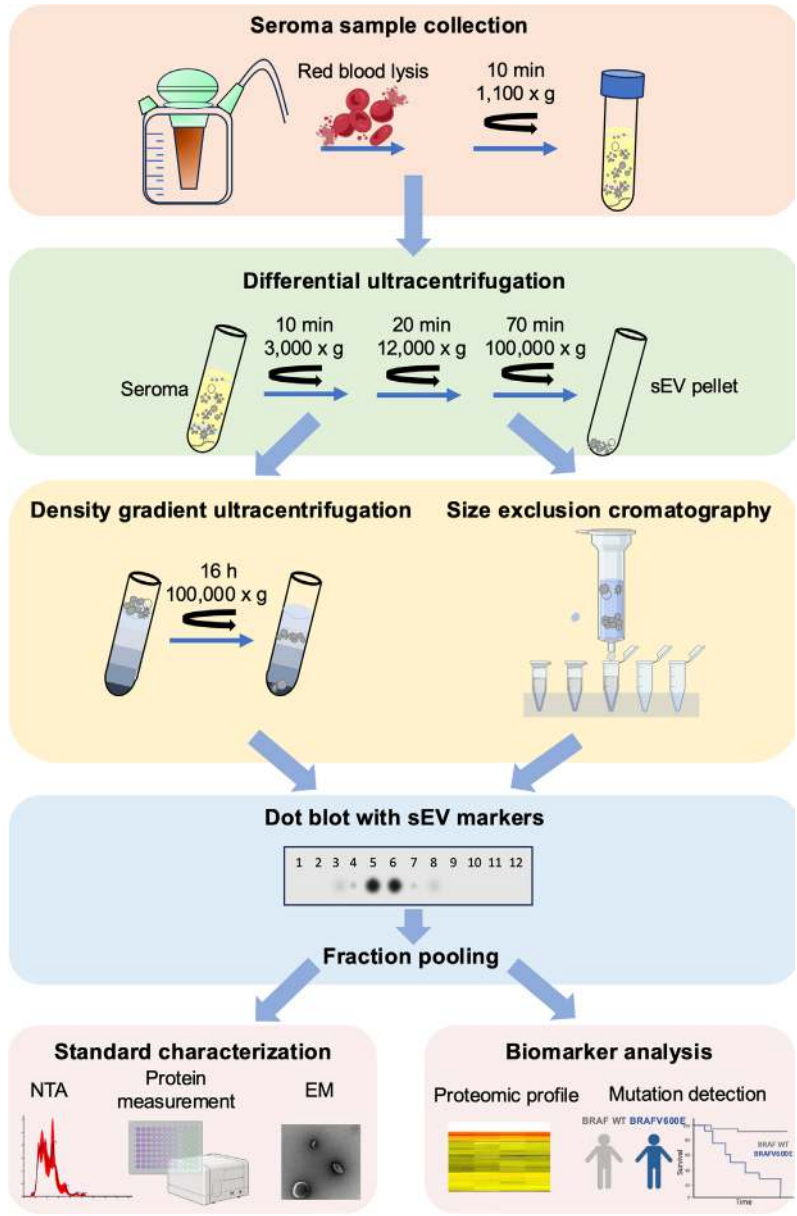


Fig. 1 Workflow of the isolation and analysis of sEVs. Differential ultracentrifugation and additional purification steps are followed by sEV characterization and biomarker discovery approaches. This figure has been partially created in https://BioRender.com

13. Place another mark on the top of each new tube, and align it with the exterior part of the rotor (*see* **Note 13**).
14. Ultracentrifuge at 100,000 × *g* for 70 min at 10°C.

15. Discard the supernatants by carefully swinging the tubes, and keep the tubes upside down for 1–2 min onto a paper towel to dry the pellets (*see* **Note 14**).
16. Wash the pellets by slowly adding 20 mL of 1× PBS along the side of the tube opposite the pellet to avoid disturbing it. Carefully place each tube into the rotor, ensuring that the mark is aligned with the exterior part of the rotor (*see* **Note 15**).
17. Centrifuge tubes at 100,000 × *g* for 70 min at 10°C.
18. Carefully discard each supernatant by gently inverting the tube. Important: the pellet contains purified sEVs. Keep each tube upside down for 2–3 min for removing any remaining liquid.
19. Resuspend the sEV pellets in 100–200 µl of 1× PBS (*see* **Note 16**).
20. Measure protein (see Sect. 3.6) and particle number by NTA (see Sect. 3.7) or other technique.

3.2 Additional Purification of sEV by Density Gradient Ultracentrifugation

1. Generate a discontinuous iodixanol gradient by sequentially layering 1.5 mL of each of the 40%, 20%, 10%, and 5% (w/v) iodixanol solutions (*see* **Note 17**).
2. Place the sEV sample obtained in Step 19 of Sect. 3.1 on top of the iodixanol gradient.
3. Centrifuge at 100,000 × *g* for 16 h at 10°C.
4. Collect fractions of 0.75 mL, starting from the top of the gradient.
5. Check fractions for sEV protein markers by dot blot, and/or measure particles by NTA (see Sects. 3.4 and 3.7).
6. Dilute sEV positive fractions (usually fractions 4, 5, and 6) in 10 mL of 1× PBS, and centrifuge at 100,000 × *g* for 70 min at 10°C (*see* **Note 18**).
7. Resuspend the pellets in 100–200 µL of 1× PBS (*see* **Note 19**).
8. Store samples (*see* **Note 20**), or proceed with analysis.

3.3 Purification of sEVs by Size Exclusion Chromatography (SEC)

As an alternative to density-gradient centrifugation, sEV samples can be purified using SEC. One column is required per sEV sample. However, the same column can be reused after cleaning.

1. Allow the qEV column(s) and 1× PBS to equilibrate to room temperature before use.
2. Prepare the Automatic Fraction Collector (AFC) by performing carousel and scale calibrations prior to sEV separation following the manufacturer's instructions.
3. Carefully remove the top and bottom caps of the qEV column.

4. Carefully, but quickly, insert the column upright into the AFC, ensuring the bottom of the column fits into the nozzle (*see* **Note 21**).
5. Once the AFC detects the column, select the following SEC parameters available on the AFC screen:
   a. Count: Number of fractions to collect.
   b. Volume: Volume of each fraction.
   c. Buffer Volume (BV): initial volume to be discarded (*see* **Note 22**).
6. Once the parameters are confirmed, mount the buffer reservoir onto the column.
7. Prior to collection, flush the qEV column with two column volumes of 1× PBS (8.5 mL) to equilibrate it.
8. Load the sEV sample obtained in Step 19 of Sect. 3.1 onto the top of the column, and allow it to fully enter the resin bed.
9. As soon as the sample is completely inside the resin bed, add the volume of 1× PBS indicated on the screen of the AFC.
10. Allow the selected BV to pass through.
11. Once the BV has been discarded, the AFC will begin to collect fractions at the preset volume.
12. Upon completion of the separation process, collect the fractions and store them at 4°C.
13. Discard or clean and rinse the column for subsequent or future use (*see* **Note 23**).
14. Perform a dot blot using antibodies against sEV markers for identifying the fractions of interest as described in Sect. 3.4. Optionally, measure the protein content in each fraction as described in Sect. 3.6.

3.4 Identification of sEV Positive Fractions by Dot Blot

This validation step is necessary after density-gradient ultracentrifugation or SEC because vesicular heterogeneity or technical issues may cause variations in the fraction distribution, depending on the sample type.

1. Spot 1 µL of each fraction obtained in Step 7 of Sect. 3.2 or in Step 12 of Sect. 3.3 onto a nitrocellulose membrane, and allow it to air-dry completely (~10 min at room temperature) (*see* **Note 24**).
2. Block the membrane with 5% nonfat dry milk in TBST for 20 min on an orbital shaker.
3. Add the primary antibody diluted in 5% nonfat dry milk in TBST, and incubate for 20 min with shaking (*see* **Note 25**).

4. Wash the membrane with TBST for 5 min under agitation. Repeat this step three times.
5. Incubate the membrane with an IRDye-conjugated secondary antibody diluted in 5% nonfat dry milk in TBST for 20 min with shaking and protection from light.
6. Wash the membrane with TBST for 5 min under agitation. Repeat this step three times.
7. Scan the membrane using an Odyssey Infrared Imaging System.
8. Analyze the signal intensity of the spots to identify the sEV-enriched fractions for subsequent downstream pooling and concentration.

3.5 Fraction Concentration After SEC or Density Gradient Ultracentrifugation

For most downstream applications, including proteomics or functional assays, it is recommended to concentrate purified sEV fractions obtained in Step 7 of Sect. 3.2 or in Step 12 of Sect. 3.3, as assessed for the presence of sEV markers using the method in Sect. 3.4.

1. Pool fractions positive for sEV markers as determined by dot blot analysis (typically fractions four to seven, depending on the sample).
2. Load the mixed fractions into an Amicon® Ultra-2 Centrifugal Filter with an Ultracel®-10k membrane (NMWL = 10 kDa).
3. Spin at 3000 × *g* for 20 min to concentrate the vesicular fraction to a final volume of 200 µL.
4. Perform further characterization of the final samples by protein and particle number measurements.

3.6 Protein Measurement of Purified sEV Samples

1. Take 5–10 µL of sEV sample, and measure sEV-associated protein concentration with a BCA assay (*see* **Note 26**).
2. Measure absorbance in a standard spectrophotometer or plate reader at 562 nm (*see* **Note 27**).

3.7 Particle Measurement

1. Dilute 1 µL of sEV samples in 1 mL of 1× PBS.
2. Determine the number and average size of particles using NTA [e.g., with a Nanosight instrument or any other particle counter device (*see* **Note 28**)].

3.8 Analysis of Purified sEVs by Electron Microscopy (EM)

1. Apply purified sEVs onto freshly glow-discharged carbon-coated 400 mesh copper EM grids at a concentration of 4×10^7 particles/mL, and incubate for 5 min at room temperature.
2. Place the grids consecutively on top of three distinct 50 µL drops of Milli-Q water, rinse gently for 2 s, and lay on the top of two different 50 µL drops of 1% uranyl acetate.
3. Stain the sample for 1 min.
4. Rinse the grids gently for 5 s, and allow them to air-dry.

5. Visualize the grids with a transmission electron microscope (*see* **Note 29**). Images can be recorded at 21,900 nominal magnification with a 4k×4k TemCam-F416 CMOS camera (Fig. 2).

3.9 Proteomic Analysis

1. Solubilize samples using 8 M urea in 100 mM Tris-HCl (pH 8.0). Samples (7.5 μg of protein amount) are digested using filter units (*see* **Note 30**).
2. Reduce with 15 mM TCEP, and alkylate the proteins with 30 mM CAA for 30 min in the dark.
3. Centrifuge the filter units at 12,000×*g* for 15 min, and discard the flow-through.
4. Remove the excess of reagents adding 2 M urea in 100 mM Tris-HCl.
5. Centrifuge the filter units at 12,000×*g* for 15 min, and discard the flow-through.
6. Sequentially digest the samples with Lys-C (protein:enzyme ratio 1:50) overnight and with trypsin (protein:enzyme ratio 1:100) for 6 h at 37°C.
7. Centrifuge the filter units at 12,000×*g* for 8 min, and keep the flow-through.
8. Desalt the resulting peptides using stage tips.
9. Perform mass spectrometry analysis (*see* **Note 31**).
10. Assess the purity of sEV preparations by performing GO-based analysis, using the Cellular Component (CC) annotation (*see* **Note 32**).
11. Probe the identified proteins against sEV repositories such as ExoCarta (www.exocarta.org), and check for the presence of well-known sEV markers such as CD9, CD63, CD81, Alix, and Syntenin.

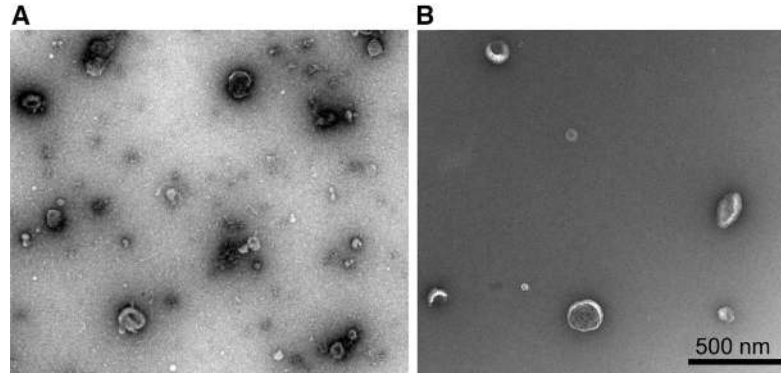


Fig. 2 Electron microscopy images of sEVs purified from exudative seroma by differential ultracentrifugation (**A**) and by differential ultracentrifugation plus iodixanol gradient ultracentrifugation (**B**)

3.10 DNA Extraction

Analysis of DNA quantity and quality, or further DNA characterization, can be performed on DNA extracted from samples obtained in Step 19 of Sect. 3.1 or in Step 3 of Sect. 3.5 (*see* **Note 33**).

1. Dilute samples from which DNA is to be extracted up to 200 µL with 1× PBS.
2. Extract DNA using the QIAamp DNA Mini kit.
3. Elute DNA from the column in 50 µL of Milli-Q water.
4. Measure DNA concentration (*see* **Note 34**) and test DNA quality (*see* **Note 35**).

3.11 Analysis of DNA Mutations (e.g., BRAF V600E/K)

sEV-associated DNA purified in Sect. 3.10 can be used for designed mutation assays. Alternatively, the approach below can be used for enrichment and analysis of genetic material through a combination of a filtration process and qPCR analysis [58].

1. Use 0.5–1 mL of initial seroma sample for co-isolation of sEV-associated RNA and DNA, along with any cfDNA (*see* **Note 36**).
2. Use the ExoLution™ Plus cfDNA + exoRNA Isolation Kit to co-isolate cfDNA + exoRNA in a single workflow.
3. Perform a reverse transcription reaction with the total purified nucleic acid from the sample.
4. Analyze both wild type and V600E/K BRAF mutant alleles by allele-specific qPCR [61].

4 Notes

1. For example, ACK lysing buffer can be purchased from many suppliers.
2. Some recommendations are:
   a. Ultracentrifuge OPTIMA XPN 100-IVD, Beckman Coulter.
   b. Rotor 50.4 Ti (Beckman-Coulter), for 4 mL polycarbonate thick-wall tubes.
   c. Rotor 70.1 Ti (Beckman–Coulter), for 13.5 mL polycarbonate thick-wall tubes.
3. Some recommendations are:
   a. For volumes up to 3.5 mL of seroma samples: 4 mL polycarbonate thick-wall tubes.
   b. For volumes up to 10 mL of seroma samples: 13.5 mL polycarbonate thick-wall tubes.

4. This material is required for an optional subsequent purification step. Purification applying a further density gradient-based procedure increases the purity of exosomes, but the yield is substantially lower.
5. This solution is needed only if additional size exclusion chromatography is performed. If necessary, degas the solution to prevent air bubble formation.
6. This kit yields more DNA than the other kits tested.
7. We recommend the Pierce BCA Protein assay kit.
8. After collecting the seroma from the patient, centrifugation and freezing of the seroma sample should be performed within 1 h to preserve the quality and avoid variability. Caution: Work with human samples carries a risk of infection if the material is not handled with care. Make sure you have the proper training and authorization to work with human samples. It is compulsory to have an approved ethical protocol before the use of any sample involving patient-derived material. Do not forget to wear required personal protection material when handling human samples.
9. We recommend collecting all samples and storing them frozen until further analysis. Procedures involving sEV isolation should ideally be performed in batches to reduce experimental variability.
10. Do not load more than 10 mL into 13.5 mL tubes or more than 3.5 mL into 4 mL tubes to prevent spillage during centrifugation. It is also important to fill at least three-quarters of the tube with the sample. If necessary, complete the volume with 1× PBS.
11. This mark will help to identify the pellet of large EVs (usually presenting a yellowish color). Try not to disturb the pellet when collecting the supernatant.
12. Depending on the rotor, the equivalence between rpm and *x* g differs. Some specific calculations for EV isolation have been published [17].
13. If the amount of sEV is low, the pellet may not be visible. The mark and orientation in the rotor help to identify the position of the pellet in the tube. For swinging-bucket rotors, the pellet is at the bottom of the tube. For fixed-angle rotors, the pellet forms along the outer wall at the bottom of the tube.
14. Do not put the tube back in the vertical position before it dries for 1 min because the remaining fluid could disturb the pellet. Important: the pellet contains sEVs. It can show a yellowish color.

15. It is very important to keep orienting the tube within the rotor since this additional washing step yields a more transparent pellet difficult to see by inexperienced investigators.
16. For resuspension, pipette up and down for at least 20 times with the pipette ejecting the liquid directly onto the pellet. Try to avoid foam formation. Sometimes, the pellet has a mucinous consistency or is difficult to resuspend. In these cases, increase the volume of 1× PBS by two to four fold. Samples can be stored at 4°C for 48 h. For longer times, samples should be stored at −80°C for at least 1 year.
17. On the bottom of the tube, add the 40% iodixanol solution. Keep layering the more diluted solutions on top of the 40% iodixanol by carefully placing the pipette where the liquid surface and the wall of the tube meet and slowly depressing the pipette plunger to allow the solution to gently fill the tube. This method will help to avoid disturbing the solution gradient. We recommend 13.5 mL polycarbonate thick-walled tubes for this method.
18. This step will help to remove the iodixanol and sucrose in the sample and concentrate the sEV content. Remember again to mark the tube for identifying the position of the pellet since it could be totally transparent after this step.
19. This sample can also be characterized for protein and particle analysis. It is also compatible with electron microscopy approaches.
20. Samples can be stored at 4°C for 48 h. For longer storage (up to at least 1 year), samples should be stored at −80°C.
21. Adjust the column position to allow the AFC to read the RFID tag.
22. We recommend: $a=12$ fractions, $b=400\,\mu L$, $c=1\,mL$. The AFC will automatically adjust the 1× PBS volume based on these parameters.
23. To clean the column, add one column volume (8.5 mL) of 0.5 M NaOH, and allow it to flow through the column until it reaches the top frit. To restore the column to its operational pH before loading another sample, flush with two column volumes of 1× PBS (8.5 ml × 2), and allow it to flow through until it reaches the frit. After the flushing step, the column is ready for reuse with additional samples. Otherwise, add 2 mL of 1× PBS containing 0.05% azide for long-term storage.
24. Mark the loading position of each SEC fraction with a pencil.
25. We recommended testing several sEV markers (e.g., TSG101, ALIX, Syntenin-1, CD9, and CD63) because their presence may be sample-dependent. Perform 1 dot blot for each EV marker.

26. Do not forget to include a standard BSA curve.
27. The expected total protein amount is highly variable depending on the source of sEVs. For plasma and seroma, 50–150 µg of total protein is expected.
28. The size range of particles is ~90–150 nm. The user may compare particles obtained in Step 19 of Sect. 3.1 with particles obtained in Step 12 of this same section to calculate the isolation yield.
29. A Tecnai 12 transmission electron microscope (Thermo Fisher Scientific Inc.) with a lanthanum hexaboride cathode operated at 120 keV can be used here. We recommend collaboration with an Electron Microscopy facility for this step and the following ones in this method. Our analysis is normally accomplished in collaboration with CNIO Electron Microscopy Unit.
30. We recommend collaboration with a Mass Spectrometry facility for this step and the following ones in this method. Our analysis is normally accomplished in collaboration with CNIO Proteomics Unit.
31. EV samples have medium/low complexity in terms of number of proteins. Hence, it is advisable to use a 60–90 min effective gradient when injecting 1–1.5 µg of total protein in a Q Exactive (Thermo) instrument or similar. The number of peptides and proteins identified is highly variable and mostly depends on the biological source of the EVs. For sEVs purified from seroma, 1000–2000 proteins are often identified using this procedure.
32. An overrepresentation of proteins in terms related to "extracellular vesicles" is expected.
33. Studies have demonstrated the presence of genomic DNA (gDNA) and nuclear proteins within exosomes and sEVs [39, 62, 63]. The mechanisms by which nuclear components are present in exosomes remain poorly understood and have been related to the maintenance of cell homeostasis or micronuclei secretion [64, 65]. Still, today there is controversy about the origin and source of DNA in sEVs. It has also been proposed that EV-associated DNA can be secreted through an autophagy- and multivesicular-endosome-dependent but exosome-independent mechanism [66]. Regardless of their origin or the underlying molecular mechanisms, tumor-derived DNA is present in sEV fractions and can be used as a biomarker to detect mutations and other tumor-associated modifications via liquid biopsy approaches in real time with high sensitivity [32, 33, 40, 41, 58].

34. DNA concentration can be measured with a fluorometer such as Qubit® 2.0.
35. DNA quality can be checked on a Bioanalyzer or a 1% agarose gel. High-quality genomic DNA shows a major band of 10–20 Kb on the gel. Circulating free DNA is characterized by bands at approximately 150, 300, and 450 bp, corresponding to DNA fragmented into nucleosome units.
36. We have collaborated with Exosome Diagnostics Inc. for these assays, using the ExoLution™ Plus extraction technology.

Competing Interests

Authors declare no competing interest.

References

1. Witwer KW, Théry C (2019) Extracellular vesicles or exosomes? On primacy, precision, and popularity influencing a choice of nomenclature. J Extracell Vesicles 8(1):1648167. https://doi.org/10.1080/20013078.2019.1648167
2. Jaiswal R, Sedger LM (2019) Intercellular vesicular transfer by exosomes, microparticles and oncosomes—implications for cancer biology and treatments. Front Oncol 9:125. https://doi.org/10.3389/fonc.2019.00125
3. Raposo G, Stoorvogel W (2013) Extracellular vesicles: exosomes, microvesicles, and friends. J Cell Biol 200(4):373–383. https://doi.org/10.1083/jcb.201211138
4. Colombo M, Raposo G, Thery C (2014) Biogenesis, secretion, and intercellular interactions of exosomes and other extracellular vesicles. Annu Rev Cell Dev Biol 30:255–289. https://doi.org/10.1146/annurev-cellbio-101512-122326
5. Tkach M, Théry C (2016) Communication by extracellular vesicles: where we are and where we need to go. Cell 164(6):1226–1232. https://doi.org/10.1016/j.cell.2016.01.043
6. van Niel G, Carter DRF, Clayton A et al (2022) Challenges and directions in studying cell-cell communication by extracellular vesicles. Nat Rev Mol Cell Biol 23(5):369–382. https://doi.org/10.1038/s41580-022-00460-3
7. Asao T, Tobias GC, Lucotti S et al (2023) Extracellular vesicles and particles as mediators of long-range communication in cancer: connecting biological function to clinical applications. Extracell Vesicles Circ Nucl Acids 4(3):461–485. https://doi.org/10.20517/evcna.2023.37
8. Wiklander OPB, Brennan M, Lötvall J et al (2019) Advances in therapeutic applications of extracellular vesicles. Sci Transl Med 11(492):eaav852. https://doi.org/10.1126/scitranslmed.aav8521
9. Gutiérrez-Vázquez C, Villarroya-Beltri C, Mittelbrunn M, Sánchez-Madrid F (2013) Transfer of extracellular vesicles during immune cell-cell interactions. Immunol Rev 251(1):125–142. https://doi.org/10.1111/imr.12013
10. Zhang J, Li H, Fan B et al (2020) Extracellular vesicles in normal pregnancy and pregnancy-related diseases. J Cell Mol Med 24(8):4377–4388. https://doi.org/10.1111/jcmm.15144
11. Mathews PM, Levy E (2019) Exosome production is key to neuronal endosomal pathway integrity in neurodegenerative diseases. Front Neurosci 13:1347. https://doi.org/10.3389/fnins.2019.01347
12. Becker A, Thakur BK, Weiss JM et al (2016) Extracellular vesicles in cancer: cell-to-cell mediators of metastasis. Cancer Cell 30(6):836–848. https://doi.org/10.1016/j.ccell.2016.10.009
13. Costa-Silva B, Aiello NM, Ocean AJ et al (2015) Pancreatic cancer exosomes initiate pre-metastatic niche formation in the liver. Nat Cell Biol 17(6):816–826. https://doi.org/10.1038/ncb3169
14. Peinado H, Aleckovic M, Lavotshkin S et al (2012) Melanoma exosomes educate bone marrow progenitor cells toward a pro-metastatic phenotype through MET. Nat Med

18(6):883–891. https://doi.org/10.1038/nm.2753
15. Hoshino A, Costa-Silva B, Shen TL et al (2015) Tumour exosome integrins determine organotropic metastasis. Nature 527(7578):329–335. https://doi.org/10.1038/nature15756
16. Imanbekova M, Sharma M, Wachsmann-Hogiu S (2025) On the dilemma of using single EV analysis for liquid biopsy: the challenge of low abundance of tumor EVs in blood. Theranostics 15(16):8031–8048. https://doi.org/10.7150/thno.115131
17. Théry C, Amigorena S, Raposo G, Clayton A (2006) Isolation and characterization of exosomes from cell culture supernatants and biological fluids. Curr Protoc Cell Biol Chapter 3(Unit 3):22. https://doi.org/10.1002/0471143030.cb0322s30
18. Yang X-X, Sun C, Wang L, Guo X-L (2019) New insight into isolation, identification techniques and medical applications of exosomes. J Control Release 308:119–129. https://doi.org/10.1016/j.jconrel.2019.07.021
19. Cantin R, Diou J, Bélanger D et al (2008) Discrimination between exosomes and HIV-1: purification of both vesicles from cell-free supernatants. J Immunol Methods 338(1-2):21–30. https://doi.org/10.1016/j.jim.2008.07.007
20. Kalra H, Adda CG, Liem M et al (2013) Comparative proteomics evaluation of plasma exosome isolation techniques and assessment of the stability of exosomes in normal human blood plasma. Proteomics 13(22):3354–3364. https://doi.org/10.1002/pmic.201300282
21. Böing AN, van der Pol E, Grootemaat AE et al (2014) Single-step isolation of extracellular vesicles by size-exclusion chromatography. J Extracell Vesicles 3:23430. https://doi.org/10.3402/jev.v3.23430
22. Nordin JZ, Lee Y, Vader P et al (2015) Ultrafiltration with size-exclusion liquid chromatography for high yield isolation of extracellular vesicles preserving intact biophysical and functional properties. Nanomedicine 11(4):879–883. https://doi.org/10.1016/j.nano.2015.01.003
23. Cheruvanky A, Zhou H, Pisitkun T et al (2007) Rapid isolation of urinary exosomal biomarkers using a nanomembrane ultrafiltration concentrator. Am J Physiol Renal Physiol 292(5):F1657–1661. https://doi.org/10.1152/ajprenal.00434.2006
24. Takov K, Yellon DM, Davidson SM (2019) Comparison of small extracellular vesicles isolated from plasma by ultracentrifugation or size-exclusion chromatography: yield, purity and functional potential. J Extracell Vesicles 8(1):1560809. https://doi.org/10.1080/20013078.2018.1560809
25. Rider MA, Hurwitz SN, Meckes DG Jr (2016) ExtraPEG: a polyethylene glycol-based method for enrichment of extracellular vesicles. Sci Rep 6: 23978. https://doi.org/10.1038/srep23978
26. Greening DW, Xu R, Ji H et al (2015) A protocol for exosome isolation and characterization: evaluation of ultracentrifugation, density-gradient separation, and immunoaffinity capture methods. Methods Mol Biol 1295:179–209. https://doi.org/10.1007/978-1-4939-2550-6_15
27. Chen J, Li P, Zhang T et al (2021) Review on strategies and technologies for exosome isolation and purification. Front Bioeng Biotechnol 9:811971. https://doi.org/10.3389/fbioe.2021.811971
28. Li G, Tang W, Yang F (2020) Cancer liquid biopsy using integrated microfluidic exosome analysis platforms. Biotechnol J 15(5):e1900225. https://doi.org/10.1002/biot.201900225
29. Calero V, Honrado C, Ainla A et al (2025) Microfluidic devices for on-chip quantification of extracellular vesicles and associated biomarkers. Extracell Vesicles Circ Nucl Acids 6(3):560–579. https://doi.org/10.20517/evcna.2025.10
30. Hassanzadeh-Barforoushi A, Sango X, Johnston EL et al (2025) Microfluidic devices for manufacture of therapeutic extracellular vesicles: advances and opportunities. J Extracell Vesicles 14(7):e70132. https://doi.org/10.1002/jev2.70132
31. Urbanelli L, Buratta S, Sagini K et al (2015) Exosome-based strategies for diagnosis and therapy. Recent Pat CNS Drug Discov 10(1):10–27. https://doi.org/10.2174/1574889810666150702124059
32. Castellanos-Rizaldos E, Grimm DG, Tadigotla V et al (2018) Exosome-based detection of EGFR T790M in plasma from non-small cell lung cancer patients. Clin Cancer Res 24(12):2944–2950. https://doi.org/10.1158/1078-0432.CCR-17-3369
33. Figueroa JM, Skog J, Akers J et al (2017) Detection of wild-type EGFR amplification and EGFRvIII mutation in CSF-derived extracellular vesicles of glioblastoma patients. Neuro Oncol 19(11):1494–1502. https://doi.org/10.1093/neuonc/nox085
34. Wang M, Yu F, Ding H et al (2019) Emerging function and clinical values of exosomal microRNAs in cancer. Mol Ther Nucleic Acids 16:791–804. https://doi.org/10.1016/j.omtn.2019.04.027
35. Jiang N, Pan J, Fang S et al (2019) Liquid biopsy: circulating exosomal long noncoding RNAs in cancer. Clin Chim Acta 495:

331–337. https://doi.org/10.1016/j.cca.2019.04.082
36. Kalishwaralal K, Kwon WY, Park KS (2019) Exosomes for non-invasive cancer monitoring. Biotechnol J 14(1):e1800430. https://doi.org/10.1002/biot.201800430
37. Chen G, Huang AC, Zhang W et al (2018) Exosomal PD-L1 contributes to immunosuppression and is associated with anti-PD-1 response. Nature 560(7718):382–386. https://doi.org/10.1038/s41586-018-0392-8
38. Pang B, Zhu Y, Ni J et al (2020) Extracellular vesicles: the next generation of biomarkers for liquid biopsy-based prostate cancer diagnosis. Theranostics 10(5):2309–2326. https://doi.org/10.7150/thno.39486
39. Thakur BK, Zhang H, Becker A et al (2014) Double-stranded DNA in exosomes: a novel biomarker in cancer detection. Cell Res 24(6):766–769. https://doi.org/10.1038/cr.2014.44
40. Yang S, Che SP, Kurywchak P et al (2017) Detection of mutant KRAS and TP53 DNA in circulating exosomes from healthy individuals and patients with pancreatic cancer. Cancer Biol Ther 18(3):158–165. https://doi.org/10.1080/15384047.2017.1281499
41. Allenson K, Castillo J, San Lucas FA et al (2017) High prevalence of mutant KRAS in circulating exosome-derived DNA from early-stage pancreatic cancer patients. Ann Oncol 28(4):741–747. https://doi.org/10.1093/annonc/mdx004
42. Garcia-Silva S, Vico-Alonso C, Meyer L et al (2023) Improved sensitivity in BRAFV600E detection in combined tissue and extracellular vesicle-based liquid biopsy in melanoma. J Invest Dermatol 143(8):1606–1610. https://doi.org/10.1016/j.jid.2023.01.025
43. Logozzi M, Angelini DF, Iessi E et al (2017) Increased PSA expression on prostate cancer exosomes in in vitro condition and in cancer patients. Cancer Lett 403:318–329. https://doi.org/10.1016/j.canlet.2017.06.036
44. Hoshino A, Kim HS, Bojmar L et al (2020) Extracellular vesicle and particle biomarkers define multiple human cancers. Cell 182(4):1044–1061. https://doi.org/10.1016/j.cell.2020.07.009.e1018
45. Van Trappen PO, Pepper MS (2002) Lymphatic dissemination of tumour cells and the formation of micrometastases. Lancet Oncol 3(1):44–52. https://doi.org/10.1016/s1470-2045(01)00621-0
46. Garcia-Silva S, Peinado H (2024) Mechanisms of lymph node metastasis: an extracellular vesicle perspective. Eur J Cell Biol 103(3):151447. https://doi.org/10.1016/j.ejcb.2024.151447
47. Leiter U, Stadler R, Mauch C et al (2016) Complete lymph node dissection versus no dissection in patients with sentinel lymph node biopsy positive melanoma (DeCOG-SLT): a multicentre, randomised, phase 3 trial. Lancet Oncol 17(6):757–767. https://doi.org/10.1016/s1470-2045(16)00141-8
48. McCaul JA, Aslaam A, Spooner RJ et al (2000) Aetiology of seroma formation in patients undergoing surgery for breast cancer. Breast 9(3):144–148. https://doi.org/10.1054/brst.1999.0126
49. Rutkowski P, Nowecki ZI, Kulik J et al (2008) Molecular staging by multimarker reverse transcriptase-polymerase chain reaction assay of lymphatic drainage and blood from melanoma patients after lymph node dissection. Melanoma Res 18(4):246–252. https://doi.org/10.1097/CMR.0b013e328307bf3f
50. Nowecki ZI, Rutkowski P, Kulik J et al (2008) Molecular and biochemical testing in stage III melanoma: multimarker reverse transcriptase-polymerase chain reaction assay of lymph fluid after lymph node dissection and preoperative serum lactate dehydrogenase level. TBr J Dermatol 159(3):597–605. https://doi.org/10.1111/j.1365-2133.2008.08710.x
51. Wlodzimierz R, Rutkowski P, Nowecki ZI et al (2004) Detection of melanoma cells in the lymphatic drainage after lymph node dissection in melanoma patients by using two-marker reverse transcriptase-polymerase chain reaction assay. Ann Surg Oncol 11(11):988–997. https://doi.org/10.1245/ASO.2004.03.023
52. Hood JL (2017) The association of exosomes with lymph nodes. Semin Cell Dev Biol 67:29–38. https://doi.org/10.1016/j.semcdb.2016.12.002
53. Pucci F, Garris C, Lai CP et al (2016) SCS macrophages suppress melanoma by restricting tumor-derived vesicle-B cell interactions. Science 352(6282):242–246. https://doi.org/10.1126/science.aaf1328
54. Srinivasan S, Vannberg FO, Dixon JB (2016) Lymphatic transport of exosomes as a rapid route of information dissemination to the lymph node. Sci Rep 6: 24436. https://doi.org/10.1038/srep24436
55. Sun B, Zhou Y, Fang Y, Li Z, Gu X, Xiang J (2019) Colorectal cancer exosomes induce lymphatic network remodeling in lymph nodes. Int J Cancer 145(6):1648–1659. https://doi.org/10.1002/ijc.32196
56. Garcia-Silva S, Benito-Martin A, Nogues L et al (2021) Melanoma-derived small extracellular vesicles induce lymphangiogenesis and metastasis through an NGFR-dependent mechanism. Nat Cancer 2(12):1387–1405. https://doi.org/10.1038/s43018-021-00272-y

57. Broggi MAS, Maillat L, Clement CC et al (2019) Tumor-associated factors are enriched in lymphatic exudate compared to plasma in metastatic melanoma patients. J Exp Med 216(5):1091–1107. https://doi.org/10.1084/jem.20181618
58. Garcia-Silva S, Benito-Martin A, Sanchez-Redondo S et al (2019) Use of extracellular vesicles from lymphatic drainage as surrogate markers of melanoma progression and BRAF (V600E) mutation. J Exp Med 216(5): 1061–1070. https://doi.org/10.1084/jem.20181522
59. Suman S, Geng L, Nevala WK et al (2026) Proteomic analysis of small extracellular vesicles from lymphatic affluents in developing premetastatic niche in melanoma. Mol Cell Proteom 25(1):101472. https://doi.org/10.1016/j.mcpro.2025.101472
60. Li ZZ, Cai ZM, Zhu WT et al (2024) Lymph node metastasis diagnosis of postoperative OSCC patients by analyzing extracellular vesicles in drainage fluid based on microfluidic isolation. J Nanobiotechnol 22(1):586. https://doi.org/10.1186/s12951-024-02846-1
61. Brinkman K, Meyer L, Bickel A et al (2020) Extracellular vesicles from plasma have higher tumour RNA fraction than platelets. J Extracell Vesicles 9(1):1741176. https://doi.org/10.1080/20013078.2020.1741176
62. Kahlert C, Melo SA, Protopopov A et al (2014) Identification of double-stranded genomic DNA spanning all chromosomes with mutated KRAS and p53 DNA in the serum exosomes of patients with pancreatic cancer. J Biol Chem 289(7):3869–3875. https://doi.org/10.1074/jbc.C113.532267
63. Lazaro-Ibanez E, Lasser C, Shelke GV et al (2019) DNA analysis of low- and high-density fractions defines heterogeneous subpopulations of small extracellular vesicles based on their DNA cargo and topology. J Extracell Vesicles 8(1):1656993. https://doi.org/10.1080/20013078.2019.1656993
64. Yokoi A, Villar-Prados A, Oliphint PA et al (2019) Mechanisms of nuclear content loading to exosomes. Sci Adv 5(11):eaax8849. https://doi.org/10.1126/sciadv.aax8849
65. Takahashi A, Okada R, Nagao K et al (2017) Exosomes maintain cellular homeostasis by excreting harmful DNA from cells. Nat Commun 8: 15287. https://doi.org/10.1038/ncomms15287
66. Jeppesen DK, Fenix AM, Franklin JL et al (2019) Reassessment of exosome composition. Cell 177(2):428–445. https://doi.org/10.1016/j.cell.2019.02.029



Chapter 14

Imaging and Analysis of Melanoma-Secreted Extracellular Vesicles in Tumor-Draining Lymph Nodes

Lucía Garrido-Miranda, Héctor Peinado and Susana García-Silva

Abstract

Small extracellular vesicles (sEVs) are key mediators of intercellular communication and play important roles in both physiological and pathological processes. In cancer, sEVs mediate communication between the tumor and its microenvironment but also contribute to metastatic organotropism and the formation of pre-metastatic niches in regional and distant organs. Lymph nodes (LNs) are central regulators of immune responses and primary sites of early metastasis, and, as such, they are critical targets for understanding cancer progression and improving immunotherapy. sEVs contribute to the conditioning of lymph nodes during pre-metastatic niche formation by altering lymphatic endothelial cell function and modulating immune cell populations, thereby promoting tumor progression. Because these interactions are complex and dynamic, their study requires in vivo models and specifically tailored sEVs-based techniques. In this chapter, we describe several approaches for studying sEVs in the LN context, including biodistribution analysis in the lymphatic system, imaging by immunofluorescence, and uptake measurement by flow cytometry.

Keywords Melanoma, Lymph nodes, Extracellular vesicles, Exosomes, Biodistribution, Imaging, Vesicle uptake

1 Introduction

Melanoma is the most aggressive form of skin cancer, and it has shown a rising incidence worldwide in recent years. Despite advancements in treatment options, the understanding of the complex mechanisms underlying melanoma progression remains a significant challenge [1]. Metastasis represents the deadliest phase of this disease [2]. Metastatic colonization depends not only on intrinsic cellular factors, such as mutations, genomic instability, or epigenetic mutations, but also on extrinsic factors that shape a permissive microenvironment in distant organs through a process that has been denominated pre-metastatic niche formation (PNM) [3]. This process that occurs concomitantly with tumor growth is characterized by multiple cellular and tissue changes, including extracellular matrix (ECM) remodeling, vascular

Kristian M. Hargadon (ed.), *Melanoma*, Methods in Molecular Biology, vol. 3089,
https://doi.org/10.1007/978-1-0716-5619-8_14,
© The Author(s), under exclusive license to Springer Science+Business Media, LLC, part of Springer Nature 2027

permeability, immune modulation, and inflammation, all of which cooperate to facilitate subsequent metastatic colonization.

Lymph nodes (LNs) are central organs in immune regulation, maintaining fluidic homeostasis, regulating immune cell trafficking, and orchestrating adaptive immune responses [4, 5]. The tumor-draining lymph nodes (TDLNs) surrounding the primary tumor are often the first sites where metastatic disease is detected [6, 7]. LN metastases can also be a cell source for subsequent dissemination to distant organs, often facilitated by tumor cells entering the systemic circulation through high endothelial venules [8, 9]. Compared to the harsh conditions of the circulatory system, the lymph offers ideal conditions for metastatic dissemination. It presents significantly less oxidative and fluid shear stress, coupled with lower flow speeds [10, 11]. Furthermore, the lymph nodes provide higher levels of glutathione and oleic acid, which notably contribute to ferroptosis resistance in tumor cells [12]. Clinically, although early-stage LN metastasis is not immediately life-threatening, its detection is strongly associated with poor prognosis. In melanoma, LN status specifically defined by the number and size of nodal metastases is considered the most accurate prognostic factor for disease staging [13, 14]. On the other hand, TDLNs play a crucial role in orchestrating antitumor immunity and are critical for achieving robust responses to immunotherapy [5].

PMN formation in TDLNs is driven by a chronic interplay between the primary tumor and the nodal microenvironment [15, 16]. This sustained communication induces extensive cellular and ECM remodeling, characterized by marked structural swelling and the active recruitment of hematopoietic cells. This continuous crosstalk triggers an unusually active lymphangiogenesis, the dilation of high endothelial venules, shifts in immune cell populations, and a hyperproliferation of reticular fiber-producing cells. These processes consequently alter LN architecture and composition [5, 7, 15]. Concurrently, lymphatic endothelial cells (LECs) undergo profound alterations in their transcriptional profiles, upregulating programs associated with proliferation, cellular and matrix adhesion, and antigen presentation machinery [17–19]. These sustained immunomodulatory signals culminate in an overwhelmingly immunosuppressive microenvironment that induces immune tolerance and actively promotes LN colonization. In this systemic communication network between the tumor and the TDLNs, extracellular vesicles (EVs) play a crucial role [16].

EVs are particles released by cells characterized by a bilipidic membrane and a cargo composed of a diverse array of biomolecules, including soluble and membrane-associated proteins, glycoproteins, lipids, nucleic acids, and metabolites, reflecting the state and origin of the secreting cell [20]. EVs display a considerable diversity in both size and origin. They can broadly be categorized into small EVs

(sEVs) and large EVs (lEVs) based on their dimensions [21]. Small EVs include vesicles such as exosomes and migrasomes, typically ranging from approximately 50–150 nm in diameter. In contrast, larger vesicles—such as microvesicles (200 nm–1 μm), apoptotic bodies (1–5 μm), exophers (~4 μm), and oncosomes (1–10 μm)—are classified as lEVs [22,23].

In addition to their multiple roles in homeostasis and pathological processes, EVs mediate also the communication between tumor cells and the tumor microenvironment (TME). For instance, EVs derived from highly metastatic melanoma cells can transfer specific cargo, such as microRNAs, to augment the proliferation and colonization capabilities of less aggressive clones [24]. Within the TME, EVs also contribute to the metabolic reprogramming of fibroblasts [25], the phenotypic modulation of macrophages toward a pro-metastatic behavior [26], and the impairment of dendritic cell differentiation [27]. These multiple effects lead to a significantly compromised antitumoral immune response. Moreover, EVs, and, in particular, exosomes, are key players in the formation of pre-metastatic niches and metastatic colonization [28]. Through the expression of specific combinations of integrins, EVs dictate metastatic organotropism, selectively facilitating tumor cell homing and uptake in target tissues [29].

In the specific context of the TDLNs, sEVs act as critical messengers traveling through lymphatic routes [30]. They are primarily captured by LECs and $CD169^+$ macrophages, although other cell types can also internalize them [31,32]. Early studies demonstrated that melanoma-derived exosomes induce transcriptional changes in LNs, including upregulation of ECM remodeling genes, inflammatory mediators, and pro-angiogenic factors such as VEGF, ultimately enhancing metastatic potential [33]. Although their binding to subcapsular sinus $CD169^+$ macrophages can initially enhance the local immune response; melanoma cells usually develop mechanisms to overcome this barrier [34].

A major consequence of sEV uptake is the induction of lymphangiogenesis and ECM remodeling. Melanoma-derived sEVs are preferentially internalized by LECs via VCAM-1/integrin αV interactions. NGFR transported by melanoma sEVs triggers signaling pathways such as MAPK and NF-κB that promote VEGFR3 activation, LEC proliferation, and lymphatic vessel formation [32, 35]. In addition to proteins such as NGFR, EV-associated miRNAs and lncRNAs regulate lymphangiogenesis through pathways involving ERK/AKT and PROX1 expression [36, 37]. Remarkably, sEVs may also contribute to ECM remodeling through their cargo containing periostin, tenascin-C, and collagen by promoting the deposition of these matrix proteins, which are known to alter LN architecture and favor metastasis [33, 38, 39]. These structural changes, together with

fibroblastic reticular cell expansion, enhance the establishment of a pro-metastatic microenvironment.

In addition to structural remodeling, tumor-derived sEVs exert broad immunomodulatory effects within LNs. LECs and macrophages act both as primary targets and as barriers limiting EV dissemination, but their functional reprogramming contributes to immune suppression. For example, antigen presentation by LECs following sEVs uptake impairs $CD8^+$ T cell responses [35], while macrophages can acquire immunosuppressive or pro-lymphangiogenic phenotypes [20, 40, 41]. Small EVs also inhibit dendritic cell maturation and function [42], promote T cell apoptosis or dysfunction via molecules such as FasL and PD-L1 [43, 44], and influence other immune populations including neutrophils and NK cells [45, 46]. Altogether, these effects reshape the LN microenvironment toward an immunosuppressive and pro-metastatic state, highlighting EVs as key mediators of LN PMN formation.

Studying sEVs in vivo in the LN context offers valuable insights into melanoma and other cancers and may also advance our understanding of other conditions such as infections and peripheral immune tolerance. Here, we present a set of tools for investigating the role of sEVs in LNs, including approaches for their visualization using fluorescent dyes, along with methods for analyzing their lymph node biodistribution and uptake using immunofluorescence and flow cytometric approaches.

2 Materials

2.1 Analysis of the Biodistribution of Melanoma-Derived sEVs in the Lymphatic System

1. 1× PBS.
2. CellVue™ NIR815 Cell Labeling Kit (Thermo Fisher Scientific).
3. Bovine serum albumin (Sigma-Aldrich).
4. 1.5 mL microcentrifuge tubes.
5. BD Micro-Fine U-100 Insulin Syringe needles 0.3 mL (BD Biosciences).
6. 8-week-old C57BL/6 mice or athymic nude mice.
7. Standard forceps.
8. Fine-tipped forceps (e.g., #5 Dumont).
9. Surgical scissors.
10. 24-well cell plates.
11. IVIS Spectrum imaging system (PerkinElmer).
12. Living Image software (PerkinElmer).
13. Infrared fluorescence scanner LI-COR Odyssey CLx (LICOR bio).

14. Image STUDIO software (LICOR bio).
15. Image analysis software (e.g., Fiji software).

2.2 Detection by Immunofluorescence of Melanoma-Derived sEVs Uptake in Mouse Lymph Nodes

1. 1× PBS.
2. DiD: DiIC$_{18}$(5) solid (1,1′-Dioctadecyl-3,3,3′,3′-Tetramethylindodicarbocyanine, 4-Chlorobenzenesulfonate Salt) [Thermo Fischer Scientific].
3. Bovin serum albumin.
4. 1.5 mL microcentrifuge tubes.
5. BD Micro-Fine U-100 Insulin Syringe needles 0.3 mL (BD Biosciences).
6. 8-week-old C57BL/6 mice or athymic nude mice.
7. Standard forceps.
8. Fine-tipped forceps (e.g., #5 Dumont).
9. Surgical scissors.
10. 16% Paraformaldehyde solution.
11. 15% (w/v) Sucrose in 1× PBS.
12. 30% (w/v) Sucrose in 1× PBS.
13. Tissue-Tek® O.C.T. Compound.
14. Tissue-Tek® Cryomold® 25 × 20 × 5 mm.
15. Isopentane (2-Methylbutane).
16. 200 mL beaker.
17. Dry ice.
18. Superfrost Plus® Gold Glass Microscope Slides.
19. Coverslips.
20. Cryostat (e.g., LEICA CM 1950 [Leica]).
21. 100 mM glycine solution in 1× PBS.
22. 0.3% Triton X-100 solution in 1× PBS.
23. Immunofluorescence (IF) blocking solution: 1% bovine serum albumin (BSA), 5% donkey serum, and 0.05% Triton X-100 in 1× PBS.
24. IF incubation solution (1% BSA and 0.05% Triton X-100 in 1× PBS).
25. 0.5 % Tween-20 in 1× PBS.
26. DAPI (4′,6-Diamidino-2-phenylindole dihydrochloride): Prepare working solution of 5 μM DAPI in 1× PBS just before use.
27. Milli-Q water.
28. Prolong Diamond® Antifade Mountant.

29. Confocal microscope [e.g., Eclipse TE2000U confocal microscope (Nikon) or TCS SP5 Leica confocal].
30. Image analysis software (e.g., Fiji software).

2.3 Analysis of Melanoma-Derived sEVs Uptake by Flow Cytometry

1. 1× PBS.
2. DiD: DiIC18(5) solid (1,1′-Dioctadecyl-3,3,3′,3′-Tetramethylindodicarbocyanine, 4-Chlorobenzenesulfonate Salt) (Thermo Fisher Scientific).
3. 1.5 mL microcentrifuge tubes.
4. 15 mL Falcon tubes.
5. 5 mL cytometry tubes.
6. RPMI-1640 medium.
7. LN Digestion Solution: RPMI-1640 medium containing 0.8 mg/mL of dispase II, 0.2 mg/mL of collagenase P, and 0.1 mg/mL of DNase I from bovine pancreas.
8. FACS buffer: 1× PBS supplemented with 1% bovine serum albumin and 2 mM EDTA.
9. Cell strainer 70 μM.
10. Mouse BD Fc Block™ (BD Pharmigen).
11. Antibodies for LN cell surface markers: anti-mouse CD45-Pacific Blue (Clone 30-F11), anti-mouse Podoplanin-AF488 (Clone eBio8.1.1), anti-mouse CD169-PE (Clone 3D6.112), anti-mouse CD31-PerCPCy5.5 (Clone MEC 13.3), anti-mouse CD11b-PE-Cy7 (Clone M1/70), and anti-mouse F4/80-APCeFluor780 (Clone BM8).
12. Non-sterile filcon cup-type filter, 50 μM (BD Bioscience).
13. DAPI (4′,6-Diamidino-2-phenylindole dihydrochloride).
14. Flow cytometer.
15. Flow cytometry analysis software (e.g., FlowJo or FCS Express).

3 Methods

3.1 Analysis of Biodistribution of Melanoma-Derived sEVs in the Lymphatic System

Specific labeling for in vivo detection can be achieved using dyes in the far-red range, which minimize interference from tissue autofluorescence. We have obtained satisfactory results with NIR815. Before staining the sEVs sample, prepare a solution containing 35% (w/v) bovine serum albumin in 1× PBS (*see* **Note 1**).

1. Dilute total (or a desired quantity of) melanoma-derived sEVs purified by ultracentrifugation or size exclusion chromatography in 1 mL of 1× PBS.
2. Add 3 μL of NIR815 to the sEVs solution, and incubate for 5 min in the dark at room temperature (*see* **Notes 2 and 3**).
3. Add 57 μL of 35% BSA, and incubate 2 min at room temperature.
4. Add 5–20 mL of sterile 1× PBS to dilute the unbound dye (*see* **Note 4**).
5. Remove the unbound dye by adding 5–20 mL of PBS and ultracentrifugate at 100,000 $\times g$ for 70 min at 10°C.
6. Carefully discard the supernatant by gently inverting the tube, and keep it upside down for 2–3 min to remove any remaining liquid (*see* **Note 5**).
7. Resuspend the sEV pellet in 100–200 μL of 1× PBS.
8. Measure particle concentration or protein concentration (*see* **Note 6**).
9. Prepare a NIR-labeled sEVs solution with a concentration of 1–5 μg of sEV protein or 10^8–10^{11} particles in 20 μL of 1× PBS per mouse (*see* **Note 7**).
10. Inject 20 μL of NIR-labeled sEVs solution intra-footpad (or 5 μL in the ear lobule) in 8-week-old C57Bl/6 or athymic nude mice using a 0.3 mL insulin syringe (*see* **Note 8**).
11. After 1 or 4 h, anesthetize the mice, and measure fluorescence in an IVIS Spectrum imaging system (*see* **Note 9**).
12. For ex vivo quantification of biodistribution, if sEVs injections were made intra-footpad, sacrifice the mice and open the ventral part of the mice and the leg, and excise the popliteal and inguinal LNs using surgical scissors, forceps, and fine-tipped forceps. If sEVs injections were made in the ear, open the neck of the mice, and excise the cervical LNs.
13. Keep the LNs in a 24-well cell plate filled with 1× PBS on ice during transport to the IVIS Spectrum imaging system.
14. Place the LNs inside the machine.
15. Adjust the settings and the field of detection to allow for zooming in on the LNs for increasing signal sensitivity.
16. Measure NIR815 fluorescence in the LNs (*see* **Note 10**). A representative image obtained by this technique is shown in Fig. 1A.
17. Return the LNs to the 24-well cell plate, and transport them to the LICOR Odyssey scanner.
18. Place each LN on a tissue to dry.

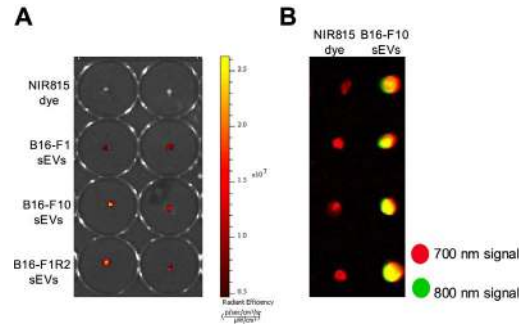


Fig. 1 (**A**), Representative IVIS image showing NIR-815-associated fluorescence in LNs from mice injected with the indicated types of labeled melanoma-derived sEVs. Signal detected in the 790 nm channel is overlaid on a photographic image of the lymph nodes. (**B**), Representative Odyssey scan of LNs from mice injected with NIR815-labeled B16-F10-derived sEVs or free NIR815 dye. The image shows the overlay of fluorescence in the 700 nm channel (red) and the 800 nm channel (green, corresponding to NIR815-associated fluorescence)

19. Arrange all the LNs to be analyzed on the Odyssey interior (*see* **Note 11**).
20. Open the iStudio program in the computer.
21. Select the area to scan, and check both 700 nm and 800 nm wavelengths (for detecting background fluorescence at 700 nm and NIR815 at 800 nm).
22. Select preview, and check how the fluorescence is detected in the automatic mode. Otherwise, exposure time and contrast settings can be determined manually. Remember to do a fast preview at low quality every time the settings are changed.
23. Perform full scanning using the high-quality mode. A representative image obtained by this technique is shown in Fig. 1B.
24. Save individual fluorescence images and session.
25. For quantification, use Fiji J software to select regions of interest around each LN and measure raw intensity/area in both 700 nm and 800 nm channels.
26. Normalize intensity measurements for each LN by obtaining the ratio between 800 nm and 700 nm channels.

3.2 Detection by Immunofluorescence of Melanoma-Derived sEVs Uptake in Mouse LNs

Specific labeling for sEVs imaging in the LNs can be performed using several dyes compatible with confocal microscopy detection (*see* **Note 12**). We have obtained the best results using DiD (Thermo Fisher Scientific), and the following method is based on this type of dye, but a similar protocol can be used with other dyes.

1. Perform the labeling of sEVs with DiD following Steps 1–9 of Sect. 3.1.
2. Inject 5 µg of DiD-labeled sEVs in a total volume of 20 µL of 1× PBS in the footpad (or 5 µL in the earlobe) of 8-week-old C57/Bl6 mice using a 0.3 mL insulin syringe.
3. After 4 or 16 h, sacrifice the animals and harvest popliteal and inguinal LNs (if injected intra-footpad) or cervical LNs (if injected in the earlobe).
4. Prepare a 4% PFA solution by diluting 10 mL of an ampule of 16% PFA in 30 mL of 1× PBS.
5. Fix LNs in 0.5–1 mL of 4% PFA solution overnight at 4°C.
6. On the next day in the morning, transfer the LNs to a 15% sucrose solution in 1× PBS.
7. In the afternoon, transfer the LNs to a 30% sucrose solution in 1× PBS.
8. On the following day, put O.C.T. into cryomolds positioned on ice.
9. Introduce the LNs into the O.C.T. in the cryomolds, and wait for 30 min.
10. Prepare a "freezing bath" by adding 100 mL of isopentane in a beaker together with some dry ice pellets.
11. After 2–3 min, take an LN-containing cryomold with the forceps, and introduce it fast into the freezing bath (*see* **Note 13**).
12. After 3 min, remove with the forceps the cryomolds, and put them into dry ice snow (preferably) or dry ice pellets.
13. After 30–60 min, transfer the cryomolds with the LNs to the −80°C freezer for storage.
14. When ready to continue the procedure, introduce the O.C.T. blocks in the cryostat to let them equilibrate to −15°C to −20°C, and set the cryostat for cutting 5–6 µm sections.
15. Place the cut sections on Superfrost microscope slides.
16. Treat slides with 100 mM glycine solution (0.5–1 mL onto the slide) for 10 min to avoid autofluorescence (*see* **Note 14**).
17. Wash three times with 1× PBS.
18. Permeabilize the specimens by incubating with 0.3% Triton X-100 solution (0.5–1 mL over each slide) for 15 min at room temperature.
19. Wash three times with 1× PBS.
20. Incubate the sections with IF blocking solution for 1 h at room temperature. We recommend adding 100–200 µL onto each slide and covering it with a paraffin stripe. Alternatively,

a hydrophobic Barrier Pap Pen can be used to delimitate the stained area.

21. Remove the IF blocking solution.
22. Add the primary antibodies diluted in IF incubation solution, cover the slides again with a paraffin stripe, and incubate them overnight at 4°C in the dark (*see* **Note 15**).
23. Wash three times with 0.5 % Tween-20 in 1× PBS (5 min for each wash).
24. Incubate the sections with secondary antibodies in IF solution by adding 100–200 µL onto the slide and covering it with a paraffin stripe for 1 h at room temperature in the dark (*see* **Note 16**).
25. Wash three times with 0.5% Tween-20 in 1× PBS (5 min for each wash).
26. Wash one time with 1× PBS.
27. Incubate the sections with 200 µL of DAPI solution for 15 min.
28. Wash three times with 1× PBS.
29. Dip each slide in Milli-Q water for 2 s and allow slides to air dry for 5 min.
30. Add a drop of mounting medium (e.g., Prolong Diamond) onto the tissue and cover it with a coverslip, taking care to avoid bubble formation.
31. Acquire images using a confocal microscope. A representative image obtained by this technique is shown in Fig. 2.
32. Analyze the images using Fiji software and the "Analyze particle" plug-in.

3.3 Analysis of Melanoma-Derived sEVs Uptake by Flow Cytometry

1. Label sEVs using DiD dye following Steps 1–9 in Sect. 3.1 (*see* **Note 17**).
2. Inject 5 µg of DiD-labeled sEVs in a total volume of 20 µL of 1× PBS in the footpad of 8-week-old C57/Bl6 mice using a 0.3 mL insulin syringe (*see* **Note 18**).
3. After 16–24 h, sacrifice the animals, and harvest the popliteal LNs.
4. Keep harvested LNs on ice in 1–2 mL of RPMI-1640 medium until the dissection procedure is complete.
5. Transfer LNs to 15 mL tubes containing 2 mL of freshly prepared LN Digestion Solution (*see* **Note 19**).
6. Incubate samples for 20 min in a water bath at 37°C, but pipette the LNs up and down with a 1 mL pipette every 5–7 min to help tissue dissociation.

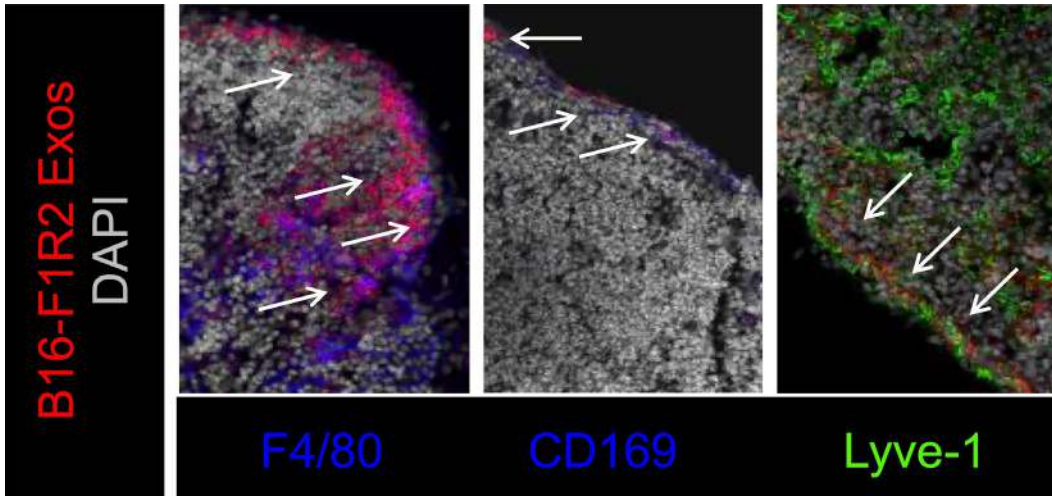


Fig. 2 Representative confocal microscopy images of popliteal lymph nodes from mice 24 h post-injection with DiD-labeled sEVs purified from B16-F1R2 melanoma cells or control animals injected with only DiD solution. Staining was performed with anti-Lyve-1, anti-CD169, and anti-F4/80 antibodies, and nuclei were counterstained with DAPI

7. After the incubation, dissociate the LNs by vigorously pipetting for 2–3 min.
8. Wait a few seconds for the undigested fragments to settle down at the bottom of the tube.
9. Transfer the supernatant to a new Falcon tube with 10 mL of FACS buffer, and keep it on ice.
10. Add 1 mL of LN Digestion Solution again to the remaining LN fragments, and incubate for another 10 min in the water bath at 37°C (*see* **Note 20**).
11. Dissociate the remaining LN fragments by vigorously pipetting for 2–3 min.
12. Transfer the sample to the previous Falcon tube with the contents of the first LN digestion in FACS buffer.
13. Pass the LN cell solution through a 70 μM cell strainer.
14. Spin Falcon tubes at 100 × *g* for 4 min at 10°C.
15. Discard supernatant, and resuspend the LN cell pellet in 100 μL of FACS buffer.
16. Take 10–20 μL of LN cell suspension for unstained and compensation controls.
17. Incubate the rest of the LN cell suspensions with 2 μL of Mouse BD Fc Block™ for 10 min on ice.
18. Spin samples at 100 × *g* for 4 min at 10°C.

19. Discard the supernatant, and add 100 µL of FACS buffer including 0.5 µL of anti-CD45-Pacific Blue, 1 µL of anti-Podoplanin-AF488, 0.5 µL of anti-CD169-PE, 0.5 µL of anti-CD31-PerCPCy5.5, 0.5 µL of anti-CD11b-PE-Cy7, and 1 µL of F4/80-APC-eFluor780.
20. Incubate for 30 min on ice.
21. Add 1 mL of FACS buffer, and spin at 100 × *g* for 4 min at 10°C to remove the antibody cocktail.
22. Discard the supernatant and add 2 mL of FACS buffer to each sample. Filter the sample through a 50 µM falcon cup filter into a FACS tube.
23. Spin at 100 × *g* for 4 min at 10°C.
24. Discard the supernatant, and add 200 µL of FACS buffer including DAPI at a final concentration of 0.2 µg/mL immediately before initiating the flow cytometry analysis.
25. Pass the control and experimental samples through the flow cytometer, and record at least $1e^6$ events to detect sufficient numbers of stromal ($CD45^-$) cells.
26. Analyze and plot results using a flow cytometry analysis software such as FlowJo or FCS Express.
27. Select the $DAPI^-CD45^-$ gate, and quantify sEVs uptake (percentage of DiD^+ cells detected with the red laser and the 660/20 band pass filter) in stromal populations such as $Podoplanin^+CD31^-$ (follicular dendritic cells), $Podoplanin^-CD31^+$ (blood endothelial cells [BEC]), $Podoplanin^+CD31^-$ [fibroblastic reticular cells (FRC)], and $Podoplanin^+CD31^+$ (lymphatic endothelial cells [LEC]), as shown in Fig. 3A **(left)** and Fig. 3B **(top)**.
28. Select $DAPI^-CD45^+$ gate, and quantify sEVs uptake in $CD11b^+CD169^+$ $F4/80^-$ subcapsular sinus (SCS) macrophages, in $CD11b^+CD169^-F4/80^+$ (medullary macrophages) and $CD11b^+CD169^+F4/80^+$ macrophages as also shown in Fig. 3A **(right)** and Fig. 3B **(bottom)**.

4 Notes

1. The BSA solution can be stored in small aliquots at −20°C for future use.
2. A concentration of 3 µM is recommended for an enhanced in vivo signal. This concentration allows labeling of 100 µg of sEVs.

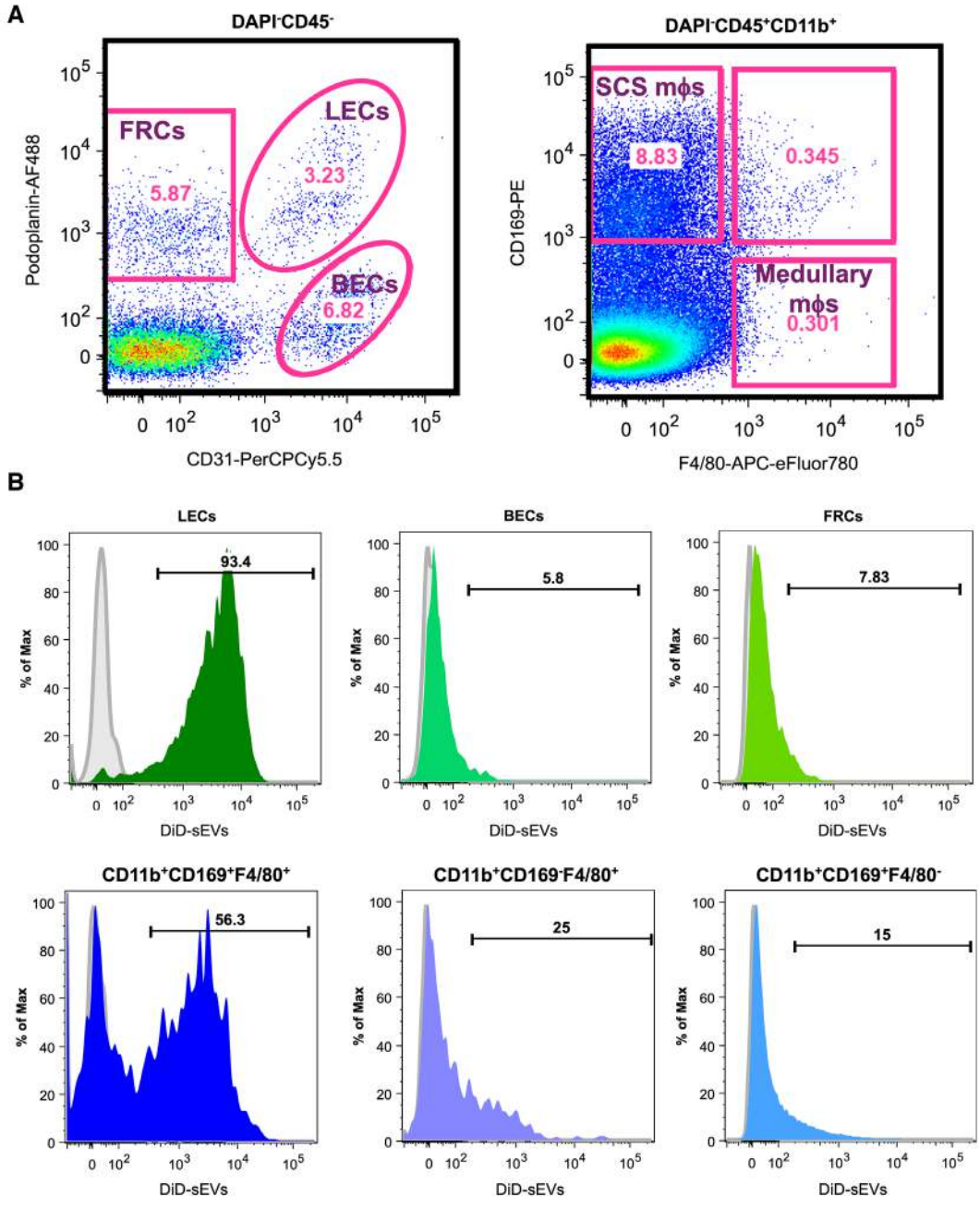


Fig. 3 (**A**), Flow cytometry plots indicating the gating strategy and selected populations for analyzing sEVs uptake in DAPI⁻CD45⁻ stromal and DAPI⁻CD45⁻CD11b⁺ macrophage populations from popliteal lymph nodes isolated from animals injected with DiD-labeled sEVs. Lymph nodes were analyzed 16 h post-injection in the footpad. (**B**), Plots showing sEV uptake in the different indicated populations measured by the percentage of cells positive for DiD fluorescence in each population as indicated in (**A**)

3. Do not forget to include an NIR815 mock control, which should be generated by adding to another tube just 1 mL of 1× PBS and 3 μL of NIR815 and performing the same steps as for the NIR815-labeled sEVs.
4. Alternatively, remove the unbound dye by purifying the sEVs sample using a SEC column with two washes of 1× PBS. Be sure to pool the sEVs' positive fractions and concentrate them, and then continue with Step 8 of Sect. 3.1.
5. Important: the pellet contains purified sEVs. Usually, a colored pellet can be appreciated on the bottom of the tube.
6. Particles can be measured with a Nanosight or similar device. For protein concentration, we recommend the bicinchoninic acid method.
7. We recommend a minimum of 1 μg of sEVs (if purified by differential ultracentrifugation) or a minimum of 10^8 particles (if purified by size exclusion chromatography).
8. Do not forget to inject control animals with the same volume of NIR815 dye-mock sample. For experiments in live animals, the thin and hairless skin of athymic nude mice is better for detecting tissue fluorescence.
9. In-Vivo Multispectral System FX (Kodak) or other imaging systems can also be used. For the IVIS Spectrum, select the fluorescence mode with a 740 nm excitation filter and a 790 nm emission filter, a medium binning, and F/stop equal to 2.
10. Once all data are recorded, images can be analyzed using the Living Image software by selecting regions of interest (ROIs) around individual LNs in sEVs-injected and NIR control mice and quantifying the intensity in each ROI.
11. Be careful to place the LNs inside the scanned area of the machine. We recommend placing the LNs as close as possible to reduce the scanned area. This approach will also reduce the time for scanning.
12. Here there is a non-exhaustive list of possible dyes for detecting sEVs by immunofluorescence: PKH67 (Sigma-Aldrich), PKH26 (Sigma-Aldrich), CFSE (Sigma-Aldrich), DiD (Thermo Fisher Scientific), and Membright dyes [47].
13. Cryomold immersion must be fast to avoid extrusion of the tissue while the O.C.T. becomes rapidly frozen. Do not forget to add additional dry ice pellets to the beaker to maintain the freezing temperature.
14. Do not allow the sections to dry completely from this step until Step 26 of this section.

15. A suggestion for primary antibodies can be anti-Lyve-1 (ab14917, Abcam) and anti-CD169-PE (Clone 3D6.112).
16. Take into account that the channel for the 633/647 is reserved for the DiD-labeled sEVs. Secondary antibodies can therefore be coupled to AlexaFluor-488 or AlexaFluor-555.
17. This method can also be adapted to other fluorescent dyes as indicated in **Note 12**.
18. Do not forget to inject only the DiD mock solution in some animals as a technical control.
19. Due to the small LN size, to obtain more reliable uptake results, it is recommended to pool 2–4 LN for each sample.
20. Pipetting up and down after 5 min will help LN dissociation.

Competing Interests

Authors declare no competing interest.

References

1. Atkins MB, Curiel-Lewandrowski C, Fisher DE et al (2021) The state of melanoma: emergent challenges and opportunities. Clin Cancer Res 27(10):2678–2697. https://doi.org/10.1158/1078-0432.CCR-20-4092
2. Gupta GP, Massague J (2006) Cancer metastasis: building a framework. Cell 127(4):679–695. https://doi.org/10.1016/j.cell.2006.11.001
3. Peinado H, Zhang H, Matei IR et al (2017) Pre-metastatic niches: organ-specific homes for metastases. Nat Rev Cancer 17(5):302–317. https://doi.org/10.1038/nrc.2017.6
4. Aspelund A, Robciuc MR, Karaman S et al (2016) Lymphatic system in cardiovascular medicine. Circ Res 118(3):515–530. https://doi.org/10.1161/CIRCRESAHA.115.306544
5. du Bois H, Heim TA, Lund AW (2021) Tumor-draining lymph nodes: at the crossroads of metastasis and immunity. Sci Immunol 6(63):eabg3551. https://doi.org/10.1126/sciimmunol.abg3551
6. Vaahtomeri K, Alitalo K (2020) Lymphatic vessels in tumor dissemination versus immunotherapy. Cancer Res 80(17):3463–3465. https://doi.org/10.1158/0008-5472.CAN-20-0156
7. Dieterich LC, Tacconi C, Ducoli L, Detmar M (2022) Lymphatic vessels in cancer. Physiol Rev 102(4):1837–1879. https://doi.org/10.1152/physrev.00039.2021
8. Brown M, Assen FP, Leithner A et al (2018) Lymph node blood vessels provide exit routes for metastatic tumor cell dissemination in mice. Science 359(6382):1408–1411. https://doi.org/10.1126/science.aal3662
9. Pereira ER, Kedrin D, Seano G et al (2018) Lymph node metastases can invade local blood vessels, exit the node, and colonize distant organs in mice. Science 359(6382):1403–1407. https://doi.org/10.1126/science.aal3622
10. Rezzola S, Sigmund EC, Halin C, Ronca R (2022) The lymphatic vasculature: an active and dynamic player in cancer progression. Med Res Rev 42(1):576–614. https://doi.org/10.1002/med.21855
11. Sleeman JP (2000) The lymph node as a bridgehead in the metastatic dissemination of tumors. Recent Results Cancer Res 157:55–81. https://doi.org/10.1007/978-3-642-57151-0_6
12. Ubellacker JM, Tasdogan A, Ramesh V et al. (2020) Lymph protects metastasizing melanoma cells from ferroptosis. Nature 585(7823):113–118. https://doi.org/10.1038/s41586-020-2623-z
13. Van Trappen PO, Pepper MS (2002) Lymphatic dissemination of tumour cells and the formation of micrometastases. Lancet Oncol 3(1):44–52. https://doi.org/10.1016/s1470-2045(01)00621-0
14. Bajaj S, Donnelly D, Call M et al (2020) Melanoma prognosis: accuracy of the American Joint Committee on Cancer staging manual eighth edition. J Natl Cancer Inst

112(9):921–928. https://doi.org/10.1093/jnci/djaa008
15. Sleeman JP (2015) The lymph node pre-metastatic niche. J Mol Med 93(11):1173–1184. https://doi.org/10.1007/s00109-015-1351-6
16. Garcia-Silva S, Peinado H (2024) Mechanisms of lymph node metastasis: an extracellular vesicle perspective. Eur J Cell Biol 103(3):151447. https://doi.org/10.1016/j.ejcb.2024.151447
17. Gkountidi AO, Garnier L, Dubrot J et al (2021) MHC class II antigen presentation by lymphatic endothelial cells in tumors promotes intratumoral regulatory T cell-suppressive functions. Cancer Immunol Res 9(7):748–764. https://doi.org/10.1158/2326-6066.CIR-20-0784
18. Santambrogio L, Berendam SJ, Engelhard VH (2019) The antigen processing and presentation machinery in lymphatic endothelial cells. Front Immunol 10:1033. https://doi.org/10.3389/fimmu.2019.01033
19. Swartz MA (2014) Immunomodulatory roles of lymphatic vessels in cancer progression. Cancer Immunol Res 2(8):701–707. https://doi.org/10.1158/2326-6066.CIR-14-0115
20. Jaiswal R, Sedger LM (2019) Intercellular vesicular transfer by exosomes, microparticles and oncosomes—implications for cancer biology and treatments. Front Oncol 9:125. https://doi.org/10.3389/fonc.2019.00125
21. Raposo G, Stoorvogel W (2013) Extracellular vesicles: exosomes, microvesicles, and friends. J Cell Biol 200(4):373–383. https://doi.org/10.1083/jcb.201211138
22. Witwer KW, Thery C (2019) Extracellular vesicles or exosomes? On primacy, precision, and popularity influencing a choice of nomenclature. J Extracell Vesicles 8(1):1648167. https://doi.org/10.1080/20013078.2019.1648167
23. D'Angelo G, Stahl PD, Raposo G (2025) The cell biology of extracellular vesicles: a jigsaw puzzle with a myriad of pieces. Curr Opin Cell Biol 94:102519. https://doi.org/10.1016/j.ceb.2025.102519
24. Kingreen T, Kewitz-Hempel S, Rohde C et al (2024) Extracellular vesicles from highly invasive melanoma subpopulations increase the invasive capacity of less invasive melanoma cells through mir-1246-mediated inhibition of CCNG2. Cell Commun Signal 22(1):442. https://doi.org/10.1186/s12964-024-01820-6
25. Yan W, Wu X, Zhou W et al (2018) Cancer-cell-secreted exosomal miR-105 promotes tumour growth through the MYC-dependent metabolic reprogramming of stromal cells. Nat Cell Biol 20(5):597–609. https://doi.org/10.1038/s41556-018-0083-6
26. Rabe DC, Walker ND, Rustandy FD et al (2021) Tumor extracellular vesicles regulate macrophage-driven metastasis through CCL5. Cancers 13(14):3459. https://doi.org/10.3390/cancers13143459
27. Grange C, Tapparo M, Tritta S et al (2015) Role of HLA-G and extracellular vesicles in renal cancer stem cell-induced inhibition of dendritic cell differentiation. BMC Cancer 15: 1009. https://doi.org/10.1186/s12885-015-2025-z
28. Sohal IS, Kasinski AL (2023) Emerging diversity in extracellular vesicles and their roles in cancer. Front Oncol 13:1167717
29. Hoshino A, Costa-Silva B, Shen TL et al (2015) Tumour exosome integrins determine organotropic metastasis. Nature 527(7578):329–335
30. Srinivasan S, Vannberg FO, Dixon JB (2016) Lymphatic transport of exosomes as a rapid route of information dissemination to the lymph node. Sci Rep 6: 24436. https://doi.org/10.1038/srep24436
31. Broggi MAS, Maillat L, Clement CC et al. (2019) Tumor-associated factors are enriched in lymphatic exudate compared to plasma in metastatic melanoma patients. J Exp Med 216(5):1091–1107. https://doi.org/10.1084/jem.20181618
32. Garcia-Silva S, Benito-Martin A, Nogues L et al. (2021) Melanoma-derived small extracellular vesicles induce lymphangiogenesis and metastasis through an NGFR-dependent mechanism. Nat Cancer 2(12):1387–1405. https://doi.org/10.1038/s43018-021-00272-y
33. Hood JL, San RS, Wickline SA (2011) Exosomes released by melanoma cells prepare sentinel lymph nodes for tumor metastasis. Cancer Res 71(11):3792–3801. https://doi.org/10.1158/0008-5472.CAN-10-4455
34. Pucci F, Garris C, Lai CP et al (2016) SCS macrophages suppress melanoma by restricting tumor-derived vesicle-B cell interactions. Science 352(6282):242–246. https://doi.org/10.1126/science.aaf1328
35. Leary N, Walser S, He Y et al (2022) Melanoma-derived extracellular vesicles mediate lymphatic remodelling and impair tumour immunity in draining lymph nodes. J Extracell Vesicles 11(2):e12197. https://doi.org/10.1002/jev2.12197
36. Zhou CF, Ma J, Huang L et al (2019) Cervical squamous cell carcinoma-secreted exosomal miR-221-3p promotes lymphangiogenesis and lymphatic metastasis by targeting VASH1. Oncogene 38(8):1256–1268. https://doi.org/10.1038/s41388-018-0511-x
37. Chen C, Luo Y, He W et al (2020) Exosomal long noncoding RNA LNMAT2

promotes lymphatic metastasis in bladder cancer. J Clin Invest 130(1):404–421. https://doi.org/10.1172/JCI130892
38. Gillot L, Lebeau A, Baudin L et al (2022) Periostin in lymph node pre-metastatic niches governs lymphatic endothelial cell functions and metastatic colonization. Cell Mol Life Sci 79(6):295. https://doi.org/10.1007/s00018-022-04262-w
39. Silvers CR, Messing EM, Miyamoto H, Lee YF (2021) Tenascin-C expression in the lymph node pre-metastatic niche in muscle-invasive bladder cancer. Br J Cancer 125(10): 1399–1407. https://doi.org/10.1038/s41416-021-01554-z
40. Huber V, Vallacchi V, Fleming V et al (2018) Tumor-derived microRNAs induce myeloid suppressor cells and predict immunotherapy resistance in melanoma. J Clin Invest 128(12):5505–5516. https://doi.org/10.1172/JCI98060
41. Sun B, Zhou Y, Fang Y et al (2019) Colorectal cancer exosomes induce lymphatic network remodeling in lymph nodes. Int J Cancer 145(6):1648–1659. https://doi.org/10.1002/ijc.32196
42. Maus RLG, Jakub JW, Nevala WK et al (2017) Human melanoma-derived extracellular vesicles regulate dendritic cell maturation. Front Immunol 8:358. https://doi.org/10.3389/fimmu.2017.00358
43. Taylor DD, Gercel-Taylor C, Lyons KS et al (2003) T-cell apoptosis and suppression of T-cell receptor/CD3-zeta by Fas ligand-containing membrane vesicles shed from ovarian tumors. Clin Cancer Res 9(14):5113–5119
44. Chen G, Huang AC, Zhang W et al (2018) Exosomal PD-L1 contributes to immunosuppression and is associated with anti-PD-1 response. Nature 560(7718):382–386. https://doi.org/10.1038/s41586-018-0392-8
45. Su X, Brassard A, Bartolomucci A et al (2023) Tumour extracellular vesicles induce neutrophil extracellular traps to promote lymph node metastasis. J Extracell Vesicles 12(8):e12341. https://doi.org/10.1002/jev2.12341
46. Vulpis E, Loconte L, Peri A et al (2022) Impact on NK cell functions of acute versus chronic exposure to extracellular vesicle-associated MICA: dual role in cancer immunosurveillance. J Extracell Vesicles 11(1):e12176. https://doi.org/10.1002/jev2.12176
47. Collot M, Ashokkumar P, Anton H et al (2019) MemBright: a family of fluorescent membrane probes for advanced cellular imaging and neuroscience. Cell Chem Biol 26(4): 600–614 e607. https://doi.org/10.1016/j.chembiol.2019.01.009



Chapter 15

Detection of Biomarkers for EMT-Associated Phenotype Switching in Melanoma-Derived Extracellular Vesicles

Quan Zhou, Jing Wang, Zhen Zhang, Matt Trau, Alain Wuethrich and Richard J. Lobb

Abstract

Melanoma cells exhibit epithelial-to-mesenchymal transition (EMT)-like phenotype switching during targeted therapy, which contributes to the development of drug resistance. Extracellular vesicles (EVs) released by melanoma cells carry surface proteins reflective of this EMT-associated transition, providing an accessible window to track therapeutic response. This chapter presents a step-by-step protocol for profiling EMT-related melanoma EV protein signatures directly from unpurified sera using a microfluidic surface-enhanced Raman scattering (SERS) biosensing platform. The method integrates melanoma-specific EV capture, alternating current-electrohydrodynamic nanomixing–enhanced binding, and multiplex SERS nanotag labeling to enable sensitive quantification of EMT surface markers in a streamlined assay. Detailed instructions for reagent preparation, SERS nanotag synthesis, biosensor fabrication and operation, spectral acquisition, and data processing are provided to support implementation in melanoma translational research laboratories. This protocol enables reproducible monitoring of EMT-like phenotypic evolution in melanoma models and patient samples and may assist future studies aiming to predict or mechanistically dissect resistance to targeted therapy.

Keywords Melanoma, Extracellular vesicles, Targeted therapy, Epithelial–mesenchymal transition, Surface-enhanced Raman scattering, Microfluidics

1 Introduction

Melanoma is characterized by remarkable cellular plasticity, enabling malignant cells to dynamically transition between proliferative and invasive states [1, 2]. Although this process is not a canonical epithelial–mesenchymal transition (EMT), it resembles EMT at the transcriptomic and proteomic levels and functionally contributes to therapy escape and tumor progression [3, 4]. The ability to monitor EMT-like phenotypic evolution is therefore critical for understanding melanoma biology and developing predictive biomarkers that can inform treatment decision-making in a more responsive timeframe than radiographic assessment or repeated tumor biopsy.

Kristian M. Hargadon (ed.), *Melanoma*, Methods in Molecular Biology, vol. 3089,
https://doi.org/10.1007/978-1-0716-5619-8_15,
© The Author(s), under exclusive license to Springer Science+Business Media, LLC, part of Springer Nature 2027

Extracellular vesicles (EVs) are promising circulating surrogates for studying EMT-like phenotypic changes in melanoma. EVs are membrane-encapsulated nanoparticles that are released by cells into circulation, and importantly, they preserve molecular information originating from their parental melanoma cells [5–9]. Surface protein signatures carried by circulating EVs can therefore reveal phenotypic transitions as they occur in vivo, making them particularly suited to capturing EMT-associated molecular shifts that may precede clinical progression [10–14]. However, direct molecular interrogation of EVs in minimally processed sera remains technically challenging due to their small size, low abundance of target-specific molecules, and interference from abundant nonvesicular particles [15].

To address these limitations, microfluidic biosensing strategies integrated with alternating-current electrohydrodynamic (AC-EHD) and surface-enhanced Raman spectroscopy (SERS) offer an opportunity to quantify EV surface biomarkers with high sensitivity, multiplex capability, and minimal sample input [16]. AC-EHD enhances target–probe interactions, while SERS enables the simultaneous quantification of multiple EMT-related markers on EVs directly from unpurified melanoma patient sera [15].

This chapter describes a protocol for characterizing EMT-associated surface protein signatures on melanoma EVs using a microfluidic SERS biosensor. The platform utilizes melanoma-specific capture antibodies against melanoma chondroitin sulfate proteoglycan (MCSP) and melanoma cell adhesion molecule (MCAM) [17], and SERS nanotag-based detection of N-cadherin, E-cadherin, thrombospondin-1 (THBS1), and ATP-binding cassette sub-family B member 5 (ABCB5)—representative markers associated with EMT-like phenotypic switching in melanoma [18–20]. The procedures provided herein include reagent preparation, SERS nanotag synthesis, biosensor fabrication and operation, spectral acquisition, and data processing. This protocol supports implementation of melanoma EV surface phenotype profiling in translational cancer research laboratories and may facilitate broader exploration of EV-based phenotypic shifts associated with melanoma progression.

Figure 1 illustrates the overall workflow for tracking EMT-like phenotype switching in melanoma EVs during MAPK inhibitor (MAPKi) treatment. Melanoma cells undergoing EMT-like transitions release EVs into circulation, where their surface molecular profiles reflect changes in cellular phenotypic state (Fig. 1A). In this assay, circulating EVs are directly interrogated from serum by selective capture using anti-MCSP and anti-MCAM antibodies immobilized on the microelectrode surface (Fig. 1B). Application of an AC field enhances molecular interactions between captured EVs and a multiplex panel of Raman nanotags targeting N-cadherin, E-cadherin, THBS1, and ABCB5. Subsequent SERS mapping enables spectral readout of EV surface protein expression (Fig. 1C). Each nanotag

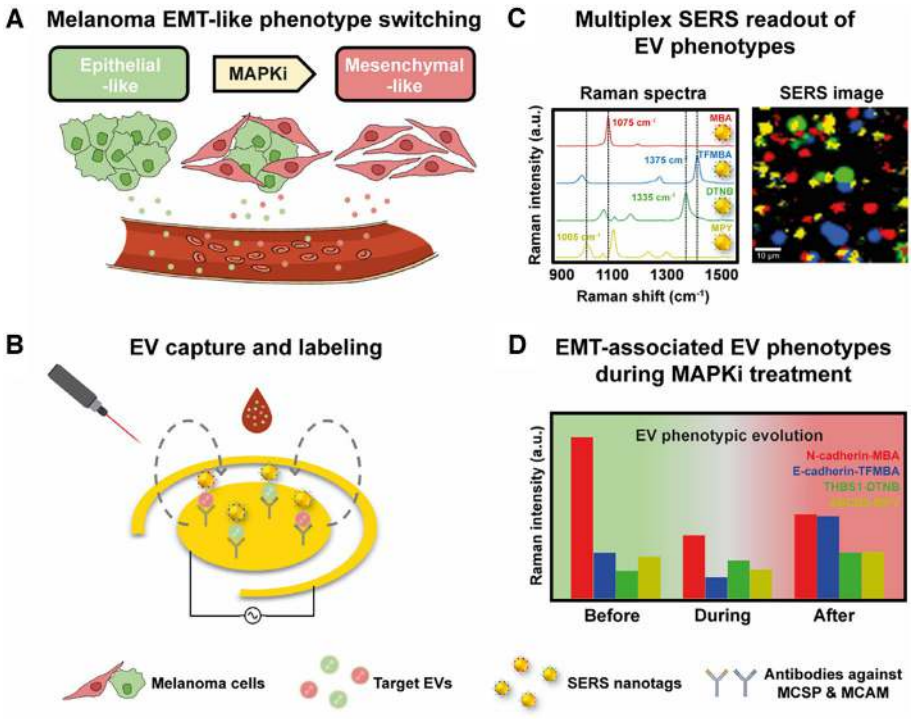


Fig. 1 Workflow for tracking EMT-like phenotype switching in melanoma extracellular vesicles during MAPKi treatment. (**A**), Melanoma cells undergoing EMT-like transitions release EVs into circulation. (**B**), Serum EVs are selectively captured using anti-MCSP and anti-MCAM antibodies on microelectrodes under an applied AC field. (**C**), Multiplex SERS nanotags targeting N-cadherin, E-cadherin, THBS1, and ABCB5 generate distinct Raman peaks to produce false-color spectral maps. (**D**), Average spectral intensities are quantified to assess EMT-associated EV phenotypic evolution. Reproduced from [1] under CC-BY license

generates a distinct Raman peak, allowing construction of false-color spectral images corresponding to the four biomarkers. Average spectral intensities extracted from these maps are used to quantify relative expression levels. This integrated workflow provides a streamlined approach to visualize and quantify EMT-associated EV phenotypic transitions in response to MAPKi exposure (Fig. 1D).

2 Materials

2.1 Cell Culture

1. Melanoma cell lines: The SK-MEL-28 cell line was obtained from American Type Culture Collection. The LM-MEL-33 and LM-MEL-64 cell lines were established at the Ludwig Institute for Cancer Research in Melbourne from patient tumor samples.
2. Complete Medium: Medium 254 supplemented with 1× Human Melanocyte Growth Supplement.

3. PLX-4720.
4. Dulbecco's phosphate-buffered saline (DPBS).
5. Cell culture flasks.
6. Sterile 0.22-μm syringe filter.

2.2 SERS Nanotag Synthesis

1. Gold (III) chloride trihydrate ($HAuCl_4$).
2. Trisodium citrate dihydrate.
3. Milli-Q ultra-pure water.
4. Cross-linking reagent: 1 mM dithiobis(succinimidyl propionate) [DSP] in dimethyl sulfoxide (DMSO).
5. Ethanol.
6. 4-mercaptobenzoic acid (MBA).
7. 2,3,5,6-tetrafluoro-MBA (TFMBA).
8. 5,5′-dithiobis (2-nitrobenzoic acid) [DTNB].
9. 4-mercaptopyridine (MPY).
10. Mouse anti-human N-cadherin (Clone 691723).
11. Mouse anti-human E-cadherin (Clone 180224).
12. Mouse anti-human THBS1 (Clone 301221).
13. Mouse anti-human ABCB5 (Clone 5H3C6).
14. 0.1% (w/v) bovine serum albumin (BSA) in water.
15. 0.1 mM phosphate-buffered saline (PBS).

2.3 Biosensor Fabrication

1. Microfluidic design software: Layout Editor L-Edit V15 (Tanner Research).
2. 5-inch soda lime chrome masks (Shenzhen Qingyi Precision Mask Making).
3. Direct write system μPG 101 (Heidelberg Instruments).
4. 4-inch Boroflat wafer (Bonda Technology Pte Ltd).
5. Sawatec SM-200 spin coater (Sawatec AG).
6. Negative photoresist AZnLOF 2020.
7. Mask aligner (EVG 620, EV Group, St Florian am Inn).
8. Developer solution: AZ726 MIF Developer.
9. Temescal FC-2000 Deposition System (Ferrotec).
10. Lift-off solution: Remover PG.
11. Polydimethylsiloxane (PDMS): SYLGARD™ 184 Silicone Elastomer Kit (Dow).

2.4 Biosensor Functionalization

1. Cross-linking reagent: 5 mM DSP in DMSO.
2. Mouse anti-human MCSP (Clone LHM-2).

3. Mouse anti-human MCAM (Clone 128018).
4. Blocking buffer: 5% (w/v) BSA in 10 mM PBS.
5. Washing buffer: 10 mM PBS.
6. Absolute ethanol.

2.5 EV Capture and Labeling

1. Signal and wave generator: waveform generator 33510B (Agilent Technologies).
2. Washing buffer: 10 mM PBS.
3. Dilution buffer: 1% (w/v) BSA in 10 mM PBS.

2.6 SERS Measurements

1. WITec Alpha 300 R microspectrometer (Oxford Instruments).
2. Data processing software: WITec Project FIVE (Oxford Instruments).
3. Background removal software: Vancouver Raman Algorithm [21].

3 Methods

3.1 Cell Culture and Conditioned Media Collection

1. Culture SK-MEL-28, LM-MEL-33, and LM-MEL-64 melanoma cell lines in Complete Medium. Maintain cells under routine culture conditions in the presence of 1 μM PLX4720 where indicated for MAPK inhibition studies.
2. Collect conditioned culture medium (CCM) at designated time points (e.g., baseline and subsequent culture intervals) (*see* **Note 1**).
3. Centrifuge CCM at 800 × *g* for 10 min at 4°C to remove cells and debris.
4. Filter the clarified CCM through a 0.22-μm syringe filter. Process immediately or store at −80°C in single-use aliquots until downstream EV analysis.

3.2 SERS Nanotag Synthesis

Figure 2 illustrates the synthesis process of gold nanoparticles and subsequent functionalization of SERS nanotags.

1. Synthesize 60 nm diameter citrate-stabilized gold nanoparticles (AuNP) using standard citrate reduction of $HAuCl_4$ [22]. Add 1 mL of 1% (w/v) trisodium citrate dihydrate to 100 mL of boiled 0.01% (w/v) $HAuCl_4$ (*see* **Note 2**). Then, boil the mixture for 20 min under magnetic stirring (*see* **Note 3**).
2. To 1 mL of synthesized AuNP suspension, add 10 μL of 1 mM Raman reporter in ethanol (MBA, TFMBA, DTNB, or

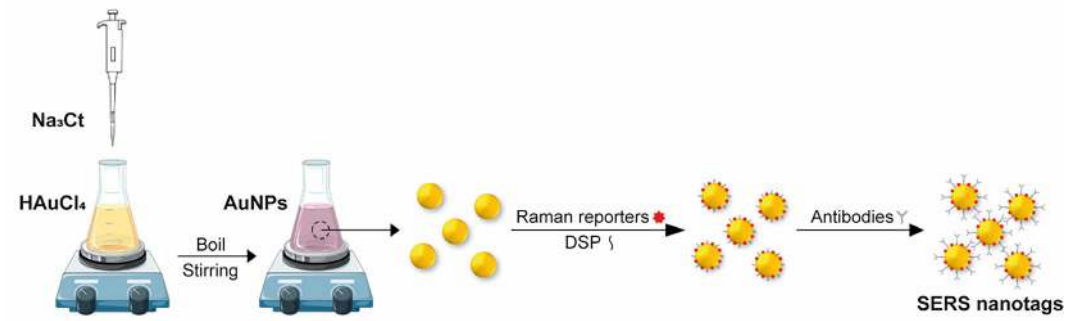


Fig. 2 Preparation of multiplex SERS nanotags. Gold nanoparticles are synthesized by citrate reduction and subsequently functionalized with Raman reporter molecules and target-specific antibodies using DSP as the crosslinker. Adapted from [1] under CC-BY license

MPY) together with 2 µL of 1 mM DSP crosslinker in DMSO. Incubate for 5 h at room temperature with gentle shaking.

3. Centrifuge at 5400 × *g* for 10 min, and discard supernatant (*see* **Note 4**).
4. Resuspend nanotags in 200 µL of 0.1 mM PBS.
5. Add 0.5 µg of specific antibody (anti–N-cadherin, anti–E-cadherin, anti-THBS1, or anti-ABCB5) to each 200 µL resuspended nanotag batch. Incubate 30 min at room temperature with gentle shaking.
6. Centrifuge at 600 × *g* for 10 min at 4°C to remove excess antibody.
7. Resuspend the pellet in 200 µL of 0.1% (w/v) BSA in water.
8. Store nanotags at 4°C until use.

3.3 Biosensor Fabrication

Figure 3 illustrates the microfabrication workflow of the patterned biosensor [23].

1. Design electrode patterns using L-Edit V15 software, and write onto five-inch soda lime chrome masks using the direct write system µPG 101 (*see* **Note 5**).
2. Coat a four-inch Borofloat wafer using Sawatec SM-200 spin coater with AZnLOF2020 negative photoresist at 510 × *g* for 30 s. Soft bake at 110°C for 2 min.
3. UV expose with mask (200 mJ cm^{-2}), and perform post-exposure bake (110°C, 1 min). Develop for 30 s in AZ 726 MIF developer (*see* **Note 6**).
4. Deposit 10 nm Ti and 200 nm Au using the Temescal FC-2000 Deposition System. Perform lift-off overnight in Remover PG (*see* **Note 7**).

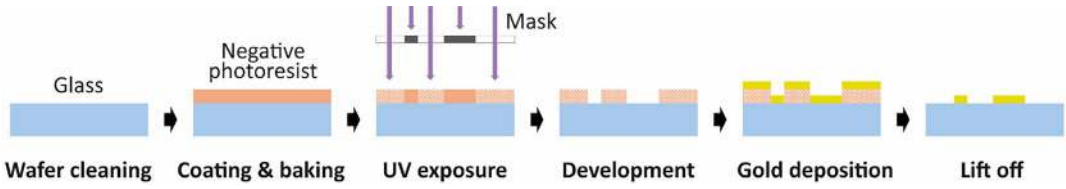


Fig. 3 Microfabrication workflow of the electrode device. A negative photoresist is patterned onto a glass wafer by photolithography, followed by metal deposition and lift-off to form titanium/gold asymmetric electrode structures. Reproduced from [23] under CC-BY license

5. Rinse wafers with isopropanol, and dry thoroughly under nitrogen.
6. Prepare a 4-mm PDMS microfluidic top slab by curing elastomer at 65°C for 2 h. Punch wells (5-mm diameter) and thermally bond PDMS to patterned wafer overnight at 65°C (*see* **Note 8**). Figure 4 shows a photo of the microfluidic biosensor with aligned PDMS on top.

3.4 Biosensor Functionalization

1. Add 20 µL of 5 mM DSP in DMSO to each microelectrode well, and incubate for 2 h at room temperature.
2. Wash once with absolute ethanol and three times with 10 mM PBS (*see* **Note 9**).
3. Add 20 µL of 5 µg/mL anti-MCSP and anti-MCAM antibody mixture in 10 mM PBS to each well. Incubate for 2 h at room temperature (*see* **Note 10**).
4. Block surfaces with 50 µL of 5% (w/v) BSA in 10 mM PBS for 2 h at room temperature.
5. Wash three times with 10 mM PBS prior to sample loading.

3.5 EV Capture and Labeling

1. Add 50 µL of sample (CCM or 1:10 diluted serum) to each functionalized well.
2. Apply AC field (500 Hz, 800 mV) for 45 min to induce nanomixing and promote EV capture.
3. Remove sample, and wash wells twice with 10 mM PBS.
4. Prepare the SERS nanotag cocktail (1:25 dilution for each nanotag) in 1% (w/v) BSA in 10 mM PBS (*see* **Note 11**). Add 25 µL of the diluted SERS nanotag cocktail, and apply the same AC field for 20 min.
5. Wash wells twice with 10 mM PBS prior to SERS measurement.

3.6 SERS Measurements

1. Acquire spectra on the WITec Alpha 300 R microspectrometer equipped with 633-nm laser and EM-CCD detector.
2. Calibrate peak position using silicon standard at 520 cm^{-1} (*see* **Note 12**).

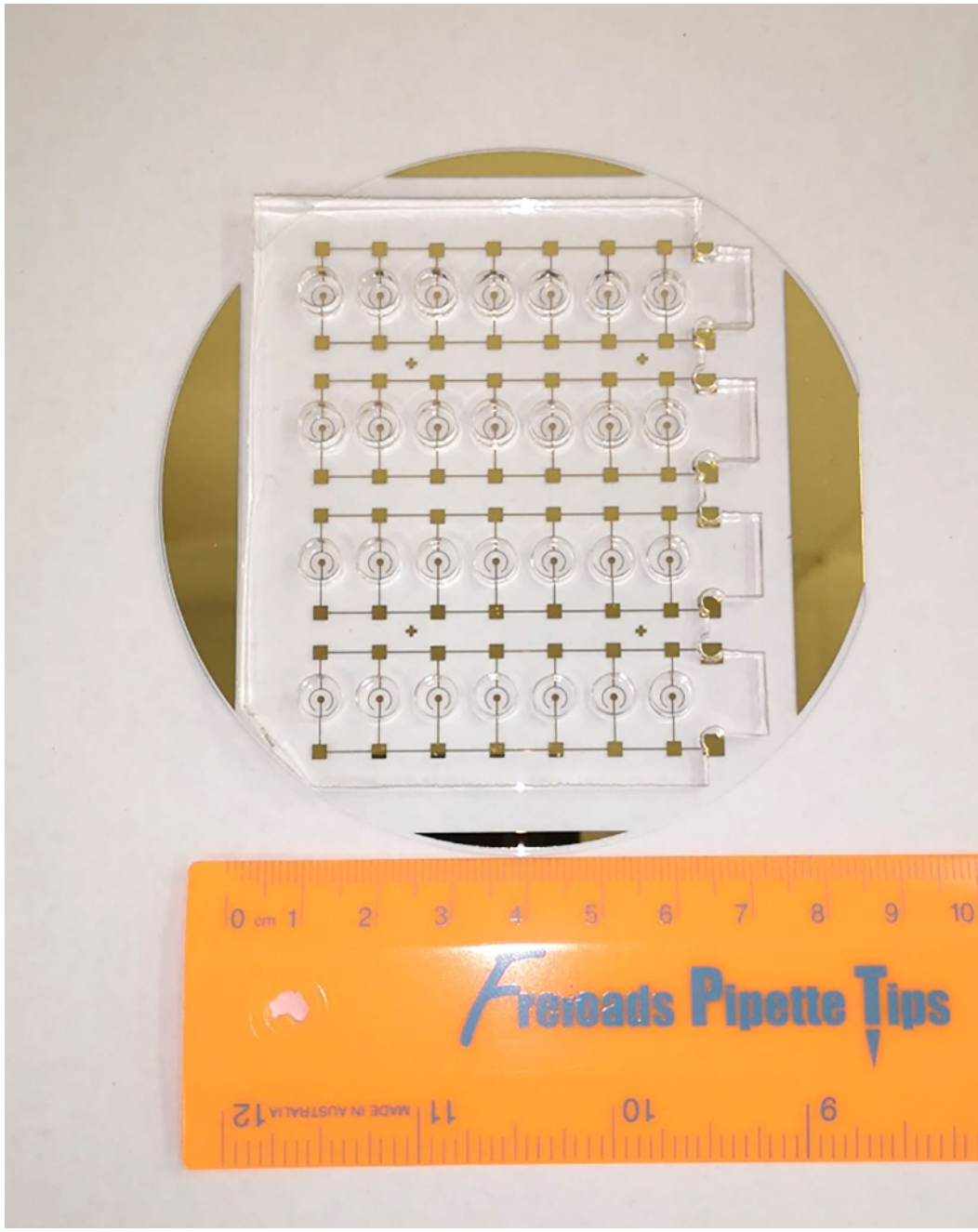


Fig. 4 Layout of the microfluidic biosensor. The device incorporates 28 asymmetric electrode pairs (inner circle diameter 1000 μm; outer ring width 120 μm) with a PDMS well-layer aligned on top to enable parallel processing of multiple liquid samples. Reproduced from [1] under CC-BY license

3. Collect spectral maps at 60 × 60 μm area (60 × 60 pixels) using a 20× objective with 50-ms integration time per pixel. Maintain laser power at 4 mW.

4. Extract average spectrum from mapped region. Remove autofluorescence background using Vancouver Raman Algorithm [21].
5. Quantify expression levels by integrating Raman intensities at 1075 (MBA), 1375 (TFMBA), 1335 (DTNB), and 1005 (MPY) cm^{-1}, corresponding to N-cadherin, E-cadherin, THBS1, and ABCB5, respectively.

4 Notes

1. CCM should be collected when cell cultures reach approximately 80% confluency.
2. Use ultrapure water for all reagent preparation, and ensure that all glassware is thoroughly cleaned prior to use.
3. The size distribution and monodispersity of synthesized gold nanoparticles may be rapidly assessed by UV–Vis spectroscopy before Raman reporter conjugation [24].
4. Centrifugation speeds may be adjusted based on pellet visibility; avoid excessive force to prevent nanoparticle aggregation.
5. Photolithography masks and wafers should be precleaned with isopropanol.
6. If photolithography development is incomplete, the development time may be extended up to 45 s as needed.
7. Acetone can be used for lift-off. Glassware should be covered during the lift-off step to minimize solvent evaporation.
8. Both the patterned wafer and the PDMS slab should be cleaned with isopropanol immediately prior to thermal bonding.
9. During biosensor functionalization and washing steps, wells should remain wet at all times. Using a multichannel pipette is recommended for consistent washing.
10. After antibody immobilization, the antibody solution does not need to be removed prior to the blocking step; blocking buffer can be added directly into the wells.
11. The dilution ratio of individual SERS nanotags can be optimized by preliminary experiments to maximize signal-to-noise ratio.
12. Maintain consistent silicon peak intensity during Raman calibration to ensure spectral comparability across samples.

Acknowledgments

A.W. acknowledges the funding support by the National Health and Medical Research Council (2034488). M.T. acknowledges the funding from the Australian Research Council (FL220100059) and the National Health and Medical Research Council (APP1185907). R.J.L. acknowledges the support by the National Health and Medical Research Council (2034433). M.T., R.J.L., and A.W. acknowledge funding from Cancer Australia (2010799). J.W. acknowledges the support from the Guiding Projects of Fujian Province (2023Y0058), the Science Fund Program for Excellent Young Scientists of Fujian (2024J09030), the Top Young Talents of Foal Eagle Program of Fujian Province, and the Joint Funds for Innovation in Science and Technology, Fujian Province (2021Y9228).

Conflict of Interest The authors have no conflicts of interest to declare that are relevant to the content of this chapter.

References

1. Zhou Q, Wang J, Zhang Z et al (2024) Tracking the EMT-like phenotype switching during targeted therapy in melanoma by analyzing extracellular vesicle phenotypes. Biosens Bioelectron 244:115819. https://doi.org/10.1016/j.bios.2023.115819
2. Arozarena I, Wellbrock C (2019) Phenotype plasticity as enabler of melanoma progression and therapy resistance. Nat Rev Cancer 19(7):377–391. https://doi.org/10.1038/s41568-019-0154-4
3. Caramel J, Papadogeorgakis E, Hill L et al (2013) A switch in the expression of embryonic EMT-inducers drives the development of malignant melanoma. Cancer Cell 24(4):466–480. https://doi.org/10.1016/j.ccr.2013.08.018
4. Pillai M, Rajaram G, Thakur P et al (2022) Mapping phenotypic heterogeneity in melanoma onto the epithelial-hybrid-mesenchymal axis. Front Oncol 12:913803. https://doi.org/10.3389/fonc.2022.913803
5. Möller A, Lobb RJ (2020) The evolving translational potential of small extracellular vesicles in cancer. Nat Rev Cancer 20(12):697–709. https://doi.org/10.1038/s41568-020-00299-w
6. Lane RE, Korbie D, Hill MM, Trau M (2018) Extracellular vesicles as circulating cancer biomarkers: opportunities and challenges. Clin Transl Med 7(1):14. https://doi.org/10.1186/s40169-018-0192-7
7. Wen SW, Lima LG, Lobb RJ et al (2019) Breast cancer-derived exosomes reflect the cell-of-origin phenotype. Proteomics 19(8):1800180. https://doi.org/10.1002/pmic.201800180
8. Xiao D, Barry S, Kmetz D et al (2016) Melanoma cell–derived exosomes promote epithelial–mesenchymal transition in primary melanocytes through paracrine/autocrine signaling in the tumor microenvironment. Cancer Lett 376(2):318–327. https://doi.org/10.1016/j.canlet.2016.03.050
9. Luan W, Ding Y, Xi H et al (2021) Exosomal miR-106b-5p derived from melanoma cell promotes primary melanocytes epithelial-mesenchymal transition through targeting EphA4. J Exp Clin Cancer Res 40(1):107. https://doi.org/10.1186/s13046-021-01906-w
10. Greening DW, Gopal SK, Mathias RA et al (2015) Emerging roles of exosomes during epithelial–mesenchymal transition and cancer progression. Semin Cell Dev Biol 40:60–71. https://doi.org/10.1016/j.semcdb.2015.02.008
11. Becker A, Thakur BK, Weiss JM et al (2016) Extracellular vesicles in cancer: cell-to-cell mediators of metastasis. Cancer Cell 30(6):836–848. https://doi.org/10.1016/j.ccell.2016.10.009
12. Kim H, Lee S, Shin E et al (2020) The emerging roles of exosomes as EMT regulators in cancer. Cells 9(4):861. https://doi.org/10.3390/cells9040861
13. Lobb RJ, Visan KS, Wu L-Y et al (2023) An epithelial-to-mesenchymal transition induced extracellular vesicle prognostic signature in

non-small cell lung cancer. Commun Biol 6(1):68. https://doi.org/10.1038/s42003-022-04350-4
14. Guo W, Wang H, Li C (2021) Signal pathways of melanoma and targeted therapy. Signal Transduct Target Ther 6(1):424. https://doi.org/10.1038/s41392-021-00827-6
15. Wang J, Kao Y-C, Zhou Q et al (2022) An integrated microfluidic-SERS platform enables sensitive phenotyping of serum extracellular vesicles in early stage melanomas. Adv Funct Mater 32(3):2010296. https://doi.org/10.1002/adfm.202010296
16. Wang J, Koo KM, Wang Y, Trau M (2019) Engineering state-of-the-art plasmonic nanomaterials for SERS-based clinical liquid biopsy applications. Adv Sci 6(23):1900730. https://doi.org/10.1002/advs.201900730
17. Tsao SC-H, Wang J, Wang Y et al (2018) Characterising the phenotypic evolution of circulating tumour cells during treatment. Nat Commun 9(1):1482. https://doi.org/10.1038/s41467-018-03725-8
18. Zeisberg M, Neilson EG (2009) Biomarkers for epithelial-mesenchymal transitions. J Clin Invest 119(6):1429–1437. https://doi.org/10.1172/JCI36183
19. Jayachandran A, Anaka M, Prithviraj P et al (2014) Thrombospondin 1 promotes an aggressive phenotype through epithelial-to-mesenchymal transition in human melanoma. Oncotarget 5(14):5782–5797. https://doi.org/10.18632/oncotarget.2164
20. Rapanotti MC, Campione E, Viguria TMS et al (2020) Stem–mesenchymal signature cell genes detected in heterogeneous circulating melanoma cells correlate with disease stage in melanoma patients. Front Mol Biosci 7:92. https://doi.org/10.3389/fmolb.2020.00092
21. Zhao J, Lui H, McLean DI, Zeng H (2007) Automated autofluorescence background subtraction algorithm for biomedical Raman spectroscopy. Appl Spectrosc 61(11):1225–1232. https://doi.org/10.1366/000370207782597003
22. Frens G (1973) Controlled nucleation for the regulation of the particle size in monodisperse gold suspensions. Nat Phys Sci 241(105):20–22. https://doi.org/10.1038/physci241020a0
23. Zhou Q, Niu X, Zhang Z et al (2024) Glycan profiling in small extracellular vesicles with a SERS microfluidic biosensor identifies early malignant development in lung cancer. Adv Sci 11(33):2401818. https://doi.org/10.1002/advs.202401818
24. Wang J, Anderson W, Li J et al (2019) A high-resolution study of in situ surface-enhanced Raman scattering nanotag behavior in biological systems. J Colloid Interface Sci 537:536–546. https://doi.org/10.1016/j.jcis.2018.11.035

Part V

Melanoma Imaging Techniques and Methods for Spatial Analysis of Melanoma Tissue



Chapter 16

Imaging and Isolation of Extravasation-Participating Endothelial and Melanoma Cells During Angiopellosis

Tyler A. Allen and Ke Cheng

Abstract

Cancer mortality is driven largely by metastatic progression rather than by primary tumor burden. The ability of circulating tumor cells (CTCs) to exit the vasculature and invade surrounding tissues—known as extravasation—is a critical and rate-limiting step in metastasis. Recent advances in high-resolution intravital microscopy have made it possible to directly visualize this process in vivo, enabling real-time imaging of individual CTCs as they interact with, transmigrate through, and recruit components of the endothelium. In this chapter, we describe intravital microscopy approaches that allow for both visualization and isolation of extravasating CTCs, as well as the endothelial cells that actively participate in their transendothelial migration. These methods provide a powerful platform for dissecting the cellular and molecular mechanisms underlying metastatic spread. Beyond mechanistic insights, the approach can also serve as a functional screening system for evaluating anticancer therapeutics that target CTC behavior, endothelial interactions, or early metastatic niche formation.

Keywords Circulating tumor cells, Metastasis, Intravital microscopy, Cancer exodus hypothesis, Extravasation, Angiopellosis, Zebrafish, Tumor infusion, Lightsheet microscopy, Tumor cell isolation

1 Introduction

Metastasis remains the leading cause of cancer-related deaths worldwide [1]. This complex process involves tumor cell(s) dissociation from the primary site, intravasation (entering) into the circulation, and extravasation (exiting) through the blood- and lymph- vessels at distant sites. The molecular mechanisms regulating this process remain poorly understood, but the process is known to depend on tumor cells' ability to transmigrate the blood vessel wall from the circulation [2–4]. Only a small percent of all tumor cells ever successfully make this journey, and even fewer actually survive following extravasation to form secondary tumors. However, this small percent of metastasis cases accounts for the overwhelming majority of cancer-related deaths [5].

Kristian M. Hargadon (ed.), *Melanoma*, Methods in Molecular Biology, vol. 3089,
https://doi.org/10.1007/978-1-0716-5619-8_16,
© The Author(s), under exclusive license to Springer Science+Business Media, LLC, part of Springer Nature 2027

Limitations of imaging technology prevent the imaging of circulating tumor cells (CTCs) in cancer patients at the needed resolution to characterize the metastasis process fully [6–9]. Our lab developed an alternative method to image CTC extravasation in real-time using a transgenic zebrafish model [10]. Zebrafish allow for unique imaging and transplantation capabilities as their embryos are both transparent and immunodeficient, allowing for the introduction, imaging, and growth of human/mammalian tumor cells [11–13]. Using this approach, we discovered that CTCs utilize the recently characterized extravasation method, *angiopellosis*, to exit blood vessels [14, 15]. Additionally, we found that CTC clusters exclusively extravasate through angiopellosis, leading to an increased propensity for tumor growth at distant sites, a phenomenon known as the *cancer exodus hypothesis* [5, 10, 14, 16].

Here, we demonstrate the use of a transgenic zebrafish model allowing for the targeted imaging and isolation of extravasation-participating endothelial cells and extravasating melanoma cells. By using light sheet microscopy, we were able to image infused melanoma cells and observe their movement and extravasation behaviors. Then, using the photo-convertible EosFP, exclusively expressed in endothelial cells and melanoma cells, we developed a method to select for extravasation-positive/participating cells [17]. These techniques are applicable to multiple cancer types and can be used to interrogate the effect of molecules, drugs, and genes at the cellular and molecular levels [16, 18–21].

2 Materials

2.1 Zebrafish Tumor Injections

1. Transgenic zebrafish lines: *Tg(fli1a:EGFP)* and *Tg(kdrl:eosFP)*.
2. E3 Medium for zebrafish embryo: 5 mM NaCl, 0.17 mM KCl, 0.33 mM CaCl2, 0.33 mM MgSO4, and 10^{-5}% Methylene Blue in ddH_2O.
3. 0.2 mM N-phenylthiourea (PTU).
4. Tricaine (3-amino benzoic acidethylester).
5. PV830 Pneumatic Pico pump and a manipulator (WPI).
6. OmniPur® Agarose, Low Melting.
7. Zebrafish Microinjection and Transplantation Kit (AgnThos).
8. Borosilicate glass capillary needles (1 mm o.d. × 0.78 mm i.d.).
9. 200 × 15 mm Petri dishes coated with 3% agarose.

2.2 Melanoma Cell Culture and Preparation

1. Tumor cell growth medium: IMDM medium supplemented with 10% (v/v) fetal bovine serum, 2 mM L-glutamine, 100 U/ml of penicillin, and100 µg/ml of streptomycin.

2. Fluorescent DiI Membrane Stain.

2.3 Isolation of Injected Melanoma Cells from Zebrafish

1. Phosphate-buffered saline (PBS) containing 50 U/mL of penicillin and 0.05 mg/mL of streptomycin (PBS/PS).
2. TrypLE™ Express Enzyme (1×).
3. Trizol.
4. Thermomixer.
5. 96-Well plate.
6. Fluorescent Microscope with adjustable field of UV-penetration/targeting.

3 Methods

3.1 Tumor Cell Injection into Zebrafish Embryo

1. Dechorionize zebrafish embryos 48 h post-fertilization (hpf) prior to injection.
2. Anaesthetize embryos with 0.016% tricaine, and position on a 200 × 15 mm Petri dish coated with 3% agarose (*see* **Notes 1 and 2**).
3. Prepare melanoma cell suspensions at a concentration of $2.0e^6$ cells/ml in PBS for injection, keep at room temperature before implantation, and implant within 2 h (*see* **Note 3**).
4. If using nonfluorescent cells, label cells with the fluorescent cell tracker DiI according to the manufacturer's instructions (*see* **Note 4**).
5. Load up to 5 μL of the cell suspension into a single borosilicate glass capillary needle (*see* **Note 5**).
6. Perform injection using a PV830 Pneumatic Pico pump and a manipulator (*see* **Notes 6 and 7**). Inject cells approximately 50 μm above the ventral end of the duct of Cuvier where it opens into the heart (Fig. 1).
7. After implantation with mammalian cells, maintain zebrafish embryos (including non-implanted controls) at 32°C (*see* **Note 8**).
8. At the conclusion of the experiment, euthanize the remaining embryos through tricaine overdose (*see* **Note 9**).

3.2 Lightsheet Imaging of Injected Zebrafish Embryos

1. Anaesthetize injected embryos using 0.016% tricaine, and then embed in 1.3% low-melting-temperature (LM) agarose prepared in E3 medium (*see* **Note 10**).
2. Suck the embryo in the agarose into a glass tube. Using a plastic mini-plunger, push the solidified agarose section containing the embryo out of the glass tube (Fig. 2; *see* **Notes 11–13**).

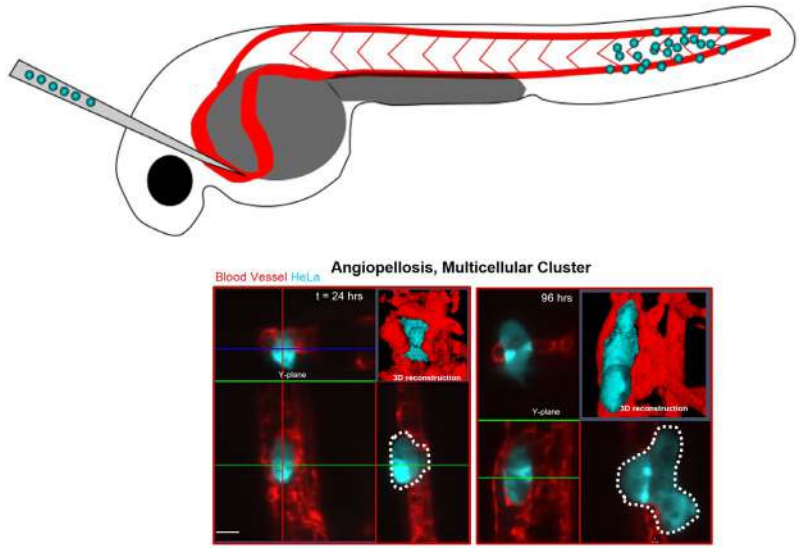


Fig. 1 Representative illustration of zebrafish tumor injection and orthographic time-lapse images of a single tumor cell cluster (cyan) following extravasation at 24 h and 96 h post-injection. Scale bar = 20 μm

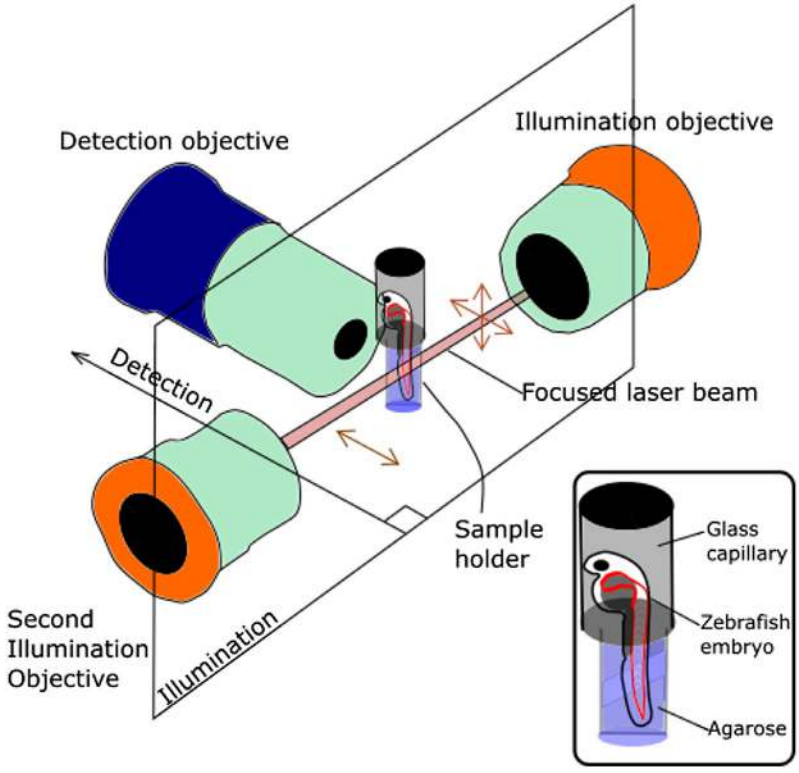


Fig. 2 Illustration of the light-sheet chamber into which zebrafish embryos were placed during the intravital time-lapse imaging

3. Fill the light sheet sample chamber with E3 medium containing 0.016% tricaine. Maintain the system temperature at 32°C throughout the imaging period.
4. Perform the fluorescent imaging using the Zeiss Lightsheet Z.1. *Z*-stacks. For timelapse (4D) images, take z-stack images every 5–15 min for a total time of up to 24 h with a step number between 50 and 200 and step size of 0.3–2.0 μm. Confirmation of injected cell migration from inside of the lumen to surrounding tissue can be done using the Zeiss ZEN software 3D retendering capability.

3.3 Isolation of Injected Tumor Cells from Zebrafish Embryos for Culturing

1. Dissect the portion of the embryo containing the extravasated tumor cells. Transfer injected embryos to PBS/PS for at least 15 min (*see* **Note 14**).
2. Refresh the PBS/PS solution once, and transfer the individual embryos to a sterile tube (embryo + 500 μL of PBS/PS) for 5 min (*see* **Note 15**).
3. Transfer the embryos to 200 μL of a 1% bleaching solution for 5 min. Then, replace the bleaching solution with PBS/PS immediately, and incubate for 5 min (*see* **Note 16**).
4. Centrifuge the embryos at 1200 × *g* for 2 min at room temperature, and discard the supernatant carefully.
5. Add 300 μl of TripLE, and incubate for 45 min at 37°C in a thermomixer, while gently mixing (*see* **Note 17**).
6. Next, pipette the embryo-TripLE mixture, with a 200-μl tip, several times up and down under sterile conditions; centrifuge immediately for 4 min at 1200 × *g* at room temperature.
7. Discard the supernatant, resuspend with 400 μl of PBS, and centrifuge again for 4 min at 1200 × *g* at room temperature.
8. Resuspend the cell pellets in 200 μl of tumor cell growth medium, and transfer cell suspension to a 96-well plate (200 μl of medium per well).
9. Allow cells to grow for at least 1 week (*see* **Note 18**).

3.4 Isolation of Extravasating Tumor Cells and Extravasation-participating Endothelial Cells for Direct Analysis

1. Inject tumor cells stably expressing EosFP into the circulation of Tg(fli1a:EGFP) or Tg(kdrl:eosFP) zebrafish embryos at 48 h post-fertilization.
2. Following the observation of CTC cluster extravasation, confirm the placement of the tumor cells as outside the blood vessel lumen using intravital microscopy (*see* **Note 19**).
3. Use targeted UV-light activation with a focused UV penetration diameter of 10 μM to photoconvert either extravasating tumor cells or extravasation-participating endothelial cells for

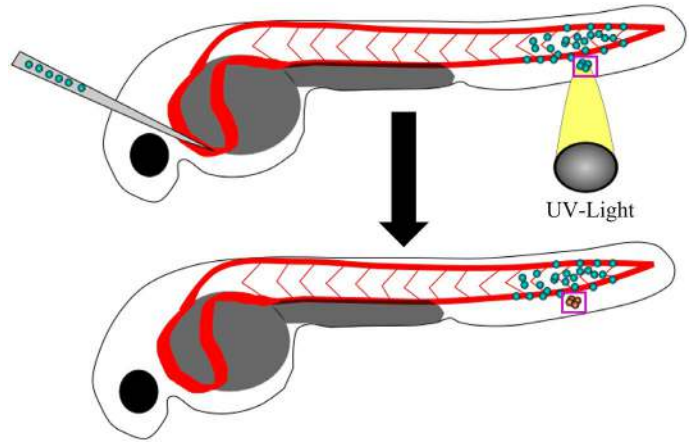


Fig. 3 Illustration of the targeted UV photo conversion of the EosFP-transduced melanoma cells following angiopellosis extravasation

at least 30 s. Visually confirm the complete transition of EosFP from GFP to RFP expression (Fig. 3; *see* **Note 20**).

4. Following activation of targeted cells, dissociate the embryos through trypsinization as previously described in Steps 1–7 of Sect. 3.3, and sort through fluorescence-activated cell sorting (FACS) directly into Trizol or a similar solution (*see* **Note 21**).

4 Notes

1. To prevent the embryo from being displaced during the injection, use an agar mold to allow the embryo to nest gently inside, with the yolk sac facing the inside of the ridge.
2. Higher amounts of tricaine will slow the heart rate and blood flow down drastically and make the injection of the cells into the circulation difficult.
3. The concentration of cells infused correlates with the type of tumor formation in the circulation. Lower concentrations will produce higher amounts of individual tumor cells, whereas higher concentrations will produce more clustered tumor cells.
4. If using a fluorescent membrane stain (such as DiO and DiI) to label the cells, be sure to wash the cells thoroughly prior to injection. If not thoroughly washed, the fluorescent particles will shed off into the blood and interfere with imaging.

5. Break the tip to create a hole just large enough to let cells comfortably out, but not too large that the solution the cells are in comes out.
6. The approximate PV830 injection parameters are: injection pressure = 300 p.s.i., holding pressure = 10 p.s.i., injection time=0.2 s. Injection parameters should be adjusted based on the size and amount of cells the investigator is aiming to inject.
7. Injected tumor cells will normally be seen entering the vasculature within 5–30 min after injection, and they begin to arrest in the vessels of the tail within 1 h of injection.
8. Normally, embryos are kept at 28°C, and the human tumor cells at 37°C. Following injection, keeping the embryos at 32°C allows for the tumor cells to survive and proliferate while also allowing the embryo to continue developing for several days.
9. Experiments were discarded when the survival rate of the control group was <80%, but some embryos will die from this process regardless.
10. 1.3% LM agarose allows for the embryo to survive for extended periods of time. This agarose percentage can be adjusted based on needed firmness.
11. Pouring the LM agarose into either an indented well or onto a piece of paraffin paper helps to suck the embryo into the tube.
12. Wait for a few moments until the LM agarose cools a bit, and place a single embryo into the melted agarose. Be careful not to place the embryo into the agarose while it is still too hot, or the fish will die. Also, LM agarose solidifies much quicker than regular agarose, so do not wait too long, because it needs to be in the liquid form for the embryos/larvae to successfully be positioned.
13. Using a glass capillary tube, specifically for Zeiss light sheet microscopes, wait at least 1 min for the agarose to solidify. If it has not completely solidified, the embryo will fall out of the tube when placed in the microscope.
14. When microdissecting the portion of the embryo, it will be extremely small— nearly invisible to the naked eye. Use care when transferring embryos, because they often will stick to the inside of tubes.
15. This step removes most contamination that would interfere with culturing the cells.
16. This step removes any additional contamination that survived the penicillin/streptomycin solution.

17. It is important to allow the embryos to incubate in the TripLE (or trypsin) for at least 40 min at 37°C. If incubated for less time, embryos will not fully dissociate, and the following steps will not work correctly.
18. It is suggested to perform this procedure with multiple injected embryos, as the success rate for culturing cells is approximately 60%, depending on cell type.
19. Light sheet microscopes are not needed for this step. Any fluorescence microscope with a DAPI wavelength and the ability to adjust the diameter of the UV-light penetration is sufficient.
20. Photo conversion will begin immediately, but for complete conversion, one must target the cells for at least 20 s or more.
21. Some of the photo-converted cells with still have trace amounts of the GFP expression along with the new RFP expression, so when using FACS, simply gating out any GFP-positive cells may remove some of the converted cells as well.

Competing Interests

The authors declare no competing interests.

References

1. Anderson RL, Balasas T, Callaghan J et al (2019) A framework for the development of effective anti-metastatic agents. Nat Rev Clin Oncol 16(3):185–204. https://doi.org/10.1038/s41571-018-0134-8
2. Miles FL, Pruitt FL, van Golen KL, Cooper CR (2008) Stepping out of the flow: capillary extravasation in cancer metastasis. Clin Exp Metastasis 25(4):305–324. https://doi.org/10.1007/s10585-007-9098-2
3. Strell C, Entschladen F (2008) Extravasation of leukocytes in comparison to tumor cells. Cell Commun Signal 6:10. https://doi.org/10.1186/1478-811X-6-10
4. Liu S, Liu M, Wang Z et al (2026) Engineering bispecific exosome activators of T cells to target immune checkpoint inhibitor-resistant metastatic melanoma. Nat Biotechnol https://doi.org/10.1038/s41587-025-02890-8
5. Aceto N, Bardia A, Miyamoto DT et al (2014) Circulating tumor cell clusters are oligoclonal precursors of breast cancer metastasis. Cell 158(5):1110–1122. https://doi.org/10.1016/j.cell.2014.07.013
6. Ambrosio M, Testa AC, Moro F et al (2020) Imaging in gynecological disease: clinical and ultrasound features of extra gastrointestinal stromal tumors (eGIST). Ultrasound Obstet Gynecol 56(5):749–758. https://doi.org/10.1002/uog.21968
7. Anfelter P, Testa A, Chiappa V et al (2020) Imaging in gynecological disease: ultrasound features of malignant ovarian yolk sac tumors (endodermal sinus tumors). Ultrasound Obstet Gynecol 56(2):276–284. https://doi.org/10.1002/uog.22002
8. Bochner F, Mohan V, Zinger A et al (2020) Intravital imaging of vascular anomalies and extracellular matrix remodeling in orthotopic pancreatic tumors. Int J Cancer 146(8):2209–2217. https://doi.org/10.1002/ijc.32759
9. Callaway NF, Mruthyunjaya P (2019) Widefield imaging of retinal and choroidal tumors. Int J Retina Vitreous 5(Suppl 1):49. https://doi.org/10.1186/s40942-019-0196-5
10. Allen TA, Asad D, Amu E et al (2019) Circulating tumor cells exit circulation while maintaining multicellularity, augmenting metastatic

potential. J Cell Sci 132(17)):jcs231563. https://doi.org/10.1242/jcs.231563
11. Lagendijk AK, Yap AS, Hogan BM (2014) Endothelial cell-cell adhesion during zebrafish vascular development. Cell Adh Migr 8(2):136–145. https://doi.org/10.4161/cam.28229
12. Liang D, Chang JR, Chin AJ et al (2001) The role of vascular endothelial growth factor (VEGF) in vasculogenesis, angiogenesis, and hematopoiesis in zebrafish development. Mech Dev 108(1-2):29–43. https://doi.org/10.1016/s0925-4773(01)00468-3
13. Wilkinson RN, van Eeden FJ (2014) The zebrafish as a model of vascular development and disease. Prog Mol Biol Transl Sci 124:93–122. https://doi.org/10.1016/B978-0-12-386930-2.00005-7
14. Allen TA, Gracieux D, Talib M et al (2017) Angiopellosis as an alternative mechanism of cell extravasation. Stem Cells 35(1):170–180. https://doi.org/10.1002/stem.2451
15. Allen TA, Cullen MM, Hawkey N et al (2021) A zebrafish model of metastatic colonization pinpoints cellular mechanisms of circulating tumor cell extravasation. Front Oncol 11:641187. https://doi.org/10.3389/fonc.2021.641187
16. Allen TA (2024) The role of circulating tumor cells as a liquid biopsy for cancer: advances, biology, technical challenges, and clinical relevance. Cancers 16(7):1377. https://doi.org/10.3390/cancers16071377
17. Wiedenmann J, Ivanchenko S, Oswald F et al (2004) EosFP, a fluorescent marker protein with UV-inducible green-to-red fluorescence conversion. Proc Natl Acad Sci U S A 101(45):15905–15910. https://doi.org/10.1073/pnas.0403668101
18. Covassin LD, Siekmann AF, Kacergis MC et al (2009) A genetic screen for vascular mutants in zebrafish reveals dynamic roles for Vegf/Plcg1 signaling during artery development. Dev Biol 329(2):212–226. https://doi.org/10.1016/j.ydbio.2009.02.031
19. Kitambi SS, McCulloch KJ, Peterson RT, Malicki JJ (2009) Small molecule screen for compounds that affect vascular development in the zebrafish retina. Mech Dev 126(5–6):464–477. https://doi.org/10.1016/j.mod.2009.01.002
20. Li Y, Zhou Y, Li B et al (2020) WDR74 modulates melanoma tumorigenesis and metastasis through the RPL5-MDM2-p53 pathway. Oncogene 39(13):2741–2755. https://doi.org/10.1038/s41388-020-1179-6
21. Yang SL, Yan S, Niu RL, Lin XK (2009) VEGF gene silencing by cytomegalovirus promoter driven shRNA expression vector results in vascular development defects in zebrafish. Genetika 45(9):1187–1193



Chapter 17

Quantitative Mapping of Organelle Positioning in Cultured Cells Using Semi-Automated Image Analysis Pipeline

Katerina Jerabkova-Roda, Vincent Hyenne and Jacky G. Goetz

Abstract

Subcellular architecture is tightly controlled and contributes to the maintenance of cell homeostasis. Organelles are regulated in size, shape, number, and position, all of which respond to changes in the extracellular environment. Lysosomes are of particular interest as they integrate various functions in the cells (nutrient sensing, metabolism, cell migration, and adhesion), serving as signaling hubs. Their function is tightly linked to their subcellular position, and deregulation of lysosome homeostasis leads to several diseases, including cancer. Therefore, methods allowing precise analysis of organelle subcellular distribution can aid in fundamental, diagnostic, and therapeutic approaches. Here, we provide a versatile image analysis pipeline using ImageJ and CellProfiler. This workflow allows for the quantification of subcellular lysosome distribution in living and fixed melanoma cells, and it is applicable to other subcellular compartments and to various cell types.

Keywords Subcellular architecture, Organelle positioning, Live-cell imaging, Immunofluorescence, Lysosomes, Radial distribution, CellProfiler, ImageJ

1 Introduction

Melanoma progression is accompanied by changes in the transcriptional program that lead to expression of matrix-degrading enzymes and to invasion and progression into metastatic stages [1]. Large efforts were made in studying the transcriptional programs of melanoma cells, yet their functional implications on the cellular level remain elusive. Tight regulation of subcellular architecture is important for maintenance of cell homeostasis. Organelles often mediate intracellular signaling events, and based on their morphology, position

Supplementary Information The online version contains supplementary material available at https://doi.org/10.1007/978-1-0716-5619-8_17

The authors "Vincent Hyenne and Jacky G. Goetz" have contributed equally.

Kristian M. Hargadon (ed.), *Melanoma*, Methods in Molecular Biology, vol. 3089,
https://doi.org/10.1007/978-1-0716-5619-8_17,
© The Author(s), under exclusive license to Springer Science+Business Media, LLC, part of Springer Nature 2027

within the cell, and contacts with other organelles, they exert different biological functions [2]. Such plasticity, although essential, also allows cancer cells to quickly adapt to the changing environment. The Golgi apparatus is responsible for protein processing and trafficking, as well as secretion of proteins forming the extracellular matrix. In cancer, its architecture oscillates between compacted and vesicular, fragmented states, which allows it to modify the tumor microenvironment and thus stimulate cancer progression via altered protein secretion of cytokines, proteases, proteoglycans, and procollagen [3]. Also, mitochondrial morphology has a direct impact on tumor growth and metastasis. Many RAS-driven cancers have fragmented mitochondria, including pancreatic [4], lung [5], liver [6], and squamous cell carcinoma [7]. In contrast, mitochondrial fusion factor Opa1 is essential for tumor cell survival in lung adenocarcinoma [5]. Furthermore, inter-organelle contacts directly impact the subcellular architecture, as lysosome–mitochondria membrane contacts can mediate mitochondria fission [8], and contacts of lysosomes with the endoplasmic reticulum (ER) can modulate lysosome motility [9]. The endo-lysosomal system has various functions, including degradation, metabolic signaling, gene regulation, plasma membrane repair, and cell adhesion and migration [10]. In response to the environment, lysosomes are able to change their position, size, number, composition, and function [11–13], which serves as a coping mechanism to adapt to homeostatic deviations such as stress (nutritional, UV, osmotic) and mechanical forces [14, 15]. Lysosomes are transported to the cell periphery along microtubules via kinesins [16], which leads to lysosome exocytosis and contributes to cancer cell invasion [12] and chemoresistance [17] (Fig. 1A).

To understand how these processes impact cancer biology and disease outcome, it is necessary to develop methods for quick and reliable assessment of organelle subcellular distribution, as this information can provide valuable insight into mechanisms of cancer progression and diagnosis. The method described herein was optimized for lysosome positioning analysis in melanoma cells, but it is applicable to any subcellular compartment marker that can be reliably labelled by live cell imaging or by immunofluorescence. To date, several approaches to quantitatively assess lysosome positioning have been developed. These include: (i) manual scoring in a blinded setup [18]; (ii) lysosome segmentation followed by distance measurements to the nucleus [19], to the cell periphery [20], to the microtubule organizing center (MTOC) [21], and to the nearest neighbor [12, 22]; (iii) segmentation and object counting near the nucleus and in the cell periphery [17]; (iv) intensity-based quantifications, calculating the perinuclear index [23, 24], the mean distribution from edge [25], and the radial distribution between cell periphery and the nucleus [12] or the centrosome [15]. These methods often use software that is not available free of charge and commonly require the use of custom-written code. Many of these methods also rely on lysosome segmentation, which

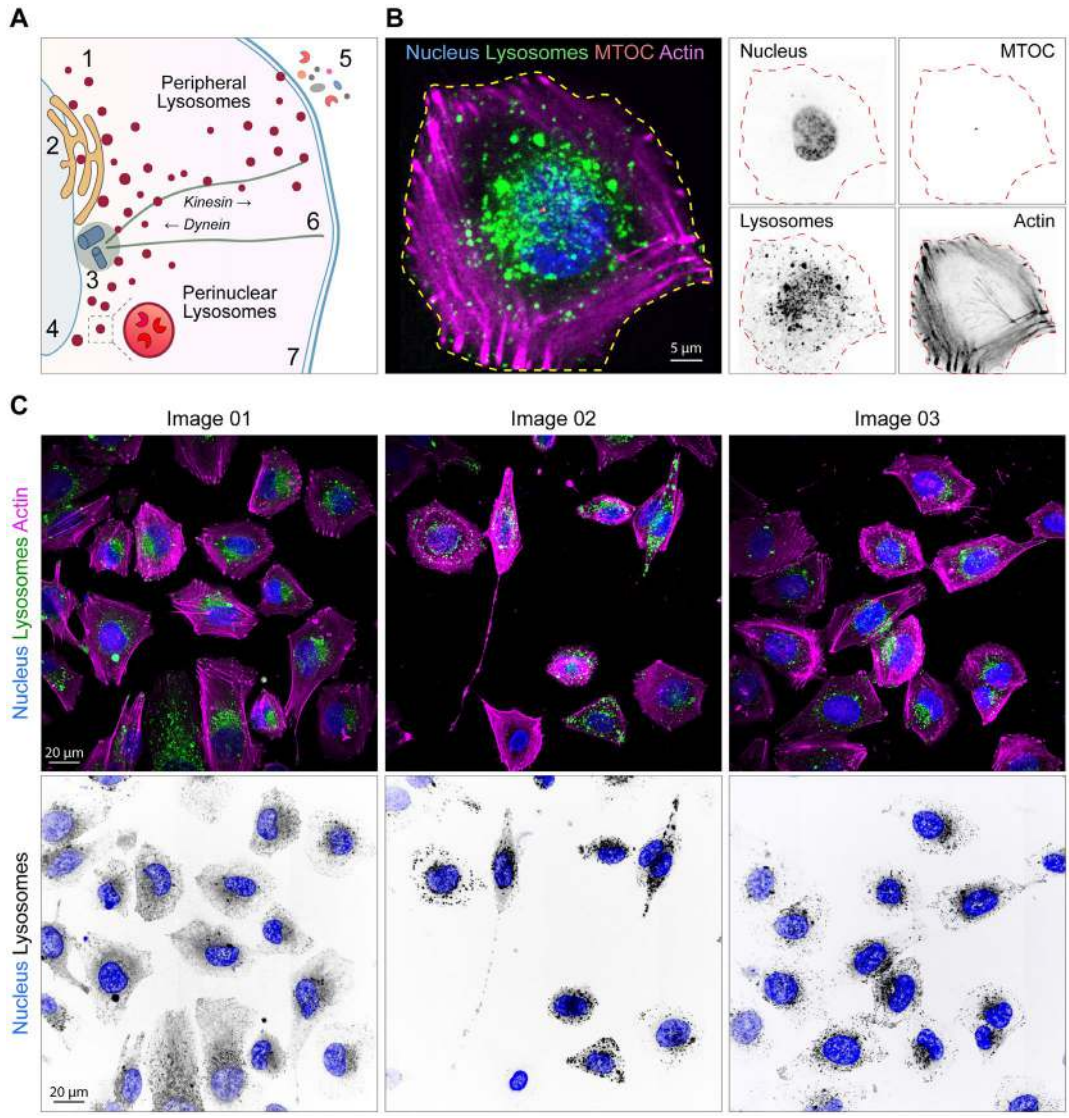


Fig. 1 Lysosome positioning in cultured melanoma cells. (**A**), Illustration of lysosomal dynamics in living cells. 1. Lysosomes, 2. Endoplasmic reticulum, 3. Centrosome, 4. Nucleus, 5. Secreted factors, lysosomal exocytosis, 6. Microtubules, 7. Plasma membrane. (**B and C**), Live-cell imaging of WM983B melanoma cells by spinning disk microscopy, maximum intensity projection. Cells are stained for lysosomes (Lysotracker green), nucleus (NucBlue), actin (SiR-Actin647, magenta), and microtubule-organizing center (stable expression of cenexin-tdTomato). (**B**), Left: Representative image of a single cell, yellow line = cell border, drawn manually. Right: Single channels showing individual markers. (**C**), Three different example images showing stained melanoma cells. Top: Composite image, merge of lysosomes (green), nucleus (blue), and actin (magenta). Bottom: Inverted fluorescent images showing the nucleus (blue) and lysosomes (gray)

can be difficult, especially when lysosomes are clustered around the nucleus. Therefore, intensity measurements represent a more versatile approach to assess lysosome subcellular distribution.

Here, we provide a robust, intensity-based analysis pipeline, using two free, open-source software, CellProfiler [26] and ImageJ/Fiji [27], together with a detailed step-by-step protocol. This protocol first describes the cell culture, cell staining, and imaging, followed by a three-step analysis pipeline: (i) cell and nucleus segmentation in ImageJ/Fiji; (ii) lysosome measurements in CellProfiler; and (iii) data visualization strategies.

2 Materials

2.1 Cell Culture, Cell Staining, and Imaging

1. Cell line: WM983B, human metastatic melanoma cell line mutant for $BRAF^{V600E}$ (*see* **Note 1**).
2. TSM medium: MCDB153 and Leibovitz's L-15 medium mixed in a 4:1 ratio, respectively, and supplemented with 2% fetal bovine serum, 1.68 mM $CaCl_2$, and 1% penicillin/streptomycin (stock 10,000 U/mL Penicillin, 10 mg/mL streptomycin).
3. Trypsin-EDTA solution (0.05% trypsin).
4. Optional: 1% EDTA (Versene) in phosphate-buffered saline (PBS), free from Ca^{2+} and Mg^{2+}.
5. 25 cm^2 flasks with filter caps.
6. Glass-bottom dishes suitable for confocal imaging with #1.5 coverslip thickness (four-chamber, 35 mm, glass-bottom dish).
7. Fibronectin coating solution: 10 μg/mL of fibronectin in water or PBS.
8. 0.4% Trypan Blue solution (to distinguish viable cells during counting).
9. Optional: Countess™ 3 Automated Cell Counter.
10. Actin Staining Solution (1×): To prepare a volume for four wells, mix 1.3 mL of TSM medium with 1.3 μL of SiR-actin probe (1:1000 dilution, without Verapamil). Prepare fresh prior to use.
11. Lysosome Staining Solution (2×): To prepare a volume for four wells, mix 1.25 mL of TSM medium with one drop of NucBlue Live Probe and 2.5 μL of Lysotracker green (from a 50 μM stock, such that the final staining concentration is 50 nM) (*see* **Note 2**). Prepare fresh prior to use.
12. Inverted Spinning Disk microscope (with a 60× objective, NA 1.2 or similar), equipped with a humidified chamber keeping the temperature at 37°C with a 5% CO_2 atmosphere (essential for live-cell imaging).

2.2 Analysis Pipeline Software

1. ImageJ/Fiji (version 1.54p, Java 21.0.7) [27].
2. MorphoLibJ ver-1.6.5.jar plugin for Fiji [28]. Downloaded from github.com/ijpb/MorphoLibJ/releases.
3. CellProfiler (version 4.2.1) [26].
4. GraphPad Prism, version 11.0.0 (84) for Windows 64-bit (GraphPad Software, Boston, MA, USA, www.graphpad.com).
5. Spreadsheet editor (Microsoft Excel or similar).

3 Methods

3.1 Cell Culture, Cell Staining, and Imaging

1. Culture the cells in a 5% CO_2 incubator at 37°C using TSM medium, and passage them 1–2 times per week at a 1:5 dilution in 25 cm^2 filter cap flasks.
2. Coat the four-compartment glass-bottom dish with fibronectin (10 μg/mL), 120 μL/coverslip, and incubate at 37°C for at least 1 h before cell seeding. Wash the dish one time with 500 μL of warm culture medium.
3. Wash cells two times with 2 ml of warm PBS, remove PBS, and add Trypsin/EDTA solution (500 μL/T25 flask). Incubate for 1 min at 37°C, and resuspend cells thoroughly in warm culture medium (5 mL/T25 flask) to achieve suspension of single cells (*see* **Note 3**).
4. Day 0: Count cells (use Trypan Blue to count the living cells, 1:1 ratio of Trypan Blue solution:single cell suspension), seed 50,000 cells per compartment, and incubate overnight at 37°C in a humidified incubator with 5% CO_2. Cells should be stained and imaged on the next day, Day 1 (*see* **Note 4**), and should be at 50%–80% confluency at the time of imaging.
5. Day 1: Stain the cells with Actin Staining Solution, using 1.3 mL per four-chamber dish in total. First, remove the culture medium, then add 300 μL of Actin Staining Solution per chamber, and incubate for 45 min at 37°C (*see* **Note 5**).
6. Preheat the microscope to stabilize the imaging chamber at 37°C with 5% CO_2 prior to imaging.
7. To stain nuclei and lysosomes, add 300 μL of Lysosome Staining Solution (2×) to each well (total volume is 600 μL/well), and incubate at 37°C for an additional 15–20 min. Following this incubation, cells are ready to be imaged (*see* **Note 6**).
8. Image cells, stained with selected markers (Fig. 1B), choosing regions where cells are not confluent (Fig. 1C), as isolated cells will be easier to segment. Acquire z-stacks of the full cell volume (z-step 0.2 μm–0.5 μm), and image at least 30 cells/

condition (~5 fields of view). Keep the same z-step and number of slices, and maintain a constant laser power and exposure time in all the images.

3.2 Analysis Pipeline

3.2.1 Step 1: Segmentation

First, segment cells and nuclei in Fiji (*see* **Note 7**). This macro saves maximum projections for each channel, generates binary masks for cells and nuclei, and saves the regions of interest (ROIs) of all segmented objects. The "Segmentation_LTrace.ijm" macro is available in the Zenodo archive [29].

1. For image preprocessing, prepare an input folder with multichannel z-stacks (three- or four-channel images are supported), saved in a TIF format.
2. Run the "Segmentation_LTrace" macro in Fiji, and select the input folder (all images in this folder will be analyzed).
3. Select the output folder (all images will be saved there). This folder will also be used as input for the next analysis step in CellProfiler.
4. Assign channels to markers for nucleus (or MTOC), target compartment (lysosomes), and cell border (actin). This macro works with three- and four-channel images (the fourth channel is not analyzed).
5. For nucleus segmentation, adjust the threshold to correctly segment all nuclei (holes will be filled in the next step using the "Fill Holes" command, and small particles will be filtered out using the "Analyze Particles" command to keep only the nuclei).
6. The cell segmentation method is based on thresholding and marker-controlled watershed (available as part of the MorphoLibJ plugin in FiJi). This macro was designed to enhance even faintly visible structures using the Enhance Local Contrast (CLAHE) command (*see* **Note 8**). Follow these steps as they appear in the macro:
   a. Adjust threshold (Li) to best capture the fine outlines of cells (holes will be filled in later steps), then adjust threshold (MinError) to have the cell area covered (eliminate holes; cells can be touching) (Fig. 2A).
   b. Cell edges are automatically created using the "Find Edges" command (Fig. 2B).
   c. Identify maxima (Fig. 2C). Important: Select "Maxima Within Tolerance" from the drop-down menu. Using "Preview," select the highest prominence number that

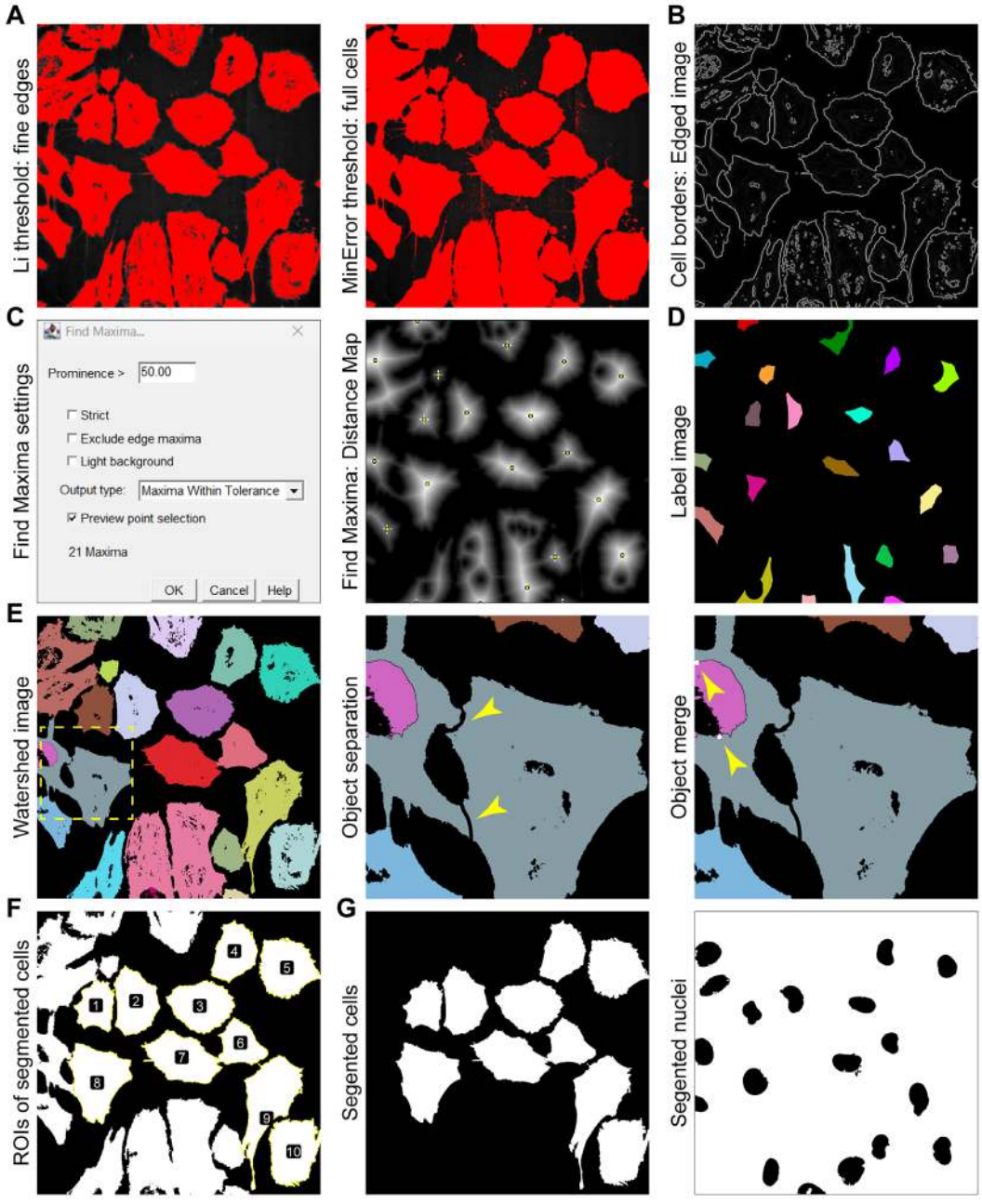


Fig. 2 Overview of analysis pipeline for Fiji (Step 1—Segmentation). (**A**), Thresholding methods for cell segmentation. (**B**), Image with cell outlines, result of Find Edges command. (**C**), Settings used to identify local maxima and thus to distinguish the individual cells. (**D**), Label image calculated from the local maxima. (**E**), Marker-controlled watershed image. Zoomed regions show examples of object separation (left) and object merge (right). (**F**), Selected cells and their ROIs, after the manual selection step. (**G**), Binary masks of segmented cells and segmented nuclei

allows identification of the individual cells. If cells are over-segmented, the prominence value is too low.

d. Marker-controlled watershed uses three images: binary cell mask (Li Threshold), Edged image (Find Edges), and Label (from Find Maxima step in Distance Map) (Fig. 2A, B, D). These images are automatically loaded to create the watershed image.

e. To refine segmentation, follow these two steps that allow for correction of segmentation errors in the original Watershed image (Fig. 2E, left). Individual objects are labeled by different colors. First, with the brush tool (size 2 pt), draw black separating lines where two cells need to be distinguished. Second, draw white lines where two objects need to be connected (Fig. 2E, right).

f. Select cells that will be analyzed for lysosome positioning. Only whole cells can be analyzed (cells spanning outside the image border should be excluded). Click on each cell with the "wand" tool, and press "t" to add this selection to the ROI manager. Repeat this step for all the cells that will be analyzed (Fig. 2F).

7. The Fiji output folder now contains three subfolders: (i) "Fluo_images_input" (containing maximum intensity projections for each channel, used in Sect. 3.2.2: **CellProfiler Analysis**); (ii) "Masks_input" (containing binary masks for segmented cells and nuclei (Fig. 2G), used in Sect. 3.3.2: **CellProfiler Analysis**); and "Other_files," which contains the ROIs of segmented objects and other images that can be used for the watershed (Edges, Label, Li threshold) or for quality control and adjustments of the segmentation (Refined binary mask, Watershed image).

3.3 Step 2: CellProfiler Analysis

1. Open the analysis pipeline "LTrace_RadialDistribution" in CellProfiler. The pipeline is available in the Zenodo archive [29], and its overview is illustrated in Fig. 3A.
2. Drag and drop the Fiji output folder to the section called "Images," and update the "NamesAndTypes" tab (Fig. 3B). Images should be automatically grouped. Verify that labels are correctly assigned to individual image sets (*see* **Note 9**).
3. Define the CellProfiler output folder in File → Preferences → Default output folder (select a path). All analysis files will be saved here.
4. The analysis pipeline generates cell and nucleus objects from the binary masks (Fiji output) and selects cells containing a single nucleus for radial distribution analysis of lysosome signal (Fig. 3C) (*see* **Note 10**).

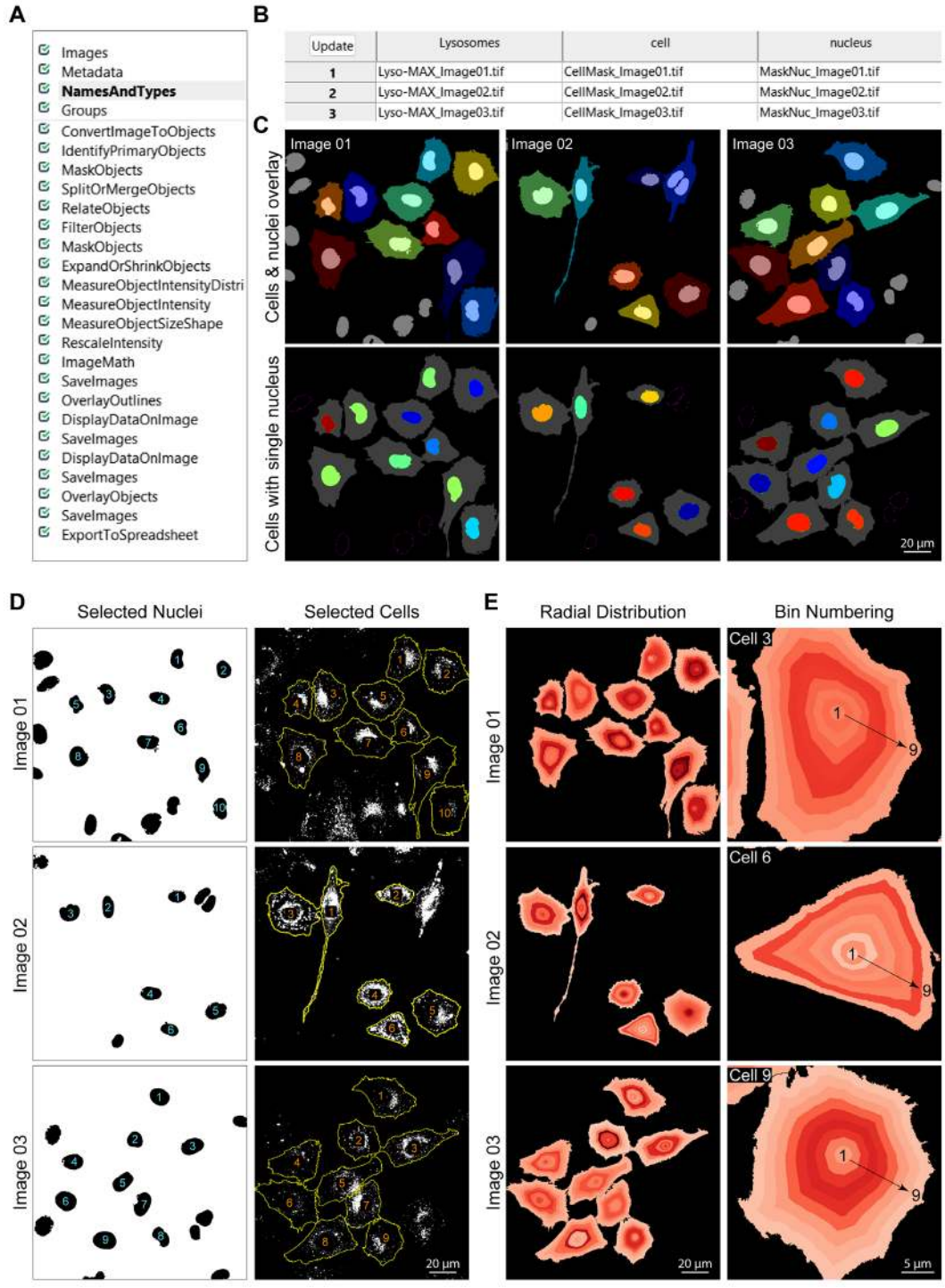


Fig. 3 Overview of the CellProfiler analysis pipeline (Step 2). (**A**), Analysis pipeline, list of all steps. (**B**), Names assigned to individual images. (**C**), Selection of cells with single nuclei for the radial distribution analysis. (**D**), Examples of CellProfiler output files. Left: the overlay image shows all segmented nuclei; numbers annotate only nuclei of analyzed cells. Right: Analyzed cells are numbered, and their outlines are overlaid on the lysosome image. (**E**), Radial distribution map is color-coded based on lysosome intensity. Dark red = high intensity. Right panel shows zoomed regions, one cell per image, showing the concentric bins, numbered from 1 (central) to 9 (peripheral)

5. The output folder contains the following:

    a. Images: (i) Cell and nuclei overlay images annotated with object numbers for each selected object (Fig. 3D). Important: Nuclei do not always have the same object number as the cells; (ii) Radial distribution maps, which represent the lysosome subcellular distribution. Each cell is divided into nine concentric segments (bins), where bin one lies close to the nucleus and bin nine lies close to the plasma membrane. Mean lysosome intensity is measured in each bin and is indicative of the lysosome localization pattern. High mean intensity value (high lysosome density) is represented by dark red color, and areas (bins) with fewer lysosomes are marked by lighter colors (Fig. 3E).

    b. Measurements: (i) "Cells_single_nuc" (This file contains measurements for the selected cells: Image and object number, file name, cell area in px = AreaShape_Area, integrated and mean lysosome intensity per cell, and Radial distribution = MeanFrac_Lysosomes bin 1–bin 9); (ii) "SelectedNuclei" (This file contains measurements for the selected nuclei: Image and object number, file name, nucleus area in px = AreaShape_Area, and several shape parameters (Compactness, Eccentricity, Form Factor, perimeter, anf major and minor axis length); (iii) Other files that are not needed for this analysis.

3.4 Step 3: Data Visualization

1. Work with the file called "Cells_single_nuc," and focus on values MeanFrac_Lysosomes" for bin 1–bin 9. These values correspond to the Radial distribution measurement. Each cell is divided into nine concentric bins, and mean lysosome intensity is provided for each bin (bin 1 = perinuclear, bin 9 = peripheral). To visualize lysosome subcellular distribution, normalize the intensity of each bin to the average intensity of bins 1–9 in each cell. Example quantification and test images are available as **Electronic Supplementary Material**.
2. Plot the normalized values in GraphPad Prism using an xy plot to visualize the lysosome distribution. As an example, we first show intensity profiles for three selected cells (Fig. 4A, B). A simplified view can be achieved by plotting area under the curve (AUC) values for the three cell regions: (i) Perinuclear (bin 1–3), (ii) Mid (bin 4–6), (iii) Peripheral (bin 7–9) (Fig. 4C). The experimental mean for each condition can be further visualized by plotting replicate values (Fig. 4D) or the individual values for each cell (Fig. 4E).
3. For quantitative assessment, plot the AUC values for individual regions: Perinuclear (bin 1–3), Mid (bin 4–6), and Peripheral (bin 7–9). AUC analysis is available in GraphPad Prism. Identify

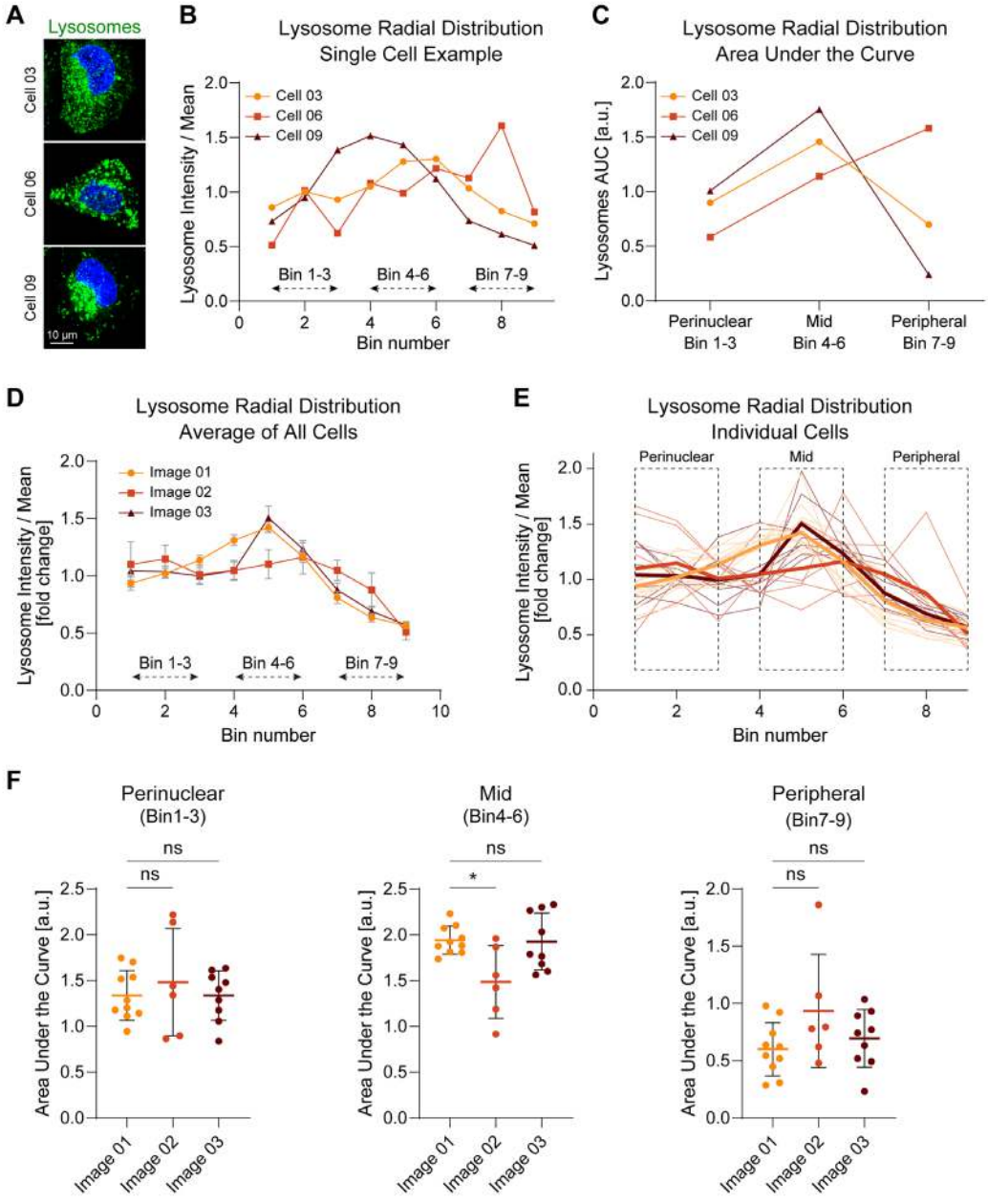


Fig. 4 Quantitative representation of lysosome subcellular distribution (Step 3). (**A**), Fluorescent images, single-cell examples, with lysosomes labeled in green and nuclei in blue. (**B**), Intensity profile for three individual cells shown as normalized radial distribution: Mean intensity in each bin, normalized to the mean intensity per cell. (**C**), Area under the curve for each cell in three different cell regions: Perinuclear, Mid, Peripheral. (**D and E**), Quantification of lysosome distribution. Image 01: $n = 10$ cells, Image 02: $n = 6$ cells, Image 03: $n = 9$ cells. Normalized radial distribution, shown as (**D**) Mean value per image and (**E**) Value per individual cells. Thick line shows the mean value per experiment. (**F**), Area under the curve quantification in the three cell regions: Perinuclear, Mid, and Peripheral, as quantified in GraphPad Prism 9. Statistics: Kruskal–Wallis with Dunn's multiple comparisons test

the smallest value in the dataset, set it as the baseline for all AUC calculations ($y = \text{MIN}$), and plot the AUC values for each region (Fig. 4F). Example quantification and test images are available as **Electronic Supplementary Material**.

4 Notes

1. The analysis described herein was optimized using a patient-derived melanoma cell line, but the protocol is suitable for any adherent cells, cancerous or noncancerous.
2. To delimit the cell borders, other dyes can be used, including SiR-Tubulin (microtubules), membrane dyes [i.e., MemGlow, CellMask, Wheat Germ Agglutinin (WGA-AlexaFluor)], or dyes staining cytoplasm (i.e., CellTrace), to name just a few. In addition, the quantification can be done on fixed samples stained by immunofluorescence, using markers for the selected compartments (i.e., LAMP1 for lysosomes, TOM20 for mitochondria, calnexin for endoplasmic reticulum, and cenexin/γ-tubulin for MTOC).
3. Cells can be washed with 1% EDTA (fast wash, or 1-min incubation at 37°C) prior to incubation with trypsin to better dissociate the cells and achieve single-cell suspension.
4. For experiments requiring gene knockdown by siRNA, seed 20,000– 30,000 cells per well, and follow the Lipofectamine RNAiMAX forward transfection protocol (24–48 h of siRNA treatment prior to the cell staining step). If reproducible cell architecture is required, cells can also be seeded on micropatterns.
5. Alternatives: (i) Cells stably expressing fluorescently tagged marker proteins can be used for live-cell imaging; (ii) Immunofluorescent labelling of selected markers can be done on fixed cells, as explained in **Note 2**.
6. To minimize autofluorescence, use cell culture medium without phenol red.
7. This step can be replaced by alternative methods for cell and nucleus segmentation that produce binary masks. Pay attention to the file names to ensure that images are properly recognized in CellProfiler. An image containing segmented cells should start with "CellMask_," and an image of segmented nuclei should start with "MaskNuc_."
8. If cells are labelled by a bright cytoplasmic marker, this step can be skipped by removing lines 171 and 180 from the macro.

9. To minimize errors, use two- or three-digit numbers (Name_01 or Name_001), and avoid using spaces in the file names.
10. This pipeline analyzes radial distribution around centers of nuclei. Distribution around MTOC is more accurate, as MTOC is not always lying at the center of the nucleus but often on the side (Fig. 1B). Segmented centrosomes can be used instead of segmented nuclei.

Acknowledgments

The work has been initially supported by the NANOTUMOR Consortium, a program from ITMO (Institut thématique multi-organisme) Cancer and ITMO BMSV (Bases moléculaires et structurales du vivant) of AVIESAN (Alliance Nationale pour les Sciences de la Vie et de la Santé, National Alliance for Life Sciences & Health) within the framework of the Cancer Plan (France). It was later supported—in the Tumor Biomechanics Lab—by INCa (Institut National Du Cancer), La Ligue contre le Cancer, ARC (Association pour la Recherche contre le Cancer), FRM (Fondation pour la Recherche Médicale), the National Plan Cancer initiative, the Region Est, INSERM, University of Strasbourg and local donators (Trailers de la Rose, Club Féminin Lampertheim, Rohan Athlétisme Saverne). We are grateful to the PIC-STRA imaging platform (CRBS, Strasbourg: P. Kessler) and members of the Tumor Biomechanics lab for their help. We acknowledge the use of ChatGPT (OpenAI, GPT-5.3; Bio-Image Analysis GPT by Robert Haase) during the initial design to decide which steps to include in the ImageJ analysis workflow. All implemented suggestions were thoroughly analyzed, validated, and verified by the authors. We also thank ChatGPT for assistance with drafting Alt Text for figures. All output was carefully reviewed and revised by the authors. We thank M. Théry (CytoMorpho Lab, Grenoble) for providing the cenexin construct to label MTOC in living cells.

Data Availability The ImageJ macro, the CellProfiler pipeline, and several example images and analysis files are available on GitHub: github.com/KJerabkovaRoda/LTrace. The ImageJ macro and the CellProfiler pipeline were deposited to the Zenodo archive: https://doi.org/10.5281/zenodo.19334736 [29]. Example images are available as **Electronic Supplementary Material**.

Conflicts of Interest The authors have no conflicts of interest to declare that are relevant to the content of this chapter.

References

1. Braeuer RR, Zigler M, Villares GJ et al (2011) Transcriptional control of melanoma metastasis: the importance of the tumor microenvironment. Semin Cancer Biol 21:83–88
2. Jerabkova-Roda K, Marwaha R, Das T et al (2024) Organelle morphology and positioning orchestrate physiological and disease-associated processes. Curr Opin Cell Biol 86:102293
3. Bajaj R, Warner AN, Fradette JF et al (2022) Dance of the Golgi: understanding Golgi dynamics in cancer metastasis. Cells 11:1484
4. Nagdas S, Kashatus JA, Nascimento A et al (2019) Drp1 promotes KRas-driven metabolic changes to drive pancreatic tumor growth. Cell Rep 28:1845–1859.e5
5. Sessions DT, Kim K-B, Kashatus JA et al (2022) Opa1 and Drp1 reciprocally regulate cristae morphology, ETC function, and NAD+ regeneration in KRas-mutant lung adenocarcinoma. Cell Rep 41:111818
6. Tian G-A, Xu W-T, Zhang X-L et al (2023) CCBE1 promotes mitochondrial fusion by inhibiting the TGFβ-DRP1 axis to prevent the progression of hepatocellular carcinoma. Matrix Biol 117:31–45
7. Kitamura S, Yanagi T, Imafuku K et al (2017) Drp1 regulates mitochondrial morphology and cell proliferation in cutaneous squamous cell carcinoma. J Dermatol Sci 88:298–307
8. Wong YC, Ysselstein D, Krainc D (2018) Mitochondria–lysosome contacts regulate mitochondrial fission via RAB7 GTP hydrolysis. Nature 554:382–386
9. Saric A, Freeman SA, Williamson C et al (2021) SNX19 restricts endolysosome motility through contacts with the endoplasmic reticulum. Nat Commun 12:4552
10. Ballabio A, Bonifacino JS (2020) Lysosomes as dynamic regulators of cell and organismal homeostasis. Nat Rev Mol Cell Biol 21:101–118
11. Eriksson I, Vainikka L, Wäster P et al (2023) Lysosomal function and intracellular position determine the malignant phenotype in malignant melanoma. J Invest Dermatol 143: 1769–1778.e12
12. Jerabkova-Roda K, Peralta M, Huang K-J et al (2025) Peripheral positioning of lysosomes supports melanoma aggressiveness. Nat Commun 16:3375
13. Sarre C, Jerabkova-Roda K, Denis V et al (2026), Selective targeting of RalA with intrabodies impairs triple negative breast cancer metastasis. bioRxiv https://doi.org/10.64898/2026.01.09.698394v1
14. Da Graça J, Delevoye C, Morel E (2025) Morphodynamical adaptation of the endolysosomal system to stress. FEBS J 292:248–260
15. Wu P-H, Onodera Y, Giaccia AJ et al (2020) Lysosomal trafficking mediated by Arl8b and BORC promotes invasion of cancer cells that survive radiation. Commun Biol 3:620
16. Pu J, Guardia CM, Keren-Kaplan T et al (2016) Mechanisms and functions of lysosome positioning. J Cell Sci 129:4329–4339
17. Machado E, White-Gilbertson S, Vlekkert Dvande et al (2015) Regulated lysosomal exocytosis mediates cancer progression. Sci Adv 1:e1500603
18. Korolchuk VI, Saiki S, Lichtenberg M et al (2011) Lysosomal positioning coordinates cellular nutrient responses. Nat Cell Biol 13:453–460
19. Steffan JJ, Snider JL, Skalli O et al (2009) Na+/H+ exchangers and RhoA regulate acidic extracellular pH-induced lysosome trafficking in prostate cancer cells. Traffic 10:737–753
20. Johnson DE, Ostrowski P, Jaumouillé V et al (2016) The position of lysosomes within the cell determines their luminal pH. J Cell Biol 212:677–692
21. Jia R, Bonifacino JS (2019) Lysosome positioning influences mTORC2 and AKT signaling. Mol Cell 75:26–38.e3
22. Mathur P, De Barros Santos C, Lachuer H et al (2023) Transcription factor EB regulates phosphatidylinositol-3-phosphate levels that control lysosome positioning in the bladder cancer model. Commun Biol 6:1–14
23. Marwaha R, Arya SB, Jagga D et al (2017) The Rab7 effector PLEKHM1 binds Arl8b to promote cargo traffic to lysosomes. J Cell Biol 216:1051–1070
24. Nair SV, Narendradev ND, Nambiar RP et al (2020) Naturally occurring and tumor-associated variants of RNF167 promote lysosomal exocytosis and plasma membrane resealing. J Cell Sci 133:jcs239335
25. Marwaha R, Manoj D, Rawal S et al (2025) Mechanosensitive dynamics of lysosomes along microtubules regulate leader cell emergence during collective cell migration. Nat Commun 17:921
26. Stirling DR, Swain-Bowden MJ, Lucas AM et al (2021) CellProfiler 4: improvements in speed, utility and usability. BMC Bioinformatics 22:433
27. Schindelin J, Arganda-Carreras I, Frise E et al (2012) Fiji: an open-source platform for biological-image analysis. Nat Methods 9:676–682
28. Legland D, Arganda-Carreras I, Andrey P (2016) MorphoLibJ: integrated library and plugins for mathematical morphology with ImageJ. Bioinformatics 32:3532–3534
29. KJerabkovaRoda (2026), github.com/KJerabkovaRoda/LTrace: v1.0 LTrace Lysosome radial distribution. Available at: https://doi.org/10.5281/zenodo.19334737, accessed Mar 30 2026.

Chapter 18

Design Strategies for Melanoma-Targeting Fluorescent Probes

Emin Sahin, Safaa Altves and Sundus Erbas-Cakmak

Abstract

Melanoma is responsible for most skin cancer-related mortalities, and clinical urgency drives the development of novel diagnostic tools. Precision diagnostics relying on fluorescence output provide many advantages, including easy and noninvasive readout and a high signal-to-noise ratio that is enabled through a change in the intensity or the wavelength of fluorescence in response to disease-associated parameters. This chapter explores the chemical design strategies for fluorescent probes, focusing on the exploitation of melanogenic enzymes, protein biomarkers, and the targeting of the dysregulated tumor microenvironment to achieve unprecedented diagnostic precision.

Keywords Melanoma probes, Design of fluorescent probes, Tyrosinase sensors

1 Introduction

Cutaneous melanoma represents a paradigmatic challenge in modern oncology: a malignancy that, while accounting for a fraction of skin cancer diagnoses, is responsible for most skin cancer-related mortalities. Between 1990 and 2021, the global incidence of melanoma surged by 182.3%, rising from approximately 107,400 cases to over 303,000 cases annually [1]. While mortality rates have stabilized in certain high-income demographics due to improved surveillance and therapies, the burden remains substantial. The disease exhibits a profound predilection for metastasis, often disseminating to the liver, lungs, bone, and brain before the primary tumor reaches a substantial size. Consequently, the margin for error in diagnosis and staging is vanishingly small [1, 2]. Conventional surveillance strategies, including ultrasonography, computed tomography (CT),, and positron emission tomography (PET), are constrained by issues of sensitivity, specificity, and radiation burden. For instance, while ultrasound offers high resolution for superficial lymph nodes, it suffers from operator dependency and a high false-positive rate (up to

Kristian M. Hargadon (ed.), *Melanoma*, Methods in Molecular Biology, vol. 3089,
https://doi.org/10.1007/978-1-0716-5619-8_18,
© The Author(s), under exclusive license to Springer Science+Business Media, LLC, part of Springer Nature 2027

5.9%), leading to unnecessary invasive procedures such as fine-needle aspiration [1]. Conversely, CT and PET/CT lack the spatial resolution to detect micro-metastases and expose patients to cumulative ionizing radiation, a nontrivial concern for younger populations or those requiring long-term surveillance [1].

The limitations detailed above have catalyzed a shift toward precision oncology, a paradigm that demands diagnostic tools capable of interrogating the tumor at the molecular level rather than merely defining its anatomical boundaries [3]. Fluorescence imaging has emerged as a frontrunner in this domain. By utilizing "smart" or activatable probes, researchers can visualize specific enzymatic activities, receptor expressions, and microenvironmental conditions (e.g., hypoxia, acidosis) in real-time with subcellular resolution [4]. These fluorescent probes are designed to have distinct photophysical properties in healthy tissue (either quenched or emitted at a different wavelength) and undergo a chemical transformation, such as cleavage, oxidation, or conformational change, only upon encountering a melanoma-specific biomarker. This "turn-on" fluorescence or spectral shift mechanism ensures a high signal-to-background ratio, enabling the detection of malignant cells that would otherwise be invisible to anatomical imaging [5]. In the first part of this chapter, distinct biomarkers associated with melanoma are summarized. In the second part, small-molecule fluorescent probes with melanoma-responsive photophysical characteristics are covered.

2 Melanoma Pathobiology Relevant to Probe Design

2.1 Melanocyte Origin, Melanogenesis, and Melanosome Biogenesis

The fidelity of a molecular probe depends on the exclusivity of its target. In melanoma, many of the most robust targets are lineage-specific proteins that are expressed during the embryonic specification of melanocytes and maintained during malignant transformation. Understanding the developmental trajectory of the melanocyte lineage from the neural crest to the terminally differentiated cell is therefore foundational for identifying antigens that are universally expressed in melanoma but absent in non-melanocytic tissues.

Melanocytes are derived from the neural crest, a transient, multipotent population of cells that arises during vertebrate neurulation. Often termed the "fourth germ layer" due to their extraordinary developmental potential, Neural Crest Cells (NCCs) undergo an epithelial-to-mesenchymal transition (EMT) at the dorsal neural tube, delaminating and migrating along defined pathways to populate diverse tissues [6, 7]. To understand the heterogeneity of melanoma, one must visualize the two distinct routes a neural crest cell can take to become a melanocyte. Recent lineage-tracing studies have refined the classical model into a dual-origin system (Fig. 1):

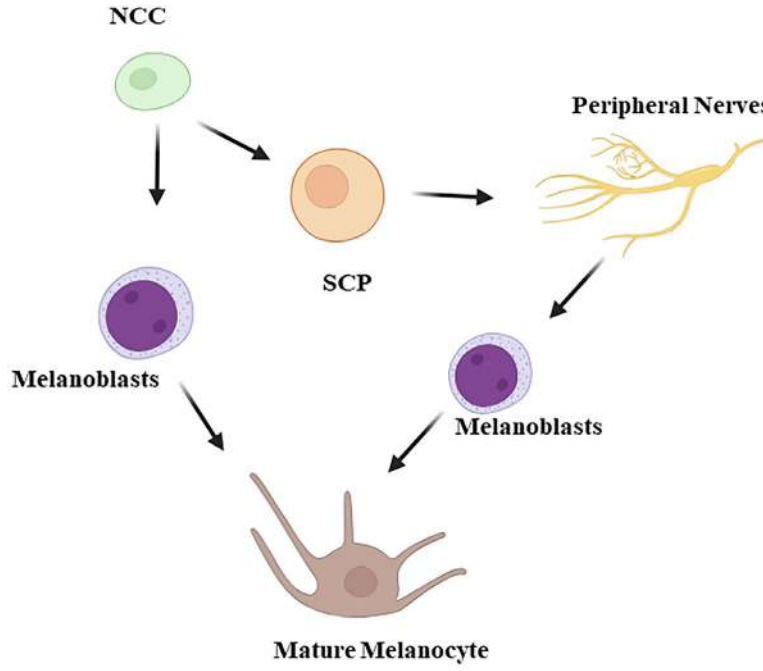


Fig. 1 Dual-origin model of melanocyte lineage specification

1. Direct Neural Crest Derivatives (The Direct Route): These cells migrate via the dorsolateral pathway, traveling between the ectoderm and the somites. They rapidly commit to the melanocytic fate, turning on lineage markers like SOX10 (SRY-Box Transcription Factor 10) and MITF (Microphthalmia-associated Transcription Factor) early to colonize the epidermis [7]
2. Schwann Cell Precursors (The Indirect Route): A significant population of melanocytes arises from Schwann Cell Precursors (SCPs). These cells initially travel ventrally to associate with developing nerve fibers. They exist in a multipotent state along the nerves and can detach to differentiate into melanocytes [7].

Melanocytes and Schwann cells share a neural-crest developmental origin, and some melanocytes arise from Schwann cell precursors along peripheral nerves. Desmoplastic (often neurotropic) melanoma commonly shows strong SOX10 and S100 immunoreactivity, so probes/markers against SOX10 or S100B can be effective in this context because these markers are shared across Schwannian and melanocytic lineages [8].

2.2 Transcription Factors as Diagnostic Markers

The molecular switch from a multipotent NCC to a committed melanoblast is governed by a gene regulatory network that remains active in melanoma. The persistence of these factors makes them critical targets for immunohistochemical probes and potentially for

genetic imaging strategies. SOX10 and MITF are among diagnostic transcription factors. SOX10 is a high-mobility group transcriptional regulator essential for the survival and maintenance of multipotency in NCCs. It is one of the earliest markers of the lineage and is required for the expression of downstream melanogenic genes. In diagnostic pathology, SOX10 is considered a pan-melanocytic marker, often more sensitive than traditional markers for spindle cell and desmoplastic melanomas [9, 10]. However, its role extends beyond specification; SOX10 creates a "permissive" epigenetic landscape for oncogenic transformation. In the context of probe design, SOX10 expression correlates with a proliferative, differentiated state. Loss of SOX10 is associated with dedifferentiation and resistance to targeted therapies, implying that SOX10-targeted probes might fail to detect highly invasive, drug-resistant subpopulations [11–13].

Regulated by SOX10 and PAX3, MITF is the "master regulator" of the melanocyte lineage. It controls the transcription of genes necessary for pigment production (Tyrosinase, TYRP1, and DCT) and melanosome structure (PMEL and MLANA). MITF operates via a "rheostat" model: intermediate levels support proliferation, high levels drive differentiation and pigmentation, and low levels promote invasion and stemness [14]. This rheostat model is critical for imaging; "high-MITF" tumors will express abundant Tyrosinase and MART-1 (good targets for enzymatic or antibody probes), while "low-MITF" tumors may lack these antigens, necessitating probes that target the neural crest stem cell markers (e.g., NGFR/p75) upregulated in this state [15, 16].

2.3 Melanosome Biogenesis: The Structural Scaffold for Probes

The defining functional characteristic of the melanocyte is the ability to synthesize melanin within specialized, membrane-bound organelles called melanosomes. Melanosomes are lysosome-related organelles (LROs) that mature through four morphologically distinct stages [17]. This maturation process creates a high density of lineage-specific proteins within the cell, offering multiple epitopes for antibody-based imaging (e.g., ^{89}Zr-labeled antibodies [18]) or targets for organelle-specific small molecules (Table 1) [19, 20].

2.4 PMEL (Premelanosome Protein) and Amyloid Formation

Stage I and II melanosomes are characterized by the presence of intralumenal fibrils derived from the protein PMEL (also known as PMEL17, GP100, or SILV). PMEL is synthesized as a transmembrane glycoprotein and cleaved in the endosome to form fragments that assemble into amyloid-like sheets [20, 21]. These fibrils serve as the scaffold upon which melanin is deposited. Because PMEL is essential for the structural integrity of the melanosome and is expressed *before* pigment synthesis begins, it is a robust target for amelanotic melanomas (which may lack melanin but still possess the organelle machinery). The monoclonal antibody HMB-45, widely used in clinical diagnostics, specifically recognizing the striated fibrils of Stage II melanosomes [22].

Table 1
Distinct morphological and molecular features at different stages of melanosomes and their relevance to probe design

Stage	Morphology	Key molecular markers	Relevance to probe design
Stage I	Spherical, vacuolar, unpigmented	PMEL (GP100), MART-1	Target for "amelanotic" melanoma detection; PMEL fibrils form the matrix.
Stage II	Ellipsoidal, striated, unpigmented	PMEL (fibrils), MART-1, TYR (inactive)	Structural proteins are abundant; ideal for immunodiagnostics (HMB-45).
Stage III	Ellipsoidal, partially pigmented	Tyrosinase (active), TYRP1, DCT	Onset of enzyme activity; target for enzyme-activatable probes.
Stage IV	Ellipsoidal, fully melanized	Melanin polymer, Rab27a	High melanin content targets benzamides and photoacoustic probes.

2.5 MART-1 (Melanoma Antigen Recognized by T-cells 1) and MC1R (Melanocortin 1 Receptor)

Also known as Melan-A, MART-1 is a transmembrane protein enriched in early-stage melanosomes. While its precise function remains partially obscure, it is thought to regulate the expression, stability, or trafficking of PMEL [23]. MART-1 is one of the most immunogenic antigens in melanoma, making it a primary target for T-cell receptor (TCR)-based therapies. For imaging, radiolabeled antibodies or peptides targeting MART-1 offer high sensitivity because the protein is abundant even in early lesions. However, like PMEL, its expression is driven by MITF, meaning it may be downregulated in dedifferentiated variants [23]. Peptide-functionalized fluorophores specifically binding to the Melanocortin1 Receptor (MC1R) are also used for selective melanoma imaging [24, 25].

2.6 Melanogenesis and Melanosome Transport

Biochemically, melanogenesis occurs within the melanosome and is strictly regulated to prevent cytosolic toxicity from reactive quinone intermediates. The enzymatic cascade process begins with the hydroxylation of L-tyrosine to L-DOPA, followed by the oxidation of L-DOPA to DOPAquinone. Both steps are catalyzed by Tyrosinase (TYR), the rate-limiting enzyme [26]. In the absence of sulfhydryls, DOPAquinone cyclizes to DOPAchrome. The enzymes TYRP1 (Tyrosinase-Related Protein 1) and DCT (DOPAchrome Tautomerase) then convert DOPAchrome into DHICA and DHI, which polymerize to form eumelanin [26]. In the presence of cysteine or glutathione, DOPAquinone reacts to form cysteinyldopas, which polymerize into pheomelanin. This pathway is mutagenic due to the generation of free radicals [26].

Once fully melanized (Stage IV), melanosomes are transported from the perinuclear region to the dendrite tips. This transport is mediated by a complex of Rab27a (a GTPase), which is upregulated

in metastatic melanoma to facilitate exosome release, making it a potential dual target for imaging invasion and pigmentation [27]. The final transfer of pigment to keratinocytes involves PAR-2 (Protease-Activated Receptor 2) signaling and is a critical step for skin pigmentation.

3 Probe Design Strategies: Responsiveness to Tyrosinase, High ROS, Metabolic Rewiring

While developmental markers define the lineage, the functional molecular features of melanoma cells (including their enzymatic activity, oxidative state, metabolic preferences, and pigment accumulation) provide the physicochemical contrast necessary for functional molecular imaging. Recent advances in chemical biology have moved beyond simple ligand-binding probes to "reaction-based" or "activatable" probes that interrogate the physiological state of the tumor.

The field of biomedical imaging has witnessed a shift toward the "rational design" of molecular probes—engineered chemical entities that integrate precise targeting capabilities, optimized photophysical properties, and responsive "smart" behaviors [28]. The development of these probes is not merely an exercise in synthetic chemistry; it is a multidisciplinary convergence of photophysics, cancer biology, and molecular engineering. The objective is to overcome the optical barriers of biological tissue scattering, absorption, and autofluorescence while exploiting the unique biochemical signatures of the melanoma microenvironment, such as upregulated tyrosinase activity, lysosomal proteases, oxidative stress, and acidic pH [29–31].

Tyrosinase (TYR) is a major molecular target for melanoma because its expression is largely restricted to the melanocytic lineage (melanocytes/melanoma; also, retinal pigment epithelium) and it is highly expressed in a large fraction of melanomas. Because TYR is an active melanosomal enzyme that catalyzes the first committed steps of melanogenesis, probe designs can exploit enzymatic amplification, where a single TYR molecule can convert many substrate (probe) molecules, potentially boosting signal compared with purely binding-based targets [32, 33]. The catalytic activity of Tyrosinase, specifically its phenol oxidase and catechol oxidase activity, has been exploited to design probes that remain "silent" (quenched or inactive) in the circulation/healthy tissue and which are activated specifically within the tumor. To achieve this goal, the following design strategies or improvements (aside from good solubility in an aqueous environment, chemical/photo-stability, and good cellular uptake) are usually addressed in the literature:

- Change in fluorescence intensity through biomarker-dependent change in the photoinduced electron transfer (PeT) efficiency

- Change in fluorescence intensity through restriction of molecular motion (i.e., Aggregation Induced Emission, AIE)
- Change in fluorescence wavelength through biomarker-dependent change in the intramolecular charge transfer (ICT)
- Overcoming the penetration limit of the light through engineering of the fluorophore structure to achieve large Stoke's shift and/or Near-IR emission
- Improving selectivity through designing biomarker-specific responsive units and/or multi-analyte sensing
- Molecular engineering to combine analyte-responsive units with the parent fluorophore (i.e., use of self-immolative linkers)

3.1 Self-Immolative Linkers in the Design of Probes

In the design of some fluorescent probes, a tyrosinase-responsive receptor unit is attached through a self-immolative linker [4-(2-aminoethyl) phenol, 3-hydroxy benzyl, or 4-hydroxy aniline], which can be spontaneously removed through linker cleavage mechanisms (Fig. 2) that include cyclization (Figs. 2a) or 1, 4 or 1, 6-elimination (Figs. 2b, c), followed by enzyme-mediated oxidation. Cyclization-dependent hydrolysis rate for 4-(2-aminoethyl) phenol-attached urea can take place within 20 min when the urea is in a diphenylamine

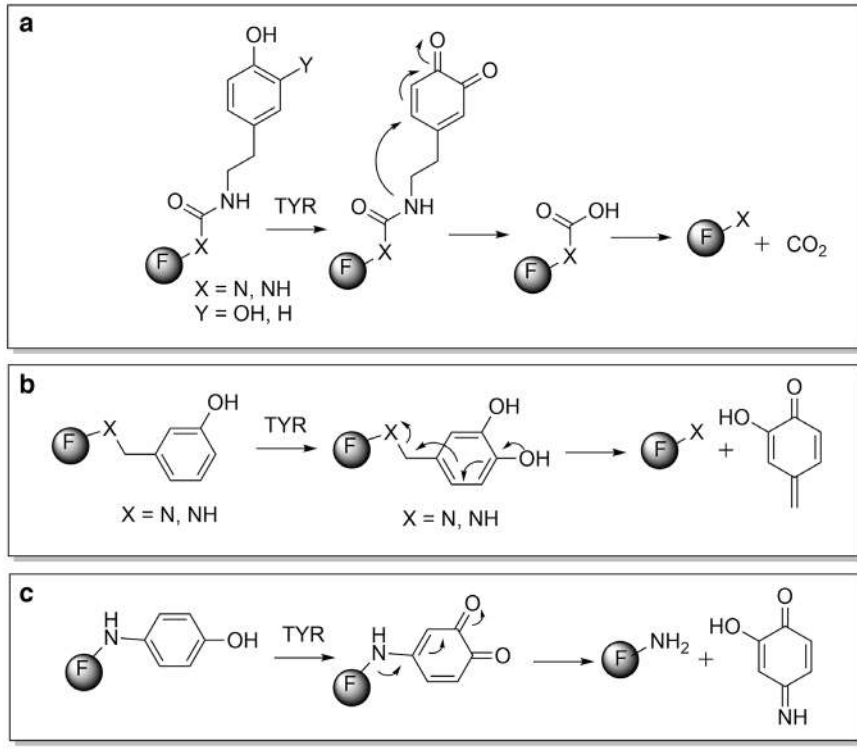


Fig. 2 Mechanism of self-immolative linker cleavage: cyclization (**a**) or elimination (**b** and **c**)

or *N*-methylaniline structure. Fluorophores are mostly functionalized on their OH or NH groups using ester, amide, or urea linkages.

3.2 Fluorescent Probes with PeT Mechanisms

The PeT mechanism relies on electron transfer in the excited state between the core fluorophore and the auxiliary group. For efficient electron transfer the donor and acceptor groups should be in close proximity. The process depends on the relative HOMO-LUMO levels of the groups when the fluorophore is in the excited state, which determines the direction and efficiency of electron transfer. Enzyme-dependent chemical modification alters the HOMO-LUMO energies and directly modulates PeT efficiency. Tyrosinase enzymes can catalyze the oxidation of phenols up to quinones, and this property is widely used to modulate PeT efficiency (Fig. 3).

One of the earlier examples of PeT-based tyrosinase fluorescence sensors (Table 2) was developed by Kim et al. [34]. **Probe 1** is a boradiazaindacene (BODIPY) fluorophore functionalized with 3,4-dihydroxyphenyl at the *meso* position. Photoinduced electron transfer from the 3,4-dihydroxyphenyl to the excited core fluorophore quenches the emission, with a calculated quantum yield (f_F) of 0.001. When the probe is incubated with melanoma biomarker tyrosinase in the presence of O_2, oxidation of the probe to quinone decreases the PeT efficiency. The resulting quinone derivative emits at 515 nm upon excitation at 465 nm with an 18-fold increase in quantum yield. The probe can detect tyrosinase as low as 0.5 nM and selectively over alcohol dehydrogenase (ADH). Bioimaging with tyrosinase-expressing B16-F10 mouse melanoma cells demonstrates the success of enzyme detection. An increase in emission upon application of melanin-stimulating hormone (α-MSH, 100 nM) was reported, and this emission is reduced when the cells are incubated with tyrosinase inhibitors kojic

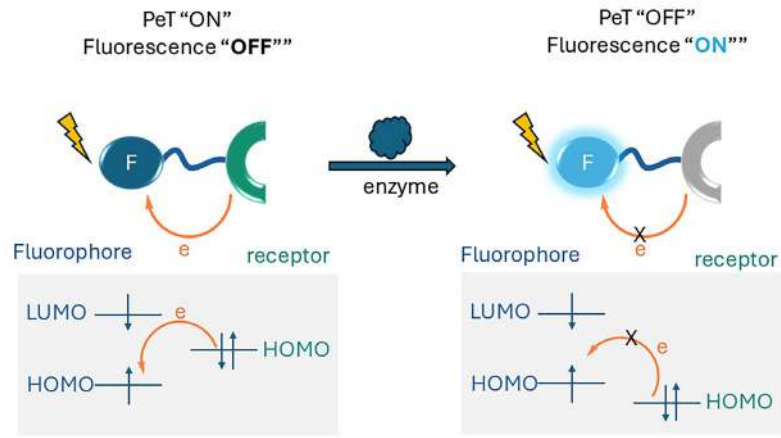


Fig. 3 Mechanism of PeT. Change in the energy levels of the receptor module on the probe by the enzymatic conversion modulates the PeT efficiency and the photophysical properties of the fluorophore unit

Table 2

Structures and photophysical properties of fluorescent TYR probes having turn-on/turn-off response through PeT or oxPeT mechanisms

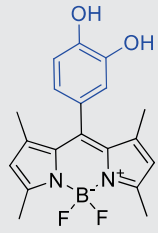
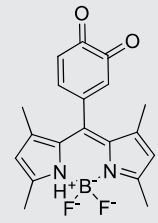
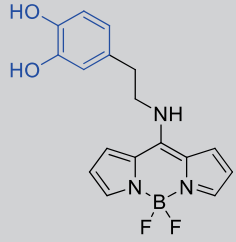
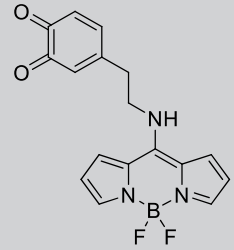
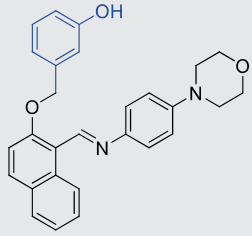
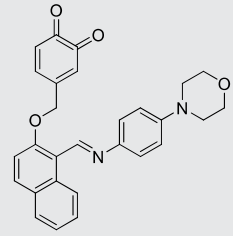
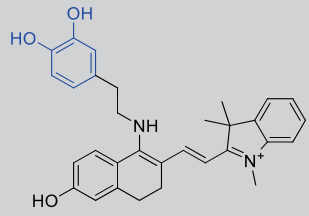
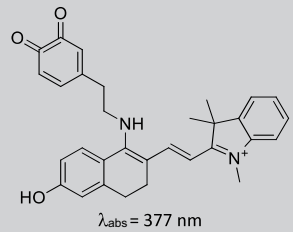
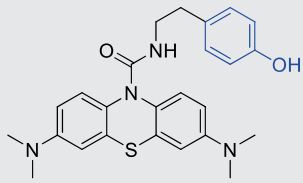
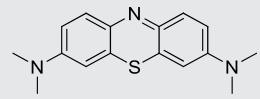
Probe no	Probe structure 1	Probe structure 2[a]	Fluorophore/ Mechanism/ LOD	Ref
1	 λ_{abs} = 496 nm λ_{fluo} = 512 nm $\Phi_F \approx 0.001$ K_m = 5.3 μM	 λ_{abs} = 498 nm λ_{fluo} = 515 nm Φ_F = 0.018	BODIPY (PeT) LOD = 0.5 nM	[34]
2	 λ_{abs} = 400 nm λ_{fluo} = 452 nm	 λ_{abs} = 400 nm λ_{fluo} = 452 nm λ_{exc} (two photon)= 740 nm	BODIPY (PeT) LOD = 0.025 U mL^{-1} 2.5×10^{-2} U mL^{-1}	[35]
3	 λ_{fluo} = 675 nm K_m = 87.35 μM	 λ_{abs} = 290 nm/480 nm λ_{fluo} = 675 nm	MNP (PeT) LOD = 0.5 U mL^{-1}	[37]

Table 2 (continued)

Probe no	Probe structure 1	Probe structure 2[a]	Fluorophore/ Mechanism/ LOD	Ref
4	 λ_{abs} = 538 nm λ_{fluo} = 629 nm Φ_F = 0.0395	 λ_{abs} = 377 nm λ_{fluo} = 629 nm	Hemicyanine (oxPeT) LOD = 0.003 U mL^{-1}	[38]
5	 K_m = 4.6 μM	 λ_{exc} = 640 nm λ_{fluo} = 706 nm	MB	[39]

[a]Probe structure 2 is the structure of the molecule generated upon TYR-mediated chemical conversion TYR-responsive units are shown in blue

acid or miconazole (100 mM or 30 mM, respectively), demonstrating tyrosinase dependency of the resulting emission.

Using a similar tyrosine-responsive unit and the same core BODIPY fluorophore, Naidu et al. reported a tyrosinase-activatable PeT-based two-photon **Probe 2** [35]. The two-photon approach is based on excitation of the probe with a longer wavelength two photons, preferentially in infrared region of the electromagnetic spectrum, in order to achieve higher tissue penetration depth. Compared to traditional imaging techniques, femtosecond laser pulses are used as excitation sources, which enable local excitation, minimum absorption by the tissue, and reduced damage. Two-photon absorption cross-section ($\sigma\Phi_F$) is an important parameter for such probes for practical applications. High $\sigma\Phi_F$ values, around 300 GM, can be achieved by using conjugated molecules with electron donor and acceptor groups [36]. Upon incubation with tyrosinase, **Probe 2** emission at 452 nm increased 12.5-fold in PBS buffer upon excitation at 400 nm, allowing the detection of 2.5×10^{-2} U mL^{-1} enzyme. Selectivity of probe for tyrosinase was evaluated using various reactive oxygen species (ROS), metal ions, all amino acids, ascorbic acid, and glutathione (GSH), and none of the analytes displayed a significant change in emissions. Two-photon imaging is achieved with 740 nm excitation in B16-F10 melanoma cells, which are either pretreated

with H_2O_2 (50 mM) to stimulate tyrosinase, or an exogenous enzyme (100 U mL^{-1}) is added. Dose-dependent decrease in the fluorescence intensity upon treatment with kojic acid (10, 50, and 100 mM) further proves the enzyme dependency of the optical response.

In a study reported by Peng et al. selective accumulation of the probes in melanosomes is achieved by incorporating a morpholine targeting unit on the fluorophore (**Probe 3**) [37]. 1-(((4-morpholinophenyl)imino)methyl)naphthalen-2-ol (MNP) is functionalized with selective tyrosinase pseudo-substrate m-phenol. 48-fold probe emission enhancement was monitored at 675 nm with a 195 nm Stokes shift when irradiated at 500 nm upon oxidation of the phenol to quinone by the tyrosinase. The detection limit of this highly sensitive PeT-based tyrosinase probe is calculated to be 0.5 U mL^{-1} and the Michaelis constant (K_m) is determined to be 87.35 mM. The probe is insensitive to ROS, biological cations, and oxidase enzymes. Fluorescence can be detected in B16-F10 cells compared to cells with low tyrosinase expression. Additionally, when the tyrosinase expression was induced in poorly invasive OCM-1A and highly invasive M619 uveal melanoma cells by preincubating the cells with 8-methoxypsoralen (50 μM) for 12 h and irradiation with UV-A (1.0 J/cm^2), significantly enhanced emission was detected. The fluorescence intensity is reduced upon treatment with kojic acid (100 mM) 3 h prior to probe application. Co-localization analysis indicates a good melanosome targeting (Pearson's correlation coefficient = 0.88). The time-dependent density functional theory (TD-DFT) calculations indicate that the HOMO level of the receptor module (*m*-hydroxy phenyl) decreases from −5.41 eV to 6.57 eV upon oxidation, hence indicating blocking of the PeT.

Li et al. used dopamine to design a selective hemicyanine-based probe with good aqueous solubility (**Probe 4**) [38]. As the tyrosinase oxidizes the catechol to dopaquinone, the fluorescence emission at 629 nm is quenched. A "turn-off" response is obtained due to an oxidative PeT (oxPeT) resulting from electron transfer from the excited fluorophore to the dopaquinone. The detection limit was determined as 0.003 U mL^{-1}. Probe selectivity was evaluated towards ions, amino acids, enzyme species, and different biomolecules, and the probe showed better selectivity for tyrosinase. In vitro experiments with HEPG2 liver cells show time-dependent decreases in emissions in the absence of kojic acid. The probe displays similar quenching in vivo in zebrafish larva.

Li et al. reported a careful optimization of the spontaneous hydrolysis rate of urea-linked TYR-responsive units on a fluorophore scaffold and decreased the response time from around 3 h to 20 min [39]. Urea with a diphenylamine or *N*-methylaniline group was determined to have a higher spontaneous hydrolysis rate and hence was selected for urea-type tyrosinase probe design (**Probe 5**). 4-(2-aminophenyl) phenol was selected as a suitable TYR-responsive unit to eliminate steric hindrance of the fluorophore on the catalytic side of the tyrosinase enzyme. Tyrosinase activity leads to intramolecular cyclization

between NH of reduced methylene blue (MB) and quinone, and the fluorescence emission increases 100-fold within 20 min at 706 nm upon excitation with 640 nm light. K_m value is calculated to be 4.6 mM. In vitro imaging potential of the probe was demonstrated in B16-F10 cells with or without 1 mM kojic acid inhibitor. A similar tyrosinase-responsive unit is used by Yan et al. with 6-acyl-N-methyl-2-naphthylamine probe achieving a TYR-dependent turn-on response [40].

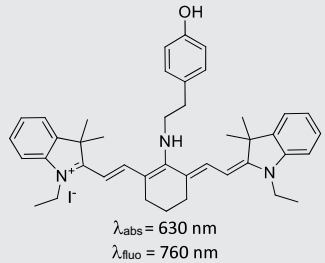
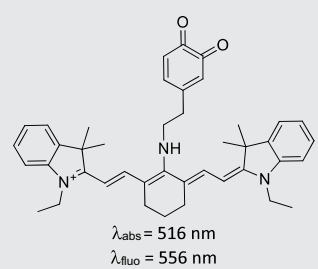
3.3 Fluorescent Probes with AIE Mechanisms

Restriction of molecular motion in the solid state or molecular assemblies can reduce dissipation of excited-state energy and lead to an enhanced emission with large Stokes shift for some probes, so called aggregation-induced emission (AIE) (Table 3) [41]. Zhang et al. developed cyanine-based **Probe 6**, substituted with phenol [42]. Upon tyrosinase-mediated oxidation to o-benzoquinone, H-aggregation is observed, leading to a ratiometric change in emission from 760 nm to 560 nm. Dynamic Light Scattering (DLS) analysis proved that the aggregation depends on tyrosinase activity, and enzyme treatment leads to a 400-fold increase in particle size. The detection limit is determined to be 0.02 U mL^{-1}. Analytes such as ions, ATP, amino acids, Bovine Serum Albumin (BSA), lysozyme, and H_2O_2 are not interfering with the fluorescence properties of the probe.

3.4 Fluorescent Probes with ICT Mechanisms

Fluorophores having substituents with electron donor and acceptor character display distinct photophysical properties, and intramolecular charge transfer (ICT) can be modulated by a chemical change on substituents (Fig. 4). Many tyrosinase fluorescent probes use this method (Table 4), mostly through caging of the electron donor group with tyrosinase-responsive units described above. Enzymatic conversion that changes the ICT character of the fluorophore usually changes the HOMO-LUMO gap, leading to a large shift in

Table 3
Fluorescent TYR probe using the AIE mechanism

Probe no	Probe structure 1	Probe structure 2[a]	Fluorophore/ LOD	Ref
6			Cyanine (AIE) LOD = 0.02 U mL^{-1}	[42]

[a]Probe structure 2 is the structure of the molecule generated upon TYR-mediated chemical conversion

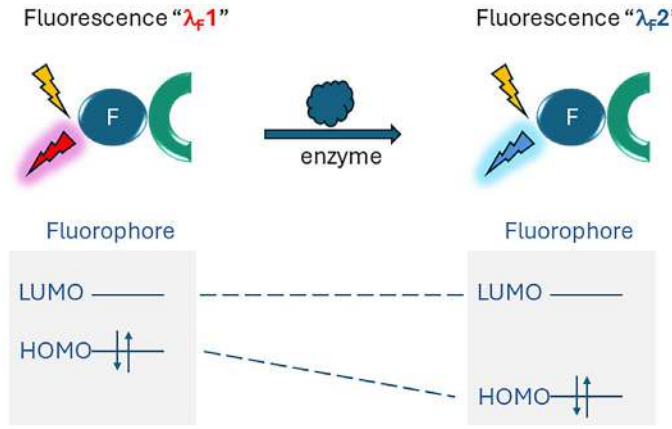


Fig. 4 Mechanism of ICT. Change in the energy levels of the fluorophore by the enzymatic conversion modulates the ICT character, leading to a change in fluorescence wavelength and/or intensity

emission or a change in emission intensity. When a fluorescence shift is observed, normalization of the emission intensities with the value at an unchanged isobestic point can yield a reliable, ratiometric output, independent of environmental perturbations.

A strong TYR-dependent fluorescence is observed in **Probe 7** when the electron-donating amine is exposed [43]. Resorufin dye is non-emissive when the hydroxyl group is caged. Wu et al. incorporate a TYR-responsive m-hydoxy phenyl substituent, which is also stable in the presence of ROS, on resorufin to obtain **Probe 8** [44]. The compound is non-emissive with a quantum yield of 0.007. Upon the tyrosinase-mediated oxidation, the resulting 3,4-dihydroxypneyl is eliminated spontaneously, leading to emission enhancement at 586 nm in PBS when excited at 550 nm. The detection limit of the probe is determined as 0.04 U mL^{-1}. Probe has no response to various potent interfering species such as inorganic salt, amino acids, some enzymes, or ROS. Probe gives strong fluorescence in tyrosinase-expressing B16-F10 melanoma cells as opposed to liver and breast cancer cells. A similar approach was used by the Sidhu group to functionalize the naphthalimide fluorophore to make **Probe 9** [45]. After the TYR-dependent cleavage, the strong donor character of the free amine enhances the ICT character of the probe, changing the emission wavelength from 467 nm to 537 nm and enabling ratiometric sensing. Limit of detection (LOD) was calculated as 0.2 U mL^{-1}. A similar naphthalimide-based fluorophore was functionalized with p-toluenesulfonamide to enable endoplasmic reticulum targeting (ER) [46]. ER-localized TYR activity was monitored in melanoma cells as the probe emission shifts from 480 nm to 550 nm. The detection limit was calculated as 5.64 U mL^{-1}. Another naphthalimide-based fluorophore was functionalized with morpholine to enable

Table 4
Structure and photophysical properties of tyrosinase probes using ICT mechanism

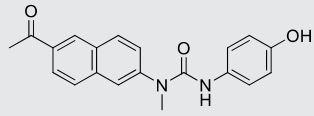
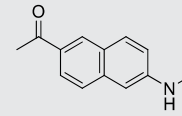
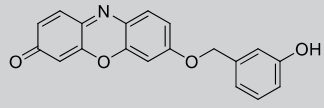
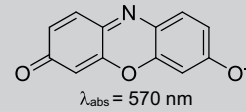
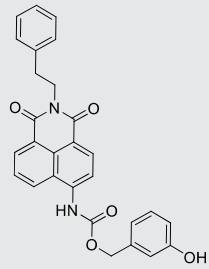
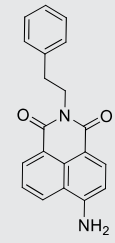
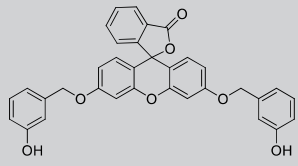
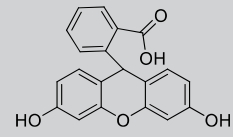
Probe No	Structure 1	Structure 2[a]	Fluorophore/ LOD	Ref.
7		 λ_{abs} = 382 nm λ_{fluo} = 503 nm λ_{exc} = 770 nm (two photon)	6-acyl-N-methyl-2-naphthylamine	[43]
8	 λ_{abs} = 470 nm $\Phi_F \approx$ 0.007 K_m = 30μM	 λ_{abs} = 570 nm λ_{fluo} = 586 nm	**Resorufin** LOD = 0.04 U mL^{-1}	[44]
9	 λ_{fluo} = 467 nm K_m = 43.5 μM	 λ_{exc} = 425 nm λ_{fluo} = 535 nm	Naphthalimide LOD = 0.2 U mL^{-1}	[45]
10	 λ_{abs} = 460 nm λ_{fluo} = 517 nm Φ_F = 0.031 K_m = 16.07 μM	 λ_{abs} = 460 nm λ_{fluo} = 517 nm Φ_F = 0.85	Fluorescein LOD = 0.127 U mL^{-1}	[48]

Table 4 (continued)

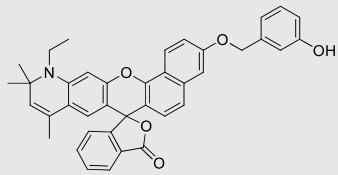
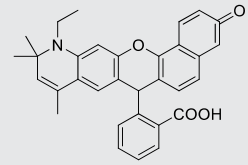
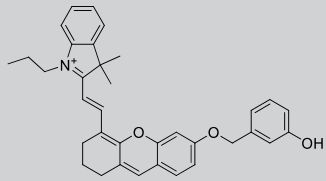
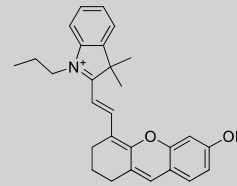
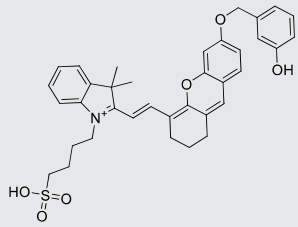
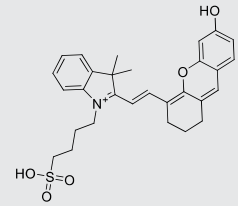
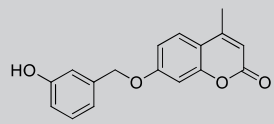
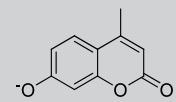
Probe No	Structure 1	Structure 2[a]	Fluorophore/ LOD	Ref.
11	 λ_{abs} = 587 nm λ_{fluo} = 650 nm Φ_F = 0.016	 λ_{abs} = 587 nm λ_{fluo} = 650 nm Φ_F = 0.22	Rhodamine LOD = 0.45 U mL^{-1}	[49]
12	 λ_{abs} = 650/600 nm λ_{fluo} = 670 nm Φ_F = 0.013	 λ_{abs} = 654/604 nm λ_{fluo} = 708 nm Φ_F = 0.20	Hemicyanine LOD = 2.76 U mL^{-1}	[50]
13	 λ_{abs} = 600 nm	 λ_{abs} = 670 nm λ_{fluo} = 708 nm Φ_F = 0.18	Hemicyanine LOD = 0.11 μ g mL^{-1}	[51]
14	 λ_{abs} = 325 nm $\Phi_F \approx$ 0.006	 λ_{abs} = 325 nm λ_{fluo} = 454 nm λ_{exc} = 740 nm (two photon)	Coumarin LOD = 0.34 U mL^{-1}	[52]

Table 4 (continued)

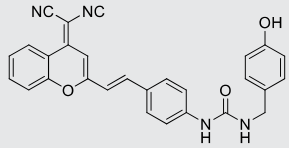
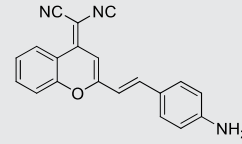
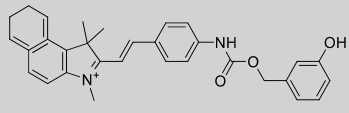
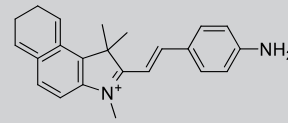
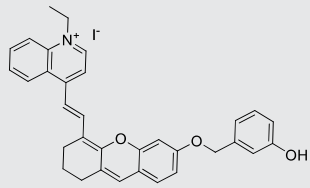
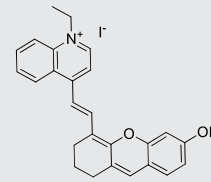
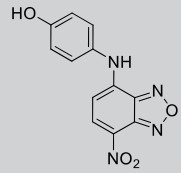
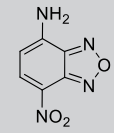
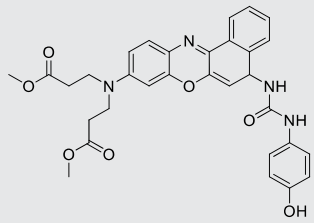
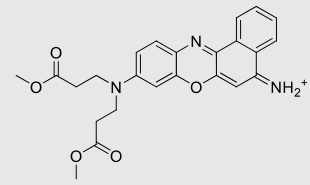
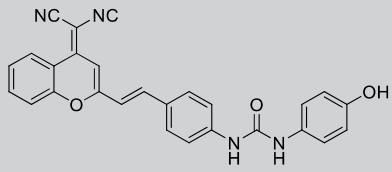
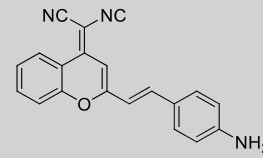
Probe No	Structure 1	Structure 2[a]	Fluorophore/ LOD	Ref.
15	 λ_{abs} = 453 nm λ_{fluo} = 570 nm	 λ_{abs} = 480 nm λ_{fluo} = 662 nm	DCM	[53]
16	 λ_{abs} = 445 nm λ_{fluo} = 580 nm Φ_F = 0.0172	 λ_{exc} = 500 nm λ_{fluo} = 580 nm Φ_F = 0.2467	*p*-aminostyryl benzindole LOD = 1.024 U mL^{-1}	[54]
17		 λ_{exc} = 610 nm λ_{fluo} = 740 nm Φ_F = 0.30	EQR LOD = 0.035 U mL^{-1}	[55]
18		 λ_{exc} = 460 nm λ_{fluo} = 540 nm	7-nitrobenzo [c] [1,2,5]oxadiazol-4-amine	[56]

Table 4 (continued)

Probe No	Structure 1	Structure 2[a]	Fluorophore/ LOD	Ref.
19	 $\lambda_{abs} \approx 510$ nm $\lambda_{fluo} = 660$ nm $\Phi_F = 0.02$	 $\lambda_{exc} = 580$ nm $\lambda_{fluo} = 660$ nm $\Phi_F = 0.23$	Phenoxazine	[57]
20	 $\lambda_{exc} = 450$ nm $\lambda_{fluo} = 548$ nm	 $\lambda_{exc} = 453$ nm $\lambda_{fluo} = 660$ nm	DCM LOD = 0.6 U mL^{-1}	[58]

[a]Probe structure 2 is the structure of the molecule generated upon TYR enzyme conversion

lysosome and lysosome-like organelles [47]. The ratiometric probe detects tyrosinase activity as low as 0.4 U mL^{-1} and can be used to monitor tyrosinase accumulation in lysosomes or lysosome-like organelles such as the melanosome. Orbital energies of fluorescein-based **Probe 10** were calculated, and a 1.52 eV decrease in HOMO-LUMO gap was determined upon TYR-mediated conversion [48]. The probe displays a strong emission at 517 nm in response to TYR. With a rhodamine-based fluorophore (**Probe 11**), Song et al. obtained TYR-induced Near-IR emission at 650 nm upon excitation at 587 nm [49]. The quantum yield of the compound increased 13.75-fold (0.016–0.22) after the enzyme-mediated elimination. The enzyme detection limit was calculated to be 0.45 U mL^{-1} for this probe. The probe has a large Stokes shift, 63 nm, which significantly eliminated self-quenching.

Hemicyanine modified with a 3-hydroxy benzyl group (**Probe 12**) displays a Near-IR emission at 708 nm when excited at 670 nm [50]. Quantum yield increases 15-fold (0.013 to 0.20) when TYR is applied, and the detection limit is 2.76 U mL^{-1}. ROS do not interfere with the fluorescence signal even at concentrations higher than physiologically relevant values. Fluorescence is detected to be 1.6-fold higher in B16-F10 melanoma cells compared to HeLA. Three-day-old

zebrafish have been used for imaging in vivo TYR. With **Probe 13**, the same scaffold bearing sulfobutyl is developed to achieve better aqueous solubility. Emission at 708 nm with quantum yield 0.18 is observed, where the detection limit is calculated to be 0.11 mg mL^{-1} [51]. TYR level has been detected in a 5-week-old BALB/c nude mouse model. Structure and photophysical properties of other 3-hydroxy-benzyl-substituted ICT probes based on coumarin (**Probe 14**), dicyanomethylene-4H-pyran (DCM, **Probe 15**), *p*-aminostyryl benzindole (**Probe 16**), and EQR with a high 130 nm Stokes shift (**Probe 17**) are also shown in Table 4 [52–56].One other group of ICT-based sensors uses 4-hydroxy phenyl urea as a TYR-responsive group (**Probes 18–20**), which spontaneously cleaves upon oxidation to quinone [57, 58]. Metastasis to the lung and spleen can also be detected with **Probe 19** in xenogeneic mouse models.

3.5 Multi-Analyte Sensing Approach

One-lock tyrosinase-detecting fluorescent probes might have false-positive results since this enzyme is also found in normal melanocytes. To deal with this problem, researchers have designed two or more analyte-sensitive probes enabling multiple biomarker detection simultaneously without interference (Tables 5 and 6). Multianalyte sensing enables sensing of more than one analyte or regioselective control over probe activity. For melanoma disease, microenvironment is widely used as a guiding diagnostic method to eliminate false positive results. Melanoma cells exist in a state of chronic oxidative stress, with basal ROS levels significantly higher than those of normal melanocytes or other skin cells [26]. This "oxidative signature" is driven by pheomelanogenesis, NADPH oxidases (NOX), or metabolic dysregulation. The synthesis of pheomelanin consumes glutathione and generates superoxide anion (O_2^-) as a byproduct [59]. Multiple NOX isoforms (including NOX5 and, in some contexts, NOX4/NOX1) have been implicated in melanoma ROS signaling. Unlike mitochondrial ROS (which is often a byproduct of inefficiency), NOX enzymes deliberately generate ROS to drive signaling pathways such as MAPK/ERK, promoting proliferation and invasion [60, 61]. During therapy adaptation, melanoma cells can rewire mitochondrial metabolism such that altered electron transport and redox balance can increase mitochondrial ROS (including superoxide), which may contribute to signaling and drug resistance [62].

Melanoma probes responsive to multiple parameters of the disease environment are usually based on caging of the heteroatoms either on the core structure of the probe or on the TYR-responsive module. For the second approach, masking of the hydroxyl group on the 3-hydroxybenzyl is widely used since the TYR-mediated oxidation of this group to 4-hydroxybenzyl is significantly attenuated when the hydroxyl group is shielded [63] Michaelis constant (K_m) for **Probe 21** in the ester form is determined to be 44.3 μM, which is 1.5 more than nonacetylated compound. Therefore, the dual-responsive (esterase and TYR) **Probe 21** displays enhanced TYR activity only when esterase

Table 5

Dual-stimuli responsive probes sensitive to melanoma marker TYR and other external or internal stimuli .

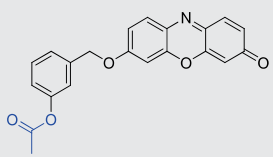
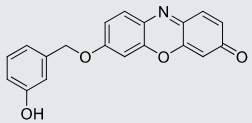
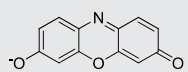
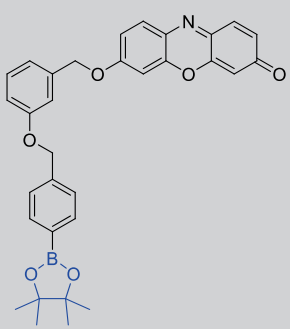
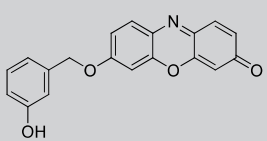
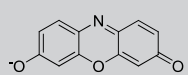
Probe no	Probe structure	Structure after exposure to stimulus 1	Structure after exposure to stimulus 2	Fluorophore/LOD	Ref.
21	 λ_{abs} = 478 nm Φ_F = 0.04 K_m = 44.3 μM	 Stimulus 1: esterase	 Stimulus 2: TYR λ_{abs} = 571 nm λ_{fluo} = 584 nm	Resorufin	[63]
22	 λ_{abs} = 478nm λ_{fluo} = 588 nm Φ_F = 0.014 K_m = 50.1μM	 Stimulus 1: H_2O_2 λ_{exc} = 550 nm λ_{fluo} = 588 nm Φ_F = 0.009 Exication 550 de yapılmış hepsinde	 Stimulus 2: TYR λ_{exc} = 550 nm λ_{fluo} = 588 nm Φ_F = 0.75	Resorufin LOD (TYR) = 0.2 13 U mL^{-1}	[64]

Table 5 (continued)

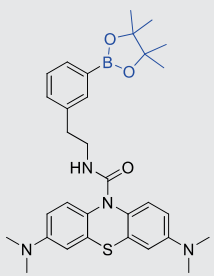
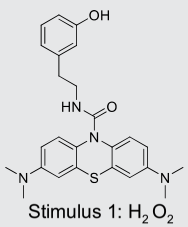
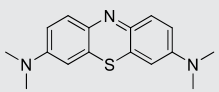
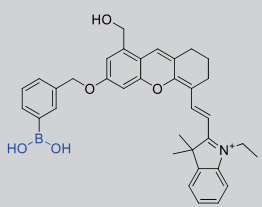
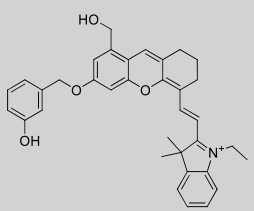
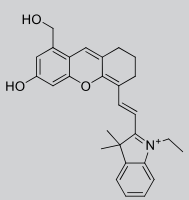
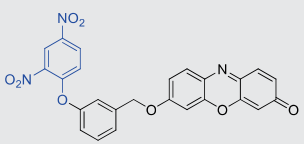
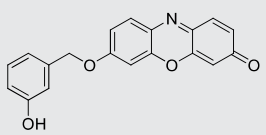
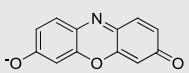
Probe no	Probe structure	Structure after exposure to stimulus 1	Structure after exposure to stimulus 2	Fluorophore/LOD	Ref.
23		 Stimulus 1: H_2O_2	 Stimulus 2: TYR λ_{exc} = 665nm λ_{fluo} = 684 nm	MB	[65]
24		 Stimulus 1: ROS	 Stimulus 2: TYR λ_{exc} = 600 nm λ_{fluo} = 715 nm	Hemicyanine LOD (TYR) = 0.73 U mL^{-1} LOD (ROS) = 120 nM	[66]
25		 Stimulus 1: H_2S	 Stimulus 2: TYR λ_{exc} = 570 nm λ_{fluo} = 574 nm Φ_F = 0.45	resorufin	[69]

Table 5 (continued)

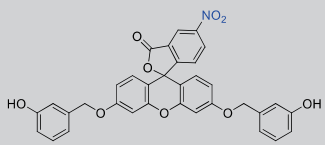
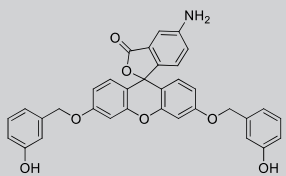
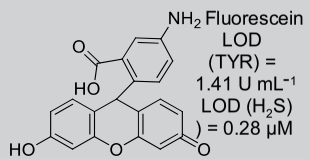
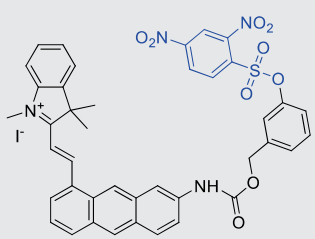
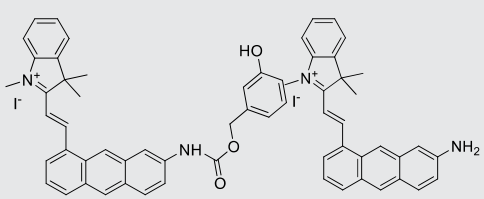
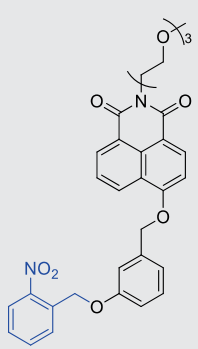
Probe no	Probe structure	Structure after exposure to stimulus 1	Structure after exposure to stimulus 2	Fluorophore/LOD	Ref.
26	 λ_{exc} = 470 nm λ_{fluo} = 517 nm Φ_F =0.023	 Stimulus 1: H_2S λ_{exc} = 470 nm λ_{fluo} = 517 nm Φ_F =0.078	 Stimulus 2: TYR λ_{exc} = 470 nm λ_{fluo} = 517 nm Φ_F = 0.56	Fluorescein LOD (TYR) =1.41 U mL^{-1} LOD (H_2S) = 0.28 µM	[70]
27	 λ_{abs} = 610/660 nm	 Stimulus 1: GSH λ_{abs} = 610/660 nm Stimulus 2: TYR λ_{abs} = 660 nm λ_{fluo} = 705 nm	 λ_{abs} = 408 nm λ_{fluo} = 468 nm		[71]

Table 5 (continued)

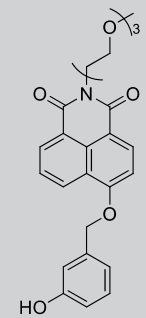
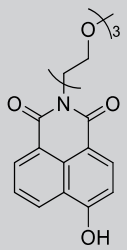
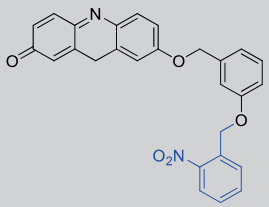
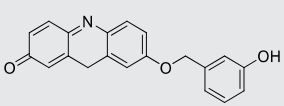
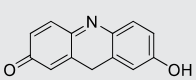
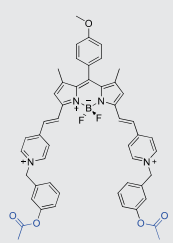
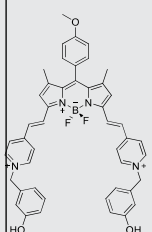
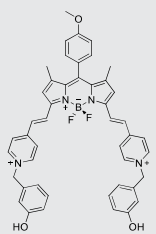
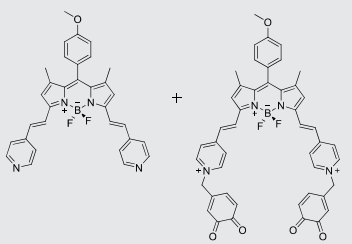
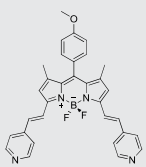
Probe no	Probe structure	Structure after exposure to stimulus 1	Structure after exposure to stimulus 2	Fluorophore/LOD	Ref.
28	 Stimulus 1: UV light	 Stimulus 2: TYR λ_{abs} = 462/451 nm λ_{fluo} = 550 nm	 λ_{abs} = 440 nm	1,8-Naphthalimide LOD = 1.9 U mL^{-1}	[72]
29	 Stimulus 1: light λ_{abs} = 470 nm	 Stimulus 2: TYR λ_{abs} = 550 nm λ_{fluo} = 586 nm	 λ_{abs} = 663 nm λ_{fluo} = 710 nm Φ_F = 0.26	Resorufin LOD = 0.08 U mL^{-1}	[73]

Table 6

Triple-stimuli responsive probe sensitive to melanoma marker TYR, esterase enzyme associated with drug resistance, and tumor marker GSH

Probe no	Probe structure	Structure after exposure to stimulus 1	Structure after exposure to stimulus 2	Structure after exposure to stimulus 3	Fluorophore/ LOD	Ref.
30	 Stimulus 1: esterase	 Stimulus 1: esterase	 Stimulus 2: TYR	 Stimulus 3: GSH λ_{abs} = 619 nm λ_{fluo} = 638 nm Φ_F = 0.84	BODIPY LOD (TYR) = 0.83 U mL^{-1}	[74]

Chemical groups highlighted in blue are sensitive to analytes/stimuli other than TYR

enzymes deacetylate the compound. The presence of both enzymes leads to a 70-fold increase in fluorescence at 584 nm. Designing probes for ROS is challenging because inflammation also generates ROS. To achieve melanoma specificity, researchers have developed "AND" logic gate (dual trigger) probes that require two simultaneous triggers: High ROS and Tyrosinase activity. For hydrogen peroxide (H_2O_2)-responsiveness, boronic acids or their pinacol esters are used. High levels of H_2O_2 in the melanoma environment oxidize the boronate ester to a phenol. The newly exposed phenol is recognized by Tyrosinase, which oxidizes it and triggers a self-immolative cleavage of the linker. Resorufin-, methylene blue-, and hemicyanine-based probes are successfully used for H_2O_2 (or ROS)/TYR dual sensing (**Probes 22–24**). For resorufin, when 3-boronate ester-modified benzyl is directly attached to the fluorophore, oxidation to quinone by high concentrations of H_2O_2 limits 1,6-elimination, and fluorescence output cannot be detected [64–67].

Cystathionine g-lyase (CSE) overexpressed in melanoma is responsible for H_2S synthesis and associated with proliferation and elevated melanin synthesis; therefore, H_2S responsiveness is also used in multi-analyte sensors [68]. For this purpose, the 2,4-dinitrophenyl group is used as a reporter unit in **Probe 25**. Upon nucleophilic attack of H_2S, this group is cleaved, exposing the TYR-responsive 3-hydroxybenzyl moiety [69]. A 30-fold increase in the fluorescence intensity at 574 nm can be obtained in the presence of both biomarkers. H_2S-mediated reduction of 6-nitrofluorescein and TYR-mediated removal of 3-hydroxy benzyl groups leads to almost 12-fold fluorescence enhancement in **Probe 26** [70]. As opposed to the dual responsive probes described above, additional responsiveness is enabled by modification of the core structure of the probe. Glutathione tripeptide (GSH), elevated in most tumors is used as a second discriminative cancer biomarker in **Probe 27**, where the thiol on the GSH attacks and cleaves dinitrobenzosulfonyl [71].

Besides the biological markers in the melanoma cells/microenvironment, external stimuli can enable regioselective probe activation and, hence, regional melanoma sensing. For this purpose, **Probes 28** and **29** were developed [72, 73]. TYR-responsive units on 1,8-naphthalimide or resorufin probes were caged with photolabile 2-nitrobenzyl groups. Although local probe activation can eliminate false positive signals from around, toxicity of UV light restricts the application of these probes.

More than two biomarkers can also be used for diagnostic purposes, yet only limited examples have been reported (Table 6). A Near-IR absorbing distyryl BODIPY-based probe (**Probe 30**) has been developed for selective melanoma sensing, and the probe is sensitive to TYR enzyme, esterase enzyme, and GSH [74]. A strong electron-withdrawing nature of the pyridinium structure on the probe enables emission at 710 nm. When the structure is converted in the presence of all three inputs, probe quantum yield increases

to 0.84, accompanied by a large 72 nm spectral shift as a result of a change in ICT character. Esterase enzyme exposes the tyrosinase-responsive group; however, TYR-mediated oxidation can generate both 3,4-dihydroxybenzyl and quinone. The former can be released spontaneously, generating the fluorescence output, whereas the quinone intermediate cannot. Glutathione is thus incorporated to reduce the quinone intermediate, further enhancing the signal. The triple analyte responsiveness has been shown in melanoma cells with the use of a thiol scavenger (dimethyl fumarate) and a TYR inhibitor (kojic acid).

3.6 Proximity Labeling

For deep-tissue imaging, retention of the signal is crucial. Small molecules often wash out of the tumor rapidly. To overcome this, a novel class of probes utilizes "Tyrosinase-Mediated Proximity Labeling" [75]. The probes contain a tyrosine mimic. Upon entering the active site of TYR, the phenolic ring is oxidized to an *ortho*-quinone. While DOPA quinone would normally cyclize to melanin, the quinone moiety on the probe is designed to be highly electrophilic. It undergoes a Michael addition or Schiff base formation with nucleophilic residues (e.g., thiol or amine groups) on proteins in the immediate vicinity of the enzyme. This covalently tethers the radioactive or paramagnetic payload to the tumor tissue [75].

4 Approaches to Overcome Tissue Penetration Depth of Light

The transition from in vitro cellular imaging to in vivo whole-body imaging introduces severe optical challenges. Biological tissue is a turbid medium that interacts with light through absorption and scattering. The design of the fluorophore module must be strictly governed by these physical parameters to achieve sufficient depth of penetration and resolution.

Historically, fluorescence imaging operated in the visible spectrum (400–700 nm), where tissue autofluorescence is high and hemoglobin absorption is maximal. The field then moved to the First Near-Infrared Window (NIR-I, 700–900 nm), where hemoglobin and water absorption are relatively low. However, the primary limiter of resolution in biological tissue is photon scattering. Scattering intensity is inversely proportional to the wavelength (λ^{-w}), where w depends on the tissue type but typically ranges from 0.4 to 1.5. Consequently, NIR-I photons still suffer significant scattering, blurring images of deep-seated tumors (e.g., >3–5 mm deep). The Second Near-Infrared Window (NIR-II, 1000–1700 nm) represents the current frontier to suppress scattering and autofluorescence [76].

Funding

S. Erbas-Cakmak acknowledges the support provided by TUBİTAK, Grant No: 221Z058, TÜBİTAK Incentive Award, METU Mustafa Parlar Foundation, and TÜBA GEBİP.

Conflicts of Interest The authors have no conflicts of interest to declare that are relevant to the content of this chapter.

References

1. Sun Y, Shen Y, Liu Q et al (2025) Global trends in melanoma burden: a comprehensive analysis from the Global Burden of Disease Study, 1990-2021. J Am Acad Dermatol 92(1):100–107
2. Maeda T, Yanagi T, Ujiie H (2023) Lessons from clinical trials on triple combination of immune checkpoint inhibitors and BRAF/MEK inhibitors in BRAF-mutant melanoma. Ann Transl Med 11(9):326
3. Brlek P, Škaro V, Hrvatin N et al (2025) Advances in precision oncology: from molecular profiling to regulatory-approved targeted therapies. Cancers 17(21):3500
4. Hettie KS, Klockow JL, Moon EJ et al (2021) A NIR fluorescent smart probe for imaging tumor hypoxia. Cancer Rep 4(5):e1384
5. Wang X, Ding Q, Groleau RR et al (2024) Fluorescent probes for disease diagnosis. Chem Rev 124(11):7106–7164
6. Kulesa PM, Kasemeier-Kulesa JC, Teddy JM et al (2006) Reprogramming metastatic melanoma cells to assume a neural crest cell-like phenotype in an embryonic microenvironment. Proc Natl Acad Sci USA 103(10):3752–3757
7. Brombin A, Patton EE (2024) Melanocyte lineage dynamics in development, growth and disease. Development 151(15):dev201266
8. Karamchandani JR, Nielsen TO, Van De Rijn M, West RB (2012) Sox10 and s100 in the diagnosis of soft-tissue neoplasms. Appl Immunohistochem Mol Morphol 20(5):445–450
9. Hou L, Pavan WJ (2008) Transcriptional and signaling regulation in neural crest stem cell-derived melanocyte development: do all roads lead to Mitf? Cell Research 18(12): 1163–1176
10. Capparelli C, Purwin TJ, Glasheen M et al (2022) Targeting SOX10-deficient cells to reduce the dormant-invasive phenotype state in melanoma. Nature Commun 13(1):1381
11. Kim J, Lo L, Dormand E, Anderson DJ (2003) SOX10 maintains multipotency and inhibits neuronal differentiation of neural crest stem cells. Neuron 38(1):17–31
12. Tacha D, Qi W, Ra S et al (2015) A newly developed mouse monoclonal SOX10 antibody is a highly sensitive and specific marker for malignant melanoma, including spindle cell and desmoplastic melanomas. Arch Pathol Lab Med 139(4):530–536
13. Abou-Hamad J, Hodgins JJ, Yakubovich E et al (2024) Sox10-deficient drug-resistant melanoma cells are refractory to oncolytic RNA viruses. Cells 13(1):73
14. Levy C, Khaled M, Fisher DE (2006) MITF: master regulator of melanocyte development and melanoma oncogene. Trends Mol Med 12(9):406–414
15. Roider E, Lakatos AIT, McConnell AM et al (2024) MITF regulates IDH1, NNT, and a transcriptional program protecting melanoma from reactive oxygen species. Scientific Rep 14(1):21527
16. Wellbrock C, Arozarena I (2015) Microphthalmia-associated transcription factor in melanoma development and MAP-kinase pathway targeted therapy. Pigment Cell Melanoma Res 28(4):390
17. Raposo G, Marks MS (2007) Melanosomes—dark organelles enlighten endosomal membrane transport. Nat Rev Mol Cell Biol 8(10):786
18. Van De Watering FCJ, Rijpkema M, Perk L et al (2014) Zirconium-89 labeled antibodies: a new tool for molecular imaging in cancer patients. Biomed Res Int 2014:203601
19. Schlessinger DI, Rahimi N, Schlessinger J (2025) Biochemistry, Melanin. StatPearls Publishing LLC.
20. Bao M, Gempeler M, Campiche R et al (2025) Melanosome transport and processing in skin pigmentation: mechanisms and targets for pigmentation modulation. Int J Mol Sci 26(17):8630
21. Watt B, Van Niel G, Raposo G, Marks MS (2013) PMEL: a pigment cell-specific model for functional amyloid formation. Pigment Cell Melanoma Res 26(3):300
22. Rothberg BEG, Moeder CB, Kluger H et al (2008) Nuclear to non-nuclear Pmel17/gp100 expression (HMB45 staining) as a discriminator between benign and malignant melanocytic lesions. Mod Pathol 21(9):1121
23. Bao M, Gempeler M, Campiche R (2025) Melanosome transport and processing in

skin pigmentation: mechanisms and targets for pigmentation modulation. Int J Mol Sci 26(17):8630
24. Tafreshi NK, Huang X, Moberg VE et al (2012) Synthesis and characterization of a melanoma-targeted fluorescence imaging probe by conjugation of a melanocortin 1 receptor (MC1R) specific ligand. Bioconjug Chem 23(12):2451–2459
25. Von Kiedrowski V, Hübner R, Kail D et al (2020) Synthesis, characterization and optimization of in vitro properties of NIR-fluorescent cyclic α-MSH peptides for melanoma imaging. J Mater Chem B 8(46):10602–10608
26. Slominski RM, Sarna T, Płonka PM et al (2022) Melanoma, melanin, and melanogenesis: the yin and yang relationship. Front Oncol 12:842496
27. Wang TT, Li ZZ, Cai Y et al (2025) Emerging roles of Rab27 proteins: from normal to cancer stem cells. Biochem Biophys Res Commun 775:152109
28. Feng Z, Tang T, Wu T et al (2021) Perfecting and extending the near-infrared imaging window. Light Sci Appl 10(1):197
29. Harada T, Sano K, Sato K et al (2014) Activatable organic near-infrared fluorescent probes based on a bacteriochlorin platform: synthesis and multicolor in vivo imaging with a single excitation. Bioconjug Chem 25(2):362–369
30. Zhan C, Cheng J, Li B et al (2018) A fluorescent probe for early detection of melanoma and its metastasis by specifically imaging tyrosinase activity in a mouse model. Anal Chem 90(15):8807–8815
31. Boussadia Z, Gambardella AR, Mattei F, Parolini I (2021) Acidic and hypoxic microenvironment in melanoma: impact of tumour exosomes on disease progression. Cells 10(12):3311
32. Zeng Z, Tan Y, Luo T et al (2025) Tyrosinase-activated MRI and PET probes for selective melanoma imaging. ACS Sens 10:3032
33. Jin W, Stehbens SJ, Barnard RT et al (2024) Dysregulation of tyrosinase activity: a potential link between skin disorders and neurodegeneration. J Pharm Pharmacol 76(1):13–22
34. Il Kim T, Park J, Park S et al (2011) Visualization of tyrosinase activity in melanoma cells by a BODIPY-based fluorescent probe. Chem Commun 47(47):12640–12642
35. Bobba KN, Won M, Shim I et al (2017) A BODIPY-based two-photon fluorescent probe validates tyrosinase activity in live cells. Chem Commun 53(81):11213–11216
36. Kim D, Ryu HG, Ahn KH (2014) Recent development of two-photon fluorescent probes for bioimaging. Org Biomol Chem 12(26):4550–4566
37. Peng M, Wang Y, Fu Q et al (2018) Melanosome-targeting near-infrared fluorescent probe with large stokes shift for in situ quantification of tyrosinase activity and assessing drug effects on differently invasive melanoma cells. Anal Chem 90(10):6206–6213
38. Li Z, Xia X, You Y et al (2021) Fast-response fluorescent probe with favorable water solubility for highly sensitive imaging of endogenous tyrosinase in living cells and zebrafish model. Chinese Chem Lett 32(5):1785–1789
39. Li Z, Wang YF, Zeng C et al (2018) Ultrasensitive tyrosinase-activated turn-on near-infrared fluorescent probe with a rationally designed urea bond for selective imaging and photodamage to melanoma cells. Anal Chem 90(6):3666–3669
40. Yan S, Huang R, Wang C et al (2012) A two-photon fluorescent probe for intracellular detection of tyrosinase activity. Chem Asian J 7(12):2782–2785
41. Cai X, Liu B (2020) Aggregation-induced emission: recent advances in materials and biomedical applications. Angew Chem Int Ed Engl 132(25):9952–9970
42. Zhang P, Li S, Fu C et al (2019) A colorimetric and near-infrared ratiometric fluorescent probe for the determination of endogenous tyrosinase activity based on cyanine aggregation. Analyst 144(18):5472–5478
43. Yan S, Huang R, Wang C et al (2012) A two-photon fluorescent probe for intracellular detection of tyrosinase activity. Chem Asian J 7:2782–2785
44. Wu X, Li X, Li H et al (2017) A highly sensitive and selective fluorescence off–on probe for the detection of intracellular endogenous tyrosinase activity. Chem Commun 53(16):2443–2446
45. Sidhu JS, Singh A, Garg N et al (2018) A highly selective naphthalimide-based ratiometric fluorescent probe for the recognition of tyrosinase and cellular imaging. Analyst 143(18):4476–4483
46. Shu D, Xie W, Liu H et al (2024) Fluorescence monitoring of refluxed tyrosinase using endoplasmic reticulum-localized enzymatic activity-based sensing. Chem Commun 60(43):5618–5621
47. Park SY, Won M, Kim JS, Lee MH (2020) Ratiometric fluorescent probe for monitoring tyrosinase activity in melanosomes of melanoma cancer cells. Sens Actuators B Chem 319:128306
48. Hu S, Wang T, Zou J et al (2019) Highly chemoselective fluorescent probe for the detection of tyrosinase in living cells and zebrafish model. Sens Actuators B Chem 283:873–880
49. Song J, Yu J, Sun K et al (2023) A high quantum yield xanthene-based fluorescent probe for the specific detection of tyrosinase and cell imaging. J Photochem Photobiol A Chem 441:114693
50. Wu X, Li L, Shi W et al (2016) Near-infrared fluorescent probe with new recognition moiety for specific detection of tyrosinase activity: design, synthesis, and application in living

cells and zebrafish. Angew Chem Int Ed Engl 55(47):14728–14732
51. Zhang J, Li Z, Tian X, Ding N (2019) A novel hydrosoluble near-infrared fluorescent probe for specifically monitoring tyrosinase and application in a mouse model. Chem Commun 55:9463–9466
52. Cui Y, Park SJ, Wu X et al (2021) Highly selective two-photon fluorescent off–on probes for imaging tyrosinase activity in living cells and tissues. Chem Commun 57:6911–6914
53. Valverde-Pozo J, Paredes JM, García-Rubiño ME et al (2023) New ICT-based ratiometric two-photon near infrared probe for imaging tyrosinase in living cells, tissues, and whole organisms. Chemosensors 11(2):145
54. Chen D, Ji Y, Sun S, Pu S (2024) A turn-on fluorescence probe for imaging tyrosinase at the wound site in broken tail of zebrafish. Bioorg Chem 146:107298
55. Wang X, Ma C (2022) A near-infrared fluorescent chemosensor with a remarkably large Stokes shift for the ultrasensitive detection of tyrosinase activity and bioimaging in living cells and mouse xenograft model. Sens Actuators B Chem 354:131211
56. Wang C, Yan S, Huang R et al (2013) A turn-on fluorescent probe for detection of tyrosinase activity. Analyst 138(10):2825–2828
57. Zhan C, Cheng J, Li B et al (2018) A fluorescent probe for early detection of melanoma and its metastasis by specifically imaging tyrosinase activity in a mouse model. Anal Chem 90(15):8807–8815
58. Li Q, Yan C, Zhang J et al (2019) Ratiometric and light-up near-infrared fluorescent DCM-based probe for real-time monitoring endogenous tyrosinase activity. Dyes Pigments 162:802–807
59. Arslanbaeva LR, Santoro MM (2020) Adaptive redox homeostasis in cutaneous melanoma. Redox Biol 37:101753
60. Savoia P, Fava P, Casoni F, Cremona O (2019) Targeting the ERK signaling pathway in melanoma. Int J Mol Sci 20(6): 1483
61. Antony S, Jiang G, Wu Y et al (2017) NADPH oxidase 5 (NOX5)—induced reactive oxygen signaling modulates normoxic HIF-1α and p27Kip1 expression in malignant melanoma and other human tumors. Mol Carcinog 56(12):2643
62. Kumar PR, Moore JA, Bowles KM et al (2021) Mitochondrial oxidative phosphorylation in cutaneous melanoma. Br J Cancer 124(1):115–123
63. Cakmak SE (2022) Development of dual enzyme responsive molecular AND logic gate. Turk J Chem 46(2):567–574
64. Guo L, Feng D, Yuan F et al (2024) A 'dual-key-and-lock' molecular probe for accurate diagnosis of melanoma. Sens Actuators B Chem 409:135572
65. Peng H, Wang T, Li G et al (2021) Dual-locked near-infrared fluorescent probes for precise detection of melanoma via hydrogen peroxide–tyrosinase cascade activation. Anal Chem 94(2):1070–1075
66. Lv R, Hang S, Zhao Y et al (2025) Reactive oxygen species (ROS)–tyrosinase cascade-activated near-infrared fluorescent probe for the precise imaging of melanoma. Anal Chem 97(7):4241–4250
67. Li H, Liu W, Zhang F et al (2017) Highly selective fluorescent probe based on hydroxylation of phenylboronic acid pinacol ester for detection of tyrosinase in cells. Anal Chem 90(1):855–858
68. Ying J, Wang Q, Jiang M et al (2020) Hydrogen sulfide promotes cell proliferation and melanin synthesis in primary human epidermal melanocytes. Skin Pharmacol Physiol 33(2):61–68
69. Almammadov T, Dirak M, Saymaz A et al (2023) A hydrogen sulfide and tyrosinase responsive dual-locked fluorophore for selective imaging of melanoma cells. Chem Commun 59(66):9972–9975
70. Ying J, Luo Z, Zhang Q et al (2026) A dual-locked fluorescent probe for imaging of human primary melanocytes and melanoma tissues via tyrosinase and hydrogen sulfide activation. Spectrochim Acta A Mol Biomol Spectrosc 350:127418
71. Wu D, Gan C, He C et al (2025) Glutathione and tyrosinase co-activated near-infrared fluorescent probes for precise detection of melanoma. Dyes and Pigments 237:112712
72. Zhang Z, Fan Z, Jiao J et al (2025) Light-controllable enzymatic emission shift for spatiotemporal ratiometric imaging of tyrosinase activity in living cells and zebrafish. Sens Actuators B Chem 433:137538
73. Yang S, Jiang J, Zhou A et al (2020) Substrate-photocaged enzymatic fluorogenic probe enabling sequential activation for light-controllable monitoring of intracellular tyrosinase activity. Anal Chem 92(10):7194–7199
74. Verirsen I, Ozsamur NG, Sahin E, Erbas-Cakmak S (2025) An information processing triple input fluorescent probe for melanoma cancer. Anal Chim Acta 1346:343769
75. Zeng Z, Tan Y, Luo T et al (2025) Tyrosinase-activated MRI and PET probes for selective melanoma imaging. ACS Sens 10(4):3023–3032
76. Zhu S, Yung BC, Chandra S et al (2018) Near-infrared-II (NIR-II) bioimaging via off-peak NIR-I fluorescence emission. Theranostics 8(15):4141



Chapter 19

Multi-Analyte Responsive Fluorescent Sensing of Pathological Cellular States in Melanoma

Safaa Altves, Emin Sahin and Sundus Erbas-Cakmak

Abstract

Melanoma progression involves multiple biomarkers and signaling pathways, and relying on a single marker can lead to incomplete or inaccurate diagnoses. Multi-analyte sensors allow simultaneous monitoring of several biomarkers, providing a more comprehensive picture of the tumor microenvironment, identifying distinct cellular states, and improving diagnostic accuracy. This chapter presents protocols that can be used for fluorescence sensing of the melanoma marker enzyme tyrosinase in conjunction with different In Vitro microenvironmental signals, including hypoxia and reactive oxygen species.

Keywords Melanoma sensing, Fluorescent sensing, Multi-analyte sensing, Tyrosinase, Melanoma microenvironment, Hypoxia, Reactive oxygen species, B16-F10

1 Introduction

Fluorescent probes provide rapid bioimaging of disease-associated parameters, and they are widely used for diagnostic and basic research purposes. Probes that detect different features of the melanoma microenvironment can greatly enhance diagnostic accuracy and highlight subtle molecular signatures during disease progression. Among microenvironmental signals, elevated levels of various reactive oxygen species (ROS) and glutathione are used as diagnostic clues besides protein biomarkers such as tyrosinase (TYR) enzyme [1]. A hypoxic microenvironment is another key parameter driving the melanoma tissue into a more aggressive form by inducing angiogenesis and invasion [2]. To mimic the melanoma microenvironment In Vitro and monitor pathological states of the disease, TYR-expressing cells, particularly the B16-F10 (murine), M14 (human), SK-MEL-1 (human), and A375 (human) melanoma cell lines, are used. Cells are induced with α-Melanocyte-stimulating hormone (α-MSH) to increase cAMP-mediated melanogenic enzymes prior to experimental setup. Chemical stimulation of TYR activity in B16-F10 melanoma

Kristian M. Hargadon (ed.), *Melanoma*, Methods in Molecular Biology, vol. 3089,
https://doi.org/10.1007/978-1-0716-5619-8_19,
© The Author(s), under exclusive license to Springer Science+Business Media, LLC, part of Springer Nature 2027

cells is also achieved using agents that elevate intracellular cAMP levels, such as forskolin, 3-isobutyl-1-methylxanthine (IBMX), or stress-inducing agents like 8-methoxypsoralen (8-MOP). Forskolin acts as a direct activator of adenylyl cyclase [3], while IBMX functions as a nonspecific phosphodiesterase inhibitor that prevents cAMP degradation [4–6]. These pathways converge on the protein kinase A (PKA)-mediated phosphorylation of the cAMP-response element-binding protein (CREB), which upregulates the transcription of microphthalmia-associated transcription factor (MITF), the master regulator of the *TYR* gene [7]. Alternatively, 8-MOP stimulates melanogenesis by mimicking UV-induced DNA damage and ROS signaling [8].

Melanoma microenvironments are characterized by elevated levels of ROS [1, 9]. High metabolic activity leads to the generation of ROS, including superoxide radical, by cytochrome P450 and NADPH oxidases in mitochondria. Superoxide radical is converted into hydrogen peroxide (H_2O_2) by superoxide dismutase. Hydrogen sulfide (H_2S)-generating cystathionine-γ-lyase (CSE) is also overexpressed in response to elevated reactive oxygen and nitrogen species. Therefore, these microenvironment clues are informative for insights into the redox state of melanoma.

For multi-analyte sensing, culture medium of TYR-expressing cells is supplied with stimulants to mimic the tumor microenvironment, such as $CoCl_2$ to yield an O_2 level lower than 2% that mimics hypoxic tumors, external ROS including H_2O_2, and H_2S. Scavengers or inhibitors are then used to verify biomarker-dependent output generation by a reconfigurable fluorescent TYR probe that can be used to discriminate different pathological cellular states (based on distinct fluorescence outputs that occur under different microenvironmental conditions). This chapter describes experimental protocols for fluorescence sensing of multiple melanoma markers In Vitro. A summary of the experimental steps is depicted in Fig. 1.

2 Materials

The method described in this chapter is for the B16-F10 mouse melanoma cell line. Similar methodologies can be applied to other melanoma cell lines, although incubation time and probe/inhibitor concentrations may require optimization. All materials should be sterile. To avoid any solvent-induced artifacts, the final DMSO concentration in the cell culture should not exceed 1%. Solutions of probe, $CoCl_2$, H_2O_2, NaHS, scavengers, and inhibitors should be freshly prepared prior to use. For experimental consistency, the incubation time and DMSO concentration in all experimental groups should be equal. Store all solutions at 4 °C unless otherwise indicated.

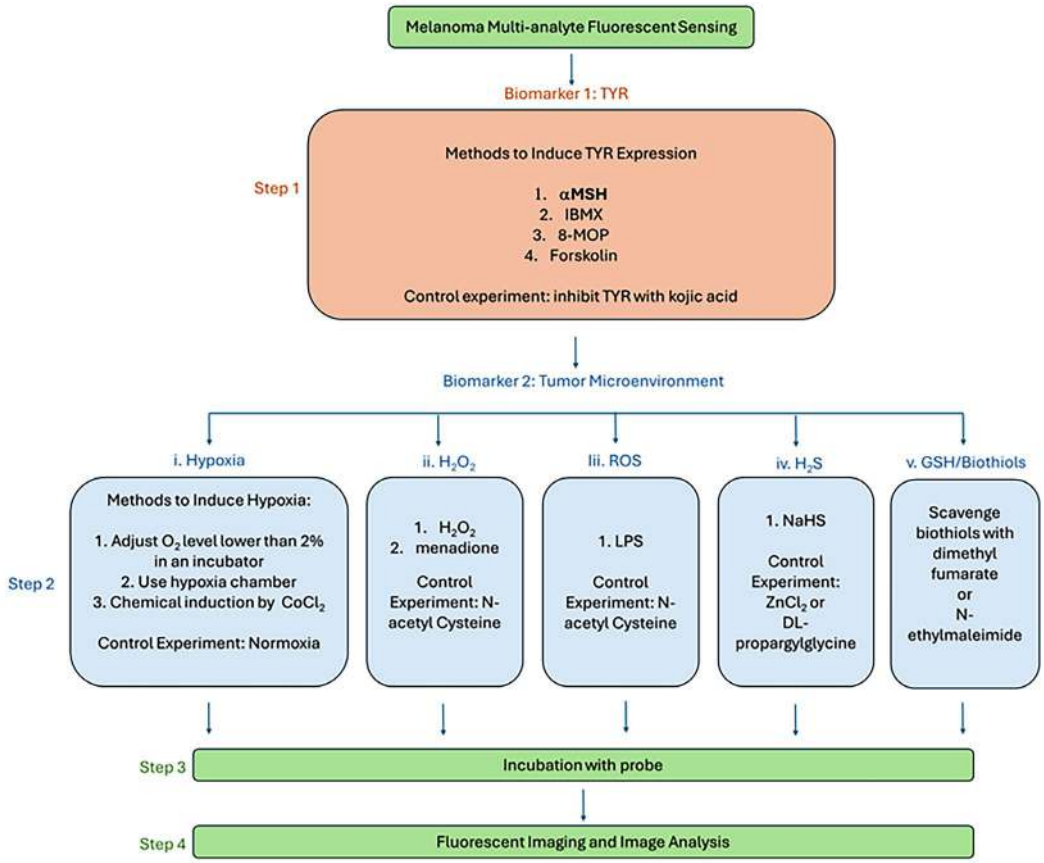


Fig. 1 Steps to follow for fluorescent multi-analyte sensing of melanoma. This method is applicable to any probe responsive to TYR and another tumor-associated biomarker. In the first step, melanoma biomarker TYR overexpression is induced either hormonally (with 50–100 nM α-MSH) or chemically (10 μM IBMX or 100 μM 8-MOP or 10 μM forskolin) for 24 h. In the second step, tumor microenvironment is mimicked with alternative conditions (hypoxia or various ROS). (i) Hypoxia can be set by adjusting oxygen level below 2% (in an incubator or in a sealed hypoxia chamber) or by applying 150–200 μM $CoCl_2$ for 48 h. (ii) If, in the second step, H_2O_2 is used as a tumor marker, external addition of H_2O_2 (100 μM) or endogenous generation of H_2O_2 with the use of 20 μM menadione are alternative methods. (iii) If the second biomarker is selected as ROS, LPS (2 μg/mL) induction for 30 min is sufficient to mimic the corresponding microenvironment. (iv) H_2S over-production can be mimicked by applying NaHS (50 μM) in the culture medium followed by 30 min incubation. (v) To evaluate the involvement of biothiols, including GSH, thiol scavengers such as dimethyl fumarate (50 μM) or *N*-ethyl maleimide (200 μM) can be added to culture medium 2 h prior to probe addition. When all the tumor markers are mimicked In Vitro, probe is applied to the cells. In the final step, fluorescent images of cells are recorded under a confocal/fluorescent microscope, and images are analyzed

1. 37 °C CO_2 incubator.
2. B16-F10 mouse melanoma cells (ATCC, CRL-6475).
3. Complete Growth Medium: Dulbecco's Modified Eagle Medium containing 4 mM L-glutamine, 4500 mg/L glucose, 1 mM sodium pyruvate, 1.5 g/L $NaHCO_3$ (*see* **Note 1**) and

supplemented with 10% heat-inactivated fetal bovine serum (FBS) and 0.1% gentamicin sulfate.

4. Trypsin-EDTA Solution, 1×: 0.25% Trypsin/0.53 mM EDTA in Hanks Balanced Salt Solution without calcium or magnesium.
5. Complete Medium containing α-MSH: Complete Growth Medium supplemented with 50–100 nM α-MSH (*see* **Note 2** for alternative chemical TYR induction methods).
6. TYR-responsive probe, such as Pyridinium-functionalized distyryl-BODIPY P2 TYR Probe or other melanoma-targeting multi-analyte responsive probes [10–15]: Stock solutions (5 mM) should be prepared in a well-dissolving solvent, such as dimethyl sulfoxide (DMSO), and the solution should be stored at −20 °C. Preparation of less dilute stock solutions using deionized water (18 MΩ-cm at 25 °C) or Phosphate Buffered Saline (PBS), pH 7.4, is recommended (*see* **Note 3**).
7. Freezing Medium: 90:10 FBS:DMSO v/v.
8. Kojic Acid (TYR Inhibitor) for negative control experiments.
9. Cell culture ware (35 mm glass-bottom culture dishes or 6-well tissue culture-treated plates).
10. Western blot reagents and supplies (*see* Sect. 3.2):
    a. RIPA Buffer.
    b. Protease inhibitor cocktail [Na_3VO_4 and phenylmethylsulfonyl fluoride (PMSF) inhibitor solutions, Elabscience E-BC-R327].
    c. BCA assay kit.
    d. 6× Laemmli loading buffer (containing β-mercaptoethanol) [Thermo J61337.AD].
    e. 10% Bis-acrylamide gels.
    f. Prestained molecular weight marker.
    g. PVDF membranes.
    h. Transfer Buffer: Prepare stock buffer solution containing 25 mM Tris base, 192 mM glycine, 20% methanol (v/v) in ddH_2O.
    i. 100% methanol.
    j. Transblot SD (Semi-dry) system.
    k. Blotting filter paper.
    l. 0.1% Tween-20 in Tris-buffered saline (TBS-T).
    m. 0.1% Tween-20 in PBS (PBS-T).
    n. Nonfat milk.

o. Anti-TYR antibody (i.e., TYR Monoclonal Antibody (T311), Thermo Fisher Scientific Catalog #35-6000).
p. Anti-β-actin antibody.
q. HRP-conjugated secondary antibody (i.e., Goat Anti-Mouse IgG (H + L) HRP, Affinity Biosciences Catalog #S0002).
r. Enhanced Chemiluminescence (ECL) reagents
s. Western Blot imager.
t. Imaging software (i.e., ImageJ or Fiji).

11. Equipment/reagents for induction of a hypoxic microenvironment, depending on the specific investigator's interests and laboratory infrastructure (see Sect. 3.3.1):
    a. Hypoxic cell culture conditions can be induced using a CO_2 incubator with the oxygen level set to lower than 2%.
    b. Alternatively, a sealed hypoxia chamber (Modular Incubator Chamber, MIC-101, Embrient) infused with a gas mixture containing 0.5% O_2, 5% CO_2, and 94.5% N_2 (for severe hypoxia) or 1% O_2, 5% CO_2, and 94% N_2 (for mild hypoxia) can be used, in which case a flow meter (SFM-3001, Embrient) to adjust gas flow rate to the chamber and 1 μm air filters (HFS-2021, Embrient) for the flow meter will also be required.
    c. 100 mM $CoCl_2$ stock solution: Prepare a 100 mM stock solution of $CoCl_2$ in sterile deionized water (18 MΩ-cm at 25 °C). Filter-sterilize the solution using a 0.22 μm syringe filter, and store at. Prepare fresh solutions prior to experiments requiring chemical induction of hypoxia.
12. Reagents for inducing/scavenging ROS (see Sect. 3.3.2): Depending on the specific investigator's interests, various reagents for inducing and scavenging ROS in cultured cells can be used, including:
    a. H_2O_2 (or menadione) for mimicking elevated H_2O_2.
    b. Lipopolysaccharide (LPS, an ROS inducer) and *N*-acetyl Cysteine (NAC, an ROS scavenger).
    c. NaHS, CSE inhibitor DL-Propargylglycine (PGG), and $ZnCl_2$ (an H_2S scavenger), for mimicking elevated H_2S.
    d. Dimethyl fumarate (DMF) and *N*-ethyl maleimide (NEM) for thiol scavenging.
13. 4% paraformaldehyde (PFA).
14. Confocal microscope.
15. Imaging software (ImageJ or Fiji).

3 Methods

3.1 Cell Maintenance and Subculturing

1. Thaw frozen B16-F10 cells by removing cryovial from liquid nitrogen or −80°C freezer and placing vials in a 37°C water bath (~1–2 min).
2. Transfer cells into a 15 mL tube containing 9 mL of warm Complete Growth Medium.
3. Centrifuge at 150–400 × *g* for 8–12 min.
4. Discard the supernatant and resuspend the pellet in 10 mL of fresh Complete Growth Medium.
5. Transfer the cell suspension to a T-25 or T-75 flask, ensuring that cells are spread all over the flask surface.
6. Incubate the flask at 37 °C in incubator maintaining 5% CO_2 humidified atmosphere.
7. Passage cells when they reach 80%–90% confluence.
    a. Aspirate the old medium, and wash the cell monolayer with 5 mL of sterile PBS to remove residual FBS.
    b. Add 1–2 mL of 0.25% Trypsin-EDTA until the entire flask surface is covered.
    c. Re-incubate cells at 37°C for 5–15 min until all the cells detach. Check the cells under the microscope.
    d. Add at least a two-fold volume (compared to Trypsin-EDTA) of Complete Growth Medium.
    e. Centrifuge cells at 150–400 × *g* and remove supernatant.
    f. Resuspend the pelleted cells in Complete Growth Medium, and split the cells to re-seed new flasks as needed. For B16-F10, a split ratio of 1:6 to 1:10 is standard every 2–3 days.
    g. To freeze stock vials of cultured cells for future use, resuspend 1×10^6 cells in 2 mL of Freezing Medium in a cryovial. Keep the cryovial at 4°C for 30 min, then move the vial to −20°C for 1 h, and later to −80°C or liquid nitrogen for long-term storage.

3.2 Induction and Verification of TYR Overexpression

1. Seed B16-F10 melanoma cells (1×10^5 cells/dish) onto 35 mm glass-bottom culture dishes or coverslips placed in a 6-well plate.
2. Incubate cells for at least 24 h at 37°C in a 5% CO_2 incubator, such that cells adhere to the plate surface and reach at least 60%–70% confluency.
3. Prepare Complete Growth Medium containing α-MSH (50-100 nM).

4. Discard the existing medium of the cell culture, and add α -MSH-containing Complete Growth Medium. Incubate the cells for 48–72 h. The medium may turn slightly brown/black due to secreted melanin (this indicates successful TYR activation). For alternative methods of chemically inducing TYR overexpression (*see* **Note 2**).
5. When conducting initial experiments with this protocol, set up an extra set of samples that can be used to verify TYR overexpression after induction by Western Blot analysis, as follows (*see* **Note 4**):

    a. Lyse cells in ice-cold RIPA buffer (containing 1% (v/v) of Na_3VO_4 and PMSF protease inhibitor cocktail) for 30 min on ice with occasional vortexing.
    b. Centrifuge samples at 14,000 × *g* for 15 min at 4 °C. Collect the supernatant.
    c. Determine protein concentration using a BCA assay.
    d. Mix 25 μg of total protein with 6× Laemmli loading buffer (containing β-mercaptoethanol) to achieve 1× Laemmli loading buffer solution, and denature samples by heating at 95°C for 5 min.
    e. For SDS-PAGE separation of proteins, load a pre-stained molecular weight marker and experimental samples into a 10% Bis-acrylamide gel [this percentage is optimal for resolving TYR (~70–84 kDa) and the β-actin control (~42 kDa].
    f. Run gel at 80 V until samples enter the resolving gel.
    g. Increase voltage to 120 V for approximately 1.5 h or until the dye front reaches the bottom.
    h. For semi-dry transfer, cut a PVDF membrane to the size of the gel. Immerse in 100% methanol for 15–30 s to activate the membrane, then rinse in distilled water and equilibrate in Transfer Buffer.
    i. In a Transblot SD (Semi-dry) system, stack the layers as follows: (i) Anode (+), (ii) Blotting Filter Paper (soaked in transfer buffer), (iii) Activated PVDF membrane, (iv) SDS-PAGE gel, (v) Blotting Filter Paper (soaked in transfer buffer), (vi) Cathode (−).
    j. Transfer at a constant current 2.5 A 25 V for 7 min.
    k. Block the membrane by incubating in 5% nonfat milk in TBS-T for 1 h at room temperature to prevent nonspecific antibody binding.

l. Incubate membrane overnight with anti-TYR antibody [i.e., TYR Monoclonal Antibody (T311), Thermo:35-6000] at the recommended dilution at 4°C.

m. Wash the membrane three times for 10 min each with PBS-T (PBS + 0.1% Tween-20).

n. Incubate membrane with HRP-conjugated secondary antibody (i.e., Goat Anti-Mouse IgG (H + L) HRP, Affinity Biosciences Cat# S0002) for 2 h at room temperature.

o. Repeat the washing step with PBS-T three times for 10 min each.

p. Apply Enhanced Chemiluminescence (ECL) reagents to the membrane for 1 min.

q. Capture signals using a cooled CCD (Charge-Coupled Device) Camera System.

r. Re-use the membrane with a validated anti-β-actin antibody to verify equal loading.

s. Perform densitometric analysis using ImageJ or Fiji. Calculate the relative expression by dividing the TYR band intensity by the β-actin band intensity for each sample.

3.3 Mimicking the Tumor Microenvironment

Following TYR overexpression (as described in Sect. 3.2), apply conditions for the microenvironment signal of interest (hypoxia or ROS). When designing experiments, include as a negative control a sample to which kojic acid is added (2 mg mL^{-1}) to the culture medium 1 h prior to probe application [16]. Because kojic acid is a TYR inhibitor, this control ensures that the fluorescent signal output in non-inhibited samples reflects distinct responsiveness of the TYR-associated probe to the microenvironmental conditions under study.

3.3.1 Mimicking Hypoxia

As a second tumor parameter to be sensed in conjunction with TYR expression, hypoxia can be used. There are three widely used methods to induce hypoxia In Vitro: adjusting O_2 level in a standard CO_2 incubator (Method A); using a hypoxia chamber (Method B); inducing hypoxia chemically (Method C). Method A is recommended since a stable hypoxic environment can be set without any chemical interference. In the absence of an incubator with adjustable O_2 settings or a hypoxia chamber, chemical induction of hypoxia with $CoCl_2$ (Method C) is also a viable alternative. Chemical induction of hypoxia with $CoCl_2$ relies on the fact that the hypoxia response in the cell is mediated through the transcription factor Hypoxia Inducible Factor 1 (HIF1α/β). HIF induces metabolic reprogramming, angiogenesis, and metastasis. Under normoxia (21% O_2), proline residue on this protein is oxidized by prolyl hydroxylase enzyme, and rapid degradation of HIF1α is observed [17]. Oxygen deprivation reduces the

degradation of the transcription factor, and transcriptional regulation by the protein can be initiated. $CoCl_2$ is a chemical hypoxia inducer, which inhibits the prolyl hydroxylase enzyme. Co^{2+} ions replace Fe^{2+} in the active site of prolyl hydroxylase enzymes (PHDs), preventing the hydroxylation and subsequent VHL-mediated proteasomal degradation of HIF-1α. $CoCl_2$ also reduces HIF1α mRNA levels [18, 19]. With this method, a hypoxic response can be generated even if the oxygen level is sufficient (21%).

1. To mimic hypoxia in a standard incubator (Method A), incubate the cells under moderate (1% O_2) to severe (0.5% O_2) hypoxia conditions for at least 12 h by adjusting the oxygen level of the incubator (*see* **Note 5** for the verification of hypoxia).
2. To mimic hypoxia using a hypoxic chamber (Method B), place the cell flask in a sealed hypoxia chamber and then flush the chamber with a gas mixture containing 0.5% O_2, 5% CO_2, and 94.5% N_2 (for severe hypoxia) or 1% O_2, 5% CO_2, and 94% N_2 (for moderate hypoxia) for 6 min [20, 21]. Use air filters to avoid contamination. The recommended flow rate is 17 L/min. Seal the chamber, and incubate the cells for at least 12 h at 37°C (*see* **Note 5** for the verification of hypoxia).
3. To chemically induce hypoxia (Method C), add the appropriate volume of 100 mM $CoCl_2$ stock solution to the cell culture medium to achieve a final concentration of 150–200 μM [22], and incubate the cells for 48 h (*see* **Note 5** for the verification of hypoxia).

3.3.2 Mimicking Elevated ROS

Increased levels of H_2O_2, H_2S, or collective ROS are another good set of secondary melanoma-associated parameters that can be sensed by multi-analyte probes. Following the TYR over-expression step described in Sect. 3.2, the following methods for specific ROS induction can be used: for H_2O_2 induction, follow Method A of this section; for general ROS induction, follow Method B of this section; for H_2S induction, follow Method C of this section; and for understanding the role of GSH/biothiols in the sensing mechanism of the probe, follow Method D of this section.

1. To mimic a microenvironment with elevated H_2O_2 (Method A), incubate the cells with H_2O_2 (100 μM) for 30 min before staining with the probe. As an alternative to H_2O_2, one can use menadione (20 μM), which is reported to induce intracellular H_2O_2 in other cells [23]. In a separate control experiment, treat cells with 200 μM NAC for 2 h to scavenge ROS [10].
2. To mimic a microenvironment with cumulative ROS overproduction, pretreat the cells with LPS (2 μg/mL) for 30 min before staining with the probe [11]. In a separate control

experiment, treat cells with 100 μM NAC for 30 min to scavenge ROS.

3. To mimic a microenvironment with elevated H_2S, treat the B16-F10 cells with NaHS (50 μM) 30 min before staining with the probe [12]. For control experiments, pretreat the cells with 200 μM DL-PGG for 6 h before probe addition to inhibit the H_2S-producing CSE enzyme [12]. An alternative negative experimental group would be incubation of cells with $ZnCl_2$ (300 μM) for 10 min to scavenge H_2S [13].
4. To study the involvement of GSH (or other biothiols) in the sensing mechanism, add thiol-scavenging DMF (50 μM) or NEM (200 μM). Incubate for 2 h at 37°C, and then stain the cells with the probe as described in Sect. 3.4 [14, 15].

3.4 Staining the Cells with the Probe

1. Remove the culture medium, and gently wash the cells twice with warm PBS (pH 7.4) to remove residual serum proteins and any reagents added in the previous steps (i.e., inhibitors, ROS inducers, etc.).
2. Dilute the probe in Complete Growth Medium, and add to the dish. The final probe concentration can be 1–20 μM (*see* **Note 6** for probe considerations, including optimum probe concentration).
3. Incubate the cells in the dark at 37°C. Incubation time depends on the probe (*see* **Note 7**).
4. Wash extracellular probe with warm PBS without phenol red.
5. For fixation, treat the cells with 4% paraformaldehyde (PFA) for 15 min at room temperature. This step can be skipped if live-cell imaging is preferred.
6. *Optional*: Another probe for staining intracellular proteins or organelles can be used at the same time for tracking the intracellular distribution of the primary probe (i.e., DAPI for nuclear staining). Criteria to consider for selecting the best probes (*see* **Note 8**).

3.5 Confocal Imaging and Analysis

1. Set the excitation and emission wavelengths according to the specific spectral characteristics of the probe.
2. To ensure accurate quantification, it is critical to maintain consistent laser power, detector gain, and offset settings across all experimental and control groups. Laser power should not exceed 2% [24]. Long-time laser exposure may bleach the probes and should be avoided. Similarly, slow scan speeds can bleach the probe.
3. Ensure that fluorescence signals are within the linear detection range on the detector by adjusting parameters to the dynamic range of the brightest sample.

4. For fluorescence quantification, utilize specialized software such as ImageJ or Fiji to measure the Mean Fluorescence Intensity (MFI). Do not analyze the fluorescence signal of the entire photo; instead, select cells individually in order to eliminate the dependency on cell density. Ensure that background subtraction is applied consistently to each image before performing comparative analysis.

4 Notes

1. If the cells are incubated in a high CO_2 atmosphere, more than 1.5 g/L $NaHCO_3$ is recommended for proper adjustment of medium pH.
2. TYR expression is regulated by cAMP. Therefore, reagents such as forskolin, IBMX, and 8-MOP can be used for chemical induction of TYR enzyme through cAMP overproduction. Forskolin (10 mM) and IBMX (10 mM) can induce 20- and 17-fold increases in TYR expression in B16 cells after 24 h incubation, respectively [25]. Co-stimulation with 1 mM forskolin and 1 mM α-MSH results in a more than seven-fold increase in TYR mRNA in B16-F10 cells [26]. 8-MOP induces stress and also activates TYR expression. A seven-fold increase in TYR activity is observed when the cells are treated with 100 mM 8-MOP [8].
3. To avoid any solvent-induced artifacts, the final DMSO concentration in the cell culture should not exceed 1%. Solutions of the probe, as well as $CoCl_2$, H_2O_2, NaHS, scavengers, and inhibitors, should be freshly prepared prior to use. For experimental consistency, the incubation time and DMSO concentration in all experimental groups should be equal.
4. Efficient solubilization from the melanosomal membrane is critical since TYR is a Type I membrane-bound protein.
5. Hypoxia can be verified using various methods. The most widely used method is analysis of HIF1a protein levels using Western Blot since low oxygen levels stabilize the protein. HIF1a overexpression can be detected using RT-PCR methods as well. Overexpression of carbonic anhydrase IX can also be analyzed using Western Blot and/or RT-PCR to verify hypoxia induction [27].
6. The solubility of the probe should be sufficient. If the probe stock solution is prepared in an organic solvent (such as DMSO), the final percentage of the DMSO must be less than 1%. The DMSO ratio in all experimental setups should be the same. The choice of probe concentration depends on

photophysical properties and toxicity of the probe. A cell viability analysis should be run using different concentrations of the probe. For imaging, nontoxic concentrations must be preferred. For probes having moderate to high fluorescence quantum yields ($\phi_F = 0.4–1$), less than 10 μM probe is sufficient to get good images. Otherwise, probe concentration can be optimized.

7. Typically, 30–60 min incubation is enough for most probes for internalization and analyte-dependent conversion.
8. Probe localization can be detected using organelle-specific probes. In case multi-analyte sensing is done together with organelle staining, organelle-specific probes should be carefully chosen. The excitation and emission spectra of the probes should not overlap the multi-analyte sensor's spectra, for reliable data collection. Additionally, either quantum yields of the dyes should be comparable, or the concentration of the dyes should be optimized to achieve signal with comparable intensities.

Acknowledgments

S. Erbas-Cakmak acknowledges the support provided by TUBİTAK, Grant No: 221Z058, TÜBİTAK Incentive Award, METU Mustafa Parlar Foundation, and TÜBA GEBİP. ES acknowledges TÜBİTAK 2211-A for PhD scholarship.

Conflict of Interest The authors have no conflicts of interest to declare that are relevant to the content of this chapter.

References

1. Arslanbaeva LR, Santoro MM (2020) Adaptive redox homeostasis in cutaneous melanoma. Redox Biol 37:101753
2. D'Aguanno S, Mallone F, Marenco M et al (2021) Hypoxia-dependent drivers of melanoma progression. J Exp Clin Cancer Res 40(1):159
3. Seamon KB, Padgett W, Daly JW (1981) Forskolin: unique diterpene activator of adenylate cyclase in membranes and in intact cells. Proc Natl Acad Sci USA 78(6):3363–3367
4. Huai Q, Liu Y, Francis SH et al (2004) Crystal structures of phosphodiesterases 4 and 5 in complex with inhibitor 3-isobutyl-1-methylxanthine suggest a conformation determinant of inhibitor selectivity. J Biol Chem 279(13):13095–13101
5. Koo JH, Kim HT, Yoon HY et al (2008) Effect of xanthohumol on melanogenesis in B16 melanoma cells. Exp Mol Med 40(3):313–319
6. Beavo JA, Rogers NL, Crofford OB et al (1970) Effects of xanthine derivatives on lipolysis and on adenosine 3',5'-monophosphate phosphodiesterase activity. Mol Pharmacol 6(6):597–603
7. Levy C, Khaled M, Fisher DE (2006) MITF: master regulator of melanocyte development and melanoma oncogene. Trends Mol Med 12(9):406–414
8. Lei TC, Virador V, Yasumoto KI et al (2002) Stimulation of melanoblast pigmentation

by 8-methoxypsoralen: the involvement of microphthalmia-associated transcription factor, the protein kinase a signal pathway, and proteasome-mediated degradation. J Invest Dermatol 119(6):1341–1349
9. Cannavò SP, Tonacci A, Bertino L et al (2019) The role of oxidative stress in the biology of melanoma: a systematic review. Pathol Res Pract 215(1):21–28
10. Peng H, Wang T, Li G et al (2022) Dual-locked near-infrared fluorescent probes for precise detection of melanoma via hydrogen peroxide-tyrosinase cascade activation. Anal Chem 94(2):1070–1075
11. Lv R, Hang S, Zhao Y et al (2025) Reactive oxygen species (ROS)-tyrosinase cascade-activated near-infrared fluorescent probe for the precise imaging of melanoma. Anal Chem 97(7):4241–4250
12. Ying J, Luo Z, Zhang Q et al (2026) A dual-locked fluorescent probe for imaging of human primary melanocytes and melanoma tissues via tyrosinase and hydrogen sulfide activation. Spectrochim Acta A Mol Biomol Spectrosc 350:127418
13. Almammadov T, Dirak M, Saymaz A et al (2023) A hydrogen sulfide and tyrosinase responsive dual-locked fluorophore for selective imaging of melanoma cells. Chem Commun 59(66):9972–9975
14. Verirsen I, Ozsamur NG, Sahin E, Erbas-Cakmak S (2025) An information processing triple input fluorescent probe for melanoma cancer. Anal Chim Acta 1346:343769
15. Wu D, Gan C, He C et al (2025) Glutathione and tyrosinase co-activated near-infrared fluorescent probes for precise detection of melanoma. Dyes Pigm 237:112712
16. Verirsen I, Uyar B, Ozsamur NG et al (2022) Enzyme activatable photodynamic therapy agents targeting melanoma. Org Biomol Chem 20(45):8864–8868
17. Bruick RK, McKnight SL (2001) A conserved family of prolyl-4-hydroxylases that modify HIF. Science 294(5545):1337–1340
18. Baser AS, Basar B, Dogan HB et al (2023) Reprograming cancer cells by a BODIPY G-quadruplex stabiliser. Chem Commun 59(83):12447–12447
19. Sahin E, Ozsamur NG, Altves S et al (2025) Reconfigurable logic operations for fluorescent sensing of drug resistant and/or hypoxic cancer cells. J Mater Chem B 13(16):4791–4795
20. Uyar B, Ozsamur NG, Celik FS et al (2023) Downregulation of gene expression in hypoxic cancer cells by an activatable G-quadruplex stabiliser. Chem Commun 59(16):2247–2250
21. Ma NY, Tinganelli W, Maier A et al (2013) Influence of chronic hypoxia and radiation quality on cell survival. J Radiat Res 54(Suppl 1):i13–i22
22. Licarete E, Sesarman A, Rauca VF et al (2017) HIF-1α acts as a molecular target for simvastatin cytotoxicity in B16.F10 melanoma cells cultured under chemically induced hypoxia. Oncol Lett 13(5):3942–3950
23. Lee JD, Nguyen A, Gibbs CE, et al (2025) Monitoring in real time and far-red imaging of H_2O_2 dynamics with subcellular resolution. Nat Chem Biol 22:556–567. https://doi.org/10.1038/s41589-025-01891-7
24. Shihan MH, Novo SG, Marchand SJL et al (2021) A simple method for quantificating confocal fluorescent images. Biochem Biophys Rep 25:100916
25. Bertolotto C, Bille K, Ortonne JP, BaUotti R (1996) Regulation of tyrosinase gene expression by cAMP in B16 melanoma cells involves two CATGTG motifs surrounding the TATA box: implication of the microphthalmia gene product. J Cell Biol 134(3):747–755
26. Galus R, Niderla J, Sladowski D et al (2010) Fluvastatin increases tyrosinase synthesis induced by-melanocyte-stimulating hormone in B16F10 melanoma cells. Pharmacol Rep 62(1):164–169
27. Wykoff CC, Beasley NJ, Watson PH et al (2000) Hypoxia-inducible expression of tumor-associated carbonic anhydrases. Cancer Res 60(24):7075–7083



Chapter 20

Radiopharmaceuticals for Melanoma Theranostics

Chao Meng, Zhen Cheng and Xiaowei Ma

Abstract

Malignant melanoma (MM) remains a formidable clinical challenge due to its high metastatic potential and the eventual emergence of resistance to current BRAF/MEK and immune checkpoint inhibitors. To address these limitations, the theranostic strategy integrating diagnostic imaging with targeted radionuclide therapy to enable personalized treatment has gained significant traction. Current research primarily exploits the overexpression of the melanocortin 1 receptor (MC1R), very late antigen-4 (VLA-4), and melanin as primary molecular targets for radiopharmaceutical development. For MC1R, α-MSH peptide analogs have been engineered with β-emitters such as ^{177}Lu and ^{90}Y for peptide receptor radionuclide therapy (PRRT), as well as α-emitters like ^{225}Ac and ^{212}Pb (β^- decay to ^{212}Bi and then emit α particles) for targeted alpha therapy (TAT), showing high specificity and rapid clearance. Concurrently, VLA-4-targeted platforms utilizing high-affinity LLP2A ligands have been optimized through PEGylation and albumin-binding strategies to enhance bioavailability and tumor retention. Beyond these primary receptors, this review evaluates alternative strategies, including copper transporter (CTR1) targeting with $^{64}CuCl_2$ and the use of gold nanocages for multimodal applications. Together, these advancements represent a critical shift toward image-guided, dosimetry-driven radionuclide therapies that may work synergistically with existing immunotherapies to improve survival in metastatic melanoma.

Keywords Melanoma, Radiopharmaceuticals, Theranostics, Melanocortin 1 receptor, Melanin, Positron emission tomography

1 Introduction

Malignant melanoma (MM), a neoplasm originating from melanocytes, constitutes the fifth most common cancer among adults in the United States. It is a highly aggressive malignancy, responsible for 75% of skin cancer-related deaths [1]. Although the prognosis for metastatic melanoma has significantly improved with the advent of novel therapies, including inhibitors targeting BRAF, MEK, and PD-L1, as well as immune checkpoint inhibitor-boosting radiotherapies such as those targeting fibroblast activation protein (FAP), many melanomas exhibit initial non-responsiveness or rapidly develop resistance within months [2]. Consequently, the theranostic approach is gaining prominence as a particularly popular new strategy for treatment.

Kristian M. Hargadon (ed.), *Melanoma*, Methods in Molecular Biology, vol. 3089,
https://doi.org/10.1007/978-1-0716-5619-8_20,
© The Author(s), under exclusive license to Springer Science+Business Media, LLC, part of Springer Nature 2027

Melanocortin 1 receptor (MC1R) and very late antigen-4 (VLA-4) are the two most commonly used targets in the diagnosis and treatment process. The promising preclinical and clinical results of new MC1R- and VLA-4-targeted peptide radiopharmaceuticals highlighted in this review present an optimistic outlook for clinical translation of receptor-targeting melanoma imaging and radionuclide therapy in the future.

2 MC1R-Targeting Theranostics

MC1R, a G-protein-coupled receptor (GPCR), is a highly attractive target for melanoma theranostics. It is densely expressed and over-expressed in approximately 80% of melanomas and their associated metastases [3, 4]. Critically, MC1R expression is generally restricted to melanocytes within the skin and hair follicles, resulting in a limited biodistribution. This limited off-target presence minimizes the risk of systemic toxicity, rendering MC1R an ideal target for systemic radiotherapy approaches [3]. Furthermore, upon ligand binding, MC1R is internalized by tumor cells, a key advantage that facilitates more effective tumor cell irradiation while simultaneously lowering organ toxicity [4].

Alpha-melanocyte stimulating hormone (α-MSH) peptide analogs are highly promising agents for melanoma-specific imaging and therapy, primarily due to their nanomolar binding affinity for MC1R [5, 6]. The development of these MSH-targeted agents follows two main therapeutic strategies: modifying the analogs with β-emitters for Peptide Receptor Radionuclide Therapy (PRRT) or employing highly potent α-particle emitters for Targeted Alpha Therapy (TAT) and targeted ablation. These radiolabeled analogs serve as both diagnostic probes for melanoma detection and as therapeutic agents.

2.1 *β-Emitters Labeled MC1R-Targeting Radiopharmaceuticals*

^{90}Y-DOTA-Re(Arg^{11})CCMSH and ^{177}Lu-DOTA-Re (Arg^{11}) CCMSH are radiolabeled peptides synthesized by Thomas P. Quinn's team in 2005. Both radiolabeled peptides displayed rapid cellular internalization and extended cellular retention [7]. The pharmacokinetics and tumor-targeting properties were determined in B16/F10 murine melanoma-bearing C57Bl/6 mice. Both radiolabeled peptides showed very rapid and high tumor uptake. ^{90}Y-DOTA-Re(Arg^{11}) CCMSH achieved its peak tumor uptake at 2 h post-injection, which was significantly higher than the ^{177}Lu analog's uptake at the same time point (the ^{177}Lu-DOTA-Re(Arg^{11})CCMSH peak tumor uptake occurred at 4 h post-injection). Tumor uptake was confirmed to be specific and receptor-mediated. The tumor uptake reduced at after 2 h post-injection. Both agents demonstrated very rapid whole-body clearance. Approximately 90% of the injected dose was washed out by 2 h post-injection, increasing to 93%–96% by 24 h. The ability of ^{177}Lu

to emit γ-rays (113 and 208 keV) makes it suitable for tumor imaging during therapy [6]. Therefore, ^{177}Lu- DOTA-Re-(Arg^{11})-CCMSH can be used as an integrated diagnostic and therapeutic drug.

The team optimized two types of radioactive peptides in 2006. A negatively charged amino acid, glutamic acid (Glu), was coupled to DOTA-Re(Arg^{11})CCMSH between DOTA and Cys at the 3rd position to generate a new peptide, DOTA-Re(Glu2, Arg^{11})CCMSH [8]. ^{90}Y-DOTA-Re (Glu^2, Arg^{11}) CCMSH and ^{177}Lu-DOTA-Re(-Glu^2, Arg^{11}) CCMSH exhibit favorable properties for radiopharmaceutical application, including rapid clearance, high and specific tumor uptake, and, most importantly, significantly reduced kidney uptake compared to the DOTA-Re(Arg11)CCMSH counterparts. This improved biodistribution leads to a superior tumor-to-kidney absorbed dose ratio, suggesting that DOTA-Re(Glu^2, Arg^{11})CCMSH is a more promising candidate for PRRT of melanoma [7]. In addition, linear peptide analogs such as ^{99m}Tc-CCMSH, ^{111}In DOTA-MSH, and ^{67}Ga-DOTA-NAPamide have the potential to serve as SPECT imaging probes [5].

2.2 MC1R-Targeted α-Particle Therapy

TAT is a compelling therapeutic approach for malignancies, such as melanoma, offering the advantage of maximizing damage to disease while minimizing toxicity to surrounding non-targeted tissues. This selectivity is attributed to the short path length and high linear energy transfer (LET) of α-particles [9].

In the context of melanoma, an α-emitting radiopharmaceutical targeting MC1R, specifically ^{225}Ac-DOTA-Ahx-MC1RL, has been successfully synthesized and demonstrated promising results in preclinical in vivo studies [10]. Comparative research investigating two therapeutic α-particle-emitting radiopharmaceuticals, ^{225}Ac-DOTA-Ahx-MC1RL (^{225}Ac-Ahx) and ^{225}Ac-DOTA-di-D-Glu-MC1RL (^{225}Ac-di-D-Glu), found ^{225}Ac-Ahx to be the more effective agent. Specifically, ^{225}Ac-Ahx exhibited significantly superior tumor growth delay and prolonged survival in a mouse model. Despite ^{225}Ac-Ahx showing higher liver uptake compared to ^{225}Ac-di-D-Glu, both compounds maintained acceptable toxicity profiles over a 7-month period, positioning both as promising and safe candidates for continued development in TAT for melanoma [9].

2.3 Innovative Platform for Integrated Theranostic Targeting of MC1R

2.3.1 The Theranostic Principle and the ^{203}Pb/^{212}Pb pair

The concept of the theranostic approach is highly attractive, involving the concurrent administration of a radiopharmaceutical pair: one labeled with a diagnostic radionuclide suitable for imaging and the other with a cytotoxic alpha- or beta-emitting radionuclide for

therapy [11]. A significant combination within this paradigm is the $^{203}Pb/^{212}Pb$ Pair.

The utility of the $^{203}Pb/^{212}Pb$ pair stems from its shared radiolabeling chemistry, which is ideal for a seamless theranostic platform. While ^{212}Pb decay chains are almost pure α- and β emitters exploited solely for radiotherapy, its diagnostic counterpart, ^{203}Pb, enables imaging via single-photon emission computed tomography (SPECT). Specifically, ^{203}Pb has a half-life of 51.9 h and emits 279 keV γ-rays, which are well-suited for SPECT imaging [12]. The ^{203}Pb-DOTA-GGNle-CycMSH$_{hex}$ is a novel α-MSH peptide designed for theranostic applications in melanoma. Its primary advantages include high binding specificity and affinity for MC1R, which is overexpressed in most melanomas, along with rapid cellular internalization and prolonged intracellular retention. Furthermore, it exhibits favorable pharmacokinetics characterized by high tumor uptake (e.g., 16.81% ± 5.48% ID/g at 2 h in B16/F10 tumors) and rapid clearance from non-target tissues, resulting in high tumor-to-background ratios. However, a notable disadvantage is the moderate radioactive accumulation in the kidneys (e.g., 5.43% ± 2.0% ID/g at 2 h), a common challenge for peptide-based agents. The main application demonstrated is the high-contrast SPECT/CT imaging of both primary flank tumors and pulmonary metastatic melanoma lesions. The future development direction focuses on transitioning this probe into a targeted α-radionuclide therapy by substituting ^{203}Pb with its therapeutic twin, ^{212}Pb, leveraging their identical radiolabeling chemistry to provide a precise, imaging-guided treatment for metastatic melanoma [12].

2.3.2 Gold Nanocages for Multimodal Theranostics

Beyond pure radiotheranostics, complex nanostructures, such as gold nanocages (AuNCs), are being investigated for multimodal applications in melanoma. Zhao et al reported on α-MSH-functionalized AuNCs, radiolabeled with ^{64}Cu [13]. The physical properties of ^{64}Cu are uniquely suited for theranostics, as it is both a positron- and β -emitter, allowing its use for both diagnosis and therapy at different dosages. AuNCs are inherently valuable as a multivalent platform due to their high surface-to-volume ratio, which facilitates the conjugation of various functional components. The conjugation of the α-MSH peptide specifically targets the highly expressed MC1R on melanoma cells, enabling sensitive and specific in vivo detection via MC1R-mediated delivery. The AuNCs were engineered to a smaller size, which successfully reduced their uptake by the Mononuclear Phagocyte System (MPS) (liver and spleen) by at least two-fold compared to larger counterparts (e.g., 50 nm AuNCs). This size reduction is crucial for optimizing in vivo pharmacokinetics and mitigating potential systemic toxicity. Furthermore, efficient PEGylation resulted in high initial blood retention, followed by a rapid decrease that favors a low background signal for imaging [13]. The AuNCs also

possess efficient photothermal conversion capability, positioning them as unique nanostructures for image-guided photothermal therapy [13]. Following injection and localization via PET/CT imaging, a near-infrared laser (NIR) can be applied to the tumor site to produce a photothermal effect, thus integrating photothermal heating with radionuclide therapy for enhanced cancer eradication [4].

3 VLA-4-Targeting Theranostics

VLA-4 is a transmembrane noncovalent heterodimer widely expressed on various malignancies, including melanoma, lymphoma, and multiple myeloma [14]. Its native ligands, fibronectin and vascular cell adhesion molecule-1 (VCAM-1), mediate VLA-4's crucial role in tumor growth, angiogenesis, and metastasis by promoting tumor cell adhesion and migration [14]. Significantly, the heightened expression of the VLA-4 integrin correlates directly with tumor progression and the development of human melanoma metastasis [15]. This critical involvement in malignancy establishes high-affinity ligands, notably LLP2A, as effective platforms for targeted drug development [16].

3.1 ^{177}Lu/^{68}Ga-DOTA-PEG4-LLP2A for Melanoma Theranostics

Preliminary studies have demonstrated that the non-PEGylated ^{111}In-DOTA-LLP2A complex achieves excellent tumor targeting, confirmed by small-animal SPECT, showing a high tumor-to-non-tumor uptake ratio [14]. Expanding on this, Carolyn J. Anderson's group evaluated the theranostic pair, ^{177}Lu- and ^{68}Ga-labeled DOTA-PEG4-LLP2A, for VLA-4-targeted radiotherapy and companion PET imaging in metastatic melanoma. The agents demonstrate high affinity for VLA-4, rapid cellular internalization, and significant tumor accumulation with high contrast, enabling the detection of metastases as small as 1–2 mm. While showing great promise for diagnosis and treatment—particularly for patients resistant to current targeted therapies—the conjugates also exhibit notable uptake in VLA-4-rich healthy organs like the spleen and bone marrow, which may limit the therapeutic window.

Collectively, these robust preclinical data support the significant potential of the ^{177}Lu-DOTA-PEG4-LLP2A and ^{68}Ga-DOTA-PEG4-LLP2A compounds as a VLA-4-targeted theranostic platform for both the diagnosis and treatment of melanoma and other VLA-4-expressing malignancies [17].

3.2 Other Probes Targeting VLA-4

Hao Wu et al developed novel VLA-4-targeting conjugates of the high-affinity ligand LLP2A by attaching ^{68}Ga-DOTA to either the Ach or Aad side chain of the molecule. In vivo evaluation demonstrated that [^{68}Ga]Ga-T-CH significantly outperformed [^{68}Ga]Ga-T-AD, achieving higher tumor uptake while maintaining comparable tumor-to-muscle ratios. To further optimize the imaging profile,

polyethylene glycol (PEG) linkers (PEG2, PEG4, PEG6) were introduced between the Ach and DOTA. Among these PEGylated probes, [^{68}Ga]Ga-T2 (featuring a PEG2 linker) yielded the most favorable in vivo distribution profile, notably increasing the tumor-to-muscle ratio by approximately three-fold compared to the non-PEGylated [^{68}Ga]Ga-T-CH [18].

In a separate development, the David M. Perrin group successfully enhanced the bioconjugate RBF 3-LLP2A by chelating it with an additional DOTA fragment. This design modification resulted in a nearly three-fold increase in tumor uptake and a greater than tenfold reduction in gastrointestinal (GI) accumulation [19].

Human serum albumin's long biological half-life is leveraged to extend the circulation time of therapeutic agents [20]. While albumin-binding agents (ABAs) have demonstrated significantly improved biodistribution, enhanced tumor targeting, and superior therapeutic efficacy compared to their non-albumin-bound counterparts, this is often coupled with a trade-off of increased hematopoietic toxicity [21].

To explore this balance, the Carolyn J. Anderson group utilized click chemistry to synthesize and characterize three novel albumin-binding, VLA-4-targeted radioconjugates: ^{177}Lu-Lu-1, ^{177}Lu-Lu-2, and ^{177}Lu-Lu-3. All three compounds exhibited favorable properties, including hydrophilicity, excellent stability, slow blood clearance, and high-affinity binding to VLA-4 receptors.

Comparative analysis revealed distinct biodistribution profiles among the analogs: Lu-3 achieved the highest tumor uptake, peaking at 48 h; Lu-2 demonstrated superior overall tumor-to-non-target tissue ratios; and Lu-1 displayed the most rapid blood clearance. This work highlights that the BCN-azide click linkage is optimal for the future development of versatile theranostic libraries that incorporate different VLA-4 ligands, albumin binders, and chelators [22].

4 Melanin Targeting Radiopharmaceuticals

Melanin represents a highly specific biomarker for malignant melanoma, enabling a targeted theranostic approach using benzamide-based radiopharmaceuticals. Although the early SPECT tracer ^{123}I-BZA2 demonstrated diagnostic utility for pigmented lesions, its clinical translation was significantly limited by a low sensitivity of approximately 39% for metastatic sites and the inherently lower spatial resolution of SPECT imaging [23, 24]. To overcome these challenges, the PET probe ^{18}F-P3BZA was developed, featuring a simplified automated synthesis via solid-phase extraction and superior melanin-binding affinity [25, 26]. Clinical studies confirm that ^{18}F-P3BZA is safe, well-tolerated, and provides exceptional

tumor-to-background contrast, achieving 100% sensitivity in detecting primary melanoma [25, 27]. Beyond diagnostic imaging, the intrinsic theranostic potential of melanin-binding agents allows for targeted radionuclide therapy (TRT) by substituting imaging isotopes with therapeutic emitters like ^{131}I or ^{212}Pb [24]. Specifically, the radiopharmaceutical ^{131}I-ICF01012 has shown significant anti-tumor efficacy in preclinical models, effectively inhibiting tumor growth and improving survival rates across both BRAF- and NRAS-mutant pigmented melanoma subtypes [28]. To further ensure clinical safety and precision, current translational protocols such as the MELRIV-1 study utilize a low-dose diagnostic scan of ^{131}I-ICF01012 for patient-specific dosimetry before administering high-activity therapeutic doses. Its primary advantages include its exceptional pharmacokinetic profile (characterized by prolonged tumor retention for up to 8 days and rapid clearance from nontarget organs, offering a potent systemic solution for polymetastatic disease) and a potential immune-activating abscopal effect. However, its efficacy is limited by the biological requirement for melanin, which may be lost in dedifferentiated tumors, and the inherent risk of radiotoxicity to healthy pigmented tissues such as the retina. Currently applied to pigmented metastatic melanoma patients who have failed standard treatments (like immune checkpoint inhibitors), the future development of this therapy focuses on establishing optimized therapeutic doses and exploring synergistic combinations with immunotherapy to enhance clinical outcomes by transforming "cold" tumors into "hot" ones through radiation-induced antigen release [29].

5 Other Theranostic Radiopharmaceuticals

The copper transporter (CTR1), which is highly expressed in both melanotic (B16/F10) and amelanotic (A375M) melanoma, is another target for melanoma theranostics. In vitro uptake was specific and effectively blocked by excess cold $CuCl_2$. PET imaging clearly visualized both tumor types with high contrast, and biodistribution confirmed sustained tumor accumulation. Radionuclide therapy with a single dose of $^{64}CuCl_2$ significantly slowed tumor growth and prolonged survival without long-term toxicity, demonstrating that $^{64}CuCl_2$ is a promising agent for both PET imaging and radiotherapy of CTR1-positive melanomas [30].

Other peptide or small-molecule theranostics include FAP-targeting agents and CXC chemokine receptor type 4 (CXCR4) targeting agents. Although mostly studied in other cancers, FAP-targeted and CXCR4-targeted radioligand therapy could theoretically be applied in melanoma stroma-rich lesions [31].

6 Conclusion and Perspectives

The field of melanoma theranostics is exceptionally promising, largely owing to intensive research into two key targets: MC1R and VLA-4. MC1R is an ideal candidate for systemic radiotherapy due to its high expression in approximately 80% of melanomas and its restricted distribution to melanocytes, which minimizes the risk of off-target toxicity. Optimizations through peptide engineering, such as with ^{177}Lu-DOTA-Re(Glu^{2}, Arg^{11})CCMSH, have significantly reduced renal uptake and enabled the integration of diagnosis and therapy via the γ-ray emission capability of ^{177}Lu. Concurrently, VLA-4, an integrin correlated with tumor progression and metastasis, has established an effective theranostic platform through high-affinity ligands like LLP2A. Optimization strategies, including PEGylation and the introduction of albumin-binding moieties, have further enhanced the biodistribution and tumor uptake of VLA-4-targeted agents, as exemplified by ^{177}Lu-Lu-3.

^{131}I-ICF01012 offers precise imaging-guided radiotherapy but is limited by tumor dedifferentiation and off-target toxicity. An alternative approach using $^{64}CuCl_2$ targets the broadly expressed copper transporter CTR1, demonstrating efficacy in both melanotic and amelanotic models with favorable pharmacokinetics and no long-term toxicity. Additionally, emerging peptide-based agents targeting FAP or CXCR4 hold theoretical potential for melanoma, particularly in stroma-rich lesions. These diverse platforms underscore a shift toward personalized, image-guided radionuclide therapy, with future directions emphasizing dose optimization and synergistic combinations with immunotherapy.

Significant advances have been made in optimizing known melanoma-targeted probes (e.g., melanin, MC1R, and integrins) through structural modifications (PEGylation, chelator substitution) to enhance binding affinity, pharmacokinetics, and tumor contrast. New targets such as CTR1, CXCR4, VLA-4, and FAP may lead to novel radiopharmaceuticals development C-6, for more specific imaging and immunotherapy monitoring. Furthermore, emerging radionuclides, including $^{155/161}$Tb,$^{203/212}$Pb, $^{44/47}$Sc, and $^{64/67}$Cu, are being developed as theranostic pairs, enabling personalized dosimetry and combined imaging-therapy strategies for melanoma.

Conflict of Interest

The authors have no conflicts of interest to declare that are relevant to the content of this chapter.

References

1. Davis LE, Shalin SC, Tackett AJ (2019) Current state of melanoma diagnosis and treatment. Cancer Biol Ther 20(11):1366–1379
2. Rouanet J, Quintana M, Auzeloux P et al (2021) Benzamide derivative radiotracers targeting melanin for melanoma imaging and therapy: preclinical/clinical development and combination with other treatments. Pharmacol Ther 224:107829
3. Filippi L, Frantellizzi V, De Vincentis G (2021) David versus Goliath: radiotheranostic nanomedicine as a weapon against melanoma. Cancer Treat Res Commun 29:100478
4. Suzuki H, Uehara T (2025) Precision targeting of the melanocortin-1 receptor with radiopharmaceuticals in metastatic melanoma. Expert Opin Ther Targets 29(9):609–612
5. Miao Y, Quinn TP (2007) Alpha-melanocyte stimulating hormone peptide-targeted melanoma imaging. Front Biosci 12:4514–4524
6. Catania A (ed) (2010) Melanocortins: multiple actions and therapeutic potential. Advances in experimental medicine and biology, Springer, New York, NY p 681
7. Miao Y, Hoffman TJ, Quinn TP (2005) Tumor-targeting properties of 90Y- and 177Lu-labeled alpha-melanocyte stimulating hormone peptide analogues in a murine melanoma model. Nucl Med Biol 32(5):485–493
8. Miao Y, Fisher DR, Quinn TP (2006) Reducing renal uptake of 90Y- and 177Lu-labeled alpha-melanocyte stimulating hormone peptide analogues. Nucl Med Biol 33(6):723–733
9. Tichacek CJ, Tafreshi NK, Kil H et al (2020) Biodistribution and multicompartment pharmacokinetic analysis of a targeted α particle therapy. Mol Pharm 17(11):4180–4188
10. Tafreshi NK, Tichacek CJ, Pandya DN et al (2019) Melanocortin 1 receptor–targeted α -particle therapy for metastatic uveal melanoma. J Nucl Med 60(8):1124–1133
11. Filippi L, Scopinaro F, Pelle G et al (2016) Molecular response assessed by (68) Ga-DOTANOC and survival after (90)Y microsphere therapy in patients with liver metastases from neuroendocrine tumours. Eur J Nucl Med Mol Imaging 43(3):432–440
12. Yang J, Xu J, Cheuy L et al (2019) Evaluation of a novel Pb-203-labeled lactam-cyclized alpha-melanocyte-stimulating hormone peptide for melanoma targeting. Mol Pharm 16(4):1694–1702
13. Zhao Y, Pang B, Detering L et al (2018) Melanocortin 1 receptor targeted imaging of melanoma with gold nanocages and positron emission tomography. Mol Imaging 17:1536012118775827
14. DeNardo SJ, Liu R, Albrecht H et al (2009) 111In-LLP2A-DOTA polyethylene glycol–targeting α4β1 integrin: comparative pharmacokinetics for imaging and therapy of lymphoid malignancies. J Nucl Med 50(4):625–634
15. Schadendorf D, Heidel J, Gawlik C et al (1995) Association with clinical outcome of expression of VLA-4 in primary cutaneous malignant melanoma as well as P-selectin and E-selectin on intratumoral vessels. J Natl Cancer Inst 87(5):366–371
16. Gai Y, Sun L, Lan X et al (2018) Synthesis and evaluation of new bifunctional chelators with phosphonic acid arms for gallium-68 based PET imaging in melanoma. Bioconjug Chem 29(10):3483–3494
17. Beaino W, Nedrow JR, Anderson CJ (2015) Evaluation of (68)Ga- and (177)Lu-DOTA-PEG4 -LLP2A for VLA-4-targeted PET imaging and treatment of metastatic melanoma. Mol Pharm 12(6):1929–1938
18. Zhou P, Wu Y, Han G et al (2025) Comparison of a series of 68Ga-Labeled DOTA-LLP2A conjugates for positron emission tomography imaging of very late antigen-4 in melanoma. Mol Pharm 22(2):1031–1041
19. Roxin Á, Zhang C, Huh S et al (2019) A metal-free DOTA-conjugated 18F-labeled radiotracer: [18F]DOTA-AMBF3 -LLP2A for imaging VLA-4 over-expression in murine melanoma with improved tumor uptake and greatly enhanced renal clearance. Bioconjug Chem 30(4):1210–1219
20. Sand KMK, Bern M, Nilsen J et al (2015) Unraveling the interaction between FcRn and albumin: opportunities for design of albumin-based therapeutics. Front Immunol 5:682
21. Pun MD, Gallazzi F, Ho K-V et al (2024) Albumin-binding lutetium-177-labeled LLP2A derivatives as theranostics for melanoma. Mol Pharm 21(6):2960–2969
22. Li L, Wirrick A, Pun MD et al (2025) Effect of click chemistry linkages on the biological behavior of albumin-binding ^{177}Lu-DOTAGA-pIBA-LLP2A analogues targeting melanoma. Bioconjug Chem 36(9):2002–2012
23. Eschbach RS et al (2018) 18F–FDG-PET/CT and diffusion-weighted MRI for monitoring a BRAF and CDK 4/6 inhibitor combination therapy in a murine model of human melanoma. Cancer Imaging 18: 2
24. Zhang X et al (2024) Melanin-targeting radiotracers and their preclinical, translational, and

clinical status: from past to future. J Nucl Med 65:19S–28S
25. Ma X et al (2019) Biodistribution, radiation dosimetry, and clinical application of a melanin-targeted PET probe,18 F-P3BZA, in patients. J Nucl Med 60:16–22
26. Hong Z et al (2021) A convenient and efficient solid phase extraction-based pathway for purification of melanin-targeted probe 18F-P3BZA. Microchem J 164:106008
27. An R, Xiang T, He F, Ma X, Wang Y (2025) Clinical value of combined 18F-FDG and 18F-P3BZA imaging in the diagnosis of melanoma. Front. Med. 12:1571929
28. Akil H et al (2021) Efficacy of targeted radionuclide therapy using [131I]ICF01012 in 3D pigmented BRAF- and NRAS-mutant melanoma models and in vivo NRAS-mutant melanoma. Cancers 13:1421
29. Thivat E, Rouanet J, Auzeloux P et al (2022) Phase I study of [131I] ICF01012, a targeted radionuclide therapy, in metastatic melanoma: MELRIV-1 protocol. BMC Cancer 22(1):417
30. Qin C, Liu H, Chen K et al (2014) Theranostics of malignant melanoma with 64CuCl2. J Nucl Med 55(5):812–817
31. Pirsan I, Piciu D (2025) Radiopharmaceuticals in malignant melanoma: a comprehensive review of diagnostic, therapeutic, and immune-related applications by PET/CT, SPECT/CT, and PET/MRI. Diagnostics 15(18):2305



Chapter 21

PET Imaging of Melanoma Using a Melanin-Targeted Probe

Xiaowei Ma and Zhen Cheng

Abstract

Melanin exists in most melanoma lesions. Melanin plays an important role in melanoma progression, metastasis, therapy response, and the overall survival of patients. Therefore, melanin is a critical target for melanoma diagnosis and therapy. Many melanin-targeting probes, such as radioisotope-labeled benzamide analogs, have been developed for melanoma diagnosis using positron emission tomography (PET). The *N*-(2-(diethylamino)-ethyl)-^{18}F−5-fluoropicolinamide (^{18}F−P3BZA) probe is one of the benzamide analogs and has been preliminarily tested for clinical diagnosis of melanoma in our recent studies. It has shown high specificity and favorable in vivo performance for PET imaging of melanoma. Herein, we describe the detailed synthesis protocol of ^{18}F−P3BZA and the PET/CT imaging procedure for animal models and patients.

Keywords Melanin, Positron emission tomography, Melanoma, Targeted probes

1 Introduction

Melanin is a dark biological pigment that is synthesized and secreted by melanocytes and melanoma cells. Most melanomas are melanotic, in which melanin pigmentation is highly increased because tyrosinase activity is significantly elevated [1, 2]. Only 2%–8% of melanomas are amelanotic (lacking either pigment on visual inspection or melanin in the pathology) [3, 4]. Many studies reported that melanin regulates epidermal homeostasis and plays an important role in melanoma metastasis, the outcome of therapy, and the overall survival of patients with metastatic melanomas [5–7].

Melanin is a highly specific biomarker for melanoma, and it allows differentiation of melanomas from other tumors. It also affects the behavior of melanoma cells and their surrounding environment by modifying cellular metabolism, generating an oxidative environment or hypoxia. Furthermore, melanin is related to immunosuppression and resistance to chemotherapies and radiotherapy [5, 6, 8]. Melanin is a very attractive target for melanoma diagnosis and therapeutic effect evaluation. A variety of radiolabeled melanin-targeting probes

Kristian M. Hargadon (ed.), *Melanoma*, Methods in Molecular Biology, vol. 3089,
https://doi.org/10.1007/978-1-0716-5619-8_21,
© The Author(s), under exclusive license to Springer Science+Business Media, LLC, part of Springer Nature 2027

have been developed for melanoma PET imaging or radionuclide therapy [9–14].

PET/CT is a powerful molecular imaging tool for melanoma diagnosis and therapy response evaluation with high sensitivity and accuracy [15, 16]. Recently, a series of radiolabeled benzamide analogs have been developed for melanin-targeted PET imaging, including N-(2-(diethylamino)-ethyl)-^{18}F-5-fluoropicolinamide (^{18}F-P3BZA) [17], *N*-(2-(dimethylamino)ethyl)-5-^{18}F-fluoropicolinamide (^{18}F-DMPY2) [18], and ^{18}F-*N*-(2-diethylaminoethyl)-4-(2-[2-ethoxy]-ethoxy)pyridine (^{18}F-PFPN) [19]. They have high targeting specificity and binding capability to melanin in melanoma. The structures and synthesis schemes are shown in Fig. 1. ^{18}F-P3BZA and ^{18}F-PFPN have been further studied to understand their radiation dosimetry and pharmaceutical kinetics in human volunteers.

Meanwhile, melanoma patients have been recruited for PET/CT imaging of melanin-targeting PET and ^{18}F-FDG PET. Studies have demonstrated that ^{18}F-P3BZA and ^{18}F-PFPN are safe and show a statistically higher specificity than ^{18}F-FDG for diagnosis of melanoma metastases [17, 19, 20]. ^{18}F-P3BZA and ^{18}F-PFPN have high potential for PET imaging of melanoma by targeting melanin. In this chapter, we describe the detailed synthesis protocol for the precursor and standard of ^{18}F-P3BZA synthesis and PET/CT imaging procedures in melanoma mouse models and patients.

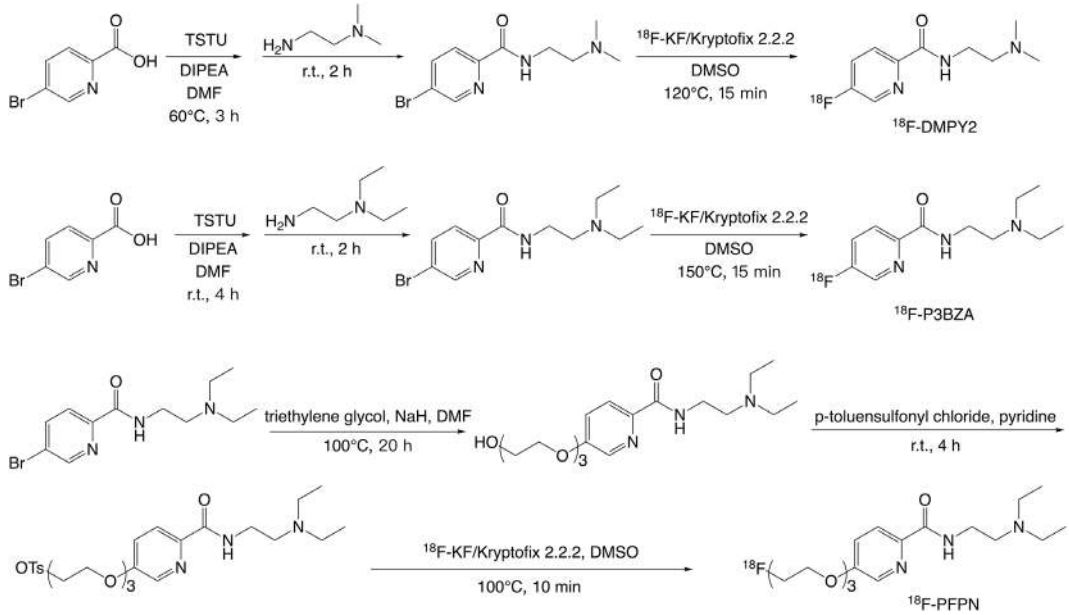


Fig. 1 The structures and synthesis schemes of the melanin-targeting probes

2 Materials

1. Chemicals for synthesis of Br-P3BZA precursor and ^{19}F-P3BZA standard compound (Fig. 2):
   a. 5-bromopyridine-2-caboxylic acid (CAS: 30766-11-1).
   b. 5-fluoropyridine-2-carboxylic acid (CAS: 107504-08-5).
   c. *N*,*N*,*N*',*N*'-tetramethyl-*O*-(*N*-succinimidyl)uronium tetrafluoroborate (TSTU) (CAS: 105832-38-0).
   d. *N*,*N*-diisopropylethylamine (DIPEA) (CAS: 7087-68-5).
   e. *N*,*N*-diethylethylenediamine (CAS: 100-36-7).
2. Dimethylformamide (DMF).
3. Anhydrous Dimethyl sulfoxide (DMSO).
4. Helium or Nitrogen.
5. Anhydrous acetonitrile.
6. Acetonitrile.
7. Ethanol.
8. Deionized water (di-water).
9. K2.2.2/K_2CO_3 solution (1 mL): 15 mg Kryptofix2.2.2 (K2.2.2) and 3.5 mg K_2CO_3 in 0.9 mL of acetonitrile and 0.1 mL of di-water. Store at 4°C and use within 1 month.
10. $^{18}F^-$, produced by a cyclotron.

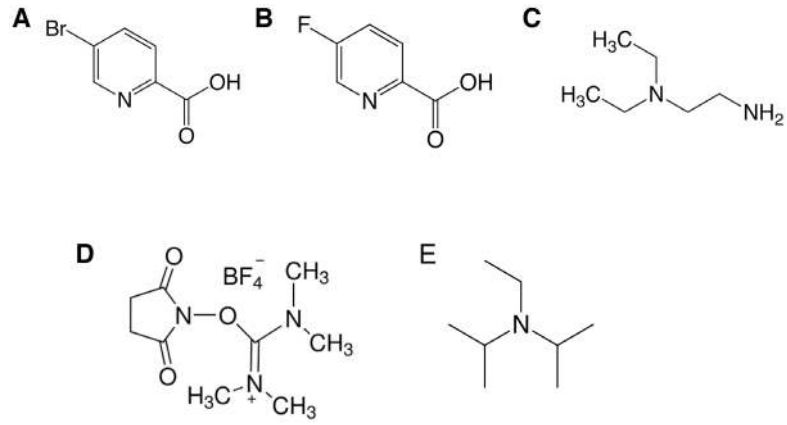


Fig. 2 The chemical structures of the materials. (**A**) 5-bromopyridine-2-caboxylic acid (CAS: 30766-11-1); (**B**) 5-fluoropyridine-2-carboxylic acid (CAS: 107504-08-5); (**C**) *N*,*N*-diethylethylenediamine (CAS: 100-36-7); (**D**) *N*,*N*,*N*',*N*'-tetramethyl-*O*-(*N*-succinimidyl)uronium tetrafluoroborate (TSTU) (CAS: 105832-38-0); (**E**) *N*,*N*-diisopropylethylamine (DIPEA) (CAS: 7087-68-5)

11. 0.01 M $(NH_4)HCO_3$ solution: Dissolve 0.79 g Ammonium bicarbonate (≥99.8%) in 1 L of Millipore water. Then filter through 0.45 μm pore-size PTFE filter.
12. Ethanol/0.01 M $(NH_4)HCO_3$ (1/4, v/v) solution: add 2 mL Ethanol to 8 mL 0.01 M $(NH_4)HCO_3$ solution.
13. Saline (0.9% NaCl).
14. QMA cartridge.
15. C18 plus Sep-Pak cartridge.
16. 0.22 μm sterile filter (PTFE).
17. Cell culture medium: Dulbecco's modified Eagle medium (DMEM) supplemented with 10% fetal bovine serum (FBS).
18. Phosphate-buffered saline (PBS).
19. Trypsin.
20. Incubator.
21. Sterile Petri dishes.
22. Hemocytometer.
23. C57BL/6 mice, 4–6 weeks old.
24. Anesthesia machine, oxygen, and isoflurane.
25. 1 cm^3 tuberculin syringe with 21 G needle.
26. Trypan Blue solution: Dilute to 0.8 mM in PBS. Store at room temperature. S for 1 month.
27. High-performance liquid chromatography (HPLC).
28. Thin layer chromatography (TLC) instrument.
29. Radioactivity detector (for detecting radioactivity of the TLC strip).
30. TLC developing solvent: Mix Methanol and $(NH_4)HCO_3$ at a 6:4 (v:v) ratio.
31. Paper or silica gel-coated sheets for TLC.
32. PET scanners (micro-PET/CT and clinical PET/CT).

3 Methods

3.1 Synthesis of the Precursor (Br-P3BZA) and Standard (^{19}F-P3BZA)

The reaction for this synthesis scheme is shown in Fig. 3. For the reagent equivalents in this reaction, *see* **Note 1**.

1. Dissolve 5-Bromopyridine-2-caboxylic acid (or 5-Fluoropyridine-2-carboxylic acid for synthesizing standard) in DMF at a concentration of ~100 nM (in 500 ′L of DMF).
2. Add TSTU to the above solution.

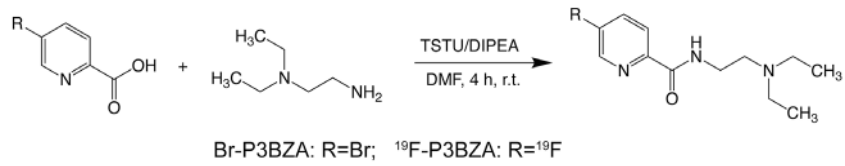


Fig. 3 Synthesis scheme of Br-P3BZA and ^{19}F-P3BZA

3. Add DIPEA to the above solution.
4. Add *N*,*N*-Diethylethylenediamine to the reaction.
5. Incubate the reaction for 2 h at room temperature (20°C–25°C).
6. Check the reaction with HPLC and mass spectrometry (MS).
7. Load the mixture onto HPLC for purification: set absorption wavelength at 254 nm. Mobile phases are acetonitrile and di-water.
8. Collect the product.
9. Check the molecular weight, structure, and purity of the product with mass spectrometry (MS), ^{1}H-NMR, ^{13}C-NMR, and HPLC.
10. Lyophilize and weigh the product.
11. Dissolve the product in 10% ethanol to make a 30 mg/mL solution.
12. Inject the solution through the 0.22 μm filter under a biosafety cabinet.
13. Recalculate the concentration with spectrometer at an absorption wavelength of 254 nm.
14. Aliquot to 3 mg per vial.
15. Lyophilize in a sterile room or in a biosafety cabinet.
16. Seal: sealed with helium protection.
17. Store at –20°C; and for animal experiment use only. For human use, the precursor must be synthesized by a manufacturer in a Good Manufacturing Practice (GMP) environment and with certifications.

3.2 Radiochemistry of the ^{18}F-P3BZA Probe

The radiochemistry of ^{18}F-P3BZA is shown in Fig. 4.

1. Dissolve 3 mg of anhydrous Br-P3BZA in 1 mL of anhydrous DMSO.
2. Prepare and place reagents and materials in the right position of the radiosynthesis module, and double-check that everything is ready (*see* **Notes 2 and 3**).
3. Produce $^{18}F^-$ on cyclotron, and transfer to the module.

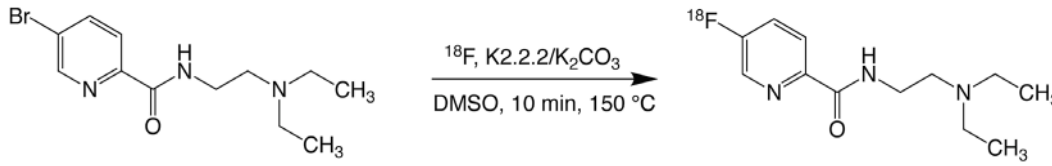


Fig. 4 The radiochemistry scheme of ^{18}F-P3BZA

4. Load $^{18}F^-$ onto QMA cartridge.
5. Elute ^{18}F from QMA with 1 mL of $K_{2.2.2}/K_2CO_3$ solution into reactor.
6. Dry the ^{18}F solution completely under helium or nitrogen flow (*see* **Note 4**).
7. Add anhydrous Br-P3BZA solution to the reactor.
8. Rapidly heat up to 150°C, and keep for 10 min.
9. Cool down the reactor to 45°C.
10. Add 6 mL of $(NH_4)HCO_3$ solution to dilute the reacted solution.
11. Transfer the solution to HPLC for purification (*see* **Note 5**).
12. Monitor the radioactive channel of the HPLC chromatography, and collect the product into an empty vial. The retention time of the product is approximately a few minutes shorter than for the precursor.
13. Dilute the product solution with 20 mL of 0.01 M $(NH_4)HCO_3$ solution.
14. Inject the mixture through a C18 plus Sep-Pak slowly (about 10 mL per minute).
15. Inject 10 mL of di-water through the C18 plus Sep-Pak slowly to remove solvent residue (about 10 mL per minute).
16. Elute desired product from the C18 plus Sep-Pak with 2 mL of Ethanol/0.01 M $(NH_4)HCO_3$ (1/4, v/v) and then 10 mL of saline, and pass through a 0.22 μm sterile filter to a sterile vial (*see* **Note 6**).
17. Mix 3.7 MBq of product with 20 μg of ^{19}F-P3BZA, and then inject into HPLC to test the retention time (*see* **Note 7**).
18. Perform routine radiopharmaceutical quality control (QC) tests (including radionuclide identity, radionuclide purity, radiochemical purity, chemical purity, visual examination, content of solvents, and sterility) of the product (*see* **Note 8**).
19. The product is ready for use once all QCs are passed.

3.3 PET/CT Imaging of Melanoma in Mouse Models

1. Grow B16F10 melanoma cells in DMEM containing 10% FBS.

2. When cells are 70%–80% confluent, remove medium and wash cells with PBS.
3. Harvest cells grown in monolayer culture during the exponential growth phase using trypsin.
4. Add culture medium and disperse cells.
5. Centrifuge cells immediately at 225 × *g* for 5 min, and wash twice with PBS.
6. Resuspend cells in PBS. Mix 20 μL of cell suspension with 20 μL of trypan blue solution, and count cell number using a hemocytometer to calculate the cell concentration. Viable cells exclude trypan blue, while dead cells are stained blue color due to trypan blue uptake.
7. Mix cells, and draw 1.0×10^6 cells (50 μL) into a syringe without a needle.
8. Clean and sterilize the lower flank of 4–6-week-old C57BL/6 mice, and subcutaneously inject B16F10 cells using a 1-cm^3 syringe with 21-G needle.
9. Start imaging experiments when the tumors have reached an average volume of 100 mm^3.
10. Anesthetize mice with 2.5% isoflurane.
11. Inject about ~3.7 MBq of ^{18}F-P3BZA (100 μL) into the mice through the tail vein.
12. Acquire PET/CT images at 20–40 min post-injection. Imaging parameters should be set according to the manual of the PET scanner.
13. Process and analyze the imaging data (*see* **Note 9**). A PET image of the melanoma in this mouse model is shown in Fig. 5.

3.4 PET/CT Imaging of Melanoma in Human Patients

Extra precautions must be taken when using the ^{18}F-P3BZA probe in clinical settings (*see* **Note 10**).

1. Recruit patients according to the clinical trial regulations.
2. Inject ^{18}F-P3BZA (3.5 MBq/kg body weight) to patient through cubital vein or hand vein.
3. Acquire PET/CT images at 20–40 min post-injection. The scan and reconstruction parameters should be set according to the manual of the PET scanner.
4. Process and analyze the imaging data. A PET image from a melanoma patient is shown in Fig. 6.

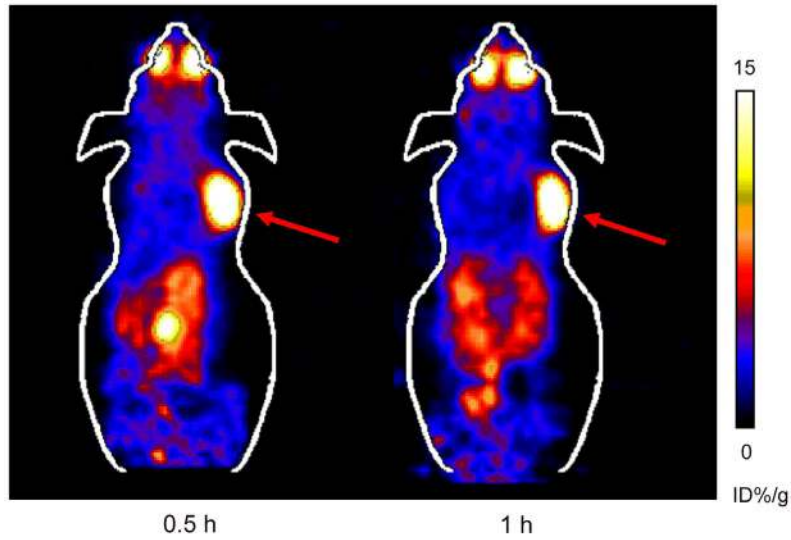


Fig. 5 Decay-corrected static micro-PET images of C57BL/6 mice bearing B16F10 melanoma tumors at 0.5 and 1 h after injection of ^{18}F-P3BZA. Tumors are indicated by arrows. ^{18}F-P3BZA physiological uptake could also be found in the eyes because of melanin distribution in the retina

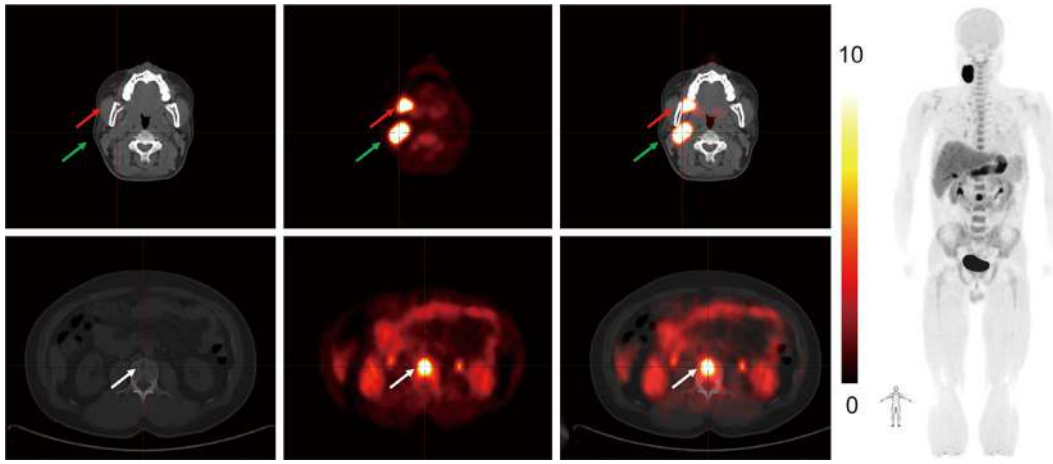


Fig. 6 PET images of a melanoma patient at 60 min after ^{18}F-P3BZA injection. The primary melanoma (red arrow), lymph node (LN) metastasis (green arrow), and bone metastasis (white arrow) could be observed on the PET imaging

4 Notes

1. The reagent equivalents for this reaction are as follows: 5-bromopyridine-2-caboxylic acid or 5-fluoropyridine-2-carboxylic acid = 1; TSTU = 1.5; DIPEA = 4; *N*,*N*-Diethylethylenediamine = 2.

2. Activate a QMA cartridge with 1 mL of ethanol, followed by 1 mL of di-water and then 10 mL of air, and then place it into the synthesis system.
3. Activate C18 cartridges with 10 mL of ethanol, followed by 10 mL of di-water, and then place them in the synthesis system.
4. The radiolabeling yield is critically dependent on the drying degree of ^{18}F and the precursor. Make sure the ^{18}F solution is completely dried. Sometimes, an extra drying with anhydrous acetonitrile is necessary.
5. The mobile phase is 20% acetonitrile and 80% 0.01 M $(NH_4)HCO_3$ solution, and a reversed-phase 5 μm C18 column is preferred. The retention time of the product is significantly shorter than that of the precursor. A prepurification step could be added to the protocol: if desired, load the diluted reaction solution onto a C18 plus Sep-Pak cartridge, and elute the C18 with 1 mL of acetonitrile followed by 5 mL of 0.01 M $(NH_4)HCO_3$. Then inject the eluate into the HPLC for further purification.
6. Sometimes the product cannot be retained on the C18 plus Sep-Pak cartridge. In that case, check the pH value (~7.5) of the solution and the ratio of acetonitrile.
7. Theoretically, the retention times on the 254 nm ultraviolet channel and radioactive channel should be the same. However, due to the dead volume of the tubing between the ultraviolet detector and radioactive detector, the retention times are different. Researchers can calculate the time difference based on the speed of the mobile phase and the volume of the tubing.
8. The TLC developing solvent is methanol and 0.01 M $(NH_4)HCO_3$ (v:v = 6:4). The R_f is between 0.5 and 0.8. For human use, the quality must be higher than the radiopharmaceutical standard.
9. The retina uptake is a distinctive property of the ^{18}F-P3BZA probe. Significant retinal uptake should be observed on successful ^{18}F-P3BZA PET imaging.
10. For human PET/CT imaging using ^{18}F-P3BZA, the precursor must be synthesized under a GMP environment and pass strict QC. Each batch of production of ^{18}F-P3BZA must be subjected to quality control according to the requirements of the radiopharmaceutical standard. Also, Institutional Review Board (IRB) approval is needed for human studies of ^{18}F-P3BZA.

Acknowledgments

This work was supported by grants from the National Natural Science Foundation of China (81501501). We acknowledge Dr. Feng He and the Xiangya Second Hospital of Central South University for testing and optimizing the radiochemistry of the ^{18}F-P3BZA based on the method published by our group.

Conflict of Interest The authors have no conflicts of interest to declare that are relevant to the content of this chapter.

References

1. Dadachova E, Casadevall A (2005) Melanin as a potential target for radionuclide therapy of metastatic melanoma. Future Oncol 1(4):541–549. https://doi.org/10.2217/14796694.1.4.541
2. Thompson JF, Scolyer RA, Kefford RF (2005) Cutaneous melanoma. Lancet 365(9460):687–701. https://doi.org/10.1016/S0140-6736(05)17951-3
3. Thomas NE, Kricker A, Waxweiler WT et al (2014) Comparison of clinicopathologic features and survival of histopathologically amelanotic and pigmented melanomas: a population-based study. JAMA Dermatol 150(12):1306–1314. https://doi.org/10.1001/jamadermatol.2014.1348
4. Gualandri L, Betti R, Crosti C (2009) Clinical features of 36 cases of amelanotic melanomas and considerations about the relationship between histologic subtypes and diagnostic delay. J Eur Acad Dermatol Venereol 23(3):283–287. https://doi.org/10.1111/j.1468-3083.2008.03041.x
5. Brożyna AA, Jóźwicki W, Roszkowski K et al (2016) Melanin content in melanoma metastases affects the outcome of radiotherapy. Oncotarget 7(14):17844–17853. https://doi.org/10.18632/oncotarget.7528
6. Slominski RM, Zmijewski MA, Slominski AT (2015) The role of melanin pigment in melanoma. Exp Dermatol 24(4):258–259. https://doi.org/10.1111/exd.12618
7. Brożyna AA, Jóźwicki W, Carlson JA, Slominski AT (2013) Melanogenesis affects overall and disease-free survival in patients with stage III and IV melanoma. Hum Pathol 44(10):2071–2074. https://doi.org/10.1016/j.humpath.2013.02.022
8. Shain AH, Bastian BC (2016) From melanocytes to melanomas. Nat Rev Cancer 16(6):345–358. https://doi.org/10.1038/nrc.2016.37
9. Roberts MP, Nguyen V, Ashford ME et al (2015) Synthesis and in vivo evaluation of [123I]melanin-targeted agents. J Med Chem 58(15):6214–6224. https://doi.org/10.1021/acs.jmedchem.5b00777
10. Cachin F, Miot-Noirault E, Gillet B et al (2014) 123)I-BZA2 as a melanin-targeted radiotracer for the identification of melanoma metastases: results and perspectives of a multicenter phase III clinical trial. J Nucl Med 55(1):15–22. https://doi.org/10.2967/jnumed.113.123554
11. Sillaire-Houtmann I, Bonafous J, Veyre A et al (2004) [Phase 2 clinical study of 123I-N-(2-diethylaminoethyl)-2-iodobenzamide in the diagnostic of primary and metastatic ocular melanoma]. J Fr Ophtalmol 27(1):34–39. https://doi.org/10.1016/s0181-5512(04)96089-5
12. Kertesz I, Vida A, Nagy G et al (2017) In vivo imaging of experimental melanoma tumors using the novel radiotracer (68)Ga-NODAGA-Procainamide (PCA). J Cancer 8(5):774–785. https://doi.org/10.7150/jca.17550
13. Garg PK, Nazih R, Wu Y et al (2017) Selective targeting of melanoma using N-(2-diethylaminoethyl) 4-[(18)F]fluoroethoxy benzamide (4-[(18)F]FEBZA): a novel PET imaging probe. EJNMMI Res 7(1):61. https://doi.org/10.1186/s13550-017-0311-2
14. Rizzo-Padoin N, Chaussard M, Vignal N et al (2016) [(18)F]MEL050 as a melanin-targeted PET tracer: fully automated radiosynthesis and comparison to (18)F-FDG for the detection of pigmented melanoma in mice primary subcutaneous tumors and pulmonary metastases. Nucl Med Biol 43(12):773–780. https://doi.org/10.1016/j.nucmedbio.2016.08.010
15. Mena E, Sanli Y, Marcus C, Subramaniam RM (2017) Precision medicine and PET/Computed Tomography in melanoma. PET Clin 12(4):449–458. https://doi.org/10.1016/j.cpet.2017.05.002
16. Petersen H, Holdgaard PC, Madsen PH et al (2016) FDG PET/CT in cancer: comparison

of actual use with literature-based recommendations. Eur J Nucl Med Mol Imaging 43(4):695–706. https://doi.org/10.1007/s00259-015-3217-0
17. Ma X, Wang S, Wang S et al (2019) Biodistribution, radiation dosimetry, and clinical application of a melanin-targeted PET probe, (18)F-P3BZA, in patients. J Nucl Med 60(1):16–22. https://doi.org/10.2967/jnumed.118.209643
18. Pyo A, Kim DY, Kim H et al (2020) Ultrasensitive detection of malignant melanoma using PET molecular imaging probes. Proc Natl Acad Sci USA 117(23):12991–12999. https://doi.org/10.1073/pnas.1922313117
19. Zhang X, Li M, Gai Y et al (2022) 18)F-PFPN PET: a new and attractive imaging modality for patients with malignant melanoma. J Nucl Med 63(10):1537–1543. https://doi.org/10.2967/jnumed.121.263179
20. Hong Z, Yu B, Xiao J et al (2021) A convenient and efficient solid phase extraction-based pathway for purification of melanin-targeted probe 18F-P3BZA. Microchem J 164:106008. https://doi.org/10.1016/j.microc.2021.106008

Chapter 22

SPECT Imaging of Melanoma Using a ^{99m}Tc-Labeled Melanin-Targeted Probe

Ji Tao, Mei Tian and Zhen Cheng

Abstract

Melanoma is a highly aggressive cutaneous malignancy characterized by a poor clinical prognosis, making early and accurate detection paramount for patient survival. Melanin, abundantly expressed in most melanoma lesions, serves as an ideal and highly specific biomarker for targeted molecular imaging. While various imaging modalities exist, single-photon emission computed tomography (SPECT) provides a highly accessible and cost-effective strategy for widespread clinical translation. From our recent studies, ^{99m}Tc-SMIC-4006 emerged as the optimal ^{99m}Tc-labeled radiotracer, demonstrating exceptional radiochemical purity, highly specific melanin binding, and superior tumor-to-blood contrast in B16F10 melanoma xenografts. Herein, we describe the detailed radiosynthesis protocol for ^{99m}Tc-SMIC-4006, alongside comprehensive procedures for its in vitro property evaluation and in vivo SPECT/CT imaging in preclinical melanoma models.

Keywords Melanin, Single-photon emission computed tomography, Melanoma, ^{99m}Technetium

1 Introduction

Malignant melanoma is an aggressive cutaneous malignancy characterized by a high metastatic potential [1, 2]. While molecular imaging with ^{18}F-FDG PET/CT is widely utilized for clinical staging, its diagnostic accuracy is often compromised by false positives stemming from local inflammation, as well as limited sensitivity toward small or hypometabolic lesions [3, 4]. These limitations underscore an urgent clinical need for imaging strategies that directly target melanoma-specific molecular signatures.

Melanin, a natural pigment overexpressed in more than 90% of melanomas as a consequence of dysregulated tyrosinase activity, has emerged as a robust and highly specific biomarker for targeted molecular imaging [5, 6]. Given its intrinsic involvement in tumor progression, immune evasion, and therapeutic resistance, melanin represents an attractive molecular target for diagnostic intervention. Radiolabeled probes designed to bind melanin, particularly

Kristian M. Hargadon (ed.), *Melanoma*, Methods in Molecular Biology, vol. 3089,
https://doi.org/10.1007/978-1-0716-5619-8_22,
© The Author(s), under exclusive license to Springer Science+Business Media, LLC, part of Springer Nature 2027

benzamide (BZA) derivatives, which engage the pigment through a dual mechanism combining electrostatic interactions and π–π stacking, offer a powerful strategy for distinguishing melanoma from other malignancies [7–9].

Although several PET-based melanin probes (e.g., ^{18}F-P3BZA) have demonstrated significant clinical utility, the high operational costs, limited accessibility of PET facilities, and short half-lives of positron-emitting isotopes underscore an urgent clinical need for cost-effective single-photon emission computed tomography (SPECT) alternatives [10]. However, early generations of ^{99m}Tc-labeled BZA probes frequently suffered from insufficient tumor retention or excessive off-target accumulation in excretory organs such as the liver and kidneys [11–13].

To overcome these pharmacokinetic limitations, we optimized the benzamide framework by introducing a morpholine ring to enhance both structural stability and target affinity, culminating in the development of a novel SPECT probe, ^{99m}Tc-SMIC-4006. Our studies have demonstrated its superior metabolic stability, highly specific melanin binding, and high tumor-to-background contrast [14]. In this chapter, we describe the detailed procedures for the radiosynthesis of ^{99m}Tc-SMIC-4006, alongside methodologies for its in vivo SPECT/CT imaging in preclinical melanoma models.

2 Materials

1. Chemicals for synthesis of precursor compound (Fig. 1):
   a. 2-(Tritylthio)ethanamine (CAS: 1095-85-8).
   b. 2-Bromoacetyl bromide (CAS: 598-21-0).
   c. 4-(2-Bromoethyl)morpholine hydrobromide (CAS: 42802-94-8).
2. Acetonitrile (CAS: 75-05-8).
3. Cesium carbonate (Cs_2CO_3) (CAS: 534-17-8).
4. Potassium iodide (KI) (CAS: 7681-11-0).

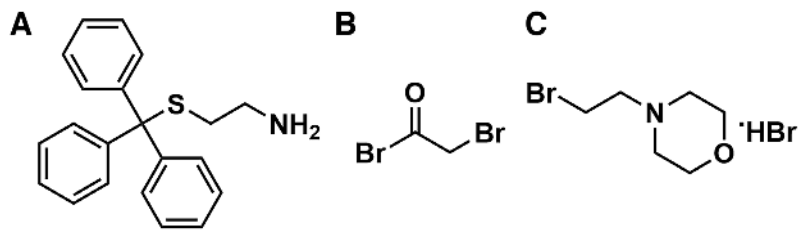


Fig. 1 The chemical structures of the materials. (**A**) 2-(Tritylthio)ethanamine (CAS: 1095-85-8); (**B**) 2-Bromoacetyl bromide (CAS: 598-21-0); (**C**) (4-(2-Bromoethyl)morpholine hydrobromide (CAS: 42802-94-8)

5. Triethylamine (Et_3N) (CAS: 121-44-8).
6. Dichloromethane (DCM) (CAS: 75-09-2).
7. Chloroform (CAS: 67-66-3).
8. Sodium bicarbonate (CAS: 144-55-8).
9. Sodium chloride (CAS: 7647-14-5).
10. Anhydrous sodium sulfate (Na_2SO_4) (CAS: 7757-82-6).
11. Petroleum ether (CAS: 8032-32-4).
12. Ethyl acetate (CAS: 141-78-6).
13. Trifluoroacetic acid (TFA) (CAS: 76-05-1).
14. Triethylsilane (TES) (CAS: 611-14-3).
15. Commercial freeze-dried kit containing sodium gluceptate (CAS: 31138-65-5), stannous chloride (CAS: 7772-99-8), and urea (CAS: 57-13-6).
16. Fresh sodium ^{99m}Tc-pertechnetate ($Na^{99m}TcO_4$) eluted with saline from a ^{99}Mo/^{99m}Tc-generator.
17. Complete cell culture medium: Dulbecco's Modified Eagle's Medium (DMEM, high glucose formulation) supplemented with 10% fetal bovine serum (FBS) and 1% Penicillin-Streptomycin.
18. Phosphate-buffered saline (PBS).
19. Rotary evaporator.
20. Lyophilizer (freeze-dryer).
21. Metal heating block.
22. Humidified cell culture incubator.
23. Animals: Female C57BL/6 mice (6–8 weeks old).
24. Anesthesia machine equipped with oxygen and isoflurane.
25. Nuclear Magnetic Resonance (NMR) spectrometer: Configured for recording ^{1}H and ^{13}C NMR spectra.
26. Liquid Chromatography-Mass Spectrometry (LC–MS) system: Equipped with a C18 reversed-phase column (2.1 mm × 100 mm, 3.5 μm) coupled to a mass spectrometer (UV detection wavelength at 254 nm).
27. Radio-High-Performance Liquid Chromatography (Radio-HPLC) system: Equipped with a flow-through γ-detector for radiochemical purity determination.
28. Animal imaging system: Small-animal single-photon emission computed tomography/computed tomography (SPECT/CT) scanner equipped with animal anesthesia machine.

3 Methods

3.1 Synthesis of the Precursor Compound 4

The reaction for this synthesis scheme is shown in Fig. 2. For the specific reagent equivalents employed in this reaction, *see* **Note 1**.

1. Dissolve 2-(tritylthio)ethanamine in chloroform (10 mL) to attain a 0.1 M concentration.
2. Add triethylamine to the mixture at 4°C.
3. Add 2-bromoacetyl bromide dropwise to the mixture at 4°C over 5 min.
4. Gradually warm the mixture to room temperature and maintain continuous stirring for 48 h.
5. Dilute the reaction mixture with dichloromethane, wash successively with saturated aqueous sodium bicarbonate and brine, and subsequently dry the organic layer over anhydrous sodium sulfate.
6. Filter the mixture, concentrate *in vacuo*, and purify the residue via flash column chromatography using a mobile phase of petroleum ether and ethyl acetate (1:1, v/v) to afford compound **2**.
7. Dissolve compound **2** in acetonitrile to obtain a 0.05 M concentration.
8. Sequentially add 4-(2-bromoethyl)morpholine hydrobromide, cesium carbonate, and potassium iodide at room temperature (*see* **Note 2**).

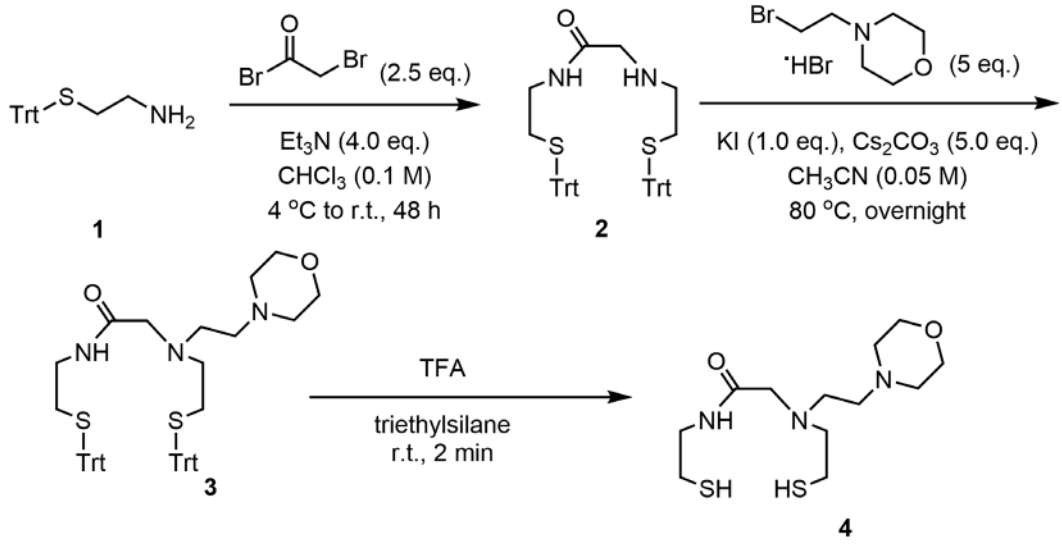


Fig. 2 Synthesis scheme of precursor compound **4**

9. Heat the mixture to 80°C under a nitrogen atmosphere, and stir overnight.
10. Monitor the reaction progression using HPLC and mass spectrometry (MS).
11. Concentrate the mixture *in vacuo*, and subject the residue to HPLC purification (absorption wavelength at 254 nm), utilizing acetonitrile and deionized water as mobile phases, to isolate compound **3**.
12. Collect the target product.
13. Verify the molecular weight, structural integrity, and purity of the product via MS, ^{1}H-NMR, ^{13}C-NMR, and HPLC.
14. Lyophilize and accurately weigh the intermediate product.
15. Dissolve compound **3** in trifluoroacetic acid (TFA) to achieve a 0.015 M concentration.
16. Vortex the solution for 2 min, followed by the dropwise addition of triethylsilane until the solution transitions from yellow to colorless (*see* **Note 3**).
17. Concentrate the reaction solution *in vacuo* via rotary evaporation to completely remove the residual TFA.
18. Dissolve the resulting residue in a defined volume of an appropriate solvent (e.g., ultrapure water), and aliquot the solution into individual single-use reaction vials based on the specific stoichiometric requirements for a single radiolabeling batch.
19. Lyophilize the aliquoted vials to absolute dryness to afford the final deprotected precursor (compound **4**).
20. Immediately seal the vials airtight, and store them at −20°C, strictly protected from light and moisture, until required for radiolabeling (*see* **Note 4**).

3.2 Radiochemistry of the ^{99m}Tc-SMIC-4006 Probe

The radiochemistry procedure of ^{99m}Tc-SMIC-4006 is shown in Fig. 3.

1. Reconstitute a commercially available freeze-dried kit, containing sodium gluceptate, stannous chloride, and urea, with 1 mL

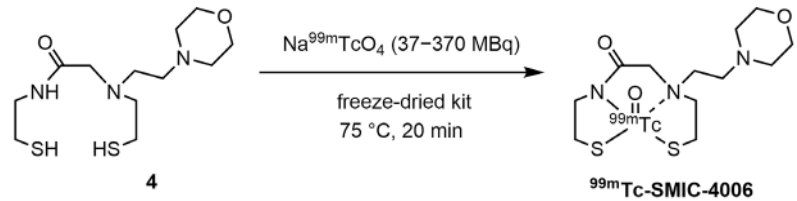


Fig. 3 The radiochemistry scheme of ^{99m}Tc-SMIC-4006

of freshly eluted sodium ^{99m}Tc-pertechnetate ranging from 37 to 111 MBq (*see* **Notes 5 and 6**).

2. Allow the vial to stand at room temperature for 1–2 min to facilitate the formation of the ^{99m}Tc-gluceptate intermediate.
3. Introduce the deprotected precursor, compound **4**, into the reconstituted kit to achieve a final reaction concentration of 12 μM (*see* **Note 7**).
4. Incubate the reaction vessel in a metal heating block at 75°C for 20 min to finalize the radiolabeling process.
5. Withdraw a small aliquot of the final product for routine quality control analysis, ensuring that the radiochemical purity strictly exceeds 95% before in vivo application.

3.3 SPECT/CT Imaging of Melanoma in Mouse Models

1. Cultivate B16F10 melanoma cell lines in complete cell culture medium.
2. Propagate the cell cultures within a standard humidified incubator maintained at 37°C with a 5% CO_2 atmosphere.
3. To establish the tumor xenografts, inoculate one million B16F10 cells (resuspended in 100 μL of serum-free medium) subcutaneously into the right shoulder flank of female C57BL/6 mice (6–8 weeks of age).
4. Monitor tumor progression regularly. Initiate the in vivo imaging studies once the subcutaneous tumors reach an approximate volume of 300 mm^3.
5. Induce and sustain deep sedation in the animal subjects using a 2.5% isoflurane–oxygen mixture.
6. Administer the radiotracer, ^{99m}Tc-SMIC-4006 (~3.7 MBq formulated in 100 μL of saline), via standard intravenous tail vein injection.
7. Perform small-animal SPECT/CTscanning at predetermined time points (e.g., 1 h, 3 h, and 6 h post-administration), utilizing instrument-specific default acquisition protocols.
8. Reconstruct and evaluate the acquired imaging data. Representative in vivo SPECT/CT visualizations of the melanoma xenograft model are presented in Fig. 4 (*see* **Note 8**).

4 Notes

1. The molar equivalents for the reagents in this reaction are as follows: 2-(tritylthio)ethanamine (1.0 equiv.), 2-bromoacetyl bromide (2.5 equiv.), and triethylamine (4.0 equiv.). The

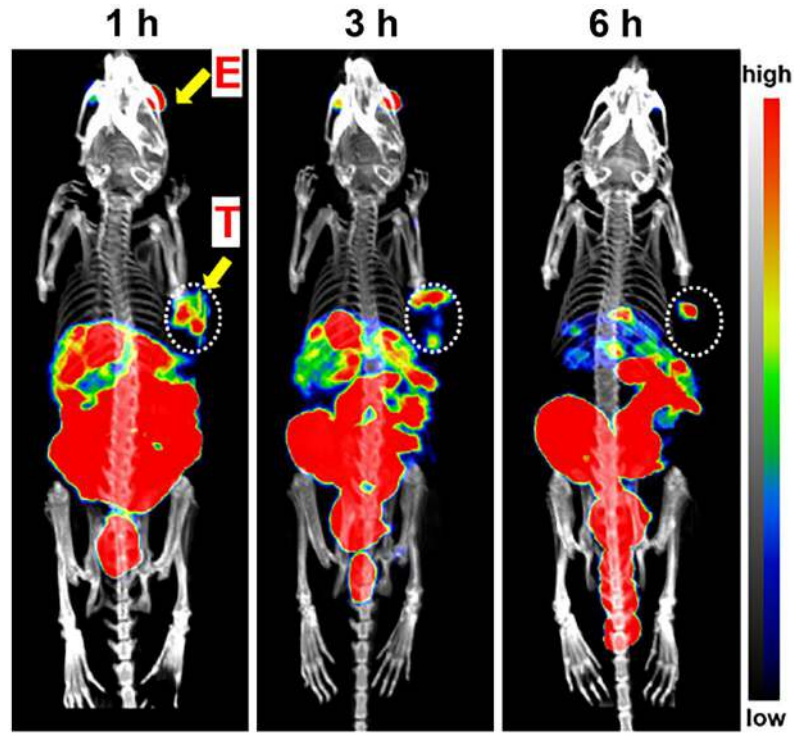


Fig. 4 Micro-SPECT/CT images of C57BL/6 mice bearing subcutaneous B16F10 melanoma xenografts at 1 h, 3 h, and 6 h post-injection of ^{99m}Tc-SMIC-4006. The tumor sites are indicated by yellow arrows and the label "T." Physiological accumulation of the radiotracer can be observed in the eyes (labeled "E"), which is consistent with the endogenous melanin expression in the retina. Note also that in this subcutaneous B16F10 model, no metastatic lesions were observed in the abdominal region at the time of imaging, as confirmed by ex vivo analysis. The abdominal signal is primarily attributable to the in vivo metabolic processing and hepatobiliary or renal excretion of the radiotracer, rather than specific uptake by metastatic tumor cells. Therefore, the abdominal accumulation reflects normal physiological clearance of the probe, not B16F10 metastasis

reaction is performed in chloroform at a substrate concentration of 0.1 M.

2. The molar equivalents for the reagents in this reaction are as follows: compound 2 (1.0 equiv.), 4-(2-bromoethyl)morpholine hydrobromide (5.0 equiv.), cesium carbonate (5.0 equiv.), and potassium iodide (1.0 equiv.).
3. Dissolving the precursor in TFA generates yellow trityl cations, indicating the cleavage of the protecting groups. Triethylsilane (TES) is added as a scavenger to reduce these reactive yellow cations into colorless triphenylmethane. Thus, the visual

transition from yellow to colorless readily confirms the complete liberation of the free thiol groups while preventing re-alkylation.

4. In situ lyophilization of pre-aliquoted solutions circumvents the severe inaccuracies of weighing microgram quantities and minimizes ambient air exposure. Because the deprotected free thiols are highly vulnerable to oxidative dimerization, this single-use strategy strictly avoids repeated freeze–thaw cycles, thereby preserving the precursor's integrity and maximizing radiochemical yield.
5. Upon addition of the ^{99m}Tc eluate, it is imperative to maintain the reaction vial in a strictly upright position and avoid any vigorous shaking or agitation. Given the micro-scale volume of the overall reaction mixture, excessive movement can cause the radioactive liquid to adhere to the upper inner walls or the rubber septum of the vial. This spatial separation removes the reactants from the bulk solution, drastically lowering the effective reaction concentration and ultimately compromising the radiochemical yield.
6. The formation of radiocolloidal impurities (typically insoluble $^{99m}TcO_2$) can occur if the reducing agent (stannous chloride) is compromised due to oxidation over time. Therefore, it is imperative to strictly verify that the commercial lyophilized kit is within its designated shelf life and has been continuously stored under proper conditions (typically 2°C–8°C) prior to reconstitution.
7. Ensure that the deprotected precursor (compound **4**) is dissolved in a suitable co-solvent system (e.g., an ethanol/saline mixture) and properly neutralized prior to addition. Maintaining the reaction mixture at an optimal pH of 6.0–7.5 is critical to facilitate efficient transchelation and preserve the efficacy of the stannous reducing agent.
8. Prominent physiological accumulation of ^{99m}Tc-SMIC-4006 in the eyes is a distinctive hallmark of this probe, driven by the high endogenous melanin expression in the retinal pigment epithelium. Consequently, clear ocular uptake serves as an intrinsic positive control, confirming both the structural integrity of the radiotracer and the overall success of the in vivo SPECT/CT imaging procedure.

Acknowledgments

This work was supported by grants from the National Natural Science Foundation of China (Grant No. U2267221) and the Natural Science Foundation of Shanghai (Grant No. 24ZR1477300).

Conflict of Interest The authors have no conflicts of interest to declare that are relevant to the content of this chapter.

References

1. Siegel RL, Giaquinto AN, Jemal A (2024) Cancer statistics, 2024. CA Cancer J Clin 74(1):12–49. https://doi.org/10.3322/caac.21820
2. Waseh S, Lee JB (2023) Advances in melanoma: epidemiology, diagnosis, and prognosis. Front Med 10:1268479. https://doi.org/10.3389/fmed.2023.1268479
3. Pijl JP, Nienhuis PH, Kwee TC et al (2021) Limitations and pitfalls of FDG-PET/CT in infection and inflammation. Semin Nucl Med 51(6):633–645. https://doi.org/10.1053/j.semnuclmed.2021.06.008
4. Wong ANM, McArthur GA, Hofman MS et al (2017) The advantages and challenges of using FDG PET/CT for response assessment in melanoma in the era of targeted agents and immunotherapy. Eur J Nucl Med Mol Imaging 44(Suppl 1):67–77. https://doi.org/10.1007/s00259-017-3691-7
5. Shi H, Cheng Z (2022) MC1R and melanin-based molecular probes for theranostics of melanoma and beyond. Acta Pharmacol Sin 43(12):3034–3044. https://doi.org/10.1038/s41401-022-00970-y
6. Wei W, Ehlerding EB, Lan X et al (2018) PET and SPECT imaging of melanoma: the state of the art. Eur J Nucl Med Mol Imaging 45(1):132–150. https://doi.org/10.1007/s00259-017-3839-5
7. Ren G, Pan Y, Cheng Z (2010) Molecular probes for malignant melanoma imaging. Curr Pharm Biotechnol 11(6):590–602. https://doi.org/10.2174/138920110792246465
8. Rouanet J, Quintana M, Auzeloux P et al (2021) Benzamide derivative radiotracers targeting melanin for melanoma imaging and therapy: preclinical/clinical development and combination with other treatments. Pharmacol Ther 224:107829. https://doi.org/10.1016/j.pharmthera.2021.107829
9. Zhang X, Lin Z, Feng Y et al (2024) Melanin-targeting radiotracers and their preclinical, translational, and clinical status: from past to future. J Nucl Med 65(Suppl 1):19S–28S. https://doi.org/10.2967/jnumed.123.266945
10. Tually P, Quinto VG, Omar Y et al (2024) Real world experience with [^{99m}Tc]Tc-HYNIC-iPSMA SPECT prostate cancer detection: interim results from the global NOBLE registry. EJNMMI Rep 8(1):43. https://doi.org/10.1186/s41824-024-00226-4
11. Friebe M, Mahmood A, Spies H et al (2000) '3+1' mixed-ligand oxotechnetium(V) complexes with affinity for melanoma: synthesis and evaluation in vitro and in vivo. J Med Chem 43(14):2745–2752. https://doi.org/10.1021/jm000050e
12. N'Dongo HWP, Raposinho PD, Fernandes C et al (2010) Preparation and biological evaluation of cyclopentadienyl-based Tc-^{99m}-complexes (Cp-R)Tc-$^{99m}CO_3$ mimicking benzamides for malignant melanoma targeting. Nucl Med Biol 37(3):255–264. https://doi.org/10.1016/j.nucmedbio.2009.11.006
13. Cheng Z, Mahmood A, Li H et al (2005) ^{99m}TcOAADT]-$(CH_2)_2$-NEt_2: a potential small-molecule single-photon emission computed tomography probe for imaging metastatic melanoma. Cancer Res 65(12):4979–4986. https://doi.org/10.1158/0008-5472.CAN-03-3093
14. Tao J, Cao R, Lei Z et al (2025) Development of ^{99m}Tc-labeled melanin-targeted probes for SPECT imaging of melanoma. Eur J Nucl Med Mol Imaging 52(11):4157–4170. https://doi.org/10.1007/s00259-025-07268-1

Chapter 23

PET Imaging of Melanoma Using a Melanocortin 1 Receptor-Targeted Probe

Tian Xiang, Mengshi Li, Nicholas J. Baumhover, Michael K. Schultz, Zhen Cheng and Xiaowei Ma

Abstract

The melanocortin-1 receptor (MC1R) is overexpressed in more than 80% of melanoma cells but is expressed at low levels in normal tissues, making it an important target for melanoma imaging and therapy. Recently, MC1R has attracted the interest of numerous researchers as a target for melanoma. Radiolabeled alpha-melanocyte-stimulating hormone (α-MSH) peptides bind specifically to MC1R and internalize into tumor cells, enabling melanoma diagnosis and therapy. Several radiolabeled α-MSH peptides have been developed. Among those, a cyclized α-MSH peptide produced via an alternative click chemistry cyclization strategy offers faster and more specific bindings to MC1R. It could be labeled with $^{203}Pb/^{212}Pb$ (VMT01) for melanoma single-photon emission computed tomography (SPECT) imaging and therapy and also could be labeled with ^{68}Ga (VMT02) for positron emission tomography (PET) imaging. Preliminary clinical imaging showed highly sensitive and specific melanoma detection. This chapter describes the synthesis of VMT02 and PET/CT imaging procedures in both mouse models and patients.

Keywords Melanocortin-1 receptor, Positron emission tomography, Melanoma, Targeted probes

1 Introduction

The melanocortin-1 receptor (MC1R) is a G protein-coupled receptor that is overexpressed in over 80% of melanoma cells while showing low expression in normal tissues, making it a promising molecular target for receptor-targeted melanoma imaging and therapy [1, 2]. Alpha-melanocyte stimulating hormone (α-MSH) and its analogs can specifically bind to MC1R, with nanomolar affinity. Upon binding to MC1R, radionuclide-labeled α-MSH peptides can be internalized into melanoma cells, enabling tumor imaging and therapy [3].

To date, various radionuclide-labeled α-MSH peptides have been synthesized for melanoma imaging and therapy. A lactam bridge-cyclized α-MSH peptide developed by Miao Y. and colleagues can be labeled with multiple radionuclides (e.g., ^{99m}Tc, ^{203}Pb,

Kristian M. Hargadon (ed.), *Melanoma*, Methods in Molecular Biology, vol. 3089,
https://doi.org/10.1007/978-1-0716-5619-8_23,
© The Author(s), under exclusive license to Springer Science+Business Media, LLC, part of Springer Nature 2027

^{111}In, and ^{177}Lu) for single-photon emission computed tomography (SPECT) imaging of melanoma and radionuclide-targeted therapy [4–6]. Building on this work, the same research group developed an MC1R-targeted positron emission tomography (PET) imaging probe (^{68}Ga-DOTA-GGNle-CycMSHhex) and, for the first time, visualized multiple lesions in two melanoma patients [7].

However, research on MC1R-targeted peptides has largely remained in the preclinical stage. Thus, the efficacy of this imaging agent in actual clinical practice remains unclear. Moreover, the probe ^{68}Ga-DOTA-GGNle-CycMSHhex employs a lactam cyclization strategy, which requires orthogonal protecting groups to protect the peptide N terminus during cyclization between aspartic acid and lysine. However, during the synthesis process, the removal of allyl/alloc protecting groups can lead to partial cleavage of the N-terminal Fmoc group, affecting synthesis yield. To address this, an alternative cyclization strategy using click chemistry, which offers faster reaction rates and higher specificity, was utilized to design and synthesize a novel α-MSH cyclized peptide (VMT01) that can be labeled with ^{203}Pb for melanoma diagnostic imaging or with ^{212}Pb for radionuclide therapy of melanoma [8, 9]. Currently, it is in the phase I/IIa clinical trial stage [10]. For PET imaging with this new α-MSH cyclized peptide, it was conjugated with DOTA for ^{68}Ga labeling and was named VMT02. Preliminary clinical imaging has been performed at the Second Xiangya Hospital of Central South University and has demonstrated sensitive and specific melanoma detection in many patients. In this chapter, we describe the synthesis protocol for the VMT02 probe and PET/CT imaging procedures in melanoma mouse models and patients.

2 Materials

1. Dichloromethane (DCM).
2. *N*,*N*-Dimethylformamide (DMF).
3. *N*,*N*-Diisopropylethylamine (DIPEA).
4. 2,6-dimethylpyridine.
5. Ascorbic acid.
6. Copper(I) bromide.
7. 2% trifluoroacetic acid (TFA) in DCM.
8. 90% aqueous TFA.
9. Fmoc-PEG2-OH.
10. Triisopropylsilane (TIS).
11. Diethyl ether/pentane (1:1, v/v).
12. Acetonitrile (ACN).

13. ACN/water (1:1, v/v).
14. Tri-tert-butyl 1,4,7,10-tetraazacyclododecane-1,4,7,10-tetraacetate (DOTA-(tBu) ester).
15. Benzotriazole-1-yl-oxy-tris-pyrrolidino-phosphonium hexafluorophosphate (PyBOP).
16. Ethanol (EtOH).
17. Deionized water (di-water).
18. Ultra-pure water.
19. HCl.
20. Sodium acetate anhydrous (NaAc) [≥99.8%].
21. 1 M NaAc buffer (pH 6.0): Dissolve 820.3 mg of NaAc in 9 mL of ultra-pure water. Add acetic acid to adjust the pH value to 6.0. Add ultra-pure water to set the volume to 10 mL. Then inject through a 0.22 μm sterile PTFE filter, and collect the filtration in a sterilized vial.
22. Saline (0.9% NaCl).
23. C18 light Sep-Pak cartridge.
24. 0.22 μm sterile filter (PTFE).
25. Cell culture medium: Dulbecco's modified Eagle medium (DMEM) supplemented with 10% fetal bovine serum (FBS).
26. Phosphate-buffered saline (PBS).
27. Trypsin.
28. Incubator.
29. Sterile Petri dishes.
30. Hemocytometer.
31. C57BL/6 mice, 4–6 weeks old.
32. Anesthesia machine, oxygen, and isoflurane.
33. 1 cm^3 tuberculin syringe with 21 G needle.
34. Trypan Blue solution: Dilute to 0.8 mM in PBS. Store at room temperature. Stable for 1 month.
35. Amino acids and other chemicals: Fmoc-AEEA-OH (PEG2), Fmoc-Lys(N3)-OH, Fmoc-L-Pra-OH, Fmoc-Nle-OH, Fmoc-His(Trt)-OH, Fmoc-Arg(Pbf)-OH, Fmoc-Trp(Boc)-OH, Fmoc-D-Phe-OH, Fmoc-Lys(Mmt)-OH, Fmoc-Rink MBHA-Resin.

3 Methods

3.1 VMT02 Synthesis

1. Perform automated Solid Phase Peptide Synthesis (SPPS) using the following parameters:

a. For resin selection, utilize Rink amide resin to ensure a C-terminal amide.
b. For assembly, synthesize the linear sequence as follows: Nle-Pra-His(Trt)-D-Phe-Arg(pbf)-Trp(Boc)-Lys(N3)-Lys(Mmt) (Fig. 1) from C- to N terminus using Fmoc-based chemistry in an automated synthesizer.
c. Perform all steps at room temperature under a nitrogen atmosphere.
d. Cycles: Alternate between Fmoc-removal (to liberate the amine) and coupling of the appropriate Fmoc-protected building blocks.
e. For N-terminal capping, after final Fmoc-group removal, acetylate the N-terminal amine.

2. Prepare the resin by washing with alternating dichloromethane (DCM) and methanol, and then dry *in vacuo*.
3. Perform the following on-resin modifications:

a. Swelling: Reswell the resin in DCM.
b. Selective Deprotection: Remove the Mmt-group from the lysine side chain by treatment with 2% TFA in DCM.
c. Linker Attachment: Couple Fmoc-PEG2-OH to the liberated side chain, followed by Fmoc-removal.

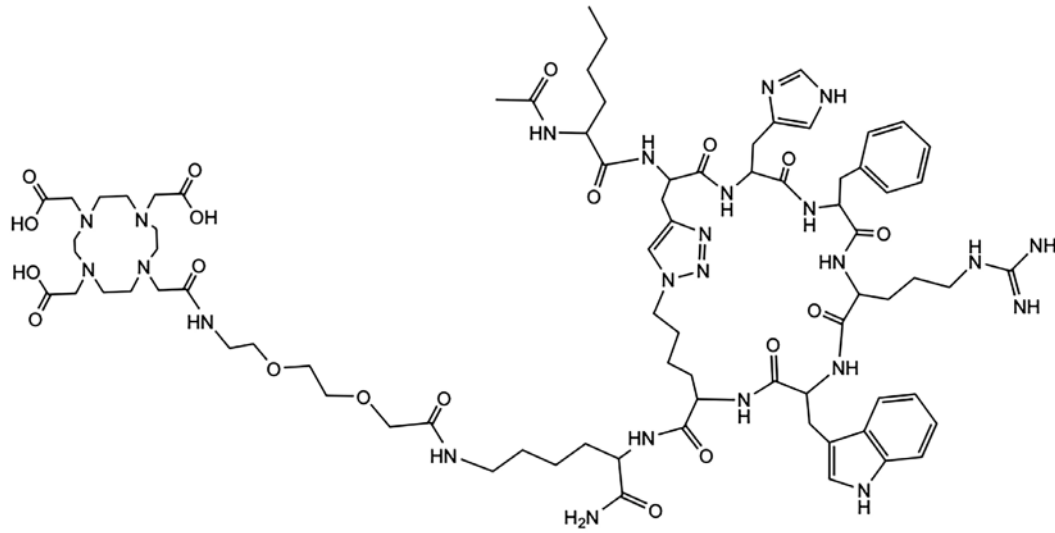


Fig. 1 Chemical structure of VMT02

4. Wash and dry the resin postmodification.
5. Perform cleavage and global deprotection as follows:
    a. Detachment: Treat the peptide-loaded resin with a TFA cocktail containing scavengers (H_2O and TIS) to detach the peptide and remove side-chain protecting groups simultaneously.
    b. Precipitate the crude peptide using pre-cooled diethyl ether/pentane (1:1, v/v).
    c. Centrifuge the suspension, remove the supernatant, and wash the pellet with the ether/pentane mixture.
    d. Air-dry the pellet, dissolve it in ACN/water (1:1, v/v), and lyophilize.
6. Perform click reaction and purification according to the following procedure:
    a. For cyclization, perform a copper-catalyzed azide-alkyne cycloaddition (click reaction) to cyclize the peptide. Uniformly suspend the linear alpha-MSH-derived peptide in DMF, followed by the addition of two volumes of DIPEA, three equivalents of 2,6-dimethylpyridine, two equivalents of ascorbic acid (dissolved in a 1:1 mixture of ultrapure water/DMF), and an equal amount of copper(I) bromide (dissolved in acetonitrile). Carry out the reaction in a flask under a nitrogen atmosphere for 2 h. Afterward, wash away the excess reagents with DMF.
    b. For the first purification, use reverse-phase HPLC (RP-HPLC) [C18 column] with a gradient of 0.05% TFA/ACN in 0.05% TFA/water.
    c. Monitor via UV detection at 215 nm.
    d. For quality control (QC), confirm fractions containing the "clicked" peptide via ESI-MS (purity > 80%).
    e. For intermediate isolation, combine pure fractions and lyophilize from ACN/water (1:1, v/v).
7. Perform DOTA coupling and final deprotection as follows:
    a. For coupling, react the peptide with DOTA-(tBu)ester in the presence of PyBOP and base. Add additional DOTA-(tBu)ester if necessary to drive the reaction to completion.
    b. Concentrate the mixture *in vacuo*, and lyophilize the DOTA(tBu)-peptide.
    c. For global deprotection, remove tBu-groups by treatment with 90% aqueous TFA.
    d. For final isolation, remove TFA and lyophilize the crude VMT02.

8. Purify crude VMT02 on standard RP-HPLC via a binary gradient of 0.05% TFA/ACN in 0.05% TFA/water coupled with C-18 columns.
9. Collect purified VMT02 peptide through fraction collector.
10. Confirm the purity and identity of the VMT02 product by standard liquid chromatography-mass spectrometry (LC–MS) analysis.

3.2 ^{68}Ga Labeling of VMT02

1. Prepare the VMT02 precursor solution by dissolving the VMT02 in ultrapure water to a concentration of 1 μg/μL).
2. Elute the ^{68}Ga from the generator with 5 mL of HCl (*see* **Note 1**).
3. Adjust the pH of the ^{68}Ga elution to 3.5–4.0 with 1 M NaAc buffer.
4. Transfer the VMT02 precursor solution to the ^{68}Ga elution (usually 1~2 μg/mCi), and check that the final pH is 3.5–4.0 (*see* **Note 2**).
5. Incubate at 95°C for 10 min.
6. Dilute the product solution with 10 mL of sterilized water.
7. Inject the mixture slowly through a C18 light Sep-Pak (about 10 mL per minute).
8. Inject 10 mL of sterilized di-water slowly through the C18 plus Sep-Pak slowly to remove solvent residue (about 10 mL/min).
9. Elute the desired product from the C18 plus Sep-Pak with 1 mL of Ethanol and then 10 mL of saline, and pass it through a 0.22 μm sterile filter to a sterile vial.
10. Inject 3.7 MBq of product to HPLC to validate the radioactive purity of the product.
11. Perform routine radiopharmaceutical QC tests (including radionuclide identity, radionuclide purity, radiochemical purity, chemical purity, visual examination, content of solvents, and sterility) of the product.

3.3 PET/CT Imaging of Melanoma in Mouse Models

Prepare melanoma xenografts by subcutaneously injecting B16F10 cells into C57BL/6 mice according to the following protocol:

1. Grow B16F10 melanoma cells in DMEM containing 10% FBS.
2. When cells are 70%–80% confluent, remove medium and wash cells with PBS.
3. Harvest cells grown in monolayer culture during the exponential growth phase using trypsin.
4. Add culture medium and disperse cells.

5. Centrifuge cells immediately at 225 × *g* for 5 min, and wash twice with PBS.
6. Resuspend cells in PBS. Mix 20 μL of cell suspension with 20 μL of trypan blue solution, and count cell number using a hemocytometer to calculate the cell concentration. Viable cells exclude trypan blue, while dead cells are stained with blue color due to trypan blue uptake.
7. Mix cells, and draw 1.0×10^6 cells (50 μL) into a syringe without a needle.
8. Clean and sterilize the lower flank of 4- to 6-week-old C57BL/6 mice, and subcutaneously inject B16F10 cells using a 1-cm^3 syringe with 21 G needle.
9. Start imaging experiments when the tumors have reached an average volume of 100 mm^3.
10. Anesthetize mice with 2.5% isoflurane.
11. Inject about ~3.7 MBq of ^{68}Ga-VMT02 (100 μL) into the mice through the tail vein.
12. Acquire dynamic PET/CT imaging from 0 to 90 min post-injection. Imaging parameters should be set according to the manual of the PET scanner.
13. Process and analyze the imaging data. A PET image of melanoma in the B16F10-C57Bl/6 mouse model is shown in Fig. 2.

3.4 PET/CT Imaging of Melanoma in Human Patients

Extra precautions must be taken when using the ^{68}Ga-VMT02 probe in clinical settings (*see* **Note 3**).

1. Recruit patients according to the clinical trial regulation.
2. Inject ^{68}Ga-VMT02 (~3.7 MBq/kg body weight) to patients through the cubital vein or hand vein.
3. Acquire PET/CT images at 30 min postinjection. The scan and reconstruction parameters should be set according to the manual of the PET scanner.
4. Process and analyze the imaging data. A PET image from a melanoma patient is shown in Fig. 3.

4 Notes

1. The concentration usually ranges from 0.05 M to 0.5 M, depending on the generator property. Check the manual of the generator to confirm the concentration of the HCl.
2. The ratio of the precursor to radioactivity is usually set as 1–2 μg to 1 mCi ^{68}Ga.

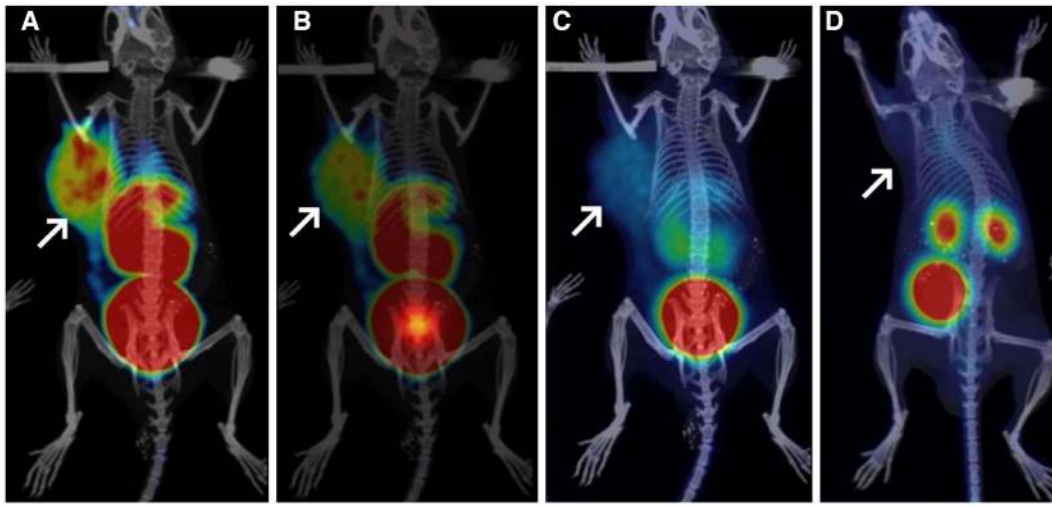


Fig. 2 The PET imaging of B16F10 xenograft mouse at 30 min **A**, 60 min **B**, 120 min (**C**), and blocking (**D**) post-injection of ^{68}Ga-VMT02. White arrows indicate the melanoma tumor

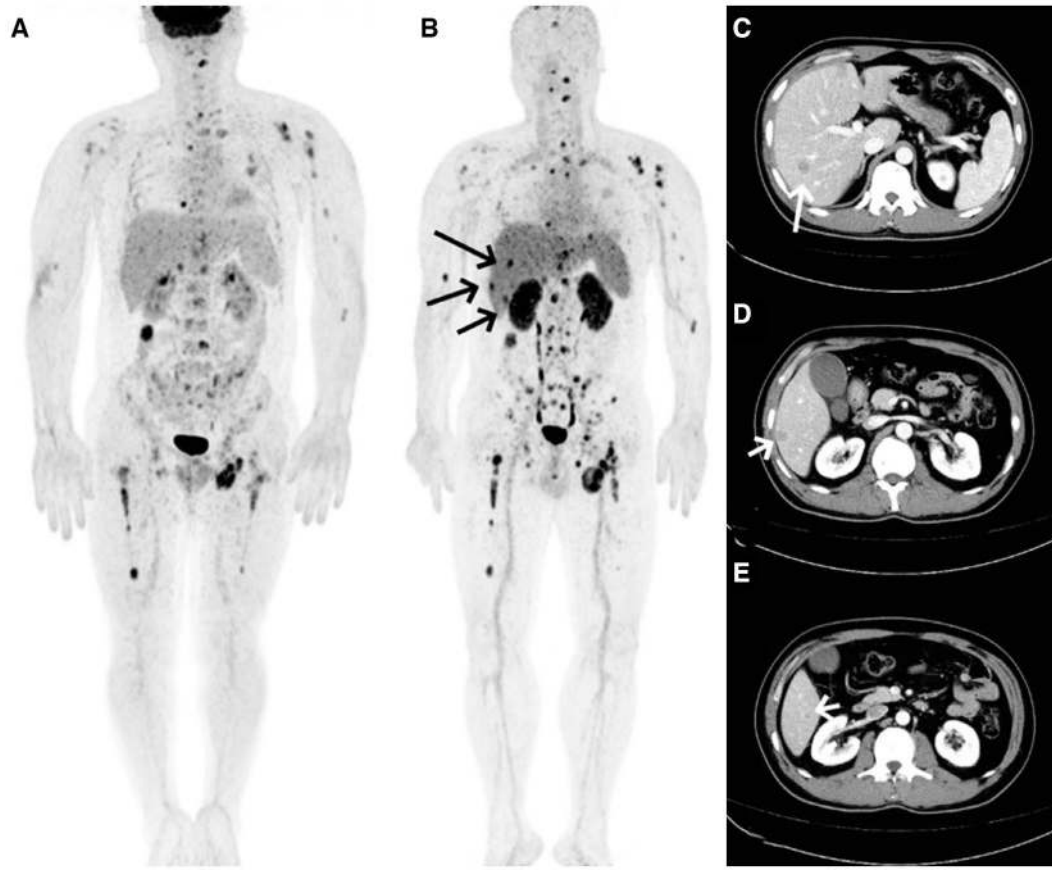


Fig. 3 The ^{18}F-FDG PET imaging (**A**) ^{68}Ga-VMT02 PET imaging (**B**) and contrast-enhanced computed tomography (CT) imaging (**C–E**) of a patient with melanoma and metastasis

3. For human PET/CT imaging using ^{68}Ga-VMT02, the precursor must be synthesized under a Good Manufacturing Practice (GMP) environment and pass strict QC. Each batch of production of ^{68}Ga-VMT02 must be subjected to QC according to the requirements of the radiopharmaceutical standard. Also, an Institutional Review Board (IRB) approval is needed for a human study of ^{68}Ga-VMT02.

Conflicts of Interest

The authors have no conflicts of interest to declare that are relevant to the content of this chapter.

References

1. Xiang T, Li H, Wang X, Su D (2025) Melanocortin-1 receptor expression as a predictive factor for postoperative outcomes in melanoma patients: a retrospective study. Front Immunol 16:1570502. https://doi.org/10.3389/fimmu.2025.1570502
2. Su DG, Djureinovic D, Schoenfeld D et al (2024) Melanocortin-1 receptor expression as a marker of progression in melanoma. JCO Precis Oncol 8:e2300702. https://doi.org/10.1200/PO.23.00702
3. Suzuki H, Uehara T (2025) Precision targeting of the melanocortin-1 receptor with radiopharmaceuticals in metastatic melanoma. Expert Opin Ther Targets 29(9):609–612. https://doi.org/10.1080/14728222.2025.2557277
4. Guo H, Miao Y (2013) Melanoma targeting property of a Lu-177-labeled lactam bridge-cyclized alpha-MSH peptide. Bioorg Med Chem Lett 23(8):2319–2323. https://doi.org/10.1016/j.bmcl.2013.02.069
5. Miao Y, Figueroa SD, Fisher DR et al (2008) 203Pb-labeled alpha-melanocyte-stimulating hormone peptide as an imaging probe for melanoma detection. J Nucl Med 49(5):823–829. https://doi.org/10.2967/jnumed.107.048553
6. Miao Y, Benwell K, Quinn TP (2007) 99mTc- and 111In-labeled alpha-melanocyte-stimulating hormone peptides as imaging probes for primary and pulmonary metastatic melanoma detection. J Nucl Med 48(1):73–80
7. Yang J, Xu J, Gonzalez R et al (2018) 68) Ga-DOTA-GGNle-CycMSH(hex) targets the melanocortin-1 receptor for melanoma imaging. Sci Transl Med 10(466):eaau4445. https://doi.org/10.1126/scitranslmed.aau4445
8. Orcutt KD, Henry KE, Habjan C et al (2022) Dosimetry of [(212)Pb]VMT01, a MC1R-Targeted alpha therapeutic compound, and effect of free (208)Tl on tissue absorbed doses. Molecules 27(18):5831. https://doi.org/10.3390/molecules27185831
9. Li M, Sagastume EA, Lee D et al (2020) 203/212) Pb theranostic radiopharmaceuticals for image-guided radionuclide therapy for cancer. Curr Med Chem 27(41):7003–7031. https://doi.org/10.2174/0929867327999200727190423
10. Morris ZS, Puhlmann M, Johnson F et al (2024) A phase I/IIa of [212Pb]VMT01 targeted a-particle therapy for unresectable or metastatic melanoma. J Clin Oncol 42(16 suppl):TPS9610. https://doi.org/10.1200/JCO.2024.42.16_suppl.TPS9610



Chapter 24

Preparation of Melanoma Tissue for Multiplex Immunofluorescence Histology Analysis of Immune Infiltration and Spatial Organization

Victoria Ann Remley, Marya Dunlap-Brown, Kelly T. Smith, Sheri Vanhoose, Sara J. Adair, Todd W. Bauer and Ileana S. Mauldin

Abstract

Immunotherapies extend survival in melanoma patients by increasing the immune system's capacity to detect tumors and mediate tumor cell death. Understanding mechanisms of antitumor immunity requires evaluating changes in immune infiltrate composition, activation, and spatial distribution within the tumor microenvironment (TME). Despite this need, relatively few methods allow for detailed analysis of both the structural organization and immunological characteristics of tumor-infiltrating immune cells in preclinical cancer models. In this chapter, we present a multiplex immunofluorescence staining approach for identifying, characterizing, and quantifying tumor-infiltrating immune cells in murine melanoma, allowing evaluation of how therapies influence immune infiltration in preclinical models.

Keywords Melanoma, Multiplex immunofluorescence Histology, IHC, Immune infiltration

1 Introduction

PD-1/PD-L1 and CTLA-4 checkpoint blockade immunotherapy have demonstrated clear clinical benefits for patients with melanoma [1, 2]. These therapies function by activating the immune system to recognize and infiltrate tumors and to drive tumor cell death [3]. Consistent with this, the extent of immune cell infiltration in primary and metastatic melanomas and the functional state of these immune subsets are strong prognostic indicators, with higher levels associated with improved survival and response to checkpoint blockade immunotherapy [3, 4]. Patients with primary melanoma exhibiting higher levels of tumor-infiltrating lymphocytes have an estimated survival of 210 months after diagnosis, compared to 190 months in those with lower immune infiltration [6]. Increased numbers of mature $CD11c^+$ dendritic cells are also associated with improved survival in primary melanoma [8–10]. In contrast, greater infiltration by

Kristian M. Hargadon (ed.), *Melanoma*, Methods in Molecular Biology, vol. 3089,
https://doi.org/10.1007/978-1-0716-5619-8_24,
© The Author(s), under exclusive license to Springer Science+Business Media, LLC, part of Springer Nature 2027

macrophages ($F4/80^+$) and regulatory T cells ($FoxP3^+$) correlate with worse outcomes, with increased $FoxP3^+$ regulatory T cells linked to a higher recurrence risk and reduced overall or progression-free survival [11–13]. In metastatic melanoma, similar patterns are observed. Higher infiltration by T and B lymphocytes is associated with better prognosis [3–5], and patients with elevated quantities of $CD3^+$, $CD4^+$,, and $CD8^+$ T cells demonstrate longer overall survival compared to those with lower lymphocyte presence [7]. The increased presence of intratumoral lymphocytes correlates with an increase in tumor PD-L1 expression in metastatic patients, as well as a response to anti-PD-1/PD-L1 immunotherapy [7].

Beyond the overall quantity of immune infiltration, spatial organization of immune cells within the tumor is also associated with survival. For example, tertiary lymphoid structures (TLS), organized immune aggregates resembling lymph nodes, are associated with improved survival and enhanced response to checkpoint blockade therapies in melanoma [14–18]. Additionally, patients with metastatic melanoma with immune cells broadly dispersed throughout their tumors have better outcomes than those with immune infiltrates confined to the tumor margin [4]. Similarly, a second study identified three patterns of immune infiltrates in melanomas and termed them Immunotype A, B, and C. Patients with Immunotype C tumors, with diffuse immune infiltrates throughout the tumor, had the longest median survival of 130 months. In contrast, those with Immunotype B tumors, characterized by immune cells primarily localized around blood vessels, had a median survival time of 23 months. Patients with Immunotype A tumors, exhibiting sparse infiltration, had the lowest median survival time of 15 months [19].

While the prognostic relevance of immune infiltrate density and spatial organization is well established in human melanomas; comparable studies assessing these factors in preclinical mouse models are limited. This gap is partly due to technical challenges, including difficulties with murine histology and the limited availability of reliable antibodies for these applications. Consequently, immune profiling in cancer mouse models is commonly performed using flow cytometry, gene expression analysis, or confocal imaging. However, each of these approaches has notable limitations: flow cytometry and gene sequencing lack spatial resolution, while confocal imaging uses frozen sections, which can compromise tissue architecture compared to paraffin-embedded sections. Expanding the study of tumor-infiltrating lymphocytes (TIL) and their prognostic relevance in preclinical models could yield valuable insights into how therapies impact immune infiltrates and enhance the translation of these findings into clinical outcomes [18, 20, 21].

Multiplex immunofluorescence histology (mIFH) overcomes many of these limitations by enabling single-cell-level analysis while preserving the spatial organization of cells within tissue. This approach allows for detailed mapping of immune cell localization

and interactions, capabilities not achievable with gene expression profiling alone [22, 23], and supports imaging that improves efficiency, conserves tissue, and reveals cellular interactions that are not accessible with single histology techniques. Furthermore, mIFH is performed on paraffin-embedded sections, thereby maintaining tissue architecture and cellular morphology, and it enables quantitative assessments of multiple immune biomarkers within a single tissue specimen. Moreover, mIFH enables quantitative analyses of immune density, immune activation, and immune distribution within the tumor microenvironment. Despite these advantages, mIFH requires substantial time and cost for panel development and validation, as well as access to specialized imaging systems and analytical software.

Here, we present a methodology for preparing melanoma tissue for mIFH analysis, along with a novel mIFH panel that can be used to characterize immune cell infiltration in preclinical murine models of melanoma and other solid tumors. This methodology permits the concurrent identification, quantification, and imaging of five immune markers: T cells (CD3), B cells (CD19), macrophages (F4/80), dendritic cells (CD11c) and regulatory T cells (FoxP3), all within a single tissue section. Collectively, this panel establishes a robust framework for analyzing TIL dynamics in melanoma and other solid tumors, both natively and in relation to immunotherapy response.

2 Materials

2.1 Tumor Inoculation and Harvesting

1. C57Bl/6J mice.
2. Murine melanoma cell lines (i.e., D4M and B16F1, as described herein).
3. 100 cc syringe with needle.
4. Sterile Phosphate-Buffered Saline (PBS) solution.
5. Digital calipers.
6. Surgical scissors.
7. Forceps.
8. 10% Neutral Buffered Formalin.
9. 70% ethanol.
10. Histology cassettes.

2.2 Tissue Processing, Embedding, and Sectioning

1. Automated tissue processor (i.e., Epredia Excelsior AS or Tissue Tek VIP 6 AI).
2. Epredia positively charges slides
3. 10% Neutral Buffered Formalin.
4. 70% ethanol.
5. 80%–90% ethanol.

6. 100% ethanol.
7. Histology cassettes.
8. Xylene.
9. Paraffin wax.

2.3 Specimen Preparation

1. Paraffin-embedded tissue specimen.
2. Tissue-Tek slide staining dishes.
3. Freshly cut 4 μm sections mounted on SuperFrost Plus Microscope Slides and dried at 30°C overnight.
4. Xylene.
5. Ethanol (EtOH).
6. 10% Neutral Buffered Formalin.
7. Epredia positively charges slides.

2.4 Immunofluorescent Staining

1. Humidified slide staining chambers.
2. Antigen Retrieval Buffer 9 (AR9) (Quanterix)
3. Antigen Retrieval Buffer DIVA (DIVA) (Quanterix)
4. Opal 7-Color Manual IHC Kit (Quanterix), includes Opals, Blocking/Antibody Diluent, HRP-conjugated Secondary Antibody that recognizes mouse or rabbit species, spectral DAPI, Antigen Retrieval Buffer 6 (AR6), and Amplification Diluent. To generate Opal stock, reconstitute the lyophilized powder in 150 μL of dimethyl sulfoxide (DMSO).
5. Monoclonal antibodies for staining (Tables 1 and 2).
6. Goat anti-Rat IgG H&L (HRP) preabsorbed (Abcam)
7. ProLong Diamond Antifade Mountant (ThermoFisher Scientific)
8. 24 × 50 mm coverslips
9. BRAND® plastic staining trough, Hellendahl pattern.

Table 1
Antibodies for immunofluorescence staining

Antibody	Clone	Supplier
CD3	SP162	Abcam
F4/80	SP115	Abcam
CD19	D4V48	Cell signaling
CD11c	EPR21826	Abcam
FOXP3	EPR22102-37	Abcam

Table 2
Immune infiltrate identification staining panel

Staining order	Antigen retrieval	Primary antibody and working dilution	Secondary antibody	Opal
1.	AR9	CD3 (1:100)	Opal anti-Ms+Rb HRP	520
2.	DIVA	F4/80 (1:100)	Opal anti-Ms+Rb HRP	540
3.	AR9	CD19 (1:50)	Opal anti-Ms+Rb HRP	650
4.	AR9	CD11c (1:100)	Opal anti-Ms+Rb HRP	570
5.	DIVA	FOXP3 (1:50)	Opal anti-Ms+Rb HRP	620
6.		DAPI		

10. Panasonic Microwave Oven with Inverter Technology and Genius Sensor, 1200 W
11. TBST Wash Buffer: Tris-buffered saline containing 0.05% Tween 20, pH 7.5.

2.5 Image Acquisition

1. Vectra 3 microscope (Quanterix) or a comparable microscope
2. inForm image analysis software (Quanterix)

3 Methods

3.1 Tumor Inoculation and Harvesting

1. Inject murine melanoma cell lines subcutaneously into the flanks of C57Bl/6J mice (*see* **Note 1**). Inject 3×10^5 D4M cells or 2×10^5 B16F1 cells in 100 µL of sterile PBS to promote tumor growth.
2. Monitor tumor growth via digital caliper measurements, where tumor volume is measured as: volume = (length × width^2)/2 [24].
3. Excise tumors at the desired point of progression based on experimental interests, and keep them in a labeled cassette submerged in 10% neutral buffered formalin for 48–72 h before long-term storage in 70% ethanol.

3.2 Tissue Processing to Prepare for Paraffin Embedding

1. Place fixed tissue into labeled histology cassettes (trim specimens to a thickness of <5 mm thick, if necessary, to fit the cassette, and orient as desired for sectioning).

2. Load cassettes into an automated tissue processor (i.e., Epredia Excelsior AS or Tissue Tek VIP 6 AI), and follow a standard overnight procedure.
3. For dehydration of tissue, expose specimens to increasing ethanol concentrations as follows:
   a. 70% ethanol (30–60 min).
   b. 80%–95% ethanol (one to two changes of fresh ethanol, 30–60 min each).
   c. 100% ethanol (two to three changes of fresh ethanol, 45–60 min each).
4. For tissue clearing, treat specimens with xylene (two to three changes of fresh xylene, 45–60 min each).
5. For infiltration, incubate specimens with molten paraffin wax at 42°C (three to four changes of fresh wax, 45–60 min each [or longer for larger samples]).
6. Remove cassettes from the processor, and keep samples in molten paraffin until embedding (do not allow specimens to cool).

3.3 Tissue Embedding

1. Preheat embedding station, molds, and paraffin to 42°C.
2. Open the tissue cassette, and transfer fixed tissue to a metal embedding mold filled with molten paraffin.
3. Orient the tissue carefully (e.g., cut the surface down for the desired plane of section; note tumor margins if relevant).
4. Place the cassette base on top of the mold as a label holder, and fill completely with molten Epredia Paraffin Type 9.
5. Transfer the mold to a cold plate or cooling tray, and allow it to solidify completely (~15–30 min).
6. Remove the solidified block from the mold (blocks can be stored at room temperature indefinitely).

3.4 Tissue Sectioning

1. Mount the paraffin block on a rotary microtome. Insert a fresh disposable blade (angle ~5°).
2. Face/trim the block at 10–20 μm until the full tissue face is exposed. Discard trimmings.
3. Cut serial sections at 5 μm thickness.
4. Float sections in a 40°C–45°C water bath to remove wrinkles.
5. Pick up sections onto Epredia positively charged or coated glass slides, ensuring flat tissue mounting with no folds.
6. Drain excess water and dry slides horizontally at 37°C–55°C for 15–60 min (or overnight at room temperature) to ensure tissue adhesion.

3.5 Deparaffinization, Rehydration, Fixation, and Antigen Retrieval

1. Prepare Tissue-Tek slide staining dishes that are filled with the following solutions: Xylene (×3 dishes), 100% EtOH, 95% EtOH, 70% EtOH, Deionized H_2O (DH2O) (×3 dishes), TBST Wash Buffer (×1 dish), 10% Neutral Buffered Formalin (×1 dish).
2. Move the slide rack from dish to dish in sequential steps, with all steps performed at room temperature, as follows (*see* **Note 2**):
    a. Xylene dish 1 (10 min).
    b. Xylene dish 2 (10 min).
    c. Xylene dish 3 (10 min).
    d. 100% EtOH (5 min).
    e. 95% EtOH (5 min).
    f. 70% EtOH (2 min).
    g. DH2O (2 min).
    h. TBST Wash Buffer (2 min).
    i. DH2O (2 min).
    j. 10% Neutral Buffered Formalin (20 min).
    k. DH2O (2 min).
3. Fill the BRAND® plastic staining trough, Hellendahl pattern, with 1× diluted AR or DIVA buffer. Use the associated AR buffer for the first antigen of interest, as detailed in Table 2. For example, the panel in Table 2 begins with a CD3 stain post AR9 antigen retrieval; AR9 Buffer would be used first.
4. Remove the slides from the DH20 immersion, and place them into the BRAND staining jar, loading the slides back-to-back, with the tissue facing outward, to fill each slot. Wait 2 min, and then discard the buffer (this serves as an AR buffer rinse).
5. Fill the chamber completely with AR buffer.
6. Microwave slides at 100% power for ~2 min, or until the buffer reaches a boil. Once boiling is achieved, stop the microwave, reduce the power setting to 20%, and continue heating for 18 min. Closely monitor the slides during the initial high-power step to ensure that the buffer does not boil off excessively, and replenish the buffer as needed (*see* **Note 3**).
7. Allow slides to cool at room temperature for 30 min, and then proceed with further staining steps or store at 4°C overnight for continuation on the following day.

3.6 Multiplex Stain

The primary antibody, antibody dilutions, secondary antibodies, and Opal dyes to be used when performing these multiplex steps below

are detailed in Table 2. Before beginning the staining protocol, dilute primary antibodies in Antibody Diluent, dilute HRP-conjugated Goat Anti-Rat Secondary antibody in Antibody Diluent at 1:100, dilute Opal stock in Amplification Diluent, and generate 1× diluted AR or DIVA buffer. Set up 12 Tissue-Tek staining dishes containing TBST Wash Buffer. The first dish should contain a clean slide rack that will be moved from dish to dish. All of these subsequent steps should be performed at room temperature.

8. Place slides into a Tissue-Tek staining dish filled with TBST, and soak for 2 min to perform a TBST wash.
9. Remove slides from TBST and place into the humidified chamber.
10. Pipette 300 µL (or enough to cover the entire tissue) of Antibody Diluent solution on each slide, and wait 10 min. This solution acts as an antibody block.
11. Discard the Antibody Diluent solution from the slide by tipping the slides over a beaker, and place the slides back into the staining chamber.
12. Pipette 300 µL of primary antibody diluted in Antibody Diluent onto each slide, and incubate for 30 min in a humidified chamber. For example, the first antigen stained for in Table 2 is CD3 diluted at 1:100 in Antibody Diluent.
13. Set up four Tissue-Tek dishes filled with TBST Wash Buffer. The first dish should contain a clean slide rack that will be moved from dish to dish.
14. After primary antibody incubation, discard the primary antibody over a beaker, and add the slides to the slide rack in TBST.
15. Place slides in the first of four Tissue-Tek dishes containing TBST and wash 4 × 2 min, transferring the slide rack to a fresh dish every 2 min.
16. Remove slides from TBST, and place them into the humidified staining chambers.
17. Pipette 300 µL of ready-to-use secondary antibody (Opal Polymer HRP or HRP-conjugated Goat anti-Rat IgG H&L preabsorbed to each slide) and stain for 10 min.
18. Discard the secondary antibody, and wash slides 4 × 2 min each in TBST.
19. Remove slides from TBST, and place them into humidified staining chambers.
20. Dilute Opal stock 1:50 in Amplification Diluent to generate Opal staining solution.
21. Pipette 300 µL of Opal staining solution to each slide, and incubate for 10 min. Use the Opal dye corresponding to each

primary antibody (see Table 2). For example, Opal 520 is used for CD3 detailed in Table 2.

22. Discard Opal solution, and wash slides 4×2 min each in TBST.
23. Rinse slides in the appropriate AR or DIVA buffer for the next antigen in the staining panel (as indicated in Table 2) for 2 min in a BRAND staining jar, and then discard the buffer. For example, in Table 2, the next antigen retrieval buffer that would be used is DIVA Buffer.
24. Refill the jar completely with DIVA Buffer. Microwave at 100% power for ~2 min until the solution begins boiling, and then microwave for 18 min at 20% power (*see* **Note 4**).
25. Allow slides to cool at room temperature for 30 min, and then proceed to do further staining steps, or store slides at 4°C overnight for continuation on the following day.
26. Repeat Steps 1–17 from this section four additional times, each time using a different primary antibody and corresponding Opal dye each cycle, until all the antigens in each panel are stained. Follow the staining order specified in Table 2, as changing the order may affect results. For example, Table 2 proceeds with F4/80/Opal 540, CD19/Opal 650, CD11c/Opal 570, and FoxP3/Opal 620.

3.7 Spectral DAPI Stain, Mount, and Coverslip

1. Set up two Tissue-Tek dishes filled with TBST Wash Buffer and two Tissue-Tek dishes filled with DH_2O. The first dish should contain a clean slide rack that will be moved from dish to dish.
2. Wash slides in DH_2O for 2 min.
3. Wash slides in TBST for 2 min.
4. Prepare the DAPI staining solution by adding two drops of spectral DAPI per mL of TBST.
5. Pipette 300 µL DAPI staining solution to each slide, and incubate for 5 min.
6. Wash slides in TBST for 2 min.
7. Wash slides in DH_2O for 2 min.
8. Transfer slides to a staining chamber, apply enough ProLong Diamond Antifade Mountant to cover the tissue, and place a coverslip.
9. Allow slides to dry overnight.
10. The next day, remove excess mountant by cleaning slides with EtOH and image with a fluorescent microscope.

3.8 Identification and Characterization of Immune Infiltrates by Immunofluorescence

Perform immunofluorescent image acquisition and analysis using a fluorescent microscope such as the Vectra 3. Perform subsequent spectral unmixing or compensation with inForm image analysis software (Quanterix) using single-stain controls. *See* **Note 5** for staining control suggestions, **Note 6** for acquisition procedures, and **Note 7** for cell enumeration procedures. Representative images corresponding to the panel in Tables 1, 2 are shown in Figs. 1 and 2.

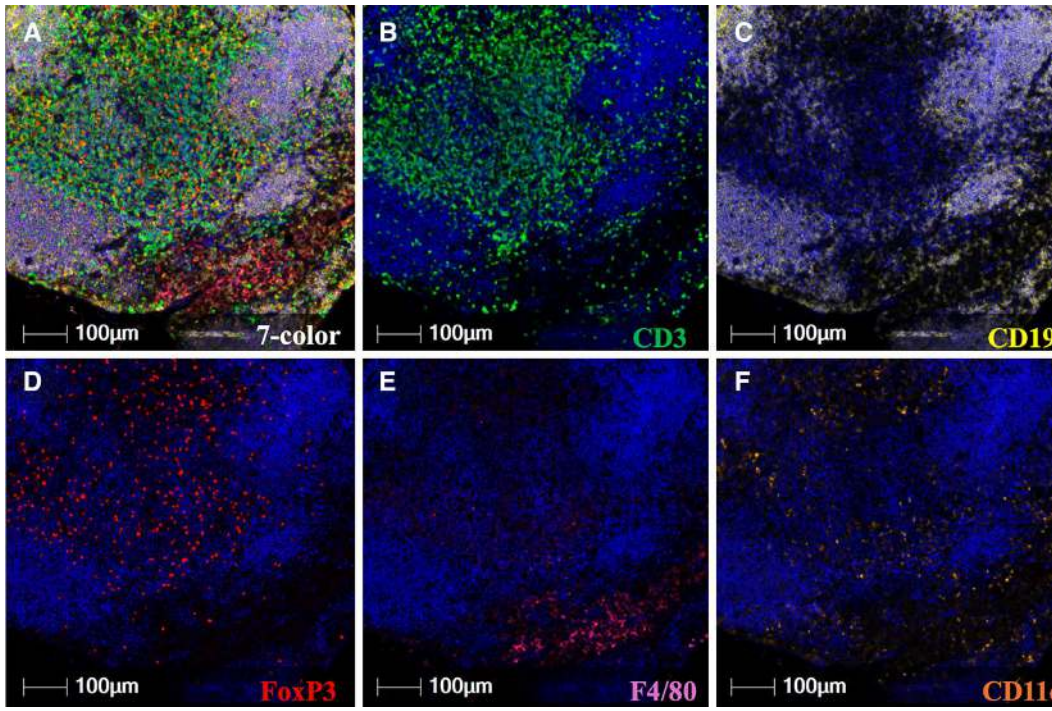


Fig. 1 Tissue specimens were stained for immunofluorescent microscopy, as outlined in Sect. 3.5–3.7, with the Immune Infiltration Panel (Table 2). Images were acquired at 20× and spectrally compensated in the inForm program (Quanterix) using single-stain positive controls. Images with a scale bar were generated using HALO software. Images (**A**–**F**) are of a murine lymph node. Scale bar = 100 µm

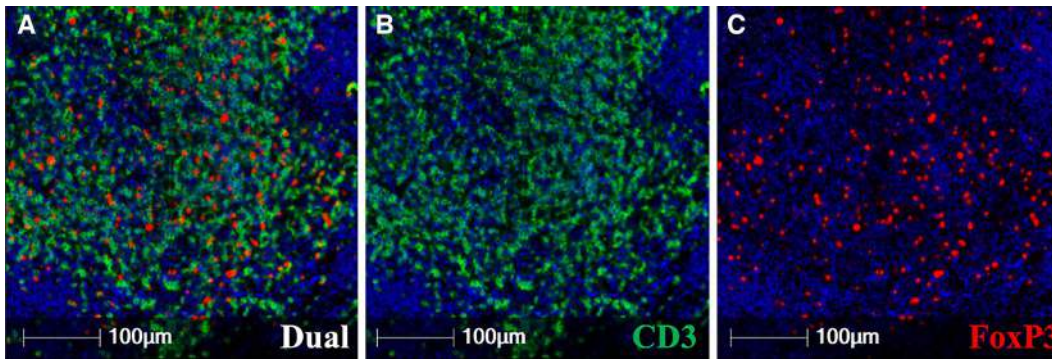


Fig. 2 Tissue specimens were stained for immunofluorescent microscopy with the Immune Infiltration Panel 1 (Table 2). Images (**A**–**C**) are zoomed-in ROIs that identify co-staining of CD3 and FoxP3 in murine lymph nodes. Scale bar = 100 µm

4 Notes

1. Cells should be in the logarithmic growth phase with a viability of at least 85%.
2. Immerse the slides in each solution, ensuring that the tissue remains fully submerged during all steps so that it does not dry out.
3. If the solution is dropping low during microwaving and the tissue is at risk of not being submerged, refill the jars, bring the solution up to a boil at 100% power, and then continue with microwaving at 20% power until the full 18 min of time has been achieved.
4. This step functions to remove the primary and secondary antibodies from the slides and prepare them for the next step.
5. For each of these panels, we recommend using murine lymph nodes as positive staining and imaging controls. These positive controls should be stained and processed alongside the other tissues of interest. Single stain controls should also be used for unmixing, as well as no Opal-stained controls in which the tissue is stained with all the reagents and goes through all steps of the protocol except for the Opal dye staining steps. Additionally, a no-primary antibody-control in which the tissue is stained with all the reagents and goes through all steps of the protocol except the primary antibody staining steps should be included. Fluorescence Minus One control (FMOs) can also be useful when developing a panel initially. Both the no Opal and no Primary Antibody controls were done in lymph node tissue. Fluorescence Minus One control (FMOs) can also be useful when developing a panel initially.
6. Whole slides should initially be scanned at 10× to identify specific regions of interest (ROI) for more detailed analysis. These ROI are then scanned at 20× magnification for cell enumeration.
7. Digital software, including Halo (Indica Labs), can be used to enumerate the cell data on the 20× scanned ROI. Annotations can be drawn around key areas to enable the enumeration of cell subsets at the specific site of interest. Enumeration of immune cells can also be done manually or by using other available software packages, such as inForm (Quanterix).

Acknowledgments

Tissue sectioning was performed by the Research Histology Core, and slide imaging and analysis were performed using microscopes and software in the Molecular Immunologic and Translational Science Core at the University of Virginia (CCSG 2P30CA044579-26).

Conflicts of Interest The authors have no competing interests to declare that are relevant to the content of this chapter.

References

1. Siddiqui I, Schaeuble K, Chennupati V et al (2019) Intratumoral Tcf1^{+}PD-1^{+}CD8^{+} T cells with stem-like properties promote tumor control in response to vaccination and checkpoint blockade immunotherapy. Immunity 50(1):195–211.e10. https://doi.org/10.1016/j.immuni.2018.12.021
2. Gide TN, Quek C, Menzies AM et al (2019) Distinct immune cell populations define response to anti-PD-1 monotherapy and anti-PD-1/anti-CTLA-4 combined therapy. Cancer Cell 35(2):238–255.e6. https://doi.org/10.1016/j.ccell.2019.01.003
3. Liang Y, Zheng Y, Zeng Y et al (2025) Immune checkpoint inhibitors in melanoma: mechanisms, immune cell interactions, and the tumour microenvironment. Front Imm 16:1691608. https://doi.org/10.3389/fimmu.2025.1691608.
4. Kümpers C, Jokic M, Haase O et al (2019) Immune cell infiltration of the primary tumor, not PD-L1 status, is associated with improved response to checkpoint inhibition in metastatic melanoma. Front Med 6:27. https://doi.org/10.3389/fmed.2019.00027
5. Kluger HM, Zito CR, Barr ML et al (2015) Characterization of PD-L1 expression and associated T-cell infiltrates in metastatic melanoma samples from variable anatomic sites. Clin Cancer Res 21(13):3052–2060. https://doi.org/10.1158/1078-0432.CCR-14-3073
6. Morrison SL, Han G, Elenwa F et al (2025) Tumor infiltrating lymphocytes in primary melanoma are associated with a better prognosis. Am J Surg 246:116243. https://doi.org/10.1016/j.amjsurg.2025.116243
7. Kakavand H, Vilain RE, Wilmott JS et al (2015) Tumor PD-L1 expression, immune cell correlates and PD-1+ lymphocytes in sentinel lymph node melanoma metastases. Mod Pathol 28(12):1535–1544. https://doi.org/10.1038/modpathol.2015.110
8. Zeng Y, Zeng Y, Yin H et al (2021) Exploration of the immune cell infiltration-related gene signature in the prognosis of melanoma. Aging 13(3):3459–3482. https://doi.org/10.18632/aging.202279
9. Selitsky SR, Mose LE, Smith CC et al (2019) Prognostic value of B cells in cutaneous melanoma. Genome Med 11(1):36. https://doi.org/10.1186/s13073-019-0647-5
10. Tucci M, Passarelli A, Mannavola F et al (2019) Immune system evasion as hallmark of melanoma progression: the role of dendritic cells. Front Oncol 9:1148. https://doi.org/10.3389/fonc.2019.01148
11. Femel J, Hill C, Illa Bochaca I et al (2024) Quantitative multiplex immunohistochemistry reveals inter-patient lymphovascular and immune heterogeneity in primary cutaneous melanoma. Front Imm 15:1328602. https://doi.org/10.3389/fimmu.2024.1328602.
12. Knol AC, Nguyen JM, Quéreux G et al (2011) Prognostic value of tumor-infiltrating Foxp3+ T-cell subpopulations in metastatic melanoma. Exp Derm 20(5):430–434. https://doi.org/10.1111/j.1600-0625.2011.01260
13. Miracco C, Mourmouras V, Biagioli M et al (2007) Utility of tumour-infiltrating CD25+ FOXP3+ regulatory T cell evaluation in predicting local recurrence in vertical growth phase cutaneous melanoma. Oncol Rep 18(5):1115–1122
14. Engelhard VH, Rodriguez AB, Mauldin IS et al (2018) Immune cell infiltration and tertiary lymphoid structures as determinants of antitumor immunity. J Immunol 200(2):432–442. https://doi.org/10.4049/jimmunol.1701269
15. Zheng L, Katyal P, Mauldin IS (2025) Methods for analysis of tertiary lymphoid structures and immune activity by multiplex immunofluorescence histology. Methods Cell Biol 199:37–49. https://doi.org/10.1016/bs.mcb.2025.03.008.
16. Lin Z, Huang L, Li S et al (2020) Pan-cancer analysis of genomic properties and clinical outcome associated with tumor tertiary lymphoid structure. Sci Rep 10(1):21530. https://doi.org/10.1038/s41598-020-78560-3
17. Lynch KT, Young SJ, Meneveau MO et al (2021) Heterogeneity in tertiary lymphoid structure B-cells correlates with patient survival in metastatic melanoma. J Immunother Cancer 9(6):e002273. https://doi.org/10.1136/jitc-2020-002273
18. Cabrita R, Lauss M, Sanna A et al (2020) Tertiary lymphoid structures improve immunotherapy and survival in melanoma. Nature 577(7791):561–565. https://doi.org/10.1038/s41586-019-1914-8
19. Erdag G, Schaefer JT, Smolkin ME et al (2012) Immunotype and immunohistologic characteristics of tumor-infiltrating immune cells are associated with clinical outcome in metastatic melanoma. Cancer Res 72(5):1070–1080. https://doi.org/10.1158/0008-5472

20. Helmink BA, Reddy SM, Gao J et al (2020) B cells and tertiary lymphoid structures promote immunotherapy response. Nature 577(7791):549–555. https://doi.org/10.1038/s41586-019-1922-8
21. Vanhersecke L, Brunet M, Guégan JP et al (2021) Mature tertiary lymphoid structures predict immune checkpoint inhibitor efficacy in solid tumors independently of PD-L1 expression. Nat Cancer 2(8):794–802. https://doi.org/10.1038/s43018-021-00232-6
22. Parra ER, Ferrufino-Schmidt MC, Tamegnon A et al (2021) Immuno-profiling and cellular spatial analysis using five immune oncology multiplex immunofluorescence panels for paraffin tumor tissue. Sci Rep 11(1):8511. https://doi.org/10.1038/s41598-021-88156-0.
23. Mezheyeuski A, Bergsland CH, Backman M et al (2018) Multispectral imaging for quantitative and compartment-specific immune infiltrates reveals distinct immune profiles that classify lung cancer patients. J Pathol 244(4):421–431. https://doi.org/10.1002/path.5026
24. Thim EA, Kitelinger LE, Rivera-Escalera F et al (2024) Focused ultrasound ablation of melanoma with boiling histotripsy yields abscopal tumor control and antigen-dependent dendritic cell activation. Theranostics 14(4):1647–1661. https://doi.org/10.7150/thno.92089.



Chapter 25

A Method for Quantifying Immune Infiltrates and Tertiary Lymphoid Structures in Murine Melanoma Tumors by Multiplex Immunofluorescence

Jackson R. Clark, Pallavi Rustogi and Ileana S. Mauldin

Abstract

The presence of tertiary lymphoid structures (TLS) and elevated levels of tumor-infiltrating lymphocytes have been linked to improved survival outcomes in several solid cancers, including melanoma. Despite this association, the precise function and immunological impact of TLS remain incompletely understood, as do factors that drive their formation and which might potentially be leveraged to enhance patient outcomes. Functional studies using murine models may help clarify the biological roles of TLS; however, relatively few methodologies currently exist that allow for detailed assessment of the structural organization and functional characteristics of TLS within solid tumors. To advance understanding of the biology underlying TLS, this chapter describes multiplex immunohistochemistry panels designed for the identification, characterization, and quantification of TLS and intratumoral immune infiltrates in melanoma. Although these methods are presented in the context of melanoma, they are broadly applicable and can be used to investigate TLS across a wide range of human cancers.

Keywords Melanoma, Tertiary lymphoid structures, Immunology, Multiplex immunofluorescence histology, IHC, Immune infiltrates, High endothelial venules

1 Introduction

Tertiary lymphoid structures (TLS) are ectopic lymphoid organs commonly found in stroma in close proximity to solid tumors or occasionally within the tumor areas themselves [1–3]. TLS are thought to develop in response to chronic inflammation. In humans, they are best identified through multiplex staining, as these structures are defined by their organization and immune cell composition. TLS share morphological similarities with conventional secondary lymphoid organs, typically containing organized and distinct T- and B-cell compartments, as well as high endothelial venule-like vessels that express peripheral node addressin (PNAd) [4, 5]. In patients with melanoma, TLS are associated with increased

Kristian M. Hargadon (ed.), *Melanoma*, Methods in Molecular Biology, vol. 3089,
https://doi.org/10.1007/978-1-0716-5619-8_25,
© The Author(s), under exclusive license to Springer Science+Business Media, LLC, part of Springer Nature 2027

survival and higher response rates to immune checkpoint blockade therapy [2, 6, 7]. Due to this favorable association in cancer and their resemblance to lymph nodes, it has been proposed that TLS support antitumor immunity by promoting tumor antigen presentation and facilitating both T-cell- and B-cell-mediated immune responses directed against local tumor antigens [8, 9]. However, in contrast, TLS in lung transplantation has been associated with increased immune tolerance, raising the possibility that TLS may exhibit functional diversity depending on the biological context [10]. Thus, the function and immunological impact of TLS remain incompletely defined.

TLS have also been identified in murine melanoma models through genetic profiling and histological analyses. Compared with TLS observed in patients, murine TLS exhibit a similar overall composition, consisting of dense B- and T-clusters associated with $PNAD^+$ vasculature [11]. However, TLS structures in mice appear to be less organized than those observed in patients, and they generally lack clearly separated T- and B-cell zones as well as germinal center formation [12]. In some murine melanoma models, TLS were previously demonstrated to develop only in intraperitoneal tumors and not in subcutaneously implanted tumors [11], which contrasts with the experience in humans. However, a recent study utilizing the B16F0 melanoma model reported the generation of TLS in subcutaneous tumors following treatment with PD-L1 blockade and CXCL13, either alone or in combination with CCL21 [13]. In that study, TLS were identified through staining for B and T cells, although co-staining with PNAd was not performed to definitively confirm TLS structures. Notably, TLS presence did not correlate with enhanced responses to PD-L1 blockade, as improved therapeutic responses was observed only in tumors treated with CXCL13 plus CCL21, but not with CXCL13 alone, despite TLS formation in both conditions [13]. These findings highlight the need for standardized approaches to improve TLS identification and characterization across murine models. In addition to CXCL13 and CCL21, lymphotoxin-β receptor ligands [14] and the cytokine LIGHT (TNFSF14/CD258) [15] have also been implicated in TLS formation in murine tumors [16]. However, whether induction of TLS with these cytokines consistently enhances antitumor immune responses or improves tumor control remains unclear, as do the mechanisms underlying these effects. Functional studies of TLS in murine models are therefore needed to better define their biological role and identify factors that drive TLS formation that could be leveraged to improve patient outcomes. Multiplex immunofluorescent histology analyses of TLS architecture, immune activity at the TLS sites, and the resulting changes in immune composition within the tumor microenvironment may help elucidate the functional impact of TLS.

Here we present two multiplex immunofluorescent histology panels optimized for the identification and quantitative characterization of murine TLS and tumor-infiltrating lymphocytes (TILs) within the tumor microenvironment (TME) [17]. The markers included in these panels enable the detection of T cells (CD3, CD4, and CD8), B cells (CD19), high endothelial venules (PNAd), proliferating cells (Ki67), and cytotoxic T cells (granzyme-b). Together, these panels provide a robust approach for identifying TLS in murine tumor tissues and for quantitatively profiling the immune composition and activation state of immune cells within TLS and in adjacent tumor and stromal regions. In addition, this multiplex framework enables spatial analysis of TLS within the tumor microenvironment and characterization of the spatial relationships among immune cell populations within tumors [18]. These approaches facilitate systematic evaluation of TLS architecture, immune activity within TLS niches, and potential associations between TLS features and tumor immune contexture and therapeutic response or overall survival. As such, these panels provide a standardized and reproducible platform for studying TLS biology and immune organization in murine tumor models.

2 Materials

2.1 Specimen Preparation

1. Paraffin-embedded tissue specimen.
2. Tissue-Tek slide staining dishes.
3. Freshly cut 4 μm sections mounted on SuperFrost Plus Microscope Slides and dried at 30°C overnight.
4. Xylene.
5. Ethanol (EtOH).
6. 10% Neutral Buffered Formalin.

2.2 Immunofluorescent Staining

1. Humidified slide staining chambers.
2. Antigen Retrieval Buffer 9 (AR9) (Quanterix).
3. Opal 7-Color Manual IHC Kit (Quanterix): includes Opals, Blocking/Antibody Diluent, HRP-conjugated Secondary Antibody that recognizes mouse or rabbit species, spectral DAPI, Antigen Retrieval Buffer 6 (AR6), and Amplification Diluent. To generate Opal stock, reconstitute the lyophilized powder in 150 μL of dimethyl sulfoxide (DMSO).
4. Monoclonal antibodies for staining (Tables 1–3).
5. Goat AntiRat IgG H&L (HRP) preabsorbed (Abcam).
6. ProLong Diamond Antifade Mountant (ThermoFisher Scientific).
7. 24 × 50 mm coverslips.

Table 1
Antibodies for immunofluorescence staining

Antibody	Clone/Catalog number	Supplier
CD3	SP162	Abcam
CD4	EPR19514	Abcam
CD8	CAL38	Abcam
CD19	D4V4B	Cell signaling
PNAd	MECA-79	Biolegend
Ki67	SP6	Abcam
Granzyme-b	Cat. no. ab4059	Abcam

Table 2
Tertiary lymphoid structure and tumor-infiltrating lymphocytes identification panel 1

Staining order	Antigen retrieval	Primary antibody and working dilution	Secondary antibody	Opal
1	AR9	PNAd (1:50)	Goat Anti-Rat IgG H&L (HRP) preabsorbed	620
2	AR9	CD4 (1:100)	Opal polymer HRP mouse + rabbit	520
3	AR9	CD8 (1:200)	Opal polymer HRP mouse + rabbit	540
4	AR9	CD19 (1:50)	Opal polymer HRP mouse + rabbit	650
5	AR9	Ki67 (1:1000)	Opal polymer HRP mouse + rabbit	570
6	AR9	Granzyme-b (1:1000)	Opal polymer HRP mouse + rabbit	690
7		DAPI		

8. Opal Staining jar (Quanterix).
9. Panasonic Microwave Oven with Inverter Technology and Genius Sensor, 1200W.
10. TBST Wash Buffer: Tris-buffered saline containing 0.05% Tween 20, pH 7.5.

2.3 Image Acquisition

1. Vectra 3 microscope (Quanterix) or a comparable microscope.
2. inForm image analysis software (Quanterix).

Table 3
Tertiary lymphoid structure and tumor-infiltrating lymphocytes identification panel 2

Staining order	Antigen retrieval	Primary antibody and working dilution	Secondary antibody	Opal
1	AR9	CD3 (1:100)	Opal polymer HRP mouse + rabbit	520
2	AR9	CD8 (1:200)	Opal polymer HRP mouse + rabbit	540
3	AR9	CD19 (1:50)	Opal polymer HRP mouse + rabbit	650
4	AR9	PNAd (1:50)	Goat Anti-Rat IgG H&L (HRP) preabsorbed	620
5	AR9	Ki67 (1:1000)	Opal polymer HRP mouse + rabbit	570
6	AR9	Granzyme-b (1:1000)	Opal polymer HRP mouse + rabbit	690
7		DAPI		

3 Methods

3.1 Deparaffinization, Rehydration, Fixation, and Antigen Retrieval

1. Prepare Tissue-Tek slide staining dishes that are filled with the following solutions: Xylene (×3 dishes), 100% EtOH, 95% EtOH, 70% EtOH, Deionized H_2O (DH2O) (×3 dishes), TBST Wash Buffer (×1 dish), 10% Neutral Buffered Formalin (×1 dish).
2. Move the slide rack containing slides from dish to dish in sequential steps, with all steps performed at room temperature, as follows (*see* **Note 1**):
   a. Xylene dish 1 (10 min).
   b. Xylene dish 2 (10 min).
   c. Xylene dish 3 (10 min).
   d. 100% EtOH (5 min).
   e. 95% EtOH (5 min).
   f. 70% EtOH (2 min).
   g. DH_2O (2 min).
   h. TBST Wash Buffer (2 min).
   i. DH_2O (2 min).
   j. 10% Neutral Buffered Formalin (20 min).
   k. DH_2O (2 min).

3. Fill the Opal staining jars with 1× diluted AR buffer. Use the associated AR buffer for the first antigen of interest, detailed in Tables 2, 3. For example, the panel in Table 2 begins with a PNAd stain post AR9 antigen retrieval; AR9 Buffer would be used first.
4. Remove the slides from the DH_2O immersion, and place them into the Opal staining jar, loading the slides back-to-back, with the tissue facing outward, to fill each slot. Wait 2 min and then discard the buffer (this serves as an AR buffer rinse).
5. Fill the chamber completely with AR buffer.
6. Microwave slides at 100% power for ~2 min, or until the buffer reaches a boil. Once boiling is achieved, stop the microwave, reduce the power setting to 20%, and continue heating for 18 min. Closely monitor the slides during the initial high-power step to ensure that the buffer does not boil off excessively, and replenish the buffer as needed (*see* **Note 2**).
7. Allow slides to cool at room temperature for 30 min, and then proceed to do further staining steps or store at 4°C overnight for continuation on the following day.

3.2 Multiplex Stain

The primary antibody, antibody dilutions, secondary antibodies, and Opal dyes to be used when performing these multiplex steps below are detailed in Tables 2 and 3. Before beginning the staining protocol, dilute primary antibodies in Antibody Diluent, dilute HRP-conjugated Goat Anti-Rat Secondary antibody in Antibody Diluent at 1:100, dilute Opal stock in Amplification Diluent, and generate 1× diluted AR buffer. Set up 12 Tissue-Tek staining dishes containing TBST Wash Buffer. The first dish should contain a clean slide rack that will be moved from dish to dish. All of these subsequent steps should be performed at room temperature.

1. Place slides into a Tissue-Tek staining dish filled with TBST, and soak for 2 min to perform a TBST wash.
2. Remove slides from TBST and place into the humidified chamber.
3. Pipette 300 µL (or enough to cover the entire tissue) of Antibody Diluent solution on each slide, and wait 10 min. This solution acts as an antibody block.
4. Discard the Antibody Diluent solution from each slide by tipping the slides over a beaker, and place the slides back into the staining chamber.
5. Pipette 300 µL of primary antibody diluted in Antibody Diluent onto each slide, and incubate for 30 min in a humidified chamber. For example, the first antigen stained for in Table 2 is PNAd diluted at 1:50 in Antibody Diluent.

6. Set up four Tissue-Tek dishes filled with TBST Wash Buffer. The first dish should contain a clean slide rack that will be moved from dish to dish.
7. After primary antibody incubation, discard the primary antibody over a beaker and add slides to the slide rack in TBST.
8. Place slides in the first of four Tissue-Tek dishes containing TBST and wash 4×2 min, transferring the slide rack to a fresh dish every 2 min.
9. Remove slides from TBST, and place them into the humidified staining chambers.
10. Pipette 300 µL of ready-to-use secondary antibody [Opal Polymer HRP or HRP-conjugated Goat Anti-Rat IgG H&L (preabsorbed) to each slide], and stain for 10 min.
11. Discard the secondary antibody, and wash slides 4×2 min each in TBST.
12. Remove slides from TBST and place into humidified staining chambers.
13. Dilute Opal stock 1:50 in Amplification Diluent to generate Opal staining solution.
14. Pipette 300 µL of Opal staining solution to each slide, and incubate for 10 min. Use the Opal dye corresponding to each primary antibody (see Tables 2 and 3). For example, Opal 620 is used for PNAd as detailed in Table 2.
15. Discard Opal solution, and wash slides 4×2 min each in TBST.
16. Rinse slides in the appropriate AR Buffer for the next antigen in the staining panel (as indicated in Tables 2 and 3) for 2 min in an Opal staining jar, and then discard the buffer. For example, in Table 2, the next AR Buffer that would be used is AR9.
17. Refill the jar completely with AR Buffer. Microwave at 100% power for ~2 min, until the solution begins boiling, and then microwave for 18 min at 20% power (*see* **Note 3**).
18. Allow slides to cool at room temperature for 30 min, and then proceed to do further staining steps, or store slides at 4°C overnight for continuation on the following day.
19. Repeat Steps 1–17 from this section five additional times, each time using a different primary antibody and corresponding Opal dye each cycle, until all of the antigens in each panel are stained. Follow the staining order specified in Tables 2 and 3, as changing the order may affect results. For example, Table 2 proceeds with CD4/Opal 520, CD8/Opal 540, CD19/Opal 650, Ki67/Opal 570, and Granzyme-b/Opal 690.

3.3 Spectral DAPI Stain, Mount, and Coverslip

1. Set up two Tissue-Tek dishes filled with TBST Wash Buffer and two Tissue-Tek dishes filled with DH_2O. The first dish should contain a clean slide rack that will be moved from dish to dish.
2. Wash slides in DH_2O for 2 min.
3. Wash slides in TBST for 2 min.
4. Prepare the DAPI staining solution by adding two drops of spectral DAPI per mL of TBST.
5. Pipette 300 μL DAPI staining solution to each slide, and incubate for 5 min.
6. Wash slides in TBST for 2 min.
7. Wash slides in DH_2O for 2 min.
8. Transfer slides to a staining chamber, apply enough ProLong Diamond Antifade Mountant to cover the tissue, and place a coverslip.
9. Allow slides to dry overnight.
10. The next day, remove excess mountant by cleaning slides with EtOH and image with a fluorescent microscope.

3.4 Identification and Characterization of TLS and TIL by Immunofluorescence

Perform immunofluorescent image acquisition and analysis using a fluorescent microscope such as the Vectra 3 or PhenoImager HT (Quanterix). Perform subsequent spectral unmixing or compensation with inForm image analysis software (Quanterix) using single-stain controls. *See* **Note 4** for staining control suggestions, **Note 5** for acquisition procedures, and **Note 6** for cell enumeration procedures. Representative images corresponding to each of the panels in Tables 2 and 3 are shown in Figs. 1, and 2, respectively.

4 Notes

1. Immerse the slides in each solution, ensuring that the tissue remains fully submerged during all steps so that it does not dry out.
2. If the solution is dropping low during microwaving and the tissue is at risk of not being submerged, refill the jars, bring the solution up to a boil at 100% power, and then continue with microwaving at 20% power until the full 18 min of time has been achieved.
3. This step functions to remove the primary and secondary antibodies from the slides and prepare them for the next step.
4. For each of these panels, we recommend using murine spleens and lymph nodes as positive staining and imaging controls. Lymph

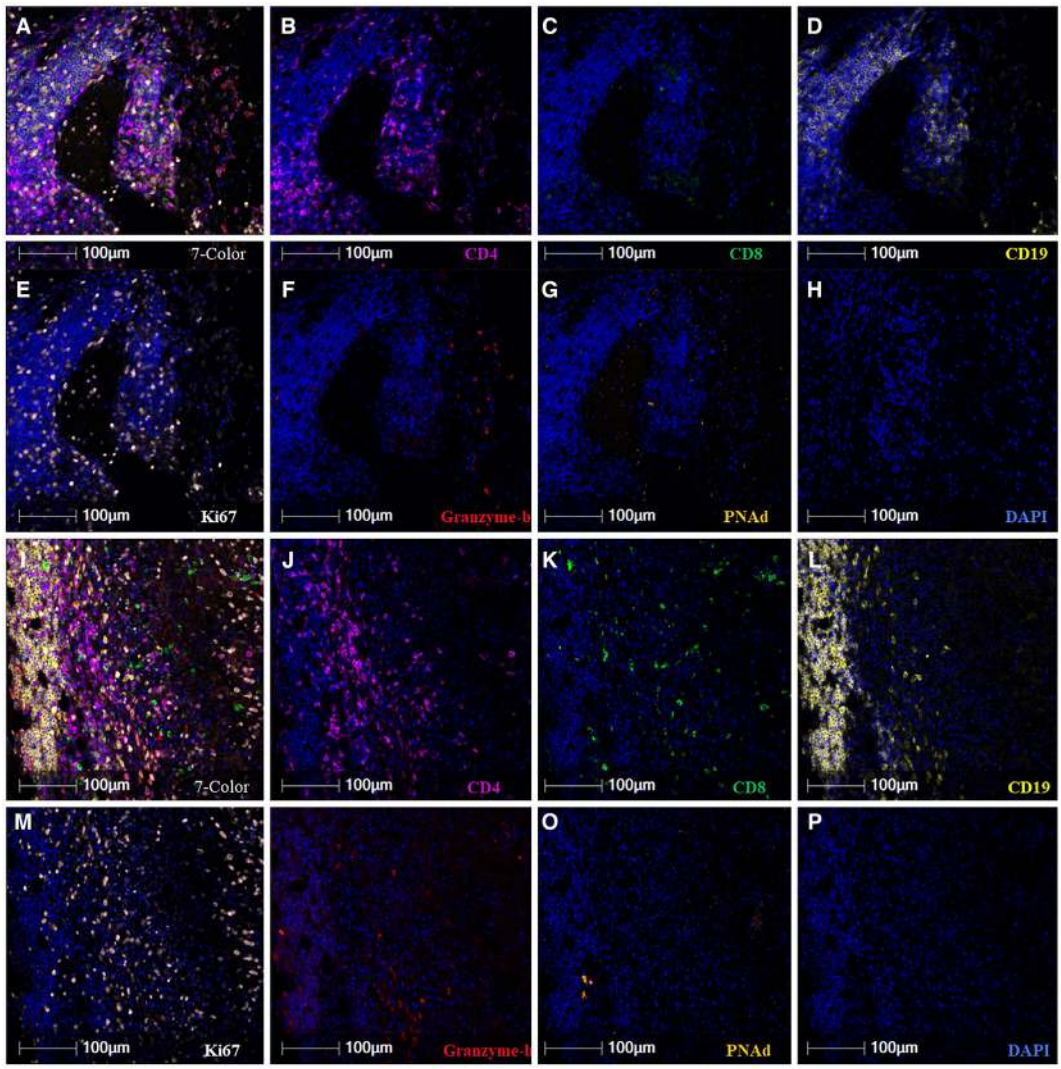


Fig. 1 Two sets of representative multiplex immunofluorescent images of tissue sections stained with Tertiary Lymphoid Structure and Tumor Infiltrating Lymphocytes Identification Panel 1 (Table 2). Panels **A**–**H** and **I**–**P** depict infiltrates in murine BPD6 subcutaneous tumors. Images were acquired at 20× and spectrally compensated in the inForm program (Quanterix) using single-stain positive controls. Images with a scale bar were generated using HALO software. Scale bar = 100 µm

nodes represent secondary lymphoid organs, which are resembled by TLS. These positive controls should be stained and processed alongside the other tissues of interest. Single stain controls should also be used for unmixing, as well as no Opal-stained controls in which the tissue is stained with all the reagents and goes through all steps of the protocol except for the Opal dye staining steps. Additionally, a no-primary-antibody control in which the tissue is stained with all the reagents and goes through all steps of the protocol except the primary antibody staining steps should

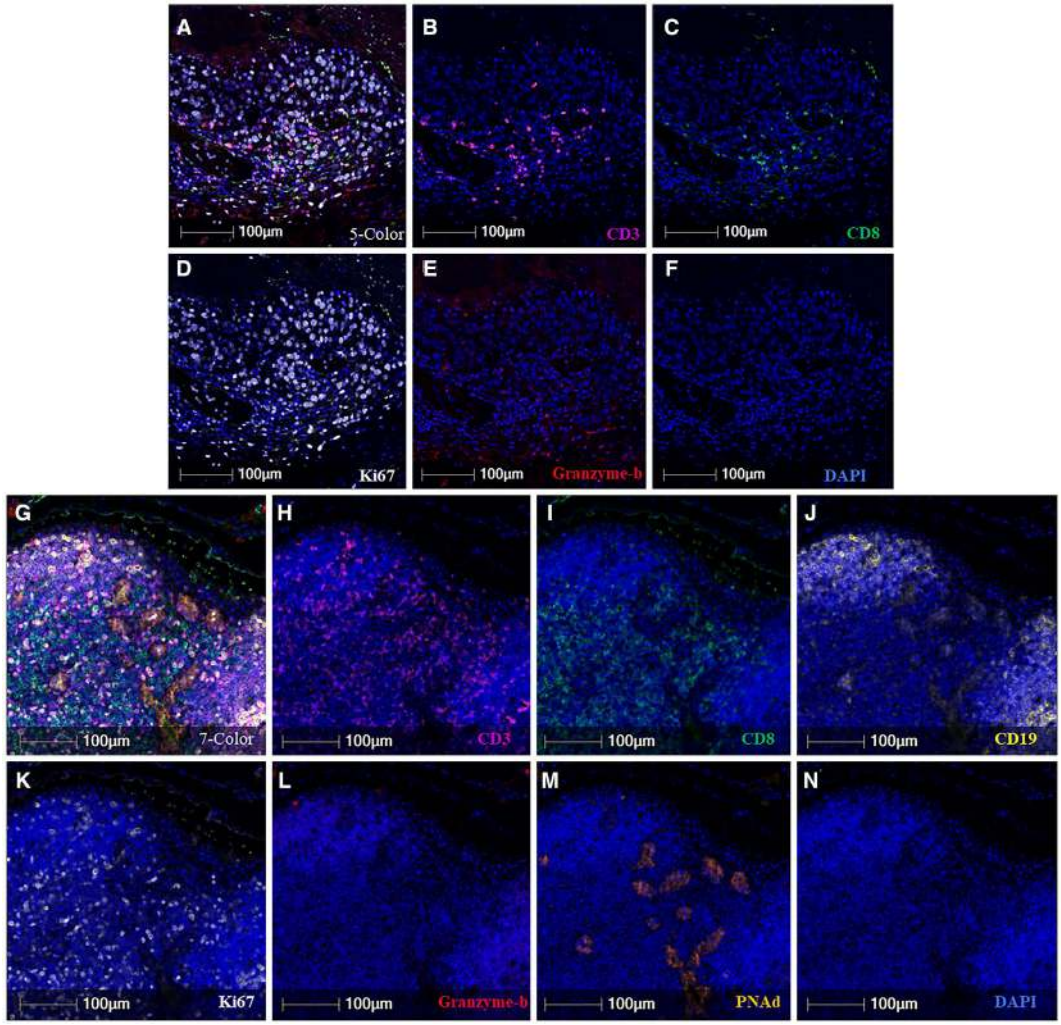


Fig. 2 Representative multiplex immunofluorescent images of tumor sections stained with Tertiary Lymphoid Structure and Tumor Infiltrating Lymphocytes Identification Panel 2 (Table 3). Panels **A**–**F** depict infiltrates in murine B16F1 subcutaneous tumors that lack TLS, and panels **G**–**N** depict a murine tumor-involved draining lymph node. Scale bar = 100 μm

be included. Fluorescence Minus One control (FMOs) can also be useful when developing a panel initially.

5. Whole slides should initially be scanned at 10× to identify specific regions of interest (ROI) for more detailed analysis. These ROI should then be scanned at 20× for cell enumeration. Potential TLS regions should be selected based on CD19 staining (B cell clusters). TLS are usually localized on the tumor border or peritumorally.
6. Digital software, including Halo (Indica Labs), can be used to enumerate the cell data on the 20× scanned ROI. Annotations

can be drawn around key areas, such as TLS, to enable the enumeration of cell subsets at the specific TLS site. Enumeration of immune cells can also be done manually or by using other available software packages, such as inForm (Quanterix).

Acknowledgments

Tissue sectioning was performed by the Research Histology Core, and slide imaging and analysis were performed using microscopes and software in the Molecular Immunologic and Translational Science Core at the University of Virginia. The authors would like to acknowledge the expertise provided by Dr. Craig L. Slingluff Jr. This work was supported by the University of Virginia Cancer Center (NIH P30 CA044579) to support the Research Histology Core and the Molecular Immunologic and Translational Sciences Core.

Conflicts of Interest The authors have no competing interests to declare that are relevant to the content of this chapter.

References

1. Schumacher TN, Thommen DS (2022) Tertiary lymphoid structures in cancer. Science 375(6576):eabf9419
2. Edmonds NL, Gradecki SE, Katyal P et al (2023) Tertiary lymphoid structures in desmoplastic melanoma have increased lymphocyte density, lymphocyte proliferation, and immune cross talk with tumor when compared to non-desmoplastic melanomas. Oncoimmunology 12(1):2164476
3. Stowman AM, Hickman AW, Mauldin IS et al (2018) Lymphoid aggregates in desmoplastic melanoma have features of tertiary lymphoid structures. Melanoma Res 28(3):237–245
4. Sawada J, Kikuchi Y, Duah M et al (2025) Simultaneous STING and lymphotoxin-beta receptor activation induces B cell responses in tertiary lymphoid structures to potentiate antitumor immunity. Nat Immunol 26(10):1766–1780
5. Engelhard VH, Rodriguez AB, Mauldin IS et al (2018) Immune cell infiltration and tertiary lymphoid structures as determinants of antitumor immunity. J Immunol 200(2): 432–442
6. Martinet L, Guellec SL, Filleron T et al (2012) High endothelial venules (HEVs) in human melanoma lesions: major gateways for tumor-infiltrating lymphocytes. Oncoimmunology 1(6):829–839
7. Sun X, Liu W, Sun L et al (2022) Maturation and abundance of tertiary lymphoid structures are associated with the efficacy of neoadjuvant chemoimmunotherapy in resectable non-small cell lung cancer. J Immunother Cancer 10(11):e005531
8. Jones GW, Jones SA (2016) Ectopic lymphoid follicles: inducible centres for generating antigen-specific immune responses within tissues. Immunology 147(2):141–151
9. Hughes CE, Benson RO, Bedaj M, Maffia P (2016) Antigen-presenting cells and antigen presentation in tertiary lymphoid organs. Front Immunol 7:481
10. Hsiao HM, Li W, Gelman AE (2016) The role of lymphoid neogenesis in allografts. Am J Transplant 16(4):1079–1085
11. Rodriguez AB, Peske JD, Engelhard VH (2018) Identification and characterization of tertiary lymphoid structures in murine melanoma. Methods Mol Biol 1845:241–257
12. Rochefort J, Marodon G, Teillaud J-L, Dieu-Nosjean M-C (2025) The Sunrise of tertiary lymphoid structures in cancer. Immunol Rev 332(1):e70046
13. Yoshimitsu M, Nakamura M, Kano S et al (2025) CXCL13 and CCL21 induce tertiary lymphoid structures and enhance the efficacy of immunotherapy for melanoma. Cancer Sci 116(8):2075–2085

14. Tang H, Zhu M, Qiao J, Fu Y-X (2017) Lymphotoxin signalling in tertiary lymphoid structures and immunotherapy. Cell Mol Immunol 14(10):809–818
15. Johansson-Percival A, He B, Li Z-J et al (2017) De novo induction of intratumoral lymphoid structures and vessel normalization enhances immunotherapy in resistant tumors. Nat Immunol 18(11):1207–1217
16. Rodriguez AB, Engelhard VH (2020) Insights into tumor-associated tertiary lymphoid structures: novel targets for antitumor immunity and cancer immunotherapy. Cancer Immunol Res 8(11):1338–1345
17. Rodriguez AB, Peske JD, Woods AN et al (2021) Immune mechanisms orchestrate tertiary lymphoid structures in tumors via cancer-associated fibroblasts. Cell Rep 36(3): 109422
18. Kumar G, Pandurengan RK, Parra ER et al (2023) Spatial modelling of the tumor microenvironment from multiplex immunofluorescence images: methods and applications. Front Immunol 14:1288802



Chapter 26

Methods for Analyzing Immune Infiltrates and Spatial Organization Within the Melanoma Microenvironment Using Multiplex Immunofluorescence

Jackson R. Clark, Kelly T. Smith, Marya Dunlap-Brown, Timothy N.J. Bullock, Craig L. Slingluff Jr. and Ileana S. Mauldin

Abstract

Immunotherapies improve survival in patients with melanoma by enhancing the immune system's ability to recognize and eliminate tumor cells. Understanding the immunological effects of these therapies requires evaluation of both changes in lymphocyte composition and activation within the tumor microenvironment (TME) as well as the spatial organization of these cells. Increased lymphocyte infiltration and distinct patterns of immune cell distribution within the TME have been associated with improved survival and enhanced response to immunotherapy in melanoma. However, relatively few methodologies currently enable detailed characterization of both the structural organization and immunological features of tumor-infiltrating lymphocytes. In this chapter, we describe multiplex immunofluorescence staining approaches for the identification, characterization, and quantification of tumor-infiltrating lymphocytes in melanoma.

Keywords Melanoma, Immune infiltrates, Spatial organization, Multiplex immunofluorescence histology, IHC

1 Introduction

Cancer immunotherapy, including cancer vaccines and immune checkpoint blockade, prolongs survival in patients with melanoma [1, 2]. These therapies primarily act by enhancing the immune system's ability to recognize cancer cells and by stimulating lymphocyte activity within the tumor microenvironment (TME) [3–5], thereby promoting immune-mediated tumor cell killing and improved tumor control. Consequently, the abundance of tumor-infiltrating lymphocytes (TIL), alterations in immune regulation, and changes in the overall composition of the TME are important indicators of therapeutic response [6, 7]. When evaluating the effects of immunotherapy, two key factors are particularly informative: (1) the composition and activation status of lymphocytic populations before and after

Kristian M. Hargadon (ed.), *Melanoma*, Methods in Molecular Biology, vol. 3089,
https://doi.org/10.1007/978-1-0716-5619-8_26,
© The Author(s), under exclusive license to Springer Science+Business Media, LLC, part of Springer Nature 2027

treatment, and (2) the spatial distribution and organization of these lymphocytes within the TME. Changes in these characteristics have been shown to have prognostic value in melanoma [6–9]. Multiplex immunofluorescence histology (mIFH) provides a powerful approach for visualizing and quantifying immune infiltrates within the TME while also enabling analysis of their activation state and spatial relationships.

TILs are a well-established prognostic marker in melanoma, with higher abundance associated with improved overall survival and increased responsiveness to PD-1 and CTLA-4 checkpoint blockade immunotherapy [9, 10]. In particular, increased infiltration of $CD8^+$ T-cells and B-cells correlates with improved survival outcomes in melanoma patients [8, 11], as does a higher ratio of effector T-cells (T-bet^+) relative to regulatory T-cells ($Foxp3^+$) [12]. Effective infiltration of T-cells into tumors depends on adhesion-dependent extravasation across the tumor vasculature and sustained retention within the tissue. Integrins, such as CD49a and CD103, play a critical role in this process by promoting lymphocyte retention in peripheral tissues and tumors. These integrins are also key markers of tissue-resident memory T-cells, which support long-term immune surveillance and enable rapid responses to infection or cancer [13]. $CD8^+$ T-cells co-expressing CD49a and CD103 have been associated with improved patient survival and enhanced response to anti-PD-1 immunotherapy [13, 14]. Beyond overall cell abundance, the spatial pattern of immune infiltration within the melanoma TME also carries prognostic significance. We have defined three histological patterns of immune cell infiltration in metastatic melanoma: an immune-desert phenotype (Immunotype A); restricted, perivascular infiltration (Immunotype B); and diffuse, widespread infiltration throughout the tumor (Immunotype C). These immunotypes account for approximately 29%, 63%, and 8% of melanoma metastases, respectively, and are associated with estimated median survival times of 15, 23, and 130 months [11].

To better characterize immune composition and organization within the TME, we describe three mIFH antibody panels designed to identify and quantitatively characterize TILs. The panels include markers for T-cells (CD3 and CD8), B-cells (CD20), melanoma cells (Sox10), and tissue-resident T-cells (CD49a, CD103). Additional markers allow for evaluation of cellular proliferation (Ki67) and immune activation states, including regulatory T cells (FoxP3), T-helper-1 T cells (T-bet), and PD-1 expression. Together, these panels provide a comprehensive approach for quantitatively profiling the immune composition and activation state of immune cells within tumor and adjacent stromal regions while enabling analysis of spatial relationships among immune cell populations within the TME. This strategy facilitates systematic assessment of changes in immune contexture by quantifying differences in immune cell density, composition, functional state, and spatial organization. Applied to

patient biopsy samples collected before and after treatment, these analyses can reveal associations between immune landscape dynamics, therapeutic response, and clinical outcomes. Overall, these panels provide a robust framework for investigating how immunotherapies reshape the TME and influence lymphocyte populations and their relationship to treatment response, clinical outcome, and patient survival.

2 Materials

2.1 Specimen Preparation

1. Paraffin-embedded tissue specimen.
2. Tissue-Tek slide staining dishes.
3. Freshly cut 4 μm sections mounted on SuperFrost Plus Microscope Slides and dried at 30°C overnight.
4. Xylene.
5. Ethanol (EtOH).
6. 10% Neutral Buffered Formalin.

2.2 Immunofluorescent Staining

1. Humidified slide staining chambers.
2. Antigen Retrieval Buffer 9 (AR9) (Quanterix).
3. DIVA Decloaker, 10× Antigen Retrieval (AR) Buffer (BioCare Medical).
4. Opal 7-Color Manual IHC Kit (Quanterix): includes Opals, Blocking/Antibody Diluent, HRP-conjugated Secondary Antibody (Opal Polymer HRP) that recognizes mouse or rabbit species, spectral DAPI, Antigen Retrieval Buffer 6 (AR6), and Amplification Diluent. To generate Opal stock, reconstitute the lyophilized powder in 150 μL of dimethyl sulfoxide (DMSO).
5. Monoclonal antibodies for staining (Tables 1–4).
6. ProLong Diamond Antifade Mountant (ThermoFisher Scientific).
7. 24 × 50 mm coverslips.
8. Opal Staining jar (Quanterix).
9. Panasonic Microwave Oven with Inverter Technology and Genius Sensor, 1200 W.
10. TBST Wash Buffer: Tris-buffered saline containing 0.05% Tween 20, pH 7.5.

2.3 Image Acquisition

1. Vectra 3 microscope (Quanterix) or a comparable microscope.
2. inForm image analysis software (Quanterix).

Table 1
Antibodies for immunofluorescence staining

Antibody	Clone/Catalog number	Supplier
CD3	MRQ-39	Cell Marque
CD8	C8144B	Dako
CD20	L26	Dako
Ki67	SP6	Abcam
PD-1	NAT105	Abcam
FoxP3	236A/E7	Abcam
Tbet	4B10	Santa Cruz
CD103 (aE)	2G5.1	Abcam
CD49a (a1)	Cat. No. ab181434	Abcam
Sox10	Cat. No. 383A-76	Cell Marque

Table 2
Integrins panel

Staining order	Antigen retrieval	Primary antibody and working dilution	Secondary antibody	Opal
1	DIVA	PD1 (1:100)	Opal polymer HRP mouse + rabbit	570
2	AR9	CD3 (1:100)	Opal polymer HRP mouse + rabbit	520
3	AR9	CD8 (1:500)	Opal polymer HRP mouse + rabbit	540
4	AR9	CD49a (a1 1:4000)	Opal polymer HRP mouse + rabbit	650
5	AR6	CD103 (aE 1:4000)	Opal polymer HRP mouse + rabbit	620
6	AR6	Ki67 (1:20)	Opal polymer HRP mouse + rabbit	690
7		DAPI		

3 Methods

3.1 Deparaffinization, Rehydration, Fixation, and Antigen Retrieval

1. Prepare Tissue-Tek slide staining dishes that are filled with the following solutions: Xylene (×3 dishes), 100% EtOH, 95% EtOH, 70% EtOH, Deionized H_2O (DH2O) (×3 dishes), TBST Wash Buffer (×1 dish), and 10% Neutral Buffered Formalin (×1 dish).

Table 3
T cell infiltration panel

Staining order	Antigen retrieval	Primary antibody and working dilution	Secondary antibody	Opal
1	DIVA	PD1 (1:500)	Opal polymer HRP mouse + rabbit	570
2	AR9	CD3 (1:100)	Opal polymer HRP mouse + rabbit	520
3	AR9	CD8 (1:500)	Opal polymer HRP mouse + rabbit	540
4	AR6	CD20 (1:2000)	Opal polymer HRP mouse + rabbit	620
5	DIVA	Sox10 (1:25)	Opal polymer HRP mouse + rabbit	650
6	AR6	Ki67 (1:20)	Opal polymer HRP mouse + rabbit	690
7		DAPI		

Table 4
Helper T cell identification panel

Staining order	Antigen retrieval	Primary antibody and working dilution	Secondary antibody	Opal
1	AR9	CD3 (1:100)	Opal polymer HRP mouse + rabbit	520
2	AR9	CD8 (1:500)	Opal polymer HRP mouse + rabbit	540
3	DIVA	FoxP3 (1:50)	Opal polymer HRP mouse+rabbit	570
4	DIVA	Tbet (1:200)	Opal polymer HRP mouse + rabbit	650
5	AR6	Ki67 (1:20)	Opal Polymer HRP mouse + rabbit	690
6		DAPI		

2. Move the slide rack containing slides from dish to dish in sequential steps, with all steps performed at room temperature, as follows (*see* **Note 1**):
   a. Xylene dish 1 (10 min).
   b. Xylene dish 2 (10 min).
   c. Xylene dish 3 (10 min).

d. 100% EtOH (5 min).
e. 95% EtOH (5 min).
f. 70% EtOH (2 min).
g. DH2O (2 min).
h. TBST Wash Buffer (2 min).
i. DH2O (2 min).
j. 10% Neutral Buffered Formalin (20 min).
k. DH2O (2 min).

3. Fill the Opal staining jars with 1× diluted AR buffer. Use the associated AR buffer for the first antigen of interest, detailed in Tables 2–4. For example, the panel in Table 2 begins with a PD1 stain post DIVA antigen retrieval; DIVA Buffer would be used first.
4. Remove the slides from the DH20 immersion, and place them into the Opal staining jar, loading the slides back-to-back, with the tissue facing outward, to fill each slot. Wait 2 min, and then discard the buffer (this step serves as an AR buffer rinse).
5. Fill the chamber completely with AR buffer.
6. Microwave slides at 100% power for ~2 min, or until the buffer reaches a boil. Once boiling is achieved, stop the microwave, reduce the power setting to 20%, and continue heating for 18 min. Closely monitor the slides during the initial high-power step to ensure that the buffer does not boil off excessively, and replenish the buffer as needed (*see* **Note 2**).
7. Allow slides to cool at room temperature for 30 min, and then proceed to do further staining steps, or store at 4°C overnight for continuation on the following day.

3.2 Multiplex Stain

The primary antibody, antibody dilutions, secondary antibodies, and Opal dyes to be used when performing these multiplex steps below are detailed in Tables 2–4. Before beginning the staining protocol, dilute primary antibodies in Antibody Diluent, dilute Opal stock in Amplification Diluent, and generate 1× diluted AR buffer. Set up 12 Tissue-Tek staining dishes containing TBST Wash Buffer. The first dish should contain a clean slide rack that will be moved from dish to dish. All of these subsequent steps should be performed at room temperature.

1. Place slides into a Tissue-Tek staining dish filled with TBST, and soak for 2 min to perform a TBST wash.
2. Remove slides from TBST, and place them into the humidified chamber.
3. Pipette 300 µL (or enough to cover the entire tissue) of Antibody Diluent solution on each slide, and wait 10 min. This solution acts as an antibody block.

4. Discard the Antibody Diluent solution from each slide by tipping the slides over a beaker, and place the slides back into the staining chamber.
5. Pipette 300 µL of primary antibody diluted in Antibody Diluent onto each slide, and incubate for 30 min in a humidified chamber. For example, the first antigen stained for in Table 2 is PD1, with anti-PD1 antibody being diluted 1:100 in Antibody Diluent.
6. Set up four Tissue-Tek dishes filled with TBST Wash Buffer. The first dish should contain a clean slide rack that will be moved from dish to dish.
7. After primary antibody incubation, discard the primary antibody over a beaker, and add slides to the slide rack in TBST.
8. Place slides in the first of four Tissue-Tek dishes containing TBST and wash 4 × 2 min, transferring the slide rack to a fresh dish every 2 min.
9. Remove slides from TBST, and place them into the humidified staining chambers.
10. Pipette 300 µL of ready-to-use secondary antibody (Opal Polymer HRP) to each slide, and stain for 10 min.
11. Discard the secondary antibody, and wash slides 4 × 2 min each in TBST.
12. Remove slides from TBST and place into humidified staining chambers.
13. Dilute Opal stock 1:50 in Amplification Diluent to generate Opal staining solution.
14. Pipette 300 µL of Opal staining solution to each slide, and incubate for 10 min. Use the Opal dye corresponding to each primary antibody (see Tables 2–4). For example, Opal 570 is used for PD1 as detailed in Table 2.
15. Discard Opal solution, and wash slides 4 × 2 min each in TBST.
16. Rinse slides in the appropriate AR Buffer for the next antigen in the staining panel (as indicated in Tables 2–4) for 2 min in an Opal staining jar, and then discard the buffer. For example, in Table 2, the next AR Buffer that would be used is AR9.
17. Refill the jar completely with AR Buffer. Microwave at 100% power for ~2 min, until the solution begins boiling, and then microwave for 18 min at 20% power (*see* **Note 3**).
18. Allow slides to cool at room temperature for 30 min, and then proceed to do further staining steps or store slides at 4°C overnight for continuation on the following day.
19. Repeat steps 1–17 from this section five additional times, each time using a different primary antibody and corresponding Opal dye, until all of the antigens in each panel are stained.

Follow the staining order specified in Tables 2–4 as changing the order may affect results. For example, Table 2 proceeds with CD3/Opal 520, CD8/Opal 540, CD49a/Opal 650, CD103/Opal 620, and Ki67/Opal 690.

3.3 Spectral DAPI Stain, Mount, and Coverslip

1. Set up two Tissue-Tek dishes filled with TBST Wash Buffer and two Tissue-Tek dishes filled with DH2O. The first dish should contain a clean slide rack that will be moved from dish to dish.
2. Wash slides in DH2O for 2 min.
3. Wash slides in TBST for 2 min.
4. Prepare the DAPI staining solution by adding two drops of spectral DAPI per mL of TBST.
5. Pipette 300 µL of DAPI staining solution to each slide, and incubate for 5 min.
6. Wash slides in TBST for 2 min.
7. Wash slides in DH2O for 2 min.
8. Transfer slides to a staining chamber, apply enough ProLong Diamond Antifade Mountant to cover the tissue, and place a coverslip.
9. Allow slides to dry overnight.
10. The next day, remove excess mountant by cleaning slides with EtOH and image with a fluorescent microscope.

3.4 Identification and Characterization of Immune Infiltrates and Spatial Organization by Immunofluorescence

Perform immunofluorescent image acquisition and analysis using a fluorescent microscope such as the Vectra 3 or PhenoImager HT (Quanterix). Perform subsequent spectral unmixing or compensation with inForm image analysis software (Quanterix) using single-stain controls. *See* **Note 4** for staining control suggestions, **Note 5** for acquisition procedures, and **Note 6** for cell enumeration. Representative images corresponding to each of the panels in Tables 2–4 are shown in Figs. 1–3, respectively.

4 Notes

1. Immerse the slides in each solution, ensuring that the tissue remains fully submerged during all steps so that it does not dry out.
2. If the solution is dropping low during microwaving and the tissue is at risk of not being submerged, refill the jars, bring the solution up to a boil at 100% power, and then continue with microwaving at 20% power until the full 18 min of time has been achieved.

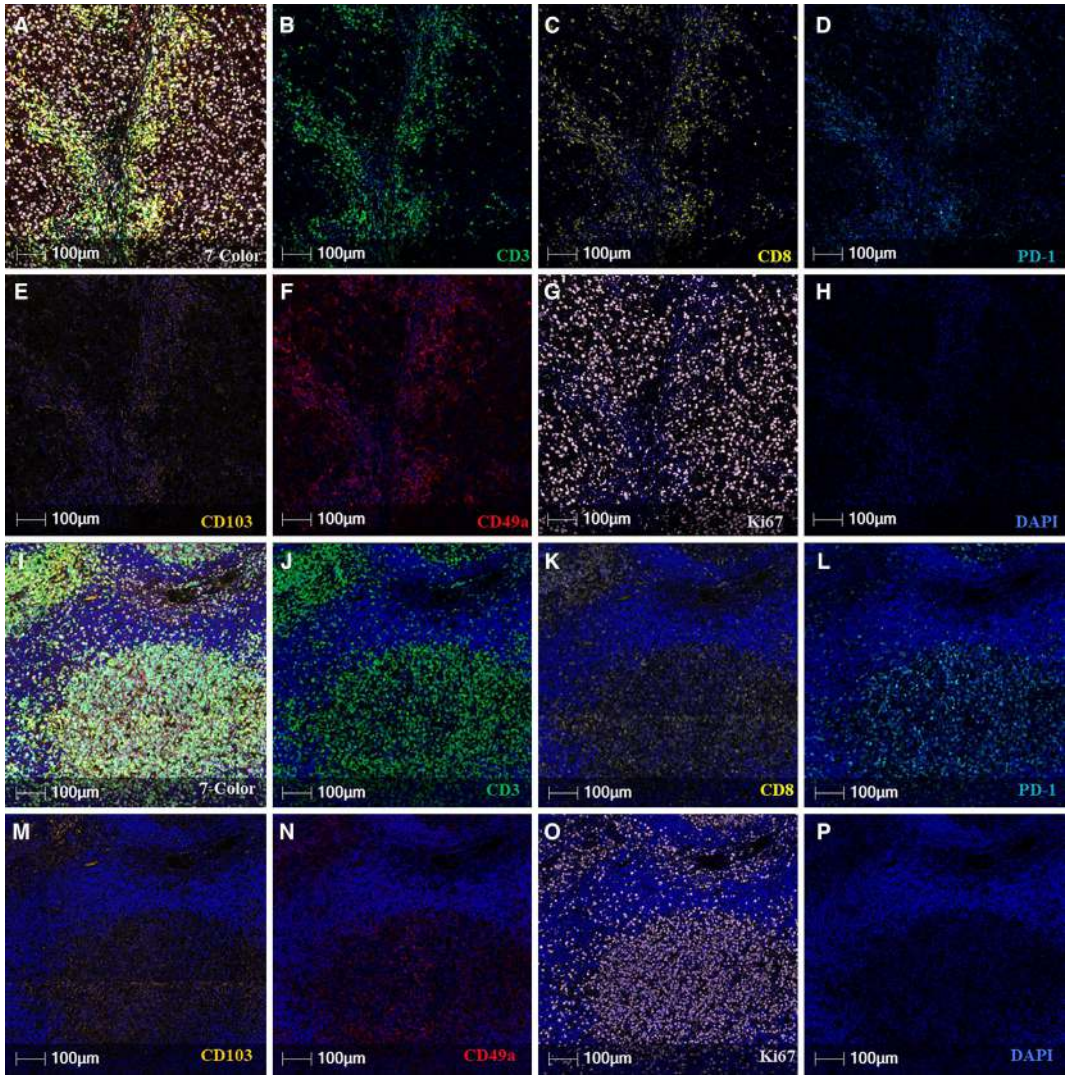


Fig. 1 Two sets of representative multiplex immunofluorescent images of lymph node sections stained with the Integrins Panel (Table 2). Panels **A**–**H** and panels **I**–**P** depict tumor-involved lymph nodes. Images were acquired at 20× and spectrally compensated in the inForm program (Quanterix) using single-stain positive controls. Scale bar images were generated in HALO software. Scale bar = 100 μm

3. This step functions to remove the primary and secondary antibodies from the slides and prepare them for the next step.
4. For each of these panels, we recommend using tumor-involved lymph nodes as positive staining and imaging controls. These positive controls should be stained and processed alongside the other tissues of interest. Single stain controls should also be used for unmixing, as well as no Opal-stained controls in which the tissue is stained with all the reagents and goes through all steps of the protocol except for the Opal dye staining steps.

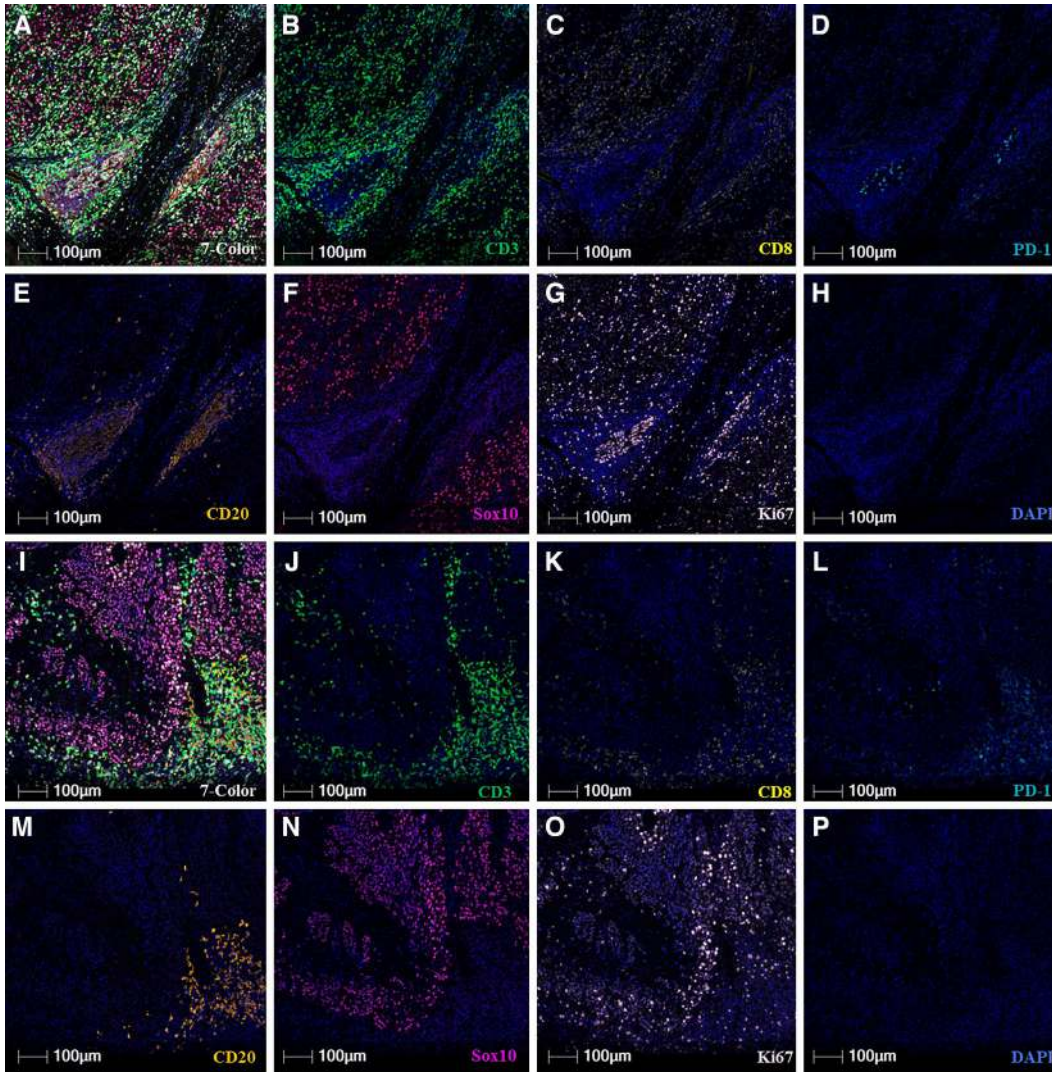


Fig. 2 Representative multiplex immunofluorescent images of lymph node sections stained with the T-cell infiltration panel (Table 3) are shown. Panels **A–H** and panels **I–P** depict tumor-involved lymph nodes. Scale bar = 100 μm

Additionally, a no-primary-antibody control in which the tissue is stained with all the reagents and goes through all steps of the protocol except the primary antibody staining steps should be included. Fluorescence Minus One controls (FMOs) can also be useful in the initial panel development.

5. Whole slides should initially be scanned at 10×, which is used to identify specific regions of interest (ROI) for more detailed analysis. These ROI should then be scanned at 20× for cell enumeration.

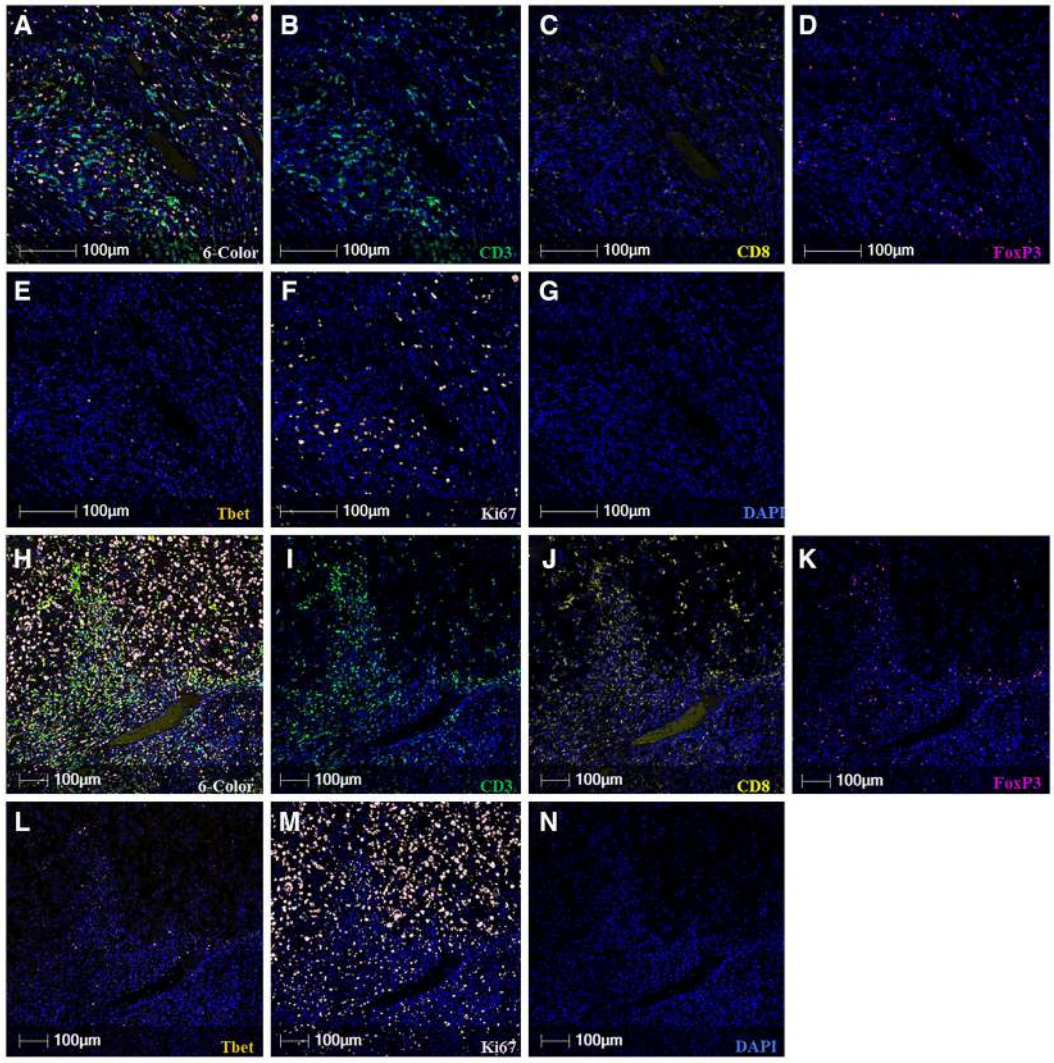


Fig. 3 Representative multiplex immunofluorescent images of lymph node sections stained with the helper T-cell identification panel (Table 4) are shown. Panels **A–H** and **G–N** depict tumor-involved lymph nodes. Scale bar = 100 μm

6. Digital software, including Halo (Indica Labs), can be used to enumerate the cell data on the 20× scanned ROI. Annotations can be drawn around key areas, such as tertiary lymphoid structures (TLS), to enable enumeration of cell subsets at the specific TLS site. However, enumeration of immune cells can also be done manually or by using other available software packages, such as inForm (Quanterix).

Acknowledgments

Tissue sectioning was performed by the Biorepository and Tissue Research Facility, and slide imaging and analysis were performed using microscopes and software in the Molecular Immunologic and Translational Science Core at the University of Virginia. This work was supported by the United States Department of Defense Translational Team Science Award (CA181046). Additional funding was provided by the University of Virginia Cancer Center (NIH P30 CA044579) to support the Office of Clinical Research, Biorepository and Tissue Research Facility, Biostatistics Core, and Molecular Immunologic and Translational Sciences Core.

Conflict of Interest The authors have no competing interests to declare that are relevant to the content of this chapter.

References

1. Ninmer EK, Zhu H, Chianese-Bullock KA et al (2024) Multipeptide vaccines for melanoma in the adjuvant setting: long-term survival outcomes and post-hoc analysis of a randomized phase II trial. Nat Commun 15(1):2570. Addendum in (2025) Nat Commun 16(1):8236
2. Wolchok JD, Chiarion-Sileni V, Rutkowski P et al (2025) Final, 10-year outcomes with nivolumab plus ipilimumab in advanced melanoma. N Engl J Med 392(1):11–22
3. Onitilo AA, Wittig JA (2020) Principles of immunotherapy in melanoma. Surg Clin North Am 100(1):161–173
4. Gaißler A, Meldgaard TS, Heeke C et al (2022) Dynamics of melanoma-associated epitope-specific CD8+ T cells in the blood correlate with clinical outcome under PD-1 blockade. Front Immunol 13:906352
5. Kristensen NP, Heeke C, Tvingsholm SA et al (2022) Neoantigen-reactive CD8+ T cells affect clinical outcome of adoptive cell therapy with tumor-infiltrating lymphocytes in melanoma. J Clin Invest 132(2):e150535
6. Ma Y, Zhang L, Liu W (2025) Immunosuppressive tumor microenvironment and advance in immunotherapy in melanoma bone metastasis. Front Immunol 16:1608215
7. Bagaev A, Kotlov N, Nomie K et al (2021) Conserved pan-cancer microenvironment subtypes predict response to immunotherapy. Cancer Cell 39(6) 845-865:e7
8. Piras F, Colombari R, Minerba L et al (2005) The predictive value of CD8, CD4, CD68, and human leukocyte antigen-D-related cells in the prognosis of cutaneous malignant melanoma with vertical growth phase. Cancer 104(6):1246–1254
9. Barnes TA, Amir E (2017) HYPE or HOPE: the prognostic value of infiltrating immune cells in cancer. Br J Cancer 117(4):451–460
10. Verdegaal EME, Verpoorte ALC, van der Kooij MK et al (2025) Effective TIL therapy for patients with checkpoint-resistant melanoma without lymphodepleting regimens requires IFNalpha. Clin Cancer Res 31(13):2628–2638
11. Erdag G, Schaefer JT, Smolkin ME et al (2012) Immunotype and immunohistologic characteristics of tumor-infiltrating immune cells are associated with clinical outcome in metastatic melanoma. Cancer Res 72(5):1070–1080
12. Knol AC, Nguyen JM, Quéreux G et al (2011) Prognostic value of tumor-infiltrating Foxp3+ T-cell subpopulations in metastatic melanoma. Exp Dermatol 20(5):430–434
13. Plunkett KR, Armitage JD, Inderjeeth A-J et al (2022) Tissue-resident memory T cells in the era of (Neo) adjuvant melanoma management. Front Immunol 13:1048758
14. Park SL, Buzzai A, Rautela J et al (2019) Tissue-resident memory CD8(+) T cells promote melanoma-immune equilibrium in skin. Nature 565(7739):366–371

Part VI

Strategies for Diagnostic and Prognostic Metabolomic/ Microbiomic Biomarker Identification for Melanoma and Computational/Bioinformatic Approaches to OMICS-Based Analysis of Melanoma



Chapter 27

Integrated Functional and Metabolomic Profiling of Melanoma Cells Treated with Redox-Active Compounds

Marcella Bonanomi and Daniela Gaglio

Abstract

Metabolic plasticity is a hallmark of melanoma progression and therapy resistance. This chapter describes a reproducible protocol for comprehensive metabolic profiling of melanoma cells exposed to redox-active compounds such as emodin and aloe-emodin. The method integrates cell proliferation assays, mitochondrial functional analysis using Seahorse extracellular flux measurements, reactive oxygen species (ROS) quantification, LC–MS-based metabolomics, stable-isotope tracing, and ^{13}C metabolic flux analysis (^{13}C-MFA). The workflow enables quantitative characterization of treatment-induced alterations in energy metabolism, redox balance, and central carbon fluxes in melanoma cell lines with distinct metabolic phenotypes. The procedures are presented in a step-by-step format suitable for researchers unfamiliar with the individual techniques and can be adapted to other cancer models or metabolic perturbations.

Keywords Melanoma, Metabolic plasticity, Seahorse assay, LC–MS metabolomics, Stable isotope tracing, ^{13}C metabolic labeling, Emodin, Aloe-emodin, Redox homeostasis

1 Introduction

Melanoma is an aggressive form of skin cancer characterized by rapid progression, early metastatic dissemination, and high mortality [1–4]. Its clinical behavior is shaped not only by oncogenic signaling pathways but also by the remarkable ability of melanoma cells to reprogram their metabolism [3, 4]. Within the same tumor, cells can differ substantially in how they generate energy, maintain redox balance, and channel nutrients into biosynthetic pathways [3, 4]. Some subpopulations adopt a predominantly glycolytic, "Warburg-like" phenotype, others rely more strongly on mitochondrial oxidative phosphorylation (OXPHOS), and many are capable of switching between these states or maintaining mixed profiles [3–6]. This metabolic plasticity provides a buffer against microenvironmental and therapeutic stress and is increasingly recognized as a key determinant of therapy resistance [1, 4–6]. Targeting metabolic vulnerabilities in melanoma requires tools that perturb and monitor metabolism in a

Kristian M. Hargadon (ed.), *Melanoma*, Methods in Molecular Biology, vol. 3089,
https://doi.org/10.1007/978-1-0716-5619-8_27,
© The Author(s), under exclusive license to Springer Science+Business Media, LLC, part of Springer Nature 2027

coordinated manner [1, 4, 7]. Natural compounds with redox-active scaffolds are attractive in this regard because they tend to influence multiple metabolic nodes simultaneously [2, 8–10]. Among these, the anthraquinones emodin and aloe-emodin have received considerable attention [1, 2, 8–10]. These molecules, originally isolated from plants such as *Rheum palmatum* and *Aloe vera*, contain a quinone core capable of accepting and donating electrons, thereby engaging in redox cycling reactions [8, 9]. By interacting with mitochondrial electron transport and other redox-sensitive targets, emodin and aloe-emodin can alter reactive oxygen species (ROS) levels, disturb NAD^+/NADH balance, and affect ATP production, which in turn modulates cell proliferation and survival [1, 9, 10].

In melanoma cells, emodin and aloe-emodin have been shown to inhibit proliferation and interfere with both glycolytic and mitochondrial pathways [1, 9, 10]. However, the exact nature of these effects depends on the pre-existing metabolic state of the cells [1–4]. For example, cell lines that are more OXPHOS-dominated at baseline may respond differently from those that are strongly glycolytic [1, 3–6]. Simple viability assays or single-parameter measurements are therefore insufficient to capture the complexity of these responses. A more informative strategy is to combine functional bioenergetic measurements with quantitative metabolomics and metabolic flux analysis, thereby linking changes in growth and survival to specific alterations in metabolic pathways [1, 7, 11–15].

This chapter describes a reproducible protocol for metabolic profiling of melanoma cells following treatment with redox-active agents, exemplified here by emodin and aloe-emodin [1, 2, 8–10]. The method integrates complementary measurements, including cell proliferation, Seahorse-based mitochondrial stress testing, reactive oxygen species (ROS) quantification, and LC–MS metabolomics, stable-isotope tracing with [U-^{13}C] substrates, and ^{13}C metabolic flux analysis (^{13}C-MFA) to characterize treatment-induced changes in cellular bioenergetics, redox balance, metabolite pools, and central carbon fluxes (Fig. 1) [1, 7, 11–18]. By collecting these readouts under matched experimental conditions, the workflow enables mechanistic interpretation beyond single-endpoint assays [1, 11–15]. The protocol has been validated in three human melanoma cell lines representing distinct metabolic phenotypes: COLO 800 and COLO 794, which display more oxidative, TCA-cycle-enriched profiles; and A375, which is more glycolytic and rapidly proliferating. Applying the same workflow across these models allows identification of both common metabolic effects of treatment and cell-line-specific adaptive responses [1, 3–7, 11–15]. Although illustrated using emodin and aloe-emodin, the procedure can readily be adapted to other redox-active compounds, cancer types, or metabolic perturbations [2, 8–15]. Detailed step-by-step instructions are provided to enable successful implementation by investigators unfamiliar with individual components of the method [2, 7, 11–15].

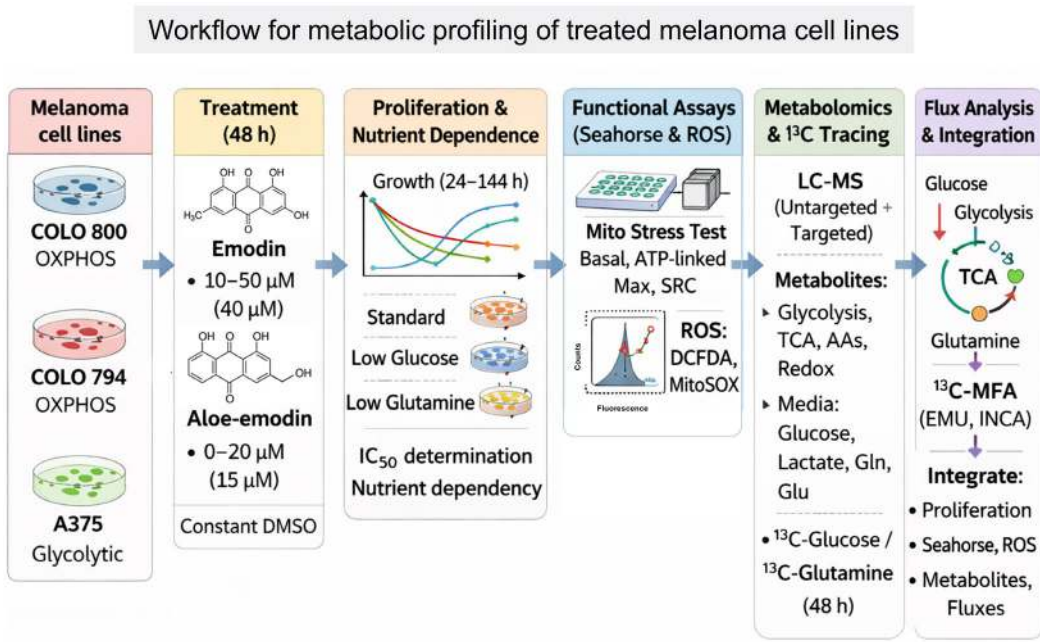


Fig. 1 Workflow for metabolic profiling. Schematic workflow illustrating the integrated metabolic profiling of melanoma cell lines treated with redox-active compounds. The diagram shows sequential steps including cell culture and compound treatment, cell proliferation analysis, Seahorse mitochondrial stress testing, reactive oxygen species quantification by flow cytometry, metabolite extraction for LC–MS analysis, and stable isotope tracing with uniformly labeled carbon substrates

2 Materials

Prepare all solutions using appropriate-grade water and reagents. For metabolomics and isotope tracing, use LC–MS-grade solvents, and handle all samples on ice or at 4°C when possible.

2.1 Cell Lines and Culture Reagents

1. Human melanoma cell lines: COLO 800, COLO 794, and A375 (or equivalent lines representing distinct metabolic phenotypes).
2. Complete Growth Medium for COLO 800 and COLO 794 melanoma cells: RPMI-1640 medium supplemented with 10% heat-inactivated fetal bovine serum (FBS), 2 mM L-glutamine, 100 U/mL of penicillin, and 100 μg/mL of streptomycin.
3. Complete Growth Medium for A375 melanoma cells: DMEM (high glucose, 25 mM ≈ 4.5 g/L) supplemented with 10% heat-inactivated FBS, 2 mM L-glutamine, 100 U/mL of penicillin, and 100 μg/mL of streptomycin.
4. Phosphate-buffered saline (PBS), pH 7.4, without Ca^{2+}/Mg^{2+}.

5. Trypsin-EDTA Solution, 1×: 0.25% Trypsin/0.53 mM EDTA in Phosphate Buffered Saline Solution without calcium or magnesium.
6. Tissue culture flasks and multiwell plates (6-, 12-, 24-, and 96-well).
7. Humidified incubator set at 37°C with 5% CO_2.
8. Dimethyl sulfoxide (DMSO), cell culture grade.
9. Hemocytometer or automated cell counter.
10. Mycoplasma test kit (recommended).

2.2 Compounds

1. Emodin from *Frangula* bark (purity ≥90%): Dissolve compound in DMSO to prepare a 500 mM stock solution. Vortex until fully dissolved. Aliquot stocks in small volumes into light-protected tubes and store at −20°C. Avoid repeated freeze–thaw cycles (*see* **Note 1**).
2. Aloe-emodin, ≥97% purity: Dissolve compound in DMSO to prepare a 500 mM stock solution. Vortex until fully dissolved. Aliquot stocks in small volumes into light-protected tubes and store at −20°C. Avoid repeated freeze–thaw cycles (*see* **Note 1**).

2.3 Seahorse and Functional Assays

1. Seahorse XF extracellular flux analyzer (e.g., XF24 or XF96).
2. Seahorse XF cell culture microplates.
3. Seahorse XF Sensor Cartridges.
4. Seahorse XF Cell Mito Stress Test Kit (oligomycin, FCCP, rotenone/antimycin A).
5. Seahorse XF Calibrant.
6. Seahorse Assay Medium: Supplement nonbuffered DMEM with 25 mM glucose, 2 mM glutamine, and 1 mM sodium pyruvate. Adjust pH to 7.4 at 37°C. Prepare fresh on the day of use.
7. Non-CO_2 incubator set at 37°C.
8. Bradford protein assay kit (or equivalent method) for post-assay normalization.
9. 1 M NaOH solution.
10. 1 M HCl solution.
11. Spectrophotometer capable of reading at 595 nm.

2.4 Redox Assays

1. DCFDA Cellular ROS Detection Kit.
2. MitoSOX™ Red mitochondrial superoxide indicator.
3. Flow cytometer equipped with FITC and PE channels and appropriate software.

2.5 Metabolomics and Isotope Tracing

1. LC–MS-grade acetonitrile.
2. LC–MS-grade water.
3. LC–MS-grade formic acid.
4. Saline solution: 0.9% NaCl.
5. Labeled Glucose ([U-$^{13}C_6$]glucose, ≥99% isotopic enrichment) Medium: Weigh [U-$^{13}C_6$]glucose and dissolve it in glucose-free culture medium (RPMI for COLO 800 and COLO 794 cells, DMEM for A375 cells) to obtain a final glucose concentration of 11 mM (for COLO 800 and COLO 794 cells) and 25 mM (for A375 cells), respectively; then add 10% FBS, 2 mM L-glutamine, 100 U/mL of penicillin, and 100 μg/mL of streptomycin. Filter sterilize before use.
6. Labeled Glutamine ([U-$^{13}C_5$]glutamine, ≥99% isotopic enrichment) Medium: Weigh [U-$^{13}C_5$]glutamine and dissolve it in glutamine-free culture medium (RPMI for COLO 800 and COLO 794 cells, DMEM for A375 cells) to obtain a final glutamine concentration of 2 mM; then add 10% FBS, 100 U/mL of penicillin, and 100 μg/mL of streptomycin. Filter-sterilize before use.
7. UHPLC system.
8. QTOF mass spectrometer with electrospray source.
9. PFP column (e.g., 2.1 × 100 mm, 2.7 μm).
10. Centrifuge for microtubes
11. Centrifugal vacuum concentrator.
12. –80°C refrigerator.
13. LC–MS vials with glass inserts and caps.
14. YSI bioanalyzer or equivalent for media glucose, lactate, glutamine, and glutamate quantification.

2.6 Software

1. Vendor-specific LC–MS data processing software (e.g., MassHunter ProFinder and VistaFlux).
2. MetaboAnalyst or equivalent web-based platform for statistical and pathway analysis.
3. INCA or similar.
4. ^{13}C-MFA software implementing the EMU framework.
5. Flow cytometry analysis software (e.g., CytExpert).
6. Standard spreadsheet and statistical software.

3 Methods

3.1 Routine Cell Culture

1. Thaw COLO 800, COLO 794, and A375 cells, and culture them according to the supplier's instructions in the appropriate Complete Growth Medium. Maintain all cultures at 37°C in a humidified incubator with 5% CO_2, and whenever possible use the same incubator for all cell lines (*see* **Note 2**).
2. Expand the cells in T-flasks until they reach 60%–70% confluency.
3. Passage cells when they reach 70%–80% confluency, using trypsin–EDTA to detach adherent cells from flasks. Avoid reaching over confluency in growth, which markedly alters metabolic profiles (*see* **Note 3**).
4. For experiments, use cells within a defined passage range (e.g., passages 5–20). After thawing, perform at least two to three passages before starting metabolomics experiments. Record passage number and date in a log.
5. Periodically test for mycoplasma and confirm cell line identity to ensure reproducibility.

3.2 Compound Treatment

1. For each experiment, on the day of treatment, thaw an aliquot of 50 mM stock emodin and aloe-emodin, and prepare a fresh 1:20 dilution of the compounds in the appropriate pre-warmed culture medium, yielding a 2.5 mM intermediate working solution for each compound. Further dilute the intermediate working solutions to reach the final concentrations required for the assays, ensuring that the final DMSO concentration is identical in all conditions (typically ≤0.1% v/v).
2. For dose–response experiments, prepare a series of concentrations (i.e., aloe-emodin 0–20 μM; emodin 0–50 μM). For mechanistic assays, select one or two working concentrations based on IC50 and long-term proliferation data (see Sect. 3.3).
3. Add emodin, aloe-emodin, or DMSO vehicle to cell cultures, and incubate for 48 h for endpoint analyses unless specified otherwise. Protect plates from light where feasible by covering them with foil.

3.3 Cell Proliferation Analysis

3.3.1 Proliferation Under Standard and Nutrient-Modified Conditions

1. Seed COLO 800, COLO 794, and A375 cells in six-well plates at a density that maintains exponential growth over the planned time course (i.e., 1.2×10^5 cells per well for COLO 800 and COLO 794 and 0.8×10^5 cells per well for A375 [*see* **Note 4**]). Allow cells to attach overnight in Complete Growth Medium.

2. At time zero, replace the Complete Growth Medium with fresh Complete Growth Medium, a low-glucose formulation (e.g., 1 mM ≈ 0.18 g/L) of the appropriate culture medium, or a low-glutamine formulation of the appropriate culture medium (e.g., 0.5 mM glutamine), depending on the desired comparison. At 24, 48, 72, and 144 h, detach cells by trypsinization, and count cells using a hemocytometer or automated counter. Record total cell number and viability.
3. Plot cell number versus time under each condition to generate proliferation curves and reveal differences in nutrient sensitivity between cell lines.

3.3.2 Proliferation Under Emodin and Aloe-Emodin Treatment

1. Seed cells in six-well plates as described in Sect. 3.3.1.
2. After 24 h, replace culture medium with Complete Growth Medium containing emodin, aloe-emodin, or DMSO at the chosen concentrations.
3. For dose—response assays, treat cells for 48 h, and then take a cell count to calculate viability relative to DMSO controls for each concentration. Fit dose–response curves to determine IC50 values.
4. For long-term proliferation studies, treat cells at working concentrations, and count them at 24, 48, 72, and 144 h. Use these results to confirm that the selected working concentrations induce substantial, but not complete, growth inhibition in order to establish a window in which metabolic changes can be observed.

3.4 Seahorse XF Mitochondrial Stress Test

1. Seed the cells in Seahorse XF plates at a density optimized for each line [i.e., 2×10^4 cells per well in XF24 plates for COLO 800 and COLO 794, 0.5×10^4 cells per well for A375 (*see* **Note 5**)]. Cells should form a uniform monolayer without reaching confluency by the time of the assay.
2. Allow cells to adhere, and then treat them with emodin, aloe-emodin, or DMSO at working concentrations for 48 h before the assay.
3. The day before the Seahorse run, hydrate the Seahorse sensor cartridge overnight in Seahorse XF Calibrant according to the manufacturer's instructions.
4. On the day of the assay, prepare fresh Seahorse Assay Medium.
5. Gently remove the culture medium from each well, wash once with pre-warmed Seahorse Assay Medium, and add fresh Seahorse Assay Medium (500 µL per well in XF24 plates).
6. Incubate the plate in a 37°C non-CO_2 incubator for 60 minutes to allow equilibration.
7. Prepare injection solutions for the Mito Stress Test as follows:

a. Oligomycin at a concentration that will yield a 1 μM final concentration when added to the sample wells.
b. FCCP at a titrated concentration yielding robust uncoupling. For melanoma cell lines, a final concentration of 1 μM is recommended (*see* **Note 5**).
c. Rotenone/antimycin A at a concentration that will yield a 0.5 μM final concentration when added to the sample wells.

8. Load oligomycin into Port A, FCCP into Port B, and rotenone/antimycin A into Port C of the sensor cartridge.
9. Run the standard Mito Stress Test protocol, acquiring several measurement cycles at baseline and after each injection. Export oxygen consumption rate (OCR) data and calculate as follows:
   a. Basal respiration = OCR before oligomycin—OCR after rotenone/antimycin A.
   b. ATP-linked respiration = OCR before oligomycin—OCR after oligomycin.
   c. Maximal respiration = OCR after FCCP—OCR after rotenone/antimycin A.
   d. Spare respiratory capacity = maximal respiration—basal respiration.
10. Normalize OCR values to protein content per well. To quantify protein content, add 50 μL of 1 M NaOH solution to each well, and incubate the plate at 37°C for 30 min. Then add 50 μL of 1 M HCl to neutralize. Measure 10 μL in 1 mL of Bradford protein assay solution, reading the absorbance at 595 nm using a spectrophotometer.

3.5 ROS Measurements by Flow Cytometry

3.5.1 Total ROS Detection with DCFDA

DCFDA (2′,7′-dichlorofluorescin diacetate) is a cell-permeable probe that can be used to detect intracellular ROS. Upon cellular entry, DCFDA is deacetylated by cellular esterases into a non-fluorescent compound that can subsequently become oxidized by ROS to form highly fluorescent DCF (2′,7′-dichlorofluorescein), which emits a fluorescent signal detectable by flow cytometry (or fluorescence microscopy).

1. Plate and treat cells in six-well plates as described in Sects. 3.3.1 and 3.3.2 (*see* **Note 6**).
2. Prepare a DCFDA working solution according to the kit instructions (20 μM in prewarmed medium).
3. Remove the culture medium, wash once with PBS, and add the DCFDA solution to cover cells (1 ml of solution in each well).

4. Incubate for 30 min at 37°C in the dark.
5. Aspirate the medium, wash cells with PBS, detach by trypsinization, and resuspend each well in 500 µl of PBS containing 5% FBS.
6. Keep samples on ice and protected from light. Acquire at least 10,000 events per sample in a flow cytometer using the FITC channel.
7. Analyze data to obtain median fluorescence intensity values, which represent total intracellular ROS levels.

3.5.2 Mitochondrial ROS (MitoSOX)

MitoSOX™ Red is a cell-permeable probe that enters cells and then accumulates within mitochondria, where it is oxidized by superoxide but not other ROS. Following its oxidation within mitochondria, MitoSOX™ Red binds to mitochondrial and nuclear DNA, leading to emission of a strong red fluorescence that can be measured by flow cytometry (or fluorescence microscopy).

1. Plate and treat cells in six-well plates as described in Sects. 3.3.1 and 3.3.2 (*see* **Note 6**).
2. Prepare a MitoSOX™ Red working solution according to the kit instructions (5 µM in prewarmed medium).
3. Remove the culture medium, wash once with PBS, and add the MitoSOX™ Red working solution to cover cells (1 ml of solution in each well).
4. Incubate for 30 minutes at 37°C in the dark.
5. Aspirate the medium, wash cells with PBS, detach by trypsinization, and resuspend each well in 500 µl of PBS containing 5% FBS.
6. Keep samples on ice and protected from light. Acquire at least 10,000 events per sample in a flow cytometer using the PE channel.
7. Analyze data to obtain median fluorescence intensity values, which represent mitochondrial superoxide levels.

3.6 Metabolite Extraction for LC–MS

Central carbon metabolic pathways, including but not limited to glycolysis, the tricarboxylic acid cycle, amino acid metabolism, and mitochondrial oxidative phosphorylation, play important roles in melanoma biology and plasticity (Fig. 2). Metabolomic profiling of melanoma cells under steady-state conditions and following exposure to various treatments can therefore provide key insights into melanoma adaptation to environmental and therapeutic stressors.

1. Seed cells in six-well plates as described in Sect. 3.3.1.
2. Treat cells with emodin, aloe-emodin, or DMSO for 48 h as described in Sects. 3.2 and 3.3.
3. At the end of treatment, place the plates on ice, and aspirate medium rapidly (*see* **Note 7**).

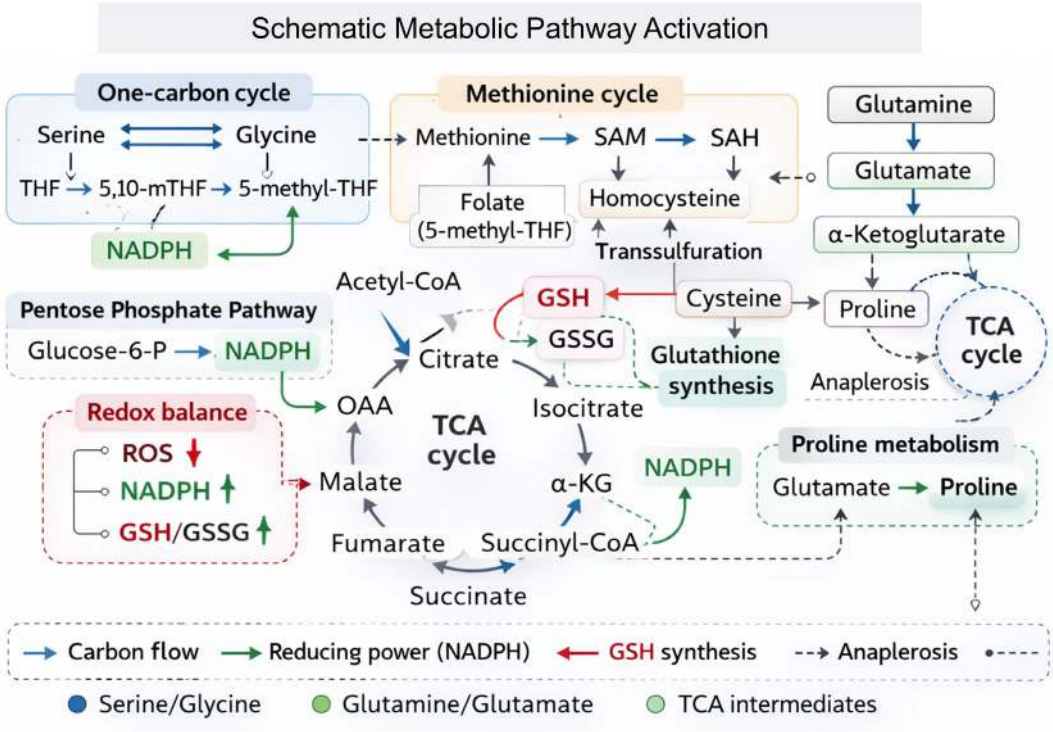


Fig. 2 Schematic metabolic pathway activation. Schematic representation of central carbon metabolic pathways in melanoma cells, highlighting glycolysis, the tricarboxylic acid cycle, glutamine metabolism, and mitochondrial oxidative phosphorylation. The diagram illustrates metabolite flow from glucose and glutamine into pyruvate, lactate, and tricarboxylic acid cycle intermediates, with arrows indicating pathway activity and redox balance connections

4. Wash cells once with ~1 ml/well of ice-cold 0.9% NaCl to remove extracellular metabolites.
5. Quickly add 500 µL of ice-cold 70:30 (v/v) acetonitrile/water solution to each well to quench metabolism.
6. Place plates at −80°C for 10 min to enhance protein precipitation and quenching.
7. Scrape cells into the acetonitrile:water solution, and transfer the suspension into pre-cooled microcentrifuge tubes.
8. Briefly sonicate on ice to facilitate extraction (two 5-second pulses at moderate power).
9. Centrifuge at 12,000 × *g* for 10 min at 4°C to remove debris and proteins.
10. Transfer the supernatant to glass inserts.
11. Dry samples in a centrifugal vacuum concentrator at 30°C until solvent is removed (~2.5 h).
12. Reconstitute dried extracts in 150 µL of LC–MS-grade water, vortex, and keep at 4°C in the autosampler until analysis.

3.7 Untargeted and Targeted LC–MS Analysis

1. Install a PFP column (2.1 × 100 mm, 2.7 μm) on an UHPLC system coupled to a QTOF mass spectrometer operating in negative-ion electrospray mode.
2. Use mobile phase A (water with 0.1% formic acid) and mobile phase B (acetonitrile with 0.1% formic acid).
3. Set a flow rate of 0.2 mL/minute and a column temperature of 35°C.
4. Run the following gradient (time, %A):
   0–2 min: 100% A
   2–4 min: 100–99% A
   4–10 min: 99–98% A
   10–11 min: 98–70% A
   11–15 min: 70% A
   15–16 min: 70–100% A
   16–21 min: 100% A (postrun)
5. Inject 15 μL of each sample.
6. Acquire spectra over m/z 60–1050 with appropriate source parameters and, if available, continuous mass calibration.
7. Include pooled quality-control samples at regular intervals.
8. Process data using dedicated software for feature detection, retention-time alignment, and annotation (untargeted analysis), as well as to extract peak areas for predefined metabolites (targeted analysis).
9. Normalize metabolite intensities to cell number or protein content.
10. Use appropriate transformations and scaling (e.g., log transformation, Pareto scaling) for statistical analysis and pathway enrichment.

3.8 Stable Isotope Tracing

1. Seed cells in six-well plates as described in Sect. 3.3.1.
2. After attachment, replace Complete Growth Medium with Labeled Glucose Medium or Labeled Glutamine Medium for stable isotope tracing (Fig. 3).
3. Add emodin, aloe-emodin, or DMSO to the labeled medium at the working concentrations. Incubate for 48 h under standard conditions, allowing isotopic labeling to approach steady state for central carbon metabolites (*see* **Note 8**).
4. At the end of labeling, extract intracellular metabolites as described in Sect. 3.6.
5. Analyze labeled samples by LC–MS using the same chromatographic conditions as for unlabeled samples.
6. Perform isotopic natural abundance correction, and obtain mass distribution vectors for selected metabolites (e.g., lactate, citrate, malate, aspartate, and glutamate).
7. Export isotopologue distributions for use in ^{13}C-MFA (*see* **Notes 9 and 10**).

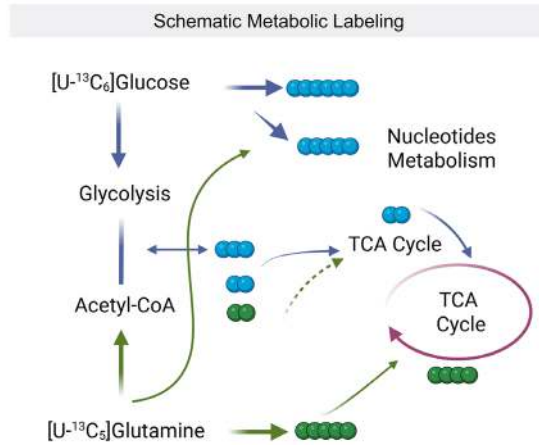


Fig. 3 Schematic metabolic labeling. Schematic illustration of stable isotope tracing in melanoma cell lines using uniformly labeled carbon substrates. The schematic shows uptake of uniformly labeled U-[$^{13}C_6$]glucose or uniformly labeled U-[$^{13}C_5$]glutamine, incorporation of labeled carbon into glycolysis, TCA cycle, and nucleotide metabolism

4 Notes

1. Emodin and aloe-emodin are light-sensitive; store stock solutions in amber tubes or wrapped in foil, and minimize light exposure during handling and incubation.
2. Maintaining all cell lines in the same incubator and under identical atmospheric conditions helps to avoid systematic biases in metabolic measurements.
3. Cell density and confluency have strong effects on nutrient and oxygen gradients and, therefore, on metabolic readouts. Keep seeding densities and harvest times as consistent as possible across experiments.
4. Initial seeding densities may require optimization for each cell line; aim for exponential growth throughout the experiment, and adjust based on observed doubling times.
5. For Seahorse assays, carefully titrate both cell density and FCCP concentration for each line before running large experiments; suboptimal conditions can mask or exaggerate treatment effects.

6. For ROS measurements, avoid overloading cells with probes, and keep staining times within recommended limits, as prolonged exposure can alter ROS levels and cell viability.
7. During metabolite extraction, work quickly and keep everything cold to minimize postharvest metabolic activity and degradation of labile metabolites.
8. In isotope tracing experiments, ensure that labeling and culture conditions are stable over the labeling period; medium exhaustion or large changes in cell density can compromise steady-state assumptions.
9. When building MFA models, start from previously validated networks whenever possible, and check identifiability by sensitivity analysis to avoid interpreting underdetermined fluxes.
10. Integration of proliferation, Seahorse, ROS, metabolite, and flux data provides a more complete picture of how emodin and aloe-emodin affect metabolic plasticity than any individual readout alone.

Conflict of Interest

The authors have no conflicts of interest to declare that are relevant to the content of this chapter.

References

1. Baldassari F, Bonanomi M, Mallia S et al (2025) Emodin and aloe-emodin reduce cell growth and disrupt metabolic plasticity in human melanoma cells. Nutrients 17:1113.
2. Atanasov AG, Zotchev SB, Dirsch VM, Supuran CT (2021) Natural products in drug discovery: advances and opportunities. Nat Rev Drug Discov 20:200–216
3. Lunt SY, Vander Heiden MG (2011) Aerobic glycolysis: meeting the metabolic requirements of cell proliferation. Annu Rev Cell Dev Biol 27:441–464
4. Pavlova NN, Thompson CB (2016) The emerging hallmarks of cancer metabolism. Cell Metab 23:27–47
5. Viale A, Pettazzoni P, Lyssiotis CA et al (2014) Oncogene ablation-resistant pancreatic cancer cells depend on mitochondrial function. Nature 514:628–632
6. Porporato PE, Filigheddu N, Pedro JMB et al (2018) Mitochondrial metabolism and cancer. Cell Res 28:265–280
7. Patti GJ, Yanes O, Siuzdak G (2012) Innovation: metabolomics: the apogee of the omics trilogy. Nat Rev Mol Cell Biol 13:263–269
8. Seigler DS (1998) Benzoquinones, naphthoquinones, and anthraquinones. In: Seigler DS (ed) Plant secondary metabolism. Springer, Boston, pp 76–93
9. Dong X, Fu J, Yin X et al (2016) Emodin: a review of its pharmacology, toxicity and pharmacokinetics. Phytother Res 30:1207–1218
10. Hsu SC, Chung JG (2012) Anticancer potential of emodin. BioMedicine 2:108–116
11. Trachootham D, Alexandre J, Huang P (2009) Targeting cancer cells by ROS-mediated mechanisms: a radical therapeutic approach? Nat Rev Drug Discov 8:579–591

12. Antoniewicz MR (2018) A guide to ^{13}C metabolic flux analysis for the cancer biologist. Exp Mol Med 50:11
13. Young JD (2014) INCA: a computational platform for isotopically non-stationary metabolic flux analysis. Bioinformatics 30:1333–1335
14. Crown SB, Antoniewicz MR (2013) Publishing ^{13}C metabolic flux analysis studies: a review and future perspectives. Metab Eng 20:42–48
15. Xia J, Wishart DS (2016) Using MetaboAnalyst 3.0 for comprehensive metabolomics data analysis. Curr Protoc Bioinformatics 55:14.10.1–14.10.91
16. Brand MD, Nicholls DG (2011) Assessing mitochondrial dysfunction in cells. Biochem J 435:297–312
17. Divakaruni AS, Brand MD (2011) The regulation and physiology of mitochondrial proton leak. Physiology 26:192–205
18. Nicholls DG (2009) Spare respiratory capacity, oxidative stress and excitotoxicity. Biochem Soc Trans 37:1385–1388



Chapter 28

Serum Peptidomic Profiling for Biomarker Discovery in Canine Oral Melanoma and Squamous Cell Carcinoma via MALDI-TOF and LC-MS/MS

Sekkarin Ploypetch, Sittiruk Roytrakul and Gunnaporn Suriyaphol

Abstract

Canine oral malignancies, particularly oral melanoma (OM) and oral squamous cell carcinoma (OSCC), present significant diagnostic hurdles due to their aggressive metastasis and the difficulty of early-stage detection. This study establishes a robust methodological workflow for identifying systemic biomarkers by analyzing the serum peptidome, a minimally invasive alternative to traditional tissue biopsies. Using a high-throughput approach that combines matrix-assisted laser desorption/ionization time-of-flight mass spectrometry (MALDI-TOF MS) for rapid screening with liquid chromatography-tandem mass spectrometry (LC-MS/MS) for precise peptide identification, we successfully differentiated early and late-stage malignancies from benign and healthy controls. Principal component analysis confirmed distinct peptidomic clusters, leading to the identification of four key proteins: FKBP4, ESRRA, IGSF10, and ABCB5. Notably, FKBP4, ESRRA, and ABCB5 were overexpressed in both late-stage OM and late-stage OSCC, while IGSF10 showed specificity for late-stage OSCC. These markers are integral to metastatic pathways and correlate with chemotherapeutic sensitivity, providing a foundation for precision diagnostic and prognostic protocols in veterinary oncology.

Keywords Peptidomics, Serum, MALDI-TOF mass spectrometry, LC-mass spectrometry/mass spectrometry, Canine oral melanoma

1 Introduction

Canine oral tumors account for approximately 6% of all canine cancers, with oral melanoma (OM) and oral squamous cell carcinoma (OSCC) being the most prevalent and aggressive malignancies. These are typically staged by size and metastasis, ranging from early-stage (EOM; Stages I and II) to late-stage (LOM/LOSCC; Stages III and IV) [1]. Peptidomics , the large-scale analysis of small protein fragments, has become a vital tool for biomarker discovery in human oncology. While proteomic profiles for canine oral tumor tissues and saliva are established [2, 3], serum-based peptidomic markers remain unreported. Given that blood circulation reflects systemic

Kristian M. Hargadon (ed.), *Melanoma*, Methods in Molecular Biology, vol. 3089,
https://doi.org/10.1007/978-1-0716-5619-8_28,
© The Author(s), under exclusive license to Springer Science+Business Media, LLC, part of Springer Nature 2027

disease and is easily accessible, serum serves as an ideal source for circulating biomarkers to enhance the diagnosis, prognosis, and therapeutic monitoring of canine oral malignancies. This protocol describes a high-throughput methodology to investigate serum peptidome-based biomarkers across a spectrum of conditions, including EOM, LOM, LOSCC, benign oral tumors (BN), chronic periodontitis (PD), and healthy controls (CTRL) [4]. The procedure involves rapid screening via matrix-assisted laser desorption/ionization time-of-flight mass spectrometry (MALDI-TOF MS) to generate peptide mass fingerprints (PMFs) and 3-dimensional principal component analysis (3D-PCA) plots (Fig. 1). The 3D-PCA allows for the visualization of distinct clusters, revealing the uniformity within groups and the differences between malignant and nonmalignant states (Fig. 2). Following the identification of significantly different peaks by ClinProTools software (Fig. 3), unique peptide sequences are analyzed and verified using liquid chromatography-tandem mass spectrometry (LC-MS/MS). For instance, peaks at m/z 1574.10, 1892.10, 2158.09, and 2182.14 Da can be sequenced to identify key proteins such as FKBP4, ESRRA, IGSF10, and ABCB5 (Fig. 4). This workflow further integrates bioinformatic tools, such as UniProtKB and STITCH, to map candidate proteins to critical oncogenic pathways—including PI3K-Akt and VEGF signaling pathways—and to evaluate their relationships with common chemotherapy drugs like doxorubicin and cisplatin [4]. This comprehensive approach provides a robust framework for discovering circulating targets in precision veterinary oncology.

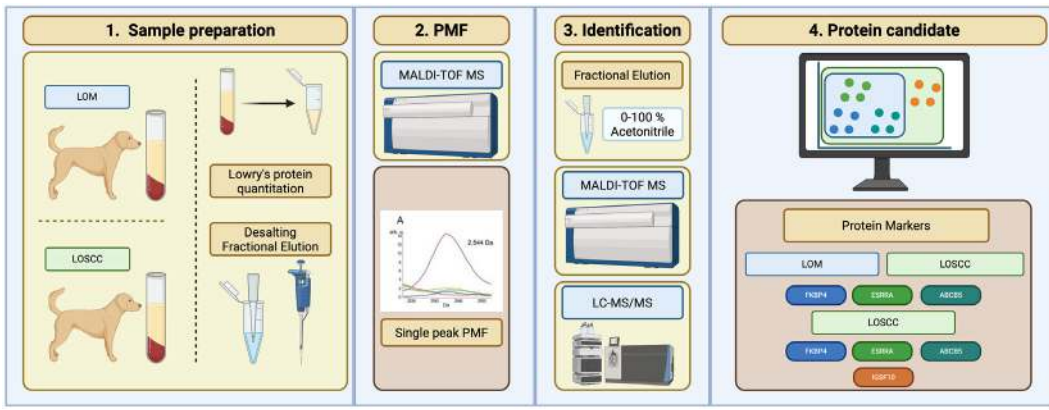


Fig. 1 Graphical overview of MALDI-TOF and LC-MS/MS protocol for profiling serum peptidomic profile used in biomarker discovery in canine oral melanoma (LOM) and squamous cell carcinoma (LOSCC). (Create by BioRender.com/Mahidol University)

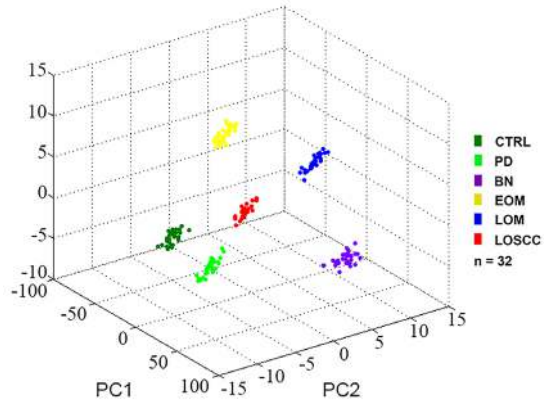


Fig. 2 Principal Component Analysis (PCA) 3D scatterplot demonstrating the differential clustering of healthy subjects (CTRL), inflammatory conditions (PD), and oral pathologies, including benign neoplasms (BN), early-stage oral melanoma (EOM), late-stage oral melanoma (LOM), and late-stage oral squamous cell carcinoma (LOSCC)

2 Materials

Prepare all solutions using HPLC-grade acetonitrile (ACN) and double-distilled deionized water unless otherwise specified.

2.1 Serum Processing and Protein Quantitation

1. Hardware and Plasticware: 4-mL serum clot activator tubes, 96-well flat-bottom plates (lidded), a microplate shaker, and an RT-2100C microplate reader.
2. Buffer: Sterile normal saline (0.9% NSS)
3. Inhibitors: Halt protease inhibitor cocktail (refrigerate at 4°C).
4. Copper-tartrate-carbonate (CTC) reagent: 0.1% $CuSO_4 \cdot 5H_2O$, 0.2% tartaric acid, 10% Na_2CO_3. Dissolve 0.2 g $CuSO_4 \cdot 5H_2O$ and 0.4 g tartaric acid in 100 mL of water. Dissolve 20 g Na_2CO_3 in 100 mL of water. Combine equal volumes (5 mL each) of these two solutions, vortex thoroughly, and maintain at 25°C.
5. Lowry assay Reagent A (Working mix): Mix 10 mL of the CTC reagent with 10 mL of 0.8 N NaOH and 20 mL of 5% sodium dodecyl sulfate (SDS) (*see* **Note 1**).
6. Lowry assay Reagent B (Folin working solution): Dilute Folin reagent with water at a 1:6 ratio (e.g., 1 mL Folin to 5 mL water). Keep at 25°C.
7. 10 mg/mL Bovine serum albumin (BSA) standard: Prepare a 10 mg/mL BSA stock in water for generating standard curves. Store at −20°C (*see* **Note 2**).

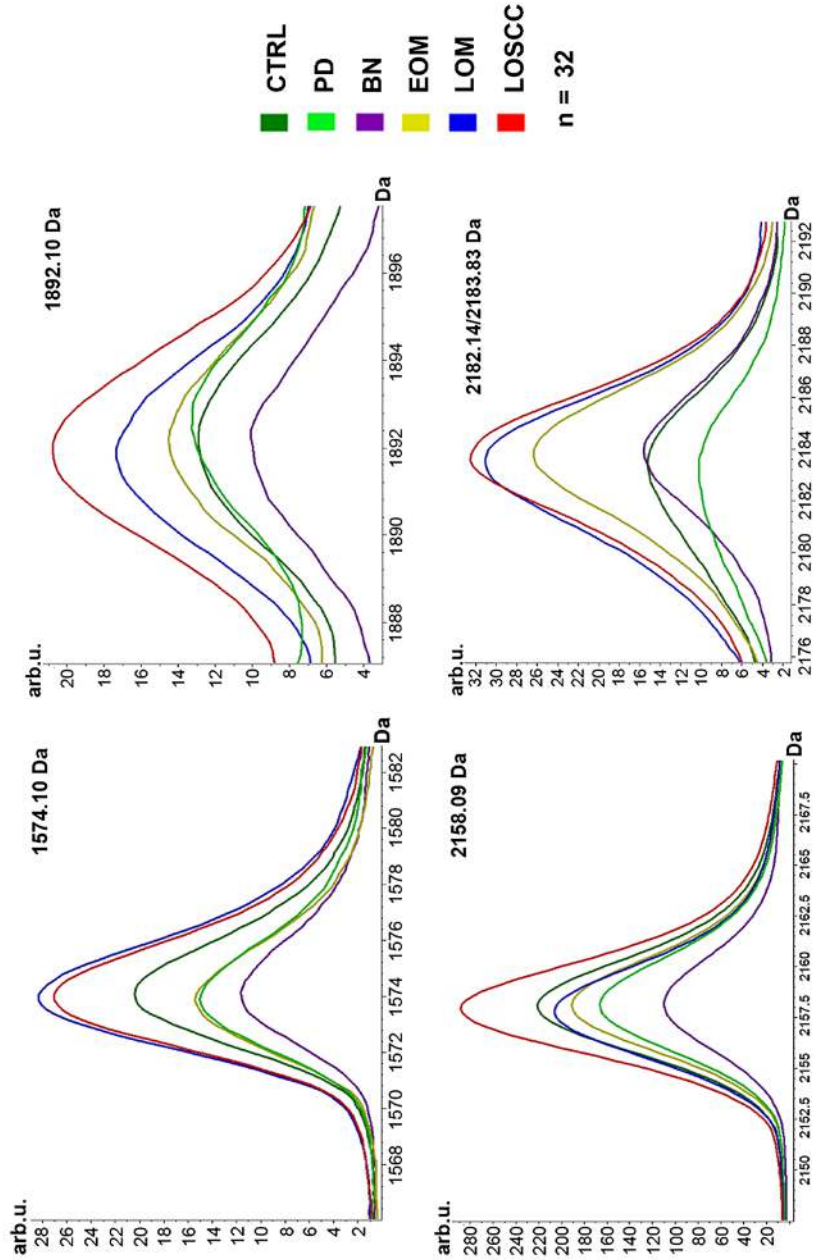


Fig. 3 Comparative analysis of significantly upregulated peptide signatures across canine oral malignancy cohorts. Data highlight the proteomic divergence between healthy/inflammatory controls (CTRL, PD) and neoplastic progressions, specifically benign tumors (BN), staged oral melanoma (EOM, LOM), and advanced oral squamous cell carcinoma (LOSCC)

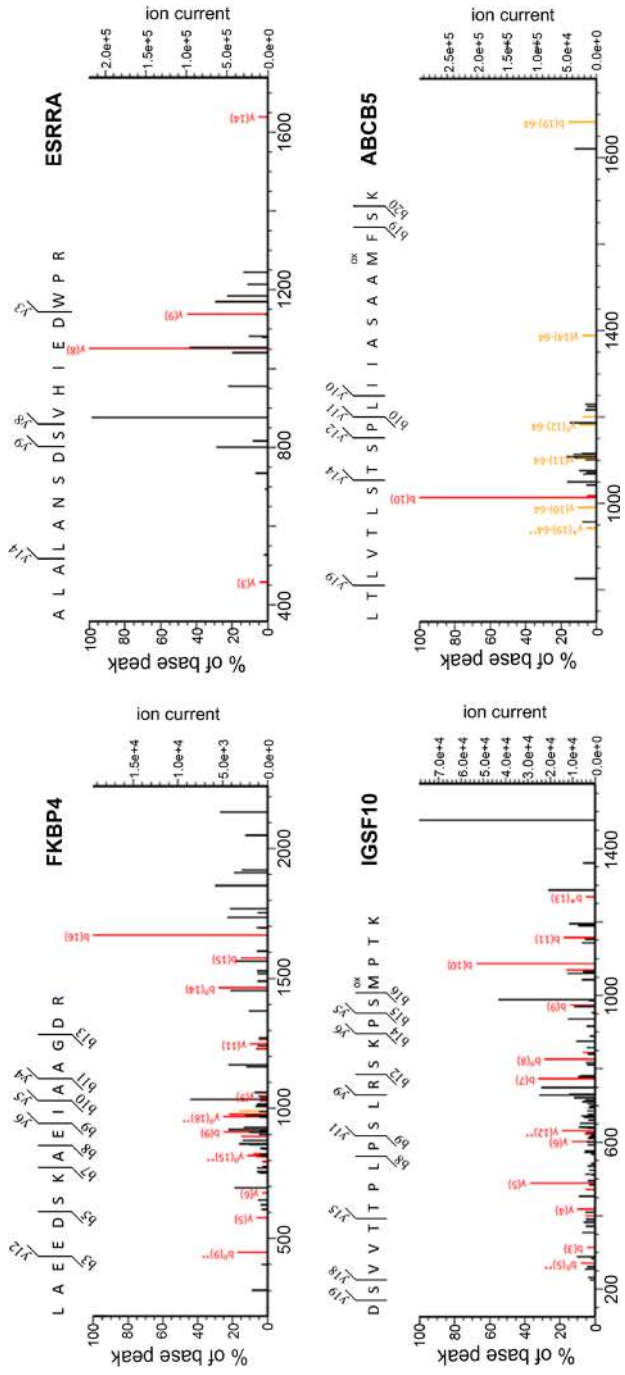


Fig. 4 Characterization of four candidate peptide peaks via high-resolution LC-MS/MS. Identified proteins include peptidyl-prolyl cis-trans isomerase FKBP4 (isoform X2), steroid hormone receptor ERR1 (ESRRA), immunoglobulin superfamily member 10 (IGSF10), and ATP-binding cassette subfamily B member 5 (ABCB5)

8. 0.1% (v/v) Trifluoroacetic acid (TFA) solution in ACN: Prepare by adding 10 μL of TFA to 10 mL of ACN. Keep at 25°C.

2.2 First and second MALDI-TOF MS

1. Instrumentation: Ultraflex III TOF/TOF MS (Bruker Daltonics) utilizing MTP384 target plates.
2. Software: Data acquisition and analysis via flexAnalysis 3.2 software and ClinProTools v.3.0 software (Bruker Daltonics).
3. CHCA matrix solution: Dissolve 10 mg of α-cyano-4-hydroxycinnamic acid in 1 mL of 5% (v/v) TFA in ACN. Keep at 25°C.
4. 5% TFA/ACN solution: Combine 50 μL of 100% TFA with 950 μL of ACN. Store at 25°C.
5. Calibration standard: Mix 1:1 of matrix solution and ProteoMass Peptide/Protein MALDI-MS Calibration Standard (*see* **Note 3**). Store at −20°C.

2.3 Desalting and Fractional Elution by ZipTip$_{C18}$ Pipette Tips

1. C_{18} micro-adsorption: ZipTip$_{C18}$ pipette tip containing reversed-phase media.
2. Wetting and equilibration: Pure ACN is used for wetting. For equilibration and washing, use 0.1% (v/v) TFA solution (1 μL TFA with 1000 μL water). Keep at 25°C.
3. Elution gradient series: Prepare 51 different ACN dilutions ranging from 0% to 100% in 0.1% TFA, spaced at equal intervals (*see* **Note 4**). Keep at 25°C.
4. High-concentration TFA: 5% (v/v) TFA in ACN. Keep at 25°C.

2.4 LC-MS/MS

2.4.1 Hardware and Columns

1. Sample containment: 2-mL HPLC autosampler vials equipped with 250-μL glass micro-inserts.
2. Sample concentration: A Speed-Vac centrifugal concentrator for solvent evaporation.
3. LC-MS system: A hyphenated system consisting of an Ultimate 3000 LC (Thermo Fisher Scientific) coupled with an HCT Ultra PTM Discovery System (Bruker Daltonics) for reversed-phase chromatography.
4. Analytical column: A PepSwift monolithic nanocolumn (dimensions: 100 μm diameter × 50 mm length) designed for nano-flow separations.

2.4.2 Bioinformatics and Data Processing

1. Data conversion: CompassXport (Bruker Daltonics) for handling mass spectrometry data files.
2. Differential analysis: DeCyder MS software (Amersham Biosciences) for MS/MS ions search.
3. Protein identification: Mascot search engine (Matrix Science).

4. Network Analysis: STITCH software (version 5.0) for analyzing protein–protein and protein–chemical interactions.

2.4.3 Mobile Phase Preparation

1. Eluent A: 0.1% formic acid (FA) in water. Prepare by adding 1 mL of formic acid (FA) to 1000 mL of HPLC-grade water. Maintain at 4°C for stability.
2. Eluent B: 0.1% FA in 50% ACN. Combine 500 mL of ACN with 500 mL of HPLC-grade water, then acidify with 1 mL of FA. Maintain at 4°C.

3 Methods

Precision and meticulous manual technique are paramount throughout the following proteomic workflows to ensure reproducibility and data integrity.

3.1 Serum Isolation

1. To collect serum, draw whole blood using a 22-gauge, 1-inch needle, and centrifuge the samples at 3000 × *g* for 15 min at 4°C.
2. To inhibit proteolysis, immediately separate the serum from the pellet, and stabilize the serum by adding a Halt protease inhibitor cocktail at a 1:100 ratio (1 µL of inhibitor per 100 µL of serum). Store stabilized aliquots at −20°C.

3.2 Protein Quantification by Modified Lowry Assay [5]

1. Dispense 2 µL of each sample into a 96-well flat-bottom plate.
2. Add 200 µL of Lowry assay Reagent A to each well.
3. Following a 30-min incubation, add 50 µL of Lowry assay Reagent B (*see* **Note 5**), and incubate for an additional 30 min.
4. Agitate the lidded plate at 180 rpm using a microplate shaker.
5. Quantify absorbance at 690 nm. Establish a standard calibration curve using BSA 2–10 µg/µL, plating 5 µL of each standard in quadruplicate (*see* **Note 2**).
6. Dilute samples to a final working concentration of 0.1 µg/µL using 0.1% TFA.
7. Store at −20°C for subsequent proteomic analysis.

3.3 First MALDI-TOF MS Analysis and Statistical Filtering

1. For matrix integration, agitate the CHCA matrix via vortex for 30 s, and combine the standardized sample (0.1 µg/µL) with the MALDI matrix at a 1:1 ratio by mixing 5 µL of the matrix supernatant with 5 µL of the analyte in a 0.6 mL tube, followed by a 30-s vortex.
2. Apply 2 µL of the mixture onto an MTP384 target plate in eight replicates to minimize technical bias.

3. Fortify each spot with 2 μL of an external calibration standard (*see* **Note 6**).
4. Analyze via Ultraflex III TOF/TOF MS in linear positive mode (mass range: 1000–5000 Da).
5. Process peptide mass spectra using flexAnalysis 3.3.
6. Execute peak analysis (1000–5000 Da) using ClinProTools v.3.0 algorithms, including Quick Classifier (QC), Different Average, Supervised Neural Network (SNN), Anderson-Darling (AD), t-test/ANOVA (TTA), Wilcoxon/Kruskal-Wallis (W/KW), and the Genetic Algorithm (GA).
7. For quality control, utilize Principal Component Analysis (PCA) to assess group homogeneity and sample uniformity.
8. Select the four most consistent replicates per sample for pooling, and subject these pooled samples to a secondary round of MALDI-TOF MS (32 replicates) to confirm consistency.
9. Identify unique peptide mass fingerprints (PMF) using the aforementioned algorithms to prioritize targets for purification using statistical algorithms of ClinProTools v.3.0 software, as mentioned in Step 6.

3.4 Peptide Enrichment via ZipTip$_{C18}$ Chromatography

1. Prime the ZipTip$_{C18}$ tips (fitted to a 200 μL pipette) with 100 μL of ACN. Repeat twice (Fig. 5) (*see* **Note 7**).
2. For equilibration, wash the tips twice with 100 μL of 0.1% TFA solution (*see* **Note 7**).
3. Aspirate and dispense 100 μL of the standardized sample four times to ensure maximum peptide adsorption to the resin in the ZipTip$_{C18}$ tip (*see* **Note 7**).
4. For fractional elution, perform a stepwise elution using an ACN gradient in 0.1% TFA. Collect 50 μL fractions (five cycles

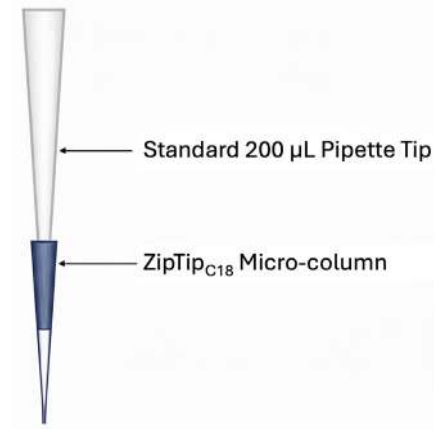


Fig. 5 Configuration of the ZipTip$_{C18}$ micro-column assembly

Table 1
Preparation of BSA standards

BSA (mg/mL)	BSA 10 mg/mL (µL)	Water (µL)
2	20	80
4	40	60
6	60	40
8	80	20
10	100	0

of 10 µL) for each concentration, starting from 0% ACN and progressing from 2% to 100% ACN (*see* **Note 7**).

5. To concentrate the samples, dry 20 µL aliquots of each fraction using a Speed-Vac, and reconstitute in 20 µL of 5% TFA.
6. Clean ZipTipC_{18} pipette tip with 100 µL of ACN.

3.5 Second MALDI-TOF MS and LC-MS/MS Identification

1. To refine the analysis, analyze the ZipTip fractions via MALDI-TOF (as described in Sect. 3.3) to determine the ACN percentage yielding the highest peak intensity for the peptides of interest.
2. In preparation for LC-MS/MS, dry 30 µL of the optimal ACN fraction via Speed-Vac. Resuspend in 30 µL of 0.1% FA, vortex for 30 s, and centrifuge at 10,000 rpm for 10 min. Transfer to HPLC vials with glass inserts (*see* **Note 8**).
3. For nanoflow separation, inject 5 µL (in triplicate) into the Ultimate 3000 LC system [6].
4. Resolve peptides on a PepSwift monolithic nanocolumn at a flow rate of 300 nL/min, using a linear gradient of 10%–70% Eluent B. Initiate the mobile phase at 10% Eluent B (90% Eluent A). Increase linearly to 70% Eluent B over 13 min. Perform a high-organic wash at 90% Eluent B between minutes 13 and 15, followed by a re-equilibration phase at 10% Eluent B from 15 to 20 min.
5. For mass spectrometry, perform electrospray ionization (positive mode) using a quadrupole ion trap (HCT Ultra PTM). Acquire fragments in data-dependent AutoMS mode (m/z 400–1500).
6. For protein identification and mapping, convert spectra to.mzXML via CompassXport.
7. Quantify signals using DeCyder MS, and identify proteins through Mascot searches against the NCBI mammalian database ($p < 0.05$) with the following criteria [7]: Taxonomy: Mammalian database; Proteolytic enzyme: trypsin;

Table 2
0%–100% ACN dilutions in 0.1% TFA solution

ACN (%)	100% ACN (μL)	0.1% TFA (μL)
0	0	150
2	3	147
4	6	144
6	9	141
8	12	138
10	15	135
12	18	132
14	21	129
16	24	126
18	27	123
20	30	120
22	33	117
24	36	114
26	39	111
28	42	108
30	45	105
32	48	102
34	51	99
36	54	96
38	57	93
40	60	90
42	63	87
44	66	84
46	69	81
48	72	78
50	75	75
52	78	72
54	81	69
56	84	66
58	87	63
60	90	60
62	93	57
64	96	54

Table 2 (continued)

ACN (%)	100% ACN (μL)	0.1% TFA (μL)
66	99	51
68	102	48
70	105	45
72	108	42
74	111	39
76	114	36
78	117	33
80	120	30
82	123	27
84	126	24
86	129	21
88	132	18
90	135	15
92	138	12
94	141	9
96	144	6
98	147	3
100	150	0

Modifications: Methionine oxidation and carbamidomethylation (variable); Mass type: Monoisotopic, unrestricted protein mass.; Tolerances: Peptide mass tolerance of 1.2 Da, MS/MS fragment tolerance of 0.6 Da; Ionization: Charge states assigned as 1+, 2+, and 3+; Cleavage: A maximum of three missed cleavage sites permitted.

8. Manually annotate particular protein information using the UniProtKB/Swiss-Prot entries (https://www.uniprot.org/).
9. Annotate identified proteins using UniProtKB/Swiss-Prot and evaluate drug–protein interactions via the STITCH 5.0 database (http://stitch.embl.de/).

4 Notes

1. Ensure the Lowry working solution (Lowry mix) is prepared immediately before each experimental session to ensure reagent stability and maintain assay sensitivity.

2. For standard curve preparation, construct a series of aqueous BSA standards at concentrations of 2, 4, 6, 8, and 10 mg/mL, following the proportions detailed in Table 1.
3. The ProteoMass MALDI-MS Calibration Kit includes the following mixture of peptides and proteins for use as calibration standards: human angiotensin II (m/z 1046), P14R (m/z 1533), human adrenocorticotropic hormone fragment 18–39 (m/z 2465), bovine insulin oxidized B chain (m/z 3465), bovine insulin (m/z 5731), and cytochrome c (m/z 12362).
4. Formulate the ACN and 0.1% TFA mixtures according to the volumetric specifications provided in Table 2.
5. Pipetting precision is particularly important at this step. Lowry assay Reagents A and B should be dispensed with care to prevent the formation of air bubbles, which can cause significant interference during spectrophotometric absorbance measurements.
6. For the purposes of internal standardization, apply 2 μL of the external calibration mixture precisely to the center of the pre-spotted analyte for each of the eight replicates.
7. Ziptip Maneuvering: Aspirate the required volume using a standard 200 μL tip, then securely attach the ZipTipC_{18} to create a tandem tip assembly for dispensing. Maintain constant pressure to prevent air from entering the C_{18} resin.
8. Sample loading: Utilize a mini centrifuge to pulse-spin the glass inserts. This eliminates air bubbles and ensures the sample is at the base. Maintain a sterile environment and wear gloves throughout this stage.

Acknowledgments

The author acknowledges financial support from Mahidol University (S.P.).

Competing Interests The authors have no conflicts of interest to declare that are relevant to the content of this chapter.

References

1. Liptak JM, Withrow SJ (2007) Cancer of the gastrointestinal tract: oral tumors. In: Withrow SJ, Vail DM, editors. Withrow and MacEwen's Small Animal Clinical Oncology, 4th ed. St. Louis: Saunders Elsevier, pp 455–475
2. Pisamai S, Roytrakul S, Phaonakrop N et al (2018) Proteomic analysis of canine oral tumor tissues using MALDI-TOF mass spectrometry and in-gel digestion coupled with mass spectrometry (GeLC MS/MS) approaches. PLoS One 13(7):e0200619
3. Ploypetch S, Roytrakul S, Jaresitthikunchai J et al (2019) Salivary proteomics of canine oral tumors using MALDI-TOF mass spectrometry

and LC-tandem mass spectrometry. PLoS One 14(7):e0219390
4. Ploypetch S, Jaresitthikunchai J, Phaonakrop N et al (2022) Utilizing MALDI-TOF MS and LC-MS/MS to access serum peptidome-based biomarkers in canine oral tumors. Sci Rep 12(1):21641
5. Waterborg JH (2009) The lowry method for protein quantitation. In: Walker JM (ed) The protein protocols handbook. Springer protocols handbooks. Humana Press, Totowa, NJ
6. Szklarczyk D, Santos A, Von Mering C et al (2016) STITCH 5: augmenting protein–chemical interaction networks with tissue and affinity data. Nucleic Acids Res 44(D1):D 380–D384
7. Johansson C, Samskog J, Sundström L et al (2006) Differential expression analysis of *Escherichia coli* proteins using a novel software for relative quantitation of LC-MS/MS data. Proteomics 6(16):4475–4485



Chapter 29

Discovery of Salivary Metabolomic Biomarkers for Canine Oral Melanoma and Squamous Cell Carcinoma via CIL LC-MS Analysis

Sekkarin Ploypetch, Xian Luo, Shuang Zhao, Gunnaporn Suriyaphol and Liang Li

Abstract

In this case-control cross-sectional study, we examined the diagnostic potential of salivary metabolomics to differentiate canine oral melanoma (OM) and oral squamous cell carcinoma (OSCC) from benign oral tumors (BN). Using high-performance chemical isotope labeling liquid chromatography-mass spectrometry (CIL LC-MS) targeting at the amine/phenol submetabolome, we analyzed saliva from 65 dogs across malignant, benign, and healthy groups. Our results revealed distinct metabolic clustering among the groups, identifying 154 significantly altered metabolites in OM and 66 in OSCC compared to BN ($P_{adj} < 0.05$). Notable biomarkers included elevated tryptophyl-threonine and decreased 1,2-dihydroxynaphthalene-6-sulfonic acid in OM, while OSCC was characterized by reduced seryl-arginine and sarcosine. These findings, and the protocol described herein that was used to obtain them, demonstrate the broad coverage of the salivary submetabolome and emphasize the potential of noninvasive metabolic profiling as a practical, high-throughput approach for accurate diagnosis of canine oral cancers in clinical settings.

Keywords Metabolomics, Saliva, Chemical isotope labeling, LC-mass spectrometry/mass spectrometry, Canine oral melanoma

1 Introduction

In veterinary oncology, oral malignancies account for about 6% of all canine neoplastic cases, with oral melanoma (OM) and oral squamous cell carcinoma (OSCC) being the most common and clinically challenging subtypes [1]. These tumors are often only detected once they reach advanced stages, making diagnosis more difficult. Although histopathological examination of biopsy tissue remains the gold standard, performing these invasive procedures requires general anesthesia, which poses significant physiological risks, especially for older dogs [1]. Salivary metabolomics, the comprehensive

Kristian M. Hargadon (ed.), *Melanoma*, Methods in Molecular Biology, vol. 3089,
https://doi.org/10.1007/978-1-0716-5619-8_29,
© The Author(s), under exclusive license to Springer Science+Business Media, LLC, part of Springer Nature 2027

analysis of small molecules in saliva, offers a promising noninvasive alternative because saliva directly contacts oral tumors and is easy to collect. While previous studies have characterized metabolomic profiles for various human cancers, the salivary metabolome of canine oral tumors remains largely unexplored. This protocol describes a high-performance chemical isotope labeling (CIL) liquid chromatography-mass spectrometry (LC-MS) method for identifying biomarkers in canine OM and OSCC. The approach focuses on the amine/phenol submetabolome, using ^{12}C-/^{13}C-dansyl chloride labeling to enhance detection sensitivity and quantification accuracy [2]. The procedure involves advanced sample normalization using liquid chromatography with ultraviolet detection (LC-UV) to account for physiological variations in saliva concentration [3]. After LC-Orbitrap analysis, light/heavy peak pairs are extracted and searched against a three-tier metabolite library [4–6]. Multivariate analysis, such as partial least squares discriminant analysis (PLS-DA), is then performed, which clearly separates benign oral tumors (BN) and healthy controls (Fig. 1). The identification of potential biomarkers such as seryl-arginine and sarcosine for OSCC, or tryptophyl-threonine for OM, further demonstrates the high diagnostic power of this approach, with area under the curve (AUC) values over 0.9 [7]. Finally, pathway enrichment analysis of data obtained with this protocol can be performed, as we have done to demonstrate that several critical metabolic pathways, such as aminoacyl-tRNA biosynthesis and arginine metabolism, are altered in the BN group [7, 8].

2 Materials

Prepare all aqueous solutions with LC-MS-grade reagents.

2.1 Saliva Processing Supplies

1. Sampling apparatus: 6-inch sterile cotton swabs with wooden handles for noninvasive saliva collection.
2. High-speed refrigerated centrifuge.
3. 1.5-mL microcentrifuge tubes.
4. Irrigation solution: Sterile 0.9% normal saline solution (NSS).
5. High-performance liquid chromatography (HPLC)-grade methanol (for protein precipitation to remove high-molecular-weight proteins).
6. Assay Plate: 96-well flat-bottom microplates equipped with lids to prevent evaporation during incubation.
7. Agitation Equipment: a microplate shaker for consistent sample homogenization during the assay.
8. Detection Instrumentation: an RT-2100C microplate reader (BioTecNika, BE) configured for automated microtiter plate spectrophotometry.

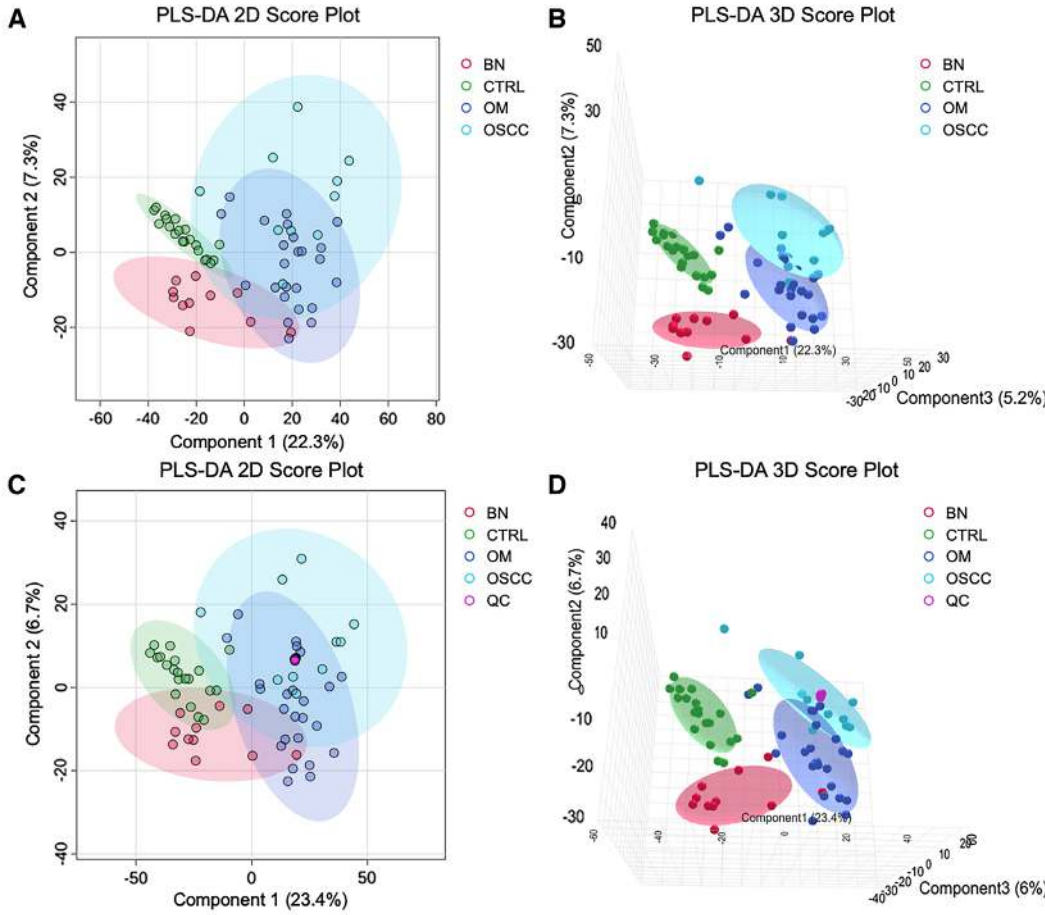


Fig. 1 Partial Least Squares-Discriminant Analysis (PLS-DA) score plots for metabolomics data. (**A**) A 2D PLS-DA score plot showing the separation of four sample groups based on Component 1 (22.3% variance) and Component 2 (7.3% variance). The groups include benign neoplasm (BN, red), control (CTRL, green), oral melanoma (OM, blue), and oral squamous cell carcinoma (OSCC, cyan). Each point represents an individual sample. (**B**) A 3D PLS-DA score plot illustrating the spatial separation of the same four groups as in (A), using the first three components. Component 1 explains 22.3% of the variance, Component 2 explains 7.3%, and Component 3 explains 5.2%. (**C**) A 2D PLS-DA score plot showing the separation of five groups, including quality control (QC, magenta), based on Component 1 (23.4% variance) and Component 2 (6.7% variance). The other four groups (BN, CTRL, OM, and OSCC) are color-coded as in (A). (**D**) A 3D PLS-DA score plot depicting the distribution of the five groups as in (C), using Component 1 (23.4% variance), Component 2 (6.7% variance), and Component 3 (6% variance) [7]

2.2 Saliva Normalization and Chemical Isotope Labeling Reagents

1. Amino acid standards (AAS18; Sigma-Aldrich, Burlington, MA, USA), serially diluted from 2 mM to 0.0625 mM (Fig. 2) (*see* **Note 1**).
2. Chemical isotope labeling kit (Catalog No. NMT-4101-KT, Nova Medical Testing Inc., Edmonton, Alberta, Canada), complete with the following reagents:

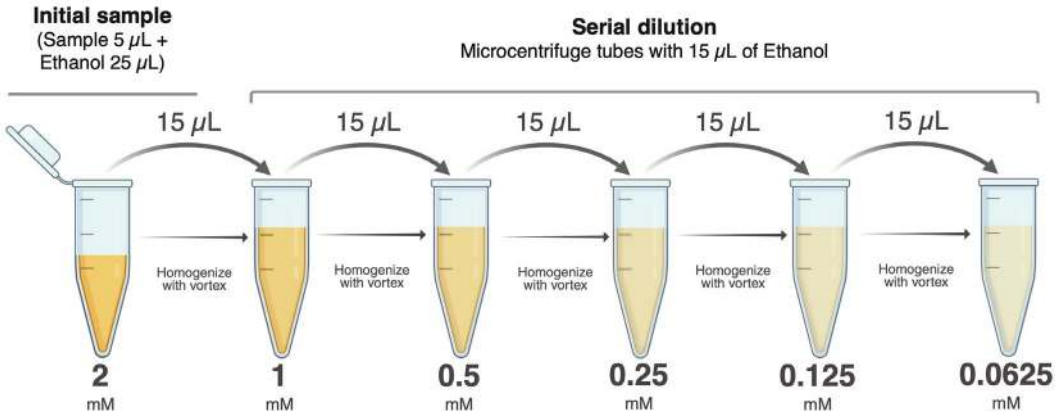


Fig. 2 Schematic workflow of the serial dilution process for amino acid standards. The initial standard solution (2 mM) was prepared by mixing 5 μL of the amino acid sample with 25 μL of ethanol. A twofold serial dilution series was then performed using microcentrifuge tubes, each prefilled with 15 μL of ethanol as the diluent. At each step, 15 μL of the solution was transferred to the next tube and mixed using a vortex mixer to ensure uniform concentration. This process produced a calibration range of six concentration points: 2, 1, 0.5, 0.25, 0.125, and 0.0625 mM

a. Labeling reagents: ^{12}C-dansyl chloride (^{12}C-DnsCl) for labeling individual specimens and ^{13}C-dansyl chloride (^{13}C-DnsCl) for pooled sample labeling, which serves as an internal standard (*see* **Note 2**).
b. Reaction buffer: Na_2CO_3/$NaHCO_3$ solution (to adjust the labeling pH).
c. 250 mM NaOH.
d. 425 mM formic acid (FA).

3. Universal retention time (RT) calibrant (Catalog No. NMT-2134-L, Nova Medical Testing Inc., Edmonton, Alberta, Canada).

2.3 Instrumentation and Supplies for Sample Processing and Analysis

1. 1220 Infinity II HPLC system (Agilent, Santa Clara, CA, USA) equipped with a Variable Wavelength Detector (VWD) for measuring total metabolite concentration.
2. Vanquish Ultra-High Performance Liquid Chromatography (UHPLC) system coupled with a Q Exactive Orbitrap mass spectrometer (Thermo Fisher Scientific, Waltham, MA, USA).
3. Mobile Phase A solvent: 0.1% (v/v) formic acid in water.
4. Mobile Phase B solvent: 0.1% (v/v) formic acid in acetonitrile (ACN).
5. Agilent ZORBAX Eclipse Plus C18 narrow bore guard analytical column (2.1 mm × 12.5 mm, 5 μm particle size).

6. Agilent ZORBAX reversed phase Eclipse Plus C18 column (2.1 mm × 10 cm, 1.8 μm particle size, 95 Å pore size).
7. MS Convert 3.0 (ProteoWizard, Palo Alto, CA, USA).
8. IsoMS Pro 1.2.20 (Novo Medical Testing Inc., Edmonton, AB, Canada).

3 Methods

Maintaining strict precision and meticulous manual protocols is essential throughout subsequent metabolomic procedures to ensure analytical consistency and the integrity of the metabolic data.

3.1 Saliva Collection and Processing

1. On the day of surgery, ensure that dogs are fasted for at least 6–8 h before sampling.
2. Rinse the mouth with sterile 0.9% NSS irrigation solution, taking care to avoid any mechanical or chemical stimulation.
3. Collect saliva using sterilized cotton swabs for 5–10 min to obtain 0.5–1.0 mL of saliva.
4. Centrifuge samples at 2600 × *g* for 15 min at 4°C to remove cellular debris.
5. Precipitate proteins overnight using a fivefold volume of HPLC-grade methanol at −20°C.
6. Centrifuge at 3000 × *g* for 30 min at 4°C and then aliquot and store supernatants at −80°C.
7. When ready to perform CIL and normalization, combine 25 μL of saliva with 12.5 μL of Na_2CO_3/$NaHCO_3$ reaction buffer solution, and then add 37.5 μL of ^{12}C-DnsCl for individual samples or ^{13}C-DnsCl for the reference or pooled sample.
8. Vortex briefly, and incubate the reaction at 40°C for 45 min.
9. Quench the reaction by adding 7.5 μL of 250 mM NaOH and incubating at 40°C for 10 min.
10. Acidify the solution using 30 μL of 425 mM FA.
11. Aliquot the supernatants, and store aliquots at −80°C until ready for metabolomic analysis.

3.2 Sample Normalization and LC-MS Analysis

1. Equilibrate an appropriate column with 100% mobile phase A before injection. Gradient: $t=0$, 100% B; $t=0.5$, 100% B; $t=1$, 100% A; $t=2.5$, 100% A.
2. Normalize samples via LC-UV using the following parameters:
   a. Injection volume: 2 μL.
   b. Flow rate: 0.65 mL/min.
   c. Detector wavelength: 338 nm.

3. Mix ^{12}C-labeled individual samples with the ^{13}C-labeled pool in equal molar amounts based on the LC-UV normalization results.
4. Generate quality control (QC) samples by mixing equal volumes of the ^{12}C-labeled and ^{13}C-labeled pools.
5. Collect samples using the following parameters:
   a. Injection volume: 7 µL
   b. LC gradient: $t = 0$ min at 25% mobile phase B; $t = 10$–13 min at 99% B; returning to 25% B at $t = 13.1$ min through 16 min.
   c. Flow rate: 400 µL/min.
   d. Column temperature: 40°C.
   e. Polarity: positive.
   f. Spray voltage of 3.6 kV; an ion transfer capillary temperature of 300°C.
   g. Scan range: 220–1000 Da (*see* **Note 3**).
   h. Resolution: 70,000.
   i. Microscan: 3.
   j. Ion injection time: 250 ms.
6. For quality assurance, randomize sample injection order, and inject QC samples after every ten injections. Inject the universal RT calibrant after every ten samples to track retention time shifts.

3.3 Data Processing and Quality Control

1. To export data, convert raw LC-MS data files (comprising 24 OM, 10 OSCC, 11 BN, 20 CTRL, 4 blanks, and 8 QC files) were initially converted to .txt format using MS Convert 3.0. For the data described herein, we performed this conversion for 24 OM, 10 OSCC, 11 BN, 20 CTRL, 4 blanks, and 8 QC files.
2. Convert the .txt files into .csv format using IsoMS Pro 1.2.20.
3. To maintain analytical integrity, track instrument performance using two main metrics:
   a. Mass accuracy: Confirm through consistent observation of background ions (Dns-ammonia) at a specific m/z of 251.0849, ensuring that distributions remain within the established reference range.
   b. LC stability: Monitor the LC system's performance and retention time consistency by injecting an RT Calibrant every ten samples, ensuring that drift stays within established reference ranges.
4. For peak pair extraction, pick ^{12}C/^{13}C peak pairs from the data using IsoMS Pro 1.2.20 according to the following parameters:

a. Retention time range: 50– 800 s.
b. Mass range: m/z 240–1000.
c. Intensity threshold: Minimum input intensity threshold of 1000.

5. For data alignment, align multiple LC-MS data files based on mass and retention time, using a tolerance of 9 s for retention time and 10 ppm for mass.
6. Impute the missing values using the Zerofilling function in IsoMS Pro.
7. To ensure high data quality, the dataset should be filtered using the following strict criteria:

a. Feature filtering: Keep features only if they appeared in at least 80% of samples within at least one experimental group.
b. Noise removal: Exclude peak pairs if their intensities in the samples were less than four times those in the blank samples.

3.4 Metabolite Identification

1. Perform a 3-Tier Library Search using the CIL library, Linked Identity (LI) library, and My Compound ID (MCID) library.
   a. Tier 1: Search peak pairs against the CIL Library (>1500 standards) based on both accurate mass and retention time (CIL library: retention time: 10 s, m/z: 10 ppm).
   b. Tier 2: Search remaining pairs against the LI Library (>9000 metabolites) based on accurate mass and predicted retention time (LI library: retention time window: 75 s, m/z: 10 ppm).
   c. Tier 3 (*see* **Note 4**): Search remaining pairs against the MCID library (8000 endogenous metabolites in 0-reaction library) and its predicted metabolite library (1-reaction and 2-reaction library) [MCID library: m/z window: 10 ppm].

3.5 Statistical Analysis, Pathway Analysis, and Biomarker Discovery

1. For univariate analysis (volcano plots), generate volcano plots to visually represent significantly altered metabolites based on fold change ($\log_2$) and negative $\log_{10}$-transformed p-values. As recommended thresholds, define a metabolite as significantly changed only if it meets all of the following criteria: p-value < 0.05; false discovery rate (FDR)-adjusted p-value (p_{adj}) < 0.05; fold change is greater than 1.5 or less than 0.67.
2. For multivariate analysis, construct two-dimensional principal component analysis (PCA) and PLS-DA score plots (Fig. 1) to provide a comprehensive visualization of the metabolic data.
3. For Pathway Enrichment Analysis, upload Tier 1 and Tier 2 metabolites, as identified in the oral cancer (OM or OSCC) vs.

benign (BN) cohorts in the example analysis presented herein, into the Metaboanalyst (https://www.metaboanalyst.ca/). Select Canis lupus familiaris (dog) (KEGG) as the pathway library for analysis and identify significantly altered pathways based on *p*-values and impact value.

4. For biomarker discovery, perform statistical modeling by executing Linear Support Vector Machine (SVM) and Receiver Operating Characteristic (ROC) analyses via MetaboAnalyst 5.0 [8] to evaluate the diagnostic power of individual or panels of metabolic biomarkers. To assess performance metrics, utilize the Area Under the Curve (AUC) and cross-validation prediction accuracy to evaluate the sensitivity and specificity of potential biomarkers. AUCs of 0.8–0.9 are excellent, and those exceeding 0.9 are outstanding diagnostic markers. Identify candidate metabolic biomarkers based on significantly changed metabolites unique to each group (via Venn diagram), prioritizing those with an AUC > 0.9 and $p < 0.05$.

4 Notes

1. AAS18 normalization: Because the metabolite concentration in saliva is highly related to dogs' hydration status, it is critical to normalize the saliva sample before LC-MS analysis.
2. To create a reference for quantification, we recommend generating a pooled sample by combining aliquots from each individual sample.
3. Mass shift correction: Since the dansyl tag introduces a mass shift of approximately 220 Da, the m/z range is specifically set to 220–1000 Da to ensure that metabolites with a native m/z below 220 are reliably detected.
4. Although the Tier 3 database includes millions of compounds generated from predicted metabolic reactions, these predicted metabolites were not used for pathway analysis in order to prioritize metabolites with higher biological confidence.

Acknowledgments

This research was supported by the TRF Research Career Development Grant (RSA5980053), alongside the 90th and 100th Anniversary of Chulalongkorn University Scholarships. Additional funding was provided by an Overseas Research Experience Scholarship for Graduate Students, as well as by the Natural Sciences and

Engineering Research Council of Canada, the Canada Foundation for Innovation, and Genome Canada.

Competing Interests The authors have no conflicts of interest to declare that are relevant to the content of this chapter.

References

1. Liptak JM, Withrow SJ (2007) Cancer of the gastrointestinal tract: oral tumors. In: Withrow SJ, Vail DM, editors. Withrow and MacEwen's Small Animal Clinical Oncology, 4th ed. St. Louis: Saunders Elsevier, pp 455–475
2. Guo K, Li L (2009) Differential 12C-/13C-isotope dansylation labeling and fast liquid chromatography/mass spectrometry for absolute and relative quantification of the metabolome. Anal Chem 81(10):3919–3932. https://doi.org/10.1021/ac900166a
3. Wu Y, Li L (2012) Determination of total concentration of chemically labeled metabolites as a means of metabolome sample normalization and sample loading optimization in mass spectrometry-based metabolomics. Anal Chem 84(24):10723–10731. https://doi.org/10.1021/ac3025625
4. Li L, Li R, Zhou J et al (2013) MyCompoundID: using an evidence-based metabolome library for metabolite identification. Anal Chem 85(6):3401–3408. https://doi.org/10.1021/ac400099b
5. Huan T, Wu Y, Tang C et al (2015) DnsID in MyCompoundID for rapid identification of dansylated amine- and phenol-containing metabolites in LC–MS-based metabolomics. Anal Chem 87(19):9838–9845. https://doi.org/10.1021/acs.analchem.5b02282
6. Huan T, Tang C, Li R et al (2015) MyCompoundID MS/MS Search: metabolite identification using a library of predicted fragment-ion-spectra of 383,830 possible human metabolites. Anal Chem 87(20):10619–10626. https://doi.org/10.1021/acs.analchem.5b03126
7. Ploypetch S, Luo X, Zhao S et al (2024) Salivary metabolomic identification of biomarker candidates for oral melanoma and oral squamous cell carcinoma in dogs. J Vet Intern Med. 38(4):2293-2304. https://doi.org/10.1111/jvim.17092
8. Pang Z, Zhou G, Ewald J et al (2022) Using MetaboAnalyst 5.0 for LC–HRMS spectra processing, multi-omics integration and covariate adjustment of global metabolomics data. Nat Protoc 17(8):1735–1761. https://doi.org/10.1038/s41596-022-00710-w



Chapter 30

Spatial Lipidomic Analysis Using Secondary Ion Mass Spectrometry (SIMS)

Simon Uzoni, John S. Fletcher and Noora Neittaanmäki

Abstract

Secondary ion mass spectrometry (SIMS) produces a mass spectral image of a sample, where each pixel in the image contains a mass spectrum from which chemical information can be extracted to provide maps of different molecules of interest. Alternatively, a chemical fingerprint of regions of interest in the image/sample can be extracted. The mass spectral image can be correlated with histological images to better understand the spatial chemistry associated with the different cell types/regions of the sample.

Keywords Secondary ion mass spectrometry (SIMS), Imaging, Lipids, Metabolites, Tissue sections, Lipidomics, Biomarkers

1 Introduction

Secondary ion mass spectrometry (SIMS) is a surface-sensitive mass spectral analysis technique that can provide detailed chemical maps of a sample. While widely used in material analysis applications for many years, SIMS has recently evolved into a powerful tool for biological analysis [1, 2]. SIMS uses an energetic (*primary*) ion beam to eject atoms and molecules from a sample surface that are detected as *secondary* ions. However, when using conventional atomic or small cluster projectile ions, the efficiency for the ejection of intact biomolecules is very low. The recent benefits for bioanalysis have been, in a large part, due to the introduction of gas cluster ion beams (GCIBs) that utilize supercooled clusters of gas atoms/or molecules that, upon impact with the sample, dissipate their energy over their many (typically several thousand) constituents, resulting in a gentler lifting of molecules from the sample surface [3]. GCIB-SIMS imaging has been demonstrated in a range of biological settings, including pre-clinical studies [4–10]. Coupled with the new ion beams, advances in sample handling (specifically cryogenic sample analysis systems) improve signal response while maintaining the

Kristian M. Hargadon (ed.), *Melanoma*, Methods in Molecular Biology, vol. 3089,
https://doi.org/10.1007/978-1-0716-5619-8_30,
© The Author(s), under exclusive license to Springer Science+Business Media, LLC, part of Springer Nature 2027

sample in a more lifelike state while exposed to the vacuum of the SIMS instrument [11–13]. In this protocol, we provide a workflow and guidance to prepare and analyze tissue samples for lipidomic research using GCIB-SIMS, together with example data obtained from an application of this approach to assess spatial lipid distribution in metastatic melanoma tissue.

2 Materials

2.1 Embedding Tissue

1. Fresh frozen tissue (*see* **Note 1**). The tissue should be frozen as soon as possible after removal to stop any biological process that will degrade the tissue.
2. Tissue-Tek® Optimum Cutting Temperature (OCT) compound.
3. Cryo-moulds.

2.2 Sectioning

1. Cryotome.
2. Argon gas (99.99% or better).
3. Tissue-Tek® OCT compound.
4. Microtome blade (C35, FEATHER Safety Razor Co., Ltd., Osaka, Japan).
5. Specimen holder.
6. Brushes.
7. Microscope slides.
8. Indium-tin-oxide (ITO)-coated microscope slides (*see* **Notes 2 and 3**).
9. Microscope slide container.
10. Dry ice.

2.3 Freeze-Dried Tissue Preparation

1. Cryotome or polystyrene box (large).
2. Argon gas (99.99% or better).
3. Dry ice.
4. Liquid nitrogen.
5. Forceps.
6. Dewar.
7. Aluminium foil.
8. Vacuum desiccator.
9. Nitrogen gas (99.99% or better, optional)

2.4 Frozen-Hydrated Tissue Preparation

1. Cryotome or polystyrene box (large with transparent lid and small).

2. Argon gas (99.99% or better).
3. Dry ice.
4. Liquid nitrogen.
5. Forceps.
6. Dewar with lid.

3 Methods

3.1 Tissue Preparation

Larger tissue pieces may be sliced without embedding, but for small specimens, embedding is typical so that the sample is easier to handle.

3.1.1 Embedding Tissue

1. Place the tissue in a cryo-mould, considering the orientation of tissue in the mold if a specific plane in the tissue is of interest.
2. Fill the mold with OCT (*see* **Note 4**), and immediately freeze.
3. Place the mold in a −80°C freezer for a few hours or overnight to ensure that the tissue is completely frozen.

3.1.2 Sectioning

SIMS probes the surface of a sample, so it is essential that tissue sections are relatively flat with the regions of interest exposed for the analysis.

1. Purge the cryotome with dry argon gas. Set the appropriate temperature for the sample holder and cutting blade, if possible, and use the appropriate microtome blade. Optimal temperature (−20°C to −25°C) and blade type can vary depending on tissue type. Cool the specimen holder on the cold block.
2. If stored, transport the tissue in a sealed container to the cryotome, keeping the sample cold with dry ice and avoiding exposure to air/moisture as much as possible.
3. Mount the tissue to the specimen holder by putting a small amount of OCT mounting medium on the holder. Lightly press and hold the tissue against the holder for a short moment for the OCT to freeze. For embedded tissues, the side of the mold with the tissue exposed should be facing away from the specimen holder.
4. Begin sectioning the tissue, and adjust the angle of the tissue block and the antiroll plate until the blade cuts the tissue evenly and the sections stay flat. Do not use any OCT on the blade (*see* **Note 5**).
5. Cut the tissue until the desired plain has been reached. Cut slowly and allow the blade to cool down between sections to avoid smearing the lipids (*see* **Note 6**).

6. Cut four consecutive sections of the tissue with 5–15 µm thickness (*see* **Notes 7–9**).
7. Mount the first and fourth sections on normal microscope slides and write the section number on slides (*see* **Note 10**).
8. Mount the second and third sections on the metal coated side of separate cold ITO-glass slides. Brushing the sections onto the conductive side of slides, heat the backside of the slide with a finger to thaw-mount the tissue sections, and quickly recool the ITO-glass slides (*see* **Note 11**).
9. Place the ITO-glass slides in individual microscope slide containers (*see* **Note 12**). Do not write on the ITO-glass slide. Instead, write information such as sample ID and section number on the microscope slide container (*see* **Note 13**).
10. Stain the consecutive tissue section mounted on an ordinary microscope slide with hematoxylin and eosin (H&E) to find the region of interest (ROI) in the tissue section.

3.1.3 Freeze-Dried Tissue Preparation

Once the tissue section is mounted to the ITO-glass slide for analysis at room temperature, the sample needs to be freeze-dried prior to insertion into the vacuum chamber of the SIMS instrument. If using a cryotome to create a cold and dry atmosphere in which to attach the ITO-glass slide with tissue to the sample holder, purge the cryotome and cool down the sample holder for the SIMS instrument on the cryobar. If a cryotome is not available or does not provide sufficient work space, purge a polystyrene box, containing a small container of dry ice, with argon, and then cool down the sample holder on the dry ice. Once cooled, transport the sealed frozen-hydrated tissue section on dry ice to the large polystyrene foam box.

1. When the sample holder is cold, mount the ITO-glass slide with the tissue on the sample holder for the SIMS instrument.
2. Put the sample holder in aluminium foil, and fold and close the foil such that it looks like a pouch, ensuring that the foil does not come in contact with the tissue (*see* **Note 14**).
3. Submerge the wrapped sample holder in a dewar with liquid nitrogen.
4. Once the boiling has stopped, quickly take the sample holder and place it in a vacuum desiccator, allowing it to slowly warm up to room temperature under vacuum for 1–3 h.
5. When the freeze-drying is complete, gently vent the vacuum desiccator with nitrogen gas, if possible, and proceed to inserting the tissue section into the SIMS instrument for analysis.

3.1.4 Frozen Hydrated Tissue Preparation

If using a SIMS instrument equipped with cryogenic sample cooling and a glove box to insert samples, the tissue section does not need

to be freeze-dried but can instead be analyzed while still containing water in a frozen hydrated state. The following steps cover when the tissue is sectioned and immediately used for analysis or the ITO-glass slide is mounted to the instrument sample holder in the cryotome.

1. Purge the cryotome with dry argon.
2. Mount the ITO-glass slide with the tissue to the sample holder for the SIMS instrument (*see* **Note 15**).
3. Plunge the sample holder with the sample into a dewar with liquid nitrogen, and place a lid on the dewar to reduce ice formation from moisture in air. Make sure that the sample holder is always covered by liquid nitrogen.
4. Once the boiling has stopped, take the dewar out of the cryotome and transport it to the SIMS instrument.

Alternatively, the following steps cover methods when using tissue sections that have either been stored or transported and a cryotome does not provide sufficient workspace or is not available close to the SIMS instrument.

1. Purge a prepared large polystyrene box containing a dewar and a smaller polystyrene box with a calm flow of dry argon, and place the sample holder in the smaller box, as shown in Fig. 1 (*see* **Note 16**).
2. Transport the sealed frozen-hydrated tissue section, cooled with dry ice, to the large polystyrene box, but wait before placing the sealed tissue section in the box.
3. Fill the smaller polystyrene box and the dewar with liquid nitrogen, and cover the larger box with a transparent lid with a small gap to let out gas (*see* **Note 17**). The dewar can also be covered with a lid.
4. When the box is completely clear of any condensed moisture, carefully slide off the lid. Open the tissue slide container in the larger box, quickly take out the ITO-glass slide with the tissue section using forceps, and mount it to the sample holder (*see* **Note 18**). Avoid quick movements that may pull moist air into the box that could condense and form ice.
5. When the ITO-glass slide is mounted to the sample holder, quickly transfer it from the smaller box to the dewar, and cover it with a lid. Now it is ready to transfer to the glove box on the SIMS instrument.

3.1.5 Frozen-Hydrated Sample Transfer to SIMS

The following steps cover inserting frozen-hydrated samples into a SIMS instrument equipped with a glove box and cryogenic sample cooling.

1. Cool down the instrument sample transfer system, sample stage, and cold trap, if available, to cryogenic temperatures

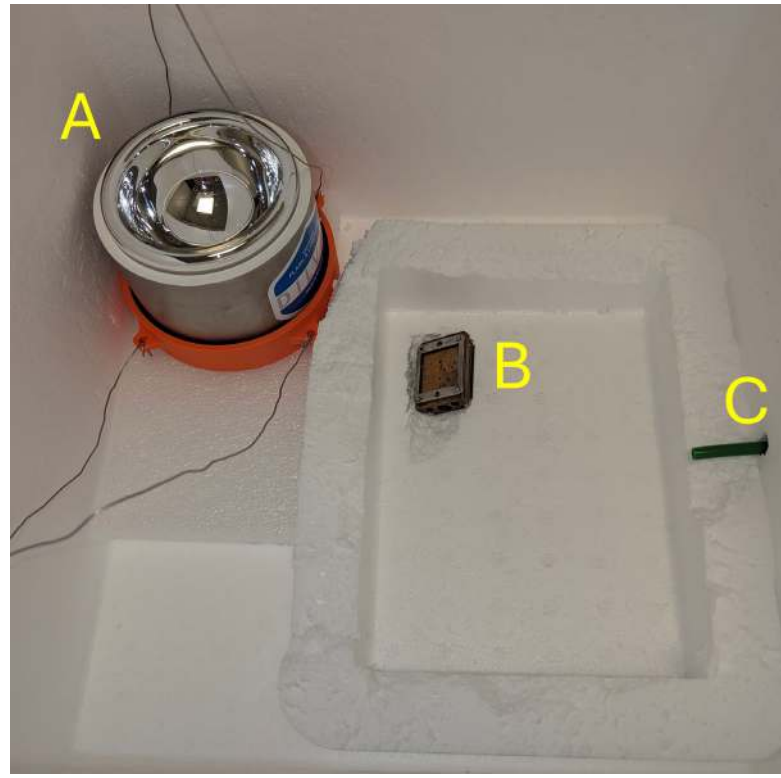


Fig. 1 Experimental setup for attaching samples to SIMS instrument sample stub with placement of the dewar (**A**), smaller polystyrene box with a sample holder (**B**), and tube for argon purging (**C**)

using liquid nitrogen. Purge the glove box attached to the SIMS instrument sample insertion system with dry argon, and allow enough time to replace the gas volume in the glovebox two to three times (*see* **Note 19**).

2. Open the glove box, and place the dewar with the sample holder in the glove box. Seal it, and wait until the argon gas has entered. Replace the gas volume in the glove box at least once (*see* **Note 20**). When no condensation mist is visible, remove the lid from the dewar.
3. Skim off any ice crystals that may be floating on the liquid nitrogen using a piece of aluminium foil.
4. Remove any ice crystals that may have landed on top of the tissue section by tilting and swirling the sample holder up and down in a circular motion while still submerged. Keep the sample holder up from the bottom of the dewar so the ice crystals do not swirl up and land on the tissue section.
5. When the ice crystals have been removed from the tissue section, tilt the sample holder, and quickly take it out of the liquid

nitrogen. Transfer the sample holder to the SIMS instrument's load lock, and close then vacuum pump the load lock (*see* **Note 21**).

6. When the pressure in the load lock is below the manufacturer's recommended value, transfer the sample holder from the load lock chamber to the analysis stage. Keep the sample holder below −143°C (130 K) to avoid ice sublimation, and keep the tissue section in a frozen-hydrated state.

3.1.6 Removal of Tissue After Analysis

Once the tissue section has been analyzed, it can still be used for other purposes, such as staining for histology. For users who wish to reuse the tissue, the following procedures should be followed:

1. Purge the glove box as described in Step 1 of Sect. 3.1.5, and cool down the cold trap.
2. Transfer the sample holder from the analysis stage to the load lock chamber.
3. Vent the load lock chamber, and remove the sample holder. If the tissue needs to remain frozen-hydrated, place the sample holder on an open container with dry ice in the glove box. Otherwise, let the sample holder warm up to room temperature.
4. Remove the ITO-glass slide, and place it in a glass slide container. Keep the container cold with dry ice while transporting (*see* **Note 22**).

3.2 SIMS Analysis

Different SIMS instruments provide different possibilities for analysing tissue sections, and the ion beams, mass analyser, and sample cooling system all have significant impact on the outcome of the analysis. It is important to evaluate the capabilities of the available SIMS instruments before proceeding with the analysis. The following information should be taken into consideration when planning the analysis methodology.

1. Ion beam selection: For the best ability to detect intact lipids, water gas cluster ion beams (H_2O-GCIBs) should be used, as this type of beam has been shown to produce the highest intensity of intact lipids but also produces a minimal amount of fragmentation, which is essential for studying lipid metabolism [13]. Liquid metal and C_{60} ion beams are less efficient for detecting intact lipids and may limit the detection range to small ions.
2. Ion beam setup: The setup of the GCIB can influence imaging resolution, analysis time (throughput), ionization efficiency, and fragmentation. Imaging resolution should be set based on the resolution needed to resolve features in a tissue section before the analysis begins. Higher resolution will resolve

smaller features, but the SIMS image will take a longer time to acquire, so both factors need to be balanced (*see* **Note 23**). The cluster size for the GCIB should be around 0.10 electron Volts (eV) per nucleon (*see* **Note 24**) for maximal ionization efficiency of intact lipids while minimizing fragmentation.

3. Experimental setup:

   a. When setting up the experiments, factors such as the instrument's ability to maintain the sample at cryogenic temperatures, recorded mass range, and surface charge compensation need to be considered. The instrument's cryogenic cooling system must be able to keep the tissue section at constant cryogenic temperatures for the entire duration of the experiment. 24-h cryogenic cooling before requiring liquid nitrogen refill provides the best possibility for analyzing all biologically interesting areas.

   b. The recorded mass range should cover all detectable lipids in the tissue. Small ions and fragment ions should also be recorded, as these can provide some information about lipid composition (*see* **Note 25**) as well as good images for visualizing features and structures in the tissue section.

   c. Surface charging can be challenging to compensate for, as it is affected by the ion beam, tissue section thickness, tissue type, and secondary ion (and electron) yield. Applying a bias voltage to the sample can offset some charging effects. This should be controlled for each tissue section using an area of tissue that is biologically similar to the ROIs. In positive ion mode, use a positive bias voltage, and in negative ion mode, use a negative bias voltage. Additionally, a low-energy electron beam should be used in combination with a negative bias voltage.

   d. A crucial parameter for SIMS analysis is the primary ion dose, which is typically measured in ions/cm^2. Firing more ions at a sample can produce more signal but may also increase molecular fragmentation and will ultimately lead to the removal of material such that the ions being detected originate from a deeper region of the initial sample. For tissue imaging, ion doses in the 10^{10}–10^{13} ion/cm^2 range are typical.

3.3 Data Analysis

1. For initial inspection, once the data have been acquired, control and adjust the calibration of the mass spectra using common lipids if necessary (*see* **Note 26**). Identify the ROIs in the SIMS images by visually comparing where individual lipids are in the tissue section to the H&E images of the same tissue section post-analysis (or a consecutive section).

2. When performing spectral analysis of ROIs in the images, mass spectra can be extracted and analyzed using statistical analysis to highlight differences in lipid composition. Principal components analysis (PCA) is usually a good starting point for analyzing the data, followed by expanded analyses with other statistical methods [14]. This approach is good when the comparison is targeted toward a known biological feature in the tissue sections.
3. The options for analyzing SIMS images are numerous, from comparing how individual lipids are distributed in the tissue section by generating and overlaying ion images of different lipids (Fig. 2) [10] to more computationally advanced methods using multivariate analysis and machine learning on entire SIMS images [15] to identify different regions based on lipid composition [8]. Image analysis allows for exploratory analysis by allowing non-ROI areas to be studied and compared, but it may require more biological knowledge when interpreting the results.
4. For peak identification, putatively assigning lipids in ToF-SIMS mass spectra using accurate mass is easiest done by starting with the heaviest detected lipid and continuing with those decreasing in mass. The detected m/z can be submitted to databases such as LIPID MAPS [15], Human Metabolomic Data Base (HMDB) [16], and SwissLipids [17], which will suggest possible lipids. There are some general trends that can

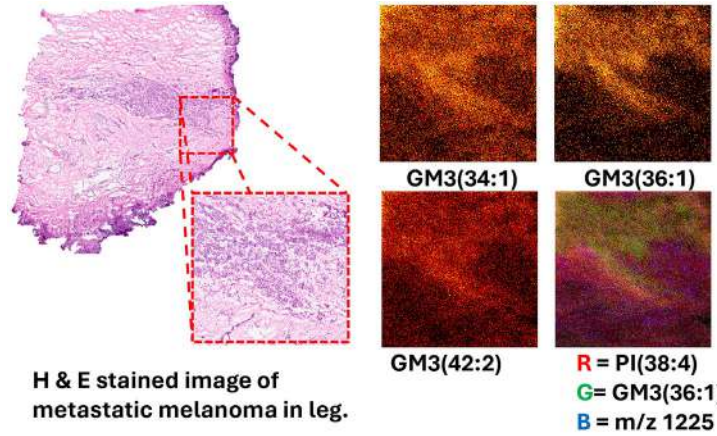


Fig. 2 H&E-stained section of metastatic melanoma in the leg with a magnified region of interest outlined by red dashed boxes analyzed using ToF-SIMS. Corresponding ToF-SIMS ion images show the spatial distributions of GM3(34:1), GM3(36:1), and GM3(42:2) correlating with the tumor. The merged image highlights colocalization patterns of PI(38:4) (red), GM3(36:1) (green), and m/z 1225 (blue)

be considered when assigning lipids based on lipid class (*see* **Note 27**).

4 Notes

1. The tissue should be frozen as soon as possible after removal to stop any biological process that will degrade the tissue.
2. Always use clean gloves when handling the ITO slides to avoid contamination that may interfere with the analysis.
3. Identify the conductive side of the ITO slide by measuring electrical resistance using a multimeter. Cut the ITO slide on the uncoated side using a scribe or glass cutting tool to a size that fits the tissue once sectioned but that also can be mounted to the sample holder of the SIMS instrument. Mark the ITO slide near the edge on the conductive side using a scribing tool or the edge of a thin flathead screwdriver. The mark must be shaped so it is very easy to know when the conductive side is facing up. The number 4 is a good shape, as it looks correct only from one side. Any scratch will also break the reflection, which also makes it easier to identify the correct side.
4. Using gelatine for embedding small or fragile tissue and carboxymethyl cellulose for larger tissue is preferred for imaging mass spectrometry, as OCT can diffuse into the tissue and smear across the tissue [18].
5. OCT contains glycerols that can smear across the sample surface [18].
6. When manually cutting the sections, use even force throughout the section in order to avoid compressing the tissue. Motorized sectioning can be useful.
7. Thinner sections provide better results as surface charging from the ion beam becomes more manageable.
8. For SIMS analysis, one section is used per ion polarity (positive and negative). The first and fourth sections are normally stained with H&E to identify the area of interest in the tissue section before the analysis. The second and third sections are used for SIMS analysis.
9. To minimize differences in tissue morphology and locations of cells between consecutive sections, the tissue can be "butterflied" such that the backside of the first section is a mirror image of the frontside of the second section.
10. Avoid using marker pens, as the ink may contain compounds that migrate and spread between surfaces.

11. This action is to stop lipids from migrating across the tissue surface.
12. Have a method to know which side the tissue section is facing in the container. For example, the tissue section could always be facing the label on the container. It is hard to identify which side of the ITO-glass slide has the tissue section when mounting frozen-hydrated samples, and there is very little time to find the correct side, as the tissue needs to be kept frost-free for the analysis.
13. Chemicals in marking pens can spread onto the ITO-glass slide and tissue and cause interference during the SIMS analysis.
14. The foil will trap dry argon around the sample and reduce the risk of any moisture in the air condensing on the sample until it reaches room temperature.
15. The ease of this step may depend on how the sample holder for the SIMS instrument is designed and how the sample is mounted. Mounting methods using screws to mechanically secure and electrically connect the sample to the sample holder can be time-consuming and finicky, as the ITO-glass slide can move when being screwed down. Using metal frames to secure and clamp the glass slide to the sample holder can be a quicker and easier method.
16. A polystyrene foam box can give much more space to mount a sample compared to the cryotome and allows for much better dexterity compared to a glove box. The box should be large enough for a dewar that fits in the glove box attached to the SIMS instrument but also large enough to hold the sample, yet also a smaller polystyrene box. Cut down the height of the smaller polystyrene box so it is deep enough to cover the sample holder with 1–2 cm of liquid nitrogen. In the larger box next to the smaller box, make a large enough hole to fit a plastic tube for purging the larger box with dry cold argon. The tube should reach just to the liquid nitrogen. The flow of argon should be low, so it does not produce turbulence in the larger box. Consider using colored polystyrene boxes, or color the interior of the boxes to avoid eye strain.
17. Do not put any dry ice in the large box, as the liquid nitrogen will condense CO_2 gas into a mist and reduce visibility.
18. Have a method for keeping track of how the tissue sections are oriented in the container, as it is difficult to see which side of the ITO-glass slide the tissue section is on without increasing the risk for ice formation on the tissue section. Ice formation could cover the tissue and block the ion beam from reaching it.

19. The purging can be helped by sealing the glove box and letting the argon pressurize and inflate the gloves. When the gloves are inflated, slightly open the glove box and push the gloves in to expel any trapped air. An O_2 sensor could also be used to monitor how much air is still left.
20. The details of this step depend on the design of the glove box. Some glove boxes may have an opening in the top to lower items into, and because the dewar's exterior is cold, there is a risk that air is cooled and falls into the glove box. Other glove boxes may have a sample lock that reduces the risk of contaminating the inert and dry atmosphere in the glove box.
21. Visible condensation or frost formation on the sample holder is a sign that moisture is still present in the glove box, indicating that the glove box may not be sealed or purged properly. In the case of frost formation on the tissue section, the transfer has failed, and the tissue section cannot be analyzed. If frost appears on the instrument's sample transfer system when loading the sample holder, do not expose it to vacuum, as the ice will sublime and may overload the pumping system.
22. Removing the ITO-glass slide is easier than mounting it; however, if more space is needed, the sample holder could be placed in a container, covered with aluminum foil, and taken back to the larger polystyrene box before removing the ITO-glass slide.
23. The tissue section can be analyzed first at a lower resolution and low primary ion dose to get an overview image of the entire tissue section before selecting which areas should be imaged at higher resolution based on lipid composition or structures seen in a consecutive section used for histological stainning.
24. eV per nucleon is calculated with the following equation (assuming singly charged ions): $\frac{V_a}{m_g n_g}$, V_a is the anode voltage for the ion beam, m_g is the molecular weight for the gas molecule, and n_g is the number of gas molecules in the gas cluster.
25. Although ion beams for SIMS are being developed to minimize fragmentation, some fragmentation does still occur. This outcome needs to be kept in mind, as fragment ions can be mistaken as small intact lipids due to sharing some chemical base structures.
26. Select multiple (minimum 3) peaks throughout the mass range to calibrate the mass spectrum, keeping 100–200 m/z between each calibration point. This calibration requires some knowledge of which lipids should be expected in the sample. Lipid fragments such as headgroups and fatty acids can be

used. The calibration peaks should all have similar intensities; avoid very intense peaks, as they may be very wide and skew the calibration. Keep some known peaks to control the accuracy of the calibration by comparing the expected m/z to the detected.

27. Lipids in the phosphatidylcholine (PC) and sphingomyelin (SM) classes are usually detected as positive ions. PC are ionized by protonation $[M+H]^+$, but also form adduct ions with sodium $[M+Na]^+$ and potassium $[M+K]^+$. PC that has formed adduct ions with Na and K can also be detected as fragment ion by losing the trimethylamine part of the headgroup, $[M+Na/K\text{-}TMA]^+$, forming a pattern that can be used to identify PC lipids. SM lipids are usually detected by forming adduct ions with Na and K [19]. Cholesterol is also a lipid that is commonly detected as a positive ion, mainly as $[M+H\text{-}H_2O]^+$ [20]. Lipids such as phosphatidylinositol (PI), phosphatidylethanolamine (PE), phosphatidylserine (PS), and phosphatidic acid (PA) are generally detected as negative ions formed by deprotonation, i.e. $[M\text{-}H]^-$ ions [19].

Acknowledgments

The authors gratefully acknowledge financial support from the Swedish State (VR grant: 2022-04498), Swedish governmental funding of clinical research (ALF), and Hudfonden.

Competing Interests The authors declare no competing interests.

References

1. Lockyer NP, Aoyagi S, Fletcher JS et al (2024) Secondary ion mass spectrometry. Nat Rev Methods Primers 4:32. https://doi.org/10.1038/s43586-024-00311-9
2. Barut I, Fletcher JS (2023) Cell and tissue imaging by secondary ion mass spectrometry. Biointerphases 18(6):061202. https://doi.org/10.1116/6.0003140
3. Yamada I, Matsuo J, Toyoda N, Kirkpatrick A (2001) Materials processing by gas cluster ion beams. Mater Sci Eng R Rep 34(6):231–295. https://doi.org/10.1016/S0927-796X(01)00034-1
4. Angerer TB, Magnusson Y, Landberg Gr, Fletcher JS (2016) Lipid heterogeneity resulting from fatty acid processing in the human breast cancer microenvironment identified by GCIB-ToF-SIMS imaging. Anal Chem 88(23):11946–11954. https://doi.org/10.1021/acs.analchem.6b03884
5. Angerer TB, Chakravarty N, Taylor MJ et al (2019) Insights into the histology of planarian flatworm *Phagocata gracilis* based on location specific, intact lipid information provided by GCIB-ToF-SIMS imaging. Biochim Biophys Acta Mol Cell Biol Lipids 1864(5):733–743. https://doi.org/10.1016/j.bbalip.2019.01.011
6. Dimovska Nilsson K, Neittaanmäki N, Zaar O et al (2020) TOF-SIMS imaging reveals tumor heterogeneity and inflammatory response markers in the microenvironment of basal cell carcinoma. Biointerphases 15(4):041012. https://doi.org/10.1116/6.0000340
7. Sämfors S, Ståhlman M, Klevstig M et al (2019) Localised lipid accumulation detected in infarcted mouse heart tissue using ToF-SIMS.

Int J Mass Spectrom 437:77–86. https://doi.org/10.1016/j.ijms.2017.09.012
8. Uzoni S, Zanchin D, Chatzikyriakos V et al (2025) Mapping the molecular landscape of human DLBCL by GCIB-SIMS. Analy Chem 97(13):7186–7194. https://doi.org/10.1021/acs.analchem.4c06594
9. Tian H, Sheraz née Rabbani S, Vickerman JC, Winograd N (2021) Multiomics imaging using high-energy water gas cluster ion beam secondary ion mass spectrometry [(H2O)n-GCIB-SIMS] of frozen-hydrated cells and tissue. Analy Chem 93(22):7808–7814. https://doi.org/10.1021/acs.analchem.0c05210
10. Neittaanmäki N, Zaar O, Cehajic KS et al (2024) ToF-SIMS imaging reveals changes in tumor cell lipids during metastatic progression of melanoma. Pigment Cell Melanoma Res 37(6):793–800. https://doi.org/10.1111/pcmr.13182
11. Shon HK, Yeun J, Lee Gs et al (2025) Cryogenic ToF-SIMS 3D imaging of SKOV3 ovarian cancer spheroids: preserving native lipid distributions with Ar cluster sputtering. J Vac Sci Technol B 43(6):064005. https://doi.org/10.1116/6.0005061
12. Angerer TB, Mohammadi AS, Fletcher JS (2016) Optimizing sample preparation for anatomical determination in the hippocampus of rodent brain by ToF-SIMS analysis. Biointerphases 11(2):02A319. https://doi.org/10.1116/1.4941064
13. Uzoni S, Zeidi S, Thoma J et al (2026) Secondary ion yield enhancement for lipids in frozen hydrated lymphoma tissue samples using water cluster SIMS. J Vac Sci Technol B 44(1):014002. https://doi.org/10.1116/6.0005143
14. Aoyagi S (2023) Application of machine learning to spectrum and image data. J Vac Sci Technology A 41(6):063202. https://doi.org/10.1116/6.0002858
15. Conroy MJ, Andrews RM, Andrews S et al (2024) LIPID MAPS: update to databases and tools for the lipidomics community. Nucleic Acids Res 52(D1):D1677–D1682. https://doi.org/10.1093/nar/gkad896
16. Wishart DS, Guo A, Oler E et al (2022) HMDB 5.0: the Human Metabolome Database for 2022. Nucleic Acids Res 50(D1):D622–D631. https://doi.org/10.1093/nar/gkab1062
17. Aimo L, Liechti R, Hyka-Nouspikel N et al (2015) The SwissLipids knowledgebase for lipid biology. Bioinformatics 31(17):2860–2866. https://doi.org/10.1093/bioinformatics/btv285
18. Yoon S, Lee TG (2018) Biological tissue sample preparation for time-of-flight secondary ion mass spectrometry (ToF–SIMS) imaging. Nano Converg 5(1):24. https://doi.org/10.1186/s40580-018-0157-y
19. Adams KJ, DeBord JD, Fernandez-Lima F (2016) Lipid specific molecular ion emission as a function of the primary ion characteristics in TOF-SIMS. J Vac Sci Technol B Nanotechnol Microelectron 34(5):051804. https://doi.org/10.1116/1.4961461
20. Piehowski PD, Carado AJ, Kurczy ME et al (2008) MS/MS methodology to improve subcellular mapping of cholesterol using TOF-SIMS. Anal Chem 80(22):8662–8667. https://doi.org/10.1021/ac801591r



Chapter 31

Unbiased Microbiome and Metabolomic Profiling of Fecal Samples from Patients with Melanoma

Animesh A. Mishra, Nicole Poulides, Aidan C. Morrill, Shuheng Gan, Gabriella Nguyen, Meagan A. Mollergren, Christina M. Zarek and Andrew Y. Koh

Abstract

Gut microbiota influence and modulate host immune responses. In preclinical cancer models, mice lacking gut microbiota have a markedly diminished response to immune checkpoint inhibitor therapy. Further, in melanoma patients, specific commensal gut microbiota have been associated with a positive clinical response to immunotherapy. In order to study the gut microbiome and metabolome, we have developed methods for fecal sample collection and processing, microbiome and metabolome profiling, and bioinformatic analysis. This protocol will be a useful tool for interrogating the taxonomic composition and functional output of a melanoma patient's gut microbiome.

Keywords Microbiome, Metabolomics, Fecal, Immunotherapy, Melanoma

1 Introduction

The gut microbiome, the trillions of microorganisms residing in the intestine, plays a pivotal role in educating and activating the immune system [1, 2]. Unleashing the immune system with immune checkpoint inhibitor therapy (ICT) has resulted in remarkable clinical efficacy in patients with previously incurable cancers, such as advanced melanoma. These two fields of cancer immunotherapy and the microbiome synergize in the intriguing notion that the gut microbiome modulates host antitumor immune responses [3–5].

Interestingly, specific gut bacteria are required for optimal response to ICT in preclinical models [4, 5]. Germ-free and antibiotic-treated mice respond poorly to ICT [4, 5]. Our group [6] and others [7–10] have shown that melanoma patients who respond to ICT therapy have a distinct gut microbiota signature compared to counterparts with disease progression. While ICT has revolutionized the treatment of patients with metastatic melanoma, a significant

Kristian M. Hargadon (ed.), *Melanoma*, Methods in Molecular Biology, vol. 3089,
https://doi.org/10.1007/978-1-0716-5619-8_31,
© The Author(s), under exclusive license to Springer Science+Business Media, LLC, part of Springer Nature 2027

portion of these patients (~40%–50%) fail to respond to ICT and have limited survival [11]. Host factors, including gut microbiota composition, likely contribute to this heterogeneity in treatment response.

To further study the relationship between host and gut microbiota, fecal samples from patients with melanoma can be collected for analysis of the gut microbiome (the gut microbiota and the genes that they harbor) and metabolome (the composite set of small molecule chemicals or metabolites). We use metagenomic shotgun sequencing (MSS) to gain insight into taxonomic and functional abundance of the gut microbiome. To gain additional insight into the functional capacity of the gut microbiome, we also utilize ultra-high performance liquid chromatography-tandem mass spectroscopy (UPLC-MS/MS) to identify metabolites. Indeed, gut microbiota-derived metabolites (e.g., short-chain fatty acids) can induce phenotypic changes in the host (i.e., dampen inflammation in the gut), even in the absence of the gut microbiota that produce them [12, 13]. Ultimately, precision editing of gut microbiota and/or gut microbiota-derived metabolites could lead to novel therapeutic approaches to augment the host antitumor immune response. Here we present a comprehensive approach to fecal sample collection and processing along with gut microbiome and metabolome profiling and analysis.

2 Materials

2.1 Fecal Sample Collection

2.1.1 Inpatient Collection

1. Falcon 50 mL conical tube, with 15–20 mL of 95% ethanol, which does not need to be molecular grade (*see* **Note 1**).
2. One biohazard specimen transport bag, 6×9 in.
3. Fisherbrand Commode Specimen Collection System: one collection receptacle and one collection bracket (*see* **Note 2**).
4. Sterile wooden tongue depressors.

2.1.2 Outpatient Collection for Gut Microbiome Profiling

1. OMNIgene GUT stool collection kit (OMR-200): OM-AC1 toilet accessory, collection tube, spatula, biohazard bag, heavy weight absorbent pad, shipping box.
2. Prepaid postage for subject's residence and tracking number (*see* **Note 3**).

2.1.3 Outpatient Collection for Gut Metabolomic Profiling

1. Fisherbrand Commode Specimen Collection System: one collection receptacle and one collection bracket.
2. One 95 kPa biohazard specimen transport bag, 10×14 inch.
3. Seven 8-ounce ice packs.

4. One Therapak refrigerated biological substance category B shipping system: cardboard box and foam cooler.
5. Heavy weight absorbent.
6. Prepaid postage for subject's residence and tracking number (*see* **Note 4**).

2.2 Fecal Sample Aliquot and Storage

1. Matrix 1.0 mL ScrewTop tubes in barcoded latch racks (*see* **Note 5**).
2. 10% bleach.
3. Sterile wooden applicator sticks.
4. Standard wood tongue depressors.
5. BioMicroLab XL9 Tube Handler.
6. Wipes (e.g., Kimtech Kimwipes).
7. Surface protector/liner (e.g., Versi-dry).
8. Personal protective equipment (PPE): lab coat, double gloves, a facemask, and protective glasses.

2.3 Genomic DNA (gDNA) Extraction

1. MagMAX Prime Viral/Pathogen NA Isolation Kit (Binding Solution, Wash I Solution, Binding Beads, Proteinase K, Elution Buffer, Proteinase K dye).
2. MagMAX Prime G+ Stool Lysis Buffer.
3. KingFisher 96 Deep-Well Plates.
4. KingFisher 96-tip combo for deep well magnets.
5. KingFisher 96 microplate.
6. KingFisher Apex with 96 Deep Well Head.
7. KingFisher Apex 96 Deep Well Heating Block.
8. 80% Ethanol solution.
9. 2-mL bead beater tubes.
10. Bead beater (e.g., TissueLyser II [Qiagen]).
11. Benchtop microcentrifuge.
12. Vortex.
13. Reagent reservoir.
14. 1.5-mL microfuge tubes.
15. Clear adhesive film.
16. 100% ethanol.

2.4 gDNA Quantification

1. Qubit Flex Fluorometer.
2. Qubit assay tubes.
3. Quant-iT dsDNA assay kit, broad range (Thermo Fisher) (*see* **Note 6**).

2.5 Sample Preparation for LC-MS Analysis

1. Ice water bath or cold packs.
2. Benchtop microcentrifuge.
3. Tissue homogenizer (e.g., Qiagen TissueLyser II).
4. Extraction solvent: Just prior to use, prepare 2 mL of extraction solvent by mixing Acetone and Isopropanol at a 2:1 ratio. Prepare 2 mL of the solvent per sample at room temperature in a fume hood (*see* **Notes 7 and 8**).
5. 2-mL screw cap microfuge tubes.
6. 2-mL screw cap vials with external threads and a silicon gasket.

3 Methods

3.1 Fecal Sample Collection

3.1.1 Inpatient Collection

1. Instruct clinical staff assisting with collection to observe the following:
   a. Prior to sample collection, the patient should empty their bladder. Collect the fecal sample without contamination of urine or toilet water.
   b. To assemble the stool collection system, remove the lid off the collection receptacle and secure the receptacle in the collection bracket.
   c. Place the stool collection system under the toilet seat.
   d. The fecal sample needs to be at least 500 mg (approximately 2.5 cm in diameter or the size of a US quarter). Any urine should be poured out of the collection receptacle so that only stool remains in the receptacle.
2. Using a sterile tongue depressor, place approximately 5 mL of feces (a maximum of 10 mL of feces) into the 50 mL conical with 95% ethanol to allow for complete immersion of the fecal sample in ethanol. This will kill gut microbiota (preventing further growth of some bacteria) while helping to preserve the fecal metabolome and nucleic acid integrity.
3. Transport fecal samples to the laboratory at room temperature in a biohazard specimen transport bag within the hour. If not possible, store samples at 4°C for up to 24 h.
4. Once the samples are received in the lab, aliquot them as described below (Sect. 3.2). If it is not possible to promptly aliquot samples, the samples can be stored in the conicals at −80°C for up to 6 months [14].

3.1.2 Outpatient Collection for Gut Microbiome Profiling

1. Provide the participants with an OMNIgene GUT stool collection kit at an appointment closest to the study collection time point (i.e., before initiation of cancer immunotherapy). This kit enables stabilized transport and storage of microbial DNA at ambient temperature for up to 60 days without the need for cold-chain processes.
2. Instruct the patient to perform the following at home (*see* **Note 9**):
   a. Prior to sample collection, the patient should empty their bladder and then collect the fecal sample without contamination of urine or toilet water.
   b. To facilitate collection of the fecal sample, install the OM-AC1 toilet accessory included in the kit. Carefully peel open the edges and affix the adhesive surface to the back of the toilet seat, close to the outer edge of the seat. Press firmly to secure it.
   c. While holding the yellow tube top, unscrew only the purple cap from the collection device and set aside for later use. The yellow tube top should not be removed, and care should be taken to avoid spilling the stabilizing liquid contained in the tube.
   d. Using the provided spatula, collect a small amount of fecal sample and transfer into the top portion of the yellow tube top. Repeat this process until the sample fills the yellow tube top. The sample should not be pushed into the tube.
   e. Scrape horizontally across the tube top to level the sample and remove any excess. Wipe clean the exterior of the tube and top with toilet paper or tissue as needed.
   f. Replace the purple cap and screw onto the yellow tube top until fully tightened.
   g. Vigorously shake the sealed tube in a back-and-forth motion for at least 30 s to ensure mixing of the fecal sample with the stabilizing solution. If large particles remain, continue shaking until they are reduced in size. Not all particles will be dissolved.
   h. The used toilet accessory may be discarded by dropping it into the toilet water, waiting 1 min for the paper to become soft, and then flushing. Alternatively, it may be discarded in the trash. The spatula should be returned to its original packaging or wrapped in toilet paper and disposed of in the trash.
   i. Place the sealed collection device with the fecal sample into a biohazard bag with a heavy-weight absorbent pad. Seal the bag, expelling as much air as possible.

j. Note the sample collection date, and include this information inside the shipping box.

k. Seal the shipping box containing the sample, and ship with the shipping label included. If the sample needs to be stored until shipping, please store at room temperature. Alternatively, samples may be brought to a scheduled appointment within a few days of collection.

3. Upon arrival at the laboratory, samples are aliquoted as described in Sect. 3.2 (*see* **Note 10**). If samples cannot be promptly aliquoted, they may be stored at −80°C in the OMNIgene Gut tube for up to 6 months.

3.1.3 Outpatient Collection for Gut Metabolomic Profiling

1. Assemble the stool collection kit with all materials listed in Sect. 2.1.3.
2. Provide subject with a stool collection kit at an appointment closest to the study collection time point (i.e., before initiation of cancer immunotherapy).
3. Instruct the patient to perform the following at home (*see* **Note 9**):
   a. Before collecting the fecal sample, place the ice packs flat in a freezer so they will be frozen solid before shipping.
   b. Prior to sample collection, the patient should empty their bladder and then collect the fecal sample without contamination of urine or toilet water.
   c. To assemble the stool collection system, remove the lid from the collection receptacle, and secure the receptacle in the collection bracket.
   d. Place the stool collection system under the toilet seat.
   e. The fecal sample needs to be at least 500 mg (approximately 2.5 cm in diameter or the size of a US quarter). Any urine should be poured out of the collection receptacle so that only stool remains in the receptacle.
   f. Snap the lid tightly onto the receptacle.
   g. Place the stool collection system on a countertop and remove the bracket by pushing down on one side at a time.
   h. Place the closed collection receptacle with the fecal sample into the biohazard bag with the heavy-weight absorbent. Seal the bag, expelling as much air as possible.
   i. Place three to four ice packs in the cooler, then add the biohazard bag and its contents, followed by the remaining ice packs on top. Place the lid on the cooler.
   j. Note the sample collection date and include this information inside the shipping box.

k. Seal the shipping box containing the cooler and sample.

l. Ship the sample on a Monday, Tuesday, or Wednesday in order to avoid potential shipping delays and/or delivery of samples on the weekend. If the sample needs to be stored until shipping, please store in a cool, dry room, refrigerator, or freezer. Do not place it in a warm or hot room. Alternatively, if the subject has an appointment within a few days of sample collection, the sample can be stored and brought to the appointment.

4. Once the sample is received in the lab, aliquot it as described in Sect. 3.2 (*see* **Note 10**).

3.2 Fecal Sample Aliquot and Storage

1. Pre-weigh the individual tubes in the Matrix 2D tube rack to obtain the empty tube weights (in mg) and 2D tube barcodes.
2. Create an Excel spreadsheet with rack ID, 2D tube barcodes, and pre-weights. Use this list going forward for making aliquots of fecal samples.
3. Dress in appropriate PPE (*see* **Note 11**).
4. Place the 2D tubes and fecal samples in separate ice receptacles.
5. Clean biosafety cabinet with 10% bleach and then cover surface with a Versi-dry surface liner.
6. Aliquot fecal samples:
   a. Prepare at least four aliquots from each sample (additional aliquots can be taken if needed and/or if sample size allows). Fill tubes with 30–50 mg of sample in each aliquot. Using all fecal samples from the OMNIgene GUT tube should yield four to six aliquots. Fecal sample from a commode for metabolomic profiling yields four to eight aliquots. Label the corresponding number of tubes with de-identified sample ID and aliquot number.
   b. Remove the cap of the 2D tube carefully. Place the inside of the cap facing upward to avoid contact with any part of the bench and potential contamination of the sample.
   c. For samples stored in OMNIgene Gut tubes, the sample may be mainly liquid. In this case, aliquot stool using a micropipette. For solid samples, use a tongue depressor or applicator stick to take the first aliquot. The tongue depressor and applicator stick may be used for all aliquots from the same sample if it is stored in the same way.
   d. Once the sample is in the tube, push any sample near the top of the tube toward the bottom. If there is any sample on the screw-top threads, wipe the tube with a clean Kimwipe to ensure that stool will not leak out and contaminate other samples in the tube rack.

e. Carefully screw the cap back onto the tube, again being careful to avoid any contact with the inside of the cap.

f. Repeat Steps b–f of this section for the remaining tubes.

7. Dispose of any remaining sample, collection materials, and other used supplies in medical biohazardous waste.
8. Weigh each 2D tube containing fecal sample, and record the weight (mg).
9. Use the tube scanner to ensure tubes are in the correct position.
10. Store the tube rack at −80°C for future use.
11. Save the final Excel sheet with tube barcodes, sample IDs, and pre- and post-weights on a secure password-protected computer.

3.3 gDNA Extraction

We utilize a high-throughput pipeline that includes the MagMAX Prime Viral/Pathogen NA Isolation kit (Thermo Fisher) and the KingFisher automated instrument platform (Thermo Fisher).

1. Set up the extraction instrument. Install a 96 deep-well heating block and 96 deep-well head on the KingFisher instrument, and load the appropriate Prime_GI script prior to sample processing (Prime_GI_APX script for the Apex instrument or Prime_GI_FLX script for the Flex instrument) (*see* **Note 12**).
2. Prepare processing plates by adding the following reagents to wells designated to contain samples or controls.

   a. Wash I Plate: Add 950 µL of Wash Solution to a KingFisher 96 Deep Well Plate.

   b. Wash II Plate: Add 950 µL of 80% Ethanol solution to a KingFisher 96 Deep Well Plate.

   c. Elution Plate: Add 200 µL of Elution Buffer to a KingFisher 96 Deep Well Plate.

   d. Tip Comb Plate: Place a KingFisher 96 tip comb for deep-well magnets in a KingFisher 96 microplate (200 µL).

   e. Label the sample plate (to be prepared in Step 9 of this section).

3. Prepare Binding Bead Mix. For each sample and control (volume 400 µL), prepare 515 µL of Binding Bead Mix by combining 500 µL of Binding Solution and 15 µL of Binding Beads (*see* **Note 13**).
4. Mix well by slow inversion, avoiding bubbles, then store at room temperature for up to 4 h.

5. Resuspend 0.1 g of fecal sample in 800 µL of MagMAX Prime Stool Lysis buffer in the bead beating tubes (*see* **Note 14**). Also prepare a negative control containing 800 µL of MagMAX Prime Stool Lysis buffer in a bead beating tube.
6. Add 20 µL of Proteinase K or Proteinase K dye mixture (*see* **Note 15**) to each tube.
7. To mix sample (or control) and buffer, use a bead beater (e.g., TissueLyser II) at 30 Hz for 3–4 min to ensure the sample is sufficiently homogenized (*see* **Note 16**).
8. Remove tubes and centrifuge at 14,000 × *g* for 2 min.
9. Aspirate 400 µL of supernatant from bead tubes to a deep-well Sample Plate, ensuring to carefully avoid the beads and fecal pellet.
10. Remix Binding Bead Mix by inversion, and add 515 µL of Binding Bead Mix to each sample in the Sample Plate. Ensure that Binding Bead Mix is viscous by frequently inverting the tube to remix.
11. Load the prepared sample and processing plates into the KingFisher instrument, ensuring the A1 plate position aligns with the instrument markings. Start the instrument using the script on the KingFisher instrument.
12. The program runs for approximately 45 min. Once complete, remove the Elution plate within 10 min to minimize evaporation of the samples. Cover the plate with clear adhesive film and place promptly on ice.
13. Purified nucleic acid may be immediately used, or the plate can be stored long-term at −20°C.
14. Assess DNA purity by spectroscopy (*see* **Note 17**) and DNA integrity by agarose gel electrophoresis (*see* **Note 18**).
15. Quantify gDNA using a fluorescence-based assay (e.g., Qubit) for subsequent MSS (*see* **Note 19**).

3.4 gDNA Sequencing

1. Submit ~500 ng to 1 µg of high purity, high integrity (e.g., nondegraded) fecal gDNA for each sample to an academic core sequencing facility or commercial sequencing company for library preparation and MSS.
2. We recommend using a short-read sequencing platform (e.g., Illumina HiSeq or NovaSeq, 150 bp pair-end reads). Typically, 40–100 million sequences are generated per sample.

3.5 Bioinformatic Analysis of MSS Data

MSS allows high-resolution characterization of complex microbial communities. There are numerous bioinformatics approaches to analyzing MSS data, and no clear consensus on the "best" method [15]. As such, we recommend that investigators consult with microbiome

bioinformatics specialists at their respective institutions. A brief description of our current MSS bioinformatics pipeline is as follows, with a schematic workflow presented in Fig. 1.

1. Perform quality control on the raw MSS data using FastQC (http://www.bioinformatics.babraham.ac.uk/projects/fastqc/) or NGS-QC (https://github.com/mjain-lab/NGSQCToolkit).
2. Remove human sequences with the NCBI BMTagger Human Contamination Screening Tool (ftp://ftp.ncbi.nlm.nih.gov/pub/agarwala/bmtagger/).
3. Perform taxonomic identification. There are a number of established approaches to taxonomic identification, including DNA-to-DNA, DNA-to-protein, or marker-based classification. DNA-to-DNA and DNA-to-protein classification compares sequence reads to respective comprehensive genomic databases, whereas marker-based classification interrogates sequence reads against a subset of specific gene families with good discriminatory power between species. We currently use unique clade-specific marker genes via a computational tool such as Metagenomic Phylogenetic Analysis, MetaPhlAn 4.0 [16] (http://huttenhower.sph.harvard.edu/metaphlan [17]) or a lowest common ancestor positioning approach to determine taxonomic composition.
4. Perform functional pathway analysis. The Kyoto Encyclopedia of Genes and Genomes (KEGG) orthology database can be

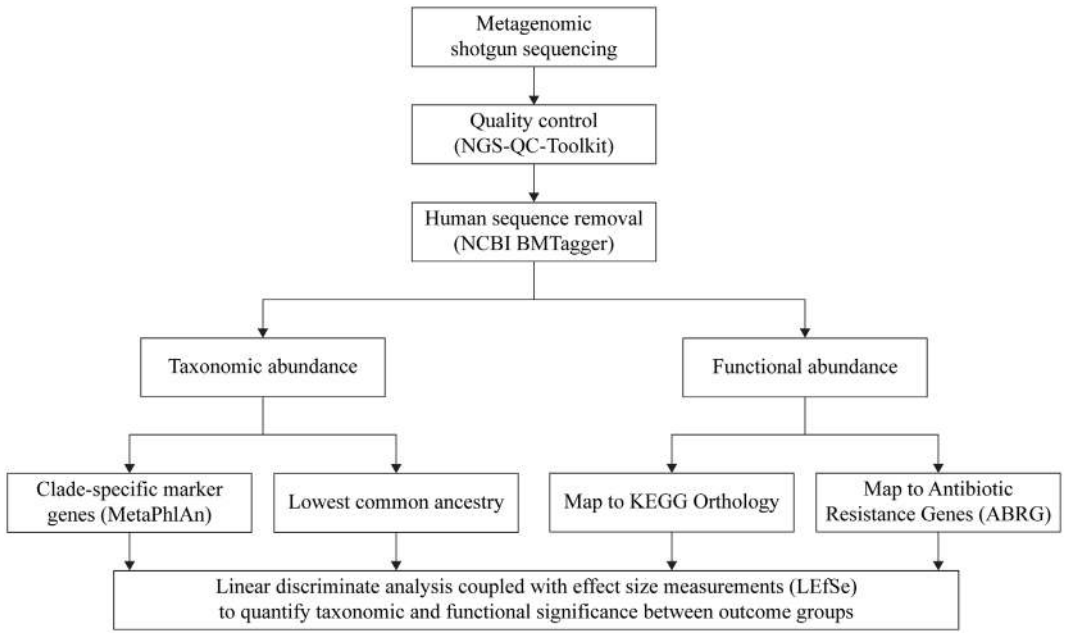


Fig. 1 Overview of bioinformatics pipeline for MSS data

used to directly map each sequence to a KEGG orthology representative sequence. The sum of sequences belonging to a particular functional pathway can then be computed. Functional pathway abundance can then be calculated using HUMAnN 2.0 [18,19] or FMAP [20], as we have done previously [21].

5. Perform taxonomic differential abundance analysis. A common goal of microbiome research is to determine if specific gut microbiota are more abundant or enriched in cohorts with a disease process or phenotype (e.g., melanoma patients who respond favorably to cancer immunotherapy versus counterparts who do not). As such, we use linear discriminant analysis coupled with effect size measurements (LEfSe) to quantify differential taxonomic and functional pathway abundance between comparison groups. LEfSe determines the statistically and biologically significant features of the identified taxa that are most likely to explain the differences between comparison groups [22]. The results can be visualized as a histogram and/or cladogram.

In summary, there are numerous approaches to determine taxonomic classification, functional pathway analysis, and differential abundance with MSS data. Of note, different bioinformatics pipelines can provide widely disparate results. Ultimately, it is important to perform follow-up experiments using suitable *in vitro* or *in vivo* models to begin to establish or determine causality and move beyond correlation and observation.

3.6 Sample Preparation for Gut Metabolomic Profiling

1. When possible, flash-freeze fecal specimens and store immediately at −80°C (*see* **Note 20**).
2. When flash-freezing of clinical fecal specimens is not feasible, particularly with outpatient collection, immerse feces into 95% ethanol, and store immediately at −80°C (within 24 h) as an acceptable alternative.

3.7 Quantification of Sample Amount

1. Label and weigh a 2-mL microfuge tube. Store at −20°C or less until needed.
2. Thaw frozen fecal samples on ice. Aliquot approximately 30–50 mg (wet weight) of feces into the pre-weighed and cooled 2-mL microfuge tube using a sterile plastic loop. Use screw-top tubes to aliquot the samples. Keep the weights between the samples as close as possible, within twofold of each other.
3. Determine the wet fecal weight by weighing the 2-mL microfuge tube with feces and subtracting the weight of the microfuge tube as determined in Step 1 of this section.
4. Snap freeze samples in liquid nitrogen, and immediately proceed to the extraction step, or store the samples at −80°C until

extraction can be performed (within 6 months). Extracting multiple or all samples on the same day reduces experimental variability.

3.8 Extraction

1. Prepare 2 mL of a 2:1 acetone:isopropanol extraction solvent (LC-MS grade) per sample, and store at room temperature in a sealable glass bottle (*see* **Notes 7 and 8**).
2. Add 300 µL of extraction solvent to each tube containing fecal matter (*see* **Note 21**).
3. Vortex each tube for 15 s twice (*see* **Note 22**).
4. Transfer supernatant to a new labeled 2-mL microfuge tube.
5. Add 300 µL of extraction solvent to the original tubes (from Step 2 of this section).
6. Vortex each tube for 15 s twice. Transfer supernatant to the labeled 2-mL microfuge tube from Step 4 of this section.
7. Centrifuge the tubes with the supernatants (from Step 4) at 13,500 × *g* at 4°C for 10 min.
8. Transfer most of the supernatant (without disturbing the pellet) to the pre-labeled 2 mL screw cap vial with silicon gasket and external thread.
9. Store at −80°C or in liquid nitrogen until ready for analysis.

3.9 Unbiased Gut Metabolomic Profiling with Ultrahigh Performance Liquid Chromatography-Tandem Mass Spectroscopy (UPLC-MS/MS)

Unbiased metabolomic profiling is often relegated to academic core facilities or commercial companies because of the challenges associated with validation of comprehensive metabolite reference libraries and the optimization needed for all categories of metabolites. Such capabilities are typically beyond the scope of individual research laboratories. Accordingly, we have used commercial companies to perform unbiased gut metabolomic profiling by UPLC-MS/MS (e.g., Metabolon and General Metabolics). Briefly, the extracted samples are split into aliquots for analysis by UPLC-MS/MS utilizing positive (two methods), negative, and polar ion modes, followed by normalization to account for differential volumes extracted. Compounds are identified by automated comparison to reference chemical library entries with subsequent visual inspection for quality control. Peaks are quantified using area under the curve. For studies spanning multiple days, a data normalization step is performed to correct variation resulting from instrument inter-day tuning differences.

3.10 Statistical Analysis of Metabolome

For statistical analyses and data display as performed in our previous study [6], any missing values are assumed to be below the limits of detection; these values are imputed with the compound minimum (minimum value imputation). Standard statistical analyses (e.g., Welch's two sample *t*-test) should be performed in ArrayStudio

(Omicsoft) on log-transformed data, with $p < 0.05$ being considered significant. An estimate of the false discovery rate (q-value) should also be calculated to account for the multiple comparisons that normally occur in metabolomics-based studies, with $q < 0.05$ being used as an indication of high confidence in a result.

4 Notes

1. Fecal samples are best preserved if flash-frozen immediately after collection. However, since this is often not feasible, the sample can be placed in ethanol, which has been shown to be a cost-effective means of preserving nucleic acid integrity [23].
2. Commode systems may vary by clinic. Follow manufacturer's instructions for proper assembly and installation.
3. In compliance with the International Air Transport Association (IATA) specifications, stool samples collected and shipped in the OMNIgene stool collection kit are classified as exempt human specimens. We recommend labeling the OMNIgene stool collection kit box (Sect. 2.1.2) with the shipping labels (details can be found on iata.org and in the required certification course) as follows:
    a. Place an Exempt Human Specimen label lengthwise on the top flap of the OMNIgene stool collection kit box.
    b. Place a printed address label (TO/FROM), tracking sticker, and prepaid postage sticker above the Exempt Human Specimen label on the top flap of the box. Ensure the name and phone number of an IATA-certified individual are present in the address lines.
    c. Record the subject ID and tracking number (or a corresponding box number) to keep track of the stool collection kit.
    d. Use clear packaging tape to secure all stickers in place.
4. Outpatient specimens collected and shipped in a commode system are classified as Biological Specimens Category B. We recommend labeling the shipping box (Sect. 2.1.3) with shipping labels (details can be found on iata.org and in the required certification course) as follows:
    a. Place the red arrow stickers in the center of opposite sides of the box.
    b. Place the UN 3373 and Biological Substance Category B stickers in the top left corner on the front of the Therapak insulated shipper. Ensure the UN 3373 and Biological

Substance Category B stickers are not on the same side as the red arrows.

c. Place the printed address label (TO/FROM) below the Biological Substance Category B sticker. The IATA requires that the shipper/receiver information be on the same side as the Biological Substance Category B sticker. They also require the name and phone number of an IATA-certified individual in the address lines.

d. On the same side as the Biological Substance Category B sticker, place a tracking sticker and the pre-paid postage sticker(s) on the outside of the top flap.

e. Record the subject ID and tracking number (or a corresponding box number) to keep track of the stool collection kit.

f. Use clear packaging tape to secure all stickers in place. The shipping box and cooler can then be reused upon return.

5. Matrix 2D tube racks and 1.0 mL ScrewTop tubes can be bought separately. The racks will need to be loaded with the tubes prior to aliquoting.
6. The Quanti-iT PicoGreen dsDNA assay kit (Thermo Fisher) is an alternative fluorescence-based assay that can be used with the Qubit Flex Fluorometer.
7. All solvents should be LC-MS-grade. Since the solvent mix is highly volatile, it is recommended to prepare the fresh solvent mix in a fume hood immediately before the extraction. Do not leave the solvent open to the air to avoid evaporation.
8. Prewash all glassware in deionized water and then prerinse measurement glassware with a small portion of the extraction solvent. Note that glassware that has been repeatedly washed using soap in a dishwasher is unsuitable for LC-MS work. Additionally, newly purchased glassware typically releases large amounts of sodium and potassium ions, so it is best to prepare fresh glassware by repeatedly rinsing with deionized water and then washing by hand. Avoid dishwashing soap/detergent.
9. We recommend providing the details in Step 2 of Sect. 3.1.2 or Step 3 of Sect. 3.1.3 on a tip sheet along with the list of contents in the stool collection kit and study contact information. This tip sheet should be given to the subject along with the stool collection kit and its list of contents, as follows:

a. For microbiome profiling: one tip sheet, one OMNIgene gut stool collection kit (with Category B sticker, paid postage, tracking information, address label), and one pair of gloves.

b. For metabolomic profiling: one tip sheet, one sample receptacle with lid, one collection bracket, one foam cooler with lid, one pair of gloves, seven ice packs, one biohazard-labeled bag containing one heavy-weight absorbent, and one cardboard shipping box (with Category B sticker, paid postage, tracking information, and address label).

10. If a sample cannot be aliquoted immediately upon receipt, label the sample with the de-identified sample ID and store at −80°C. The location of the sample should be recorded in a lab notebook or other secure place for future reference.
11. Wear a lab coat, two layers of gloves, a face mask, and protective glasses. If gloves or other PPE are contaminated during sample processing, change between samples. If sensitive to smell, consider spraying the inside of the facemask with perfume prior to donning.
12. The Prime_GI scripts can be found on Kingfisher's website.
13. Include a 10% volume excess when preparing Binding Bead Mix for multiple samples. Volumes listed here do not include additional coverage.
14. Bead beating tubes should contain both 0.1 mm beads (for lysis of bacterial cells) and 0.5 mm beads (for lysis of fungal cells).
15. An optional step is to use Proteinase K dye to allow for tracking of samples that have already had Proteinase K added. If desired, combine 10 μL of proteinase K dye with 1 mL of Proteinase K in a 1.5 mL tube, and vortex before aliquoting to the samples.
16. If the sample is not sufficiently homogenized in the first round, the tube adaptor should be rotated 180°, and the 3-min homogenization protocol should be repeated.
17. For optimal success with MSS, fecal gDNA should have an A260/280 ratio > 1.7 and an A260/230 ratio > 1.0.
18. A tight band of high molecular weight DNA indicates high integrity, whereas smearing indicates degraded DNA.
19. For gDNA quantification, a fluorescence-based assay (e.g., Qubit) is required for downstream applications such as MSS. Spectrophotometric methods of quantification, such as NanoDrop, are not as accurate, as results can be affected by the detection of single-stranded DNA or other contaminants.
20. Given the high volatility of certain gut metabolites, flash-freezing of fecal specimens and immediate storage at −80°C will ensure the most accurate snapshot of the gut metabolome. Left at room temperature for even several minutes,

the metabolomics profile of the fecal specimen can change drastically.

21. The number of samples processed at once should be limited to the maximum number of samples that can fit into the centrifuge.
22. The fecal matter should break apart after vortexing. If fecal matter does not break apart, the sample should be vortexed again.

Acknowledgments

This work was supported by NIH grants R01 CA231303 (to A.Y.K.) and K24 AI123163 (to A.Y.K.) and the University of Texas Southwestern Medical Center and Children's Health Cellular and ImmunoTherapeutics Program (to A.Y.K.).

Competing Interests The authors have no conflicts of interest to declare that are relevant to the content of this chapter.

References

1. Spor A, Koren O, Ley R (2011) Unravelling the effects of the environment and host genotype on the gut microbiome. Nat Rev Microbiol 9(4):279–290. https://doi.org/10.1038/nrmicro2540
2. Hooper LV, Littman DR, Macpherson AJ (2012) Interactions between the microbiota and the immune system. Science 336(6086):1268–1273. https://doi.org/10.1126/science.1223490
3. Iida N, Dzutsev A, Stewart CA et al (2013) Commensal bacteria control cancer response to therapy by modulating the tumor microenvironment. Science 342(6161):967–970. https://doi.org/10.1126/science.1240527
4. Sivan A, Corrales L, Hubert N et al (2015) Commensal *bifidobacterium* promotes antitumor immunity and facilitates anti-PD-L1 efficacy. Science 350(6264):1084–1089. https://doi.org/10.1126/science.aac4255
5. Vétizou M, Pitt JM, Daillère R et al (2015) Anticancer immunotherapy by CTLA-4 blockade relies on the gut microbiota. Science 350(6264):1079–1084. https://doi.org/10.1126/science.aad1329
6. Frankel AE, Coughlin LA, Kim J et al (2017) Metagenomic shotgun sequencing and unbiased metabolomic profiling identify specific human gut microbiota and metabolites associated with immune checkpoint therapy efficacy in melanoma patients. Neoplasia 19(10):848–855. https://doi.org/10.1016/j.neo.2017.08.004
7. Chaput N, Lepage P, Coutzac C et al (2017) Baseline gut microbiota predicts clinical response and colitis in metastatic melanoma patients treated with ipilimumab. Ann Oncol 28(6):1368–1379. https://doi.org/10.1093/annonc/mdx108
8. Gopalakrishnan V, Spencer CN, Nezi L et al (2018) Gut microbiome modulates response to anti-PD-1 immunotherapy in melanoma patients. Science 359(6371):97–103. https://doi.org/10.1126/science.aan4236
9. Matson V, Fessler J, Bao R et al (2018) The commensal microbiome is associated with anti-PD-1 efficacy in metastatic melanoma patients. Science 359(6371):104–108. https://doi.org/10.1126/science.aao3290
10. Routy B, Le Chatelier E, Derosa L et al (2018) Gut microbiome influences efficacy of PD-1-based immunotherapy against epithelial tumors. Science 359(6371):91–97. https://doi.org/10.1126/science.aan3706
11. Larkin J, Chiarion-Sileni V, Gonzalez R et al (2015) Combined nivolumab and ipilimumab or monotherapy in untreated melanoma. N Engl J Med 373(1):23–34. https://doi.org/10.1056/NEJMoa1504030
12. Mathewson ND, Jenq R, Mathew AV et al (2016) Gut microbiome-derived metabolites

modulate intestinal epithelial cell damage and mitigate graft-versus-host disease. Nat Immunol 17(5):505–513. https://doi.org/10.1038/ni.3400
13. Smith PM, Howitt MR, Panikov N et al (2013) The microbial metabolites, short-chain fatty acids, regulate colonic Treg cell homeostasis. Science 341(6145):569–573. https://doi.org/10.1126/science.1241165
14. Carroll IM, Ringel-Kulka T, Siddle JP et al (2012) Characterization of the fecal microbiota using high-throughput sequencing reveals a stable microbial community during storage. PLoS One 7(10):e46953. https://doi.org/10.1371/journal.pone.0046953
15. Ye SH, Siddle KJ, Park DJ, Sabeti PC (2019) Benchmarking metagenomics tools for taxonomic classification. Cell 178(4):779–794. https://doi.org/10.1016/j.cell.2019.07.010
16. Blanco-Miguez A, Beghini F, Cumbo F et al (2023) Extending and improving metagenomic taxonomic profiling with uncharacterized species using MetaPhlAn 4. Nat Biotechnol 41(11):1633–1644. https://doi.org/10.1038/s41587-023-01688-w
17. Segata N, Waldron L, Ballarini A et al (2012) Metagenomic microbial community profiling using unique clade-specific marker genes. Nat Methods 9(8):811–814. https://doi.org/10.1038/nmeth.2066
18. Abubucker S, Segata N, Goll J et al (2012) Metabolic reconstruction for metagenomic data and its application to the human microbiome. PLoS Comput Biol 8(6):e1002358. https://doi.org/10.1371/journal.pcbi.1002358
19. Franzosa EA, McIver LJ, Rahnavard G et al (2018) Species-level functional profiling of metagenomes and metatranscriptomes. Nat Methods 15(11):962–968. https://doi.org/10.1038/s41592-018-0176-y
20. Kim J, Kim MS, Koh AY et al (2016) FMAP: functional mapping and analysis pipeline for metagenomics and metatranscriptomics studies. BMC Bioinformatics 17(1):420. https://doi.org/10.1186/s12859-016-1278-0
21. Simms-Waldrip TR, Sunkersett G, Coughlin LA et al (2017) Antibiotic-induced depletion of anti-inflammatory Clostridia is associated with the development of graft-versus-host disease in pediatric stem cell transplantation patients. Biol Blood Marrow Transplant 23(5):820–829. https://doi.org/10.1016/j.bbmt.2017.02.004
22. Segata N, Izard J, Waldron L et al (2011) Metagenomic biomarker discovery and explanation. Genome Biol 12(6):R60. https://doi.org/10.1186/gb-2011-12-6-r60
23. Song SJ, Amir A, Metcalf JL et al (2016) Preservation methods differ in fecal microbiome stability, affecting suitability for field studies. mSystems 1(3):e00021–16. https://doi.org/10.1128/mSystems.00021-16



Chapter 32

Assessment of Cell-Free MicroRNA by NGS Whole Transcriptome Analysis in Cutaneous Melanoma Patients' Blood

Kevin D. Tran, Rebecca Gross, Negin Rahimzadeh, Shanthy Chenathukattil, Dave S. B. Hoon and Matias A. Bustos

Abstract

MicroRNAs (miRs) are small RNA molecules (18–22 nucleotides) that regulate the transcriptome at a post-transcriptional level by affecting the expression of specific genes. This regulatory mechanism is critical to maintain cell homeostasis and specific functions. Aberrant expression of miRs has been associated with pathobiological processes, including cancer. There are few technologies available that are able to profile whole-genome miR expression using minimal amounts of blood samples and without the need for time-consuming extraction steps. Here, we describe the HTG EdgeSeq miR Whole Transcriptome Assay (WTA) in serum and plasma samples. To identify specific cell-free miR (cfmiR) patterns, we have first focused on the analysis of normal donor samples and have then compared these to patients with cutaneous melanoma. The identification of specific cfmiR for melanoma patients will allow for better patient surveillance during targeted and/or checkpoint inhibitor immunotherapy (CII) treatment.

Keywords miRNA, Metastatic melanoma, Serum, Plasma, miR Whole Transcriptome Assay

1 Introduction

Metastatic melanoma is a rapidly progressing cancer that can metastasize to distant organs such as the liver, lung, and brain, with an increasing incidence [1–3]. Early detection of melanoma metastasis remains a key factor for treatment decisions such as targeted therapy, checkpoint inhibitor immunotherapy (CII), and radiological or surgical interventions [2, 3]. In the past few years, new CII have significantly improved survival outcomes for metastatic melanoma patients and have become the standard of care [2, 3]. However, there is still a need for biomarker assay development, as this would allow for the evaluation of disease progression in melanoma patients undergoing treatment [2, 3].

Kristian M. Hargadon (ed.), *Melanoma*, Methods in Molecular Biology, vol. 3089,
https://doi.org/10.1007/978-1-0716-5619-8_32,
© The Author(s), under exclusive license to Springer Science+Business Media, LLC, part of Springer Nature 2027

Detection assays of cell-free nucleic acids (cfNA) found in the blood of patients with metastatic cutaneous melanoma have improved in recent years, particularly in circulating cell-free DNA (cfDNA) to target specific mutations [4–6]. However, the detection of cfDNA in the blood is still limited due to degradation. On the contrary, microRNAs (miRs) are short stable RNA molecules (18–22 nucleotides) that can control gene expression post-transcriptionally [7]. Specific miRs are found in both the serum and plasma of cutaneous melanoma patients, as our group and others have demonstrated [8–12].

Several diagnostic and prognostic cfmiRs have been proposed as biomarkers, both individually and in combination, for assessment of cutaneous melanoma patients. However, the specificity of diagnostic and prognostic cfmiRs identified in melanoma and other solid tumors is of major concern. Single cfNA biomarkers are not reliable for detection due to specificity and frequency. This is because most of the cfmiRs are associated with normal physiological functions and/or are associated with other diseases [7]. To increase the specificity of cfmiRs as biomarkers, we focused on the identification of cfmiRs signatures in melanoma patients compared to normal cancer-free blood samples [7–9]. In this regard, we used the HTG WTA probe-based and Next-Generation Sequencing (NGS)-based detection platform. HTG WTA is designed to detect 2083 miRs with minimal sample input requirements, reduced preprocessing isolation steps, and high reproducibility.

Using HTG WTA, we described the profiling of serum and plasma samples taken from normal healthy donors to identify cfmiR signatures, and we have performed a comparative analysis of these signatures with those obtained from melanoma patients. With this approach, we found that specific cfmiRs are differentially expressed (DE) in normal (cancer-free) donor plasma and serum samples (Fig. 1) and that specific cfmiRs are found in plasma samples from

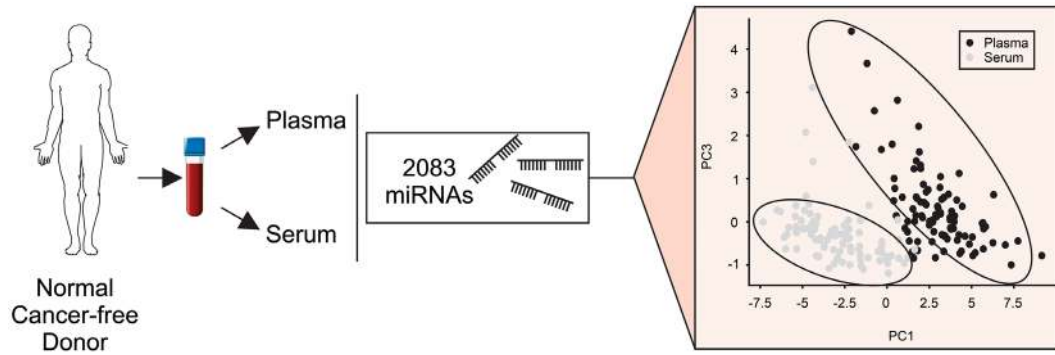
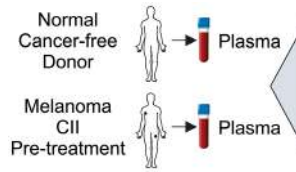


Fig. 1 Comparison of the cfmiR profiles between normal serum and plasma samples. Shown is a principal component analysis (PCA) plot for the top 100 cfmiRs DE in serum compared to plasma samples of normal (cancer-free) donors. The figure shows that the top 100 cfmiRs may distinguish serum from plasma samples in this analysis



Probe	Mean Normalized Pre-CII	Mean Normalized Normal	Fold Change Pre-CII vs Normal	Adj p-value
miR-6816-3p	615	46	12.64	1.68E-83
miR-1234-3p	594	76	7.57	4.02E-52
miR-662	277	44	6.06	1.45E-51
miR-4745-3p	1813	112	14.87	2.58E-51
miR-4649-3p	141	16	8.60	1.74E-42

Fig. 2 cfmiRs serve as markers for cutaneous melanoma treatment. The top five differentially expressed cfmiRs in pretreatment samples of melanoma patients receiving CII compared to plasma samples of normal (cancer-free) healthy donors. This is a list of cfmiRs that were found DE in the pretreatment plasma samples of melanoma patients receiving CII. The approach described herein will allow evaluation of these cfmiRs over time and may identify cfmiR biomarkers that can be used to monitor therapeutic efficacy and tumor response during the course of treatment

pretreatment melanoma patients receiving CII treatment when compared to plasma samples obtained from normal (cancer-free) donors (Fig. 2). This technology may therefore lead to the identification of cfmiR biomarkers that can be evaluated over time to monitor therapeutic efficacy and tumor response during the course of treatment.

2 Materials

2.1 Serum Isolation

1. Corvac™ red/grey mottled stopper serum separator tubes (referred to as tiger-top tubes).
2. BD Vacutainer™ Venous Blood Collection Tubes: SST™ Serum Separation Tubes: Conventional Stopper (referred to as redtop tubes).
3. Serum Filter Fisherbrand™ 16 mm OD X 2-3/4 Inch.
4. 2 ml transfer pipettes.
5. 2 ml sterile cryovials.

2.2 Plasma Isolation

1. BD Vacutainer™ Glass Blood Collection Tubes: Buffered Sodium Citrate (referred to as blue-top tubes).
2. 15 ml conical polypropylene centrifuge tubes.
3. Glass or plastic transfer pipettes.
4. 2 ml sterile cryovials.

2.3 Library Preparation and Cleanup

1. HTG EdgeSeq instrument (HTG Molecular).
2. HTG Edge System software (HTG Molecular).
3. HTG EdgeSeq miRNA sample prep pack containing biofluids lysis buffer, plasma lysis buffer, and proteinase K (HTG Molecular).
4. HTG EdgeSeq assay reagent pack and HTG EdgeSeq plate pack containing sample plate and stop plate (HTG Molecular).

5. Pipette tip pack.
6. Parafilm®.
7. Human brain total RNA.
8. 10 mM dNTP.
9. Hemo Klentaq® reaction buffer (5×): When diluted to 1× with other reaction reagents, this buffer contains 60 mM Tricine, 5 mM $(NH_4)_2SO_4$, 3.5 mM $MgCL_2$, 6% glycerol, and pH 8.7 (at 25°C).
10. Hemo Klentaq® DNA polymerase.
11. Molecular biology grade water.
12. HTG EdgeSeq sequencing tag pack containing forward and reverse primers (HTG Molecular).
13. AMPure XP beads.
14. DynaMag™-96 Side Skirted magnet.
15. 200 proof ethanol.
16. 10 mM Tris-HCl buffer, pH 8.0.
17. 1.5 ml LoBind tubes.
18. Twin.tec® PCR plate 96, unskirted, clear.
19. Microseal "B" seal.
20. T100™ Thermal cycler or any modern equivalent thermal cycler.
21. Orbital shaker with planar mixing orbit for 1.5 ml centrifuge tubes.

2.4 Library Quality Check

1. High Sensitivity (HS) D1000 ScreenTape.
2. HS D1000 sample buffer (Agilent Technologies Inc., proprietary buffer).
3. HS D1000 DNA ladder.
4. 2200 TapeStation Instrument (Agilent Technologies Inc.).
5. 8-strip optical tube.
6. 8-strip optical Cap.
7. Loading tips (1 pk).
8. KAPA library Quant kit (Illumina) universal qPCR mix kit.
9. Multiplate® PCR plates™ 96-well.
10. Tween 20.
11. 1 M Tris-HCl buffer, pH 8.0.
12. DNA dilution buffer: 10 mM Tris-HCl, pH 8.0 + 0.05% Tween 20.
13. Thermocycler Real-Time PCR Detection System.

2.5 Next-Generation Sequencing

1. HTG EdgeSeq Library Calculator Input Template (HTG Molecular).
2. HTG EdgeSeq RUO Library Calculator (HTG Molecular).
3. MiSeq™ instrument (Illumina).
4. NextSeq™ 550 instrument (Illumina).
5. MiSeq® V3 (150 Cycle) kit (Illumina).
6. NextSeq 500/550 Mid Output kit v2.5 (75 cycles) (Illumina).
7. NextSeq Accessory Box v2 (Illumina).
8. *PhiX* Control v3 Library (Illumina).
9. 10 mM Tris-HCl buffer, pH 8.5.
10. 200 mM Tris-HCl buffer, pH 7.0.
11. 2 N NaOH.
12. 2 N HCl.
13. HTG EdgeSeq ILM Seq primer kit containing ILM MiSeq primer, HTG ILM NextSeq Index primer, and ILM NextSeq Read1 primer (HTG Molecular).
14. HTG EdgeSeq Parser software (HTG Molecular).

3 Methods

3.1 Serum Isolation

1. Collect blood in tiger-top tubes, and centrifuge at 1300 × *g* at room temperature (RT) for 10 min (*see* **Notes 1 and 2**). Proceed to Step 7.
2. Collect blood in redtop tube. Remove the redtop cap while keeping the 7 ml vacutainer inside the sterile biological safety cabinet. Discard the redtop cap.
3. Using a transfer pipette, transfer serum from the spun-down serum separator tube to the 7 ml redtop vacutainer. Avoid poking the gel layer with the transfer pipette.
4. Discard the transfer pipette and serum separator tube.
5. Obtain a serum filter. Avoid touching the bottom filter portion.
6. Insert the serum filter into the 7 ml vacutainer, and push it down without covering the entire mouth of the serum filter. Be careful not to overflow the serum filter.
7. Use a new transfer pipette to transfer the filtered serum from the serum filter (or serum for tiger top tubes) to a 2 ml sterile cryovial (*see* **Note 3**).
8. Discard the serum filter, 7 ml vacutainer, and transfer pipette.
9. Store all 2 ml serum cryovials at −80°C for long-term storage.

3.2 Plasma Isolation

1. Centrifuge the bluetop tube at 1300 × *g* for 10 min at RT (*see* **Note 2**).
2. Gently remove the bluetop tube from the centrifuge to a tube rack.
3. Slowly transfer the plasma from the bluetop tube to a 15 ml conical polypropylene centrifuge tube (*see* **Note 4**).
4. Centrifuge the 15 ml conical centrifuge tube containing plasma at 1300 × *g* for 10 min at RT (*see* **Note 2**).
5. Transfer the clarified plasma from the 15 ml conical centrifuge tube to a 2 ml sterile cryovial.
6. Store all 2 ml plasma cryovials at −80°C.

3.3 Library Preparation and Cleanup

1. Remove cryovials from freezer. Thaw isolated serum/plasma on ice until completely defrosted. Pipette to mix the samples thoroughly to obtain a homogenous sample (*see* **Notes 5 and 6**).
2. Thaw biofluids lysis buffer (for serum) and/or plasma lysis buffer (for plasma) by placing the tubes on a 50°C heat block for 30 min to ensure complete solubility of any buffer precipitates.
3. Aliquot 15 µl of serum/plasma into a separate 1.5 ml LoBind tube.
4. Prepare to lyse the samples by adding 15 µl of biofluids lysis buffer or plasma lysis buffer into each serum or plasma sample, respectively. Add 3 µl of proteinase K to each sample and pipette to mix thoroughly. Quick spin for 5 s to collect the residual lysis buffer at the bottom of the tube.
5. Lyse the samples by incubating on a preheated 50°C orbital shaker set to 500 rpm for 3 h (*see* **Note 7**).
6. Aliquot 25 µl of lysate per well into an HTG sample plate (*see* **Note 8**). Load the HTG EdgeSeq Instrument with sample plate, stop plate, HTG WTA reagent cartridge, and pipette tips according to the schematic provided by the HTG Edge System software. Initiate the run according to the HTG EdgeSeq user manual. Allow the HTG WTA to perform automated probe capture for 20 h.
7. Following the 20-h processing period, remove the samples now located in the stop plate. Store the samples at −20°C until they are ready for library preparation, or move onto library preparation steps immediately (*see* **Note 9**). Clean the instrument according to the HTG EdgeSeq User Manual.
8. Carefully mix samples in the stop plate with a pipette set to 10 µl to obtain a homogenous aqueous mixture (*see* **Note 10**).

9. Prepare the PCR mixture on ice in a twin.tec® PCR plate using 21 µl of master mix (0.6 µl of 10 mM dNTP, 6 µl of 5× Hemo *Klentaq*® Reaction buffer, 2.4 µl of Hemo *Klentaq*® DNA Polymerase, and 12 µl of molecular biology grade water), 6 µl of primers from HTG EdgeSeq sequencing tag pack (3 µl of forward primer, 3 µl of reverse primer), and 3 µl of sample (*see* **Note 11**). Seal plate with a Microseal® 'B' seal.
10. On a preheated thermal cycler, run PCR using the following settings:
    a. 95°C for 4 min.
    b. 95°C for 15 s, 56°C for 45 s, 68°C for 45 s (repeat for 16 total cycles).
    c. 68°C for 10 min.
    d. Hold at 4°C.
11. Perform library cleanup by thoroughly pipetting to mix 37.5 µl of AMPure XP beads with 15 µl of PCR-amplified libraries in a new twin.tec PCR Plate. Incubate for 5 min at RT.
12. In the meantime, prepare 400 µl of 80% ethanol per sample (*see* **Note 12**).
13. Place plate on a DynaMag™ 96 Side Skirted Magnet for 2 min or until the supernatant becomes completely clear.
14. While still on the magnetic plate, remove supernatant without disturbing the library-bound beads, and add 200 µl of 80% ethanol to wash. Incubate at RT for 30 s (*see* **Note 13**).
15. Repeat 80% ethanol wash for a total of two washes.
16. Remove supernatant (ethanol) and let the beads dry on the magnet for 2 min (*see* **Note 14**).
17. Remove the plate from the magnet, and thoroughly resuspend the beads with 40 µl of 10 mM Tris-HCl, pH 8.0 to elute libraries.
18. Incubate at RT for 2 min.
19. Place the plate back on the magnet for 2 min or until the supernatant becomes completely clear.
20. Without disturbing the beads, transfer the supernatant (containing libraries) to a new plate (*see* **Note 15**).
21. Store at −20°C for up to 2 weeks, or −80°C for longer storage until ready to sequence.

3.4 Library Quality Check

1. Perform library fragment-size analysis by first allowing the Agilent HS D1000 Screentape and reagents to equilibrate to RT for 30 min. Vortex and quick spin the Agilent HS D1000 sample buffer and HS D1000 DNA ladder for at least 5 s.

2. Pipette and mix 2 µl of each library and 2 µl of sample buffer into each well of the 8-strip optical tube. Briefly vortex and quick spin for 5 s.
3. Load Agilent 2200 TapeStation Instrument with 8-strip tubes, loading tips, and equilibrated HS D1000 ScreenTape. Initialize the instrument program as specified in the Agilent 2200 TapeStation System User Manual.
4. Confirm the library fragment size is between 150 and 170 base pairs (bp).
5. To quantitate the libraries, perform qPCR with the KAPA Library Quant kit Universal qPCR mix kit.
6. Thaw Universal qPCR master mix and standards in a 4°C refrigerator (*see* **Note 16**).
7. Prepare 30 ml of DNA dilution buffer (10 mM Tris-HCl, pH 8.0 + 0.05% Tween 20) by mixing 29.55 ml of molecular-grade water, 300 µl of 1 M Tris-HCl, pH 8.0, and 150 µl of 10% Tween 20 (*see* **Note 17**).
8. Prepare a 10,000× dilution series for each sample by diluting the samples by 100× (2 µl of sample + 198 µl of DNA dilution buffer) twice in a twin.tec PCR plate. Carefully mix the samples in between dilutions.
9. Prepare 16 µl of master mix (12 µl of qPCR master mix and 4 µl of molecular-grade water) per sample, standard, and non-template control (NTC, negative control) (*see* **Note 18**).
10. Aliquot 16 µl of master mix into each well of the Multiplate® PCR plates™. Add 4 µl of the respective sample [library, standard, or DNA dilution buffer (NTC)] into respective wells.
11. Perform qPCR under the following conditions:
    a. 95°C for 5 min.
    b. 95°C for 30 s, 60°C for 45 s (repeat for 35 total cycles).

3.5 Library Normalization, Pooling, and Next-Generation Sequencing

1. Remove MiSeq® V3 (150 Cycle) kit or NextSeq 500/550 Mid Output kit v2.5 (75 cycles) from −20°C storage, and place reagent cartridge and HT1 buffer in a water bath at RT to thaw before beginning preparations for NGS (*see* **Note 19**). Remove HTG ILM MiSeq primer (MiSeq) or HTG ILM NextSeq index primer and ILM NextSeq Read1 primer (NextSeq) to thaw on ice.
2. Fill out the HTG EdgeSeq Library Calculator Input Template with the sample concentrations as determined by the qPCR results. Select the correct sequencing instrument (MiSeq or NextSeq), and input the intended final loading concentration into the HTG EdgeSeq RUO Library Calculator software. Upload the input template into the software, and generate the pooling and denaturing protocol.

3. Quantitated libraries are diluted, normalized, pooled, and denatured according to the protocol generated by the HTG EdgeSeq RUO Library Calculator software. The following steps are performed with calculated volumes provided in the protocol generated by the HTG EdgeSeq RUO Library Calculator software.
4. Dilute libraries with 10 mM Tris-HCl, pH 8.5.
5. Pool diluted libraries together.
6. Denature the normalized pool of libraries with 2 N NaOH for 8 min at RT.
7. Add cold HT1 buffer. Invert the tube to mix.
8. Neutralize the NaOH with 2 N HCl. Vortex to mix well and quickly spin for 5 s.
9. Dilute and denature stock *PhiX* Control v3 libraries by adding 5 µl of 0.2 N NaOH to 5 µl of 4 nM *PhiX*. Vortex to mix, and quick spin for 5 s.
10. Incubate at RT for 5 min.
11. Add 5 µl of 200 mM Tris-HCl, pH 7.0 to neutralize the NaOH.
12. Dilute *PhiX* to 20 pM by adding 985 µl of prechilled HT1 buffer (*see* **Note 20**).
13. Dilute 20 pM *PhiX* to 12.5 pM by adding 32.5 µl of 20 pM *PhiX* to 19.5 µl of HT1 buffer.
14. Spike denatured libraries with 12.5 pM *PhiX* control libraries at the volume specified by the HTG-generated protocol.
15. Heat denature pooled libraries and *PhiX* at 98°C for 4 min.
16. Immediately chill on ice for a minimum of 5 min.
17. Load the entire denatured library pool and custom primer into the reagent cartridges of the respective MiSeq® V3 (150 Cycle) kit or NextSeq 500/550 Mid Output kit v2.5 (75 cycles) as instructed in the HTG user manual (*see* **Note 21**).
18. Load sequencer as instructed in the respective Illumina system guide (*see* **Notes 22 and 23**).
19. After sequencing, generate FASTQ files by uploading the sequencing run files and sample sheet into the Illumina Local Run Manager module (*see* **Note 24**).
20. Upload FASTQ files and sample sheet (*see* **Note 23**) into the HTG EdgeSeq Parser software, and begin parsing and alignment. Save the generated.xls file, which includes the final counts for 2083 miRs per sample, for use in downstream data analysis.

3.6 Data Analysis

Data analysis will depend on the specific needs and experimental goals of the user. In general, though, data analysis for the sequenced miRs includes the following steps: (1) raw data processing and quality check, (2) mapping miRs to 2083 reference miRs, (3) acquiring read counts for each miR respectively, (4) identification of DE miRs, and (5) performing exploratory analysis for comparisons of DE miRs. The HTG platform accounts for the first four steps of this analysis. Exploratory analysis using datasets obtained from the HTG Reveal software can be performed in the interactive platform Jupyter (https://jupyter.org). Some of the python libraries/packages used for this analysis include scikit-learn (https://scikit-learn.org/) for data classification; Matplotlib (https://matplotlib.org/) for generating 2D plots; Seaborn (https://seaborn.pydata.org/) for creating hierarchically clustered heatmaps; NumPy (https://numpy.org/); and SciPy (https://www.scipy.org/) for statistical analysis.

4 Notes

1. Allow blood specimens to sit for 1 h at RT before processing them for serum isolation. Process blood under a clean HEPA-filtered laboratory hood (BSL2 or higher level) to avoid contamination.
2. During centrifugation, label cryovials with the specimen number, protocol ID, and the date the blood was drawn.
3. Cap tightly, and do not exceed the 1.8 ml volume of each cryovial.
4. Avoid disturbing/pipetting the solid blood layer near the top surface of the plasma.
5. Turn on and set up the HTG Instrument according to the HTG EdgeSeq user manual before processing the blood specimens.
6. Designate the human brain total RNA as the experimental positive control. Leave one well empty on the sample plate to load the positive control.
7. A heat block can be used instead of the orbital shaker, but samples must be mixed every hour.
8. There are three formats of HTG plates (8-, 24-, or 96-well sample plates), and selection is made according to the number of samples.
9. Take care not to invert the stop plate. If done, it will spill the samples and risk cross-contamination. If storing at −20°C, parafilm the lid to prevent frost from entering the plate.

10. The HTG EdgeSeq instrument performs a denaturation oil overlay on the samples in the stop plate. Mix the samples while taking care to avoid aspirating the oil overlay. Mixing the oil into the aqueous sample may inhibit downstream PCR amplification.
11. Arrange forward and reverse primers to ensure unique barcode combinations for each sample. For example, for 24 samples, 3 forward × 8 reverse primers allow for 24 unique forward–reverse primer combinations.
12. Prepare extra ethanol accounting for pipetting errors to ensure there is enough for all samples, including the standard and NTC.
13. Use a multichannel pipette when working with more than 8 samples at a time to prevent the beads from drying while working.
14. Do not allow beads to over-dry. Look for a matte finish on the beads. Cracks are indicative of over-drying and will lead to lower library yields.
15. Use a 20 µl pipette to reduce bead carryover.
16. Add 1 ml of 10× primer mix to 5 ml of qPCR master mix upon first use of the qPCR with the KAPA Library Quant kit Universal qPCR mix kit. Also, the qPCR master mix is light-sensitive.
17. Prepare 10% Tween 20 by diluting 15 µl of stock Tween 20 with 135 µl of molecular-grade water.
18. Perform qPCR on samples, standards, and NTC in at least duplicates.
19. For 24 samples, use MiSeq™ instrument and reagents. For 96 samples, use NextSeq™ 550 instrument. For NextSeq kits, HT1 buffer is provided in the NextSeq accessory box v2.
20. 20 pM denatured *PhiX* may be stored at −20°C for up to 2 weeks. Save and store extra *PhiX* for other HTG WTA sequencing runs. *PhiX* is the positive sequencing control.
21. For MiSeq runs, load custom primer ILM MiSeq primer. For NextSeq runs, load HTG ILM NextSeq index primer and ILM NextSeq Read1 primer.
22. Set-up sequencing parameters to be 1 × 50 bp read length for either instrument. MiSeq® V3 kit (150 cycle) is the lowest cycle kit validated with HTG WTA.
23. The sample sheet for either the MiSeq or NextSeq runs is located in the "Reports" tab of the HTG Edge System software. This sample sheet may be used for setting up MiSeq (required) or NextSeq (optional) runs.

24. The MiSeq™ instrument has automatic FASTQ generation. Local Run Manager is only required for NextSeq sequencing. Alternatively, if the user has an Illumina BaseSpace account, FASTQ generation may occur automatically for NextSeq runs.

Acknowledgments

The authors thank the Department of Translational Molecular Medicine staff at JWCI for their kind advisory and technical assistance. This work was supported by Dr Miriam and Sheldon G. Adelson Medical Research Foundation to DSBH, Gonda Foundation to DSBH, and Rosalie and Harold Brown Foundation to MAB.

Competing Interests The authors have no conflicts of interest to declare that are relevant to the content of this chapter.

References

1. Siegel RL, Kratzer TB, Wagle NS et al (2026) Cancer statistics, 2026. CA Cancer J Clin 76(1):e70043. https://doi.org/10.3322/caac.70043
2. Weiss SA, Wolchok JD, Sznol M (2019) Immunotherapy of melanoma: facts and hopes. Clin Cancer Res 25(17):5191–5201. https://doi.org/10.1158/1078-0432.Ccr-18-1550
3. Knight A, Karapetyan L, Kirkwood JM (2023) Immunotherapy in melanoma: recent advances and future directions. Cancers 15(4):1106. https://doi.org/10.3390/cancers15041106
4. Charbel N, Rizkallah J, Bal MN et al (2026) Circulating tumor DNA in melanoma: advances in detection, clinical applications, and integration with emerging technologies. Int J Mol Sci 27(3):1569. https://doi.org/10.3390/ijms27031569
5. Lin SY, Chang SC, Lam S et al (2020) Prospective molecular profiling of circulating tumor cells from patients with melanoma receiving combinatorial immunotherapy. Clin Chem 66(1):169–177. https://doi.org/10.1373/clinchem.2019.307140
6. Lanidou E, Hoon D (2018) Circulating tumor cells and circulating tumor DNA as a real time liquid biopsy approach. In: Wittner C, Rafai N, Horvath R (eds) Tietz textbook of clinical chemistry and molecular diagnostics, 6th edn. Elsevier, St. Louis, MO, pp 1145–1155
7. Mumford SL, Towler BP, Pashler AL et al (2018) Circulating microRNA biomarkers in melanoma: tools and challenges in personalised medicine. Biomolecules 8(2):21. https://doi.org/10.3390/biom8020021
8. Bustos MA, Tran KD, Rahimzadeh N et al (2020) Integrated assessment of circulating cell-free microRNA signatures in plasma of patients with melanoma brain metastasis. Cancers 12(6):1692. https://doi.org/10.3390/cancers12061692
9. Bustos MA, Gross R, Rahimzadeh N et al (2020) A pilot study comparing the efficacy of lactate dehydrogenase levels versus circulating cell-free microRNAs in monitoring responses to checkpoint inhibitor immunotherapy in metastatic melanoma patients. Cancers 12(11):3361. https://doi.org/10.3390/cancers12113361
10. Van Laar R, Lincoln M, Van Laar B (2018) Development and validation of a plasma-based melanoma biomarker suitable for clinical use. Br J Cancer 118(6):857–866. https://doi.org/10.1038/bjc.2017.477
11. Fleming NH, Zhong J, da Silva IP et al (2015) Serum-based miRNAs in the prediction and detection of recurrence in melanoma patients. Cancer 121(1):51–59. https://doi.org/10.1002/cncr.28981
12. Leidinger P, Keller A, Borries A et al (2010) High-throughput miRNA profiling of human melanoma blood samples. BMC Cancer 10:262. https://doi.org/10.1186/1471-2407-10-262



Chapter 33

High-Throughput Identification of miRNA–Target Interactions in Melanoma Using miR-CATCHv2.0

Andrea Marranci, Romina D'Aurizio, Milena Rizzo, Catherine M. Greene and Laura Poliseno

Abstract

MicroRNAs (miRNAs) have the potential to regulate the expression of nearly every transcript in the cell, making the identification of miRNA–mRNA target interactions crucial for understanding their role in diverse biological processes. However, the identification of the miRNAs that regulate a given mRNA remains a challenge. Here, we describe miR-CATCHv2.0, an innovative method for the high-throughput identification of the miRNAs physically interacting with an mRNA of interest. We further highlight how miR-CATCHv2.0 overcomes key limitations of both current computational predictions and existing experimental strategies, enabling a more accurate and comprehensive characterization of physiologically relevant miRNA–mRNA interactions.

Keywords MicroRNAs, microRNA–target interaction, Post-transcriptional regulation, High-throughput

1 Introduction

Post-transcriptional regulation of mRNAs is a fundamental mechanism in every cellular process and is largely mediated by noncoding RNAs, particularly microRNAs (miRNAs) [1] and RNA-binding proteins (RBPs) [2]. miRNAs are endogenous, short, single-stranded noncoding RNAs (21–25 nt) that bind to their target mRNAs through sequence complementarity and recruit proteins, including Argonaute, to form the RNA-induced silencing complex (RISC), which inhibits translation of the target mRNAs. In the vast majority of cases, miRNAs inhibit protein production by translational repression or mRNA degradation [3], though in some cases they can sustain their target expression by inducing RNA stability or translation [4, 5].

Since their discovery in the late 1990s, an increasing amount of experimental evidence has clearly established that miRNAs are involved in several cellular processes and, as a consequence, that

Kristian M. Hargadon (ed.), *Melanoma*, Methods in Molecular Biology, vol. 3089,
https://doi.org/10.1007/978-1-0716-5619-8_33,
© The Author(s), under exclusive license to Springer Science+Business Media, LLC, part of Springer Nature 2027

their deregulation is associated with different diseases, including melanoma [6] and other cancers [7–9]. In cancer, miRNAs have been reported to regulate the expression of both tumor-suppressor genes and oncogenes, thus acting as oncogenes or tumor suppressors themselves. Through this regulation, they modulate crucial phenotypes such as proliferation, cell death, and invasion [10]. Moreover, miRNAs represent important tools in diagnostics, monitoring, and therapeutics [11, 12].

The identification of miRNA-target interactions is a prerequisite for a full understanding of their biological role in the cell and, despite the advancements of recent years, remains a challenging issue [13, 14]. Computational prediction tools, based on seed sequence complementarity, thermodynamic stability, structural accessibility, and evolutionary conservation, are widely used and easily scalable [15, 16]. However, these approaches are limited by high false-positive rates (25%–70%) and may fail to catch some true noncanonical or context-specific interactions that do not follow the algorithmic "rules" [15, 17]. For this reason, experimental approaches can directly identify miRNAs physically bound to an RNA of interest and overcome the limitations of these in silico approaches.

Several experimental approaches have been developed to investigate miRNA–mRNA interactions and can be broadly divided into global and mRNA-target-centered strategies. Global methods, based on Argonaute cross-linking and immunoprecipitation (CLIP)—including HITS-CLIP, PAR-CLIP, iCLIP, and enhanced CLIP (eCLIP) [18–20]—enable transcriptome-wide mapping of RISC binding sites. Ligation-based techniques such as CLASH [21] and CLEAR-CLIP [22] further allow the identification of chimeric miRNA–mRNA hybrids, providing direct evidence of physical interactions. Although these approaches offer high-throughput, genome-wide resolution, they are not specifically tailored to study interactions associated with a single transcript of interest.

mRNA-centered methods for studying miRNA–mRNA interactions can be divided into two main strategies: (1) overexpression or exogenous administration of the RNA target as a bait for miRNAs, and (2) capture of endogenous mRNAs along with their bound miRNAs. In the first strategy, the transcript of interest—typically the 3'UTR—is fused to MS2 RNA hairpin motifs [23, 24] or introduced as a 3'-end biotinylated molecule [25], allowing selective isolation of associated miRNAs. While highly effective, these approaches rely on ectopic expression, which may alter the transcript's physiological regulation. The second strategy targets endogenous mRNAs without perturbing their natural expression. The miR-CATCH technique [26–32] uses biotinylated oligonucleotide probes complementary to the target mRNA to selectively pull it down along with associated miRNAs, providing a faithful representation of physiologically relevant interactions.

Here, we describe the technique miR-CATCHv2.0 that was coupled with small-RNA sequencing [33, 34] and used for the first time in melanoma to identify miRNA regulators of the *BRAF-X1* transcript isoform [35, 36] and has since been successfully used in other contexts [37]. This innovative upgrade of the miR-CATCH approach takes advantage of a cross-linking step, RNA fragmentation by sonication, and two sets of biotinylated tiling probes (ODD and EVEN), resulting in strong enrichment of target-related miRNAs for subsequent identification by small-RNA sequencing. Besides providing a detailed step-by-step description of the miR-CATCHv2.0 procedure, this chapter provides an *ad hoc* analytical workflow for processing sequencing data and describes several molecular assays for validating the microRNA-mediated regulation of the transcript of interest.

2 Materials

2.1 Materials for miR-CATCHv2.0 Protocol

For all buffer preparations, use concentrated stock solutions. Treat water and concentrated stock solutions (Tris-HCl and NaCl) with diethyl pyrocarbonate (DEPC) to neutralize RNAse (*see* **Note 1**), then use those solutions for buffer preparation.

1. 1% formaldehyde solution in PBS. Always prepare fresh from paraformaldehyde powder (*see* **Note 2**).
2. 1.25 M glycine solution in PBS.
3. 3' biotinylated DNA probes (3' BIOTEG oligos).
4. Basic Local Alignment Search Tool (BLAST), available at https://blast.ncbi.nlm.nih.gov.
5. ChIRP Probe Designer software, available at https://www.biosearchtech.com/chirpdesigner.
6. Hybridization Buffer: 750 mM NaCl; 1% sodium dodecyl sulfate (SDS); 50 mM Tris-HCl, pH 7.0; 1 mM EDTA; 15% formamide. Treat concentrated NaCl stock solution and water with DEPC to neutralize RNAse (*see* **Note 1**), then use those solutions for buffer. Adjust pH before adding EDTA and SDS. Supplement buffer just before use by adding fresh formamide, 1 mM PMSF, 1× protease inhibitor cocktail, and 80 U/ml RNasin.
7. Lysis Buffer: 50 mM Tris-HCl, pH 7.0; 5 mM EDTA; 1% SDS. Adjust pH before adding EDTA and SDS. To make complete Lysis Buffer from this unsupplemented Lysis Buffer, add 1 mM phenylmethylsulfonyl fluoride (PMSF), 1× protease inhibitor cocktail, and 80 U/ml of RNasin fresh before use where required.

8. Magnet.
9. mfold Web Server, available at http://unafold.rna.albany.edu/?q=mfold.
10. Proteinase K Buffer: 100 mM NaCl; 10 mM Tris-HCl, pH 7.0; 1 mM EDTA; 0.5% SDS. Follow the recommendation stated above for preparation.
11. Proteinase K.
12. Sonicator.
13. Streptavidin magnetic beads (i.e., Dynabeads MyOne Streptavidin C1).
14. Supplies for cell culture.
15. TE Buffer: 1 mM EDTA, pH 8.0; 10 mM Tris-Cl, pH 8.0.
16. Wash Buffer: 2× Saline Sodium Citrate (SSC) Buffer; 0.5% SDS. Dilute commercially available SSC buffer stock solution with DEPC water, and add SDS. Add 1 mM PMSF before use.

2.2 Materials for Small-RNAseq (Library Construction and Sequencing)

1. Mini-Protean® (MP) apparatus (BIO-RAD).
2. 5% MP TBE gel—50 µl (BIO-RAD) (*see* **Note 3**).
3. Bioanalyzer 2100 (Agilent).
4. General lab supplies.
5. High Sensitivity DNA Kit (Agilent).
6. Kapa Library Quantification Kit (Roche).
7. MiSeq sequencer (Illumina).
8. MiSeqReagent Kit V3 150 cycle (Illumina).
9. Nanosep MF centrifugal device with GHP membrane and 0.45 µm pore size (PALL Life Science) (*see* **Note 3**).
10. PhiXControl V3 Kit (Illumina).
11. SuperScript II Reverse Transcriptase (Thermo Fisher Scientific).
12. T4 RNA Ligase 2, Deletion Mutant (Epicentre, Lucigen).
13. TruSeq® Small RNA Library preparation kit (Illumina).

2.3 Hardware and Software for Bioinformatic Analysis

As prerequisites, a computer running an UNIX-based operating system with at least 4 GB of RAM is needed, with the following installed software:

1. SAMtools, which can be downloaded at https://www.htslib.org/download/.
2. Burrows-Wheeler Aligner (BWA), available at http://bio-bwa.sourceforge.net.

3. R, which can be downloaded at CRAN (https://cran.r-project.org) and, eventually, RStudio [38], the open-source integrated development environment (IDE) for R.

2.4 Materials for miRNA Validation Assays

1. Actinomycin D.
2. Anti-HA Sepharose beads.
3. Dual-Glo® Luciferase Assay System.
4. Luminometer.
5. Lipofectamine 2000 transfection reagent.
6. miRNA mimics.
7. miRNeasy Micro Kit (Qiagen).
8. NT2 Buffer: 50 mM Tris-HCl, pH 7.5; 150 mM NaCl; 1 mM $MgCl_2$; 0.05% NP-40. Follow the recommendations for buffer preparation stated above. When required, supplement the base buffer to make complete NT2 Buffer by adding Protease Inhibitor Cocktail, RNAse OUT (RNAse inhibitor), and 10 mM DTT prior to use.
9. pMIR-report Vector.
10. pMS2 Vector.
11. pMS2-BP Vector.
12. Polyethylenimine (PEI) transfection reagent.
13. Polysome Buffer: 20 mM Tris-HCl, pH 7.5; 100 mM KCl; 5 mM $MgCl_2$; 0.5% NP-40. Follow the recommendations for buffer preparation stated above. Prior to use, supplement the base buffer to make a complete polysome buffer by adding a Protease Inhibitor Cocktail, RNAse OUT (RNAse inhibitor), and 10 mM dithiothreitol (DTT).
14. Bradford protein assay kit.
15. pRL-TK Vector.
16. qRT-PCR primers, including those for Firefly and Renilla Luciferase mRNAs:
    a. Firefly Forward primer (5'-3'): CCCGCCGCCGTTGTTGTTTTGG
    b. Firefly Reverse primer (5'-3'): CGCGCAACTTTTTCGCGGTTGT
    c. Renilla Forward primer (5'-3'): GAAAGTGAAGGGCCTGCACTTC
    d. Renilla reverse primer (5'-3'): CACTGCTCGTTCTTCAGCACCC
17. QuantiTect Reverse Transcription Kit (Qiagen).
18. QuikChange II Site-directed Mutagenesis Kit (Agilent).

19. Restriction enzymes for cloning.
20. Trizol.

3 Methods

For all steps of the miR-CATCHv2.0 protocol, refer to the schematic representation in Fig. 1.

3.1 miR-CATCHv2.0

3.1.1 Probe Design and Preparation

Before starting with probe design, investigators should check carefully the length, sequence, and expression of the RNA target that they wish to study in their biological system (*see* **Note 4**).

1. Design probes for the capture of the RNA of interest using the ChIRP Probe Designer online software. Probes should be 20 nt long and designed to specifically target loci every ~100 nt along the transcript (Fig. 1a, b).
2. Check the probes to avoid using those that show noticeable matches to off-target genes, using BLAST to evaluate complementarity against the genome of interest.
3. Avoid probes that form thermodynamically stable self-dimers, which can be assessed using the mfold Web Server.
4. Design probes to have an extended spacer arm (triethyleneglycol) plus a biotin (Biotin-TEG) molecule at their 3' ends (many companies can synthesize ready-to-use oligos with this functionalization).
5. Once ordered, resuspend lyophilized probes in TE buffer following the manufacturer's instructions. Pool the *Odd* |probes and pool the *Even* probes, bringing each probe set to a 100 μM final concentration.

3.1.2 Cross-Linking

1. Harvest 1×10^7 cells into a 50 ml tube, and wash once with PBS (depending on the morphology and on the availability of the cells, a lower number can be used) (Fig. 1c). Harvest also the same amount of cells for a pellet to be used as a baseline (precapture sample for a total miRNome or further qRT-PCR analyses).
2. Prepare 10 ml of fresh 1% formaldehyde in PBS from paraformaldehyde powder (*see* **Note 2**).
3. Centrifuge the cells, and resuspend the pellet with 10 ml of 1% formaldehyde in PBS. Incubate the tube on a shaker for 10 min at room temperature.
4. Quench the reaction by adding 1 ml of 1.25 M glycine solution, and incubate for 5 minutes at room temperature.

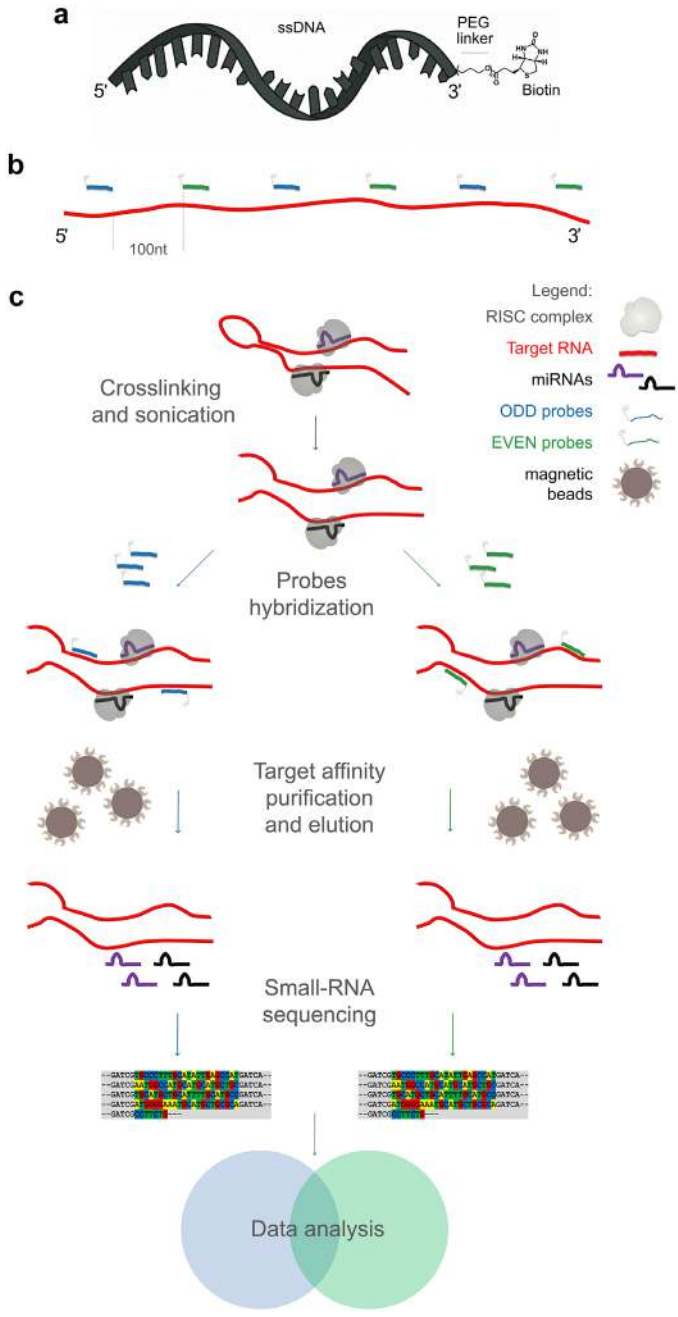


Fig. 1 miR-CATCHv2.0 experimental protocol. **a** Schematic illustration of 3' biotinylated DNA probes (3' BIOTEG oligos). **b** Schematic representation of antisense biotinylated tiling probe location in reference to target RNA sequence. Probes are located approximately 100 nt apart along the target sequence and are pooled into "ODD" and "EVEN" sets based on their position. **c** Workflow of miR-CATCHv2.0 protocol. Cells are cross-linked and lysed by sonication to obtain RNA fragmentation. ODD probes and EVEN probes are used for independent target RNA captures. miRNA:target complexes are purified using magnetic streptavidin beads, and, after stringent washes, RNA is eluted and processed for small RNA-seq

5. Centrifuge at 2000 × *g* for 5 min at 4°C. Discard supernatant.
6. Resuspend the pellet with 50 ml of ice-cold PBS, and centrifuge at 2000 × *g* for 5 min at 4°C. Discard supernatant.
7. Resuspend the cell pellet in 600 µl of ice-cold PBS, and transfer to a 1.5 ml screw-cap microtube. To harvest any remaining cells in the 50 ml tube, add an extra 600 µl of ice-cold PBS to the tube and transfer that volume to the same 1.5 ml screw-cap microtube.
8. Centrifuge at 2000 × *g* for 5 min at 4°C, and discard the supernatant (remove carefully all the supernatant using a 20 µl pipette).
9. Flash-freeze the cell pellet in liquid nitrogen.
10. **Stopping point:** the flash-frozen cell pellet can be stored at −80 °C until use.

3.1.3 Lysis and Sonication

1. Quickly thaw the cell pellets at room temperature, and flick to dislodge. Spin down the pellet at 2000 × *g* for 3 min at 4°C. Remove any supernatant using a 20 µl pipette.
2. Resuspend the pellet in 1 ml of complete Lysis Buffer, and transfer the solution to a V-bottom 15 ml tube (*see* **Note 5**). Place the tube in an ice water bath with constant convection during the sonication.
3. Put the sonicator probe in the tube, and sonicate for 12 rounds at 70% amplitude for 30 s pulses, with 45 s cool-down pauses in between. During this step, RNA fragments should reach a length between 200–1000 nt. Different types of cells may need a different number of rounds of sonication to obtain this range (*see* **Notes 5 and 6**). Flash freeze the samples in liquid nitrogen, and store at −80°C.
4. **Stopping point:** flash-frozen lysate can be stored at −80°C until use.

3.1.4 Hybridization of Probes (Capture)

1. Thaw tubes of lysate at room temperature, and collect together sonicated lysates to have a minimum of 1 ml for the ODD capture and 1 ml for the EVEN capture.
2. Wash 60 µl (30 µl for each pool of probes) of streptavidin magnetic beads three times with 1 ml of unsupplemented Lysis Buffer, and resuspend the beads in 60 µl of complete Lysis Buffer (*see* **Note 7**).
3. Add 30 µl of beads to 1 ml of lysate in a 1.5 ml tube, and incubate in a 37°C hybridization oven for 30 min under constant upside/down mixing on a rocker.
4. Clear the lysate from beads twice, using the magnetic stand and new 1.5 ml tubes, and then transfer the lysate to a 5 ml round-bottom tube (*see* **Note 8**).

5. Add 2 ml of supplemented Hybridization Buffer and a total amount of 100 pmol of probes (1 µl from the 100 µM stock probe pool) to each tube (one tube for *Odd* probes and one tube for *Even* probes).
6. Incubate the tubes under constant upside/down mixing in a 37°C hybridization oven for 4 h.
7. Wash 200 µl of beads three times with 1 ml of unsupplemented Lysis Buffer and resuspend in 200 µl of supplemented Lysis Buffer (*see* **Note 7**).
8. Add 100 µl of beads to the ODD and to the EVEN capture, and place again the tubes in the hybridization oven for 30 min at 37°C under constant upside/down mixing.
9. Pellet the beads with the magnet, and resuspend them in 1 ml of wash buffer prewarmed to 37°C.
10. Transfer beads/buffer to a new 1.5 ml tube. Wash again the 5 ml tube with an additional 300 µl of Wash Buffer to collect any remaining beads, and add this volume to the 1.5 ml tube. Place the tubes under constant upside/down mixing in a 37°C hybridization oven for 5 min.
11. Wash the beads another four times as described above, using 1 ml of prewarmed Wash Buffer for a total of five washes (*see* **Note 9**).
12. Spin down beads after the last wash, and remove all remaining wash buffer using a micropipette.

3.1.5 Target Affinity Purification and Elution

1. Resuspend the beads in 185 µl of Proteinase K Buffer, and add 15 µl of 20 mg/ml Proteinase K. Treat in the same way a sample of the original lysate, as an input control.
2. Incubate the samples at 45°C for 1 h under constant and vigorous agitation.
3. Incubate the samples at 95°C for 10 min.
4. Add 1 ml of Trizol directly to the beads (and input), vortex, and incubate for 10 min at room temperature.
5. Store at −80°C, or proceed with RNA isolation using the miRNeasy Micro Kit (or equivalent kit) by following the manufacturer's instructions (*see* **Note 10**).
6. Using an aliquot of purified RNA, assess the enrichment of the target RNA over the precaptured samples (total RNA) by qRT-PCR. Then, perform small RNA-seq, qRT-PCR, and other analyses as desired, or store RNA at −80°C.

3.2 Small RNA-Seq

For next-generation sequencing (NGS), we use the Illumina platform, generating cDNA libraries with the TruSeq® Small RNA Library Preparation Kit and sequencing samples on a MiSeq sequencer (Fig. 2).

In the procedure below, only the steps differing from the standard Illumina protocol are described in more detail. Where we add these details, we refer to the specific Illumina protocol and underline the steps (i.e., step 1) from the publicly available TruSeq® Small RNA Library Prep Reference Guide (Document #15004197).

1. Lyophilize the RNA samples obtained with the miR-CATCHv2.0 procedure to reduce the volume to 5 µl.
2. Use 5 µl of RNA for the ligation of 3' (RA3) and 5' (RA5) adapters (step 1, Ligate Adapters).
3. Use 6 µl of the adapters-ligated RNA (step 1) for reverse transcription (step 2, Reverse Transcribe Libraries) and amplification (step 3, Amplify Libraries) steps. Perform all steps following the manufacturer's instruction of the Illumina protocol. During the amplification step, increase the number of cycles to 15. To pool and run together in a single lane of the MiSeq sequencer the ODD and EVEN samples of more than one independent capture (three in our case), use one specific RNA PCR Primer index (RPI) for each sample during

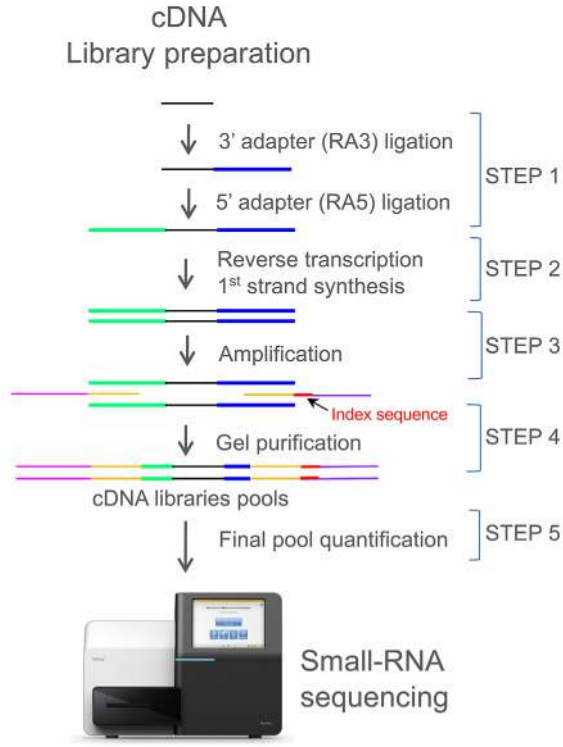


Fig. 2 Small RNA-seq. Schematic representation of the generation of the library for small RNA-seq (see Sect 3.2 for details)

amplification (step 3). At the end, one cDNA library (50 µl) for each sample will be obtained.

4. Pool the cDNA libraries obtained from the ODD and EVEN samples (50 µl + 50 µl) of the same capture, and perform size selection (step 4, Purify cDNA Construct) using a 5% MP TBE gel (50 µl), 1× TBE buffer, and MP apparatus. Load and run the pools according to the Illumina protocol. Each pool must be loaded in more than one well, and the gel slice excised from the wells belonging to the same pool is further processed following the Illumina protocol (*see* **Notes 11 and 12**).
5. Concentrate the pools using the protocol described in the "Concentrate Final Library" paragraph of the Illumina protocol (we do not use the 1× pellet paint NF co-precipitant). Importantly, the fragmented gel slices of the different pools must be shaken overnight with 300 µl of ultrapure water to increase cDNA elution. At the end, size-selected/purified pools are obtained.
6. To check the quality of the pools (*step 5*, Check Libraries), load 1 µl of each pool onto a High Sensitivity DNA chip (Agilent), and run the chip in the Bioanalyzer 2100 following the manufacturer's indication. The resulted peak must be ~147 bp.
7. On the basis of the molarity estimated by the Bioanalyzer, construct a "final pool" composed of an equimolar quantity of the pools of the independent captures.
8. Before sequencing, evaluate the "final pool" molarity by qRT-PCR, using the Kapa Library Quantification Kit according to the manufacturer's protocol (*see* **Note 13**).
9. Process the "final pool" for sequencing, following the Illumina protocol (Preparing Libraries for Sequencing on the MiSeq). We sequence 18 pm (*see* **Note 13**) of the "final pool" on a MiSeq V3 flow cell (MiSeq reagent kit V3 150 cycle), using the "FASTQ only" workflow in single read mode (36 bp) on a MiSeq sequencer.

3.3 Bioinformatic Analysis

In this section we describe how to select miRNAs that are likely physically bound to the RNA of interest, starting from the full set of miRNAs identified by small-RNA sequencing (as described in Sect. 3.2). A schematic representation of the analytical workflow is shown in Fig. 3 and encompasses three main steps: #1. target-abundance scaling correction, #2. miR-CATCHv2.0 miRNAs selection, and #3. classification of miR-CATCHv2.0 enriched miRNAs (refer to #1, #2, and #3 in Fig. 3).

The identification of miRNAs and their quantification from a small-RNA seq experiment is not part of this protocol, which is devoted to the peculiarities of analyzing miR-CATCHv2.0 experiments. Many different bioinformatic tools have been developed

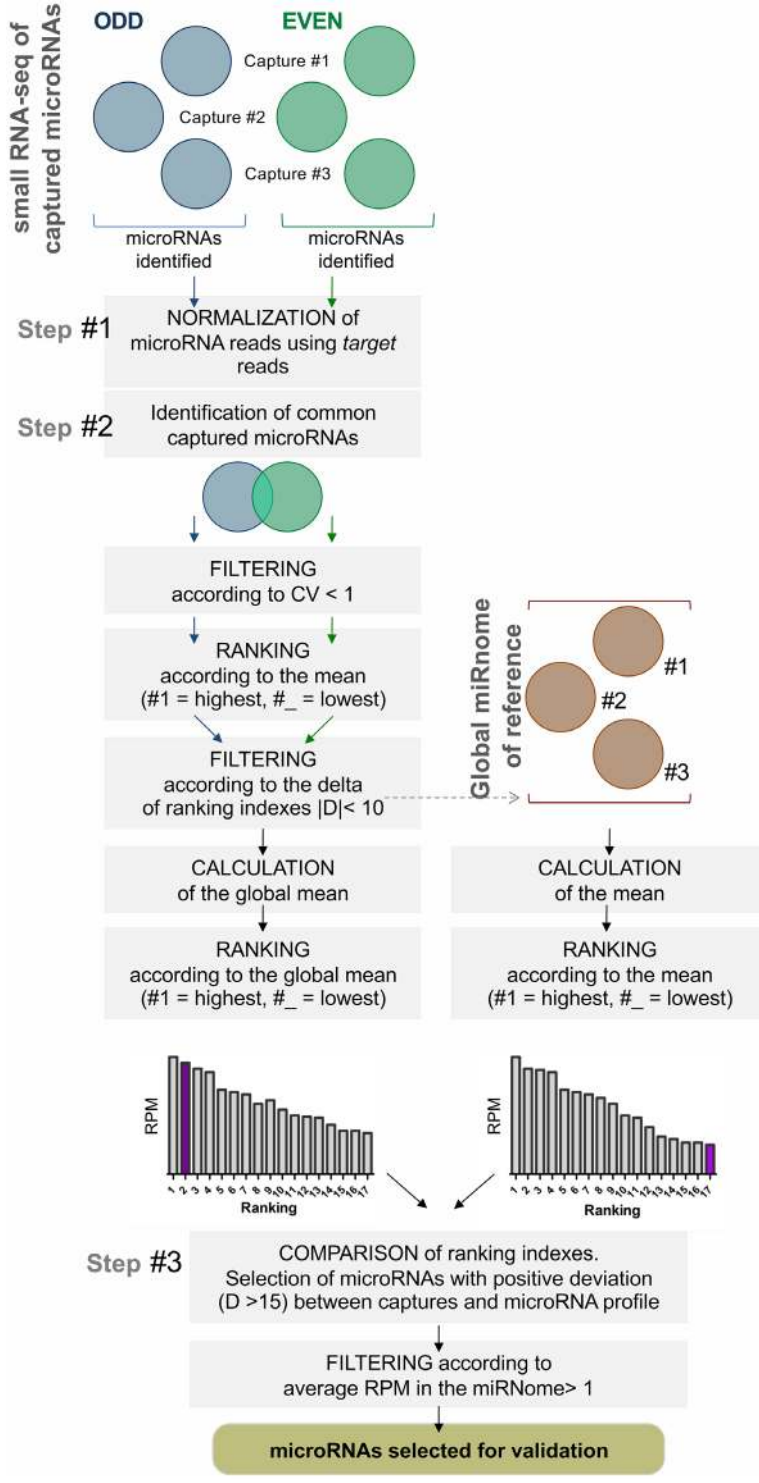


Fig. 3 Bioinformatic analysis of the microRNAs identified through small RNA-seq. Schematic representation of the analytical steps followed to select the microRNAs to be validated (see text for details)

in the last decades for the analysis of small RNA high-throughput sequencing data. Most of them are stand-alone tool suites to be run locally with separated or combined features, such as reads preprocessing, mapping, and differential expression analysis, e.g., mirExpress [39], miRDeep2 [40], or miRanalyzer [41]. Web platforms with integrated tools for independent pipelines are also available, such as sRNAtoolbox [42]. Details on these procedures have been previously described [43].

The standard output of all miRNA identification tools is a reads count (expression units) matrix of each miRNA per sample (rows per columns), which provides a digital measure of the abundance of a miRNA/gene. Furthermore, most of the tools also provide the library size normalized counts, which are necessary to remove technical biases in sequenced data due to the different size of libraries produced by nonuniform depth of sequencing (higher sequencing depth produces higher read counts for genes expressed at the same level). The normalized read counts matrix, Reads Per Million (RPM), is the input data of the analytical workflow that we describe in this section (*see* **Note 14**).

Before proceeding with the downstream analysis, one should check the quality of the produced data. Indeed, the pool of ODD probes and that of EVEN probes can show differences in binding efficiencies, resulting in a subset of microRNAs being identified by only one pool (*see* **Note 15**).

3.3.1 Target Abundance Scaling Correction

The first step (Fig. 3, #1) of the analysis accounts for the influence of the abundance of miRNAs by the relative abundance of the captured target, e.g., ×1 3'UTR. Since all RNA molecules are cut into small pieces during the sonication step, the target mRNA is also captured by the small-RNA sequencing library procedure and can be quantified by counting the number of reads aligning to its sequence for each capture sample. To identify and quantify the sequenced reads of the target, use the BWA alignment tool with the following command lines starting from the .fasta file with the sequence of the target and the .fastq file with the sequenced reads of each capture sample:

```
>bwaindex 3UTR_BRAF-X1.fa
>bwaaln 3UTR_BRAF-X1.fa115-ODD9_S1_L001_R1_001.T.fastq >
     115-ODD9.sai
>bwasamse 3UTR_BRAF-X1.fa115-ODD9.sai 3UTR_BRAF-X1.fa |
samtools   view -S -b -o 115-ODD9.bam -
>samtoolsflagstat115-ODD9.bam >115-ODD9.stat
```

In the .stat output file there is the total number of reads of the library and the number of mapped reads to calculate the normalized counts for the target (RPM_T) (*see* **Note 14**). Calculate the target scaled counts of each miRNA using those values as scaling factors for the original miRNAs, RPM, and the formula:

$$RPM, Target\ scaled\ of\ a\ microRNA = \frac{RPM\ of\ a\ microRNA}{RPM_T}$$

3.3.2 miR-CATCHv2.0 miRNAs Selection

The lists of miRNAs identified by ODD and EVEN probes must be compared to select only those that: 1) are common to both capture probe sets; 2) show low-variance among replicates of the same probe set; and 3) are concordant between ODD and EVEN captures. The selection steps described below could be implemented using R codes, starting from a normalized count matrix of miRNAs from a miR-CATCHv2.0 experiment (Fig. 3, #2). In the working example used here, we use the normalized count matrix from GEO accession number GSE117640, which can be downloaded from the GEO repository through the link: https://www.ncbi.nlm.nih.gov/geo/query/acc.cgi?acc=GSE117640. The page shows details about the full dataset, which includes 6 samples (ODD and EVEN probe captures for the 3 independent experiments and the scrambled probes captures). The GSE117640_rpm.txt.gz is a tab-delimited file with a matrix with normalized RPM values for each identified miRNA for each sample, by rows and columns, respectively.

1. Load the tab-delimited file with microRNA RPMs:

```
>GSE117640_rpm <- read.delim2("~/Downloads/
GSE117640_rpm.txt")
```

2. Load precalculated RPM_T (from Sect. 3.3.1), and scale miRNAs RPMs using the equation in Sect. 3.3.1:

```
>RPM_T<- c(599.67,291.88,489.48,496.67,12.09,189.44,
274.47)
>miR-CATCH.target<- data.frame((1/
RPM_T)*GSE117640_rpm[,-1])
```

3. Select miRNAs identified in both capture probe sets:

```
>indODD<- grep("ODD",colnames(miR-CATCH.target))
>indEVEN<- grep("EVEN",colnames(miR-CATCH.target))
>miR-CATCH.common<-
   miR-CATCH.target[which(rowSums(miR-CATCH.
   target[,indODD])!=0&
   rowSums(miR-CATCH.target[,indEVEN])!=0),]
```

4. Calculate the Coefficient of Variation (CV) and the mean of each miRNA in the three captures performed with the same pool of probes, ODD and EVEN, separately. CV is the standard deviation divided by the mean and is useful to evaluate stability across samples:

```
>miR-CATCH.STAT<-
   data.frame("mean.ODD"=apply(miR-CATCH.
   common[,indODD],1,mean),
   "sd.ODD"=apply(miR-CATCH.common[,indODD],1,sd),
   "mean.EVEN"=apply(miR-CATCH.
   common[,indEVEN],1,mean),
   "sd.EVEN"=apply(miR-CATCH.common[,indEVEN],1,sd))
```

5. Starting from the initial common miRNAs, select those with CV < 1 in both set of pools:

```
>indS<- which(miR-CATCH.STAT$sd.ODD/miR-CATCH.
STAT$mean.ODD< 1 &
   miR-CATCH.STAT$sd.EVEN/miR-CATCH.STAT$mean.EVEN< 1)
>miR-CATCH.S<- miR-CATCH.STAT[indS,]
```

6. Rank them in descending order according to their mean values, separately, in the three ODD and the three EVEN captures:

```
>miR-CATCH.S.rank<- cbind(miR-CATCH.S,
   "rank.mean.ODD"=c(nrow(miR-CATCH.S)-rank(miR-
   CATCH.S$mean.ODD)+1),
   "rank.mean.EVEN"=c(nrow(miR-CATCH.S)-rank(miR-
   CATCH.S$mean.EVEN)+1))
```

7. Compare the ranks to select miRNAs with concordance mean, i.e., for which the ranks differ less than 10 positions (*see* **Note 16**) between ODD and EVEN captures:

```
>miR-CATCH.S2 <-
   miR-CATCH.S.rank[which(abs(miR-CATCH.S.rank$rank.
   mean.ODD -
   miR-CATCH.S.rank$rank.mean.EVEN)<10),]
```

3.3.3 Classification of miR-CATCHv2.0 Enriched miRNAs by Comparison with the miRNome

To pinpoint which miRNAs are enriched in the miR-CATCHv2.0 captured experiments, the relative abundance of the selected miRNAs has to be compared with that obtained from a total small-RNAseq as background (Fig. 3, #3). For example, in one of our recent publications [33], we used the RPM counts of miRNAs identified in two different full small-RNAseq experiments that are present in the GEO repository with accession number GSE117641. The GSE117641_a375-dmso.rpm.txt.gz supplementary file, which is downloadable from https://www.ncbi.nlm.nih.gov/geo/query/acc.cgi?acc=GSE117641, includes RPM-based expression levels of miRNAs for A375 melanoma cells treated with DMSO for 48 h.

1. Load the tab-delimited file with miRNA RPMs:

```
>GSE117641_rpm <-
read.delim2("~/Downloads/GSE117641_a375-dmso.rpm.txt")
```

2. Extract RPM counts for the previously selected miR-CATCHv2.0 miRNAs (from Sect. 3.3.2) and merge data:

```
>mergeData<-
   data.frame(miR-CATCH.common[row.names(miR-CATCH.
   S2),-5],
   GSE117641_rpm[row.names(miR-CATCH.S2),])
```

3. Discard undetected miRNAs in full miRNomes:

```
>indNA<- which(is.na(mergeData$a375_I) &
is.na(mergeData$a375_II))
>mergeDataF<- mergeData[-indNA,].
```

4. Calculate the global mean for miR-CATCHv2.0 and full miRNomes, separately:

```
>mean.mC<- rowMeans(mergeDataF[,1:6])
>mean.full<- rowMeans(mergeDataF[,7:8])
```

5. Rank (*see* **Note 17**) and compare the full miRNome versus miR-CATCHv2.0:

```
>mean.compare<- data.frame(mean.mC,mean.full,
   "rank.mean.miR-CATCH"=c(length(mean.mC)-rank
   (mean.mC)+1),
   "rank.mean.full"=c(length(mean.full)-rank(mean.
   full)+1))
```

6. Finally, the enriched miRNAs are those showing positive deviations:

```
>enrich.mirna<- cbind(mergeData2,mergeData2$rank.
mean.full - mergeData2$rank.mean.miR-CATCH)
```

3.4 Validation of miRNA–Target Interactions Identified by miR-CATCHv2.0

A key step after miRNA identification by miR-CATCHv2.0 is the validation of their effective binding to the target under study. Here, we present MS2-TRAP and a luciferase reporter assay as "gold standard" tools to directly validate the physical association between miRNA and target at the molecular level. Moreover, we present useful experiments to study the miRNAs that increase/decrease mRNA stability or translation.

3.4.1 MS2-TRAP

MS2-tagged RNA affinity purification (MS2-TRAP) is an effective tool to validate miR-CATCHv2.0 identified miRNAs. The protocol is based on the artificial expression of the RNA of interest together with several MS2 binding sites (BS, 12–24 copies), which allow the pull-down of the target together with the bound miRNAs (RNA immunoprecipitation [RIP]). The RIP is performed using an engineered

MS2 binding protein (MS2-BP) that is fused with a reporter gene (usually GFP or YFP) and with an antibody epitope tag (HA-tag); this chimeric protein can bind the MS2 repeats and can be easily precipitated with antibody conjugated beads. Here, we present the MS2-TRAP used for miR-CATCHv2.0 validation (Fig. 4a) [33].

1. Clone the RNA target in a suitable plasmid containing 12–24 MS2 RNA tags; following the indication by Yoon et al. [23], put the insert upstream of the MS2 RNA tags.
2. Co-transfect the plasmid expressing the MS2-tagged RNA plus the plasmid expressing the MS2-BP into a cell line of choice. The transfection protocol depends on the cell line and

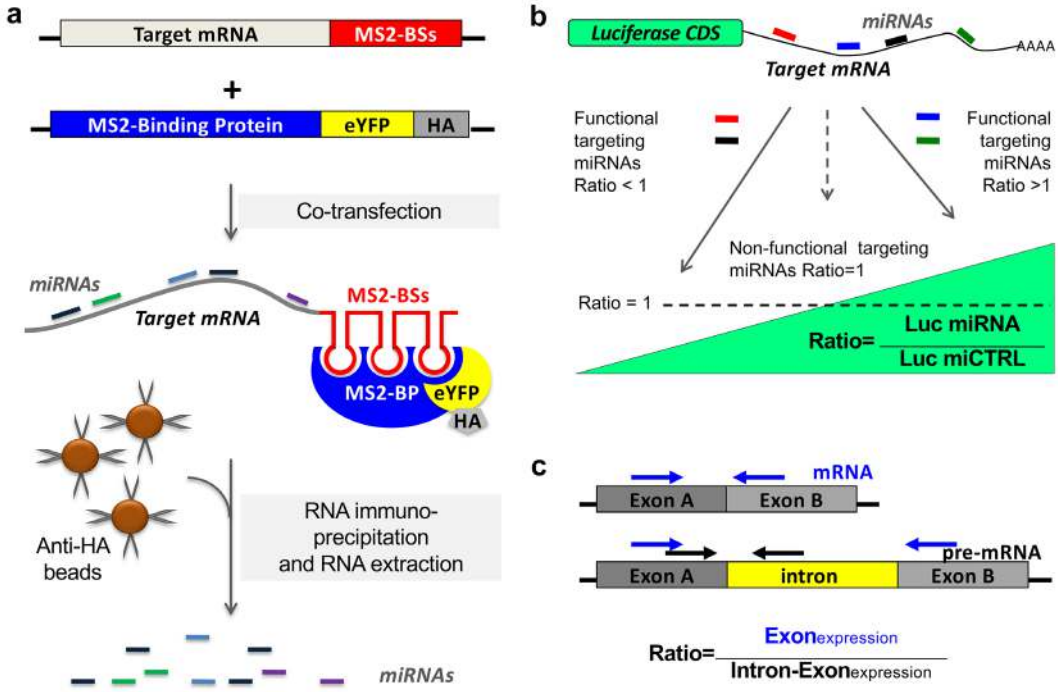


Fig. 4 Experimental validation of miRNAs identified by miR-CATCHv2.0. **a** Schematic representation of the MS2-tagged RNA affinity purification (MS2-TRAP) assay. Cells are co-transfected with 2 plasmids: the pMS2-target plasmid (*top*) expresses the target RNA sequence plus 12 copies of the MS2 binding site (BS), which is characterized by a defined secondary structure; the pMS2-BP plasmid (*bottom*) expresses the MS2-binding protein (MS2-BP) fused with the HA-Tag and eYFP. MS2-BP binds to the MS2-target RNA sequence and can be efficiently precipitated, together with endogenous miRNAs physically bound to the transcript, using anti-HA antibody-conjugated beads. **b** Schematic representation of the Luciferase reporter assay. The target sequence is cloned in a dedicated vector downstream of the stop codon of the Luciferase coding sequence (*top*). This plasmid is co-transfected with miRNA mimics (and a control mimic, mi-CTRL) in HCT116 Dicer-/- cells. miRNAs that functionally interact with the target RNA induce a decrease or increase in luciferase activity (*bottom*). **c** The ratio between the expression of mRNA and premRNA is useful to determine the impact of a miRNA on mRNA stability (degradation or stabilization). The cartoon shows how to design qRT-PCR primers for mRNA (exon-exon primers, blue arrows) and premRNA (intron-exon primer, black arrows) quantification.

the transfectant reagent used. Briefly, the conditions used in our lab are the following:

a. Seed 2×10^6 A375 melanoma cells in a 10 cm dish, and culture overnight.
b. The next day, transfect cells using 24 μg of plasmids (12 μg of pMS2-BP + 12 μg of pMS2-targetRNA) and 45 μl of 0.02 mM PEI as transfection reagent.
c. In parallel, also perform the transfection of the control sample, using 12 μg of pMS2-BP + 12 μg of pMS2 empty vector.

3. 24 h later, collect the cells from each dish as a single pellet (approximately 8×10^6–1×10^7cells in our case), and wash twice with ice-cold PBS. **Stopping point:** pellets can be stored at -80 °C until use.
4. Lyse the pellet with 600 μl of complete polysome buffer for 5 min on ice.
5. Clarify the lysate by centrifugation at 15,000 × *g* for 15 min at 4°C, and transfer the supernatant to a new 1.5 ml tube.
6. Use part of the supernatant to quantify the protein content by using a Bradford protein assay (or a similar assay).
7. Prepare 600 μl of lysate at the final protein concentration of 2 mg/ml using complete Polysome Buffer.
8. For each sample, reconstitute 25 μl of anti-HA-Tag Sepharose Bead Conjugate in 1 ml of NT2 Buffer. Spin down the beads by centrifugation for 1 min at 2500 × *g*), and remove the supernatant (*see* **Note 8**).
9. Wash beads twice with 1 ml of NT2 Buffer by pulsing in a centrifuge (1 min, 2500 × *g*).
10. Remove the supernatant, and resuspend the beads in 50 μl of complete NT2 Buffer (*see* **Note 8**).
11. Add 25 μl of beads to 500 μl of lysate, and incubate at room temperature for 4 h on an orbital shaker. Save the remaining 100 μl of lysate for further analysis at −80°C.
12. After incubation, wash beads 5 times with 1 ml of ice-cold NT2 buffer by pulsing in the centrifuge (1 minute, 2500 × g), and remove the supernatant with a pipette.
13. Add 1 ml of Trizol directly to the beads (and to the lysate, if needed), and incubate for 10 min at room temperature.
14. Store at −80°C, or proceed with RNA isolation using the miRNeasy Micro Kit (or equivalent kit) by following the manufacturer's instructions (*see* **Note 10**).

3.4.2 Luciferase Reporter Assay

The Luciferase reporter assay is a sensitive and quantitative method to assess the direct interaction between a certain miRNA and its putative target. The RNA of interest (generally the 3'UTR) is cloned downstream of the Firefly Luciferase coding sequence (CDS) in an appropriate plasmid and, when a miRNA binds the target sequence, an alteration of the Firefly Luciferase activity (compared to a control) is measured by a luminometer. A reduced Luciferase activity for the target mRNA indicates that the miRNA is capable of binding the target sequence and inhibiting reporter translation or mediating RNA degradation [3, 5]; conversely, increased Luciferase activity compared to control is indicative of a miRNA-target interaction that leads to stabilization or improved translation of the mRNA target [4, 5] (Fig. 4b). There are many available plasmids (pMIR-report, pGL3-luciferase reporter, etc.) and commercial kits for Luciferase reporter assays. We suggest using a dual system reporter assay where both Firefly (reporter) and Renilla (internal control) luciferase can be measured to avoid artifacts related to sample loading. For the Dual system reporter assay, choose a plasmid that expresses both Firefly and Renilla Luciferase or, alternatively, co-transfect two separate expression vectors (for example, pMIR-report for Firefly and pRL-TK for Renilla). Before starting, choose carefully the cell line in which to perform the assay, because it is preferable to use a cell line that expresses low levels of the miRNA of interest so that the endogenous miRNA will contribute only marginally to the regulation of the reporter gene. Moreover, some cell lines are more prone to transfection procedures, and a good transfection efficiency is crucial to improve the reproducibility of the results. In our lab, we found the use of the HCT116Dicer-/-cell line to be very convenient, since this cell line lacks the majority of mature miRNAs.

1. Clone the sequence of the 3'UTR of interest downstream of the STOP codon of the Luciferase CDS in a suitable plasmid for a Luciferase reporter assay.
2. Seed 7.5×10^4 HCT116 Dicer-/- cells/well in a 24-well plate. Seed triplicate wells for every miRNA to be tested, including the control mimic mi-CTRL (*see* **Note 18**).
3. The next day, transfect the cells with 50 ng of Luciferase reporter plasmid (pMIR-report) and 10 ng of Renilla-expressing plasmid (pRL-TK), plus 1.5 µl of 20 µM miRNA mimics (described in Sect. 3.4.4), using Lipofectamine 2000 as per the manufacturer's instructions (*see* **Note 19**).
4. 24 h after transfection, use the Dual-Glo® Luciferase Assay System (or equivalent) to perform the Luciferase assay, following the manufacturer's protocol (briefly reported below).
5. Lyse the cells with the buffer supplied in the kit.
6. Transfer 20 µl of clarified cellular lysate into a 96-well white plate, and make duplicates for each sample.

7. Acquire Firefly and Renilla Luciferase luminescence using a luminometer.
8. Calculate the Firefly/Renilla Luciferase activity ratio for each sample; luciferase ratio of the miRNA mimic data can be normalized over the Luciferase ratio of the control mimic (the control value will be set at 1). Functional miRNAs will induce a decrease (<1) or increase (>1) of the normalized Firefly/Renilla ratio compared to the control mimic.

Once miRNA target interaction is validated by the luciferase reporter assay, the same assay is also useful to assess the exact binding site of the miRNA (miRNA recognition element, MRE). As reported above, functional miRNAs induce a normalized Firefly/Renilla ratio <1 or >1 compared to the control mimic (Fig. 4b), so mutagenesis/deletion of the sequence of the MRE will lead to a normalized Firefly/Renilla ratio near a value 1.

There are many mechanisms by which miRNAs can pair with their targets, and these are mainly summarized in two categories: interactions through the miRNA seed sequence (a conserved heptametrical sequence situated at positions two to seven at the miRNA 5′-end, usually defined as "canonical" binding) and interactions that do not involve or only partially involve the seed sequence ("seedless" binding). The MRE in the target sequence can be predicted by using several bioinformatic tools; however, to choose the appropriate one, it is important to take into account that the miR-CATCHv2.0 protocol reveals both "canonical" and "seedless" miRNA target interactions. RNAhybrid tool [44] (https://bibiserv.cebitec.uni-bielefeld.de) is very useful for this purpose, because it finds, in a kind of domain mode, the minimum free energy (mfe) hybridization of miRNA-target interaction, independently of the mechanism of interaction. Once predicted, the bases that allow the pairing between the miRNA and the RNA target can be deleted or mutated (three to six bases) by using a commercial kit (QuikChange II Site-directed Mutagenesis Kit or equivalent) and following the manufacturer's instructions. Moreover, taking into consideration that a miRNA can have more than one binding site in the target sequence, we suggest predicting at least three binding sites and starting the mutagenesis/test from the site with the lowest mfe value. In some cases, the rescue of a normalized Firefly/Renilla ratio near to a value of one can be observed only when more than one predicted binding site is mutated/deleted.

3.4.3 Relative Translational Efficiency Assay

The relative translational efficiency (RTE) assay is a useful tool to evaluate the impact of a miRNA on target translation (inhibition/enhancement) [45]. The experiment is based on the Luciferase Reporter assay reported above, with the only difference being that an extra replicate for each condition is transfected and is used for RNA extraction, followed by qRT-PCR quantification of Firefly and Renilla mRNAs.

1. Seed 7.5×10^4 HCT116 Dicer-/-cells/well in a 24-well plate. Seed 4 wells of replicates for every miRNA to be tested, including the control mimic.
2. The next day, transfect the cells with 50 ng of Luciferase reporter plasmid (pMIR-report) plus 10 ng of Renilla-expressing plasmid (pRL-TK) plus 1.5 μl of 20 μM miRNA mimics using Lipofectamine 2000 as per the manufacturer's instructions.
3. 24 h after the transfection, collect the cells from 3 wells for the Dual Luciferase Reporter assay (as described in Sect. 3.4.2), and collect the cells of the extra well for RNA extraction.
4. Extract the RNA using Trizol reagent as per the manufacturer's instructions (other RNA extraction kits can also be used).
5. Use 1 μg of RNA for cDNA retrotranscription using the QuantiTect Reverse Transcription Kit (or equivalent) as per the manufacturer's protocol.
6. Perform the qRT-PCR of Firefly and Renilla genes using primers as indicated in Sect. 2.4 (*see* **Note 20**).
7. Use the data of Firefly and Renilla expression and Firefly and Renilla Luciferase activity for each sample to calculate the RTE using the formula: $RTE = [RLU_{miRNA}^{Fluc/RLuc} / RNA_{miRNA}^{Fluc/RLuc}] / [RLU_{miCTRL}^{Fluc/RLuc} / RNA_{miCTRL}^{Fluc/RLuc}]$, where RLU = Relative LuciferaseUnits, Fluc = FireflyLuciferase, and Rluc = RenillaLuciferase. An RTE value >1 indicates that the miRNA increases the translation of the target without affecting its mRNA stability; on the other hand, an RTE value <1 is indicative of translational repression.

3.4.4 Analysis of Target Expression After miRNA Overexpression

miRNAs are capable of inhibiting (or, less frequently, of enhancing) gene expression by acting both at the RNA and at the protein level [3, 4]. Therefore, measuring target expression levels after miRNA mimic transfection (by qRT-PCR and/or western blot) is another way to validate miRNA target interaction at the functional level.

A "microRNA mimic" is a double-stranded short-interfering RNA. One strand has the sequence of the desired mature miRNA. The other strand (complementary to the mature miRNA) can be modified by mutations to favor the incorporation of the miRNA-like strand into RISC [46]. Moreover, a "UU" or "TT" overhang is added on both strands at the 3′ end. miRNA mimics can be designed as described above, though many companies sell ready-to-use mimics. In all the experiments, a control mimic (mi-CTRL, *see* **Note 18**) needs to be included. Several mi-CTRL sequences can be found in published papers or in online repositories. Cell lines should be transfected with an appropriate transfection reagent; in our lab we successfully use Lipofectamine 2000™ as per the manufacturer's instructions for many melanoma cell lines (A375, 501 MEL, etc.).

Cell pellets are collected at 24 h post-transfection for RNA extraction and subsequent qRT-PCR analysis of target mRNA, or at 48 h post-transfection for protein extraction and western blot analysis of target expression.

3.4.5 Analysis of mRNA Target Stability After miRNA Overexpression by qRT-PCR

The understanding of mRNA target stability is very helpful to demonstrate that a miRNA can induce RNA degradation or stabilization, and it can easily be assessed through qRT-PCR analysis. Those analyses can be performed by two independent methods: measurement of the ratio of mature mRNA target/premRNA target and measurement of target expression over time after inhibition of de novo synthesis of the RNA (using the drug Actinomycin D).

In the first method, mature mRNA target and premRNA target are quantified by qRT-PCR of exons and introns. Such qRT-PCR is performed using 2 primer pairs, one that amplifies an exon–exon junction and the other that amplifies an exon-intron junction (Fig. 4c, *see* **Note 21**). This analysis is carried out 24 h after cells have been transfected with miRNA mimics, and the ratio of the expression of exon–exon/exon-intron is normalized over the control mimic group (mi-CTRL, *see* **Note 18**). A ratio <1 indicates that the miRNA induces degradation of the mature mRNA, whereas a ratio >1 is indicative of mRNA stabilization.

In the second method, inhibition of de novo RNA synthesis using Actinomycin D allows one to measure the effect of a certain miRNA on target RNA stability over time. Cells are transfected with miRNA mimics and mi-CTRL. For each mimic, one well is transfected for each time point (we suggest 4 time points). After 24 h, cells are treated with Actinomycin D (before use, check that the right concentration for the cell line is used; for A375 cells, we use 10 μg/ml). Cells are harvested at the desired time points (we use 0, 2, 4, and 8 h) for RNA extraction, and qRT-PCR of the target is performed. Data is plotted as a curve of expression (y-axis) and time (x-axis). For miRNAs that induce mRNA degradation, a rapid decrease of target expression is observed compared to the control, while the opposite trend is observed for miRNAs that stabilize their target.

4 Notes

1. DEPC treatment neutralizes RNAses. Add 0.1% DEPC to the water that will be used to make the described solutions, and let it stand for 1 h or more. Then autoclave and let cool to room temperature prior to use. Do not autoclave the final buffers.
2. We suggest making fresh formaldehyde solutions before starting the miR-CATCHv2.0 protocol. Commercially available and ready-to-use formaldehyde solutions can be used, but

be aware of some preservatives that may affect miR-CATCH v2.0 results.

3. We use TBE polyacrylamide gel from BIO-RAD instead of 6% Novex TBE gels (Thermo Fisher Scientific) because the BIO-RAD electrophoretic apparatus is available in our lab. For the same reason, we use the Nanosep MF centrifugal device with GHP membrane and 0.45 μm pore size (PALL Life Science) instead of 5 μm filter tubes (IST Engineering).
4. Be sure about the length and the sequence of the RNA of interest: the transcript under study can bear multiple mRNA isoforms; 3'UTRs can be shorter or longer compared to the sequence reported in the repositories; the transcript may not be expressed in the chosen cellular or biological context. Transcript length, sequence, and expression can be checked by using freely available RNA-seq data or by using PCR techniques [amplification of the fragment of interest from a cDNA sample (plus sequencing)]. Examples can be found in our recent studies [35, 36].
5. For a good reproducibility of miR-CATCHv2.0 results, a good reproducibility of the sonication step is needed. The volume of the sample and shape of the tube have an impact on this step; thus, always use the same sample volume and the same kind of tube (we use 15 ml V-bottom tubes). Moreover, a permanent marker sign on the top side of the sonicator probe can allow the operator to place tubes in the same position during sonication (the sonicator probe should always be at the same distance from the bottom of the tubes).
6. Different cell lines require different sonication conditions to reach an RNA fragmentation between 200–1000 nt. Find the best sonication condition for the selected cell line. Collect several fixed pellets as described in Sect. 3.1.2, and perform a range of incremental rounds of sonication (at least 3, 6, 9, and 12 rounds), then extract RNA and run it on an agarose gel to observe fragment size (for optimal sonication, a smear of fragments should be visualized between 200 and 1000 single-strand RNA marker bands). For more details about optimizing sonication, see also Supplementary Information from our recent study [33].
7. To be sure to add the same amount of beads to each sample, we suggest that users work with an extra volume of beads (add 10%–15% to the initial volume), taking into account this extra volume for bead resuspension after washes.
8. This step is important to eliminate molecules that bind non-specifically to the beads before the pull-down.
9. To ensure the reproducibility of this step, we encourage the use of a timer for washing steps. Wait 1 min to allow the magnetic separation of the beads, then remove the supernatant

and resuspend the beads. Be sure that the buffer is prewarmed when required.

10. We recommend the use of an appropriate kit for extraction of short RNAs.
11. When the pools (ODD plus EVEN samples of the same capture) are loaded in the TBE gel, the band is usually very faint. To be sure to collect the correct gel slice, it is important to cut the gel exactly below the 160 bp and above the 145 bp CRL marker bands. Particularly, it is important to avoid the 125 bp band that represents the adapters-dimers: a contamination of adapters-dimers could decrease the quantity of reads of miRNAs. The eventual contamination can be evaluated after the Bioanalyzer run as an additional peak at about 125 bp.
12. Given the low quantity of the starting material (captured RNA), it is extremely important to generate a high number of total reads to have sequencing as deep as possible. To do that, it is crucial to perfectly quantify the "final pool" that is loaded in the flow cell for sequencing. In our hands, qRT-PCR quantification is the most reliable method.
13. We load near the maximum molarity allowed of the "final pool" in the flow cell, i.e., 20 pM. In our hands, this molarity produces a cluster density far below the overclustering risk (about 1200 cluster density). Therefore, we suggest using a high molarity even in the first sequencing experiment.
14. For library size normalization, the normalized abundance unit is Reads Per Million (RPM) of mapped reads, which is calculated as:

$$RPM\ of\ a\ microRNA = \frac{Numberofreads\ mapped\ to\ the\ microRNA \times 10^6}{Total\ numberofmapped\ reads\ from\ the\ given\ library}$$

15. For sample quality control, it is important to check the robustness of the quantification of the miRNAs identified by both pools of probes by calculating the Pearson's correlation of the log10-scaled normalized RPM value for each independent experiment.
16. This is not an absolute threshold, rather it is relative to the peculiarities of the two datasets, mostly influenced by the specific binding efficiency of ODD and EVEN probes.
17. Note that the ranking is descending, i.e., #1 is the most abundant.

18. The mi-CTRL harbors a sequence that does not recognize any transcript in the cell and is used as a control for miRNA mimics in transfection experiments.
19. Every cell line is different, and it is therefore crucial to determine the best transfection conditions and reagents before starting the protocol.
20. The qRT-PCR reaction should be optimized for the reagent and the machine available in one's lab before starting the protocol. Detailed conditions used in our lab are available in our recent publication [33].
21. During primer design, be sure that the chosen intron is not a retained intron. Check an online genome browser (https://www.ensembl.org/index.html), or assess by experimental techniques.

Conflict of Interest

The authors have no conflicts of interest to declare that are relevant to the content of this chapter.

References

1. Chen K, Rajewsky N (2007) The evolution of gene regulation by transcription factors and microRNAs. Nat Rev Genet 8(2):93–103. https://doi.org/10.1038/nrg1990
2. Mitchell SF, Parker R (2014) Principles and properties of eukaryotic mRNPs. Mol Cell 54(4):547–558. https://doi.org/10.1016/j.molcel.2014.04.033
3. Iwakawa H-O, Tomari Y (2015) The functions of microRNAs: mRNA decay and translational repression. Trends Cell Biol 25(11):651–665. https://doi.org/10.1016/j.tcb.2015.07.011
4. Orang AV, Safaralizadeh R, Kazemzadeh-Bavili M (2014) Mechanisms of miRNA-mediated gene regulation from common downregulation to mRNA-specific upregulation. Int J Genomics 2014:970607. https://doi.org/10.1155/2014/970607
5. Gilot D, Migault M, Bachelot L et al (2017) A non-coding function of TYRP1 mRNA promotes melanoma growth. Nat Cell Biol 19(11):1348–1357. https://doi.org/10.1038/ncb3623
6. Kunz M (2013) MicroRNAs in melanoma biology. Adv Exp Med Biol 774:103–120. https://doi.org/10.1007/978-94-007-5590-1_6
7. Acunzo M, Romano G, Wernicke D, Croce CM (2015) MicroRNA and cancer—a brief overview. Adv Biol Regul 57:1–9. https://doi.org/10.1016/j.jbior.2014.09.013
8. Fattore L, Costantini S, Malpicci D et al (2017) MicroRNAs in melanoma development and resistance to target therapy. Oncotarget 8(13):22262–22278. https://doi.org/10.18632/oncotarget.14763
9. Luo C, Weber CEM, Osen W et al (2014) The role of microRNAs in melanoma. Eur J Cell Biol 93(1-2):11–22. https://doi.org/10.1016/j.ejcb.2014.02.001
10. Garzon R, Fabbri M, Cimmino A et al (2006) MicroRNA expression and function in cancer. Trends Mol Med 12(12):580–587. https://doi.org/10.1016/j.molmed.2006.10.006
11. Iorio MV, Croce CM (2012) MicroRNA dysregulation in cancer: diagnostics, monitoring and therapeutics. A comprehensive review. EMBO Mol Med 4(3):143–159. https://doi.org/10.1002/emmm.201100209
12. Mirzaei H, Gholamin S, Shahidsales S et al (2016) MicroRNAs as potential diagnostic and prognostic biomarkers in melanoma. Eur J Cancer 53:25–32. https://doi.org/10.1016/j.ejca.2015.10.009
13. Tarang S, Weston MD (2014) Macros in microRNA target identification: a comparative analysis of in silico, in vitro, and in vivo

approaches to microRNA target identification. RNA Biol 11(4):324–333. https://doi.org/10.4161/rna.28649
14. Poliseno L, Pandolfi PP (2015) PTEN ceRNA networks in human cancer. Methods 77:41–50. https://doi.org/10.1016/j.ymeth.2015.01.013
15. Laganà A (2015) Computational prediction of microRNA targets. Adv Exp Med Biol 887:231–252. https://doi.org/10.1007/978-3-319-22380-3_12
16. Demirci MDS, Yousef M, Allmer J (2019) Computational prediction of functional microRNA–mRNA Interactions. Methods Mol Biol 1912:175–196. https://doi.org/10.1007/978-1-4939-8982-9_7
17. Peterson SM, Thompson JA, Ufkin ML et al (2014) Common features of microRNA target prediction tools. Front Genet 5:23. https://doi.org/10.3389/fgene.2014.00023
18. O'Connor S, Murphy EA, Szwed SK et al (2021) AGO HITS-CLIP reveals distinct miRNA regulation of white and brown adipose tissue identity. Genes Dev 35(9-10):771–781. https://doi.org/10.1101/GAD.345447.120
19. Stebel S, Breuer J, Rossbach O (2022) Studying miRNA–mRNA interactions: an optimized CLIP-protocol for endogenous Ago2-protein. Methods Protoc 5(6):96. https://doi.org/10.3390/mps5060096
20. Chou C-H, Lin F-M, Chou M-T et al (2013) A computational approach for identifying microRNA-target interactions using high-throughput CLIP and PAR-CLIP sequencing. BMC Genomics 14 Suppl1(Supll1):S2. https://doi.org/10.1186/1471-2164-14-S1-S2
21. Gray LA, Turner PC, Renne R (2021) Modified cross-linking, ligation, and sequencing of hybrids (qCLASH) to identify microRNA targets. Curr Protoc 1(10):e257. https://doi.org/10.1002/cpz1.257
22. Moore MJ, Scheel TKH, Luna JM et al (2015) miRNA–target chimeras reveal miRNA 3′-end pairing as a major determinant of Argonaute target specificity. Nat Commun 6:8864. https://doi.org/10.1038/ncomms9864
23. Yoon JH, Srikantan S, Gorospe M (2012) MS2-TRAP (MS2-tagged RNA affinity purification): tagging RNA to identify associated miRNAs. Methods 58(2):81–87. https://doi.org/10.1016/j.ymeth.2012.07.004
24. Braun J, Misiak D, Busch B et al (2014) Rapid identification of regulatory microRNAs by miTRAP (miRNA trapping by RNA in vitro affinity purification. Nucleic Acids Res 42(8):e66. https://doi.org/10.1093/nar/gku127
25. Shi M, Han W, Spivack SD (2013) A quantitative method to identify microRNAs targeting a messenger RNA using a 3′UTR RNA affinity technique. Anal Biochem 443(1):1–12. https://doi.org/10.1016/j.ab.2013.08.002
26. Hassan T, Smith SGJ, Gaugan K et al (2013) Isolation and identification of cell-specific microRNAs targeting a messenger RNA using a biotinylated anti-sense oligonucleotide capture affinity technique. Nucleic Acids Res 41(6):e71. https://doi.org/10.1093/nar/gks1466
27. Vencken S, Hassan T, McElvaney NG et al. (2015) miR-CATCH: microRNA capture affinity technology. Methods Mol Biol 1218:365–373. https://doi.org/10.1007/978-1-4939-1538-5_23
28. De Santi C, Vencken S, Blake J et al (2017) Identification of MiR-21-5p as a functional regulator of mesothelin expression using microRNA capture affinity coupled with next generation sequencing. PLoS One 12(1):e0170999. https://doi.org/10.1371/journal.pone.0170999
29. Palfi A, Hokamp K, Hauck SM et al (2016) MicroRNA regulatory circuits in a mouse model of inherited retinal degeneration. Sci Rep 6:31431. https://doi.org/10.1038/srep31431
30. Griffith A, Kelly PS, Vencken S et al (2018) miR-CATCH identifies biologically active miRNA regulators of the pro-survival gene XIAP, in Chinese hamster ovary cells. Biotechnol J 13(3):e1700299. https://doi.org/10.1002/biot.201700299
31. Zeni A, Grasso M, Denti MA (2022) Identification of miRNAs bound to an RNA of interest by microRNA capture affinity technology (miR-CATCH). Methods Mol Biol 2404:207–218. https://doi.org/10.1007/978-1-0716-1851-6_11
32. Ragusa M, Barbagallo D, Chioccarelli T et al. (2019) CircNAPEPLD is expressed in human and murine spermatozoa and physically interacts with oocyte miRNAs. RNA Biol 16(9):1237–1248. https://doi.org/10.1080/15476286.2019.1624469
33. Marranci A, D'Aurizio R, Vencken S et al (2019) Systematic evaluation of the microRNAome through miR-CATCHv2.0 identifies positive and negative regulators of BRAF-X1 mRNA. RNA Biol 16(7):865–878. https://doi.org/10.1080/15476286.2019.1600934
34. Marranci A, D'Aurizio R, Rizzo M et al (2021) High-throughput identification of miRNA-target interactions in melanoma using miR-CATCHv2.0. Methods Mol Biol 2265:487–512. https://doi.org/10.1007/978-1-0716-1205-7_35
35. Marranci A, Tuccoli A, Vitiello M et al (2015) Identification of BRAF 3'UTR isoforms in

melanoma. J Invest Dermatol 135(6):1694–1697. https://doi.org/10.1038/jid.2015.47
36. Marranci A, Jang Z, Vitiello M et al (2017) The landscape of BRAF transcript and protein variants in human cancer. Mol Cancer 16(1):85. https://doi.org/10.1186/s12943-017-0645-4
37. Martins M, Galfrè S, Terrigno M et al (2021) A eutherian-specific microRNA controls the translation of Satb2 in a model of cortical differentiation. Stem Cell Reports 16(6):1496–1509. https://doi.org/10.1016/j.stemcr.2021.04.020
38. Racine JS (2012) RStudio: a platform-independent IDE for R and Sweave. J Appl Econom 27(1):167–172. https://doi.org/10.1002/jae.1278
39. Wang WC, Lin FM, Chang WC et al (2009) MiRExpress: analyzing high-throughput sequencing data for profiling microRNA expression. BMC Bioinformatics 10:328. https://doi.org/10.1186/1471-2105-10-328
40. Friedländer MR, MacKowiak SD, Li N et al (2012) MiRDeep2 accurately identifies known and hundreds of novel microRNA genes in seven animal clades. Nucleic Acids Res 40(1):37–52. https://doi.org/10.1093/nar/gkr688
41. Hackenberg M, Rodríguez-Ezpeleta N, Aransay AM (2011) MiRanalyzer: an update on the detection and analysis of microRNAs in high-throughput sequencing experiments. Nucleic Acids Res 39(Web Server issue):W132–138. https://doi.org/10.1093/nar/gkr247
42. Aparicio-Puerta E, Lebrón R, Rueda A et al (2019) SRNAbench and sRNAtoolbox 2019: intuitive fast small RNA profiling and differential expression. Nucleic Acids Res 47(W1):W530–W535. https://doi.org/10.1093/nar/gkz415
43. Fu X, Dong D (2018) Bioinformatic analysis of MicroRNA sequencing data. Methods Mol Biol 1751:109–125. https://doi.org/10.1007/978-1-4939-7710-9_8
44. Rehmsmeier M, Steffen P, Höchsmann M, Giegerich R (2004) Fast and effective prediction of microRNA/target duplexes. RNA 10(10):1507–1517. https://doi.org/10.1261/rna.5248604
45. Lin C-C, Liu L-Z, Addison JB et al (2011) A KLF4–miRNA-206 autoregulatory feedback loop can promote or inhibit protein translation depending upon cell context. Mol Cell Biol 31(12):2513–2527. https://doi.org/10.1128/mcb.01189-10
46. Tuccoli A, Vitiello M, Marranci A et al (2016) Methods for the identification of PTEN-targeting microRNAs. Methods Mol Biol 1388:111–138. https://doi.org/10.1007/978-1-4939-3299-3_9

Part VII

Methods for Preclinical and Clinical Development/ Characterization of Melanoma Diagnostics and Therapeutics



Chapter 34

Characterization of an Anti-Tryptophan 2,3-Dioxygenase Monoclonal Antibody and Use in a Melanoma Model

Summer Sedano, Kaylend Manley, George C. Prendergast, Marie R. Webster and Lisa D. Laury-Kleintop

Abstract

Monoclonal antibodies have served as research tools to characterize specific proteins and biomolecules to understand their role in biological processes and disease. However, because of nonspecific reactivity with other components in samples, specific reactivity can be difficult to interpret. Using web-based tools, standard hybridoma technology, and standard immunostaining methods, we describe the development of a tryptophan 2,3-dioxygenase 2 (TDO2)-targeted antibody with high specificity. In addition to providing a unique reagent needed as a research tool to investigate the role of TDO2 in preclinical models and human tissue samples, herein we provide methods to characterize TDO2 expression in human tissue samples and murine disease models. We note also that the general protocol described in this chapter will be useful to investigators interested in developing monoclonal antibodies against other targets of interest as well.

Keywords Tryptophan 2, 3-Dioxygenase, Monoclonal antibody, Melanoma, Yumm cell line, Knock-out, Western blotting, Immunostaining

1 Introduction

Studies suggest that the tryptophan catabolizing enzyme tryptophan 2,3-dioxygenase (TDO2) is overexpressed in many tumors, in parallel with the other tryptophan catabolizing enzymes indoleamine 2,3-dioxygenase 1 and 2 (IDO1 and IDO2) [1, 2]. Additionally, TDO2 has been directly implicated as a pathogenic contributor to immune escape and metastasis [3, 4]. While deeper study of TDO2 in cancer is clearly justified, limited tools are available to characterize protein expression in murine models and human tissue samples. An example is the now discontinued antibody that was used previously to characterize TDO2 expression in human glioma and meningioma tissue sections [5].

To meet a scientific need, a TDO2-specific antibody was generated by utilizing an approach previously used to generate

Kristian M. Hargadon (ed.), *Melanoma*, Methods in Molecular Biology, vol. 3089,
https://doi.org/10.1007/978-1-0716-5619-8_34,
© The Author(s), under exclusive license to Springer Science+Business Media, LLC, part of Springer Nature 2027

murine-specific antibodies against IDO1 and IDO2 [6, 7]. Using web-based analytical tools and online databases, an antigenic region for human and mouse TDO2 was identified, and the generated anti-TDO2 antibody was validated using murine and human tissues. Herein, we provide a description of the methods used to generate and characterize the anti-TDO2 antibody, demonstrating methods to characterize TDO2 expression in human tissue samples and murine disease models.

2 Materials (*see* Note 1)

2.1 Common Disposables

1. Immulon two HB Microtiter plates.
2. 96-well Tissue Culture plates with lid.
3. 100 mm Tissue Culture dishes.
4. 70 μm cell strainer.
5. Glass slides.
6. Coverslips (24 mm × 50 mm, No. 1.5 thickness).

2.2 Equipment

1. Bio-Tek Instruments Synergy 2 (Winooski, VT).
2. Bio-Rad Chemidoc imaging system (Hercules, CA).
3. Zeiss Axiovert 200 M (White Plains, NY).
4. Nikon Confocal C2 (Melville, NY).

2.3 Immunization Reagents

1. Freunds Complete Adjuvant.
2. Freunds Incomplete Adjuvant.
3. 0.9% injectable sodium chloride.

2.4 Cells and Reagents

1. Cell line Sp2/0-Ag14 (ATCC CRL-1581).
2. ClonaCell™-HY Hybridoma Kit (StemCell Technologies).
3. Dulbecco's Modified Eagle's Medium (DMEM).
4. Medium A: DMEM containing 10% low-endotoxin fetal bovine serum (FBS) only.
5. Medium B: DMEM without FBS, penicillin/streptomycin (100×), or 2-mercaptoethanol.
6. Medium C: DMEM containing 10% FBS, 1% penicillin/streptomycin (100×), and 60 μM 2-mercaptoethanol.
7. Polyethylene Glycol (PEG) reagent; Hybri-Max™, 50% (w/v), average mol wt 1450, 0.2 μm filtered, BioReagent.
8. Hypoxanthine-aminopterin-thymidine (HAT) selection medium.

9. Red cell lysis buffer (StemCell Technologies).
10. Keyhole limpet hemocyanin (KLH).
11. Carbonate buffer: 8.7 mM $NaCO_3$, 1.2 mM $NaHCO_3$pH 9.6.
12. ELISA blocking buffer: 1% bovine serum albumin (BSA) in phosphate-buffered saline (PBS) with 0.02% Tween 20.
13. 2,2′-azino-bis(3-ethylbenzothiazoline-6-sulfonic acid) (ABTS) single solution (Invitrogen).
14. Phosphate citrate buffer (Sigma/Aldrich).
15. 50% Hydrogen peroxide.
16. AffiniPure Fab Fragment goat-antimouse IgG (H+L).
17. Normal goat serum.
18. Horseradish Peroxidase (HRP) AffiniPure™ Goat AntiMouse IgG, Fcγ fragment specific.
19. Lightning Link DyLight 550.
20. Optimal cutting temperature (OCT) solution for cryosectioning tissue.
21. Cy3 goat antimouse IgG.
22. Prolong Gold with DAPI.
23. Radioimmunoprecipitation assay buffer (RIPA) lysis buffer.
24. Protease Inhibitor Cocktail Set 3 (Millipore).
25. Phosphatase Inhibitor Cocktail Set 2 (Millipore).
26. Dithiothreitol (DTT).
27. Tris-buffered saline with 0.1% Tween 20 (1× TBST).
28. 5% nonfat milk in 1× TBST.
29. Nitrocellulose membrane filter paper.
30. Pierce™ enhanced chemiluminescence substrate.

3 Methods

3.1 Peptide Design

1. Use web-based tools and databases to identify antigenic regions within a protein that would be targetable by monoclonal antibodies. Previously, we implemented this approach to generate antibodies against the small GTPase RhoB, IDO1, and IDO2 [6–8].
2. If it is important to develop an antibody that recognizes human and murine sequences, compare sequence homology between human and murine protein sequences. Use amino acid sequences with high interspecies homology to generate

an antibody that will recognize human and mouse proteins. However, if the reverse is needed, identify dissimilar regions across species in order to generate an antibody that can distinguish between human and mouse proteins.

3. After identifying unique amino acid regions, use publicly available crystal structures or predicted structures generated by web-based prediction sites such as iTasser [9] or Alphafold [10] to determine whether the identified regions are located on the surface of the structure. Figure 1 includes the sequence alignment of human and mouse TDO2, the crystal structures for both the single polypeptide and tetrameric TDO2, and the identified sequence that was used as the target for antibody generation. For our analysis, we used previously reported crystal structures for TDO2 [11–13]. In our work and studies

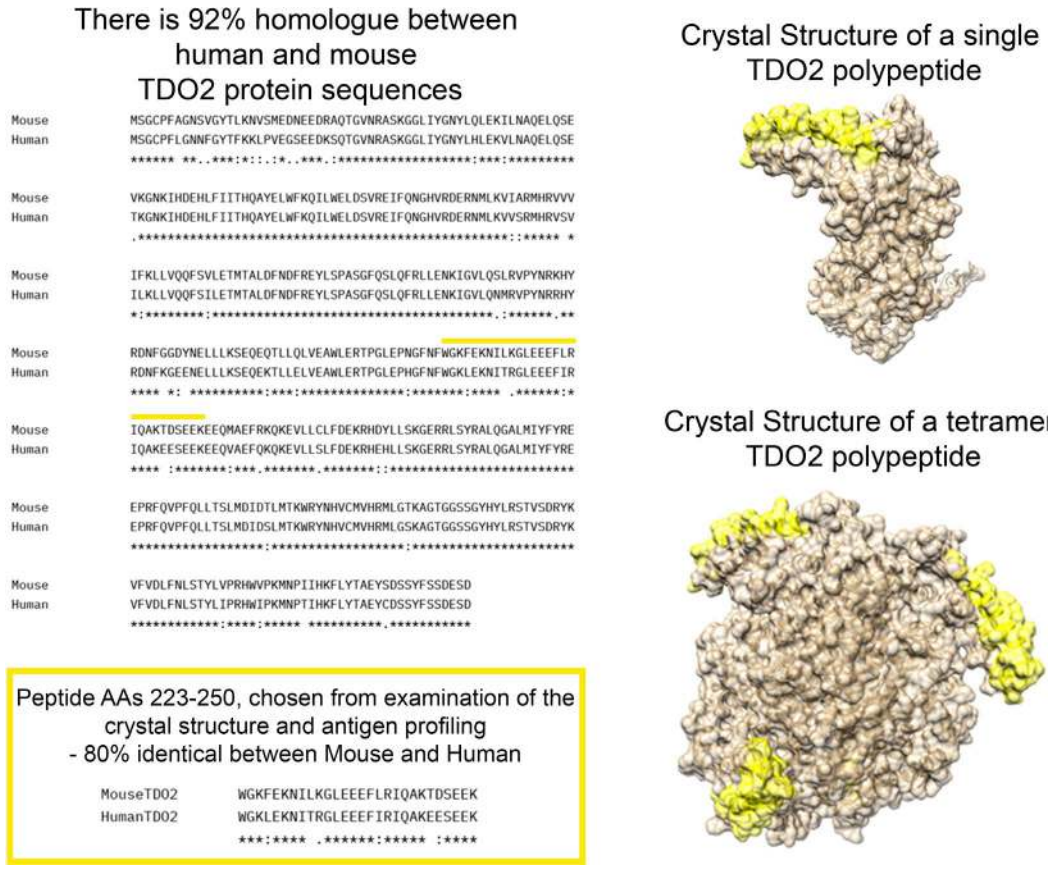


Fig. 1 Amino acid sequence, crystal structure, and antigen comparisons for human (accession no. NP_005642.1) and mouse (accession no. NP_064295.2) TDO2. Alignment was done using the Multiple Sequence Comparison by Log-Expectation (MUSCLE) web-based software (https://www.ebi.ac.uk/jdispatcher/msa/muscle). Crystal structure images were generated using analyses reported [11–13] and the UCSF CHIMERA program (https://www.cgl.ucsf.edu/chimera) [21]

reviewed by others, peptides of approximately 20–30 amino acids produce target-specific, high-affinity monoclonal antibodies [6–8, 14]. The peptide shown in Fig. 1 comprises 28 amino acids and was used as the immunogen to generate the monoclonal antibody characterized in subsequent figures.

4. Following sequence selection, synthesize two versions of the peptide using a commercial source, with one being a conjugated peptide and the other being an unconjugated peptide. The peptide with an N-terminal cysteine is conjugated to keyhole limpet hemocyanin (KLH) to provide an animal immune response and to prevent degradation, and amidation of the carboxyl terminus is included in the synthesis. The KLH-conjugated peptide will be used to immunize mice. The unconjugated peptide will be used in subsequent ELISA assays and should have N-terminal acetylation and C-terminal amidation for stability.

3.2 Immunization and Titer Assessment

Since the preferred fusion partner cell line was derived from a plasmacytoma isolated from the BALB/c strain [15], BALB/c mice are routinely used to produce monoclonal antibodies. However, in the past we have also had success producing antibodies using animals available on different genetic backgrounds that were genetically deficient for the target protein [8].

1. Perform the initial immunization in animals as a subcutaneous dose in an emulsion of 50 μg of the KLH-conjugated peptide and 100 μl of complete Freund's adjuvant.
2. 10–14 days after the first immunization, provide a second boost immunization by administering subcutaneously another 50 μg of the same peptide-KLH immunogen emulsified with 100 μl of incomplete Freund's adjuvant (*see* **Note 2**).
3. Approximately 20–28 days after the first dose of immunogen, draw blood to determine the titer of the elicited antibodies against the unconjugated peptide. Serum titers for immunogen-reactive immunoglobulin G (IgG) are measured using the ELISA assay (see Sect. 3.4). Data presented in Fig. 2 demonstrate the IgG titers after immunization with the conjugated peptide identified in Fig. 1.
4. Assess immunoreaction to KLH to confirm that the immune response is to the peptide, not the carrier protein.
5. Based on the titer of antipeptide antibodies, additional immunization doses of the conjugated peptide in incomplete Freund's adjuvant may be necessary to obtain a satisfactory serum titer of 1:10,000–1:100,000 for the peptide.
6. Once an optimal serum titer is reached, arrange a date for the fusion of the splenocytes and fusion partner cell line.

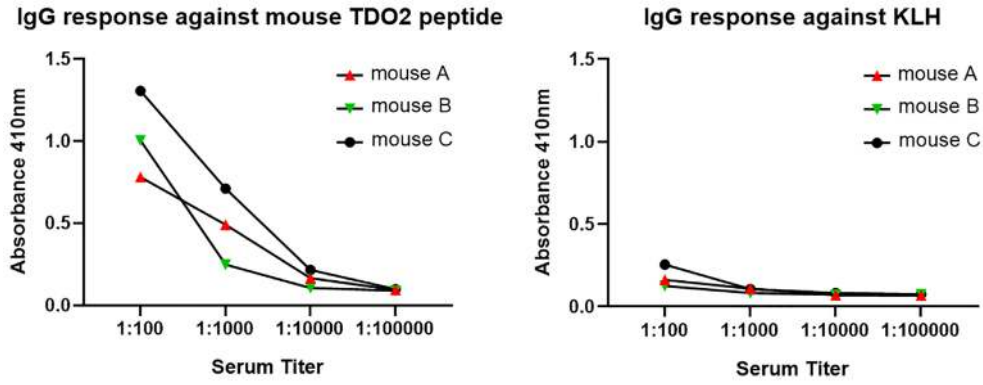


Fig. 2 ELISA results of the serum titers to the mouse TDO2-Peptide or KLH. Serum was diluted in bovine serum albumin phosphate-buffered saline at concentrations indicated on the graphs. Signal at high serum dilutions indicates a strong immune response. The graph compares the titers from individually immunized mice to the antigenic peptide coated to the ELISA plate (100 ng of peptide). Antibody from the serum bound to the fixed peptide was detected with an antimouse IgG Fc-specific horseradish peroxidase-conjugated antibody and substrate

7. Administer a final boost of immunogen 3 days before the fusion. Perform this final dosing as an intravenous injection of 50 µg of KLH-conjugated peptide in sterile 0.9% injectable sodium chloride retro-orbitally or via the tail vein at a total volume of 100 µl. The final dose should be given to the animal(s) with the highest serum titer to the immunogen.

3.3 Generation of Hybridomas

Fusion of the splenocytes and plasmacytoma cell line can be performed using the protocol supplied by StemCell Technologies for the ClonaCell™-HY Hybridoma Kit. Alternatively, investigators may use the method outlined below. For either protocol, maintain standard practices for cell culture under sterile conditions.

1. Approximately 2 weeks prior to fusing the spleen cells and plasmacytoma cells, begin propagating the Sp2/0-Ag14 cells in Medium C.
2. Six days before performing the fusion, culture 1×10^6 Sp2/0-Ag14 cells in 50 ml of Medium C.
3. Three days later (3 days before performing the fusion), prepare duplicate T75 flasks with 5×10^6 Sp2/0-Ag14 cells in 35 ml of growth Medium C in each flask.
4. One day prior to fusion, add an additional 15–20 ml of medium C to the two T75 flasks prepared in **step 3**.
5. Continue with the procedure below, which is a modification of the protocol from the StemCell Technologies ClonaCell™-HY Hybridoma Kit and uses one reagent, ClonaCell™-HY Medium D.

6. Just prior to performing the fusion, prewarm the PEG reagent (*see* **Note 3**), Medium A, Medium B, and Medium C to 37°C.
7. Place a 37°C water bath inside the Laminar flow cabinet.
8. Isolate splenocytes from the mouse with the highest serum titer against the peptide.
    a. Remove the spleen, and isolate splenocytes by passing the spleen through a 70 μm cell strainer using Medium B.
    b. Pellet cells at 500 × *g* for 5 min, and resuspend in red cell lysis buffer (2 ml/spleen).
    c. Incubate for 8 min at room temperature.
    d. Wash splenocytes with 20 ml of Medium B, and centrifuge at 500 × *g* for 5 min.
    e. Resuspend cells in Medium B (10 ml/spleen), and determine the number of splenocytes per ml (*see* **Note 4**).
9. Determine the cell count of the Sp2/0-Ag14 cells grown in the T75 flasks. Remove an appropriate number of cells, spin down, and resuspend with 30 ml of Medium B. The number of Sp2/0-Ag14 cells to use for fusion is determined using a ratio of 5:1 Splenocytes:sp2/0-Ag14. Optimal cell numbers are approximately 1×10^8:0.2×10^8.
10. Wash each cell type separately twice, with 30 ml of Medium B, to remove FBS.
11. Combine the splenocytes and Sp2/0-Ag14 cells into a 50 ml conical tube at the recommended 5:1 ratio for a final wash in 30 ml of Medium B.
12. Place the combined cell pellet in the 37°C water bath in the Laminar flow cabinet, and perform the following steps slowly:
    a. Add 1 ml of PEG reagent over the course of 1 min.
    b. Gently stir the PEG reagent and cells for 1 min.
    c. In increments of 1 ml/min, add a total of 4 ml of Medium B while stirring the contents of the tube over 4 min.
    d. In increments of 2 ml/min, add a total of 10 ml of Medium B while stirring the contents of the tube over 5 min.
    e. Allow the tube to sit in the water bath for 10 min.
    f. In increments of 15 ml/min, add a total of 30 ml of Medium A while stirring over 2 min.
    g. Allow the tube to sit in the water bath for 15 min.
    h. Centrifuge for 7 min at 400 × *g*.
    i. Gently resuspend the cell pellet with 30 ml of Medium A.

j. Centrifuge for 7 min at 400 × *g*, and remove the liquid.

k. Resuspend the washed cells in 50 ml of Medium C, and transfer the suspension into a T75 culture flask.

l. Incubate the suspended cells at 37°C in a 5% CO_2 tissue culture incubator.

13. ~24 h following the fusion, warm Medium D from the StemCell Technologies ClonaCell™-HY Hybridoma Kit for 15 min in a 37°C water bath placed in a laminar flow cabinet.
14. Collect the fused cells from the T75 flask, and pellet cells by centrifugation for 7 min at 400 × *g*.
15. Resuspend the pellet with 10 ml of Medium A.
16. Combine the 10 ml of cells in medium A with 90 ml of Medium D, and slowly mix by rotating the bottle to limit bubble formation.
17. Plate 10 ml of the cell suspension into a 100 mm cell culture dish, finishing with 10 culture dishes, each containing 10 ml.
18. Incubate the dishes at 37°C in a 5% CO_2 tissue culture incubator.
19. After 10–14 days of incubation, harvest hybridoma colonies by pipetting 10 µl of a colony of cells into separate wells of a 96-well culture plate filled with 200 µl of Medium C supplemented with 1× HAT selection medium. Fill approximately ten 96-well plates with colonies.
20. Screen the supernatant in each well ~3–4 days later by ELISA for IgG reactive to the target protein, as described in Sect. 3.4.

3.4 Screening the Hybridomas by ELISA

An ELISA protocol is used to evaluate both serum titers (see Sect. 3.2) and target reactivity of the resulting IgG secreted by the generated hybridomas.

1. Coat Immulon 2 HB plates with the immunogen peptide (1 µg/ml in 1× carbonate buffer, 100 µl per well) and incubate the plate at 4°C or room temperature overnight. The number of plates should match the number of 96-well culture plates with colony hybridomas. Perform all subsequent steps at room temperature.
2. The next day, remove the coating peptide solution from the wells of the ELISA plates, and block the wells with ELISA blocking buffer for 1–2 h.
3. Remove the blocking solution from the plates, and add 100 µl of the hybridoma supernatant (or diluted serum if titering serum antibody as described in Sect. 3.2) into appropriate wells, and incubate the plate for 1–2 h. Include negative control wells that contain 100 µl of fresh medium C (or diluted serum from

an unimmunized animal). Also setup positive control wells for hybridoma testing using a 1:100 dilution of immunized serum that previously reacted to the coated antigen.

4. Wash the plate(s) three times with 1× PBS, and after the last wash, tap the plate(s) on a paper towel to remove excess buffer.
5. Dilute the detection (secondary) antibody (goat antimouse Fc linked to HRP) to 0.1 μg/ml in ELISA Blocking Buffer, add 100 μl to each well, and incubate the plate(s) for 1 h.
6. Wash the plate(s) three times with 1× PBS, and after the last wash, tap the plate(s) on a paper towel to remove excess buffer.
7. Add 100 μl of the ABTS Single Solution substrate (prepared by the manufacturer's instructions) to each well to initiate the enzyme reaction, and incubate for 10–20 min at room temperature (*see* **Note 5**).
8. Measure the optical density (OD) of the solution in the wells at 410 nm in a plate reader. Hybridomas secreting reactive IgG are identified as having OD readings approximately three times higher than the negative control samples.
9. After hybridomas that are secreting antipeptide antibodies have been identified, propagate the hybridomas by subcloning and culturing methods as per the manufacturer's suggested methods outlined in the ClonaCell™-HY Hybridoma Kit protocol.

3.5 Analysis of the Hybridomas

3.5.1 Immunostaining Tissues Using Fluorescent Conjugates

1. Select and isolate appropriate tissue-type(s) that express the target protein of interest from wild-type (WT) mice for analysis. If available, isolate the same tissue(s) from knockout (KO) mice genetically deficient for the target protein of interest.
2. Embed tissues in OCT solution, flash freeze with liquid nitrogen, and store at −80°C (*see* **Note 6**).
3. Prepare cryosections of the frozen tissue at ~5 μm thickness on glass slides. Prepare enough sections so that one hybridoma supernatant is tested on both a WT tissue section and KO section, or, if gene-deficient tissue is not available, prepare a section for incubation with cell culture medium only.
4. Perform all subsequent steps at room temperature.
5. Fix tissue sections with ice-cold acetone for 5 min.
6. Wash slides three times with PBS (~10 min for each wash).
7. Block tissue sections first with 40 μg/ml of Fab fragment goat-antimouse IgG (H+L) in 1× PBS for 1 h.

8. Remove the Fab solution, and then block the tissue sections using 10% normal goat serum in PBS for approximately 30 min–1 h.
9. Incubate the blocked sections with the hybridoma supernatant for approximately 1 h at room temperature.
10. Wash the sections three times with PBS (~10 min for each wash).
11. To detect target-reactive hybridoma IgG, incubate tissue sections for ~1 h with 3–4 μg/ml of antimouse secondary antibody conjugated with an appropriate fluorophore in PBS. Incubate the sections in the dark to protect the fluorophore.
12. Wash slides three times with PBS (~10 min for each wash).
13. Mount coverslips (24 mm × 50 mm, No. 1.5 thickness) over the tissue sections using Prolong Gold with DAPI.
14. Analyze the fluorescent signal using an epifluorescent microscope, and compare the signal for a selected hybridoma IgG between tissue from a WT and KO animal (*see* **Note 7**).

3.5.2 Western Blotting

1. Select and isolate appropriate tissue-type(s) that express the target protein of interest from wild-type (WT) mice for analysis. If available, isolate the same tissue(s) from knockout (KO) mice genetically deficient for the target protein of interest.
2. Flash freeze tissues with liquid nitrogen, and store at −80°C (*see* **Note 8**).
3. Prepare tissue extracts on ice in cold RIPA lysis buffer containing protease and phosphatase inhibitors and dithiothreitol (DTT) [8] using a polytron blender at a ratio of 10× the weight of the tissue (Example: 100 mg is prepared in 1 ml of lysis solution) (*see* **Note 9**).
4. Centrifuge extracts at 14,000 × *g* for 15 min at 4°C, collect the supernatant (lysate), and analyze a small aliquot for protein concentration using a standard method such as the Bradford reagent and Bio-Rad manufacturer instructions. Store extracts at −80°C until ready for SDS-PAGE.
5. Separate equal amounts of protein for each tissue extract (50–100 μg/lane) by standard SDS-PAGE and blot to nitrocellulose membrane filter paper. Prepare one membrane per hybridoma supernatant to be tested.
6. Block membrane(s) in 5% nonfat milk dissolved in 1× TBST, rocking for at least 1 h at room temperature.
7. Incubate membrane(s) with hybridoma supernatant at 4°C overnight.
8. Perform all subsequent steps at room temperature.

9. After incubation with the supernatant, wash the membranes(s) are washed with 1× TBST three times, approximately 10 min per wash.
10. To detect target-reactive hybridoma IgG, incubate membrane(s) with HRP-conjugated goat antimouse Fc secondary antibody (diluted 1:1000 in blocking buffer) for 1 h.
11. Following three washes with 1× TBST wash buffer, treat the membrane(s) with Pierce™ ECL Western Blotting Substrate, and perform image acquisition using an imaging system such as the Bio-Rad ChemiDoc imaging system.

3.5.3 Confirmation of Immunostaining and Western Blotting Methods

To validate the approach for monoclonal antibody generation and forward the understanding of TDO2 in disease models, we present below the characterization of an anti-TDO2 antibody generated with the methods described herein.

1. In Fig. 3 (panels A and B), immunostaining results of mouse liver tissue are presented. Staining with the anti-TDO2 antibody or mouse isotype control IgG was performed on liver tissue from WT and KO animals [16]. The images compare the binding of the antibodies to tissue from WT (panel A) or TDO2-deficient (panel B) animals. In panel C, we present immunostaining results to demonstrate the ability of the anti-TDO2 antibody to detect TDO2 in tissue sections from human liver. Anti-TDO2 IgG was also used in the Western blotting protocol, and results are shown in panel D. This antibody detected a band of the appropriate molecular weight that was not present in liver tissue extracts from KO mice.
2. To demonstrate the potential of using the antibody to detect TDO2 expression in murine models, we present data in Fig. 4 using the Yumm1.7 murine melanoma model [17]. Yumm1.7 cells were injected subcutaneously into aged (>52 weeks old) male C57Bl/6 mice as previously described [18]. This model has been utilized to study changes in melanoma progression, therapy response, and outgrowth of dormant cells due to changes in the aging microenvironment [18–20]. About 5 weeks following subcutaneous injection, the tumors were removed, sliced, and sections were embedded in OCT and frozen or flash frozen for protein analysis. Tumor sections and protein lysates were prepared as described above. Following western blotting analysis, presented in panel A, TDO2 protein expression was detected in tumor tissue extracts isolated from tumor-bearing animals. Extracts from normal liver from WT and KO animals were included in the analysis. In panel B, immunofluorescent staining results are presented using the antibody on tissue prepared from the melanoma tumor sample #1 indicated in panel A. Taken together, the western and

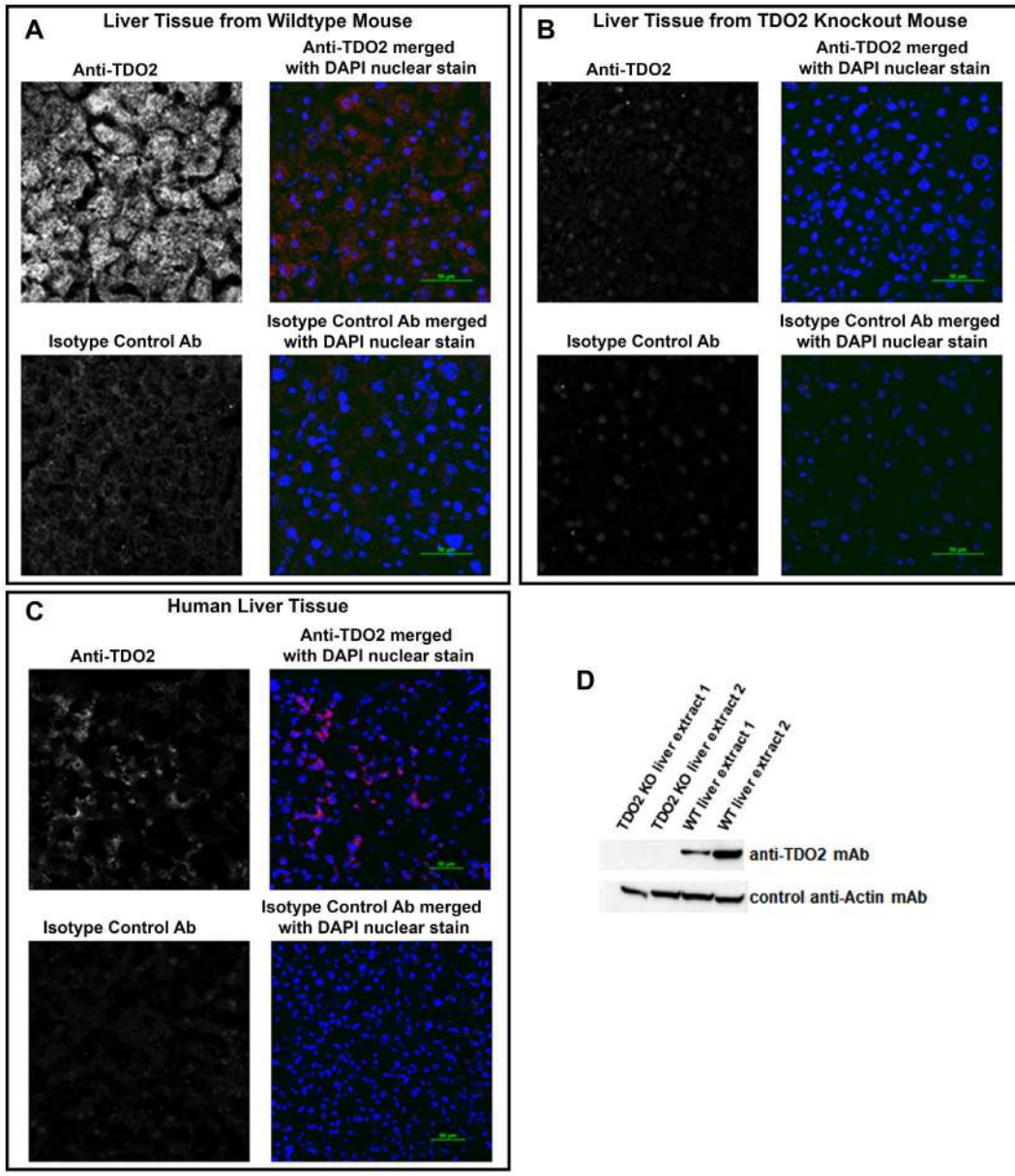


Fig. 3 Immunostaining results using anti-TDO2 antibody. In panels (**A**) and (**B**), immunostaining of mouse liver tissue is presented. Purified antibody or mouse isotype control IgG was conjugated with the DyLight 550 (Abcam) fluorophore. The DAPI fluorophore was included in the mounting medium to detect nuclei in the frozen tissue sections. The staining of an isotype control antibody was used to set the exposure level of the camera so that the staining comparison could be made between the WT and KO tissue. The images compare the binding of the antibodies to either liver tissue from WT (**A**) or TDO2-deficient (**B**) animals. (**C**), Immunostaining analysis on human liver tissue sections. The scale bar is indicated on the images. (**D**), Western blotting analysis is shown for tissue extracts (100 μg per lane) separated by standard denaturing gel electrophoresis and immunoblotted for TDO2 using the anti-TDO2 antibody. An antibody to detect the control protein Actin was used to show that protein was loaded in all lanes. TDO2 protein expression was detected in the liver tissue extracts isolated from WT but not TDO2-deficient mice

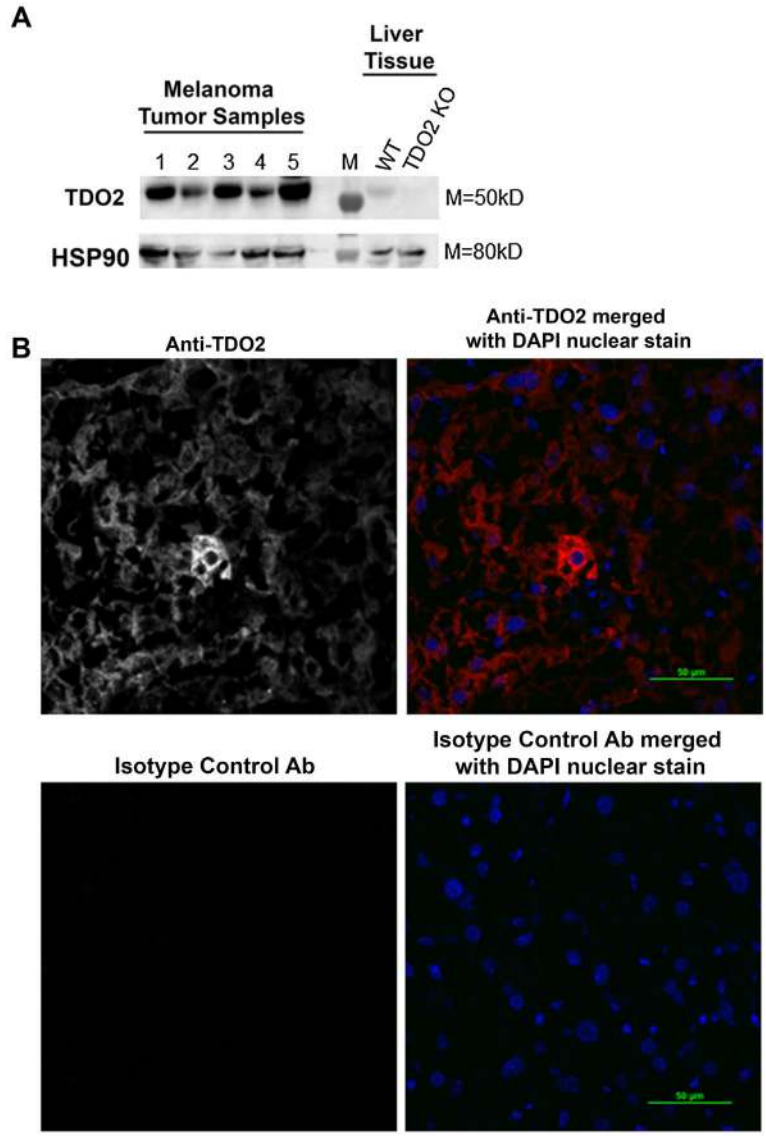


Fig. 4 TDO2 Expression in the Yumm Mouse Melanoma Model as measured with the anti-TDO2 antibody. (**A**), Western blotting analysis is shown for tissue extracts (100 μg per lane) separated on a 10% acrylamide gel by SDS-PAGE and immunoblotted for TDO2. TDO2 protein expression was detected in the tumor tissue extracts, and an antibody to detect the control protein HSP90 was used to show that protein was loaded in all lanes. (**B**), TDO2 immunostaining results on tissue prepared from the melanoma tumor sample #1 indicated in panel (**A**). Conjugated purified antibody or mouse isotype control IgG was used. The staining of an isotype control antibody was used to set the exposure level of the camera. The confocal images compare the binding of the antibodies to tumor tissue. The scale bar is indicated on the images

immunostaining results suggest the TDO2 is highly expressed in the Yumm melanoma model, and expression may be variable within the tumor.

4 Notes

1. Routinely used products and reagents are listed, and comparable products from various sources can be used unless otherwise noted. Manufacturer instructions should be followed for all selected products and reagents.
2. When handling Freund's adjuvants, wear appropriate personal protective equipment (PPE) to minimize the risk of skin/eye contact and potential irritation.
3. When handling PEG, wear appropriate PPE to minimize skin/eye contact and potential irritation. Another PEG reagent option is ClonaCell™-HY PEG (StemCell Technologies).
4. A hemocytometer or Coulter counter can be used to determine the number of cells per ml of medium.
5. Because ABTS can be an irritant, avoid skin/eye contact by using appropriate PPE
6. When performing several of the steps during the immunostaining procedure, such as using OCT and acetone, wearing PPE is recommended to avoid skin/eye contact, and following manufacturer instructions is recommended. Additionally, because acetone is a flammable liquid, be aware of heat sources. Tissue that has been fixed and paraffin embedded may also be used to characterize antibodies secreted from hybridomas.
7. When acquiring images to determine the reactivity of a monoclonal antibody, set the base camera exposure to the intensity from a section stained with either cell culture medium or murine isotype control IgG, or from the tissue isolated from a gene-deficient animal. When using mouse IgG, an appropriate concentration of 1 μg/ml can be used to compare staining intensity between the hybridoma IgG and this negative control.
8. To characterize positive reactivity of a hybridoma IgG in western blot analyses, it may be necessary to compare samples from cell lines that express or do not express the protein of interest. Extracts from cell lines that express (or that have been engineered to overexpress) the protein target (such as HEK 293 cells) can substitute for tissue extracts.
9. RIPA lysis buffer generally contains chemicals, such as DTT or beta-mercaptoethanol, that necessitate wearing PPE and

having proper ventilation. Consult the supplier's product information for specifications.

Acknowledgments

Support for this work was provided by the Lankenau Medical Center Foundation, Main Line Health Systems, and grant funds from the PA Department of Health. We are grateful to Drs. Christiane Opitz and Michael Platten for providing the TDO2 transgenic mouse.

Conflicts of Interest The authors have no conflicts of interest to declare that are relevant to the content of this chapter.

References

1. Muller AJ, Manfredi MG, Zakharia Y et al (2019) Inhibiting IDO pathways to treat cancer: lessons from the ECHO-301 trial and beyond. Semin Immunopathol 41(1):41–48
2. Theate I, van Baren N, Pilotte L et al (2015) Extensive profiling of the expression of the indoleamine 2,3-dioxygenase 1 protein in normal and tumoral human tissues. Cancer Immunol Res 3(2):161–172
3. D'Amato NC, Rogers TJ, Gordon MA et al (2015) A TDO2-AhR signaling axis facilitates anoikis resistance and metastasis in triple-negative breast cancer. Cancer Res 75(21):4651–4664
4. Opitz CA, Litzenburger UM, Sahm F et al (2011) An endogenous tumour-promoting ligand of the human aryl hydrocarbon receptor. Nature 478(7368):197–203
5. Guastella AR, Michelhaugh SK, Klinger NV et al (2018) Investigation of the aryl hydrocarbon receptor and the intrinsic tumoral component of the kynurenine pathway of tryptophan metabolism in primary brain tumors. J Neurooncol 139(2):239–249
6. Merlo LMF, Grabler S, DuHadaway JB et al (2017) Therapeutic antibody targeting of indoleamine-2,3-dioxygenase (IDO2) inhibits autoimmune arthritis. Clin Immunol 179: 8–16
7. Thomas S, DuHadaway J, Prendergast GC, Laury-Kleintop L (2014) Specific in situ detection of murine indoleamine 2, 3-dioxygenase. J Cell Biochem 115(2):391–396
8. Mandik-Nayak L, DuHadaway JB, Mulgrew J et al (2017) RhoB blockade selectively inhibits autoantibody production in autoimmune models of rheumatoid arthritis and lupus. Dis Model Mech 10(11):1313–1322
9. Yang J, Yan R, Roy A et al (2015) The I-TASSER Suite: protein structure and function prediction. Nat Methods 12(1):7–8
10. Jumper J, Evans R, Pritzel A et al (2021) Highly accurate protein structure prediction with AlphaFold. Nature 596(7873):583–589
11. Álvarez L, Lewis-Ballester A, Roitberg A et al (2016) Structural study of a flexible active site loop in human indoleamine 2,3-dioxygenase and its functional implications. Biochemistry 55(19):2785–2793
12. Lewis-Ballester A, Forouhar F, Kim S-M et al (2016) Molecular basis for catalysis and substrate-mediated cellular stabilization of human tryptophan 2,3-dioxygenase. Sci Rep 6:35169
13. Pham KN, Yeh SR (2018) Mapping the binding trajectory of a suicide inhibitor in human indoleamine 2,3-dioxygenase 1. J Am Chem Soc 140(44):14538–14541
14. Trier NP, Hansen P, Houen G (2019) Peptides, antibodies, peptide antibodies and more. Int J Mol Sci 20(24):6289
15. Kohler G, Milstein C (1975) Continuous cultures of fused cells secreting antibody of predefined specificity. Nature 256(5517):495–497
16. Lanz TV, Williams SK, Stojic A et al (2017) Tryptophan-2,3-Dioxygenase (TDO) deficiency is associated with subclinical neuroprotection in a mouse model of multiple sclerosis. Sci Rep 7:41271
17. Meeth K, Wang JX, Micevic G et al (2016) The YUMM lines: a series of congenic mouse melanoma cell lines with defined genetic alterations. Pigment Cell Melanoma Res 29(5):590–597

18. Webster MR, Fane ME, Alicea GM et al (2020) Paradoxical role for wild-type p53 in driving therapy resistance in melanoma. Mol Cell 77(3):633–644.e5
19. Alicea GM, Rebecca VW, Goldman AR et al (2020) changes in aged fibroblast lipid metabolism induce age-dependent melanoma cell resistance to targeted therapy via the fatty acid transporter FATP2. Cancer Discov 10(9):1282–1295
20. Fane ME, Chhabra Y, Alicea GM et al (2022) Stromal changes in the aged lung induce an emergence from melanoma dormancy. Nature 606(7913):396–405
21. Pettersen EF, Goddard TD, Huang CC et al (2004) UCSF Chimera—a visualization system for exploratory research and analysis. J Comput Chem 25(13):1605–1612



Chapter 35

Analytical Assessment of Fc-Receptor Binding of Therapeutic IgG1 Antibodies: A Surface Plasmon Resonance Approach

Silvia M. Bacot, Nozomi Sakakibara, Jessica Dement-Brown, Jordan D. Pritts, Devira Friedman, Kamai Patterson, Caroline Taylor, Jennifer Swisher, Gunther H. Boekhoudt, Venkateswara Simhadri, Carole Sourbier, V. Ashutosh Rao, Gerald M. Feldman and Tao Wang

Abstract

This manuscript describes the development and validation of a surface plasmon resonance (SPR)-based analytical method for characterizing Fc–Fcγ receptor (Fc–FcγR) interactions of therapeutic IgG1 antibodies. Using the Biacore T200 platform, binding kinetics between FcγRIIIa (F176 variant) and rituximab were evaluated as a proof-of-principle model. The assay enables real-time, label-free determination of association (ka), dissociation (kd), and equilibrium dissociation constant (K_D) values. The method incorporates defined sample preparation, chip conditioning, and kinetic analysis workflows and was validated in accordance with ICH Q2(R2) guidance. Intra- and inter-assay variability for kinetic parameters did not exceed 25%, and the established K_D range for the rituximab reference standard was 1.40–4.04 μM. This validated SPR approach provides a robust analytical platform for assessing Fc–Fcγ R binding interactions relevant to antibody-dependent effector functions, supporting antibody product characterization, comparability assessments, and quality control throughout the therapeutic antibody lifecycle.

Keywords Therapeutic antibody, Surface plasmon resonance, Antigen-binding fragment, Potency, Crystallizable fragment, Crystallizable fragment receptor, Effector functions

1 Introduction

1.1 Background and Scientific Rationale

Therapeutic monoclonal antibodies, including anti-CTLA-4 antibodies and antiprogrammed cell death protein 1 (PD-1) antibodies, represent a rapidly expanding class of biopharmaceuticals for the treatment of various malignancies, autoimmune conditions, and other diseases [1, 2]. In addition to direct effects mediated by binding of the Fab (antigen-binding fragment) region to target antigens, the

Kristian M. Hargadon (ed.), *Melanoma*, Methods in Molecular Biology, vol. 3089,
https://doi.org/10.1007/978-1-0716-5619-8_35,
© The Author(s), under exclusive license to Springer Science+Business Media, LLC, part of Springer Nature 2027

interaction between the crystallizable fragment (Fc) region of antibodies and Fc receptors (FcRs) represents a potentially important determinant of antibody therapeutic efficacy and safety. This interaction governs key effector functions including antibody-dependent cell-mediated cytotoxicity (ADCC), complement-dependent cytotoxicity (CDC), antibody-dependent cellular phagocytosis (ADCP), regulation of B cell activation, and modulation of antibody half-life through the neonatal FcR (FcRn).

Among effector functions, the interaction between therapeutic antibodies and Fc gamma receptor IIIa (FcγRIIIa) is particularly significant for ADCC activity. For example, mounting evidence indicates that the Fc region of ipilimumab, an IgG1 antibody, binds to FcγRIIIa (CD16) on natural killer (NK) cells and other effector cells. This binding event leads to selective depletion of CTLA-4-expressing cells, particularly regulatory T cells (Tregs) in the tumor microenvironment,resulting in enhanced anti-tumor immunity [3, 4]. Therefore, characterization of the binding affinities of Fc–FcR interactions is essential for understanding therapeutic efficacy and ensuring product quality. Notably, FcγRIIIa displays a well-characterized polymorphism at amino acid position 176 (equivalent to 158 in the mature protein), where phenylalanine (F176) and valine (V176) allelic variants exhibit distinct IgG1-binding affinities and functional responses (*see* **Note 1**). This polymorphism has been associated with differential clinical outcomes, as patients carrying the high-affinity V/V genotype generally demonstrate improved therapeutic responses and progression-free survival when treated with IgG1 antibodies such as rituximab, trastuzumab, or cetuximab, compared with those carrying the low-affinity F/F genotype [5–10].

1.2 Current Analytical Challenges

Traditional immunoassays such as ELISA provide endpoint measurements and require enzyme labeling, while flow cytometry, though capable of kinetic studies through time-course experiments, typically uses fluorescent labeling and cannot provide continuous label-free real-time binding dynamics. Surface plasmon resonance (SPR) has emerged as a promising analytical platform for studying Fc–FcR interactions due to its unique capabilities for continuous kinetic monitoring. SPR optical detection technology offers advantages in enabling comprehensive kinetic characterization of molecular interactions in real-time and without labeling requirements. SPR can determine association (k_a) and dissociation (k_d) rate constants, as well as equilibrium dissociation constant (K_D), providing insights into binding mechanisms and complex stability across concentration ranges from nanomolar to micromolar [11].

For robust regulatory scientific applications, analytical methods for product characterization and control are generally expected to demonstrate performance attributes including sensitivity, specificity, repeatability, intermediate precision, reproducibility, and robustness [12]. These performance attributes confirm that the analytical

procedures are suitable for their intended purpose and can reliably detect and quantify amounts of and differences in Fc–FcR interactions across different lots, formulations, or manufacturing conditions, supporting multiple phases of the product lifecycle, including product development and postmarket activities. The capability to measure complex binding scenarios makes SPR uniquely suited for investigating the binding behaviors observed in Fc–FcR systems. These capabilities are particularly relevant when assessing how modifications to the Fc region, such as glycosylation changes or amino acid substitutions, impact receptor binding profiles. Moreover, SPR technology has been reported in the literature to be used in stability and comparability studies of therapeutic antibodies and biosimilars [13–16].

1.3 Objectives and Scope of Protocol

This work describes the development and validation of an analytical method using the Biacore T200 Surface Plasmon Resonance system for measuring binding affinities (K_D) between FcγRIIIa (F176 variant) and a proof-of-principle IgG1 therapeutic anti-CD20 monoclonal antibody (rituximab). Notably, this protocol utilizes a chip featuring a preimmobilized dextran surface with a short oligonucleotide designed to bind biotin, optimized for protein–protein interaction analysis. While the methodology is based on protocols adapted from both Cytiva and Acro Biosystems [17, 18], this protocol focuses on the experience gained during assay development, optimization, and validation. The method encompasses sample preparation procedures and SPR analytical protocols specifically designed to characterize IgG1 Fc domain–FcγRIIIa interactions with precision and reliability. Figure 1 illustrates the mechanism of the analytical method used for measuring Fc-mediated binding of rituximab to biotinylated FcγRIIIa (F176) by SPR. Importantly, though this protocol describes the application of this technology to the analysis of the anti-CD20 antibody rituximab, it can readily be adapted to the analysis of any monoclonal antibody, including those currently in use and in development for the treatment of melanoma.

2 Materials

2.1 Equipment

1. Biacore Cytiva T200.
2. Nano-drop, Thermo Scientific Nanodrop 2000.
3. Beckman Coulter Centrifuge, Allegra 6KR.

2.2 Reagents and Supplies

Reagents and supplies may vary, as these recommendations are only for informational purposes.

1. HBS-EP + Buffer (10×): 10× Biacore running buffer (Cytiva, BR100669).
2. 7 mm Biacore tube (Cytiva, BR100212).

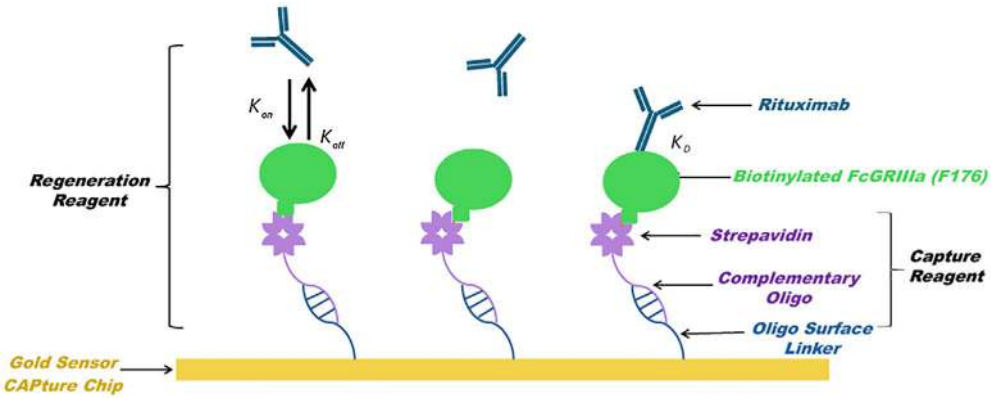


Fig. 1 Schematic of SPR biosensor setup for kinetic analysis of rituximab-FcγRIIIA interaction. The SPR sensor chip features a gold surface coated with a dextran matrix containing covalently attached oligonucleotide surface linkers. During the capture phase, a complementary oligonucleotide conjugated to streptavidin is injected as the capture reagent, forming stable hybridization complexes with the surface-bound oligonucleotides. Biotinylated human FcγRIIIA receptor (F176 polymorphic variant) is subsequently captured as the ligand through high-affinity biotin–streptavidin interactions. Rituximab, a monoclonal antibody, is then injected as the analyte, and its binding to the surface-immobilized FcγRIIIA receptor is monitored in real-time through changes in refractive index detected by surface plasmon resonance. Following each binding cycle, regeneration reagent is applied to remove the complementary oligonucleotide and all associated binding partners, effectively regenerating the sensor surface for subsequent measurements. Real-time binding kinetics enable determination of the association rate constant (k_a), dissociation rate constant (k_d), and equilibrium dissociation constant (K_D) for comprehensive characterization of the antibody–receptor interaction

3. Bovine serum albumin (BSA).
4. Biotin CAPture Kit, Series S (Cytiva, 28920234).
5. Regeneration solution: Mix three parts regeneration stock 1 (8 M Guanidine HCl) with one part regeneration stock 2 (1 M NaOH) from the Biotin CAPture kit. Prepare fresh before use.
6. Deep well 96-well microplate.
7. Sample tray and reagent rack type 2 (Cytiva, BR100482).
8. 25 μg of Biotinylated hCD16a (F176) (Acro Biosystems, CDA-H82E8).
9. PD Minitrap G25 Spin Desalting Columns (Cytiva, 28918007).
10. Rituximab (Roche)—Reference standard (RS).

3 Methods

3.1 Receptor Preparation

1. Prior to receptor reconstitution, centrifuge the vial at ~200 × *g* in a 50 mL tube to force the lyophilized material out of the cap.

2. Reconstitute the FcγRIII (F176) receptor (*see* **Notes 2** and **3**) in 250 µL of sterile/ultra-filtered water. Incubate for 30–60 min at room temperature with occasional manual mixing by inversion (do NOT vortex or mix vigorously).
3. To achieve a final reconstituted solution containing 0.1% BSA (w/v) as a stabilizer, add 500 µL of 0.15% w/v BSA solution in sterile water, and mix by gentle inversion. Alternatively, add 75 µL of 1% w/v BSA solution and dilute to 750 µL with sterile water.
4. Aliquot receptor in 1.5 mL microfuge tubes at a concentration of no less than 1 µg of receptor/tube, and store at −80°C. This reagent is single-use only and should not undergo freeze/thaw cycles.

3.2 Running Buffer Preparation

1. Prepare 1× Biacore running buffer (RB) by diluting the 10× buffer 1:10 in distilled water (1× RB does not need to be made fresh and can be used for multiple runs).
2. Filter and degas the prepared 1× Biacore RB using a 0.22 µm PES filter unit by leaving it on the vacuum filter for ~30 min.

3.3 Regeneration Solution Preparation

1. Prepare fresh regeneration solution by mixing three parts regeneration stock 1 (8 M Guanidine HCl) with one part regeneration stock 2 (1 M NaOH) from the Biotin CAPture kit.
2. Pipette 200 µL of the mixed regeneration solution into a 7 mm Biacore vial. Place the regeneration solution vial in the Biacore reagent rack for the three successive injections to condition the chip.

3.4 Antibody Preparation

1. To buffer exchange rituximab RS into 1× Biacore running buffer (1× RB) (*see* **Note 4**), begin by removing the top and bottom caps of two PD Minitrap G25 columns, and allow the storage solution to flow out by gravity.
2. Fill the column with 1× RB, allowing it to enter the packed bed completely by gravity flow. Discard the flow-through into a waste collection tube.
3. Repeat this procedure twice more, each time allowing the liquid to enter the bed completely before adding the next column volume (three column volumes is ~8 mL).
4. Add 0.5 mL of the 10 mg/mL antibody in formulation buffer to each column, allowing it to enter the bed completely. Discard the flow-through.
5. Place a fresh collection tube under the column.
6. Elute by adding 1.0 mL of 1× RB and collecting 1.0 mL of the eluate. Any eluate in excess of 1.0 mL will contain ions from the formulation buffer (*see* **Note 5**).

7. Measure antibody concentration by using the Nanodrop 2000.
8. Aliquot 250 µL of RS in 1.5 mL microfuge tubes, and store at −80°C until ready to use (*see* **Note 6**).

3.5 Chip Preparation (see Note 7)

1. Allow the sealed chip from the kit to come to room temperature for 30 min to reduce condensation.
2. Label two 50 mL conical tubes with the chip lot number from the cassette chip pouch.
3. Open the chip pouch and eject the chip from its cassette into a conical tube filled with sterile ultrapure water.
4. Hydrate the chip at room temperature overnight.
5. After rehydration, store the chips in 1× RB in a 50 mL conical tube at 4°C when not in use.

3.6 Chip Conditioning (see Note 8)

1. Run 1× RB through the instrument for a minimum of 2 h to equilibrate the system to the new buffer before docking the chip.
2. Remove the solution from the conical tube housing the chip, and wash both sides of the chip with fresh 1× RB (~ 20 mL).
3. Dry both sides of the plastic containing the sensor chip with a low-lint wipe, being careful to avoid touching the recessed gold chip surface. Be careful not to leave any dust on the recessed gold chip surface, as it may interfere with the detector prism within the instrument.
4. Open Biacore Control Software.
5. Click "Eject Chip."
6. Remove the maintenance chip.
7. Store the chip inside its corresponding cassette.
8. Select "New Chip," and enter the pertinent information, including chip type and lot number.
9. Manually shut the chip compartment door, and then click on "Dock Chip."
10. To condition the chip, perform three successive 1 min injections of regeneration solution over all surfaces at a 30 µL/min flow rate, with 1 min gaps between each successive injection.
11. The chip is now ready for running the kinetic assay.

3.7 Kinetic Run (Performed in Triplicate)

The assay consists of three separate kinetic measurements preceded by the startup cycles described above. The assay format and cycles are designed and controlled using Biacore T200 Control Software and saved as a Wizard Template.

1. Add three startup cycles into the wizard template for the triplicate runs.

2. Prepare the assay materials on a deep-well Biacore-compatible low-binding microplate with 0.5 mL wells.
3. Prepare Analyte (rituximab) for serial dilution by first diluting the monoclonal antibody to a concentration of 10,000 nM in 1× RB.
4. Prepare three separate sets of twofold serial dilutions for nine concentrations (10,000, 5000, 2500, 1250, 625, 312.5, 156.25, 78.125, and 0 nM) in 1× RB. Perform dilutions directly onto the plate, starting with 300 µl of the highest concentration and transferring 150 µl serially to lower concentrations. Two samples of the lower concentration are included in the plate as quality control.
5. To prepare the Receptor (Ligand), thaw an aliquot of Fcγ RIIIa/CD16a (F176) at 2–8°C, and briefly centrifuge at 228 × *g* for 30 s in a tabletop unit to force all liquid into the bottom of the tube (this aliquot cannot be reused once thawed and must be used within 16 h).
6. Dilute the receptor stepwise to 0.1 µg/mL with 1× RB; 900 µL is needed per triplicate run in an experiment.
7. Aliquot the receptor into two 7 mm Biacore tubes, one with 120 µL (100 µL + 20 µL extra) and the second with 720 µL (700 + 20 µL extra).
8. The plate layout is predefined by the assay file in the Control Software, on the Wizard Template, and consists of three dilution lanes and a corresponding series of CAPture reagent wells. The assay file is also preprogrammed as to how much running buffer is necessary for the analysis.
9. Briefly centrifuge the plate and tubes to ensure all the reagents are gathered at the bottom of the well or tube.
10. Insert the plate and tubes into the Biacore rack, and load the rack on the instrument
11. Begin assay run.
12. Triplicate assay running time should be approximately 15 h.

3.8 Assay Cycle

The assay can be broken down into "cycles" that consist of the following four basic steps, which were integrated into the Wizard Template. The steps are briefly described below (*see* **Note 9**):

1. Biotin CAP Reagent Injection: The Biotin CAP Reagent (found in the CAPture kit) is injected for 60 s at a flow rate of 2 µL/min over both active and reference surfaces.
2. Ligand capture: the ligand (receptor) is injected over the active surface (either S2 or S4 regions of the chip) at a flow rate of 5 µL/min for ~50 s to reach a target capture level of

13–20 RU. The reference region of the chip (either S3 or S1 regions) has no ligand (receptor) capture.

3. Analyte injection and dissociation: analyte is injected over both reference and active surfaces at a flow rate of 30 µL/min for an association phase of 100 s. The dissociation phase (when only 1× RB is flowing over the surface) follows analyte injection and lasts for 210 s at a flow rate of 30 µL/min.
4. Regeneration: regeneration is performed at the end of each cycle to remove all captured receptors along with any bound ligand. The chip is regenerated in regeneration solution at a flow rate of 10 µl/min for 120 s. Include an extra wash with 1× RB after the last regeneration injection.

3.9 Kinetic Analysis (see Note 10)

1. For interpretation of the assay, it is essential for precision that each kinetic run be assessed using the same criteria in the same manner.
2. Each set of nine dilutions makes up one independent replicate and must be analyzed separately using the kinetics function in the Biacore Evaluation Software from the results file for the run described above.
3. Select "kinetics surface bound" from the menu, then select one of the three replicates of the nine dilutions series (labeled 1–3 in the software).
4. Deselect one of the duplicates of the lowest concentration.
5. Select "kinetics" at the bottom right of the window to move forward.
6. In the window showing the normalized sensorgrams, remove the peaks in the data corresponding to the injection start and end using the right-click cursor (it should show a black box over the data to be removed). These peaks represent the changes in protein concentration during buffer transitions. The removed portion should be 1 s before and after each of the buffer transition peaks, and this editing must be repeated for each separate triplicate run.
7. In the subsequent data analysis window, the appropriate binding model for the interaction must be selected for kinetic fitting. The "1:1 binding" (Langmuir) model was chosen in our analysis, consistent with established methodologies in the scientific literature for characterizing elementary molecular interactions. This model assumes a single, independent binding event between one ligand and one analyte molecule and is widely used for determining binding affinity constants [19, 20].
8. After choosing the appropriate binding model, use the software to perform the curve-fitting to completion to determine

the kinetic parameters. A report will be generated for that dilution series with all the kinetic information and a residuals plot showing the deviation from the binding model.

9. Repeat these steps for the other two replicates of the dilution series.

3.10 Confirmation of System Suitability Criteria

1. The system suitability criteria are deemed to be acceptable as long as the T200 Evaluation software's Quality Control parameters are met. Confirm that these parameters have been met by going to the Quality Control tab and identifying that there are green check marks for the following criteria:
   a. "Kinetic constants are within instrument specifications."
   b. "Kinetic constants appear to be uniquely determined."
2. The R_{max} value represents the theoretical maximum response units (RU) achieved when the sensor surface is fully saturated with analyte. This parameter is directly proportional to the ligand immobilization level and depends on the fraction of immobilized ligand that remains functionally active and accessible for analyte binding. For this assay, R_{max} should typically fall within 20–50 RU to ensure optimal signal-to-noise ratio while avoiding mass transport limitations [19]. While R_{max} values should be reasonably consistent between experimental replicates (typically within ±20%), minor variations are acceptable since the analysis software normalizes binding responses to the actual immobilization level during kinetic fitting. Significant deviations in R_{max} may indicate surface degradation, incomplete regeneration, or changes in ligand activity [21].
3. The residuals plot (Chi^2 values of experimental vs. fitted data) should be within the ±3 × standard deviation (SD) limits.
4. U-values should be between 1 and 15.
5. Calculate the average and standard deviation of the triplicate run of the K_D obtained. Calculate the relative standard deviation (RSD) or coefficient of variation (%CV) by dividing the standard deviation by the average of triplicate K_D values, multiplied by 100.
6. In the case of unexpected and/or suspected system suitability failures (e.g., appearance of a large sharp peak, potentially due to bubbles), the triplicate run should be repeated after an appropriate regeneration step.

3.11 Confirmation of Sample Suitability Criteria

1. Based on the conditions described herein and using multiple runs, a K_D for the rituximab Reference Standard was determined to be between 1.40 μM and 4.04 μM (*see* **Note 11**).
2. Chi^2 should be ≤10% R_{max}.

3.12 Assay Validation

When FcR effector function is one of the mechanisms of action for a therapeutic antibody, SPR method validation can potentially support product characterization. For detailed assay validation principles, we followed **ICH Q2(R2)** *Validation of Analytical Procedures: Text and Methodology Guidance for Industry* (2022). A summary of the assay validation characteristics and respective acceptance criteria tested is provided in Table 1.

Table 1
Summary of validation characteristics and respective acceptance criteria

Validation characteristics	Acceptance criteria
Specificity 1) Rituximab reference material (IgG1, positive control) 2) Nivolumab reference material (IgG4, negative control)	1) Each experiment with RS should pass the system suitability criteria 2) Rituximab reference material K_D should be within 1.40 μM–4.04 μM Note: twenty percent of the established reference value is generally acceptable 3) Nivolumab should fail sample suitability
Precision Repeatability (intra-assay precision) • One analyst performing three independent SPR runs from independent preps (i.e., dilution series) on different days Intermediate Precision (inter-assay precision) • Two analysts performing three independent experiments each (three independent SPR runs per independent experiment), totaling 18 experiments, using two different chips each (four chips total) Precision and reproducibility should be separate Reproducibility • Same as above, precision/intermediate precision • Typically, different laboratories	1) Each experiment should pass the system suitability criteria 2) The intra-assay variability between three independent runs of k_a, k_d, K_D, and R_{max} on a single day by a single analyst should not exceed 25%. The following portion should go only with the reproducibility part, separate from the precision acceptance criteria. 3) The inter-assay precision of k_a, k_d, K_D, and R_{max} values by two analysts over different days should not exceed more than 25%. The following portion should go only with the reproducibility part, separate from the precision acceptance criteria. This is conducted when experiments are performed on a second Biacore instrument. Experiments should also pass sample suitability criteria
Robustness Influence of different lots: • Biotinylated FcγRIIIa • Rituximab	1) The K_D range should be within 3 × SD of RS 2) The %CV of three independent runs should not be more than 25% for the kinetic parameters (k_a, k_d, and K_D) and R_{max}
Method capability range for intended purpose: Influence of +2%–+10% difference in afucosylated glycans	1) The %CV of three independent runs should not be more than 25% for the kinetic parameters (k_a, k_d, and K_D) and R_{max} 2) Up to 10% difference in afucosylation has acceptable precision (defined above) and linearity ($R^2 > 0.98$)

4 Notes

1. In this manuscript, residue numbering refers to the full-length protein (F176/V176), corresponding to position 158 in the mature protein.
2. Generally, we have observed minor lot-to-lot variations of the commercially available Fc receptors. Therefore, it is recommended that appropriate robustness studies and new lot qualification testing (with predefined acceptance criteria) be conducted to confirm comparable binding kinetics prior to use.
3. Whenever possible, a single receptor lot should be used to evaluate multiple antibody drugs to support comparability or analytical similarity assessments. However, the use of multiple Fc receptor lots may be necessary due to reagent availability or for validation purposes. In such cases, experiments should be carefully designed to ensure sufficient replicates and the inclusion of RS to monitor accuracy and reproducibility across receptor lots. These different lots of receptors will be considered acceptable as long as the %CV across runs for the RS is <25%.
4. Prepare all samples in the same running buffer to minimize bulk shift differences that can cause significant errors in SPR measurements.
5. Buffer exchange can alternatively be performed by centrifugation or using dialysis cassettes.
6. New RS lots must be validated prior to use.
7. This chip preparation step is only necessary when using a brand-new chip.
8. Implement this conditioning step when using a new chip or whenever a chip is reused after being stored.
9. The assay cycle requires attention to the following key steps to ensure accuracy and high-quality data:
    a. Preinjection phase: allow sufficient time (typically 30–60 s) for a stable baseline before analyte injection. Monitor for baseline drift, which should be minimal (<0.1 RU/min) for reliable kinetic analysis. Ensure the 1× RB has equilibrated through the system and the temperature is stable. Any buffer changes should be allowed to fully equilibrate before starting the cycle.
    b. Sample injection (association phase): use consistent injection volumes and durations across all concentrations. Typical injection times range from 60 to 300 s, depending on the binding kinetics and required signal

levels. Maintain a constant flow rate during injection to ensure reproducible mass transport conditions. Avoid flow rate changes during the association phase, as this affects binding kinetics. Verify actual analyte concentrations through independent methods, when possible, as errors in concentration significantly impact kinetic parameter determination.

c. Dissociation phase: the buffer chase duration should allow adequate time for dissociation monitoring, typically 2–10 min, depending on the expected dissociation rate. Faster dissociating complexes require shorter monitoring periods with higher data collection frequency. Continue with a consistent flow rate during dissociation to maintain stable conditions and prevent rebinding effects.

d. Regeneration phase: use the mildest effective regeneration conditions to preserve ligand activity while ensuring complete analyte removal. Verify complete return to baseline after regeneration. Incomplete regeneration leads to slower apparent association rates and systematic errors. To assess surface stability, monitor for loss or increase in binding capacity over multiple cycles, which indicates surface degradation or incomplete regeneration.

e. Inter-cycle considerations: include adequate buffer washes between regeneration and the next injection to remove residual regeneration solution and re-establish baseline conditions. Allow consistent timing between cycles to ensure thermal equilibrium and to minimize systematic variations. Monitor real-time sensorgrams for anomalies such as injection artifacts, air bubbles, or unusual binding profiles that may indicate technical problems.

f. Cycle optimization: for preliminary optimization, conduct initial cycles with test concentrations to optimize injection time, dissociation time, and regeneration conditions before collecting final data. Run control cycles by including periodic buffer-only injections and by repeating concentration measurements to assess system stability and reproducibility throughout the experiment.

10. When conducting kinetic analyses, the following should be taken into consideration, as proper attention to these steps will significantly improve the quality and reproducibility of the kinetic measurements in SPR experiments:

a. Kinetic model selection: Choose appropriate binding models (e.g., 1:1, bivalent, heterogeneous) based on the molecular interaction, and validate model assumptions.

b. Quality assessment: evaluate residuals, chi-squared values, and parameter confidence intervals to assess fit quality and parameter reliability (all of which are established in the Biacore Evaluation Software).

11. This K_D was based on the average ±3 SD with limited data.

5 Conclusion

In summary, surface plasmon resonance (SPR) has emerged as one of the primary analytical methods for characterizing Fc–Fcγ receptor (Fc–FcR) interactions, owing to its capability to measure binding kinetics and affinities in real time without the need for labeling [5, 20, 22]. SPR can provide quantitative insights into both on-rate (k_a) and off-rate (k_d) constants, enabling greater detail in quality attributes for assessment of antibody effector function and comparability across therapeutic candidates and biosimilars. Several factors can influence the accuracy and reproducibility of SPR measurements, including the quality and purity of the IgG and receptor proteins, the flow rate of the analyte solution, the surface density of immobilized receptor, and the buffer composition [21, 23]. Interactions can also be affected by nonspecific binding or mass transport limitations if experimental parameters are not carefully optimized [24]. Therefore, appropriate control of assay conditions ensures reliable and interpretable Fc–FcR binding data.

The assay development framework described here provides a suitably robust and reproducible surface plasmon resonance (SPR) analytical procedure for evaluation of Fc–Fcγ receptor (Fc–FcR) binding interactions. The principles and procedures described in this section are generally applicable to the assessment of binding characteristics between various Fc regions and Fc receptors and, more broadly, to the characterization of protein–protein interactions relevant to therapeutic antibody development and product quality control.

Acknowledgments

Devira Friedman and Kamai Patterson and Caroline Taylor are fellows in the Research Participation Program at the Center for Drug Evaluation and Research, administered by the Oak Ridge Institute for Science and Education through an interagency agreement between the U.S. Department of Energy and the U.S. Food and Drug Administration. This research received no external funding.

This research was supported by FDA CDER OPQ BsUFA III Regulatory Science Pilot Program. This article reflects the views of the authors and does not necessarily reflect those of the U.S. Food and Drug Administration. Any mention of commercial products is for clarification only and is not intended as approval, endorsement, or recommendation.

Conflicts of Interest The authors have no conflicts of interest to declare that are relevant to the content of this chapter.

References

1. Lu R-M, Hwang Y-C, Liu IJ et al (2020) Development of therapeutic antibodies for the treatment of diseases. J Biomed Sci 27(1):1. https://doi.org/10.1186/s12929-019-0592-z
2. Paul S, Konig MF, Pardoll DM et al (2024) Cancer therapy with antibodies. Nat Rev Cancer 24(6):399–426. https://doi.org/10.1038/s41568-024-00690-x
3. Romano E, Kusio-Kobialka M, Foukas PG et al (2015) Ipilimumab-dependent cell-mediated cytotoxicity of regulatory T cells ex vivo by nonclassical monocytes in melanoma patients. Proc Natl Acad Sci 112(19):6140–6145. https://doi.org/10.1073/pnas.1417320112
4. Romano E, Kusio-Kobialka M, Foukas PG et al (2014) FcgRIIIA (CD16)-expressing monocytes mediate the depletion of tumor-infiltrating Tregs via Ipilimumab-dependent ADCC in melanoma patients. J Immunother Cancer 2(Suppl 3):O14. https://doi.org/10.1186/2051-1426-2-S3-O14
5. Bruhns P, Iannascoli B, England P et al (2009) Specificity and affinity of human Fcγ receptors and their polymorphic variants for human IgG subclasses. Blood 113(16):3716–3725. https://doi.org/10.1182/blood-2008-09-179754
6. de Taeye SW, Bentlage AEH, Mebius MM et al (2020) FcγR binding and ADCC activity of human IgG allotypes. Front Immunol ume 11:740. https://doi.org/10.3389/fimmu.2020.00740
7. Koene HR, Kleijer M, Algra J et al (1997) Fcγ RIIIa-158V/F polymorphism influences the binding of IgG by natural killer cell FcγRIIIa, independently of the FcγRIIIa-48L/R/H phenotype. Blood 90(3):1109–1114. https://doi.org/10.1182/blood.V90.3.1109
8. Cartron G, Dacheux L, Salles G et al (2002) Therapeutic activity of humanized anti-CD20 monoclonal antibody and polymorphism in IgG Fc receptor FcγRIIIa gene. Blood 99(3):754–758. https://doi.org/10.1182/blood.V99.3.754
9. Aoyama M, Tada M, Ishii-Watabe A (2022) FcγRIIIa-158V/F polymorphism affects the performance of FcγRIIIa-related bioassay. Biochem Biophys Res Commun 608:149–155
10. Musolino A, Naldi N, Bortesi B et al (2008) Immunoglobulin G fragment C receptor polymorphisms and clinical efficacy of trastuzumab-based therapy in patients with HER-2/neu–positive metastatic breast cancer. J Clin Oncol 26(11):1789–1796. https://doi.org/10.1200/JCO.2007.14.8957
11. Motsa BB, Stahelin RV (2023) A beginner's guide to surface plasmon resonance. Biochem 45(1):18–22. https://doi.org/10.1042/bio_2022_139
12. Guideline I (2022) Validation of analytical procedures Q2 (R2). ICH, Geneva, Switzerland
13. Singh SK, Pokalwar S, Bose S et al (2018) Structural and functional comparability study of anti-CD20 monoclonal antibody with reference product. Biologics 12:159–170. https://doi.org/10.2147/btt.S187744
14. Wang S, Wang Y, Li Z et al (2024) Early determination of potential critical quality attributes of therapeutic antibodies in developability studies through surface plasmon resonance-based relative binding activity assessment. Mabs 16(1):2374607. https://doi.org/10.1080/19420862.2024.2374607
15. Rathore A, Dash R (2019) Real-time characterization of biotherapeutics and comparability of biosimilars. BioPharm Int 32(3):34–39
16. Kirchhoff CF, Wang XM, Conlon HD et al (2017) Biosimilars: key regulatory considerations and similarity assessment tools. Biotechnol Bioeng 114(12):2696–2705. https://doi.org/10.1002/bit.26438
17. Cytiva. (2023). Biotin CAPture Kit: Instructions for Use (Document No. 28924234 AG, V:13)
18. ACROBiosystems. Biotinylated Human Fc gamma RIIIA / CD16a (F176) Protein,

Avitag™,His Tag (Cat. No.CDA-H82E8) in house SPR Protocol (Biotin CAP). Newark (DE): ACROBiosystems, 2022
19. Karlsson R, Fält A (1997) Experimental design for kinetic analysis of protein-protein interactions with surface plasmon resonance biosensors. J Immunol Meth 200(1–2): 121–133
20. Rich RL, Myszka DG (2000) Advances in surface plasmon resonance biosensor analysis. Curr Opin Biotechnol 11(1):54–61
21. Myszka DG (1999) Improving biosensor analysis. J Mol Recognit 12(5):279–284
22. Schuck P (1997) Use of surface plasmon resonance to probe the equilibrium and dynamic aspects of interactions between biological macromolecules. Annu Rev Biophys Biomol Struct 26:541–566. https://doi.org/10.1146/annurev.biophys.26.1.541
23. Karlsson R, Michaelsson A, Mattsson L (1991) Kinetic analysis of monoclonal antibody-antigen interactions with a new biosensor based analytical system. J Immunol Meth 145(1–2):229–240
24. Cooper MA (2002) Optical biosensors in drug discovery. Nat Rev Drug Discov 1(7):515–528. https://doi.org/10.1038/nrd838



Chapter 36

In Vivo Reversible Electroporation for Melanoma Therapy

Namita Nanda and Joseph J. Skitzki

Abstract

Reversible Electroporation (rEP) has been a venerable in vitro lab technique for the transfection of cells. Recent in vivo applications of rEP for manipulating tumors and forcing tumor cell expression of proteins of interest are being explored in clinical trials. The ability to perform in vivo rEP in the lab can create translational opportunities and study mechanisms for optimal outcomes in patients. A general protocol is described and may serve as a template for melanoma researchers.

Keywords Reversible electroporation, Irreversible electroporation, Plasmids, Melanoma, Tumor

1 Introduction

The phenomenon of exposing cells to an electrical field to increase cell membrane permeability was first reported in 1968 [1]. Electroporation is the term for applying an external electrical field that increases the cellular transmembrane potential of the lipid bilayer to a threshold that generates pores in the cell membrane [2]. Electroporation can either preserve cell viability (reversible) or lead to cell death (irreversible) and is dependent upon the applied electrical pulse duration and voltage. Typically, reversible nanopores are formed in the cell membrane after eight electrical square wave pulses with a duration of 100 μs applied at 100–1000 V [3]. When the electrical field is removed, the transmembrane potential begins to return to normal and the generated pores reseal over the course of seconds to minutes [4, 5]. The maintenance and subsequent closure and repair of the generated membrane pores is an active cellular process akin to wound healing, and the kinetics are mostly dependent upon pore size [6]. This reversible electroporation (rEP), also known as electro permeabilization or electro transfection has both in vitro and in vivo applications [2]. Contrarily, if the electrical field is sustained with 80–100 pulses at a higher voltage (~3000 V), the cell cannot compensate to recover and undergoes cell death. This irreversible

Kristian M. Hargadon (ed.), *Melanoma*, Methods in Molecular Biology, vol. 3089,
https://doi.org/10.1007/978-1-0716-5619-8_36,
© The Author(s), under exclusive license to Springer Science+Business Media, LLC, part of Springer Nature 2027

electroporation (IRE) has in vivo applications for the clinical ablation of tumors to induce multiple mechanisms of cell death, including apoptosis, necrosis, necroptosis, and/or pyroptosis [6].

Reversible electroporation has been a keystone of in vitro gene transfection of cell cultures by having DNA of interest, typically in the form of a plasmid, present in cell media and taking advantage of the temporary cell membrane pores [7]. Interestingly, the applied electrical field that creates the reversible cell membrane pores also acts as a driver of negatively charged DNA through the pores [2]. The first successful in vitro gene transfer using rEP was reported in 1982 [8]. Unlike viral vectors, which are typically limited to less than 7 kb for DNA transfer, advantages of rEP include the ability to transfect larger and/or multiple DNA segments (or larger molecules), the ability to affect any cell type at any stage of the cell cycle, and avoidance of viral products [2]. In vivo applications, mostly in tumor tissues, have become more common over the last few decades in both preclinical and clinical use [9]. An early example is improved delivery of bleomycin, which is a relatively large, hydrophilic chemotherapy that relies on carrier-mediated transport across the cell membrane. To enhance the uptake and targeting to tumor tissue, bleomycin could be injected intravenously followed by rEP of a tumor with improved responses noted preclinically [10] and clinically, including melanoma tumors [11]. Several rEP platforms have been used in cancer patients and appear well-tolerated, with mild transient injection site pain or contraction of the underlying muscle being most commonly reported [12]. Since rEP is an evolving treatment modality with the potential for immediate clinical translation in the field of melanoma [13–17], preclinical protocols may serve as a starting point for a variety of translational studies. For simplicity, the following preclinical murine protocol will focus on plasmid rEP similar to reported studies [18] and clinical trials [19] designed to immunologically alter the tumor microenvironment.

2 Materials

1. Syngeneic murine melanoma cell line (e.g., B16, YUMM [20]) or patient-derived xenograft models [21] (*see* **Note 1**).
2. Mouse model appropriate for tumor type selected. The C57BL/6 mouse strain is utilized for B16 and YUMM melanoma cell lines.
3. Plasmid(s) designed for experimental purposes (e.g., IL-2 cytokine or other protein of interest driven by a promoter sequence [e.g., CMV promoter]) and engineered with a tag for identification of successful transfection (e.g., GFP)

(Fig. 1). Commercial plasmid design and manufacturing companies are now commonplace and relatively inexpensive.

4. Dedicated reversible electroporation generators designed for in vivo laboratory use: A nonexhaustive list of commercially available examples includes BTX (Harvard Apparatus), ELGEN1000 (Inovio Pharmaceuticals), Super Electroporator NEPA21 Type II (Nepagene), as well as other proprietary or adapted platforms. The interface with tumor tissue is usually in the form of needle arrays with varying sizes and configurations available for tumor size, type, location, and depth (Fig. 2).
5. 1 ml syringes.
6. 27-gauge needles (or smaller).
7. 70% ethanol.
8. Isoflurane.
9. Buprenorphine.
10. Saline.
11. Opthalmic ointment.
12. Micro-Bead sterilizer system.
13. Warming pad.

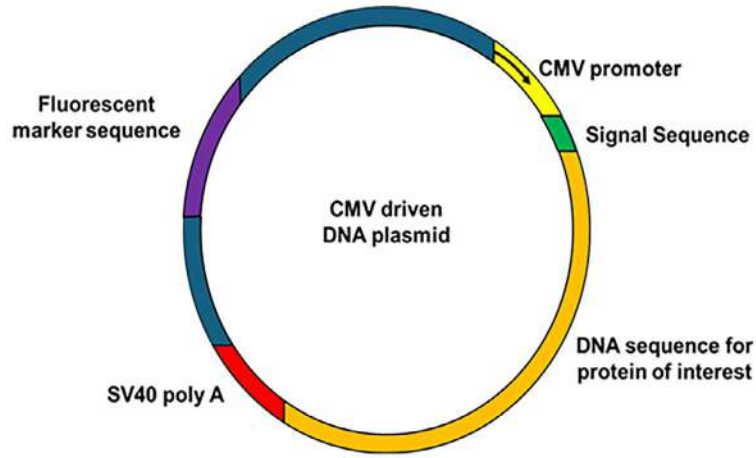


Fig. 1 An overly simplified schematic of a plasmid demonstrating a DNA sequence driven by a CMV promoter and ending in a polyA tail. Plasmid design can include several encoding regions for multiple proteins, linker regions for multiunit proteins, and unique markers to track successful transfection. Plasmids can be used individually or in combinations for their desired effect

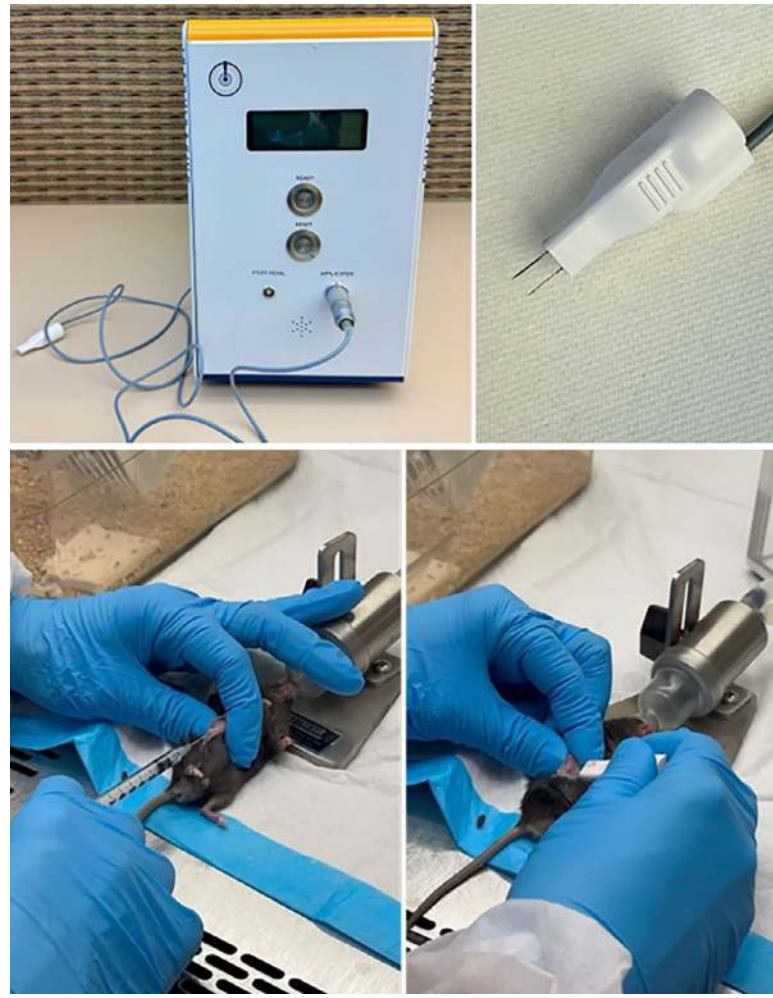


Fig. 2 Representative image of the reversible electroporator device (top left) used for plasmid delivery and the needle probe (top right), which is connected to the device and that is inserted directly into the tumor mass to administer the calibrated electrical pulse. The mouse is first injected with 100 μl of plasmid DNA (bottom left), and then rEP is performed (bottom right)

3 Methods

All procedures should be approved by the local Institutional Animal Care and Use Committee (IACUC) and conform with the requirements and ethics associated with live vertebrate animal experimentation (as well as any other applicable local, state, or national guidelines).

3.1 Tumor Growth Study (Mice Bearing Flank Tumor)

1. On day 0, harvest cultured melanoma cells, and keep cells on ice during the inoculation procedure (*see* **Note 2**).

2. Prior to tumor inoculation, 70% EtOH can be used as a topical disinfectant and air dried completely before injection (hair can be shaved as well if necessary).
3. Load tumor cells into a 1 ml syringe with a 27-gauge needle or smaller.
4. Inoculate mice with tumor cells (e.g., 2×10^5 up to 1×10^6 B16 cells) by subcutaneous injection in the flank. The injection volume can be up to 200 µl (or less, depending upon concentration and desired number of cells).
5. Monitor tumor growth over time using calipers, and calculate the tumor volume using standard formulas.

3.2 Plasmid Injection and rEP

On day 7, when tumors reach >40 mm^3 in size (typically ~100 mm^3 for rEP initiation), mice are ready for plasmid injection and rEP. All procedures should be performed in a sterile environment (animal surgical bio bubble) using sterile techniques. Sterile instruments should be used (sterilize surgical instruments with a Micro-Bead sterilizer system between mice), and staff should be garbed in a gown, cap, mask, boots, and sterile gloves.

1. Anesthetize mice with isoflurane induction (~4%), followed by maintenance (~2%). Commence with the procedure only when a proper level of anesthesia is achieved (diminished pedal withdrawal to stimuli [toe pinch]).
2. Apply ophthalmic ointment to the mouse eyes. Mucous membrane color and respiration rates should be used to determine the animal's well-being during and after the procedure of electroporation.
3. Prep the tumor site with 70% ethanol, and allow the site to completely air dry before injecting the plasmid DNA of interest (shave hair as well if necessary).
4. Load a 1–2 mg/ml solution of plasmid DNA into a 1 ml syringe with a 27-gauge (or smaller) needle.
5. Inject the anesthetized mice intratumorally with 50–100 µl of the 1–2 mg/ml solution of plasmid DNA. The same syringe can be applied to multiple tumor injections if necessary (*see* **Note 3**).
6. For the rEP procedure, place anesthetized mice on a warming pad with the tumor exposed and accessible for the probe.
7. Place the electrode of the probe into the tumor mass, making sure the needle probe has penetrated the tumor tissue and the electrode is activated at the generator. Typical settings of the generator are eight electrical square wave pulses with a duration of 100 µsec applied at 100–1000 V (*see* **Notes 4–6**).

8. Remove the electrode after delivering the electroporation pulses.
9. If bleeding is noted from the electrode entry site, compress gently with a cotton ball applicator.
10. Return animals to cages when fully alert.
11. Following the procedure, give all animals buprenorphine (0.05 mg/kg) and saline (0.5 ml) subcutaneously with a 27-gauge needle for analgesia/hydration.
12. Observe animals, and keep subjects warm, using a warm water pad, until recovery. Additional buprenorphine or normal saline can be injected as needed.
13. Place surgery cage cards after the procedure.
14. Depending on investigator interests, a cohort of mice may also receive immunotherapy/other therapies to evaluate the potential synergy between rEP and therapies of interest. Administration of these additional therapies should follow approved dosing and scheduling parameters.
15. From day 7 until the end ofthe experiment, mice should be evaluated for localized skin necrosis or burn at probe insertion sites. The tumor and overlying skin should also be monitored post-procedure, as ulceration is possible. The application of a topical antibiotic should be considered if necessary.
16. From day 14 onward, plasmid injections and rEP can be repeated (at most weekly).
17. Euthanize mice when the tumor size is >2 cm or when mice exhibit any morbidity, such as tumor ulceration, lethargy, over 15% weight loss, and diarrhea.
18. Tumor tissue may be harvested and evaluated for expression of any marker (e.g., GFP to confirm successful transfection); ELISA, Luminex, or hPLC to detect expression of the protein of interest; or any other potential functional readouts (e.g., IL-2 and cell proliferation). Additionally, flow cytometric and immunofluorescence analysis of the tumors may also be performed to assess the spatial distribution of immune cells and their phenotypes within the tumor microenvironment.

4 Notes

1. Syngeneic tumor lines in immunocompetent hosts permit the study of immune phenomena that may not be possible in xenograft models. Also, various knockout variants can be used to dissect mechanistic detail.

2. Cells suspended in HBSS with phenol red help visually ensure that the injection did not leak out. Subcutaneous tunneling of the needle tract creates consistency and mitigates leakage. Matrigel can be used to promote tumor formation but is not necessary—consistency is the most important aspect of tumor inoculation for uniform tumor generation. During the process of injecting multiple mice, the syringe can be inverted and turned to keep the concentration consistent (i.e., avoid concentration or clumping of cells by gravity). To ensure injected cells were most likely viable, the remainder of any noninjected volume can be checked in the lab with trypan blue on a hemocytometer to examine viability.
3. The location of injection should be within the tumor as much as possible to prevent plasmid loss. Moving the needle slowly through the tumor while injecting can disperse the plasmid across a wider area. Multiple injections can be performed if the tumor is large. Empty vector plasmid should be used as a control or, at a minimum, the same volume of vehicle should be delivered.
4. Each generator has specific settings that may vary based on tumor tissue and size. If necessary, one can rEP multiple areas of the tumor to make sure the entire area is "covered." Clinical generators may have the ability to optimize pulse settings based upon tissue impedance and proprietary software.
5. Electrical pulses may cause muscle contraction, and the duration is typically a few seconds.
6. Importantly, no flammable material should be near the probe during pulse delivery, as rEP is a potential fire hazard. Alcohol or prep should be completely dry, hands should be kept away from probes during rEP, and rEP should be avoided near high oxygen flow.

Competing Interests

All authors certify that they have no affiliations with or involvement in any organization or entity with any financial interest or nonfinancial interest in the subject matter or materials discussed in this manuscript.

References

1. Sale AJ, Hamilton WA (1968) Effects of high electric fields on micro-organisms. 3. Lysis of erythrocytes and protoplasts. Biochim Biophys Acta 163(1):37–43. https://doi.org/10.1016/0005-2736(68)90030-8
2. Campelo SN, Huang PH, Buie CR, Davalos RV (2023) Recent advancements in electroporation technologies: from bench to clinic. Annu Rev Biomed Eng 25:77–100. https://doi.org/10.1146/annurev-bioeng-110220-023800

3. Justesen TF, Orhan A, Raskov H et al (2022) Electroporation and immunotherapy-unleashing the abscopal effect. Cancers 14(12):2876. https://doi.org/10.3390/cancers14122876
4. Saulis G (1999) Kinetics of pore disappearance in a cell after electroporation. Biomed Sci Instrum 35:409–414
5. Kotnik T, Rems L, Tarek M, Miklavcic D (2019) Membrane electroporation and electropermeabilization: mechanisms and models. Annu Rev Biophys 48:63–91. https://doi.org/10.1146/annurev-biophys-052118-115451
6. Batista Napotnik T, Polajzer T, Miklavcic D (2021) Cell death due to electroporation—a review. Bioelectrochemistry 141:107871. https://doi.org/10.1016/j.bioelechem.2021.107871
7. Potter H, Heller R (2010) Transfection by electroporation. Curr Protoc Mol Biol 121:9.3.1–9.3.13. https://doi.org/10.1002/0471142727.mb0903s92
8. Neumann E, Schaefer-Ridder M, Wang Y, Hofschneider PH (1982) Gene transfer into mouse lyoma cells by electroporation in high electric fields. EMBO J 1(7):841–845. https://doi.org/10.1002/j.1460-2075.1982.tb01257.x
9. Campana LG, Daud A, Lancellotti F et al (2023) Pulsed electric fields in oncology: a snapshot of current clinical practices and research directions from the 4th World Congress of electroporation. Cancers 15(13):3340. https://doi.org/10.3390/cancers15133340
10. Mir LM, Orlowski S, Jr. Belehradek J, Paoletti C (1991) Electrochemotherapy potentiation of antitumour effect of bleomycin by local electric pulses. Eur J Cancer 27(1):68–72. https://doi.org/10.1016/0277-5379(91)90064-k
11. Sersa G, Cufer T, Paulin SM et al (2012) Electrochemotherapy of chest wall breast cancer recurrence. Cancer Treat Rev 38(5):379–386. https://doi.org/10.1016/j.ctrv.2011.07.006
12. Lambricht L, Lopes A, Kos S et al (2016) Clinical potential of electroporation for gene therapy and DNA vaccine delivery. Expert Opin Drug Deliv 13(2):295–310. https://doi.org/10.1517/17425247.2016.1121990
13. Canton DA, Shirley S, Wright J et al (2017) Melanoma treatment with intratumoral electroporation of tavokinogene telseplasmid (pIL-12, tavokinogene telseplasmid). Immunotherapy 9(16):1309–1321. https://doi.org/10.2217/imt-2017-0096
14. Zhang L, Dong S, Teng F et al (2025) Pulsed electric fields: a sharp sword in the battle against cancers. Front Immunol 16:1682539. https://doi.org/10.3389/fimmu.2025.1682539
15. Cucu CI, Giurcaneanu C, Popa LG et al (2021) Electrochemotherapy and other clinical applications of electroporation for the targeted therapy of metastatic melanoma. Materials 14(14):3985. https://doi.org/10.3390/ma14143985
16. Ahmad MU, Walsh A, Kirane A (2024) Review of role of surgery with electroporation in melanoma: chemotherapy, immunotherapy, and gene delivery. J Clin Med 13(13):3828. https://doi.org/10.3390/jcm13133828
17. Ferioli M, Perrone AM, De Iaco P et al (2024) Clinical insights and future prospects: a comprehensive narrative review on immunomodulation induced by electrochemotherapy. Curr Oncol 31(10):6433–6444. https://doi.org/10.3390/curroncol31100478
18. Lee JY, Nguyen B, Mukhopadhyay A et al (2022) Amplification of the CXCR3/CXCL9 axis via intratumoral electroporation of plasmid CXCL9 synergizes with plasmid IL-12 therapy to elicit robust anti-tumor immunity. Mol Ther Oncolytics 25:174–188. https://doi.org/10.1016/j.omto.2022.04.005
19. Algazi AP, Twitty CG, Tsai KK et al (2020) Phase II trial of IL-12 plasmid transfection and PD-1 blockade in immunologically quiescent melanoma. Clin Cancer Res 26(12):2827–2837. https://doi.org/10.1158/1078-0432.CCR-19-2217
20. Klinke DJ 2nd, Gould A, Pirkey A et al (2025) A functional comparison of two transplantable syngeneic mouse models of melanoma: B16F0 and YUMM1.7. Biol Open 14(9):bio062175. https://doi.org/10.1242/bio.062175
21. Kuzu OF, Nguyen FD, Noory MA, Sharma A (2015) Current state of animal (mouse) modeling in melanoma research. Cancer Growth Metastasis 8(Suppl 1):81–94. https://doi.org/10.4137/CGM.S21214



Chapter 37

Lipoplex Nanoparticle-Based RNA Delivery to 3D Melanoma Spheroids

Rüdiger Rudolf, Tiziana Cesetti, Florian Keller and Mathias Hafner

Abstract

Lipoplex nanoparticle-based vaccination technologies have shown tremendous efficiency for in vivo transfection during the COVID-19 pandemic and also hold promise for treating melanoma. While pharmacodynamics and pharmacokinetics need careful in vivo and clinical testing, other parameters of drug performance can be assessed with in vitro systems as well. Spheroids composed of more than one cell type can serve to assess drug penetration, cell-type specificity, and transfection efficiency at an early stage of drug development.

Keywords CCD-1137Sk, Fibroblast, HaCaT, Keratinocyte, LPX, Melanoma cell, SK-MEL-28, Spheroid, Transfection

1 Introduction

Lipoplex (LPX) nanoparticles are powerful mRNA transfer agents and have served as a novel kind of vaccine during the SARS-CoV-2 coronavirus pandemic [1, 2]. The principle of mRNA-based vaccination is generally applicable to a range of disorders, including the treatment of cancer and melanoma [3–6]. However, to achieve an efficient drug profile, it is crucial for therapeutics to reach specific cell types or tissues and in large quantities. Owing to their tunable molecular characteristics, LPX have shown their capability to target select organs, such as lung or spleen, and specific cell types, such as antigen-presenting cells [6–9]. The latter are of particular relevance, as they are capable of triggering systemic immune responses. In other cases, local approaches might be more favorable, e.g., for addressing specifically tumor cells in a defined tumor region endowed with several different other cell types, i.e., stroma. In any case, organ- and/or cell-type-specific targeting, good penetration even in dense tissue settings, and high transfection efficiency are characteristics that are elementary for a successful treatment with

Kristian M. Hargadon (ed.), *Melanoma*, Methods in Molecular Biology, vol. 3089,
https://doi.org/10.1007/978-1-0716-5619-8_37,
© The Author(s), under exclusive license to Springer Science+Business Media, LLC, part of Springer Nature 2027

LPX. While certain aspects of drug profiling, including toxicity testing, pharmacodynamics, and pharmacokinetics, largely depend on in vivo assays and clinical trials, the high cost and molecular complexity of LPX-mRNA vaccines require more simple and yet reliable early compound screening models. Coculture spheroids, composed of cancer and tumor stroma cells, can fulfill several of these criteria. They allow investigators to assess cell-type specificity, penetration, and transfection efficiency due to their composition of different cell types, three-dimensional morphology, and relatively easy implementation of quantitative analysis. Furthermore, they are easy to scale up, set up, and cultivate.

The triculture spheroids described herein, composed of CCD-1137Sk fibroblasts, HaCaT keratinocytes, and SK-MEL 28 melanoma cells, showed in previous studies a reliable recapitulation of basic features of early melanoma, such as the loss of keratinocyte differentiation, melanoma cell invasion, and augmented ABCB5 expression in external melanoma cells upon cytostatic treatment [10–12]. Furthermore, this spheroid model yielded insights into the penetration, cell-type specificity, and transfection efficiency of LPX carrying EGFP mRNA [13]. Expanding on this recent study, this protocol gives a detailed account of the methodological aspects of spheroid and LPX generation, transfection, imaging, and data analysis.

2 Materials

2.1 Cell Lines and Reagents

Prepare all solutions, and work with all cell lines under sterile conditions.

1. Cell lines: Human fibroblast cell line CCD-1137Sk, human keratinocyte cell line HaCaT, and human malignant melanoma cell line SK-MEL-28.
2. Standard CCD-1137Sk Medium: Iscove's Modified Dulbecco's Medium (IMDM) with L-glutamine, supplemented with 10% fetal bovine serum (FBS) and 1% penicillin/streptomycin. Store at 4°C.
3. Standard Medium for HaCaT and SK-MEL-28 cell lines: Dulbecco's modified Eagle medium (DMEM), formulated with high glucose (4.5 g/L), L-glutamine, and sodium pyruvate and supplemented with 10% FBS and 1% penicillin/streptomycin. Store at 4°C.
4. Cryoconservation medium: standard IMDM or DMEM (depending on the cell line) supplemented with 20% FBS and 5% dimethylsulfoxide (DMSO). Prepare fresh prior to cryopreservation.
5. Dulbecco's Phosphate-Buffered Saline (PBS): Store at 4°C.

6. PBS containing 1% FBS.
7. 1× Trypsin–EDTA Solution: 0.25% Trypsin/0.53 mM EDTA in Hanks Balanced Salt Solution without calcium or magnesium. Store at −20°C.
8. GlutaMAX™ Supplement, added in case of the usage of basal media without L-Glutamine to match 580 mg/mL: Store at −20°C.
9. Penetration Buffer: 0.2% Triton X-100, 0.3 M glycine, and 20% DMSO in PBS.
10. Blocking Buffer: 0.2% Triton X-100, 1% bovine serum albumin Fraction V (BSA), and 10% DMSO in PBS.
11. Washing buffer: 0.2% Tween20, 10 μg/mL of heparin, and 1% BSA in PBS.
12. D-Sucrose: Store at −20°C.
13. Agarose.
14. Paraformaldehyde.
15. Sodium azide.
16. Glycerol.
17. Urea.
18. FSC 22 Frozen Section Medium.
19. Mowiol.
20. DRAQ5 Fluorescent Probe Solution: Store at 4°C.
21. 40,6-Diamidine-20-phenylindole dihydrochloride (DAPI): Store at −20°C.
22. Quadrol.
23. DOTMA (R-1,2-di-O-oleoyl-3-trimethylammonium propane).
24. DOPE (1,2-Dioleoyl-sn-glycero-3-phosphoethanolamine).

2.2 Equipment and Supplies

1. T-75 cell culture flasks.
2. Greiner flat-bottom 96-well plate.
3. μ-Slide: 18-well, flat, uncoated chamber slide.
4. Centrifuge.
5. CO_2 incubator.
6. Vertical shaker.
7. Vi-Cell XR Cell Viability Analyzer (Beckman Coulter).
8. Menzel Cover Glasses 24 × 60 mm, thickness I.
9. Scissors to trim pipette tips.
10. Leica TCS SP8 DMi8 microscope (Leica Microsystems GmbH).
11. ImageJ software.

12. Leica Application Suite X software (LAS X; Leica Microsystems GmbH).
13. Nicomp ZLS Z3000 nanoparticle size analyzer.

3 Methods

3.1 Preparation of Spheroids

Sects. 3.1.1–3.1.4 describe the procedures to generate monoculture and triculture spheroids of fibroblasts, keratinocytes, and melanoma cells. All procedures should be performed under sterile conditions using a laminar flow hood, and cells should be maintained at 37°C in 5% CO_2 unless stated otherwise.

3.1.1 Preparation of CCD-1137Sk Monoculture Spheroids

1. Prior to spheroid generation, cultivate the CCD-1137Sk cells for at least two passages. Avoid overgrowth and undergrowth of the cells (*see* **Note 1**).
2. Remove the medium, and wash the cells with PBS.
3. Add 1× Trypsin–EDTA solution to remove the cells from the T-75 cell culture flask. Incubate cells at 37°C with 5% CO_2 for 2–4 min.
4. Inhibit trypsin activity by adding 8 mL of Standard CCD-1137Sk Medium.
5. Check cell viability using a Vi-Cell XR Cell Viability Analyzer. Cell viability should be >92%.
6. Seed CCD-1137Sk cells (1×10^4 cells/well) into a 96-well cell-repellent U-bottom plate (*see* **Note 1**).
7. Centrifuge the cells for 4 min at $500 \times g$ in order to favor the positioning of the cells in the center of the U-shaped well, and incubate the spheroids for 96 h at 37°C with 5% CO_2.
8. Change 75% of the medium every 48 h. Aspirate it carefully, not to remove the spheroid.

3.1.2 Preparation of HaCaT Monoculture Spheroids

1. Prior to spheroid generation, cultivate the HaCaT cells for at least two passages. For optimal cultivation and reproducibility, avoid overgrowth and undergrowth of the cells (*see* **Note 2**).
2. Remove the medium, and wash the cells with PBS.
3. Add 1× Trypsin–EDTA solution to detach the cells from the T-75 cell culture flask. Incubate cells at 37°C with 5% CO_2 for 5–10 min.
4. Inhibit trypsin activity by adding 8 mL of Standard HaCaT Medium.
5. Check cell viability using a Vi-Cell XR Cell Viability Analyzer. Cell viability should be >92%.

6. Seed HaCaT cells (1×10^4 cells/well) into a 96-well plate.
7. Centrifuge the cells for 4 min at $500 \times g$, and incubate the spheroids for 96 h at 37°C with 5% CO_2.
8. Change 80% of the medium every 48 h.

3.1.3 Preparation of SK-MEL-28 Monoculture Spheroids

1. Prior to spheroid generation, cultivate the SK-MEL-28 cells for at least two passages. For optimal cultivation and reproducibility, avoid overgrowth and undergrowth of the cells (*see* **Note 2**).
2. Remove the medium, and wash the cells with PBS.
3. Add 1× Trypsin–EDTA solution to detach the cells from the T-75 cell culture flask. Incubate cells at 37°C with 5% CO_2 for 2–4 min.
4. Inhibit trypsin activity by adding 8 mL of Standard SK-MEL-28 Medium.
9. Check cell viability using a Vi-Cell XR Cell Viability Analyzer. Cell viability should be >92%.
5. Seed SK-MEL-28 cells (1×10^4 cells/well) into a 96-well plate.
6. Centrifuge the cells for 4 min at $500 \times g$, and incubate the spheroids for 96 h at 37°C with 5% CO_2.
7. Change 80% of the medium every 48 h.

3.1.4 Preparation of Triculture Spheroids

1. Prior to spheroid generation, cultivate the individual cell lines for the melanoma tri-culture for at least two passages. For optimal cultivation and reproducibility, avoid overgrowth and undergrowth of the cells (*see* **Note 2**).
2. Prior to coculture, remove the medium and wash the cells with PBS.
3. Add 1× Trypsin–EDTA solution to detach the cells from their T-75 cell culture flasks. Incubate CCD-1137Sk and SK-MEL-28 at 37°C with 5% CO_2 for 2–4 min. HaCaT cells need a 5–10 min incubation at 37°C with 5% CO_2 to detach.
4. Inhibit trypsin activity by adding 8 mL of standard medium as appropriate for the particular cell lines.
5. Before starting the tri-culture, check cell viability using a Vi-Cell XR Cell Viability Analyzer. The viability of the cells should be higher than 92%.
6. To prepare the first layer of the tri-culture melanoma model, seed CCD-1137Sk (1×10^4 cells/100 µL of standard CCD-1137Sk medium) in each well of a 96-well cell-repellent U-bottom plate.
7. Centrifuge the cells for 4 min at $500 \times g$, and incubate the spheroids for 72 h at 37°C with 5% CO_2.

8. Change 80% of the medium every 48 h.
9. After 3 days, seed HaCaT (1×10^4 cells/well) and SK-MEL-28 (2.5×10^3 cells/well) cells to the already formed CCD-1137Sk spheroids (achieve a 150 µL/well total volume of standard medium for HaCaT and SK-MEL-28 cells, composed of 50 µL of each cell-specific medium).
10. Centrifuge the cells for 4 min at $500 \times g$, and incubate the spheroids for 96 h at 37°C with 5% CO_2.
11. Change 80% of the medium every 48 h, using a mixture of the three media in a 1/3 proportion.

3.2 LPX Assembly

This section describes the procedure to produce LPX for transfecting spheroids with EGFP mRNA. LPX containing EGFP-reporter-mRNA was obtained from BioNTech [13] and was prepared according to the following method:

1. Condition mRNA encoding eGFP, provided in a HEPES/EDTA buffer (10 mM/0.1 mM), with a sodium chloride solution to arrive at a sodium chloride concentration of 224 mM and an RNA concentration of 0.2 mg/mL (~0.66 mM).
2. Mix the conditioned RNA one-to-one (v/v) with cationic liposomes consisting of DOTMA and DOPE in a 2:1 molar ratio using the ethanol injection technique.
3. For quality control, determine the sizes of the LPX by using dynamic light scattering measurements.

3.3 LPX Treatment

1. 48 h after spheroid formation, carefully remove FBS out of the culture medium by performing the following steps on each well:
   a. Remove 100 µL of medium, and add up to 150 µL of PBS.
   b. Remove 150 µL, and add 150 µL of PBS.
   c. Remove 150 µL, and add up to 150 µL of medium without FBS.
   d. Remove 160 µL, and add 50 µL of medium without FBS, followed by another 10 µL of LPX, mixed according to the follow-up description.
2. To transfect spheroids with LPX, incubate cells with 10 ng/µL of LPX in serum-free DMEM for 24 h at 37°C in 5% CO_2.
3. After the 24-h LPX treatment, wash spheroids with PBS three times for 5 min each, and then fix with paraformaldehyde solution (4% in PBS) for 30 min at room temperature.
4. For further processing, carefully transfer spheroids to 1.5 mL tubes by using a P1000 pipet with a cut-off tip (*see* **Note 3**).

3.4 Optical Clearing

This section describes the method to render the spheroids optically transparent to allow whole mount analysis, i.e., without physical sectioning (*see* **Note 4**).

1. Quench spheroids for 1 h at 37°C with 0.5 M glycine.
2. Incubate for 30 min at room temperature in Penetration Buffer.
3. Wash with PBS containing 1% FBS.
4. Incubate for 2 h at 37°C in Blocking Buffer.
5. Incubate in DRAQ5 overnight at 37°C with gentle shaking for nuclear staining.
6. Wash five times for 5 min each in Washing Buffer at room temperature.
7. Wash with ddH_2O.
8. Set refractive index to 1.456 with DMSO, urea, quadrol, sucrose, and glycerol (88%) for 48 h at constant room temperature.
9. Mount cleared spheroids on 18 well μ-slides in the same solution.

3.5 Confocal Fluorescence Analysis

1. Turn on the computer, microscope, and corresponding devices, followed by starting the microscope operational software (e.g., LASX in confocal xyz mode). Initialize the stage.
2. Switch to the 10× air objective and fluorescence mode. Move the sample into the field of view in the *xy*-direction by using DRAQ5 fluorescence as a guide. Put the bottom of the sample (the one that is closer to the objective) into focus.
3. Inside the dye manager of LASX, select AlexaFluor488 and DRAQ5. Set resolution to 1024 × 1024 pixels and a speed of 400–600 Hz.
4. Start the live view for confocal scanning to adjust fine settings for laser intensity and gain. Using photomultiplier tubes as detectors, we recommend starting at 1%–1.5% laser intensity and a gain of 550–650 V, with subsequent fine-tuning for each fluorophore as necessary (*see* **Note 5**).
5. Define the beginning (bottom of sample) and end (top of sample) of the z-stack, and set the step size to 1 μm (*see* **Note 6**).
6. Execute the imaging process.

3.6 Data Analysis

This section describes the quantitative analysis of the fluorescence microscopy data to yield the fraction of EGFP-positive cells per condition. All following procedures use ImageJ software.

1. Select the confocal images of a single optical plane in the center of each spheroid.

2. Threshold the areas of EGFP fluorescence signals by adjustment to negative controls, i.e., spheroids transfected with LPX devoid of mRNA.
3. Threshold the DRAQ5-positive areas.
4. Normalize the EGFP data to the total area of DRAQ5 signals.

4 Notes

1. It is important that plastic be cell-repellent so that the cells do not attach to the plastic, which will allow the cells to spontaneously aggregate when they are close to each other.
2. Avoid too high or too low confluence of the cell lines. Subculture CCD-1137Sk cells between 2×10^4 and 7×10^4 cells/cm^2. HaCaT cells grow best at a density between 1×10^4 cells/cm^2 and 3×10^4 cells/cm^2. HaCaT cells should not be allowed to overgrow in order to avoid their differentiation. Subculture SK-MEL-28 cells between 4×10^4 cells/cm^2 and 7×10^4 cells/cm^2. Too low seeding density can result in anoikis or slow growth and should be avoided.
3. For transferring spheroids, also when embedded in glycerol, use a P1000 pipet and cut 3 mm from the tip to enlarge the opening to obviate any damage to the spheroids and prevent the formation of air bubbles.
4. Between each working step, except when culturing in a 96-well plate, allow the spheroids to settle down to the bottom of the tube. This ensures that no spheroids are lost between the individual steps.
5. Overexposure of pixels will affect segmentation and should be avoided whenever possible. The outside of spheroids will sometimes appear brighter than inside, and internal signals will decrease with imaging depth.
6. Upon using a galvanometric stage, the imaging range might be too limited to accommodate the whole sample. Alternatively, z-wide in the LASX software can be used to increase the z-range. However, beware of damaging the optics.

Acknowledgments

This work was funded by the German Federal Ministry of Education and Research (BMBF) as part of the Innovation Partnership M^{2}Aind project DrugsData (13FH8I09IA) within the framework

Starke Fachhochschulen–Impuls für die Region (FH-Impuls). This research project is a part of the Forschungscampus M²OLIE and funded by the German Federal Ministry of Education and Research (BMBF) within the Framework Forschungscampus: public–private partnership for innovations. This study was funded by the DFG, grant INST874/9-1.

Competing Interests The authors have no conflicts of interest to declare that are relevant to the content of this chapter.

References

1. Pastor F, Berraondo P, Etxeberria I et al (2018) An RNA toolbox for cancer immunotherapy. Nat Rev Drug Discov 17:751–767. https://doi.org/10.1038/nrd.2018.132
2. Pascolo S (2021) Vaccines against COVID-19: priority to mRNA-based formulations. Cells 10:2716. https://doi.org/10.3390/cells10102716
3. Pascolo S (2004) Messenger RNA-based vaccines. Expert Opin Biol Ther 4:1285–1294. https://doi.org/10.1517/14712598.4.8.1285
4. Bahl K, Senn JJ, Yuzhakov O et al (2022) Preclinical and clinical demonstration of immunogenicity by mRNA vaccines against H10N8 and H7N9 influenza viruses. Mol Ther 30:2874. https://doi.org/10.1016/j.ymthe.2022.07.013
5. Pardi N, Hogan MJ, Pelc RS et al (2017) Zika virus protection by a single low-dose nucleoside-modified mRNA vaccination. Nature 543:248–251. https://doi.org/10.1038/nature21428
6. Kranz LM, Diken M, Haas H et al (2016) Systemic RNA delivery to dendritic cells exploits antiviral defence for cancer immunotherapy. Nature 534:396–401. https://doi.org/10.1038/nature18300
7. Grabbe S, Haas H, Diken M et al (2016) Translating nanoparticulate-personalized cancer vaccines into clinical applications: case study with RNA-lipoplexes for the treatment of melanoma. Nanomedicine 11:2723–2734. https://doi.org/10.2217/nnm-2016-0275
8. Rosigkeit S, Meng M, Grunwitz C et al (2018) Monitoring translation activity of mRNA-loaded nanoparticles in mice. Mol Pharm 15:3909–3919. https://doi.org/10.1021/acs.molpharmaceut.8b00370
9. Enzlein T, Schumacher J, Geisel A et al (2026) Multiplexed spatial screening of extrahepatic lipid-based nanoparticles for in vivo messenger RNA targeting. J Control Release 392:114728. https://doi.org/10.1016/j.jconrel.2026.114728
10. Klicks J, Maßlo C, Kluth A et al (2019) Novel spheroid-based co-culture model mimics loss of keratinocyte differentiation, melanoma cell invasion, and drug-induced selection of ABCB5-expressing cells. BMC Cancer 19:402. https://doi.org/10.1186/s12885-019-5606-4
11. Nürnberg E, Vitacolonna M, Klicks J et al (2020) Routine optical clearing of 3D-cell cultures: simplicity forward. Front Mol Biosci 7:7–20. https://doi.org/10.3389/fmolb.2020.00020
12. Schäfer MEA, Klicks J, Hafner M, Rudolf R (2021) Preparation, drug treatment, and immunohistological analysis of tri-culture spheroid 3D melanoma-like models. Methods Mol Biol 2265:173–183. https://doi.org/10.1007/978-1-0716-1205-7_13
13. Schäfer MEA, Keller F, Schumacher J et al (2022) 3D melanoma cocultures as improved models for nanoparticle-mediated delivery of RNA to tumors. Cells 11:1026. https://doi.org/10.3390/cells11061026



Chapter 38

Assessing the Antitumor Immune Effects of Gut Microbiota in a Preclinical Melanoma Model

Parastoo Sabaeifard, Wenling Li, Priscilla Del Valle, Rebecca Suet-Yan Chiu, Jana Dakour, Nicole Poulides, Shuheng Gan, Jake N. Lichterman, Christina M. Zarek, Xiaowei Zhan and Andrew Y. Koh

Abstract

Antitumor immune responses are regulated by a multitude of factors, including the gut microbiota. Specific bacterial taxa and metabolites have been correlated with improved responses to immune checkpoint inhibitor therapy in melanoma patients. Gut microbiota and microbiota-derived metabolites can modulate antitumor immune responses by increasing antigen presentation capabilities and enhancing cytotoxic T-cell effector functions. To assess the effects of gut microbiota on antitumor immune responses, we optimized the following protocols focused on immune checkpoint inhibitor therapy in a preclinical melanoma model. Analysis of tumor-infiltrating and circulating lymphocytes, bacterial translocation and growth, and immune cell activation provides a foundation for microbiota/cancer immunology research.

Keywords Immune checkpoint inhibitor therapy (ICT), Immune profiling, Microbiota, Bacterial translocation, Melanoma

1 Introduction

The gut microbiota is a central regulator of local and systemic immunity and a key determinant of antitumor responses, particularly in immunogenic cancers such as melanoma [1]. Preclinical and clinical studies show that commensal microbes and/or their metabolites shape tumor progression, tumor immune infiltration, cytokine networks, and the efficacy of immune checkpoint therapies (ICTs) [2]. In melanoma, specific bacterial taxa induce enhanced dendritic cell (DC) maturation, improved antigen presentation, increased cytotoxic T-cell responses, and superior responsiveness to PD-1/PD-L1 and CTLA-4 blockade [3, 4].

Mechanistically, gut microbes and their metabolites orchestrate antitumor immunity through effects on antigen presentation, lymphoid tissue priming, effector cell differentiation, and cytokine

Kristian M. Hargadon (ed.), *Melanoma*, Methods in Molecular Biology, vol. 3089,
https://doi.org/10.1007/978-1-0716-5619-8_38,
© The Author(s), under exclusive license to Springer Science+Business Media, LLC, part of Springer Nature 2027

signaling [4–7]. Beneficial commensals, such as *Bifidobacterium*, promote DC activation and cross-presentation of tumor antigens, supporting robust $CD8^+$ T-cell responses [8]. Microbial metabolites and pattern-recognition signals modulate T-cell polarization, inflammatory tone, and immune checkpoint expression within the tumor microenvironment [9–12]. Fecal microbiota transplantation of defined microbial consortia can transfer antitumor immune phenotypes across hosts, demonstrating that the microbiome is an active and transmissible driver of tumor control [1, 13].

Our work shows that ICT drives lymph node remodeling and gut bacterial translocation to secondary lymphoid organs and tumors, where microbial signals directly enhance antigen presentation and T-cell activation. Specifically, DCs traffic live bacteria to the lymph nodes, where DC priming with highly translocated species promotes increased $CD8^+$ T cell anti-tumor cytokine production. ICT then induces lymph node remodeling, which facilitates gut microbiota translocation into the bloodstream, tumor-draining lymph nodes, and tumor [14]. This is one potential mechanism by which gut microbiota can translocate to tumor-draining lymph nodes (TDLNs) and tumors. Additionally, there is growing evidence that specific tumor types harbor distinct gut microbiota [15, 16]. These findings underscore the value of integrating analyses of microbial translocation with immune profiling in preclinical melanoma models to understand how the gut microbiota shapes therapeutic responses.

This chapter presents experimental strategies to dissect microbiota-driven antitumor immunity using the B16-F10 melanoma model in combination with ICT. In addition to outlining methods for measuring microbial burden and translocation, DC stimulation, and T-cell activation, we provide detailed methodology for multiparameter immune profiling and assessment of antigen restriction within mesenteric lymph nodes (MLNs). Together, these approaches provide a comprehensive framework for linking microbial signals to systemic antitumor immunity and for advancing microbiome-based strategies to enhance cancer immunotherapy.

2 Materials

2.1 Expansion and Preparation of B16-F10 Cells for Implantation

1. B16-F10 cells (ATCC, CRL-6475; RRID:CVC_0159).
2. Complete DMEM: Dulbecco's Modified Eagle's medium (DMEM) containing 10% heat-inactivated fetal bovine serum (FBS).
3. Centrifuge.
4. CO_2 incubator.
5. Cell culture flasks (T75 or T175).

6. TrypLE™ Express enzyme.
7. Sterile 50 mL conical tubes.
8. Dulbecco's Modified Eagle's Medium (DMEM), no FBS.
9. Cell counter slides.
10. Trypan blue.
11. Hemacytometer or automated cell counter.
12. 2 mL microcentrifuge tubes.
13. Ice bucket with ice.

2.2 Subcutaneous Tumor Cell Implantation

1. Vortex mixer.
2. 1 mL BD tuberculin syringe with detachable 27G×½ in needle.
3. Isoflurane.
4. Isoflurane murine vaporizer system (e.g., E-Z Anesthesia EZ-SA800 Single Animal System).
5. Alcohol prep pads.
6. Electric shaver.

2.3 Posttumor Implantation Treatments

1. Antibiotic water: Sterile water supplemented with penicillin G (1500 U/mL) and streptomycin (2 mg/mL) for microbiota depletion (*see* **Note 1**). Add to light-protected water bottles.
2. InVivoMAb α-mouse PD-1 (clone RMP1-14, CD279, Bio X Cell).
3. InVivoMAb α-mouse CTLA-4 (clone 9D9, CD152, Bio X Cell).
4. Sterile PBS.
5. Ice bucket.
6. 1 mL BD tuberculin syringe with detachable 27G×½ in needle.

2.4 Melanoma Model Analysis

1. Calipers.
2. CO_2 chamber for euthanasia.

2.5 Immune Profiling

2.5.1 Tissue Collection for Flow Cytometry

1. 2 mL Eppendorf tubes.
2. Complete DMEM.
3. Surgery tools: Scissors and forceps.
4. 70% ethanol.
5. Ice bucket.
6. Analytical scale.

2.5.2 Murine Serum Collection for Cytokine Analysis

1. CO_2 chamber for euthanasia.
2. 70% ethanol, in a spray bottle.
3. Sterile surgical scissors and forceps.
4. 25–27 G needles (1 per mouse).
5. 1 mL syringes (1 per mouse).
6. Serum separation tubes (1 per mouse) (*see* **Note 2**).
7. Ice bucket.
8. O-ring 1.5 mL tubes.
9. –80°C freezer.

2.5.3 Preparation of Tumor Cell Suspensions

1. Razor blades.
2. Miltenyi Biotec gentle MACS Dissociators.
3. Miltenyi Biotec Tumor Dissociation Kit: Contains Enzyme D, Enzyme R, Enzyme A, Buffer A.
4. Tumor dissociation buffer: 1.35 mL of Complete DMEM, 100 µL of Enzyme D, 10 µL of Enzyme R, and 12.5 µL of Enzyme A. Volumes indicated are for dissociation of a single tumor; scale up as needed.
5. Miltenyi Biotec gentleMACS™ C Tubes.
6. Complete DMEM.
7. PBS.
8. Miltenyi MACS® SmartStrainers (70 µm).
9. 50 mL conical tubes.
10. 15 mL conical tubes.
11. Percoll: Prepare solutions of 40% and 80% Percoll in PBS.
12. 1× RBC lysis buffer (*see* **Note 3**).
13. Ice bucket.

2.5.4 Preparation of MLNs, TDLNs, and Spleen Cell Suspensions

1. 10 mL syringe without needles.
2. 100 mm Petri dish.
3. PBS, no Mg^{2+} or Ca^{2+}.
4. Strainers (70 µm).
5. 15 mL conicals.
6. 1× RBC lysis buffer.
7. Ice bucket.

2.5.5 Surface Staining for Flow Cytometry

1. 2 mL Eppendorf tubes.
2. V-bottom 96-well plates.
3. Falcon 15 mL conical tubes for antibody master mix preparation.

Table 1
Suggested surface antibodies for tissue flow cytometry

Lymphocytes	CD45
T cells	CD3
	CD4
	CD8
	CD25
NK cells	NK1.1
B cells	CD19
Myeloid cells	Ly6C
	Ly6G
	CD11b
	F4/80
	CD11c

4. Fluorescence-activated cell sorting (FACS) buffer: PBS containing 2% heat-inactivated FBS and 2 mM EDTA.
5. Antibodies (see Table 1).
6. Cell viability dye (e.g., Zombie Yellow or Ghost Dye).
7. Flow cytometer.

2.5.6 T-cell Stimulation and Intracellular Cytokine Staining for Flow Cytometry

1. U-bottom 96-well plates.
2. BioLegend activation cocktail: Contains PMA, ionomycin, and brefeldin A (*see* **Note 4**).
3. Stimulation RPMI: RPMI containing 50 µM 2-mercaptoethanol, 50 ng/mL PMA, 750 ng/mL ionomycin, and 10 µg/mL brefeldin A.
4. PBS, no Mg^{2+} or Ca^{2+}.
5. FACS buffer.
6. BioLegend Cytofast Fix/Perm Buffer Set: Contains Fix/Perm buffer and Perm Wash.
7. diH_2O.
8. Intracellular antibodies (see Table 2 and **Note 5**).

2.5.7 Transcription Factor Staining

1. BioLegend True-Nuclear™ Transcription Factor Buffer Set: Contains Fix Concentrate, Fix Diluent, Perm Buffer.
2. diH_2O.
3. FACS buffer.
4. Transcription factor antibodies (see Table 2).

Table 2
Suggested antibodies for intracellular cytokine and transcription factor staining

Cytokines	Transcription factors
IFN-γ	T-bet
IL-4	GATA3
IL-17A	RORγt
	Foxp3

2.5.8 Tumor Tissue Lysate Preparation for Cytokine Analysis

1. R&D Systems Cell Lysis Buffer 2.
2. 15 mL conical tubes.
3. Roche cOmplete, Mini Protease Inhibitor Cocktail (tablets) (*see* **Note 6**).
4. SIGMAFAST Phosphatase Inhibitor Tablets.
5. 2 mL Eppendorf tubes (1 per tumor).
6. Ice bucket.
7. Analytical balance.
8. Tissue homogenizer: Qiagen TissueLyser II.
9. 50 mL conical tubes.
10. 70% ethanol.
11. Sterile distilled water.
12. Kimwipes.
13. Microcentrifuge.
14. O-ring 1.5 mL microcentrifuge tubes.

2.5.9 Bulk Cytokine Analysis

1. Ice bucket.
2. Luminex assay platform, reagents, and standards (e.g., Mouse Luminex Discovery Assay, R&D Systems).
3. Bio-Rad Luminex 200.
4. Microcentrifuge tubes.
5. Vortex mixer.

2.6 DC and T Cell Stimulation Assays

2.6.1 In vivo Expansion of Mouse Splenic DC

1. B16-FLT3L cells (RRID:CVCL_IJ12).
2. Complete Abx DMEM: DMEM containing 10% heat-inactivated FBS, 1× Antibiotic-Antimycotic (penicillin, streptomycin, and Gibco Amphotericin B), and 2 mM L-glutamine.
3. Sterile 50 mL conical, filled with 15 mL of sterile RPMI.

4. Surgical tools: forceps, scissors.
5. Ice bucket.

2.6.2 DC Isolation

1. Petri dishes.
2. 70 μm cell strainer.
3. 10 mL syringe.
4. Red blood cell (RBC) lysis buffer.
5. Sterile 1× PBS.
6. Sterile 15 mL conical tubes.
7. $CD11c^+$ magnetic cell separation kit (*see* **Note 7**).
8. Sterile RPMI.
9. Complete RPMI: RPMI 1640 containing 10% FBS, penicillin (100 U/mL), and streptomycin sulfate (100 μg/mL).
10. Trypan blue.
11. Automated cell counter or hemacytometer.

2.6.3 DC Activation Assay

1. 96-well U-bottom cell culture plates.
2. Complete RPMI.
3. 2 mL microcentrifuge tubes.

2.6.4 Naïve T Cell Isolation and CFSE Labeling

1. Sterile 1.5 mL microcentrifuge tubes.
2. RPMI.
3. Naïve T cell magnetic bead isolation kit (e.g., EasySep™ Mouse Naïve $CD4^+$ T Cell Isolation Kit).
4. Invitrogen CFSE Cell Division Tracker Kit: Contains lyophilized CellTrace CFSE staining dye and DMSO. Prior to use, prepare a 5 mM CFSE stock solution by adding 36 μL of DMSO to a vial of lyophilized CellTrace CFSE staining dye.
5. Sterile PBS, pH 7.4.
6. Lonza X-VIVO® 15 Serum-free Hematopoietic Cell Medium.
7. 15 mL conical tubes.

2.6.5 Activated DC and Naïve T Cell Coculture

1. Lonza X-VIVO® 15 Serum-free Hematopoietic Cell Medium.
2. 96-well U-bottom cell culture plates.
3. Stimuli of interest (e.g., bacterial lysate, LPS).
4. OVA 257-264 peptide (e.g., Sigma-Aldrich S7951 Ovalbumin (257-264) chicken) or OVA 323-339 peptide (*see* **Note 8**).

2.7 Surgical Removal of Secondary Lymphoid Organs

1. Isoflurane murine vaporizer system (e.g., E-Z Anesthesia EZ-SA800 Single Animal System).
2. Carprofen (5 mg/kg; injectable).

3. 1 mL syringes with 27 G needles.
4. Sterile eye lube (Optixcare).
5. Sterile cotton swabs.
6. Electric clippers.
7. Hair removal cream (Veet).
8. Betadine.
9. 70% ethanol.
10. Sterile surgical drapes.
11. Sterile gauze pads.
12. Sterile saline.
13. Sterile surgical tools: scissors, forceps.
14. Cauterizer.
15. 5-0 polyglycolic acid (PGA) absorbable sutures.
16. Triple antibiotic ointment: Bacitracin Zinc, Neomycin Sulfate, Polymyxin B Sulfate (*see* **Note 9**).
17. Recovery Heat Block: Set to 37°C–38°C, and cover with a sterile surgical drape.
18. Buprenorphine (0.05 mg/kg; injectable).
19. Postoperative scoring sheets.

2.8 Determination of Antigen Restriction Capacity of MLNs

2.8.1 Bacterial Preparation

1. GFP-expressing *E. coli* (e.g., harboring pZe21-RBSmod + sfGFP) (*see* **Note 10**).
2. Tryptic Soy Broth (TSB).
3. Kanamycin sulfate (50 mg/mL), 1000× solution.
4. 250 mL Erlenmeyer flask (autoclaved).
5. Shaking incubator (set at 37°C).
6. Sterile 50 mL conical tubes.
7. Sterile PBS, ice-cold.
8. Spectrophotometer (*see* **Note 11**).
9. Ice bucket.

2.8.2 MLN Bacterial Injections, Tissue Collection, and Bacterial Enumeration

1. Insulin syringes (27G needles).
2. Sterile syringes with 27G needles.
3. Sterile PBS.
4. 2 mL Eppendorf tubes with 500 µL of ice-cold PBS.
5. Analytical scale.

6. Dissection tools: Scissors, forceps.
7. Heparinized tubes.
8. Hand-held homogenizer (e.g., OMNI International TISSUE MASTER 125).
9. 1.5 mL sterile microcentrifuge tubes.
10. TSA plates containing 50 μg/mL of kanamycin.
11. Incubator: 37°C.
12. Imaging system (e.g., Bio-Rad ChemiDoc MP Imaging System with Alexa 488 detection) (*see* **Note 12**).

2.9 Single-Cell Multiplex Cytokine Profiling of T Cells

2.9.1 Lymphocyte Isolation and Overnight IL-2 Conditioning

1. Complete RPMI supplemented with L-glutamine (2 mM) and β-mercaptoethanol (50 μM). Filter sterilize (0.22 μm) and warm to 37°C before use.
2. Frosted slides.
3. PBS (Ca^{2+}/Mg^{2+} free).
4. 70-μm strainer.
5. 15 and 50 mL conical tubes.
6. Trypan blue.
7. Recombinant murine IL-2 (1 μg/mL working concentration).
8. 24-well plates.

2.9.2 $CD8^+$ T-cell Magnetic Isolation and Stimulation

1. $CD8^+$ cell isolation magnetic beads (*see* **Note 13**).
2. Isolation buffer: PBS containing 0.5% BSA and 2 mM EDTA.
3. Complete RPMI.
4. Trypan Blue.
5. Anti-mouse CD3ε (clone 145-2C11).
6. Anti-mouse CD28 (clone 37.51).
7. 24-well plates.
8. PBS (Ca^{2+}/Mg^{2+} free).

2.9.3 IsoCode Chip Preparation and Cell Loading

1. IsoCode Chips (store −20°C).
2. CodePlex Reagent Box (4°C).
3. P10 filtered tips (supplied tips).
4. P10 pipette.
5. Complete RPMI.

2.9.4 Single-Cell Incubation, Detection, and Analysis

1. Cover Tape (One per chip).
2. Cover Tape Applicator (One per kit).
3. Calibration Chip.
4. IsoLight Instrument.
5. IsoSpeak software.

2.10 Bacterial Translocation Detection

2.10.1 Preparation of Media and Plates

1. Brain Heart Infusion (BHI)/Blood Agar: Add 37 g of BD BHI broth mix and 15 g of BD Difco™ Plate Count Agar to 900 mL of distilled water. Stir continuously on a magnetic stirrer to avoid clumping. Heat and stir until the solution is fully dissolved. The solution should look clear. Add distilled water to reach a total volume of 1 L. Autoclave the mixture at 121°C for 45 min. Cool media to 45–50°C. Add 50 mL of defibrinated sheep blood. Swirl to mix. Using a flame or laminar flow hood to keep plates sterile while pouring and cooling, pour ~20 mL of media into each sterile Petri dish, and allow plates to solidify at room temperature. Store plates inverted at 2–8°C.
2. Vitamin Solution: Dissolve 2.0 mg of Biotin, 2.0 mg of Folic acid, 10.0 mg of Pyridoxine-HCl, 5.0 mg of Thiamine-HCl × 2 H_2O, 5.0 mg of Riboflavin, 5.0 mg of Nicotinic acid, 5.0 mg of D-Ca-pantothenate, 0.10 mg of Vitamin B_{12}, 5.0 mg of p-Aminobenzoic acid, and 5.0 mg of Lipoic acid in 1 L of water, and filter sterilize with 0.22 μm filter.
3. Modified Yeast Casitone Fatty Acids (YCFA) broth (1×): To 900 mL of distilled water, add 10 g of casitone, 2.5 g of yeast extract, 5 g of glucose, 45 mg of $MgSO_4 \times 7H_2O$, 90 mg of $CaCl_2 \times 2H_2O$, 0.45 g of K_2HPO_4, 0.45 g of KH_2PO_4, 0.9 g of NaCl, 1 mg of resazurin, 1.9 mL of acetic acid, 0.7 mL of propionic acid, 90 μL of iso-butyric acid, 100 μL of n-valeric acid, and 100 μL of iso-valeric acid. Boil for 10 min while stirring. Cool to room temperature while gassing with 100% CO_2. Add 4 g of $NaHCO_3$, 1 g of L-cysteine-HCl, and 10 mg of hemin. Adjust pH to 6.7–6.8. Adjust volume to exactly 1.0 L with distilled water. In an anaerobic chamber, distribute 10 mL of solution per Hungate tube, and autoclave at 121°C for 30 min. Aseptically add 100 μL of Vitamin Solution per 10 mL of medium.
4. YCFA plates: Prepare 2× modified YCFA broth and 2× agar (autoclaved). Mix both solutions together in a 1:1 ratio.
5. CME0151 agar: Add 52.5 g of Reinforced Clostridial Agar (RC Agar) [Dehydrated] to 1 L of distilled water. Boil the

mixture while stirring to dissolve the powder. Autoclave media at 121°C for 15 min. Allow the medium to cool to approximately 50°C. Pour ~20 mL of medium into each sterile Petri dish. Allow plates to solidify at room temperature, and store inverted at 2–8°C.

6. Distilled or deionized water.
7. Heat-resistant bottles.
8. Magnetic stir bars.
9. Stirring hotplate.
10. Autoclave.
11. Sterile Petri dishes.
12. pH meter.
13. NaOH and HCl.
14. Hungate tube.
15. 0.22 μm filters.
16. CO_2 bubbler.
17. Anaerobic chamber.

2.10.2 Enumeration of Bacteria from Tissues

1. Sterile 2 mL screw-cap microcentrifuge tubes.
2. Sterile reduced PBS: Keep sterile PBS in the anaerobic chamber for one week to remove oxygen.
3. Sterile 5-mm borosilicate glass beads.
4. Analytical balance.
5. 2.5-liter portable anaerobic chamber.
6. Anaerobic gas packs.
7. Qiagen TissueLyser II.
8. BHI/blood plates.
9. YCFA plates.
10. CME0151 plates.
11. Anaerobic chamber.

2.10.3 gDNA Extraction from Tissue

1. Sterile 2 mL O-ring microcentrifuge tubes.
2. Liquid nitrogen.
3. Sterile Petri dishes.
4. Razor blades.
5. 0.1 mm and 0.5 mm zirconia/silica beads: Mix in a 1:1 ratio.
6. Buffer A: Combine 8 mL of 5 M NaCl, 8 mL 1 M of Tris base, 800 μL of 0.5 M RNase-free EDTA, 60 mL of 20% SDS, and 123.2 mL of Milli-Q water. Filter sterilize and store at room temperature.

7. Phenol:Chloroform:Isoamyl alcohol (25:24:1) [pH 7.9].
8. Qiagen TissueLyser II.
9. 5 Prime Phase Lock Gel tubes
10. 1.5 mL DNase/RNase-free microcentrifuge tubes.
11. Molecular biology grade Isopropanol.
12. 3 M sodium acetate, pH 5.5.
13. Molecular biology grade, 200 proof ethanol.
14. Tris-EDTA with RNase: Combine 2.5 mL of 1 M Tris (pH 8.0), 1.0 mL of 500 mM EDTA, 10 μL of 100 mg/mL RNase, 46.5 mL of DEPC water. Store at 4°C.
15. Qiagen QIAquick PCR Purification Kit.
16. Quanti-iT PicoGreen dsDNA Assay Kit.
17. Fluorescent plate reader or Qubit.
18. Nanodrop.

2.10.4 16S Library Preparation and Sequencing

1. 96-well plates.
2. Invitrogen Accuprime *Pfx* Supermix.
3. 515F Forward primer: 5′-*AATGATACGGCGACCACCGA GATCTACAC*-NNNNNNNN-**TATGGTAATT-GT-GTGCCAGCMGCCGCGGTAA**-3′.
4. 926R Reverse primer: 5′-*CAAGCAGAAGACGGCATACG A G A T*- N N N N N N N N - **A G T C A G T C A G - C C - GGACTACHVGGGTWTCTAAT**-3.
5. PCR-grade water.
6. Plate seals.
7. Thermocycler.
8. 2% agarose gel with ethidium bromide.
9. 100 bp DNA ladder.
10. 1 kb DNA ladder.
11. Electrophoresis power supply.
12. UV light source/imager.
13. Beckman Coulter AMPure XP beads.
14. DNase and RNase-free 1.5 mL snap cap tubes.
15. Agilent Technologies D1000 ScreenTape for DNA analysis kit.
16. KAPA Biosystems KAPA Library Quantification Kit for Illumina Platforms.
17. Thermocycler with qPCR capabilities.

18. Illumina MiSeq Reagent Kit v2 (500-cycle): Contains reagent cartridge, HT1 Hybridization (Hyb) buffer, PR2 Incorporation buffer, and flow cell.
19. Water bath, 20–25°C.
20. 0.2 N NaOH.
21. Illumina PhiX v3 control library.
22. Paper towels.
23. Chemical fume hood.
24. PCR tubes.
25. Read 1 Sequencing Primer: 5′-TATGGTAATT-GT-GTGCC AGCMGCCGCGGTAA-3′.
26. Read 2 Sequencing Primer: 5′-AGTCAGTCAG-CC-GGAC TACHVGGGTWTCTAAT-3′.
27. Index Read Primer: 5′-ATTAGAWACCCBDGTAGTCCGG CTGACTGACT-3’.
28. Extra-long 20 μL filter tips.
29. Milli-Q water.
30. Lint-free wipes (e.g., Kimwipes).
31. 100% ethanol.
32. Illumina MiSeq System.

3 Methods

3.1 Preclinical Tumor Model of B16 Melanoma and Immune Checkpoint Therapy

3.1.1 Expansion of B16-F10 Cells

1. Thaw 5×10^6 B16-F10 cells into complete DMEM. Wash cells once with complete DMEM before moving into a T75 flask. Grow B16-F10 cells at 37°C, with 5% CO_2.
2. Expand B16-F10 cells in complete DMEM using T75 or T175 flasks, depending on the number of mice to be injected. For 40 mice, one T175 flask should be an excessive number of cells.
3. Harvest cells at a low passage number (preferably <10) when cultures reach approximately 70%–80% confluence.

3.1.2 Preparation of B16-F10 Cells for Implantation

1. Aspirate growth medium from the culture flask and discard. Wash cells once with 5–10 mL of sterile PBS.
2. Add 3 or 5 mL (for T75 and T175 flask, respectively) of TrypLE™ Express enzyme to detach cells, and incubate at 37°C until detachment is complete.
3. Add 10–15 mL of complete DMEM to neutralize the enzyme. Resuspend the cells, and transfer to a conical tube.
4. Centrifuge the cell suspension for 5 min at $500 \times g$, 20–25°C. Discard the supernatant.
5. Resuspend the cell pellet in DMEM only, and determine cell concentration:
   a. Mix an aliquot of the cell suspension with trypan blue.
   b. Load the mixture onto a cell counter slide.
   c. Count cells using an automated cell counter or hemacytometer.
6. Adjust the cell suspension with DMEM only (no FBS) to a final concentration of 1×10^5 cells per 100 µL per mouse for implantation.
7. Transfer the cell suspension to 2 mL microcentrifuge tubes to facilitate collection with the syringe needle.
8. Keep cells on ice until ready for implantation.

3.1.3 Subcutaneous Tumor Cell Implantation

1. Select 6- to 8-week-old female C57BL/6 mice. Female mice are used for two reasons. First, B16-F10 tumors grow much faster in male mice compared to female mice, which makes therapeutic experiments challenging. Second, male mice are more aggressive than female mice, which can result in physical damage to cutaneous tumors leading to early cessation of experiments.
2. Gently vortex the cell suspension before loading the syringe to maintain a uniform single-cell suspension.
3. Prepare syringes containing the cell suspension, removing any air bubbles. One syringe can be shared between five mice.
4. Anesthetize mice using an approved isoflurane inhalation protocol (*see* **Note 14**).
5. Once the mouse is fully anesthetized and immobile, shave the hair from the right flank.
6. Clean the area with an alcohol prep pad.
7. Inject 100 µL of the cell suspension subcutaneously into the right flank.
8. Monitor mice until full recovery from anesthesia.

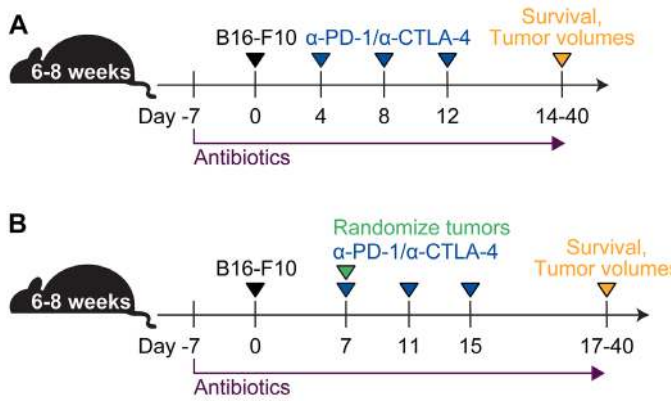


Fig. 1 Treatment timings for B16 melanoma tumor model. **(A)** ICT treatment timing without tumor size randomization. **(B)** ICT treatment timing with tumor size randomization

3.1.4 Microbiota Depletion with Antibiotics

1. Provide antibiotic drinking water to mice assigned to the microbiota-depleted groups starting 7 days before B16-F10 tumor implantation.
2. Check water levels regularly and replace antibiotic water every 2–3 days.

3.1.5 Immune Checkpoint Blockade

1. Prepare α-PD-1 and α-CTLA-4 antibodies in sterile PBS at the appropriate concentration to deliver 200 μg per mouse (*see* **Note 15**).
2. Keep antibodies on ice at all times.
3. Administer antibodies via intraperitoneal (i.p.) injection on days 4, 8, and 12 after tumor implantation (Fig. 1A) or the same day as tumor randomization (*see* **Note 16**) (Fig. 1B).

3.1.6 Melanoma Model Analysis

1. Determine tumor volume every day after tumors reach 100 $mm^3 \pm 20$ mm^3. Euthanize mice when tumor diameter exceeds 2 cm in any dimension or tumor volume ≥ 1800 mm^3.
2. Complete survival curves. Loss of survival is defined as death (with moribund mice being euthanized) or when tumor diameter exceeds 2 cm in any dimension, requiring euthanasia.

3.2 Immune Profiling: Flow Cytometry of the Tumor/Secondary Lymphoid Tissues and Serum Cytokine Analysis

3.2.1 Tissue Collection for Flow Cytometry

1. For tumors, pre-weigh 2 mL Eppendorf tubes containing 1 mL of Complete DMEM, and keep them on ice (*see* **Note 17**).

2. For spleens, TDLNs, and MLNs, dissect the whole tissues from mice, and place each into an ice-cold 2 mL tube containing 1 mL of Complete DMEM. Spray surgery tools with 70% ethanol and wipe between each mouse (*see* **Note 18**).
3. Dissect tumors from mice, and immediately submerge them into ice-cold Eppendorf tubes.
4. Weigh the Eppendorf tubes containing the tumors on an analytical scale, and calculate the tumor weight by subtraction.

3.2.2 Murine Serum Collection for Cytokine Analysis

1. Euthanize mice by CO_2 inhalation (*see* **Note 19**).
2. Spray the mouse down with 70% ethanol, and skin the mouse. Make a vertical abdominal incision, cut the sternum, and expose the heart.
3. Using a 25–27G needle with a 1 mL syringe, aspirate ≥400 μL of blood from the heart. Alternatively, blood can be drawn from the abdominal aorta.
4. Transfer whole blood into a serum separation tube. Use one tube per mouse.
5. Let the blood clot for 30 min at room temperature.
6. Centrifuge at 1300 × *g* for 10 min at 4°C.
7. Aspirate serum from the top layer. Be careful not to aspirate the gel layer under the serum.
8. Make 50 μL aliquots of serum in O-ring tubes to prevent evaporation. Keep the serum on ice while aliquoting to preserve the cytokines.
9. Store at –80°C until cytokine analysis. Avoid repeated thaws, using each aliquot only once.

3.2.3 Preparation of Tumor Cell Suspensions

1. Prepare Miltenyi Biotec gentleMACS™ C Tubes by adding 1472.5 μL of tumor dissociation buffer to each tube.
2. Transfer tumors and Complete DMEM to a Petri dish, and mince the tumors with a razor blade into the smallest possible pieces. Transfer all tissue and media into the prepared Miltenyi Biotec gentleMACS™ C Tubes.
3. Dissociate tumor tissue using the Miltenyi Biotec gentleMACS Dissociator at 37°C for 40 min. Use the gentleMACS program Soft/Medium (1 × "m_impTumor_03") for tumor dissociation.
4. Quench digestion by adding 10 mL of Complete DMEM, and then filter the suspension through a Miltenyi MACS® SmartStrainer (70 μm).
5. Centrifuge filtrate at 400 × *g* at 4°C for 10 min.
6. Remove the supernatant, and wash the cell pellet with 10 mL of PBS.

7. Centrifuge at 400 × *g* at 4°C for 10 min.
8. Resuspend the cell pellet in 1 mL of RBC lysis buffer, and incubate at room temperature for 1 min to remove erythrocytes.
9. Wash cells with 10 mL of PBS, and centrifuge at 400 × *g* at 4°C for 10 min.
10. During centrifugation, add 5 mL of 80% Percoll to separate 15 mL conical tubes per each tumor (*see* **Note 20**).
11. Resuspend cell pellets in 5 mL of 40% Percoll solution, and carefully overlay onto the 80% Percoll solution in the 15 mL conical tubes (*see* **Note 21**).
12. Centrifuge at 350 x *g* at 20–25°C for 20 min with slow acceleration (*see* **Note 22**) and no brake to prevent mixing of gradient layers.
13. Collect only the visible cell band at the 40%/80% interface using a narrow pipette tip. Avoid aspirating excess Percoll. Wash the cells gently and promptly with PBS to maintain viability.
14. Resuspend cells in 200 μL of PBS.
15. Keep cells on ice until flow cytometry staining.

3.2.4 Preparation of MLNs, TDLNs, and Spleen Cell Suspensions

1. For each tissue, place a 70 μm sterile cell strainer on a Petri dish and add 5 mL of PBS. Transfer one tissue to the strainer, and mash MLNs, TDLNs, and spleens using the plunger of a 10 mL syringe. Collect all PBS, and filter through the same 70 μm sterile cell strainer onto the Petri dish to make a single cell suspension.
2. Wash the cell strainer and plunger with an additional 10 mL of ice-cold PBS (final volume should be ~15 mL).
3. Collect the cell suspension from the Petri dish, and transfer it to a 15 mL conical tube.
4. Centrifuge at 400 × *g* at 4°C for 10 min, and resuspend the cell pellet in ice-cold PBS.
5. Keep the MLN and TDLN cell suspensions on ice until flow cytometry staining. Proceed to Step 6 for splenic cell preparation.
6. Resuspend the splenocyte pellet in 1 mL of RBC lysis buffer, and incubate at room temperature for 1 min to remove erythrocytes.
7. Add 14 mL of PBS to stop the reaction, and centrifuge at 400 × *g* at 4°C for 10 min.
8. Wash cells with 10 mL of PBS, and centrifuge at 400 × *g* at 4°C for 10 min.

9. Resuspend cells in 200 µL of PBS.
10. Keep the cell suspensions on ice until flow cytometry staining.

3.2.5 Surface Staining for Flow Cytometry

1. Transfer single-cell suspensions into a V-bottom 96-well plate, and centrifuge at 400 × *g* at 4°C for 10 min.
2. Perform one wash with PBS.
3. Stain for live/dead cells with Zombie Yellow or Ghost Dye (1:1000 dilution; 200 µL per well) for 15 min at room temperature, protected from light.
4. Wash once with FACS buffer and centrifuge at 400 × *g* for 5 min.
5. Block Fc antibody receptors on antigen-presenting cells using anti-CD16/32 Fc block (1:50 dilution) prepared in FACS buffer. Add 50 µL per well, and incubate for 10 min on ice, protected from light.
6. Prepare the surface antibody cocktail in FACS buffer. Use 1:200 dilution for most surface markers, except F4/80 (1:100). Subtract volume of antibodies from volume of FACS buffer to keep dilutions as accurate as possible (*see* **Note 23**).
7. Add 50 µL of surface antibody cocktail directly to each well containing Fc block (final volume 100 µL), mix gently by pipetting, and incubate for 30 min at room temperature in the dark. The final dilutions of the antibodies will be 1:400 (for most antibodies) and 1:200 (for F4/80).
8. Add 100 µL of FACS buffer to each well, and wash by centrifugation at 400 × *g* for 5 min.
9. Wash once with 180 µL of FACS buffer.
10. Run the plate on the flow cytometer.

3.2.6 T-Cell Stimulation and Intracellular Cytokine Staining for Flow Cytometry

1. For intracellular staining, transfer cells to U-bottom 96-well plates, and spin down at 400 × *g* at 4°C for 10 min. Aspirate supernatant (*see* **Note 24**).
2. Add 200 µL of Stimulation RPMI to each well, and incubate at 37°C in a 5% CO_2 incubator for 4.5–5 h (*see* **Note 25**).
3. Wash cells with PBS and centrifuge at 400 × *g* for 10 min, then proceed with surface staining as described in Sect. 3.2.5, Steps 1–9.
4. Perform intracellular staining using the Cytofast Fix/Perm Buffer Set (*see* **Notes 26 and 27**).
5. Add 100 µL of 1× Fix/Perm buffer to each well, mix thoroughly by pipetting, and incubate for 20 min at room temperature in the dark.

6. Add 100 µL of 1× Perm Wash buffer to each well, and centrifuge at 500 × *g* for 5 min at room temperature. Discard supernatant.
7. Add 200 µL of Perm Wash buffer, and perform two additional washes at 500 × *g* for 5 min at room temperature.
8. Prepare the intracellular antibody cocktail in 1× Perm Wash buffer using a 1:50 dilution for all anti-cytokine antibodies.
9. Add 100 µL of intracellular antibody cocktail to each well, and mix thoroughly by pipetting.
10. Incubate for 45 min at room temperature in the dark.
11. Wash once with 100 µL of Perm Wash buffer, and centrifuge at 500 × *g* for 5 min at room temperature. Discard supernatant.
12. Wash once with FACS buffer, and centrifuge at 500 × *g* for 5 min at room temperature. Discard supernatant, and resuspend cells in 200 µL of FACS buffer per well.
13. Run plate on flow cytometer.

3.2.7 Transcription Factor Staining

1. Proceed with surface staining as described in Sect. 3.2.5, Steps 1–9 (*see* **Note 28**).
2. Prepare the True-Nuclear™ Transcription Factor Buffer Set according to the manufacturer's instructions.
3. Add 200 µL of 1× Fixation buffer to each well, mix thoroughly, and incubate for 45 min at room temperature in the dark.
4. Wash cells three times with 1× Permeabilization buffer. Centrifuge at 500 × *g* for 5 min at room temperature for each wash.
5. Prepare transcription factor antibody cocktail in Perm Wash buffer using a 1:50 dilution for most transcription factors; RORγt requires a 1:25 dilution. Add 100 µL per well.
6. Incubate for 45 min at room temperature in the dark.
7. Add 100 µL of Perm Wash buffer, and wash once, centrifuging at 500 × *g* for 5 min at room temperature.
8. Wash 1–2 times with FACS buffer, and resuspend in 200 µL of FACS buffer.
9. Run the plate on the flow cytometer.
10. Analyze data with flow cytometry analysis software according to Table 3 (*see* **Note 29**).

3.2.8 Tumor Tissue Lysate Preparation for Cytokine Analysis

1. Prepare lysis buffer by aliquoting 10 mL of R&D Lysis Buffer 2 into a 15 mL tube and adding one protease inhibitor tablet and one phosphatase inhibitor tablet. Allow to dissolve at room temperature. Vortex, if needed.

Table 3
Suggested panel for immune phenotyping

Immune cell population	Markers
$CD8^+$ T cell	$CD45^+$ $NK1.1^-$ $CD3^+$ $CD8^+$ $CD4^-$
$CD4^+$ T cell	$CD45^+$ $NK1.1^-$ $CD3^+$ $CD4^+$ $CD8^-$
B cell	$CD45^+$ $NK1.1^-$ $CD3^-$ $CD19^+$
NK cell	$CD45^+$ $CD3^-$ $NK1.1^+$
Monocyte	$CD45^+$ $NK1.1^-$ $CD3^-$ $CD19^-$ $Ly6C^+$ $Ly6G^-$
Neutrophil	$CD45^+$ $NK1.1^-$ $CD3^-$ $CD19^-$ $Ly6C^+$ $Ly6G^+$
Macrophage	$CD45^+$ $NK1.1^-$ $CD3^-$ $CD19^-$ $Ly6C^+$ $Ly6G^-$ $CD11b^+$ $F4/80^+$
DC	$CD45^+$ $NK1.1^-$ $CD3^-$ $CD19^-$ $Ly6C^+$ $Ly6G^-$ $F4/80^-$ $CD11c^+$
Th1 $CD4^+$ T cell	$CD45^+$ $NK1.1^-$ $CD3^+$ $CD4^+$ $CD8^-$ T-bet^+ IFN-γ^+
Th2 $CD4^+$ T cell	$CD45^+$ $NK1.1^-$ $CD3^+$ $CD4^+$ $CD8^-$ $GATA3^+$ IL-4^+
TH17 $CD4^+$ T cell	$CD45^+$ $NK1.1^-$ $CD3^+$ $CD4^+$ $CD8^-$ RORγt^+ IL-$17A^+$
Treg	$CD45^+$ $NK1.1^-$ $CD3^+$ $CD4^+$ $CD8^-$ $CD25^+$ $Foxp3^+$

2. Add 400 µL of lysis buffer to 2 mL Eppendorf tubes (one per tumor), and place on ice. Pre-weigh each filled tube.
3. Prepare tissue homogenizer cleaning setup: Fill two 50 mL conicals with 40 mL of 70% ethanol and one 50 mL conical with 40 mL of sterile distilled water.
4. Dissect and isolate tumors (*see* Sect. 3.2.1, Steps 1, 3-4), but use the tubes filled with tumor lysis buffer.
5. Place each tumor into its pre-weighed 2 mL tube and weigh. Record the tumor weight for cytokine normalization.
6. Homogenize tumors using a TissueLyser II (30–60 s per tumor).
7. Clean homogenizer between samples: Immerse in 70% ethanol (twice), then distilled water, running the device during each wash. Wipe dry with Kimwipes before next use.
8. Incubate homogenized samples on ice for 30 min, agitating gently every 5 min.
9. Centrifuge samples at 21,000 × *g* for 15 min at 4°C.
10. Collect supernatant containing cytokines, and aliquot 50 µL into O-ring 1.5 mL tubes.
11. Store lysate aliquots at –80°C until bulk cytokine analysis.

3.2.9 Bulk Cytokine Analysis

1. Thaw murine serum or tumor lysate aliquots on ice.
2. Perform multiplex cytokine analysis using the Luminex platform (e.g., Mouse Luminex Discovery Assay, R&D Systems).

3. Load samples and standards per manufacturer's instructions.
4. Run on a Bio-Rad Luminex 200 or equivalent instrument.
5. Normalize raw cytokine concentrations to tumor weight for tissue lysates.

3.3 DC and T Cell Stimulation Assays

3.3.1 In vivo Expansion of Mouse Splenic DC

1. Follow steps in Sects. 3.1.1 and 3.1.2 to expand and prepare B16-FLT3L cells for implantation. Grow B16-FLT3L cells in Complete Abx DMEM. Prepare 5×10^6 cells per 100 µL per mouse for implantation.
2. Collect spleens 10–16 days after tumor implantation. Remove whole spleen and place in a 50 mL conical with 15 mL of RPMI. Keep on ice (*see* **Note 30**). Pool spleens from multiple mice in the same tube.

3.3.2 DC Isolation

1. Place a sterile 70 µm cell strainer in a Petri dish containing sterile RPMI.
2. Place a harvested spleen onto the strainer and mash the tissue using the plunger of a 10 mL syringe. Wash the strainer with RPMI to ensure most of the cells are collected. Use one strainer per spleen to avoid clogging.
3. Collect the cell suspension, and transfer it to a 15 mL conical tube.
4. Centrifuge for 5 min at 300 × *g* at room temperature, and discard the supernatant.
5. Add 1 mL of RBC lysis buffer, and incubate for 1 minute at room temperature (*see* **Note 31**).
6. Add 14 mL of PBS, and centrifuge for 5 min at 300 × *g*.
7. Repeat Steps 5 and 6 until the cell pellet appears white.
8. Isolate $CD11c^+$ DC using magnetic cell separation according to the manufacturer's instructions.
9. Resuspend isolated cells in Complete RPMI medium, and count the cells.

3.3.3 DC Activation Assay

1. Plate 1×10^5 freshly isolated DC per well (100 µL per well) in a 96-well U-bottom plate in Complete RPMI.
2. Add ligands or stimuli of interest to induce DC activation (*see* **Note 32**). 100 µL is a good working volume to add; the total volume in the well should be 200 µL after the stimuli are added.
3. Incubate cells for 6 h at 37°C in a 5% CO_2 incubator.
4. Centrifuge the plate at 300 × *g* for 5 min at room temperature.

Table 4
Suggested antibodies for DC and T cell stimulation assays

DC antibodies	$CD8^+$ T cell antibodies	$CD4^+$ T cell antibodies
CD11c	Live/dead stain	Live/dead stain
MHCII	CD3	CD3
CD40	CD8	CD4
CD80	CD69	CD25
CD86	Granzyme B	IFNγ
	IFNγ	TNFα

5. Collect 150 μL of the supernatant for cytokine analysis (see Sect. 3.2.9). Assess DC activation markers by flow cytometry. Follow steps for surface staining in Sect. 3.2.5. Use the markers for DC found in Table 4.

3.3.4 Naïve T Cell Isolation and CFSE Labeling

1. Collect spleens from naive mice in 1.5 mL microcentrifuge tubes with 1 mL of RPMI on ice (*see* **Note 30**). Use one tube per mouse.
2. Follow Steps 1–4 in Sect. 3.3.2 to isolate splenocytes. Keep the cells from each spleen separate.
3. Isolate naïve $CD4^+$ or $CD8^+$ T cells, based on your experimental question, using a naïve T cell magnetic bead isolation kit. Follow the manufacturer's instructions.
4. Centrifuge the isolated T cells at 300 × *g* for 5 min at room temperature.
5. Aspirate the supernatant, and resuspend the T cell pellet at 1×10^7 cells/mL in sterile PBS.
6. Add 1 μL of 5 mM CFSE solution per 2.5 mL of cell suspension.
7. Incubate for 10 min at room temperature in the dark.
8. Stop the reaction by adding five times the original staining volume of PBS.
9. Centrifuge at 300 × *g* for 5 min at room temperature.
10. Aspirate the supernatant, and resuspend the pellet with X-VIVO 15 medium at a concentration of 1.25×10^6 cells/mL.

3.3.5 Activated DC and Naïve T cell co-culture

1. Expand and isolate DC following the steps in Sects. 3.3.1 and 3.3.2. Resuspend isolated DC in X-VIVO 15 medium.
2. Plate 50 μL of the cell suspension (2.5×10^3 DC/well in X-VIVO 15 medium) in a 96-well U-bottom plate.

3. Add 50 µL of 40 µg/mL bacterial lysate or stimuli of interest to the appropriate wells.
4. Add 50 µL of 40 µg/mL OVA peptide to the appropriate wells.
5. Bring the total volume of each well to 200 µL with X-VIVO 15 medium.
6. Mix thoroughly, and incubate the plate for 6 h at 37°C in a 5% CO_2 incubator.
7. After 6 h of incubation, wash the plate with pulsed DC twice with X-VIVO 15 medium.
8. Resuspend DC with 100 µL of X-VIVO 15 medium.
9. Add 100 µL of naïve OT-I $CD8^+$ T cells to each well.
10. Incubate the plate for 5–7 days at 37°C in a 5% CO_2 incubator (*see* **Note 33**).
11. Follow steps in Sects. 3.2.5, 3.2.6, and 3.2.7 for surface staining, intracellular staining, and transcription factor staining. For intracellular staining, do not stimulate the cells with PMA, brefeldin A, and ionomycin. See Table 4 for recommended flow markers.

3.4 Surgical Removal of Secondary Lymphoid Organs

1. Set up an appropriate melanoma mouse model according to Sect. 3.1.
2. On day 7 post-implantation, select mice with tumor volumes of $100 \pm 20\,mm^3$ for randomization of the following procedures:
   a. MLN resection.
   b. Spleen resection.
   c. TDLN resection (right inguinal lymph nodes if tumors were injected into the right flank).
   d. Sham surgery (incision only, do not disturb the organs).
3. Anesthetize mice with vaporized isoflurane.
4. Administer carprofen (5 mg/kg, intraperitoneal) for pain management.
5. With a sterile cotton swab, apply eye lube to the eyes of the mouse to prevent dryness.
6. Remove abdominal fur using electric clippers, then finish with hair removal cream. Wipe off hair removal cream with a dampened paper towel. Incomplete removal of the hair removal cream will result in chemical burns.
7. Clean surgical site with betadine and 70% ethanol.
8. Drape mice with sterile surgical towels, and make approximately an inch-long longitudinal abdominal incision.

9. Gently mobilize intestines and place onto sterile, saline-moistened gauze.
10. Resect target organ(s) using sterile scissors. Immediately cauterize the affected areas and any major vessels that were ruptured.
11. Suture the peritoneum and then the skin with absorbable 5-0 PGA sutures (*see* **Note 34**).
12. Apply triple antibiotic ointment to the incision.
13. Discontinue anesthesia and monitor mice on a Recovery Heat Block. Monitor mice until they are fully awake and ambulatory.
14. Transition mice to a heated cage upon regaining mobility (*see* **Note 35**). Monitor closely for pain or lethargy.
15. Four hours post operation, check the mice and administer buprenorphine (0.05 mg/kg, subcutaneously).
16. Administer carprofen (5 mg/kg, intraperitoneal) 12 h post-operation.
17. For three days post operation, administer carprofen (5 mg/kg, intraperitoneal) twice a day (every 12 h).
18. During daily checks, if mice are not recovering or moribund, euthanize immediately.
19. Proceed with downstream applications such as tumor volume measurement, survival analysis, or flow cytometry.

3.5 Determination of Antigen Restriction Capacity of MLNs

3.5.1 Bacterial Preparation

1. Set up an appropriate melanoma mouse model according to Sect. 3.1. Complete steps in **Note 36** before starting this protocol.
2. Keep all materials and reagents as sterile as possible.
3. Inoculate GFP-expressing *E. coli* into 40 mL of Tryptic Soy Broth containing kanamycin (50 μg/mL) the day before bacteria will be injected into the mice.
4. Incubate cultures aerobically at 37°C for 24 h with shaking (250 RPM).
5. Transfer whole bacterial culture to 50 mL sterile conical tubes.
6. Centrifuge at 2000 x *g* for 10 min at 4°C.
7. Carefully discard the supernatant without disturbing the pellet.
8. Resuspend the bacterial pellet in 20 mL of ice-cold, sterile PBS.

9. Repeat Steps 6–8 twice (for a total of three washes) to remove residual media and antibiotics.
10. After the final wash, resuspend bacteria in 10 mL of sterile PBS, and read the optical density (OD_{600}).
11. Calculate the colony-forming units (CFU) based on OD_{600}, and resuspend bacteria at a concentration of 1×10^7 CFU per 20 μL (*see* **Note 36**).
12. Keep bacterial suspension on ice until use. Proceed immediately to inject the bacteria in the MLNs.

3.5.2 MLN Bacterial Injections

1. Perform GFP$^+$ *E. coli* injection one day after the final immune checkpoint therapy dose.
2. Perform abdominal surgery according to Steps 3–9 in Sect. 3.4.
3. Inject 1×10^7 GFP-expressing *E. coli* (in 20 μL) directly into the one or two nodes of MLN using an insulin syringe. Ensure minimal leakage and tissue disruption during injection.
4. Complete the surgery and follow-up care according to Steps 11–18 in Sect. 3.4.

3.5.3 Tissue Collection and Bacterial Enumeration

1. Before tissue collection, pre-weigh the 2 mL collection tubes (filled with PBS).
2. At 24 h post-MLN injection, euthanize mice according to approved protocols.
3. Collect the following samples under sterile conditions:
   a. Peripheral blood by cardiac puncture. Follow Steps 1–4 in Sect. 3.2.2, except transfer the blood to heparinized tubes to prevent coagulation.
   b. Dissect tumors and place in sterile 2 mL Eppendorf tubes containing 500 μL of ice-cold PBS.
   c. Dissect TDLNs and place in sterile 2 mL Eppendorf tubes containing 500 μL of ice-cold PBS.
4. Weigh the tubes with TDLNs and tumors to determine the weight of the tissues.
5. Homogenize tumor and TDLNs thoroughly using a sterile hand-held homogenizer. For OMNI International TISSUE MASTER 125, use speed setting 6.
6. Prepare serial dilutions of tissue homogenates and blood samples in sterile PBS (*see* **Note 37**).
7. Plate tissue homogenates and blood onto TSA plates containing kanamycin.
8. Incubate plates aerobically at 37°C for 24 h.

9. After incubation, identify GFP-expressing colonies using an appropriate imaging system with excitation at 488 nm and emission at 510 nm (detection for GFP).
10. Count colonies and calculate CFU:
    a. per gram of TDLNs.
    b. per gram of tumor.
    c. per mL of blood.
11. Record and analyze bacterial dissemination across tissues.

3.6 Single-Cell Multiplex Cytokine Profiling of T Cells

3.6.1 Animal Treatment and Tissue Collection

1. Implant the mice with B16 melanoma cells, and treat with antibiotics and ICT according to Sect. 3.1.
2. Harvest MLNs and TDLNs into 5 mL of ice-cold RPMI, following steps in Sect. 3.2.1.

3.6.2 Lymphocyte Isolation and Overnight IL-2 Conditioning

1. Mechanically dissociate nodes using frosted slides. Use sterile PBS to collect the cells.
2. Filter the cell suspension through a 70 μm strainer.
3. Centrifuge the cell suspension at $400 \times g$ for 5 minutes at 4°C.
4. Resuspend the pellet in 5 mL of Complete RPMI.
5. Pool samples within each group, and count viable cells.
6. Adjust the cell concentration to 1×10^6 cells/mL.
7. Add IL-2 to the cells for a final concentration of 1 μg/mL.
8. Add 1 mL of cell suspension to each well of a 24-well plate.
9. Incubate the cells for 12–16 h at 37°C in a 5% CO_2 incubator.

3.6.3 $CD8^+$ T Cell Magnetic Isolation and Stimulation

1. The next morning, collect the cells and wash them with 10 mL of isolation buffer.
2. Isolate $CD8^+$ cells using magnetic beads, following the kit instructions.
3. Elute $CD8^+$ cells and count.
4. Assess purity by flow cytometry (optional).
5. Coat 24-well plates with stimulatory antibodies. Mix α-CD3 and α-CD28 to a concentration of 2 μg/mL in PBS. Add 500 μL/well, and incubate the plate for 2 h at 37°C.
6. Dump or aspirate the plates. Wash twice with PBS.
7. Seed 5×10^5 cells/well in 1 mL of Complete RPMI.
8. Incubate the T cells for 48 h at 37°C in a 5% CO_2 incubator.

3.6.4 IsoCode Chip Preparation and Cell Loading (see Note 38)

1. Remove chips from −20°C, and thaw for 60–75 min at room temperature before opening. Keep sealed until loading.
2. Harvest cells and wash twice in Complete RPMI.
3. Remove the thawed chips from the bag, and place them on a flat surface, keeping the protective blue film on the bottom throughout the entire loading and sealing process to protect the glass slide (*see* **Note 39**).
4. Using provided P10 filter tips, dispense 5.5 µL of sample per well (approximately 30,000 cells).
5. Load strictly in numerical order (1–20); complete each row before next to minimize the risk of cross-contamination (*see* **Notes 40–42**).
6. Wells 5, 6, 15, and 16 are reserved for background controls and must not be loaded with a sample. Use only Complete RPMI as background control.
7. Inspect through the glass: fill must reach at least 75% of the distance between the well inlet and the first sample divider (*see* **Note 43**).

3.6.5 Single-Cell Incubation and Detection

1. Peel liner from Cover Tape.
2. Align using white rubber seals. Use a Cover Tape applicator with moderate pressure until slight indents appear (*see* **Note 44**).
3. On the IsoLight instrument:
   a. Select CodePlex Secretome.
   b. Load Calibration Chip in position 4, with CAL facing up. This step is essential, as the calibration chip provides the standard curve data required for IsoSpeak software to generate results in pg/mL.
4. Remove blue protective film from the bottom of the chip.
5. Load chips with the white seals facing up. Handle chips only by the sides or the barcode tab; do not touch the glass slide or the white rubber seals.
6. Ensure all reagent tubes are secure and the waste bottle is at least half empty.
7. Press “Start Assay” and close the chip tray by pressing “Close Chip Tray.” The chip is imaged for single-cell localization and incubated for 16 h at 37°C with 5% CO_2.
8. After the 16-h incubation, enzyme-linked immunosorbent assay detection is performed by IsoLight to determine which combination of proteins are secreted by each single cell.

3.6.6 Multiplex Cytokine Data Analysis

1. Analyze data using IsoSpeak software (*see* **Note 45**).
2. Determine cytokine combinations per cell.
3. Define polyfunctional cells, defined as ≥2 cytokines per cell.

3.7 Bacterial Translocation Detection

Bacterial translocation can be tested by culturing tissue lysate for aerobic and anaerobic bacteria, as well as by performing 16S rRNA gene sequencing to identify species in the tissues. In the case of culturing tissue lysates, place media and plates in an anaerobic chamber one week before use to make them "semi-anaerobic" (*see* **Note 46**).

3.7.1 Enumeration of Bacteria from Tissues

1. For every tissue from each mouse that will be analyzed, fill a 2 mL microtube with 500 µL of sterile PBS and one sterile 5-mm borosilicate glass bead.
2. Weigh the filled tubes before collecting tissues.
3. Follow the steps in Sect. 3.2.1 to harvest MLNs, spleen, TDLNs, and tumors. Place the harvested tissues in the tubes with the glass beads from Steps 1 and 2 of this section.
4. Place the samples inside a 2.5 L portable anaerobic chamber with an anaerobic gas pack. Keep the samples at anaerobic conditions during the collection and transportation processes.
5. Weigh the sample tubes on an analytical scale, and calculate the tumor weight by subtraction.
6. Homogenize the tissues using a TissueLyser II at 30 Hz for 3 min.
7. Prepare serial dilutions (up to 10^4) of each tissue homogenate in sterile reduced PBS.
8. Plate 10 µL replicates of each dilution on BHI/blood, YCFA, and CME0151 agar plates. Plate all replicates for one dilution on the same plate.
9. Incubate the plates at 37°C under anaerobic conditions (in an anaerobic chamber) and aerobic conditions (regular incubator) for 24–72 h.
10. When the colonies are large enough to count, quantify colonies, and calculate the CFU/mg of tissue for each sample as follows:

$$\frac{\text{Number of colonies} \times \text{Dilution factor } (10^x) \times \text{ Total volume}}{\text{Tissue weight (mg)} \times \text{ Volume plated}}$$

3.7.2 gDNA Extraction from Tissue

1. Label and weigh the empty 2 mL O-ring tubes, and record the weights. Prepare one tube for each tissue.
2. Follow steps in Sect. 3.2.1 to harvest MLNs, spleen, TDLNs, and tumors. Place the harvested tissues in the pre-weighed, empty 2 mL O-ring tubes.

3. Immediately flash freeze the harvested tissues in liquid nitrogen.
4. Weigh the sample tubes, and determine tissue weights. Move quickly to avoid thawing of samples.
5. Store the samples at −80°C until processing.
6. Thaw the tissues on ice. Keep on ice as much as possible.
7. In a sterile petri dish, grind the tissue using a scalpel blade and sterile tweezer until you get a uniform, semi-solid paste. Work quickly to limit time at room temperature.
8. Place the tissue back into its designated tube, and add ~0.5 mL of 0.1 mm and 0.5 mm zirconia/silica beads. Place the tube back on ice.
9. Add 710 μL of Buffer A (for gDNA extraction) and 500 μL of phenol/chloroform/isoamyl alcohol.
10. Lyse the cells by mechanical disruption with a TissueLyser (20 Hz for 1.5-3 min).
11. Centrifuge at 6800 × *g* for 3 min at room temperature.
12. Collect the aqueous phase (clear, top layer), and transfer it to a Phase Lock Gel tube. Be careful not to disturb the interphase layer beneath the aqueous layer.
13. Add 500 μL of phenol–chloroform–isoamyl alcohol to the aqueous layers in the Phase Lock Gel tubes. Invert the tubes three times to mix.
14. Centrifuge at 16,000 × *g* for 5 min at room temperature.
15. Transfer aqueous phase to a fresh 1.5 mL tube. Expect to collect ~500 μL.
16. Precipitate DNA from the aqueous phase by adding an equal volume of isopropanol (~500 μL) and 10% volume of 3 M sodium acetate (~50 μL).
17. Incubate overnight at −20°C or for 1 h at −80°C.
18. Centrifuge at 18,000 × *g* for 20 min at 4°C.
19. Remove and discard the supernatant. Be careful not to aspirate the DNA pellet.
20. Wash the pelleted DNA once with 500 μL of 100% ethanol.
21. Centrifuge at 18,000 × g for 2 min at 4°C.
22. Remove and discard all the ethanol. Air dry the pellet for 10–15 min.
23. Resuspend the dried DNA pellets in 200 μL of Tris-EDTA with RNase.
24. Incubate at 37°C for 30 min.

25. Column-purify the crude DNA extracts with the Qiagen QIAquick PCR Purification Kit. Follow the manufacturer's instructions.
26. Purified DNA may be used immediately or may be stored long term at −20°C.
27. Quantify gDNA using a fluorescence-based assay (Quanti-iT PicoGreen dsDNA assay kit).
28. Assess purity of DNA by spectroscopy with a Nanodrop (*see* **Note 47**).

3.7.3 16S Library Preparation and Sequencing

1. Prepare PCR reactions in a 96-well plate. Combine the following, in order: 17 μL of Accuprime *Pfx* Supermix, 20 ng of purified DNA from Sect. 3.7.2, and 1000 nM of each primer (*see* **Note 48**).
2. Perform two rounds of PCR amplification on a thermocycler with the following program: 95°C for 2 min; 30 cycles: 95°C for 20 s, 55°C for 15 s, 72°C for 5 min; 72°C for 10 min; 4°C hold.
3. Verify the products on a 2% agarose gel. Include 100 bp and 1 kB ladders on the gel. Run at 175 V for 60 min, and look for 400–430 base pair bands.
4. Normalize and clean up the samples with the AMPure XP beads. Follow the manufacturer's instructions.
5. Pool each plate into a single tube. Combine 5 μL of each normalized sample.
6. Perform quality control for each pooled plate using the D1000 ScreenTape for DNA analysis electrophoresis. Follow the manufacturer's instructions.
7. Quantify the separate pooled plate libraries with the KAPA Library Quantification kit. Follow the manufacturer's instructions.
8. Combine the pooled plate libraries in one tube to make your final sample library. Ensure that each pooled plate library has an equal final concentration.
9. Remove a 500-cycle reagent cartridge from the −20°C freezer. Place it in a room temperature water bath for one hour. Place the Hyb buffer tube in a 4°C refrigerator. While the reagent cartridge is thawing, perform Steps 10–14 of this section.
10. Prepare fresh 0.2 N NaOH.
11. To a 1.5 mL tube, add 10 μL of sample library and 10 μL of 0.2 N NaOH. To a separate tube, add 2 μL of PhiX control library, 3 μL of PCR grade water, and 5 μL of 0.2 N NaOH. Pipette to mix (*see* **Note 49**).

12. Incubate the tubes at room temperature for 5 min. Immediately add 980 μL of ice-cold Hyb buffer to the sample library tube and 990 μL of Hyb buffer to the PhiX control library tube (*see* **Note 50**).
13. Use Hyb buffer to further dilute both the sample library and PhiX control library to 4 pM for a v2 kit. Up to 8 pM can be loaded for a v3 kit (*see* **Note 51**). The final concentration of the solution loaded is 4.0 pM: 3.6 pM sample library, 0.4 pM PhiX control library, and 0.000515 N NaOH.
14. For a 15% PhiX run, combine 850 μL of 4.0 pM sample library and 150 μL of PhiX control library in a final tube. Vortex.
15. When the reagent cartridge has thawed, dry the bottom with a paper towel. Invert the cartridge repeatedly to check that each well is thawed and to mix the reagents. Place in a chemical fume hood.
16. Using a clean 1000 μL pipette tip, break the foil covering wells 12, 13, 14, and 17 of the reagent cartridge. Use a new tip each time.
17. Load 600 μL of the final Libary/PhiX solution into well 17 on the reagent cartridge.
18. Place 3 μL of the 100 μM Read 1 Sequencing Primer(s) into a clean PCR tube. Repeat in separate tubes for the Index Primer(s) and Read 2 Sequencing Primer(s).
19. Use an extra-long 20 μL tip to transfer the 3 μL of Read 1 Sequencing Primer to the bottom of well 12, and pipette to mix. Repeat this process, spiking the Index Primer into well 13 and the Read 2 Sequencing Primer into well 14.
20. Set the reagent cartridge aside. Unbox the flow cell and PR2 bottle.
21. Thoroughly rinse the flow cell with Milli-Q water. Carefully dry it by blotting with lint-free wipes. Give special attention to the edges and points of intersection between the glass and plastic.
22. Wet a new wipe with 100% alcohol, and wipe the glass on both sides, avoiding the rubber intake ports. Visually inspect the flow cell to ensure there are no blemishes, particles, or fibers on the glass.
23. Transfer the reagent cartridge, flow cell, PR2 bottle, and flash drive with the sample sheet to the MiSeq instrument. Copy the sample sheet from the flash drive to a folder on the MiSeq desktop.
24. Follow on-screen instructions to load the flow cell, reagent cartridge, and PR2 bottle. Empty and replace the waste bottle.

25. Ensure the machine recognizes the correct sample sheet. Verify the run parameters.
26. Wait for the MiSeq to perform its pre-run checks, and press start. If the pre-run check fails, try wiping down the flow cell again.
27. Run the library on a short-read sequencing platform (e.g., Illumina MiSeq, ~250 bp pair-end reads). Typically, 5000–20,000 sequences are generated per sample.

3.7.4 16S Sequencing Bioinformatic Analysis

16S rRNA gene sequencing is a widely used high-throughput approach for profiling microbial community composition and diversity. Numerous bioinformatic pipelines and parameter choices are available for 16S data analysis, and analytical decisions depend on experimental design and sequencing characteristics (e.g., targeted 16S region, amplicon length, single-end vs paired-end reads, and read length, etc). QIIME 2 [17] is a well-established and widely adopted platform for 16S data analysis. It provides well-written documentation and an active, well-organized user forum, making it suitable for beginners. We provide a brief analysis workflow for demultiplexed sequences below and a schematic overview in Fig. 2.

1. Assess raw sequence quality using FastQC (http://www.bioinformatics.babraham.ac.uk/projects/fastqc/) and MultiQC [18]. Perform the quality check for each sequence file with FastQC, and summarize results across all samples with MultiQC to identify systematic sequencing issues.
2. Remove sequencing adapters and primers, or trim low-quality ends using the QIIME 2 plugin `qiime cutadapt` [19], followed by rechecking the trimming results with `qiime demux summarize`.
3. Denoise sequences, and infer amplicon sequence variants (ASVs) using DADA2 [20] (via the plugin `qiime dada2`). DADA2 performs quality filtering, error model learning, chimera removal, and exact sequence inference to generate (ASVs).
4. Perform taxonomy annotation using the QIIME 2 plugin `qiime taxa`. Taxonomy is assigned to ASVs using a pre-trained naïve Bayes taxonomy classifier against the SILVA 138 rRNA 99 SSU reference database [21] for the targeted 16S region (`q2-feature-classifier classify-sklearn`).
5. Build a phylogenetic tree. Align all ASV sequence using MAFFT [22], and construct a phylogenetic tree with FastTree [23] (via `qiime phylogeny align-to-tree-mafft-fasttree`) for phylogeny-based diversity analyses (e.g., Faith's PD [24], UniFrac beta diversity [25]).

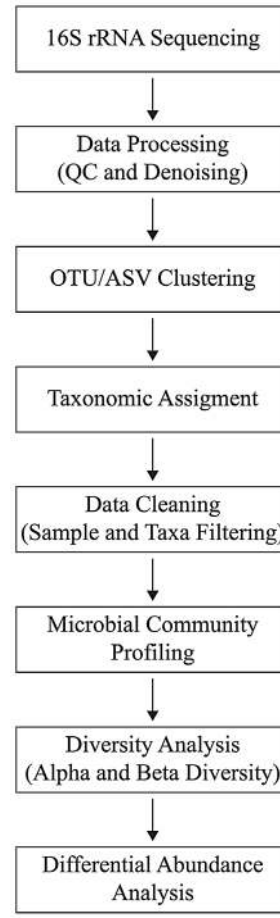


Fig. 2 Schematic overview of 16S bioinformatics pipeline

6. Integrate data into a phyloseq object for downstream analysis. Import the ASV table, taxonomy table, sample metadata, and phylogenetic tree into R using the package `qiime2R` (https://github.com/jbisanz/qiime2R), and combine them into one data file for the package `phyloseq` [26] to facilitate microbiome profile preprocessing and analyses.
7. Identify and remove contaminants. Apply the R package `decontam` [27] to detect and remove contaminant ASVs, including potential human-associated or reagent-derived sequences. This step is especially important in low microbial biomass samples, such as tumors or lymph nodes.
8. Filter low-quality samples and low-abundance ASVs. Remove samples with low read counts to reduce noise and improve statistical robustness. In addition, filter rare ASVs that occur in very few samples or are supported by extremely low read

counts (e.g., singletons), as these features are more likely to represent sequencing artifacts or residual errors rather than true biological taxa. Filtering thresholds for both samples and ASVs should be determined based on the characteristics of the microbial community, sequencing strategy, and study objectives.

9. Summarize and compare community composition using taxonomic stacked bar plots. Collapse the ASV abundance table to relative abundances at selected taxonomic levels (e.g., phylum, family, or genus) and generate stacked bar plots to provide an intuitive overview of microbiome composition. This visualization facilitates comparison of dominant and minor taxa across samples or experimental groups, helps identify large-scale compositional shifts, and serves as an important exploratory step to guide downstream diversity and differential abundance analyses.
10. Assess taxonomic diversity within and between samples. Quantify within-sample (alpha) diversity using metrics such as observed ASVs, Shannon index, Simpson index, and Faith's phylogenetic diversity to describe microbial richness and evenness. Evaluate between-sample (beta) diversity using dissimilarity metrics (e.g., Bray–Curtis [28], weighted and unweighted UniFrac), visualize patterns using ordination methods such as principal coordinates analysis (PCoA) [29], and compare group-level differences in community composition using permutational multivariate analysis of variance (PERMANOVA) [30]. The diversity metrics are calculated with R package `phyloseq` and `btools` (https://github.com/twbattaglia/btools/). The PCoA is performed using `ape::pcoa` [31] and PERMANOVA is performed using `vegan::adonis2` (https://vegandevs.github.io/vegan/).
11. Perform differential abundance analysis. Identify microbial taxa whose relative abundances are significantly different between experimental conditions, clinical outcomes, or environmental variables. This analysis is commonly used to identify taxa potentially contributing to observed phenotypic differences and to generate biologically relevant hypotheses. Multiple statistical methods are available (e.g., LEfSe [32], ANCOM-BC2 [33], and MaAsLin 3 [34]). These methods differ across multiple dimensions, including underlying statistical assumptions, normalization strategies, approaches to compositional data, covariate adjustment, and sensitivity to data sparsity. As no single method is universally optimal, results should be interpreted with caution.

4 Notes

1. Other antibiotics may be used, depending on the experimental question.
2. We recommend 5 mL BD Vacutainer Venous Blood Collection Tubes or BD Microtainer Blood Collection Tubes (SKU 365978).
3. We recommend using eBioscience 1× RBC Lysis Buffer, but it can be made using an ACK lysis buffer recipe.
4. The BioLegend activation cocktail should be stored at −80°C and protected from repeated freeze–thaw cycles. Do not reuse aliquots.
5. Avoid using conjugated antibodies for intracellular cytokine markers.
6. These tablets inhibit serine proteases, cysteine proteases, and metalloproteases. Comparable proteinase inhibitors should also work.
7. Any positive selection $CD11c^+$ cell isolation kit can be used. Magnetic cell isolation kits from Miltenyi Biotec and STEMCELL Technologies are options.
8. Use OVA 257-264 for OTI $CD8^+$ T cell stimulation and OVA 323-339 for OTII $CD4^+$ T cell stimulation.
9. The triple antibiotic ointment can be the generic or Neosporin.
10. Another fluorophore, such as RFP, can be used. Adjust all detection methods accordingly.
11. Any machine that can read the optical density of bacterial culture is suitable. Blank the instruments with the buffer or medium in which the cells are suspended.
12. The imaging system must be able to excite at 488 nm and detect emission at 510 nm (GFP or Alexa 488).
13. Magnetic cell isolation kits from Miltenyi Biotec and STEMCELL Technologies have worked successfully with this protocol.
14. For the E-Z Anesthesia EZ-SA800 Single Animal System, an isoflurane flow rate of 3–4 is typically used.
15. α-PD-1 and α-CTLA-4 antibodies have different concentrations for each lot from Bio X Cell, so calculations for specific lots will need to be completed each time.
16. To randomize tumors, measure the tumor volume with calipers. Tumor volumes are calculated using measurements from a digital caliper and the following formula: $(\text{length} \times \text{width}^2)/2$. Select mice with tumor volumes 100 ± 30 mm^3. Generally,

B16 tumors are at the appropriate size for randomization around 7–9 days post implantation. Expect to only use 50%–60% of the mice implanted with B16 tumors.

17. Maintain tissues and cell suspensions on ice whenever possible to preserve cell viability.
18. Collect TDLNs prior to tumor excision to minimize tissue damage. When collecting MLNs, remove surrounding non-lymphoid tissue as soon as possible to improve cell viability.
19. To successfully perform a cardiac puncture, euthanize mice one at a time. As soon as the mouse stops breathing completely, follow the protocol to collect blood.
20. Alternatively, immune cells can be isolated by pelleting through 40% Percoll. For this method, resuspend the tumor homogenate in 5 mL of 40% Percoll, and centrifuge at 350 × *g* at 20–25°C for 20 min with slow acceleration and no brake. Collect the pellet at the bottom of the tube. This method can save time when working with ten or more tumors.
21. Ensure all Percoll solutions are at the same temperature. Slowly layer the 40% Percoll cell suspension onto the 80% Percoll solution along the tube wall using a low pipetting speed to avoid disturbing the interface.
22. Pick the acceleration setting that is about half of the max acceleration. For example, on a centrifuge with a max acceleration of setting 9, we use setting 5.
23. When using multiple Brilliant Violet (BV) dyes, add 10 μL of BV stain buffer per well, and subtract the same volume from the total FACS buffer volume.
24. Cytokine staining and transcription factor staining should not be performed on the same sample.
25. Optimal stimulation time is 4.5–5 h. The minimum is 4 h, and the maximum is 6 h.
26. Dilute fixation and permeabilization buffers according to the manufacturer's instructions using diH_2O.
27. Apply the same staining and fixation/permeabilization procedures to compensation controls when performing intracellular staining.
28. No stimulation is required for transcription factor staining.
29. Flow data can be analyzed with FlowJo, NovoExpress, FCS Express, OMIQ, or other softwares.
30. Make sure the tissues are submerged in the medium. Increase the volume of medium, as needed.
31. Do not expose cells to RBC lysis buffer for longer than 5 min, as it could reduce the viability.

32. Purified LPS can be used as a positive control for DC stimulation (100 μL of 1 μg/mL LPS per well).
33. Depending on the stimuli of interest, dosage and timing will need to be optimized.
34. Nonabsorbable monofilament nylon (5-0 monofilament nylon nonabsorbable sutures) and veterinary surgical adhesive (Covetrus) can be used for skin closure.
35. Heat a clean cage upon a heat block set at 37°F–38°F.
36. To determine CFU from OD_{600} readings, complete the following steps for each bacterial strain and growth medium that will be used experimentally before initiating the main experiment:
    a. Inoculate GFP-expressing *E. coli* into 40 mL of Tryptic Soy Broth containing kanamycin (50 μg/mL) for 18–24 h.
    b. Prepare serial dilutions (in triplicate) of GFP-expressing *E. coli* culture (1:2; 1:4; 1:8; 1:16; 1:32), and read OD_{600}.
    c. For each dilution prepared above (step b), dilute further to 1:10; 1:100; $1:10^3$; $1:10^4$; $1:10^5$; $1:10^6$; $1:10^7$; and $1:10^8$ in Tryptic Soy Broth + kanamycin.
    d. Plate streaks of each dilution prepared above by adding 10 μL in a drop to a TSA plate containing kanamycin. Tilt the plate so all the drops slide down the plate in a streak. Complete duplicates for each dilution. Each plate can hold two drops.
    e. Count colonies for one dilution from (c) that is in a countable range (10–200 colonies), and determine CFU.
    f. For each dilution from (b), average the CFU for all six technical repeats (the duplicates for each triplicate of that dilution). Create a standard curve for average CFU based on the OD_{600} readings from step (b). Use this curve to determine CFU for experimental cultures.
37. Dilutions will need to be optimized for each experiment. We recommend initially trying a 1:5 dilution for blood (one part blood, four parts diluent); 1:5 and 1:10 for TDLN homogenates; and 1:10, 1:50, and 1:100 for tumor homogenates.
38. The sequence of these steps is critical! Do not deviate from the order presented.
39. Handle chips only by sides or barcode tab; never touch the glass or seal centers.
40. To load samples, insert the tip firmly to create a seal, dispense only to the first stop, hold for 2 s, and remove the tip slowly.

41. To prevent air bubbles: Always use a new P10 tip for each well. Fully thaw and mix samples. For pipetting technique, insert the tip firmly, dispense only to the first stop, hold for ~2 s, and release the plunger only after withdrawing the tip. Use only the P10 tips supplied with the kit.
42. Wells must be loaded strictly in consecutive order (1–20), completing each row fully before moving to the next. Deviating from this sequence or pairing incorrectly can disrupt internal fluidics and cause chip failure. Avoid pipetting into unlabeled vent holes, as this can cause chip malfunction.
43. If wells are underfilled (<75% of the chamber length), lightly tap the chip or use a clean P10 tip to promote filling, but do not apply excessive force.
44. Improper Cover Tape sealing can result in sample leakage, data loss, instrument damage, cross-contamination, chip malfunction, and software errors. Avoid touching the center holes of the seals, pipetting into vent holes, or misapplying the tape. Apply the Cover Tape using the applicator with moderate pressure until slight indents appear, and then inspect the sample fill lengths and dividers through the glass slide to ensure proper sealing and no contamination.
45. Any loading error or contamination from incorrect sequencing must be documented on the sample loading template, and affected wells should be excluded from final IsoSpeak analysis.
46. This "semi-anaerobic" method is not suitable for obligate anaerobes that are extremely sensitive to oxygen exposure. We recommend buying anaerobic media and plates from Anaerobe Systems for obligate anaerobes.
47. For optimal success with 16S analysis, fecal gDNA should have an A260/280 ratio > 1.7 and an A260/230 ratio > 1.0.
48. Primers listed in Sect. 2.11.4 include a MiSeq primer (in italics), a unique 8-base barcode (NNNNNNNN), and the 16S bacterial primer (in bold).
49. NaOH concentration on the flow cell must remain under 0.001 N. Adjusting the concentration of the NaOH used to denature the DNA to 0.1 N may be necessary if the sample library concentration is 1 nM or below.
50. The 20 pM PhiX can be frozen and used for subsequent runs.
51. Example calculations for sample library and Phix control library dilutions:
    a. (1.45 nM library × 10 ul) + (0.2 N NaOH × 10 ul) + 980 ul Hyb = 14.5pM Lib, 0.002 N NaOH.

b. (14.5pM lib×275.86 ul)+724.14 ul Hyb=4.0pM lib, 0.00055 N NaOH.
c. [(10 nM PhiX×2 ul)+3 ul HO]+(0.2 N NaOH × 5 ul)+990 ul Hyb=20pM PhiX, 0.001 N NaOH.
d. (20pM PhiX×200 ul)+800 ul Hyb=4.0pM PhiX, 0.0002 N NaOH.
e. (4.0pM Lib × 900 ul)+(4.0pM PhiX×100 ul)=solution loaded.

Competing Interests

The authors have no conflicts of interest to declare that are relevant to the content of this chapter.

References

1. Gopalakrishnan V, Spencer CN, Nezi L et al (2018) Gut microbiome modulates response to anti-PD-1 immunotherapy in melanoma patients. Science 359(6371):97–103. https://doi.org/10.1126/science.aan4236
2. Zitvogel L, Daillere R, Roberti MP et al (2017) Anticancer effects of the microbiome and its products. Nat Rev Microbiol 15(8):465–478. https://doi.org/10.1038/nrmicro.2017.44
3. Matson V, Fessler J, Bao R et al (2018) The commensal microbiome is associated with anti-PD-1 efficacy in metastatic melanoma patients. Science 359(6371):104–108. https://doi.org/10.1126/science.aao3290
4. Bautista J, Villegas-Chavez JA, Bunces-Larco D et al (2025) The microbiome as a therapeutic co-driver in melanoma immuno-oncology. Front Med 12:1673880. https://doi.org/10.3389/fmed.2025.1673880
5. Lu Y, Yuan X, Wang M et al (2022) Gut microbiota influence immunotherapy responses: mechanisms and therapeutic strategies. J Hematol Oncol 15(1):47. https://doi.org/10.1186/s13045-022-01273-9
6. Xie M, Li X, Lau HC, Yu J (2025) The gut microbiota in cancer immunity and immunotherapy. Cell Mol Immunol 22(9):1012–1031. https://doi.org/10.1038/s41423-025-01326-2
7. Baruch EN, Wang J, Wargo JA (2021) Gut microbiota and antitumor immunity: potential mechanisms for clinical effect. Cancer Immunol Res 9(4):365–370. https://doi.org/10.1158/2326-6066.Cir-20-0877
8. Sivan A, Corrales L, Hubert N et al (2015) Commensal *Bifidobacterium* promotes antitumor immunity and facilitates anti-PD-L1 efficacy. Science 350(6264):1084–1089. https://doi.org/10.1126/science.aac4255
9. Liu H, Xiong X, Zhu W et al (2025) Gut microbial metabolites in cancer immunomodulation. Mol Cancer 25(1):8. https://doi.org/10.1186/s12943-025-02521-5
10. Lei W, Zhou K, Lei Y et al (2025) Gut microbiota shapes cancer immunotherapy responses. NPJ Biofilms Microbiomes 11(1):143. https://doi.org/10.1038/s41522-025-00786-8
11. Zeng L, Qian Y, Cui X et al (2025) Immunomodulatory role of gut microbial metabolites: mechanistic insights and therapeutic frontiers. Front Microbiol 16:1675065. https://doi.org/10.3389/fmicb.2025.1675065
12. Vétizou M, Pitt JM, Daillère R et al (2015) Anticancer immunotherapy by CTLA-4 blockade relies on the gut microbiota. Science 350(6264):1079–1084. https://doi.org/10.1126/science.aad1329
13. Routy B, Le Chatelier E, Derosa L et al (2018) Gut microbiome influences efficacy of PD-1-based immunotherapy against epithelial tumors. Science 359(6371):91–97. https://doi.org/10.1126/science.aan3706
14. Choi Y, Lichterman JN, Coughlin LA et al (2023) Immune checkpoint blockade induces gut microbiota translocation that augments extraintestinal antitumor immunity. Sci Immunol 8(81):eabo2003. https://doi.org/10.1126/sciimmunol.abo2003
15. Dohlman AB, Klug J, Mesko M et al (2022) A pan-cancer mycobiome analysis reveals fungal involvement in gastrointestinal and lung

tumors. Cell 185(20):3807–3822.e3812. https://doi.org/10.1016/j.cell.2022.09.015
16. Nejman D, Livyatan I, Fuks G et al (2020) The human tumor microbiome is composed of tumor type-specific intracellular bacteria. Science 368(6494):973–980. https://doi.org/10.1126/science.aay9189
17. Bolyen E, Rideout JR, Dillon MR et al (2019) Reproducible, interactive, scalable and extensible microbiome data science using QIIME 2. Nat Biotechnol 37(8):852–857. https://doi.org/10.1038/s41587-019-0209-9
18. Ewels P, Magnusson M, Lundin S, Kaller M (2016) MultiQC: summarize analysis results for multiple tools and samples in a single report. Bioinformatics 32(19):3047–3048. https://doi.org/10.1093/bioinformatics/btw354
19. Martin M (2011) Cutadapt removes adapter sequences from high-throughput sequencing reads. EMBnet J 17(1):10–12. https://doi.org/10.14806/ej.17.1.200
20. Callahan BJ, McMurdie PJ, Rosen MJ et al (2016) DADA2: high-resolution sample inference from Illumina amplicon data. Nat Methods 13(7):581–583. https://doi.org/10.1038/nmeth.3869
21. Chuvochina M, Gerken J, Frentrup M et al (2026) SILVA in 2026: a global core biodata resource for rRNA within the DSMZ digital diversity. Nucleic Acids Res 54(D1): D334–D341. https://doi.org/10.1093/nar/gkaf1247
22. Katoh K, Misawa K, Kuma K, Miyata T (2002) MAFFT: a novel method for rapid multiple sequence alignment based on fast Fourier transform. Nucleic Acids Res 30(14):3059–3066. https://doi.org/10.1093/nar/gkf436
23. Price MN, Dehal PS, Arkin AP (2010) FastTree 2–approximately maximum-likelihood trees for large alignments. PLoS One 5(3):e9490. https://doi.org/10.1371/journal.pone.0009490
24. Faith DP (1992) Conservation evaluation and phylogenetic diversity. Biol Conserv 61(1):1–10. https://doi.org/10.1016/0006-3207(92)91201-3
25. Lozupone C, Knight R (2005) UniFrac: a new phylogenetic method for comparing microbial communities. Appl Environ Microbiol 71(12):8228–8235. https://doi.org/10.1128/AEM.71.12.8228-8235.2005
26. McMurdie PJ, Holmes S (2013) phyloseq: an R package for reproducible interactive analysis and graphics of microbiome census data. PLoS One 8(4):e61217. https://doi.org/10.1371/journal.pone.0061217
27. Davis NM, Proctor DM, Holmes SP et al (2018) Simple statistical identification and removal of contaminant sequences in marker-gene and metagenomics data. Microbiome 6(1):226. https://doi.org/10.1186/s40168-018-0605-2
28. Bray JR, Curtis JT (1957) An ordination of the upland forest communities of Southern Wisconsin. Ecol Monogr 27(4):325–349. https://doi.org/10.2307/1942268
29. Legendre P, Gallagher ED (2001) Ecologically meaningful transformations for ordination of species data. Oecologia 129(2):271–280. https://doi.org/10.1007/s004420100716
30. Anderson MJ (2001) A new method for non-parametric multivariate analysis of variance. Austral Ecol 26(1):32–46. https://doi.org/10.1111/j.1442-9993.2001.01070.pp.x
31. Paradis E, Schliep K (2019) ape 5.0: an environment for modern phylogenetics and evolutionary analyses in R. Bioinformatics 35(3):526–528. https://doi.org/10.1093/bioinformatics/bty633
32. Segata N, Izard J, Waldron L et al (2011) Metagenomic biomarker discovery and explanation. Genome Biol 12(6):R60. https://doi.org/10.1186/gb-2011-12-6-r60
33. Lin H, Peddada SD (2024) Multigroup analysis of compositions of microbiomes with covariate adjustments and repeated measures. Nat Methods 21(1):83–91. https://doi.org/10.1038/s41592-023-02092-7
34. Nickols WA, Kuntz T, Shen J et al (2026) MaAsLin 3: refining and extending generalized multivariable linear models for meta-omic association discovery. Nat Methods. Online Ahead-of-Print. https://doi.org/10.1038/s41592-025-02923-9



Chapter 39

Generation of Murine Chimeric Antigen Receptor T Cells for Adoptive T Cell Therapy for Melanoma

Amorette Barber

Abstract

Expression of chimeric antigen receptors enables T cells to be redirected toward melanoma-associated antigens in an MHC-independent manner. Retroviral transduction can be used to introduce these receptor constructs into murine $CD4^+$ and $CD8^+$ T cells. Here, we outline the generation of retroviral supernatants and the activation, transduction, expansion, and selection of murine T cells expressing the chimeric-PD1 receptor. This protocol can be adapted for any murine chimeric antigen receptor construct.

Keywords Immunotherapy, T cell, Melanoma, Chimeric antigen receptor, Retroviral transduction, Mouse

1 Introduction

Adoptive transfer of chimeric antigen receptor (CAR) T cells has achieved notable clinical success in several cancers, including B-cell acute lymphoblastic leukemia, diffuse large B-cell lymphoma, and multiple myeloma [1, 2]. CAR T-cell therapy for melanoma is also under active investigation, with several melanoma-associated antigens being targeted, including c-Met, CD70, GD2, VEGFR2, MAGE-A3, HER2, MART-1, NY-ESO-1, MUC1, and PD-1 ligands [3, 4]. Many preclinical CAR T-cell studies rely on syngeneic mouse cancer models to evaluate the safety and efficacy of CAR T-cell therapies before moving into human clinical trials.

Retroviral transduction provides a rapid and cost-effective approach to genetically engineer cells, and use of this technique has enabled the field of cellular engineering for adoptive cell therapy in cancer and other diseases to advance. Retroviral transduction of murine CD4+ and CD8+ T cells is commonly used to stably express TCR or CAR constructs in activated murine T cells for immunotherapy [5–7]. Compared with human T cells, achieving efficient retroviral gene transfer and robust expansion in murine primary T

Kristian M. Hargadon (ed.), *Melanoma*, Methods in Molecular Biology, vol. 3089,
https://doi.org/10.1007/978-1-0716-5619-8_39,
© The Author(s), under exclusive license to Springer Science+Business Media, LLC, part of Springer Nature 2027

cells presents several challenges. Herein, we describe an optimized protocol for efficient transduction of primary murine T cells with a chimeric antigen receptor targeting the ligands for the PD-1 receptor. We utilized high-titer ecotropic retroviral supernatants expressed using the GP2-293 cell line and a Moloney Murine Leukemia Virus (MMLV)-derived retroviral vector to allow efficient transduction of murine T cells [4]. We also describe optimized conditions for T cell activation and timing of retroviral exposure, both of which are essential for efficient retroviral infection/integration and T cell expansion/survival [5–7]. In addition, we describe parameters of T cell culture conditions, specifically the concentration of IL-2, selection of transduced T cells using G418 resistance, and isolation of viable transduced murine T cells using Histopaque-1083. Through use of these optimized techniques, we were able to attain efficient transduction and expression of the CAR in highly viable and functional primary murine T cells that can be used as an immunotherapy for melanoma. The murine chimeric PD1 (chPD1) antigen receptor consisting of the extracellular domain of the PD1 receptor fused to the cytoplasmic domains of the Dap10 costimulatory receptor and CD3ζ was utilized to demonstrate the murine T cell transduction protocol described here [4, 8, 9]. This protocol can be easily adapted for expression of alternative murine CAR constructs.

2 Materials

Prepare all reagents under sterile conditions. Prepare and store all reagents at 4°C unless otherwise noted. Follow all appropriate disposal and safety procedures for a BSL-2 protocol.

2.1 Retroviral Supernatant Production

1. GP2-293 packing cell line.
2. pVSV-G envelope vector.
3. MMLV-retroviral plasmid with wild-type- or chimeric-PD1 CAR gene (or other CAR construct) and G418 resistance gene.
4. Xfect polymer transfection reagent.
5. Retro-X concentrator.
6. Complete DMEM medium: DMEM medium supplemented with 10% heat-inactivated fetal bovine serum, 100 U/mL penicillin, 100 μg/mL streptomycin, 1 mM pyruvate, 10 mM Hepes, and 0.1 mM nonessential amino acids. Remove 65.5 mL of medium from a 500 mL bottle of DMEM medium (*see* **Note 1**). To the remaining 435 mL of DMEM medium, add 5 mL of 10,000 U/mL stock solution of Penicillin-Streptomycin, 5 mL of 1 M stock solution of HEPES, 5 mL of 100× stock solution of Nonessential amino acids (NEAA), and 50 mL of heat-inactivated fetal bovine serum.

2.2 T cell Isolation and Activation

1. Complete RPMI medium: RPMI medium supplemented with 10% heat-inactivated fetal bovine serum, 100 U/mL penicillin, 100 μg/mL streptomycin, 1 mM pyruvate, 10 mM Hepes, 0.1 mM nonessential amino acids, and 50 μM 2-mercaptoethanol. Remove 65.5 mL of media from a 500 mL bottle of RPMI media (*see* **Note 1**). To the remaining 435 mL of RPMI medium, add 5 mL of 10,000 U/mL stock solution of Penicillin-Streptomycin, 5 mL of 1 M stock solution of HEPES, 5 mL of 100× stock solution of Nonessential amino acids (NEAA), 500 μL of a 50 mM stock solution of 2-mercaptoethanol, and 50 mL of heat-inactivated fetal bovine serum (*see* **Note 2**).
2. Cell Culture Phosphate Buffered Saline: 1×, pH 7.4.
3. ACK lysing buffer: 155 mM NH_4Cl, 10 mM $KHCO_3$, and 0.01 mM EDTA.
4. 1 mg/mL of Concanavalin A (ConA) in sterile H_2O. Store at −20°C.

2.3 Transduction, Expansion, and Selection of T cells

1. 10 mg/mL of Polybrene in sterile H_2O. Store at −20°C.
2. 10,000 IU/mL of recombinant human interleukin-2 (rhu IL-2) in sterile H_2O. Store at −20°C.
3. 50 mg/mL of G418 Sulfate in sterile H_2O.
4. Histopaque-1083.

3 Methods

Carry out all procedures at room temperature in a BSL-2 certified biosafety cabinet under sterile conditions unless otherwise noted. All plastics and reagents should be sterile.

3.1 Retroviral Supernatant Production

1. Add GP2-293 cells (5×10^6) in 10 mL of complete DMEM to a 100 mm cell culture dish.
2. Culture cells in a humidified incubator set at 37°C with 5% CO_2 for 24 h (*see* **Note 3**).
3. Dilute 15 μg of MMLV-retroviral plasmid DNA containing gene for chimeric-PD1 CAR construct in 300 μL of Xfect Reaction buffer. Repeat this step to dilute the plasmid with the wild-type PD1 CAR construct.
4. Dilute 15 μg of pVSV-G envelope vector in 300 μL of Xfect Reaction buffer.
5. Combine the diluted retroviral plasmid from Step 3 and the diluted pVSV-G plasmid from Step 4 into one tube and vortex for 5 s.

6. Add 9 μL of Xfect polymer to the plasmid mixture. Mix well by vortexing for 10 s.
7. Incubate the mixture at room temperature for 10 min.
8. Add the mixture dropwise to the GP-293 cells.
9. Gently rock the plate back and forth to mix well.
10. Culture cells in a humidified incubator set at 37°C with 5% CO_2 for 12 h.
11. Remove the media from the cells and replace with 10 mL of fresh complete DMEM.
12. Culture cells in a humidified incubator set at 37°C with 5% CO_2 for an additional 24 h.
13. Transfer the retroviral supernatants into 50 mL conical tubes. Centrifuge the supernatants at 500 × *g* for 10 min.
14. Transfer the supernatants to a new 50 mL conical tube being careful to avoid the cell pellet. Add 1 volume of Retro-× concentrator for three volumes of retroviral supernatant. Mix gently by inversion.
15. Incubate overnight at 4°C.
16. Centrifuge mixture at 1500 × g for 45 min at 4°C.
17. Remove and discard supernatant, being careful not to disturb pellet. Gently resuspend the pellet with complete DMEM using 1/10th of the original volume of retroviral supernatant that was concentrated.
18. Fresh retroviral supernatants can be used to transduce T cells or can be stored at −80°C.

3.2 T Cell Activation

1. Remove the spleen from one euthanized mouse (*see* **Note 4**) and immediately place the spleen into 5 mL of complete RPMI medium in a 15 mL conical tube.
2. Invert the 15 mL conical tube multiple times, and quickly pour the medium and spleen into a sterile 60 mm cell culture treated dish.
3. Dissociate the spleen by pressing down on the spleen with the back of a sterile 5 mL syringe and moving the syringe in a circular motion, pressing the spleen gently against the bottom of the dish. Continue this until the spleen is dissociated and no large pieces of the spleen remain.
4. Transfer the cell suspension (splenocytes) into a 15 mL conical tube. Add 5 mL of PBS to the dish, gently swirl the dish, and transfer the PBS to the 15 mL conical tube with the splenocyte suspension.
5. Centrifuge the splenocytes in the 15 mL conical tube at 500 × *g* for 5 min (*see* **Note 5**).

6. Discard the supernatant and dissociate the cell pellet (*see* **Note 6**).
7. To lyse the red blood cells, add 3 mL ACK lysis buffer to cells and invert tube to mix cells. Incubate at room temperature for 3 min.
8. Add 10 mL of PBS to the splenocytes and invert the tube multiple times to mix.
9. Place a 70 μm cell strainer in the opening of a 50 mL conical tube. Pour the splenocyte suspension over the cell strainer to remove large pieces of tissue. The filtered splenocyte suspension will be in the bottom of the 50 mL conical tube.
10. Transfer 30 mL of PBS over the top of the cell strainer to wash the top of the strainer.
11. Centrifuge the splenocytes in the 50 mL conical tube at 500 × *g* for 5 min.
12. Discard the supernatant and dissociate the cell pellet. Add 30 mL of PBS to the suspended cells and invert the tube multiple times to mix cells.
13. Centrifuge the splenocytes in the 50 mL conical tube at 500 × *g* for 5 min.
14. Discard the supernatant and dissociate the cell pellet. Resuspend the splenocytes by adding 40 mL of complete RPMI media. Invert the tube multiple times to mix.
15. Add 10 μg of ConA to four 25 cm^2 vented tissue culture flasks. We add 10 μL of a 1 mg/mL stock solution to obtain a final concentration of 1 μg/mL ConA (*see* **Note 7**).
16. Using a sterile pipet, transfer 10 mL of the splenocyte suspension to each of the four 25 cm^2 vented tissue culture flasks. Each of the four flasks should have 10 mL of splenocyte suspension and a final concentration of 1 μg/mL ConA.
17. Place the flasks horizontally in a humidified incubator set at 37°C with 5% CO_2. Incubate the splenocytes with ConA for 18 h (*see* **Note 8**).

3.3 Retroviral Transduction of T Cells

1. Using a sterile pipet, remove medium and cells in suspension from the 25 cm^2 flasks and transfer to two 50 mL conical tubes. Media and cells from the four flasks can be combined in the conical tubes.
2. Add 10 mL of cold PBS to each flask. Gently swirl the PBS in the flask and transfer the PBS into the two 50 mL conical tubes used in Step 1.
3. Centrifuge the conical tubes at 500 × *g* for 5 min.
4. Thaw chimeric PD1 (chPD1) and wild-type PD1 (wtPD1) ecotropic retroviral supernatants expressed using the EcoPack

2-293 cell line and concentrated using RetroX Concentrator in a 37°C water bath (*see* **Note 9**).

5. Resuspend cells in retroviral supernatant at a concentration of 1×10^6 cells/mL. Divide cells between the two retroviral constructs. Typically, 10 mL of retroviral supernatant is needed per construct.
6. Add 8 μg/mL of Polybrene to each tube of cells. A stock of 10 mg/mL is typically used. For 10 mL of viral supernatant, 8 μL of Polybrene is added.
7. Add 25 IU/mL of rhu IL-2 to each tube of cells. A stock of 10,000 IU/mL rhu IL-2 is typically used.
8. Mix cells well by inverting the tube multiple times.
9. Transfer 2 mL of cells into each well of a tissue-culture-treated 12-well plate. Use one 12-well plate per construct.
10. Seal plates with parafilm.
11. Centrifuge the plates at $1500 \times g$ at 32°C for 1 h.
12. Remove plates from centrifuge, and remove parafilm.
13. Incubate the plates in a humidified incubator set at 37°C with 5% CO_2 for 7 h (*see* **Note 10**).
14. Using a sterile pipet, resuspended cells in each well and transfer to a 50 mL conical tube. Cells with the same construct can be combined in one conical tube.
15. Add 1 mL of cold PBS to each well, and transfer the PBS to the conical tube with the cells.
16. Centrifuge the conical tubes at $500 \times g$ for 5 min.
17. Discard the supernatant, and dissociate the cell pellet. Transfer 50 mL of complete RPMI media to each tube.
18. Add 25 IU/mL of rhu IL-2 to each tube of cells. For 50 mL of medium, 12.5 μL of rhu IL-2 should be added.
19. Transfer cells into one 75 cm^2 vented tissue culture flask per construct.
20. Incubate the flasks horizontally in a humidified incubator set at 37°C with 5% CO_2 for 24 h.

3.4 T Cell Expansion and Selection

1. Add complete RPMI medium and rhu IL-2 to maintain cells between 0.5×10^6 cells/mL and 2×10^6 cells/mL (*see* **Note 11**). Typically, 50 mL of complete RPMI medium and 25 IU/mL of rhu IL-2 are added to each flask.
2. To begin cell selection, add 0.5 mg/mL of G418 to each flask. We add 1 μL of a 50 mg/mL stock solution per mL of medium.
3. Gently swirl contents of flasks to mix. Transfer ½ (50 mL) of medium with cells to a new 75 cm^2 flask. There should be two flasks for each construct.

4. Incubate the flasks horizontally in a humidified incubator set at 37°C with 5% CO_2 for 24 h.
5. Add complete RPMI medium, 25 IU/mL of rhu IL-2, and 0.5 mg/mL of G418 in a similar manner as the previous step. Depending on how many cells are needed at the end of the procedure, all of the cells may be kept, or ½ of the cells may be discarded.
6. Incubate the flasks horizontally in a humidified incubator set at 37°C with 5% CO_2 for 48 h.
7. Warm Histopaque-1083 to room temperature (*see* **Note 12**).
8. Pour cells from the culture flasks into 50 mL conical tubes, keeping the cells for each construct separate.
9. Add 15 mL of cold PBS into each flask. Swirl flask gently, and pour PBS into 50 mL conical tubes.
10. The flasks can be set aside and reused at the end of this step, or the used flasks can be discarded and new flasks can be used.
11. Centrifuge the cells in the 50 mL conical tubes at 500 × *g* for 5 min.
12. Discard the supernatants and disassociate the cell pellets.
13. For each construct, add 20 mL of complete RPMI medium to the cells. Combine the cell pellets with this 20 mL of medium so that there is one tube of cells per construct.
14. Set the speed of the pipet-controller to slow. Insert the sterile pipet into the tube of cells and place the sterile pipet tip at the bottom of the tube. Slowly underlay cells with 10 mL of Histopaque-1083. Make sure the interface is not disturbed during this process.
15. Centrifuge the cells at 360 × *g* for 20 min at room temperature with no brake on the centrifuge.
16. Transfer 35 mL of PBS to a 50 mL conical tube.
17. Using a sterile pipette, slowly harvest the cells at the interface between the medium and Histopaque. Transfer cells to the 50 mL conical tube with 35 mL of PBS. Continue collecting the cells until the cloudy interface is collected. Repeat this process for each construct.
18. Centrifuge the cells in the 50 mL conical tubes at 500 × *g* for 5 min.
19. Discard supernatant and dissociate cell pellet. Add 50 mL of PBS and centrifuge cells at 500 × *g* for 5 min.
20. Discard supernatant, and dissociate cell pellet. Add complete RPMI medium and 25 IU/mL of rhu IL-2 to culture cells at 0.5×10^6 cells/mL. Typically, this requires 100 mL of medium at this step; however, it will depend on how many cells were discarded during the culture procedure.

21. Add cells to 75 cm^2 flasks with 25 IU/mL rhu IL-2 and 50 mL of complete RPMI medium in each flask.
22. Incubate cells at 37°C with 5% CO_2 for 48 h or until use in an assay.
23. Confirm cell surface expression of CAR using flow cytometry. Antitumor efficacy of T cells can also be tested in in vitro or in vivo assays. Transduced T cells are commonly used for in vitro cytotoxicity or cytokine assays (Fig. 1) or in vivo tumor burden assays (Fig. 2).

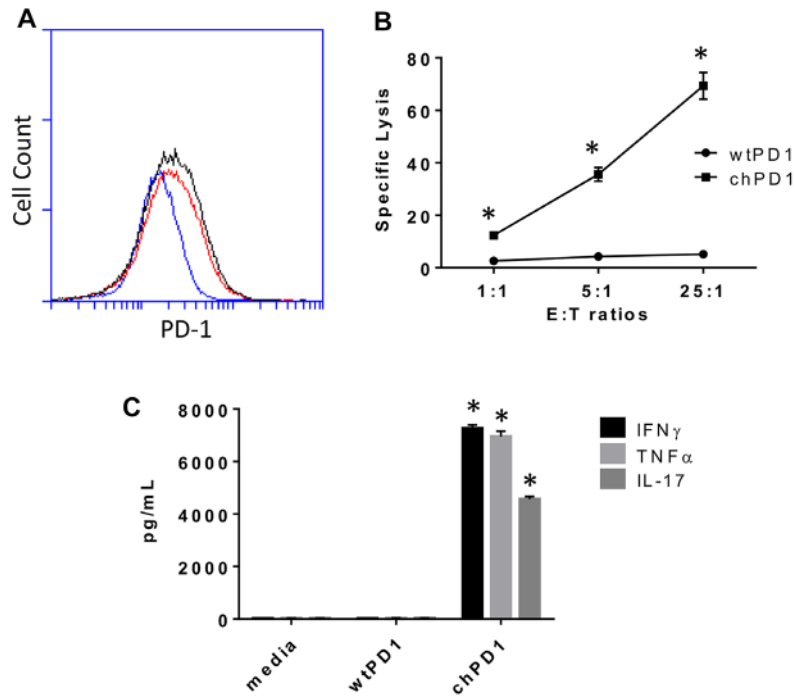


Fig. 1 ChPD1-expressing T cells lyse melanoma cells and secrete proinflammatory cytokines. (**A**) Activated murine T cells expressing wtPD1 (red) or chPD1 (black) constructs were stained with anti-PD1 antibodies and analyzed using flow cytometry. Nontransduced T cells (blue) were also used as a control. (**B**) WtPD1 (circles) or chPD1 (squares) T cells were used as effector cells with B16 melanoma cell targets at the indicated E:T ratios (1:1, 5:1, 25:1), and cell lysis was measured using an LDH assay. ChPD1 T cells had significantly higher specific lysis at all E:T ratios compared to wtPD1 T cells (*$p < 0.001$). (**C**) B16 melanoma cells were cultured with medium or with wtPD1- or chPD1-expressing T cells. After 24 h, secretion of cytokines was measured in cell-free supernatants by LEGENDPlex analysis. chPD1 T cells produced higher levels of proinflammatory cytokines compared to wtPD1 T cells when cultured with B16 melanoma cells (*$p < 0.0001$). Data are presented as mean + SD and are representative of at least three experiments

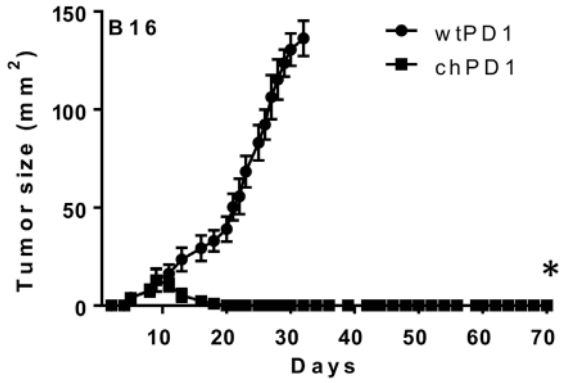


Fig. 2 ChPD1-expressing T cells reduce melanoma tumor burden and increase survival in vivo. B16-F1 tumor cells (10^5) were injected subcutaneously into mice on day 0. Mice were treated i.v. with two doses of wtPD1 (circles) or chPD1 (squares) T cells (5×10^6) after 10 and 13 days and tumor burden and survival were measured ($n = 6$). chPD1 T cells significantly reduced melanoma tumor burden and increased survival compared to wtPD1 T cells ($^*p < 0.01$). Data are presented as mean ± SD and are representative of three independent experiments

4 Notes

1. DMEM and RPMI media need to be removed from the bottle before adding the supplements to account for the volume of supplements added. For a 500 mL bottle of medium, 65.5 mL of supplements are added; therefore, 65.5 mL of medium needs to be removed. This volume can be adjusted according to the size of the medium bottle and volume of supplements added. The 65.5 mL of unsupplemented medium can be discarded or stored at 4°C and used as a medium for washes in later steps of the procedure.
2. 2-mercaptoethanol is an essential reducing agent for T cells. However, this compound degrades quickly when diluted, and fresh 2-mercaptoethanol should be added to the complete RPMI medium bottle every 2 weeks. Adjust the amount added based on the volume of medium in the bottle to maintain a final concentration of 50 μM 2-mercaptoethanol.
3. GP2-293 cells should be 80%–90% confluent when they are transfected with the plasmids.
4. Splenocytes should be isolated from the syngeneic mouse strain based on the melanoma model that us being used. For example, use C57BL/6 mice if you are using the B16 melanoma model.
5. Centrifuge acceleration and deceleration should be set to maximum for all steps unless otherwise indicated.

6. It is important to completely dissociate the pellet before adding new medium. Techniques used to dissociate the pellet can be to flick the tube firmly with your fingers or gently tap the tube on the table surface.
7. ConA is sticky and will settle out of solution. It is important to vortex the ConA stock solution right before use. It is also important to add the ConA directly to each flask.
8. To maximize transduction efficiency, splenocytes need to be cultured with ConA for 18–22 h.
9. Concentrated retroviral supernatants can be prepared prior to T cell transduction. Store retroviral supernatants at −80°C and thaw directly before T cell transduction.
10. Prolonged exposure to Polybrene is toxic to T cells. Therefore, it is essential to only culture the T cells with retroviral supernatants and Polybrene for a total of 8 h (1 h in the centrifuge and 7 h in the incubator).
11. When culturing the transduced T cells, the cell concentration needs to not be below 0.5×10^6 cells/mL and not be above 2×10^6 cells/mL throughout the entire cell culture procedure.
12. Histopaque-1083 is light and temperature sensitive. Store this reagent in the dark by wrapping the bottle in aluminum foil and store at 4°C.

Acknowledgments

This work was supported in part by Longwood University's Faculty Research Grants and Department of Biological and Environmental Sciences.

Competing Interests The author has no conflicts of interest to declare that are relevant to the content of this chapter.

References

1. Brudno JN, Maus MV, Hinrichs CS (2024) CAR T cells and T-cell therapies for cancer: a translational science review. JAMA 332(22):1924–1935
2. Patel KK, Tariveranmoshabad M, Kadu S et al (2025) From concept to cure: the evolution of CAR-T cell therapy. Mol Ther 33(5):2123–2140
3. Rosa CM, Vancheswaran A, Ariyan CE (2024) T-cell immunotherapy for melanoma. Surg Oncol 57:102160
4. Kintz H, Nylen E, Barber A (2020) Inclusion of Dap10 or 4-1BB costimulation domains in the chPD1 receptor enhances anti-tumor efficacy of T cells in murine models of lymphoma and melanoma. Cell Immunol 351:104069
5. Kurachi M, Kurachi J, Chen Z et al (2017) Optimized retroviral transduction of mouse T cells for in vivo assessment of gene function. Nat Protocol 12(9):1980–1998
6. Zhong S, Malecek K, Perez-Garcia A et al (2010) Retroviral transduction of T-cell receptors in mouse T-cells. J Vis Exp 44:2307
7. Eremenko E, Taylor ZV, Khand B et al (2021) An optimized protocol for the retroviral

transduction of mouse CD4 T cells. STAR Protoc 2(3):100719
8. Lynch A, Hawk W, Nylen E et al (2017) Adoptive transfer of murine T cells expressing a chimeric-PD1-Dap10 receptor as an immunotherapy for lymphoma. Immunology 152(3):472–483
9. Parriott G, Deal K, Crean S et al (2020) T cells expressing a chimeric-PD-1-Dap10-CD3zeta receptor reduce tumor burden in multiple murine syngeneic models of solid cancer. Immunology 160(3):280–294



Chapter 40

Retroviral Transduction of Human T Cells with a Chimeric Antigen Receptor Targeting PD-1 Ligands for Melanoma Immunotherapy

Amorette Barber

Abstract

T cells are able to target melanoma-associated antigens in an MHC-independent manner through the expression of chimeric antigen receptors. Using retroviral transduction, these receptor constructs can be efficiently delivered into human $CD4^+$ and $CD8^+$ T cells. In this protocol, we describe the production of retroviral supernatants along with the activation, transduction, expansion, and selection of human T cells engineered to express a chimeric PD-1 receptor. This method can be readily adapted for any human chimeric antigen receptor construct.

Keywords Immunotherapy, T cell, Melanoma, Chimeric antigen receptor, Retroviral transduction, Human

1 Introduction

Chimeric antigen receptor (CAR) T-cell therapy has transformed the treatment for several hematologic malignancies, and expanding this approach to melanoma is an active and promising area of research [1, 2]. Driven by a growing set of targetable tumor antigens, including CSPG4, CD70, GD2, VEGFR2, c-Met, HER2, TYRP1, MAGE-A3, Gp100, MART-1, NY-ESO-1, and PD-1 ligands, ongoing efforts aim to develop CAR T-cell strategies capable of overcoming the unique immunologic and microenvironmental barriers posed by melanoma [3–6].

Retroviral transduction of T cells has been central to advancing cellular engineering approaches for adoptive cell therapy in cancer and other diseases [7–9]. This is a rapid and cost-effective method for genetically modifying cells and is widely employed to achieve stable expression of TCR or CAR constructs in human $CD4^+$ and $CD8^+$ T cells. However, retroviral transduction of human T cells does have several challenges, including low transduction efficiency,

Kristian M. Hargadon (ed.), *Melanoma*, Methods in Molecular Biology, vol. 3089,
https://doi.org/10.1007/978-1-0716-5619-8_40,
© The Author(s), under exclusive license to Springer Science+Business Media, LLC, part of Springer Nature 2027

the requirement for robust T-cell activation and division, and limited stability of retroviral vectors [8, 9]. We describe an optimized protocol for efficiently transducing primary human T cells with a chimeric antigen receptor that targets ligands of the PD-1 receptor. Using high-titer retroviral supernatants produced in GP2-293 cells together with a Moloney Murine Leukemia Virus (MMLV)–derived vector, we achieved robust and reliable gene transfer into activated human T cells. We also describe optimized conditions for T-cell activation and timing of retroviral exposure, both of which are essential for efficient retroviral infection and integration and T-cell expansion and survival [8, 9]. In addition, we outline key parameters for T-cell culture, including the concentration of IL-2, use of G418 resistance for selecting transduced cells, and isolation of viable engineered T cells with Ficoll-Paque Plus. Using these optimized techniques, we achieved efficient transduction and robust expression of the CAR in highly viable, functional primary human T cells. To demonstrate the protocol, we employed a human chimeric PD-1 (chPD1) receptor composed of the extracellular domain of PD-1 fused to the cytoplasmic signaling domains of the Dap10 costimulatory receptor and CD3ζ [5, 6]. This protocol can be readily adapted for the expression of alternative human CAR constructs.

2 Materials

Prepare all reagents under sterile conditions. Prepare and store all reagents at 4°C unless otherwise noted. Follow all appropriate disposal and safety procedures for a BSL-2 protocol.

2.1 Retroviral Supernatant Production

1. GP2-293 packing cell line
2. pVSV-G envelope vector
3. MMLV-retroviral plasmid with wild-type- or chimeric-PD1 CAR gene (or other CAR construct) and G418 resistance gene
4. Xfect polymer transfection reagent
5. Retro-X concentrator
6. Complete DMEM medium: DMEM medium supplemented with 10% heat-inactivated fetal bovine serum, 100 U/mL penicillin, 100 μg/mL streptomycin, 1 mM pyruvate, 10 mM Hepes, and 0.1 mM nonessential amino acids. Remove 65.5 mL of medium from a 500 mL bottle of DMEM medium (*see* **Note 1**). To the remaining 435 mL of DMEM medium, add 5 mL of 10,000 U/mL stock solution of penicillin–streptomycin, 5 mL of 1 M stock solution of HEPES, 5 mL of 100× stock solution of nonessential amino acids (NEAA), and 50 mL of heat-inactivated fetal bovine serum

2.2 T-Cell Isolation and Activation

1. Complete RPMI medium: RPMI medium supplemented with 10% heat-inactivated fetal bovine serum, 100 U/mL penicillin, 100 µg/mL streptomycin, 1 mM pyruvate, 10 mM Hepes, 0.1 mM nonessential amino acids, and 50 µM 2-mercaptoethanol. Remove 65.5 mL of media from a 500 mL bottle of RPMI media (*see* **Note 1**). To the remaining 435 mL of RPMI medium, add 5 mL of 10,000 U/mL stock solution of penicillin–streptomycin, 5 mL of 1 M stock solution of HEPES, 5 mL of 100× stock solution of nonessential amino acids (NEAA), 500 µL of a 50 mM stock solution of 2-mercaptoethanol, and 50 mL of heat-inactivated fetal bovine serum (*see* **Note 2**).
2. Cell Culture Phosphate-Buffered Saline: 1×, pH 7.4.
3. 125 µg/mL of purified antihuman CD3 antibodies (clone HIT3a).
4. 10,000 IU/mL of recombinant human interleukin-2 (rhu IL-2) in sterile H_2O. Store at −20°C.

2.3 Transduction, Expansion, and Selection of T Cells

1. 10 mg/mL of polybrene in sterile H_2O. Store at −20°C.
2. 50 mg/mL of G418 Sulfate in sterile H_2O.
3. Ficoll–Paque Plus.

3 Methods

Carry out all procedures at room temperature in a BSL-2 certified biosafety cabinet under sterile conditions unless otherwise noted. All plastics and reagents should be sterile.

3.1 Retroviral Supernatant Production

1. Add GP2-293 cells (5×10^6) in 10 mL of complete DMEM to a 100 mm cell culture dish.
2. Culture cells in a humidified incubator set at 37°C with 5% CO_2 for 24 h (*see* **Note 3**).
3. Dilute 15 µg of MMLV-retroviral plasmid DNA containing the gene for chimeric-PD1 CAR construct in 300 µL of Xfect Reaction buffer. Repeat this step to dilute the plasmid with the wild-type PD1 CAR construct.
4. Dilute 15 µg of pVSV-G envelope vector in 300 µL of Xfect Reaction buffer.
5. Combine the diluted retroviral plasmid from Step 3 and the diluted pVSV-G plasmid from Step 4 into one tube and vortex for 5 s.
6. Add 9 µL of Xfect polymer to the plasmid mixture. Mix well by vortexing for 10 s.
7. Incubate the mixture at room temperature for 10 min.

8. Add the mixture dropwise to the GP-293 cells.
9. Gently rock the plate back and forth to mix well.
10. Culture cells in a humidified incubator set at 37°C with 5% CO_2 for 12 h.
11. Remove the media from the cells and replace with 10 mL of fresh complete DMEM.
12. Culture cells in a humidified incubator set at 37°C with 5% CO_2 for an additional 24 h.
13. Transfer the retroviral supernatants into 50 mL conical tubes. Centrifuge the supernatants at 500 × *g* for 10 min (*see* **Note 4**).
14. Transfer the supernatants to a new 50 mL conical tube, being careful to avoid the cell pellet. Add 1 volume of Retro-X concentrator for three volumes of retroviral supernatant. Mix gently by inversion.
15. Incubate overnight at 4°C.
16. Centrifuge mixture at 1500 × *g* for 45 min at 4°C.
17. Remove and discard supernatant, being careful not to disturb the pellet. Gently resuspend the pellet with complete DMEM using 1/10th of the original volume of retroviral supernatant that was concentrated.
18. Fresh retroviral supernatants can be used to transduce T cells or can be stored at −80°C.

3.2 T-Cell Activation

1. Resuspend 2×10^7 human peripheral blood mononuclear cells (PBMCs) in 20 mL of complete RPMI medium in a 50 mL conical tube for a final concentration of 10^6 cells/mL.
2. Add 1 μg/mL of purified antihuman CD3 antibody (clone HIT3a) to the PBMCs. For 20 mL of PBMCs, we add 6.25 μL of a 125 μg/mL stock solution of antihuman CD3 antibodies.
3. Add 50 IU/mL of rhu IL-2 to the tube of PBMCs. A stock of 10,000 IU/mL rhu IL-2 is typically used.
4. Invert the tube slowly multiple times to mix.
5. Transfer the PBMC mixture to one 75 cm^2 vented tissue culture flask.
6. Place the flask horizontally in a humidified incubator set at 37°C with 5% CO_2. Incubate the PBMCs with anti-CD3 antibodies and rhu IL-2 for 3 days (*see* **Note 5**).

3.3 Retroviral Transduction of T Cells

1. Using a sterile pipet, remove medium and cells in suspension from the 75 cm^2 flask and transfer to one 50 mL conical tube.

2. Add 10 mL of cold PBS to the flask. Gently swirl the PBS in the flask, and transfer the PBS into the 50 mL conical tube used in Step 1.
3. Divide the cell mixture evenly into two 50 mL conical tubes. Each tube should have 15 mL of the PBMC mixture.
4. Centrifuge the conical tubes at 500 × *g* for 5 min.
5. Thaw chimeric PD1 (chPD1) and wild-type PD1 (wtPD1) retroviral supernatants expressed using the GP2-293 cell line and concentrated using RetroX Concentrator in a 37°C water bath (*see* **Note 6**).
6. Resuspend cells in retroviral supernatant at a concentration of 10^6 cells/mL. Divide cells between the two retroviral constructs. Typically, 10 mL of retroviral supernatant is needed per construct.
7. Add 8 μg/mL of polybrene to each tube of cells. A stock of 10 mg/mL is typically used. For 10 mL of viral supernatant, 8 μL of polybrene is added.
8. Add 50 IU/mL of rhu IL-2 to each tube of cells.
9. Mix cells well by inverting the tube multiple times.
10. Transfer 2 mL of cells into each well of a tissue-culture-treated 12-well plate. Use one 12-well plate per construct.
11. Seal plates with parafilm.
12. Centrifuge the plates at 1500 × *g* at 32°C for 1 h.
13. Remove plates from centrifuge, and remove parafilm.
14. Incubate the plates in a humidified incubator set at 37°C with 5% CO_2 for 7 h (*see* **Note 7**).
15. Using a sterile pipet, resuspend cells in each well, and transfer to a 50 mL conical tube. Cells with the same construct can be combined in one conical tube.
16. Add 1 mL of cold PBS to each well, and transfer the PBS to the conical tube with the cells.
17. Centrifuge the conical tubes at 500 × *g* for 5 min.
18. Discard the supernatant, and dissociate the cell pellet. Transfer 20 mL of complete RPMI medium to each tube for a final cell concentration of 0.5×10^6 cells/mL.
19. Add 50 IU/mL of rhu IL-2 to each tube of cells. For 20 mL of medium, 10 μL of rhu IL-2 should be added.
20. Transfer cells into one 75 cm^2 vented tissue culture flask per construct.
21. Incubate the flasks horizontally in a humidified incubator set at 37°C with 5% CO_2 for 48 h.

3.4 T-Cell Expansion and Selection

1. Add complete RPMI medium and rhu IL-2 to maintain cells between 0.5×10^6 cells/mL and 2×10^6 cells/mL (*see* **Note 8**). Typically, 20 mL of complete RPMI medium and 50 IU/mL of rhu IL-2 are added to each flask.
2. To begin cell selection, add 0.5 mg/mL of G418 to each flask. We add 1 μL of a 50 mg/mL stock solution per mL of medium.
3. Incubate the flasks horizontally in a humidified incubator set at 37°C with 5% CO_2 for 24 h.
4. Add complete RPMI medium, 50 IU/mL of rhu IL-2, and 0.5 mg/mL of G418 in a similar manner as the previous step. Gently swirl contents of flasks to mix. Transfer half (30 mL) of the medium with cells to a new 75 cm^2 flask. There should be two flasks for each construct.
5. Depending on how many cells are needed at the end of the procedure, all of the cells may be kept, or half of the cells may be discarded.
6. Incubate the flasks horizontally in a humidified incubator set at 37°C with 5% CO_2 for 48 h.
7. Warm Ficoll-Paque Plus to room temperature (*see* **Note 9**).
8. Pour cells from the culture flasks into 50 mL conical tubes, keeping the cells for each construct separate.
9. Add 15 mL of cold PBS into each flask. Swirl the flask gently, and pour PBS into 50 mL conical tubes.
10. The flasks can be set aside and reused at the end of this step, or the used flasks can be discarded and new flasks can be used.
11. Centrifuge the cells in the 50 mL conical tubes at $500 \times g$ for 5 min.
12. Discard the supernatants and disassociate the cell pellets.
13. For each construct, add 20 mL of complete RPMI medium to the cells. Combine the cell pellets with this 20 mL of medium so that there is one tube of cells per construct.
14. Set the speed of the pipet controller to slow. Insert the sterile pipet into the tube of cells and place the sterile pipet tip at the bottom of the tube. Slowly underlay cells with 10 mL of Ficoll-Paque Plus. Make sure the interface is not disturbed during this process.
15. Centrifuge the cells at $400 \times g$ for 30 min at room temperature with no brake on the centrifuge.
16. Transfer 35 mL of PBS to a 50 mL conical tube.
17. Using a sterile pipette, slowly harvest the cells at the interface between the medium and Ficoll-Paque Plus. Transfer cells to

the 50 mL conical tube with 35 mL of PBS. Continue collecting the cells until the cloudy interface is collected. Repeat this process for each construct.

18. Centrifuge the cells in the 50 mL conical tubes at 500 × *g* for 5 min.
19. Discard supernatant and dissociate cell pellet. Add 50 mL of PBS and centrifuge cells at 500 × *g* for 5 min.
20. Discard supernatant, and dissociate cell pellet. Add complete RPMI medium and 50 IU/mL of rhu IL-2 to culture cells at 0.5×10^6 cells/mL. Typically, this requires 50 mL of medium at this step; however, it will depend on how many cells were discarded during the culture procedure.
21. Add cells to 75 cm^2 flasks with 50 IU/mL rhu IL-2 and 50 mL of complete RPMI medium in each flask.
22. Incubate cells at 37°C with 5% CO_2 for 48 h or until use in an assay.
23. Confirm cell surface expression of CAR using flow cytometry. Antitumor efficacy of T cells can also be tested in in vitro assays. Transduced T cells are commonly used for in vitro cytotoxicity or cytokine assays (Fig. 1).

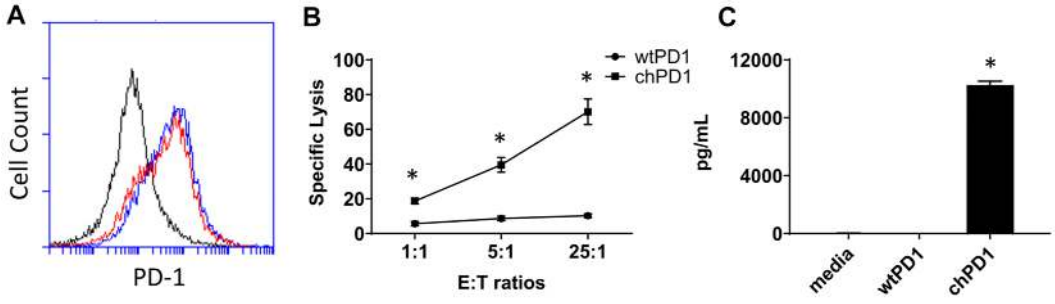


Fig. 1 Human chPD1-expressing T cells lyse melanoma cells and secrete IFNγ. (**A**), Activated human T cells expressing wtPD1 (red) or chPD1 (blue) constructs were stained with anti-PD1 antibodies and analyzed using flow cytometry. Nontransduced T cells (black) were also used as a control. (**B**), WtPD1 (circles) or chPD1 (squares) T cells were used as effector cells with A-375 melanoma cell targets at the indicated E:T ratios (1:1, 5:1, and 25:1), and cell lysis was measured using an LDH assay. ChPD1 T cells had significantly higher specific lysis at all E:T ratios compared to wtPD1 T cells (*$p < 0.001$). (**C**), A-375 melanoma cells were cultured with medium or with wtPD1- or chPD1-expressing T cells. After 24 h, secretion of IFNγ was measured in cell-free supernatants by ELISA. chPD1 T cells produced higher levels of IFNγ compared to wtPD1 T cells when cultured with A-375 melanoma cells (*$p < 0.0001$). Data are presented as mean + SD and are representative of at least three experiments

4 Notes

1. DMEM and RPMI media need to be removed from the bottle before adding the supplements to account for the volume of supplements added. For a 500 mL bottle of medium, 65.5 mL of supplements are added; therefore, 65.5 mL of medium needs to be removed. This volume can be adjusted according to the size of the medium bottle and volume of supplements added. The 65.5 mL of unsupplemented medium can be discarded or stored at 4°C and used as a medium for washes in later steps of the procedure.
2. 2-mercaptoethanol is an essential reducing agent for T cells. However, this compound degrades quickly when diluted, and fresh 2-mercaptoethanol should be added to the complete RPMI medium bottle every 2 weeks. Adjust the amount added based on the volume of medium in the bottle to maintain a final concentration of 50 μM 2-mercaptoethanol.
3. GP2-293 cells should be 80%–90% confluent when they are transfected with the plasmids.
4. Centrifuge acceleration and deceleration should be set to maximum for all steps unless otherwise indicated.
5. Human PBMCs should be cultured with purified antihuman CD3 antibodies and rhu IL-2 for 3 days for maximum retroviral transduction efficiency. It is important to not disturb the flask during this time to allow for maximum T cell activation to occur.
6. Concentrated retroviral supernatants can be prepared prior to T cell transduction. Store retroviral supernatants at −80°C, and thaw directly before T cell transduction.
7. Prolonged exposure to polybrene is toxic to T cells. Therefore, it is essential to only culture the T cells with retroviral supernatants and polybrene for a total of 8 h (1 h in the centrifuge and 7 h in the incubator).
8. When culturing the transduced T cells, the cell concentration needs to not be below 0.5×10^6 cells/mL and not be above 2×10^6 cells/mL throughout the entire cell culture procedure.
9. Ficoll-Paque Plus is light sensitive. Store this reagent in the dark by wrapping the bottle in aluminum foil.

Funding

This work was supported in part by Longwood University's Faculty Research Grants and Department of Biological and Environmental Sciences.

Conflicts of Interest The author has no conflicts of interest to declare that are relevant to the content of this chapter.

References

1. Posey AD, Young RM, June CH (2024) Future perspectives on engineered T cells for cancer. Trends Cancer 10(8):687–695
2. Khan SH, Choi Y, Veena M et al (2025) Advances in CAR T cell therapy: antigen selection, modifications, and current trials for solid tumors. Front Immunol 15: 1489827
3. Kharasakhal O, Maher J (2026) CAR-T cell immunotherapy of malignant melanoma. Expert Rev Clin Immunol 22(1):43–59
4. Rosa CM, Vancheswaran A, Ariyan CE (2024) T-cell immunotherapy for melanoma. Surg Oncol 57:102160
5. Kintz H, Nylen E, Barber A (2020) Inclusion of Dap10 or 4-1BB costimulation domains in the chPD1 receptor enhances anti-tumor efficacy of T cells in murine models of lymphoma and melanoma. Cell Immunol 351: 104069
6. Parriott G, Deal K, Crean S et al (2020) T cells expressing a chimeric-PD-1-Dap10-CD3zeta receptor reduce tumor burden in multiple murine syngeneic models of solid cancer. Immunology 160(3):280–294
7. Edes I, Clauss J, Stahn R et al (2022) TCR and CAR engineering of primary human T cells. Methods Mol Bio 2521:85–93
8. Koste L, Beissert T, Hoff H et al (2014) T-cell receptor transfer into human T cells with ecotropic retroviral vectors. Gene Ther 21(5):533–538
9. Jaballah SA, Ali LM, Jehad MA et al (2025) Retroviral vector technology for gene therapy: history, current landscape, and future prospects. J Mol Biol 437(24):169473

INDEX

A

Adipocytes 19, 85–93
Angiopellosis 242, 246
Animal models
  horse 13
  mouse
    genetically engineered mice 6, 9
  swine 15
    libechov minipig 15
    munich miniature swine troll 15
    sinclair miniature swine 15
  zebrafish 16

B

Biodistribution 212, 214–215, 308–309, 312–314
Bioinformatics
  next-generation sequencing
    metagenomic shotgun 449
  RNA-sequencing 145, 481, 484
Biomarker
  lipidomics 428
  metabolomics 417
  peptidomics 403–404
  salivary biomarker 418
  serum biomarker 191, 228, 404
Bioprinting 19, 146–147

C

Cancer exodus hypothesis 242
Canine oral melanoma 404
Cell adhesion
  integrin 311
Cell culture
  3D cell culture
    hydrogel 143–144, 147
    tumor spheroid 18
  cell lines
    B16-F1 ..... 6, 26–28, 42, 49, 53, 56, 60–61, 66
    B16-F10 ..... 6, 294
    CCD-1137Sk 542, 544–546, 548
    D5.1G4 ..... 49, 53, 56–57, 60–61, 66
    HaCaT 86, 92, 139, 542, 544–546, 548
    SK-MEL-28 ..... 229, 231, 542, 545–546, 548
    SV-LEC 96–98, 103
    YUMM 10–11, 534
    YUMMER 11
Cell invasion 86, 116, 118, 121, 252, 542
Cell migration
  transwell assay 116
  wound healing 107–108, 111, 116
  wound scratch 108–109, 111
Circulating tumor cells (CTCs) 242, 245
Co-culture 18, 59–60, 68, 86–87, 89–93, 99, 545, 557, 572
Crosstalk 210

D

Diagnostic 174, 191, 266–268, 282, 288, 293, 308–310, 312–313, 329, 340, 418, 424, 460, 472
Drug screening 542

E

Electroporation
  irreversible electroporation 533–534
  reversible electroporation 533–539
Epithelial–mesenchymal transition (EMT) 115–116, 227–229, 266
Exosomes 172–175, 177–186, 189–191, 201, 203, 211, 270
Extracellular matrix (ECM) 5, 18–19, 85–86, 96, 107–108, 133–134, 136–137, 140, 143, 209–211, 252
Extracellular vesicles (EVs) 19, 171–174, 181, 189–192, 202–203, 210–212, 228–229, 231, 233
Extravasation 241–242, 244–246, 376

F

Fibroblasts 18–19, 85–91, 93, 134, 136, 139–140, 211, 542, 544

Kristian M. Hargadon (ed.), *Melanoma*, Methods in Molecular Biology, vol. 3089,
https://doi.org/10.1007/978-1-0716-5619-8,

© The Editor(s) (if applicable) and The Author(s), under exclusive license to Springer Science+Business Media, LLC, part of Springer Nature 2027

Flow cytometry 38, 50, 57, 61, 73–74, 76, 81, 96–97, 99, 103, 116, 118–119, 122, 214, 218, 220–221, 350, 391, 393, 396–397, 518, 553–555, 565, 567–569, 572, 574, 576, 598, 609
FOXC2 ..... 26, 28, 36–40, 43–44, 116–119, 121–122

G

Genetic engineering
  CRISPR-Cas9
    CRISP-ID 44–45
    gRNA design 28, 31, 39–40
  expression vector 48
  gene editing 26, 42, 45
  gene knockout 9, 26, 30, 38–40, 42

H

Heterogeneity 4, 7–8, 18
High endothelial venules (HEV) 210, 363, 365
Hypoxia 85, 148, 266, 295, 297, 300–301, 303, 317

I

Imaging
  cellprofiler 254–255, 262
  computed tomography 265, 330–331, 334–335, 344–347
  imagej 254
  immunofluorescence 216, 222, 252
  intravital microscopy 245
  lightsheet microscopy 242–243
  live-cell imaging 254, 262
  melanoma probes
    fluorescent probes 266, 293, 295
    multi-analyte sensing 282, 294–295, 304
    tyrosinase sensors 270, 272, 275, 329
  multiplex immunofluorescence histology 350–351
  positron emission tomography 265, 272, 325, 330, 340, 344–345, 347
  single-photon emission computed tomography
    ^{99m}technetium 330, 331, 334–335, 340
  theranostics
    radiopharmaceuticals 308–309, 312–314
Immune infiltration
  tumor infiltrating lymphocyte 349–350, 376, 551
In *vitro* modeling 5, 134
Iodixanol gradient 193, 196, 199

K

Keratinocytes 11, 18–19, 85–87, 89–91, 93, 134, 136–138, 140, 270, 542, 544

L

Limiting dilution cloning 30, 33, 42, 44–45, 55
Liquid biopsy blood
  plasma 190
  serum 190
Lymphadenectomy 192, 194
Lymphatic drainage 192
Lymphatic endothelium 96
Lymphatic exudate 192, 194
Lymph node (LN) 7, 12, 14–15, 61–62, 64–65, 68, 95–96, 100–101, 145, 192, 210–219, 221–223, 265, 350, 358–359, 364, 370, 372, 383–385, 552, 573, 583

M

Malignant melanoma (MM) 5, 10, 116, 307, 312, 329, 542
Mass spectrometry
  liquid chromatography-mass spectrometry/mass spectrometry 391, 404, 407–408, 411, 444
  matrix-assisted laser desorption/ionization time-of-flight mass spectrometry 404, 408–411
  secondary ion mass spectrometry 427–438
Matrix metalloproteinase (MMP) 86
Melanin 3, 6, 48, 85, 268–269, 272, 288–289, 299, 312–314, 317–318, 324, 329–330, 335–336
Melanocortin 1 receptor (MC1R) 269, 308–310, 314, 339–340
Metabolism
  central carbon flux 390
  chemical isotope labeling
    ^{13}C metabolic labeling 420
  glucose uptake 73, 78, 80
  LC–MS metabolomics 390
  metabolite 398, 418
  2-NBDG 73–74, 78, 81
  redox homeostasis
    aloe-emodin 390
    emodin 390
  seahorse assay 390, 392
  stable isotope tracing 390–391, 399–400
Metastasis 6–8, 10, 12–13, 15–18, 73, 107, 115, 209–211, 241–242, 252, 265, 282, 300, 311, 314, 317, 324, 335, 346, 403, 459, 501
Microbiome
  bacterial translocation 552
  fecal sampling 442, 444–445
  gut microbiota 441–442, 451, 551–552
Microfluidics 116, 191–192
MicroRNA (miRNA)
  miR-CATCHv2.0 ..... 473, 476, 479, 481, 483, 485–487, 490, 493

Monoclonal antibody 50–51, 60, 268, 297, 300, 505, 514, 517, 519–520, 523
Mutations
BRAF 4, 7, 10, 19, 191
NRAS 4, 10, 14

O

Optical 16, 270, 275, 289, 462, 466, 518, 547

P

Plasmid 6, 27–28, 30–32, 41, 43, 50, 52–54, 56–57, 61, 63, 65–66, 148, 487–489, 491, 534–539, 592–594, 599, 604–605, 610
Plasticity 73, 115, 143, 171, 227, 252, 389, 397, 401
Post-transcription regulation 471

R

Rapid exosome isolation using size exclusion chromatography (REIUS) 172–174, 177
Reactive oxygen species (ROS) 270, 274–275, 277, 281–282, 284, 288, 293–295, 297, 300–302, 390–392, 396–397, 401
Retroviral transduction 591, 595, 603, 606, 610

S

Sequencing
next-generation sequencing 460, 466, 478
sanger sequencing 29, 36–37, 44
Size exclusion chromatography (SEC) 172–175, 178–180, 185, 190, 196–198, 201–202, 215, 222
Skin organ constructs (SOCs) 116, 134–140
Spatial organization 350, 376, 382
Stromal cells 12, 86, 90–92, 172
Subcellular architecture
lysosomes 251–252, 254, 260
organelle positioning 251–252
radial distribution 252, 260–261
Surface-enhanced Raman scattering (SERS) 228–233, 235
Surface plasmon resonance (SPR) 518–520, 526–529

T

Tertiary lymphoid structures (TLS) 350, 363–367, 370–373, 385
Therapy
adoptive cell transfer 7, 47, 591, 603
cancer vaccine
lipoplex nanoparticle 541
mRNA vaccine 542
chimeric antigen receptor therapy 591–592, 603–604
gene therapy 591, 604
immune checkpoint blockade
CTLA-4 ..... 349, 376, 551, 565
PD-1 ..... 349, 376, 551 , 565
PD-L1 ..... 349, 364, 551
immunotherapy 47, 86, 313–314, 349, 351, 375–376, 441, 445–446, 451, 538, 552, 591–592
targeted therapy 86, 459
therapeutic antibody 517–519, 526, 529
Transcription factor 4, 26, 40, 116, 145–146, 148–149, 151, 267–268, 300–301, 555–556, 569, 573, 586
Transcriptome
NGS whole transcriptome analysis 460, 464, 469
Tryptophan 2,3-dioxygenase (TDO2) 501–502, 504, 506, 511–514
Tumor antigen
cancer/testis antigen 48
melanocyte differentiation antigen 48
neoantigen 48, 50, 55, 57, 60, 64
Tumor cell isolation 242, 245, 593, 604–605
Tumor immunity
B cell 365, 372, 376
CD4+ T cell
helper T cell 350
regulator T cell 518
CD8+ T cell
cytotoxic T lymphocyte 7, 14, 47, 350
dendritic cell 211–212, 349, 351, 551
macrophage 211–212, 350–351
Tumor infusion 60, 242
Tumor microenvironment (TME) 13, 19–20, 85–86, 96, 116, 171–172, 211, 252, 294–295, 300, 351, 364–365, 375–377, 518, 534, 538, 552

U

Ultracentrifugation 174, 190, 195–199, 215, 222
Ultrafiltration 173, 178–180, 185
Ultrasound 265
Ultraviolet (UV) light 3, 11–12, 14, 29, 245, 248, 288, 562

V

Vesicle uptake 211–212

W

Western blotting 92, 193, 510–513

X

Xenograft transplantation 6, 8, 13, 16–17